



HAL
open science

Multicomponent reactions with lawsone scaffold: towards antiparasitic and diversely biologically active compounds

Christina Koumpoura

► **To cite this version:**

Christina Koumpoura. Multicomponent reactions with lawsone scaffold: towards antiparasitic and diversely biologically active compounds. Parasitology. Université Paul Sabatier - Toulouse III, 2023. English. NNT: 2023TOU30226 . tel-04471368

HAL Id: tel-04471368

<https://theses.hal.science/tel-04471368>

Submitted on 21 Feb 2024

HAL is a multi-disciplinary open access archive for the deposit and dissemination of scientific research documents, whether they are published or not. The documents may come from teaching and research institutions in France or abroad, or from public or private research centers.

L'archive ouverte pluridisciplinaire **HAL**, est destinée au dépôt et à la diffusion de documents scientifiques de niveau recherche, publiés ou non, émanant des établissements d'enseignement et de recherche français ou étrangers, des laboratoires publics ou privés.



THÈSE

**En vue de l'obtention du
DOCTORAT DE L'UNIVERSITÉ DE TOULOUSE
Délivré par l'Université Toulouse 3 - Paul Sabatier**

**Présentée et soutenue par
Christina KOUMPOURA**

Le 16 novembre 2023

**Réactions multicomposants de lawsone: vers des composés
antiparasitaires et diversement actifs sur le plan biologique**

Ecole doctorale : **SDM - SCIENCES DE LA MATIERE - Toulouse**

Spécialité : **Chimie-Biologie-Santé**

Unité de recherche :

LCC - Laboratoire de Chimie de Coordination

Thèse dirigée par

Anne ROBERT et Michel BALTAS

Jury

M. Bruno FIGADÈRE, Rapporteur

M. Rachid BENHIDA, Rapporteur

Mme Elisabeth DAVIOUD-CHARVET, Examinatrice

M. Alexander DOMLING, Examineur

Mme Anne ROBERT, Directrice de thèse

M. Michel BALTAS, Co-directeur de thèse

Mme Florence BEDOS-BELVAL, Présidente

AKNOWLEDGEMENTS

First of all, I would like to thank all the members of my jury: B. Figadère, R. Benhida, F. Bedos-Belval, E. Davioud-Charvet and A. Dömling for taking the time to evaluate my thesis manuscript and my research work as specialists in the field. It is a pleasure to see that three years of really hard work have finally led to a fruitful scientific discussion, with promising results and good prospects.

A really big "thank you" comes from the bottom of my heart and goes straight to my two supervisors. I probably need a chapter to explain how much I have learned alongside them and how grateful I am to have been given the opportunity to work with them both. Anne Robert is the mother of the team, she takes care of everything, she is never tired and she can assure you just by looking you in the eye. There have been hard times, there have been good times and she has always been there looking at me, just shaking her head and I have felt this security that something will come out of it in the end! Anne, thank you for calming me down when I was stressed, thank you for pointing me in the right direction when I didn't know which way to go and felt lost, and of course thank you for teaching me to pay attention to detail! Yes, details make all the difference in science, you were right.

What can I say about Michel Baltas... I still remember his call when I was accepted for this position. "You will be with us next year! ". Michel was always there for me, even when he was on holiday or at a family dinner. I cannot find the right words for someone who supported every silly idea I had, never said no to buying the most expensive reagent for just one test, and literally forced me to become better every day. I am also grateful for his confidence in leaving me on my own at times, when I felt it was my turn to show the way! I enjoyed it a lot and that made me grow!

I will never forget the support I received from all the permanent members of the team. Jean-Michel kept me up to date with the latest bibliography on malaria, Lucie and Françoise taught me parasitology and Françoise never refused any mission I wanted to take part in. It is something that I never took for granted and is very much appreciated.

I owe a special thanks to Michel Nguyen for his patience, kindness and availability, and of course for all his honest advice on the scientific and non-scientific discussions we had over the years. I would also like to thank all my colleagues with whom I have spent time in the lab. I have fond memories with each and every one of you: Stone, Bruna, Katarina, Anthony, Naomie, Anna, Chloé, Nadja, Marco, Maxime, Jana, Naka, Anissa and Imen. I really feel that I have become real friends with some of you and that we have broken through the "colleague" barrier. Thank you for the good times!

All my respect goes to F. Benoit-Vical, P. M. Loiseau, M. R. Pasca, S. Chopra and their research groups for testing our compounds against different pathogens. Special thanks to A. Garcia-Sosa for teaching me how to perform the docking studies during my short stay in Estonia. I have discovered a whole new world and fell in love with it! I am also grateful for the collaboration with J-M Sotiropoulos, as the DFT studies were necessary to support our experimental results.

Now let's get out of the lab! I cannot find the right words to express my gratitude for meeting all these amazing kind people: Yael, Vlad, Oleksandr, Marine, Massimo, Nargiz, Azadeh, Ion, Onkar and Livia. I made real friends who were there to celebrate the good moments, but also to put me "out of my misery" when things seemed to be going wrong. All the coffee breaks and short trips, all the "just one beer" that turned into very long party nights, really kept me sane and motivated. Thank you for your emotional support and I am so proud of all you Doctors and future Doctors!

At home... there was Alex! Alex was there from the time I woke up until the time I came home from the lab (sometimes very late). I don't know how many times he must have heard "I'm quitting tomorrow!!!" during those 3 years, but the answer was always the same "Honey, you can do this and I'm just here for you". And he was! He was there to support me, to advise me, to make me a very nice meal after a very long day and to force me to see the good side of every difficulty. He became my family and he was there, solid, every day, with kind words and kind deeds, without judging me, just understanding me. A paragraph is not enough to dedicate to this man I am grateful to have in my life. And he completely changed it!

But where are the Greeks? Well, now I live in France, but a part of my heart is always back home, where I have people I love so much. Special thanks to my dearest friends Pantelis, Nikos, Nikoletta, Antonis and Elisabeth for all their support over the years and I promise that now that this is coming to an end, I will try to visit them more often!

Finally, and very importantly, I would like to thank my family, my parents: Yiasemi, Leonidas and my sister: Panayiota, for all the love and support they have given me throughout my childhood and all my university studies. I am grateful for pushing me to leave my comfort zone and for inspiring me to always try for the best.

Well, everyone says that a PhD is a very hard process, there is a lot of stress and so much work and it is a dark period! I will be honest, it is. But there have been so many colors and so many fantastic days that I will never forget as I had all of you by my side! Thank you!

Bonne lecture!

To my family: Yiasemi, Leonidas and Panayiota

To Alexandre

TABLE OF CONTENTS

List of abbreviations	1
Résumé de thèse	5
Chapter 1: General Introduction	33
1.1 Vector-borne parasitic diseases in humans	35
1.2 Malaria	36
1.2.1 Vector	37
1.2.2 Pathogen: <i>Plasmodium</i> spp.	37
1.2.3 Symptoms	39
1.2.4 Malaria treatment: chemotherapy and drug resistance	39
1.2.5 <i>Plasmodium</i> mitochondrial targets	43
1.2.6 Atovaquone: a bc1 inhibitor	45
1.3 Leishmaniasis	45
1.3.1 Vector	46
1.3.2 Pathogen: <i>Leishmania</i> spp.	46
1.3.3 Symptoms	48
1.3.4 Leishmaniasis treatment and drug resistance	48
1.4 Naphthoquinones and the lawsone scaffold	49
1.5 Multicomponent reactions	52
1.5.1 The history of MCRs	52
1.5.2 MCRs and Medicinal Chemistry	55
1.6 Objectives	56
1.7 References	57
Chapter 2: Lawsone in domino reaction with aldehydes and alkyl-isocyanides: synthetic approaches and biological activities	65
2.1 Introduction	67
2.1.1 Naphthofuroquinones and biological activities	67
2.1.2 The synthetic procedures leading to naphthofuroquinones (NFQs)	71
2.2 Results and discussion	79
2.2.1 Chemistry-Synthesis	79
2.2.1.1 Reaction conditions for optimization studies	79
2.2.1.2 Structure characterization of model compound 2.69	82
2.2.1.3 Substrate scope for domino multicomponent reaction	85

2.3 Biological and <i>in silico</i> evaluation of the synthesized series	93
2.3.1 Activities against <i>P. falciparum</i> and <i>in silico</i> studies	93
2.3.2 Activities against <i>L. donovani</i>	105
2.3.3 Activities against other pathogens	111
2.4 Conclusion and Perspectives	112
2.5 Experimental Part	115
2.5.1 Materials and methods	115
2.5.2 Synthetic protocols	116
2.5.3 Compounds characterization	117
2.5.4 Computational and docking experiments	129
2.6 References	131
Chapter 3: Lawsone in Biginelli reaction with aldehydes and (alkyl)ureas: synthetic approaches and biological activities	135
3.1 Introduction	137
3.1.1 3,4-Dihydropyrimidinones exhibit diverse biological activities	137
3.1.2 One step synthesis of 3,4-dihydropyrimidinones : The Biginelli reaction	141
3.1.3 Multi-step synthesis of fused 3,4-dihydropyrimidinone-naphthoquinones	148
3.2 Results and discussion (Part I)	149
3.2.1 Chemistry-Synthesis	149
3.2.1.1 Reaction conditions optimization studies	149
3.2.1.2 Structure characterization of model compound 3.43	153
3.2.1.3 Substrate scope for the mechanochemically activated Biginelli-type reaction	154
3.2.1.4 X-ray diffraction analysis of compound 3.61	156
3.2.1.5 The reaction with <i>p</i> -anisaldehyde	157
3.2.1.6 Cyclization attempts of Biginelli-linear 3.43 and 3.46 in solution	159
3.2.1.7 Theoretical studies	161
3.2.1.8 Cyclization attempts of Biginelli-linear 3.46 via activation of the 2-hydroxy function	165
3.3 Biological and <i>in silico</i> evaluation of the Biginelli-linear series	167
3.3.1 In silico evaluation against mitochondrial targets of <i>P. falciparum</i>	168
3.3.2 Biological evaluation of Biginelli-linear series	179
3.4 Results and discussion (Part II)	181
3.4.1 Chemistry-Synthesis of <i>O</i> -methylated Biginelli-linear compounds	182

3.4.1.1	Reaction conditions for optimization studies	182
3.4.1.2	Structure characterization of monomethylated compound 3.72	183
3.4.1.3	Synthesis of a small library of O-methylated Biginelli-linear derivatives	185
3.5	Biological and <i>in silico</i> evaluation of the O-methylated Biginelli-linear series	187
3.5.1	Activities against <i>P. falciparum</i> <i>in vitro</i> and <i>in silico</i> studies	187
3.5.2	Activities against <i>L. donovani</i>	195
3.5.3	Activities against various microorganisms	198
3.6	Conclusion and Perspectives	200
3.7	Experimental Part	202
3.7.1	Materials and methods	202
3.7.2	Synthetic protocols and compounds characterization	203
3.7.3	Docking experiments	230
3.8	References	231
4.1	General Conclusion	236
ANNEXES		240

LIST OF ABBREVIATIONS

μw	microwaves
2D NMR	two-dimensional NMR
ACN	acetonitrile
AcOEt	ethyl acetate
ACTs	artemisinin-based combination therapies
AIM	action and investment to fight malaria
ART	artemisinin
ATQ	atovaquone
Boc	<i>tert</i> -butyl carbamate
CAN	ammonium cerium (IV) nitrate
CL	cutaneous leishmaniasis
CQ	chloroquine
Cy	cyclohexyl
cyt	cytochrome
DBU	1,8-diazabicyclo(5.4.0)undec-7-ene
DCE	1,2-dichloroethane
DCM	dichloromethane
DDQ	2,3-dichloro-5,6-dicyano-1,4-benzoquinone
DEA	diethyl amine
DES	deep eutectic solvent
DFT	density functional theory
DHA	dihydro-artemisinin
DHODH	dihydroorotate dehydrogenase
DHPM	3,4-dihydropyrimidinone
DMF	<i>N,N'</i> -dimethyl formamide
DMSO	dimethyl sulfoxide
EDDA	ethylenediaminediacetic acid
ESI	electrospray ionization
ETC	electron transport chain
EtOH	ethanol
FCC	flash column chromatography
FDA	food and drug administration

GR	glutathione reductase
GTS	global technical strategy for malaria
h	hour(s)
HCl	hydrochloric acid
Hex	hexane
HMPA	hexamethylphosphoramide
HPLC	high performance (or pressure) liquid chromatography
HRMS	high resolution mass spectrometry
IL	ionic liquid
IR	infrared
LC	liquid chromatography
LDA	lithium diisopropylamide
M	million(s)
MCR(s)	multicomponent reaction(s)
MeOH	methanol
min	minute(s)
ML	mucosal leishmaniasis
MMV	medicines for malaria venture
MS	mass spectrometry
NBS	<i>N</i> -bromosuccinimide
NFQ	naphthofuroquinone
NMP	<i>N</i> -methyl-2-pyrrolidone
NMR	nuclear magnetic resonance
PDB	protein data bank
PE	petroleum ether
pTSA	<i>para</i> -toluenesulfonic acid
py	pyridine
Q	ubiquinone
QH ₂	ubiquinol
RA	reversing agent
RDS	rate-determining step
R _f	retention factor
rt	room temperature
SARs	structure-activity relationship studies

THF	tetrahydrofuran
TI	therapeutic index
TLC	thin layer chromatography
TMAF	tetramethyl ammonium fluoride
TMS	tetramethylsilane
TR	trypanothione reductase
UV	ultraviolet
VBDs	vector-borne diseases
VL	visceral leishmaniasis
WHO	world health organization
XCV	<i>N</i> -[(1 <i>R</i>)-1-(5-cyano-1 <i>H</i> -pyrazol-3-yl)ethyl]-3-methyl-4-{1-[6(trifluoromethyl)pyridin-3-yl]cyclopropyl}-1 <i>H</i> -pyrrole-2-carboxamide

Résumé de thèse

1. Introduction

Les maladies parasitaires à transmission vectorielle

Les maladies parasitaires à transmission vectorielle (MTVs) sont des maladies causées par des parasites, transmis à l'homme et/ou à l'animal, par des vecteurs (ou hôtes intermédiaires). Elles représentent plus de 17 % de l'ensemble des maladies infectieuses au monde et causent plus de 700 000 décès par an. Elles sont essentiellement répandues dans les zones tropicales et subtropicales. Elles touchent de manière disproportionnée les populations les plus pauvres, et contribuent également à maintenir la pauvreté [1].

De nos jours, la distribution accrue des MTVs dans le monde est le résultat de nombreux facteurs tels que l'augmentation du tourisme international, le commerce, l'urbanisation non planifiée, l'immigration, l'importation de denrées alimentaires, le manque de sensibilisation du public et le non-respect des principes d'hygiène de base [1,2]. Les grandes épidémies de maladies à transmission vectorielle ont affecté les populations du monde entier, car elles font des victimes et chargent les systèmes de santé nationaux. En outre, elles peuvent parfois provoquer des souffrances chroniques chez les victimes, ce qui peut entraîner une stigmatisation sociale des patients et de leurs familles [2]. Malgré les progrès économiques, sociaux et technologiques réalisés depuis le 19^{ème} siècle, les maladies à transmission vectorielle sont toujours considérées comme un problème majeur de santé publique, et pas seulement pour les sociétés impactées. Parmi toutes les maladies parasitaires à transmission vectorielle, les deux maladies le plus impactantes sont principalement le paludisme (malaria) et la leishmaniose car elles sont très infectieuses et les plus répandues au monde et depuis peu aux pays européens du sud [3,4]. Mes recherches porteront sur la conception et la synthèse de nouvelles molécules à activité antiparasitaire.

Le paludisme et les médicaments utilisés

Le paludisme est une maladie parasitaire transmise par des moustiques femelles du genre *Anopheles*. Ces moustiques sont des hôtes intermédiaires infectés par les parasites *Plasmodium*, qu'ils transmettent à l'homme et aux animaux lors d'un repas sanguin. Parmi les cinq espèces infectant l'homme, *P. falciparum*, *P. vivax*, *P. ovale*, *P. malariae* et *P. knowlesi*, les plus répandues sont *P. falciparum* et *P. vivax*. L'espèce responsable de l'immense majorité des décès est *P. falciparum*. En 2019, le nombre de cas de paludisme aurait dépassé les 220 millions, causant 400.000 décès, principalement en Afrique [5,6]. Même si des vaccins sont actuellement en phase de tests cliniques ou en cours de développement [7], les chimiothérapies classiques restent les méthodes principales pour lutter contre le paludisme.

Deux familles de médicaments peuvent être distinguées : la chloroquine et les dérivés d'artémisinine (utilisés seuls ou en combinaison avec d'autres agents antipaludiques).

Actuellement, le traitement causé par *P. falciparum* est une Combinaison Thérapeutique à base d'Artémisinine (CTA). Il s'agit d'une combinaison à dose fixe de deux médicaments, un dérivé de l'artémisinine (**1.3**) (souvent l'artésunate (**1.5**) ou l'artémether (**1.4**)) et un dérivé à plus longue durée d'action comportant une structure quinoléine (amodiaquine (**1.8**), méfloquine (**1.9**), pipéraqine (**1.10**)) ou une autre aromatique (pyronaridine (**1.13**), luméfántrine (**1.11**)) (Fig. R.1) [8]. Malheureusement, la résistance émergente à l'artémisinine qui est le médicament le plus efficace, et en général aux ACTs, s'est maintenant répandue dans les régions du sud de l'Asie et en Afrique, ce qui rend les perspectives de traitement du paludisme très inquiétantes [9].^{a1}

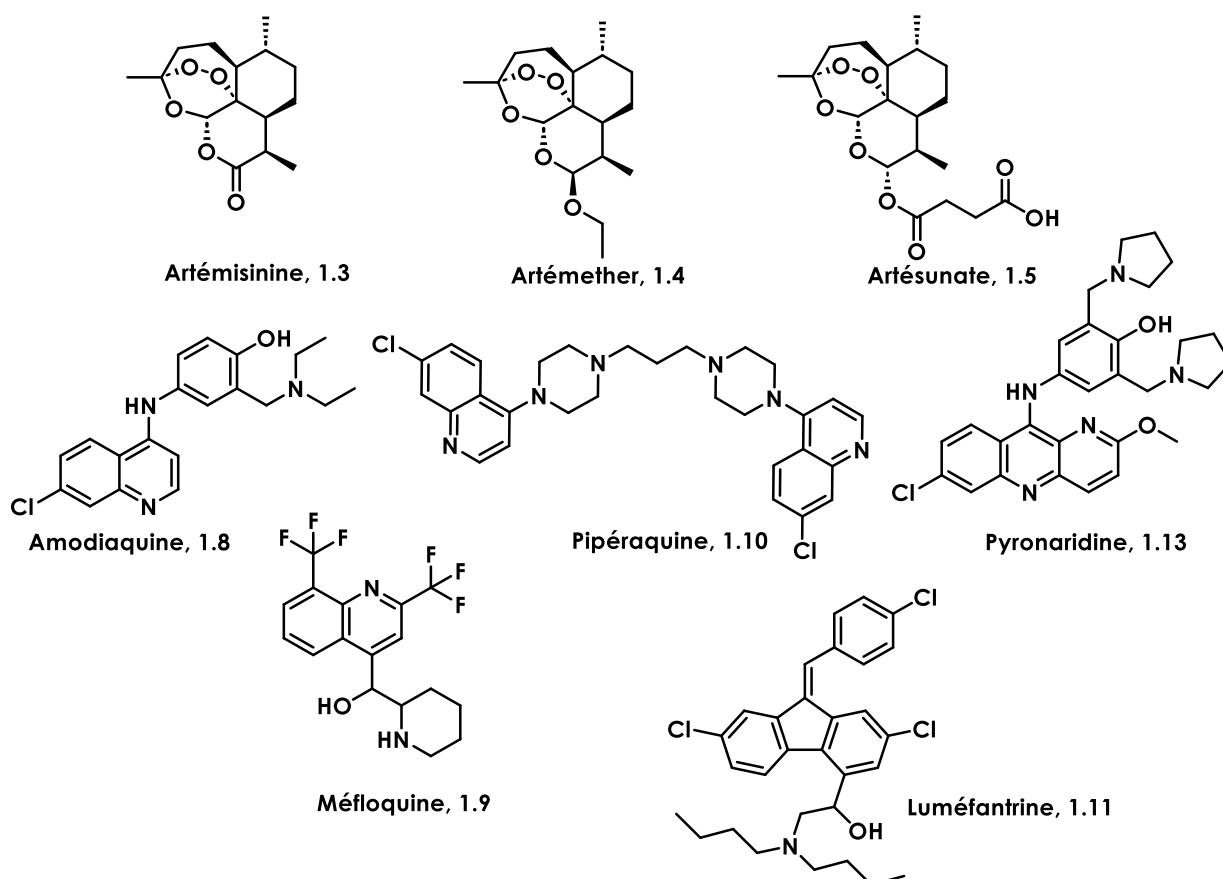


Figure R.1. Les médicaments utilisés comme traitements contre le paludisme, dans le cadre des CTAs.

La résistance principale à l'artémisinine est due à l'habilité de parasites à entrer dans un état de quiescence pour échapper aux médicaments utilisés. Lors de l'arrêt du traitement les parasites quiescents se réveillent et peuvent proliférer à nouveau [10, 11]. Les projections épidémiologiques indiquent qu'en 2040, le niveau de résistance parasitaire en Afrique

^{a1} La numérotation des composés est exactement la même que dans la thèse.

imposera de changer d'arsenal thérapeutique car les médicaments actuellement en développement ne sont pas adaptés au traitement de parasites quiescents. Pour anticiper cette situation, il faudra développer des molécules spécifiques, fondées sur la compréhension de ce mécanisme de résistance par quiescence.

Les cibles mitochondriales chez *Plasmodium*

La chaîne respiratoire mitochondriale joue un rôle essentiel à la survie du parasite chez l'hôte et elle reste active quand les parasites entrent dans leur état dormant. La mitochondrie contient deux principales cibles enzymatiques essentielles qui sont aussi liées biochimiquement : le cytochrome bc1 et l'enzyme dihydroorotate déshydrogénase (DHODH) [12].

Le cytochrome bc1 est un hétérodimère multi-sous-unités localisé dans la membrane mitochondriale interne. La composition des sous-unités peut varier selon les organismes vivants. Le cytochrome bc1 possède un domaine catalytique contenant trois sous-unités essentielles : le cytochrome c, le cytochrome c1 et la protéine fer-soufre de Rieske. Bc1 est l'élément clé du processus de transfert d'électrons mitochondrial brièvement décrit comme suit : l'ubiquinol est oxydé en ubiquinone Q_0 dans le site oxydatif, ce qui entraîne la libération de deux protons dans l'espace intermembranaire. L'ubiquinone est ensuite réduite en ubiquinol Q_i dans le site réducteur, en reprenant deux protons de la matrice [13]. Dans le parasite, l'ubiquinone oxydée de bc1 est utilisée par la dihydroorotate déshydrogénase pour générer de l'orotate qui est un intermédiaire essentiel dans la biosynthèse de la pyrimidine. Alors que la plupart d'organismes utilisent à la fois les voies *de novo* et de récupération pour générer des pyrimidines, *Plasmodium* ne dispose pas des gènes nécessaires à ce dernier processus, ce qui fait de la synthèse *de novo* de la pyrimidine une voie essentielle à sa survie [14]. Pour cette raison, le cytochrome bc1 et l'enzyme DHODH sont deux cibles primordiales de chimiothérapie antipaludique.

L'atovaquone et son mécanisme d'action

L'atovaquone (Fig. R.2, **1.35**) est un médicament antipaludique comportant une structure 2-hydroxy-1,4-naphtoquinone (ou lawsone, **1.35**), qui cible le complexe cytochrome bc1. L'atovaquone est utilisée en association avec le proguanil (Malarone) pour le traitement de la malaria causée par *Plasmodium falciparum* (y compris *P. falciparum*/*P. vivax* résistants à la chloroquine). C'est un analogue de l'ubiquinone qui agit comme un inhibiteur compétitif du site Q_0 du cytochrome bc1 [15]. Malheureusement, le développement de mutations ponctuelles dans le site Q_0 du cytochrome bc1 du parasite entraîne l'émergence rapide de souches résistantes à l'atovaquone, ce qui réduit considérablement son efficacité antipaludique [16].

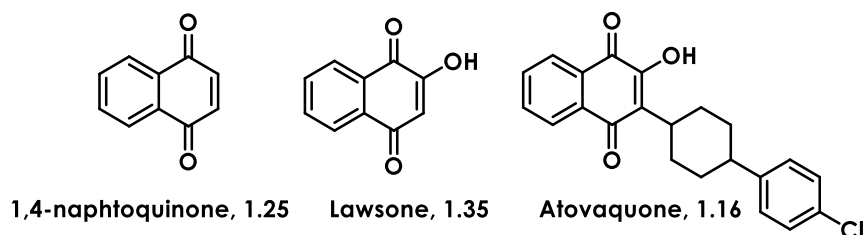


Figure R.2. L'atovaquone est une molécule antipaludique qui cible le complexe bc1 de la mitochondrie de *Plasmodium*.

La leishmaniose et les médicaments utilisés

La leishmaniose est une maladie parasitaire négligée, à transmission vectorielle, causée par des parasites appartenant à la famille des *Trypanosomatidae* et au genre *Leishmania spp.* Cette maladie infectieuse menace plus de 350 millions de personnes à travers le monde, dans 98 pays, avec 12 millions de cas rapportés chaque année. L'incidence annuelle de la leishmaniose est estimée à environ 0.2 à 0.4 millions de cas déclarés pour la forme viscérale qui est une forme létale en absence de traitement [17]. La thérapie, dominée durant de nombreuses années par l'utilisation des médicaments ayant pour base l'antimoine (Sb) comme traitement de première intention, est actuellement peu efficace [18]. Au cours des vingt dernières années, plusieurs autres médicaments sont utilisés afin de lutter contre cette maladie menaçante tels que : les antimoniés pentavalents (SbV) (**1.18-1.19**), la miltéfosine (**1.21**), la paromomycine (**1.22**) et l'amphotéricine B (**1.20**) (Fig. R.3).

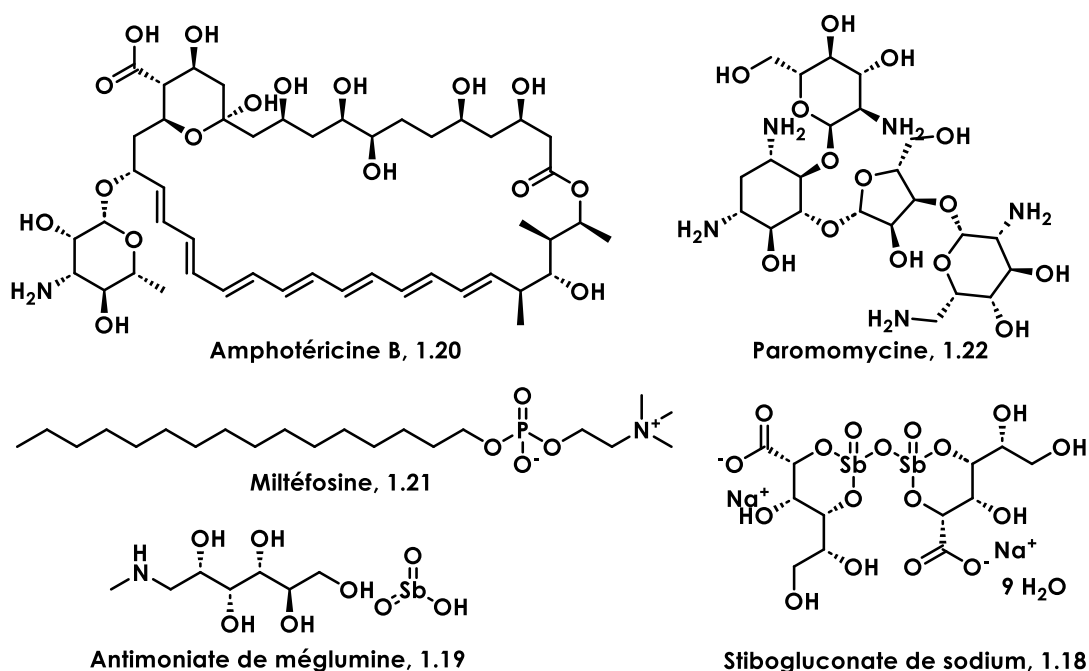


Figure R.3. Les médicaments utilisés comme traitements contre la leishmaniose.

Malheureusement, une chimiorésistance a été observée et signalée chez des patients traités par de l'antimoniate de méglumine. L'augmentation alarmante du nombre d'isolats

cliniques résistants de *Leishmania major* apparus, constitue une menace majeure pour la santé publique et il est donc indispensable de mettre au point de nouveaux médicaments [19].

Les activités biologiques variées de naphthoquinones

Les naphthoquinones sont largement répandues dans la nature et elles ont été étudiées depuis l'Antiquité pour leurs activités pharmacologiques. Les naphthoquinones naturelles ont toujours été une source d'inspiration pour les chimistes qui cherchent à synthétiser de nouvelles molécules bioactives. À cet égard, de nombreux dérivés synthétiques de la 1,4-naphthoquinone ont été signalés pour leurs activités antipaludiques [20]-[22] (composés **1.27-1.29**), leishmanicides [23],[24] (composés **1.30-1.31**), anticancéreuses [25] (composé **1.32**), antibactériennes [26] (composé **1.33**), antivirales [27] (composé **1.34**) (Fig. R.4).

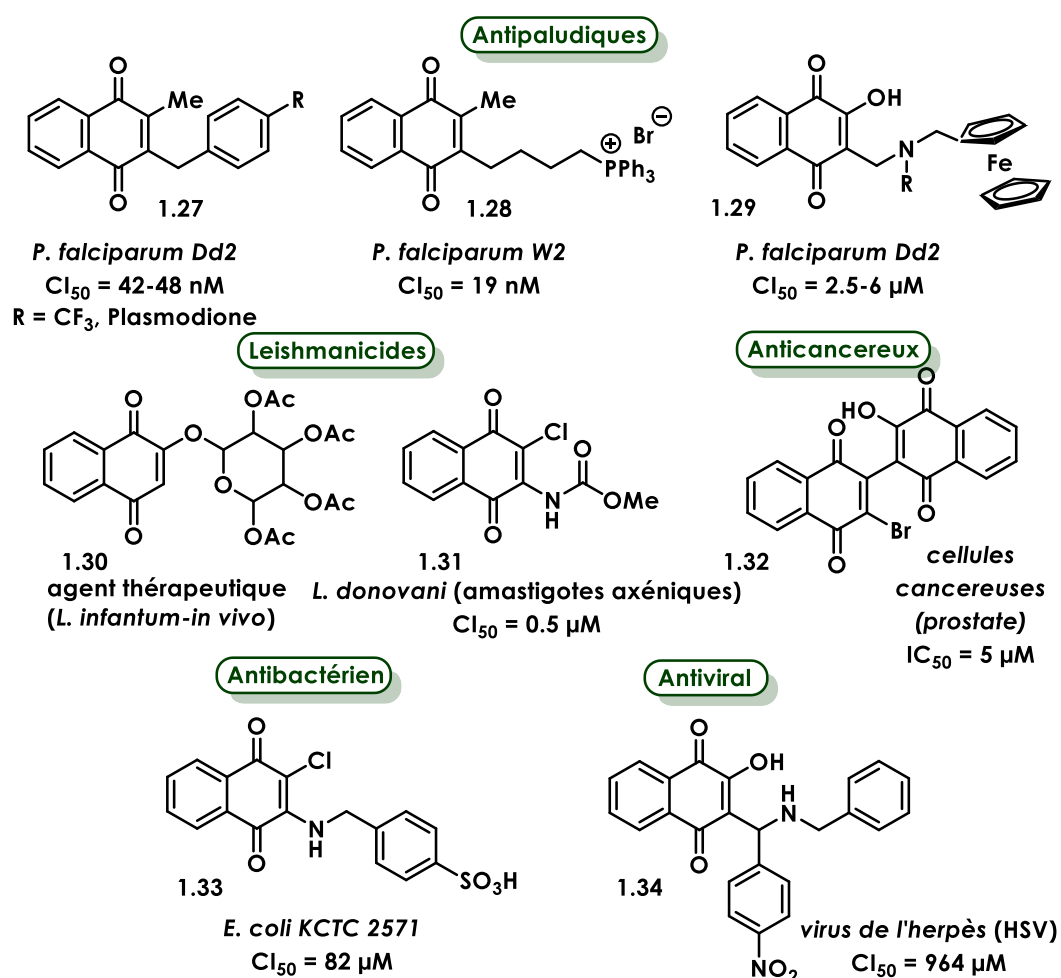


Figure R.4. Quelques exemples de 1,4-naphthoquinones synthétiques avec des activités biologiques variées.

Un outil des chimistes organiciens vers les composés bioactifs : les réactions multicomposants

Les réactions à composants multiples (RCM) sont des méthodes de synthèse qui peuvent conduire à un seul produit à partir de trois réactifs ou plus, en une seule étape, par le biais d'une cascade de réactions élémentaires [28]. La popularité des RCMs réside dans la simplicité et la polyvalence des procédures expérimentales qui ouvrent l'accès à une large gamme de produits, grâce aux possibilités multiples de combinaisons de réactifs. Le premier exemple rapporté de ces réactions, la synthèse de Strecker d'aminonitriles à partir d'aldéhydes, est apparue dès 1850 et a été peu après développée industriellement pour produire de la méthionine, un acide aminé commun utilisé notamment comme matière première pour la synthèse de médicaments [29]. Il n'a pas fallu longtemps pour que d'autres RCM basées sur le carbonyle soient développées. Parmi elles, la réaction célèbre de Mannich, qui produit des β -aminocarbonyles à partir d'un aldéhyde non énolisable, d'une amine primaire ou secondaire et de formaldéhyde via un intermédiaire iminium [30] et la réaction de Biginelli qui produit des dihydropyrimidinones à partir d'un aldéhyde, d'un β -cétoester et d'une urée [31]. Ces réactions produisent des briques de synthèse importantes pour la chimie médicinale et la synthèse de produits chimiques hétérocycliques. Parallèlement, les RCM basées sur l'isocyanure, faites pour la première fois par Passerini en 1921, sont également devenues un outil dans l'industrie pharmaceutique afin de former des produits qui contiennent un α -acyloxy amide [32]. Une autre RCM basée sur la réactivité de l'isocyanure est la condensation d'Ugi. Cette réaction implique un aldéhyde, une amine, un acide carboxylique et un isocyanure. Elle permet la préparation rapide de dérivés d' α -aminoacylamides, qui servent essentiellement à la recherche de candidats de médicaments en générant de vastes bibliothèques de composés [33].

Les dernières années une recherche active sur les RCM est développée en raison de la nature simple de l'approche qui élimine les étapes multiples d'isolation/purification, fournit une économie d'atomes élevée, limite la génération d'intermédiaires potentiellement toxiques et minimise les déchets. Les RCM ont émergé comme un outil puissant pour la synthèse organique durable, gagnant un intérêt croissant dans la recherche de méthodes respectueuses de l'environnement car elles peuvent intégrer la plupart de critères de la chimie verte [28].

Dans ce contexte, nous sommes intéressés à élaborer de familles de molécules portant le motif 1,4-naphtoquinone en utilisant des nouvelles approches de synthèse. Nous aimerions évaluer ensuite leur activité biologique essentiellement antiparasitaire contre *Plasmodium falciparum* et *Leishmania donovani*. De plus, nous sommes intéressés à étudier *in silico* les bibliothèques focalisées obtenues contre les deux cibles mitochondriales de *P. falciparum* bc1 et DHODH dont la structure de protéines en rayons-X est déjà bien connue. Les méthodologies

de synthèse que nous souhaiterions mettre en œuvre sont de type des réactions multicomposants impliquant la lawsone.

2. Vers des composés antiparasitaires à l'aide de la réaction domino impliquant la lawsone

Parmi les classes différentes de quinones, les naphtoquinones et en particulier les naphtofuroquinones (NFQs) ont suscité un intérêt croissant pour leurs activités pharmacologiques en tant qu'agents antiparasitaires [34-35], anticancéreux [36], antimicrobiens [37] etc. (Fig. R.5). Ces composés peuvent être isolés à partir de sources naturelles ou être obtenus par des approches de synthèse nécessitant de nombreuses étapes et présentant des rendements médiocres.

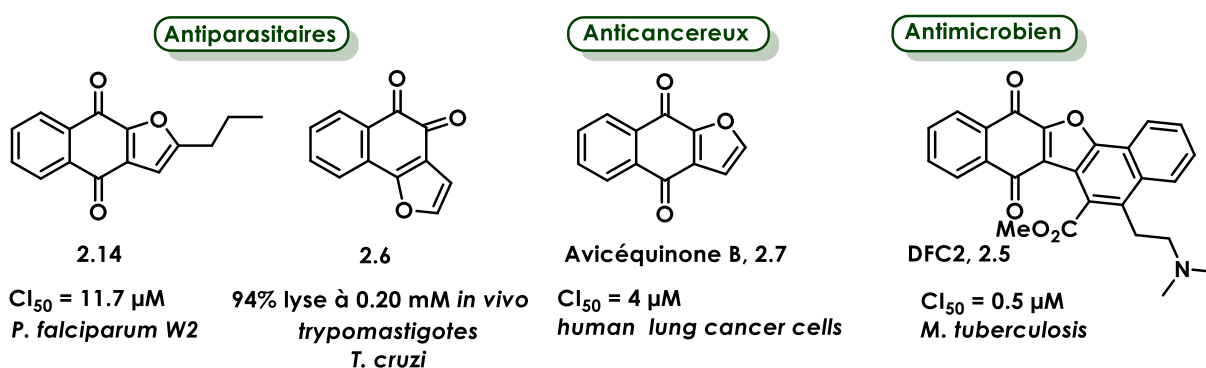


Figure R.5. Les naphtofuroquinones possèdent des activités biologiques variées.

Les quatre voies principales de synthèse des naphtofuroquinones sont présentées dans le Schéma R.1.

La première voie de synthèse est basée sur l'addition [1,4] d'énolates de lithium à des 1,4-naphtoquinones thio-substituées **2.36**, conduisant à la formation de la *para*-naphtofuroquinone attendue **2.41**. Le groupe thio-phenyl en C-2 de la molécule **2.36** joue un rôle crucial pour la détermination de la régiosélectivité de cette réaction. Cependant, cette voie de synthèse utilise des étapes multiples, des temps de réaction longs et des solvants toxiques donnant un rendement total faible (voie i, Schéma R.1) [38].

La deuxième méthode fait intervenir le nitrate d'ammonium cérique (CAN) et un alcène terminal qui par réaction d'oxydation avec la lawsone permet la formation de liaisons C-C produisant des dihydronaphtofuroquinones **2.50**. Elle nécessite ensuite une étape d'oxydation supplémentaire afin d'obtenir les naphtofuroquinones attendues **2.7**. Cette méthode de sélectivité peu contrôlée, fournit des mélanges de deux produits (voie ii, Schéma R.1) [39].

Le couplage de Sonogashira a également été testé afin de construire ce type de motif. Cette préparation en une étape de naphtofuroquinones a été testée en utilisant

l'hétéroannulation médiée par des métaux de transition tels que Pd ou Cu. Bien que le couplage de Sonogashira semble idéal en termes d'économie d'atomes, l'efficacité de cette réaction s'est avérée assez limitée en termes de substitution d'alcynes utilisés. De plus, le temps de réaction varie de façon importante en fonction de la nature du substituant R (voie iii, Schéma R.1) [40].

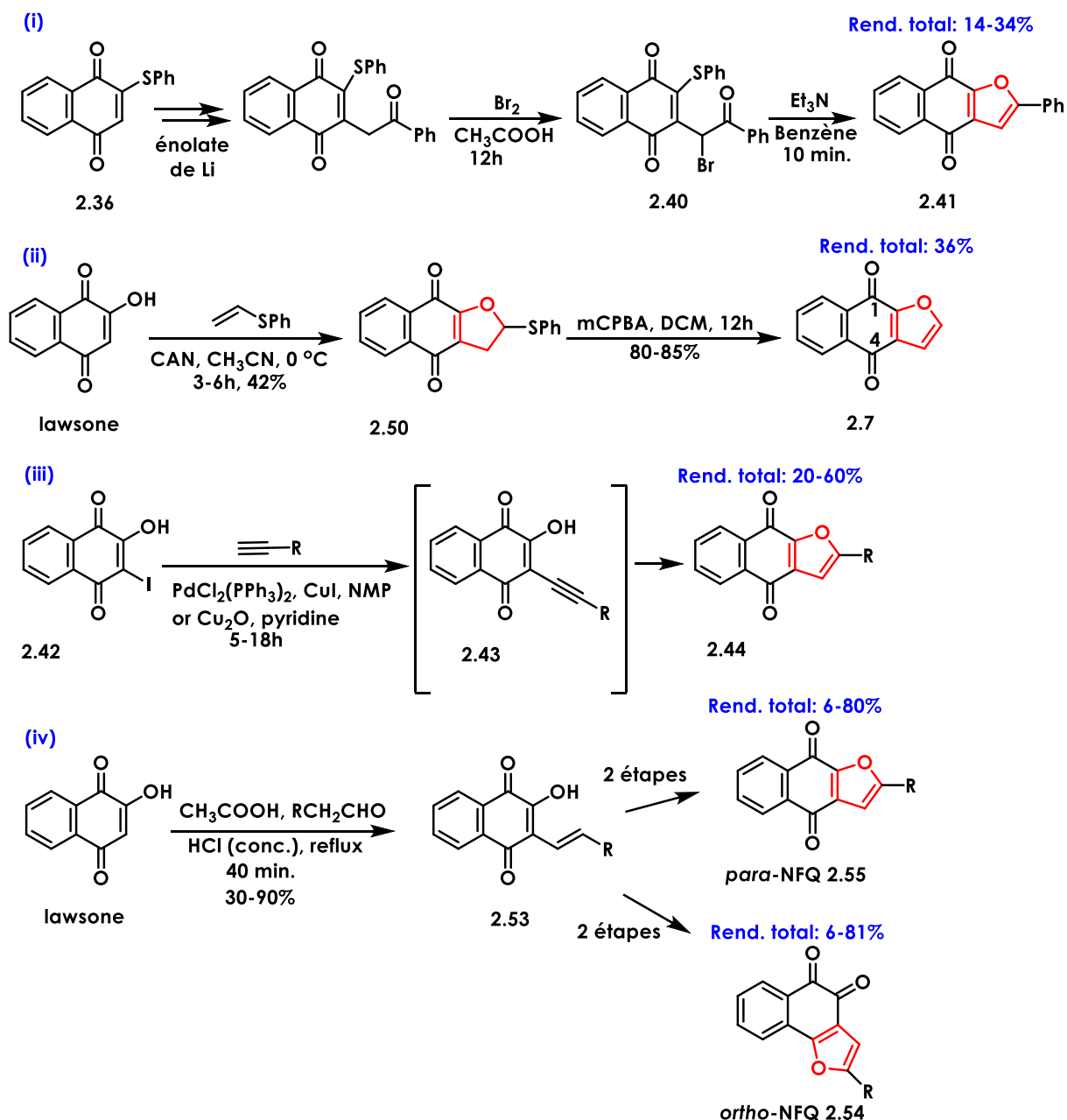


Schéma R.1. Procédures de synthèse des naphtofuroquinones.

Enfin, une méthode proposée par Borgati *et al.* décrit la synthèse sélective de *para*- et *ortho*-naphtofuroquinones en trois étapes à partir de lawsone. Une condensation aldolique entre la lawsone et des aldéhydes, selon une méthode adaptée de Hooker a donné une série de 1'-alcenyl-1,4-naphthoquinones **2.53** avec des rendements compris entre 6% et 81%

(Schéma R.1, voie iv). Les naphthofuroquinones sont préparés ensuite par cyclisation oxydative à partir de **2.53** en utilisant $\text{Hg}(\text{OAc})_2$. Les auteurs ont pu favoriser la formation de l'*ortho*- (**2.54**) ou de la *para*-naphthoquinone (**2.55**) en modifiant le temps de réaction de la deuxième étape. Lorsque les mélanges réactionnels ont été traités avec HCl 2N pendant 15 min, la formation de produits cinétiques (*ortho*) a été favorisée, tandis que la formation de produits thermodynamiques (*para*) a été favorisée lors de temps de réaction plus longs (3 h) [34].

Parmi tous les composés synthétisés, la série des *para*-naphthofuroquinones s'est avérée en général plus active que la série des *ortho*-naphthofuroquinones contre *Plasmodium falciparum*. La naphthofuroquinone **2.14** (Fig. R.5) a présenté la valeur Cl_{50} la plus faible de la série contre la souche W2, résistante à la chloroquine. En outre, les études de docking décrites proposent que ces composés agissent comme inhibiteurs du cytochrome bc1 ou de la DHODH [34].

Dans le but d'introduire également des substituants aminés sur le motif naphthofurane, des équipes ont également travaillé à l'élaboration de 2-amino-naphtho[2,3-b]furan-4,9-diones. Teimouri *et al.* [41] ont rapporté une condensation à trois composants en une seule étape entre la lawsone, un aldéhyde et un isocyanure d'alkyle à reflux dans du toluène. Plus tard, Jiménez-Alonso *et al.* [42] ont décrit une méthode utilisant l'acide éthylène diamine diacétique (EDDA) comme catalyseur, réduisant ainsi le temps de réaction.

Dans le cadre de cette thèse (Chapitre II), nous avons réalisé une étude détaillée de la réaction domino entre la lawsone, des aldéhydes et des isocyanures. Dans un premier temps, nous avons effectué une étude en utilisant une réaction modèle entre la lawsone, le 4-chlorobenzaldéhyde et l'isocyanure de *tert*-butyle dans le but de trouver les conditions optimales car il n'y a pas d'étude similaire pertinente utilisant la lawsone comme réactif [43]. Les méthodes différentes d'activation testées (méthode classique en reflux, irradiation micro-ondes et activation thermique) et la variation de tous les paramètres expérimentaux (solvant, temps de réaction, équivalents des trois réactifs, catalyseur) ont permis de trouver les conditions optimales pour cette réaction spécifique (Schéma R.2).

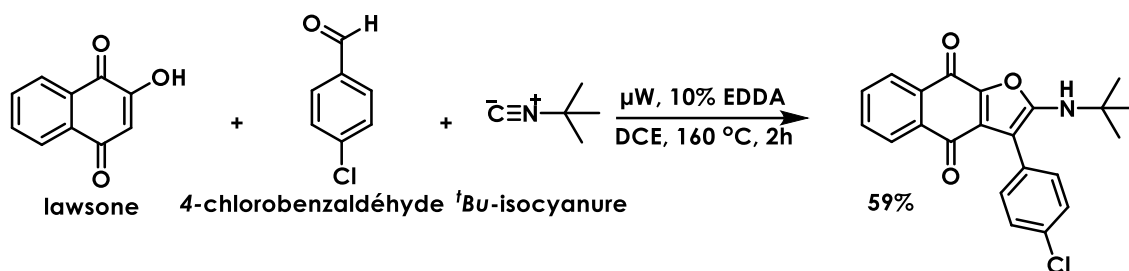
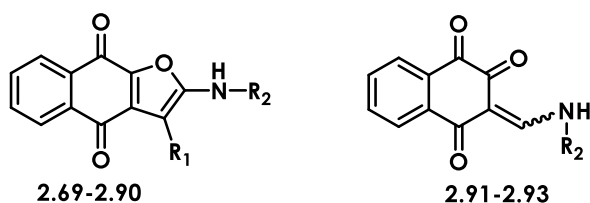


Schéma R.2. Réaction domino modèle utilisée avec ses conditions optimales.

Les conditions optimales trouvées de cette réaction domino sont : une solution équimolaire de trois réactifs (lawsone/aldéhyde/isocyanure, 1 :1 :1) dans du dichloroéthane (DCE) à 160

°C pendant 2 h sous irradiation micro-ondes, en présence de 10 mol% d'acide éthylènediaminodiacétique (EDDA) comme catalyseur. Une série de naphtofuroquinones a été synthétisée en utilisant le même protocole expérimental et en variant l'aldéhyde et l'isocyanure. La réaction est compatible avec tous les types d'aldéhydes utilisés (carbaldéhydes de pipéridine *N*-substitués, benzaldéhydes portant des substituants électro-attracteurs ou donneurs, aldéhydes portant des cycles hétérocycliques). Dans certains cas, pour des aldéhydes pas suffisamment électrophiles, nous avons observé et isolé un autre produit secondaire issu du seul couplage entre la lawsone et l'isocyanure avec un rendement entre 40-50 %. Il s'agit des structures des naphtoénaminodiones jamais décrites auparavant, obtenues en mélange de deux isomères *E* et *Z* dans un rapport 50:50. Ces deux types des structures ont été confirmés par un set détaillé d'analyses RMN 2D. Tous les produits obtenus sont présentés dans le Tableau R.1.

Tableau R.1. Liste de produits obtenus en utilisant la réaction multicomposants domino.



Produit	R ₁	R ₂	Rend. (%)	Produit	R ₁	R ₂	Rend. (%)
2.69			59	2.84			12
2.73			30	2.85			45
2.74			55	2.86			55
2.75			25	2.87			40

2.76			30	2.88			nd
2.77			35	2.89			8
2.78			19	2.90			30
2.79			52	2.91	-		40
2.80			53	2.92	-		50
2.81			46	2.93	-		nd
2.82			42				
2.83			40				

Une librairie focalisée de 19 nouvelles naphtofuroquinones a été ainsi synthétisée. Ces produits sont obtenus en une seule étape sous irradiation micro-ondes. Bien que présentant des rendements modérés, la réaction est complètement sélective, ne fournissant que des *para*-naphtofuroquinones diversement substituées. La réaction est aussi très « flexible », permettant l'utilisation d'aldéhydes et d'isocyanures très variés. Tous les produits ont été isolés

et caractérisés par des techniques spectroscopiques. L'analyse par rayons X (Fig. R.6) et par RMN 2D de la molécule **2.69** a permis la caractérisation non ambiguë de la structure de la naphtofuoroquinone, qui a ensuite été utilisée pour caractériser par analogie tous les produits obtenus de cette série.

Tous les produits de la série ci-dessus ont été évalués *in vitro* contre *Plasmodium falciparum*, *Leishmania donovani* et *Mycobacterium tuberculosis*. Leur affinité pour bc1 et DHODH a été évaluée *in silico* par docking. La structure modélisée AlphaFold2 de l'enzyme du cytochrome Q7HP03 a été utilisée pour caractériser les interactions prévues entre les composés et la cible bc1 (PDB Ref : 4PD4). Pour la cible DHODH, la structure cristalline à rayons X de cette enzyme du *Plasmodium falciparum* a été extraite de la PDB (Ref : 7L01) avec une résolution adéquate pour les études de docking. Les résultats les plus intéressants sont résumés dans le Tableau R.2.

En ce qui concerne les activités antipaludiques, la fonction 2-hydroxy de l'atovaquone joue un rôle crucial dans l'interaction de ce médicament avec sa cible bc1, et la modification de cette interaction est à l'origine de la résistance du parasite à l'atovaquone. La modulation chimique de cette position peut donc permettre de contourner la résistance à ce médicament, qui est le cas pour les deux séries de nos molécules synthétisées : les naphtofuoroquinones et énaminodiones. La série de naphtofuoroquinones s'est révélée avoir des valeurs de CI_{50} plus basses ou au même niveau que la série de *para*-naphtofuoroquinones de Borgati *et al.* [34]. La naphtofuoroquinone **2.80** et les deux énaminodiones **2.91** et **2.92** ont présenté les activités les plus intéressantes contre *Plasmodium falciparum* avec des valeurs de CI_{50} dans la gamme 1.5-2.5 μ M sur la souche F32-ART résistante à l'artémisinine. Il convient toutefois de noter que les naphtofuoroquinones portant le motif *N*-benzyl pipéridine (**2.79**, **2.80**, **2.85** et **2.90**) ont donné les valeurs de CI_{50} les plus intéressantes contre *P. falciparum*, quelle que soit la substitution du groupe amino (*n*-butyl, *tert*-butyl, cyclohexyl). Ceci est cohérent avec les études de docking, car les molécules **2.80**, **2.85** et **2.90** ont donné de très bons scores de docking sur les deux cibles bc1 et DHODH (Tableau R.2).

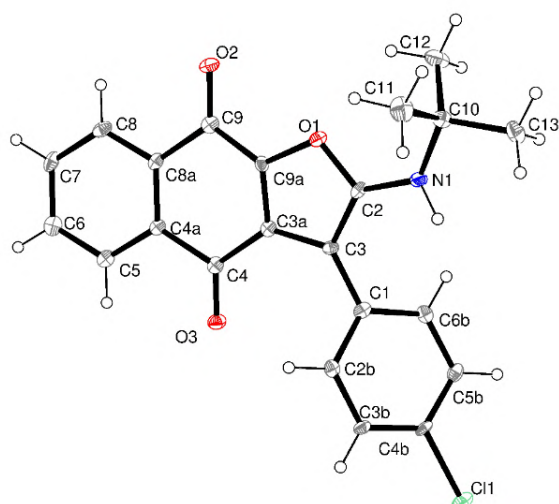


Figure R.6. La structure par diffraction de rayons-X de monocristaux de la molécule **2.69**.

Tableau R.2. Evaluation *in vitro* et *in silico* de certaines naphtofuoroquinones et naphtho-énaminodiones synthétisées.

Composé	<i>P. falciparum</i> F32-ART Cl ₅₀ (µM)	IS ^a	<i>L. donovani</i> LV9 Intramacroph. Cl ₅₀ (µM)	IS ^b	<i>M. tuberculosis</i> H37Rv MIC (µM)	Score docking <i>Pfbc1</i> (kcal/mol)	Score docking <i>PfDHODH</i> (kcal/mol)
2.79	> 10	-	7.0	7.0	> 147	-8.9	-9.4
2.80	2.5	34	-	-	9	-12.2	-11.0
2.81	11.0	4.5	9.4	5.8	39	-9.5	-8.2
2.82	6.0	>16	-	-	> 147	-8.8	-9.0
2.85	3.6	10	-	-	17-34	-6.4	-9.3
2.90	4.0	6	-	-	18	-10.8	-9.3
2.91	1.4	>36	3.5	>28.5	62-124	α= -7.2 α'= -7.0	α= -7.0 α'= -7.0
2.92	1.9	>26	6.3	7.3	> 147	α= -7.5 α'= -7.3	α= -7.1 α'= -7.5
Lawson	> 10	-	6.3	7.0	> 147	-6.5	-6.6
Atovaquone	0.001	6000	11.1	3.9	> 147	-12.1	-10.7
Streptomycine	-	-	-	-	0.25	-	-
Miltéfosine	-	-	1.5	15.5	-	-	-

^a Contre des cellules Vero. ^b Contre des cellules Hep GAA16.

Contre le parasite *Leishmania*, les composés **2.79** et **2.81** de la famille des naphtofuoroquinones ont des valeurs de Cl₅₀ inférieures à 10 µM (7 et 9.4 µM respectivement), ce qui est proche de la Cl₅₀ du médicament de référence, la miltéfosine (Cl₅₀ = 1.5 µM). Parmi les naphtho-énaminodiones, la molécule **2.91** s'est avérée très active contre *L. donovani* ayant une valeur de Cl₅₀ = 3.5 µM et une meilleure valeur d'indice de sélectivité que le médicament utilisé comme référence.

Contre *Mycobacterium tuberculosis*, la plupart de composés de la famille des naphtofuroquinones sont inactifs. Seul le composé **2.80** a une valeur de MIC inférieure à 10 μM (9.0 μM), alors le médicament de référence, la streptomycine a une MIC de 0.25 μM (Tableau R.2). Une modification des substitutions du squelette de ces molécules est donc essentielle pour améliorer les activités.

3. Synthèse des dérivés de lawsone à l'aide de la réaction multicomposants de Biginelli

La pyrimidine est le constituant le plus important de toute la famille de diazines, car ce système hétérocyclique est très répandu et essentiel dans des systèmes biologiques variés. Le noyau de pyrimidine est présent dans des vitamines telles que la riboflavine, la thiamine, et dans des acides nucléiques comme la thymine, la cytosine et l'uracile [44]. Dans le domaine de la chimie médicinale, les dérivés de la pyrimidine, et spécialement les dérivés de dihydropyrimidinones (DHPM), sont très bien connus pour leurs activités thérapeutiques comme agents antipaludiques [45-47], leishmanicides [48], antimicrobiens [49] etc. (Fig. R.7).

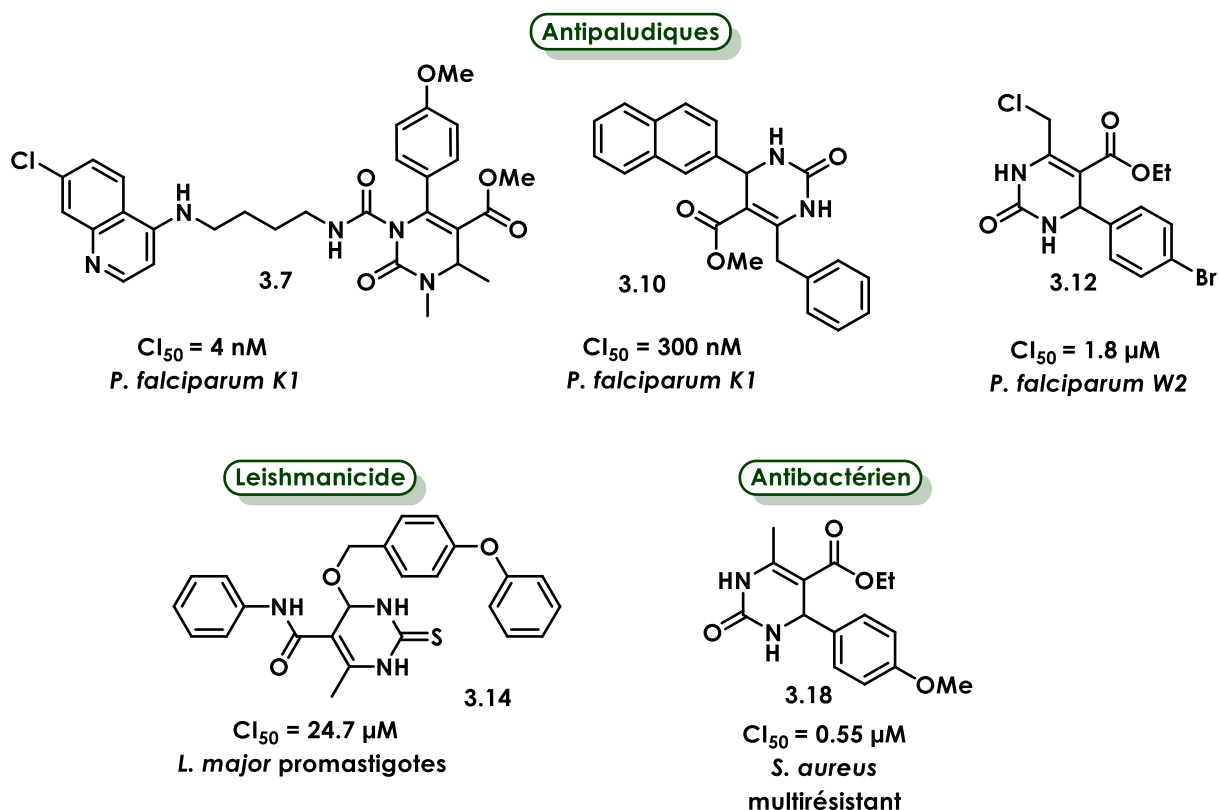


Figure R.7. Dihydropyrimidinones avec des activités biologiques intéressantes.

Dans le but de synthétiser des molécules ayant une activité biologique potentielle contre les deux parasites *Plasmodium falciparum* et *Leishmania donovani* nous avons cherché à synthétiser des dérivés tricycliques lawsone-DHPM. Ces motifs DHPM peuvent être obtenus en utilisant la réaction multicomposants de Biginelli. Cette réaction résulte de la condensation de

trois composants : un β -cétoester, une urée et un benzaldéhyde pour former le produit cyclisé 4-aryl-3,4-dihydropyrimidine-2(1H)-one (DHPM) [31]. Au cours des dernières décennies, des conditions expérimentales variées ont été proposées pour améliorer le rendement de cette réaction : utilisation de catalyseurs à base d'acides de Brønsted ou de Lewis, de liquides ioniques (LI), de solvants eutectiques (DES) ou excès de l'un des trois réactifs [50].

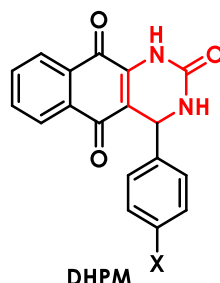


Figure R.8. Dérivés lawsone-DHPM souhaités.

Trois mécanismes sont proposés pour une réaction Biginelli classique : (i) la voie de l'iminium qui commence par la condensation de l'aldéhyde et de l'urée pour former une liaison iminium C-N, suivie de l'addition nucléophile du β -cétoester ; (ii) la voie de l'énamine, c'est-à-dire la réaction de l'urée et du β -cétoester pour former une liaison C-N d'énamine, qui réagit ensuite avec l'aldéhyde et (iii) la synthèse de l'intermédiaire de Knoevenagel, où l'aldéhyde et le β -cétoester forment une liaison C-C avant de réagir avec l'urée (Schéma R.3) [51]. Il convient de noter ici que l'étape déterminant la vitesse de la réaction (RDS) est la formation de la liaison C-N pendant l'étape finale de cyclisation intramoléculaire pour les deux mécanismes (i) et (ii), et la coupure de la liaison C-O pendant la réaction de Knoevenagel pour le mécanisme (iii) (Schéma R.3). Une préférence pour un de ces trois mécanismes peut apparaître en fonction des conditions expérimentales et des substituants des réactifs, ce qui peut favoriser un RDS par rapport à un autre [51].

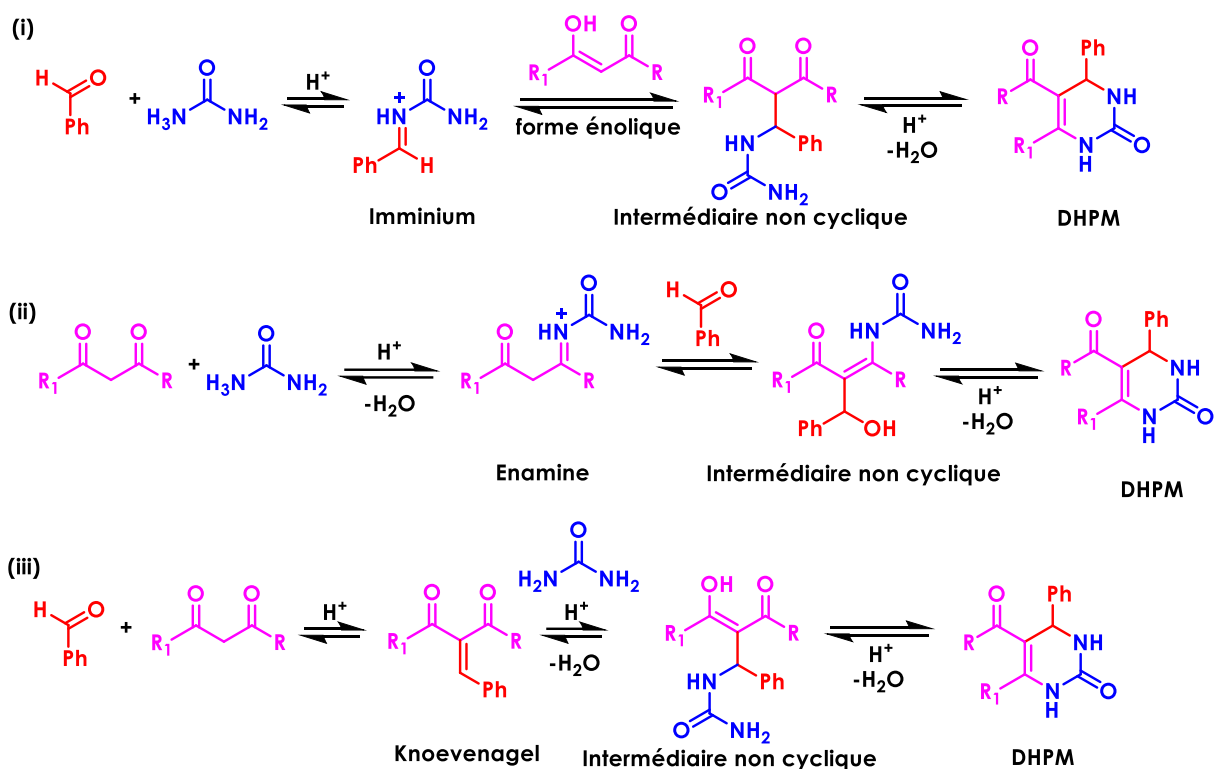


Schéma R.3. Les trois mécanismes proposés pour la réaction de Biginelli.

Pour déterminer les conditions optimales, la réaction de la lawsone avec le 4-chlorobenzaldéhyde et l'urée a été utilisée comme modèle. Nous avons d'abord utilisé des conditions conventionnelles dans des solvants protiques courants (EtOH). Puis, la réaction a été conduite dans des liquides ioniques (IL) ou des solvant eutectiques (DES). Ensuite, la réaction a été activée par irradiation par micro-ondes ou par mécano-chimie. Malheureusement, en aucun cas nous n'avons obtenu le dérivé de DHPM souhaité (Schéma R.4).

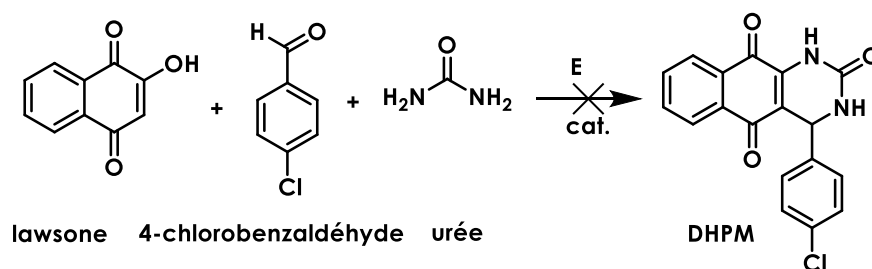


Schéma R.4. La réaction modèle utilisée pour mettre en place les conditions optimales.

Au lieu de cela, deux produits ont été obtenus : le produit linéaire de Biginelli (**3.43**) et le produit formé par l'addition de Michael entre la lawsone et le benzaldéhyde (**3.44**). Dans ce dernier cas, l'urée ne participe pas à la réaction (Schéma R.5).

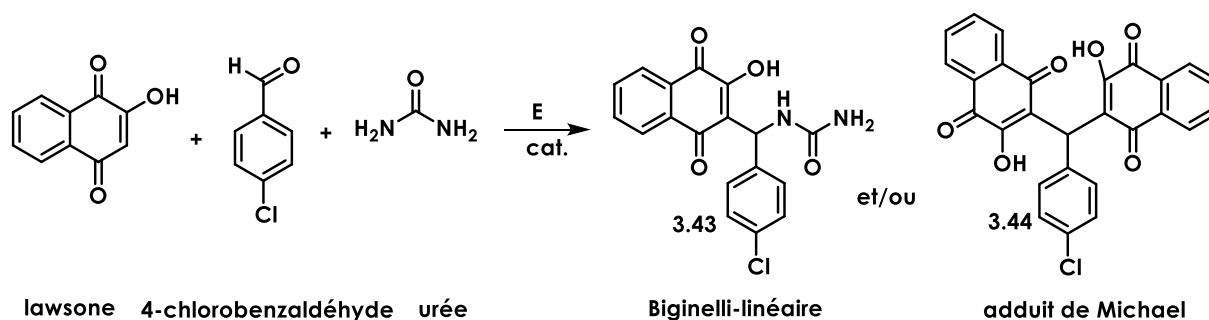


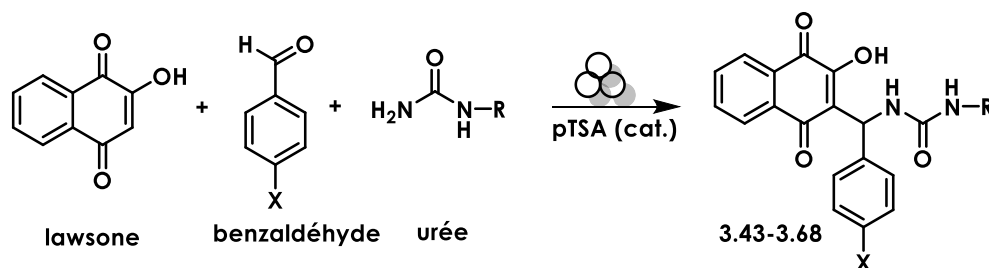
Schéma R.5. Les produits obtenus lors de la réaction de la lawsone avec le 4-chlorobenzaldéhyde et l'urée.

C'est la première fois qu'un produit non cyclique de la réaction de Biginelli est isolé. Ce produit **3.43** a été totalement caractérisé par RMN 2D.

En faisant varier les méthodes d'activation, les catalyseurs et le temps de réaction, nous avons pu favoriser la formation de l'un ou l'autre des produits **3.43** et **3.44**. Lors de l'utilisation de solvants protiques et de DES ou IL, la formation de l'adduit de Michael **3.44** a été favorisée, conduisant à des rendements de 40-47%. Lorsque la réaction a été activée par des moyens mécano-chimiques, le produit linéaire de Biginelli a été formé exclusivement. Après un simple lavage à l'eau, il a été isolé avec des rendements excellents de 90-95%, en une seule étape, sans l'utilisation des solvants organiques et sans purification sur colonne. Les meilleures conditions sont : les trois réactifs en proportions lawsone/benzaldéhyde/urée (1:1:1.5), l'acide *p*-toluène sulfonique (20 mol%) comme catalyseur, dans un broyeur planétaire à billes Pulverisette 7 (2 cycles de 40 min à 800 rpm dans une jarre d'oxyde de zirconium).

Ayant en mains les conditions optimales de l'obtention du composé de Biginelli linéaire **3.43**, nous avons exploré le spectre des substrats de cette réaction multicomposants, en utilisant des benzaldéhydes diversement substitués en position *para*, et des urées *N*-substituées. Les résultats sont présentés dans le Tableau R.3.

Tableau R.3. Les produits Biginelli-linéaires obtenus par activation mécano-chimique.



Produit	X	R	Rend. (%)
3.43	Cl	H	90

3.46	F	Et	63
3.47	Cl	Et	62
3.48	Br	Et	70
3.49	I	Et	70
3.50	NO ₂	Et	85
3.51	CF ₃	Et	90
3.52	CH ₃	Et	70
3.54	F	<i>n</i> -Bu	81
3.55	Cl	<i>n</i> -Bu	85
3.56	Br	<i>n</i> -Bu	95
3.57	NO ₂	<i>n</i> -Bu	90
3.58	CF ₃	<i>n</i> -Bu	80
3.60	F	CH ₂ C≡CH	83
3.61	Cl	CH ₂ C≡CH	73
3.62	Br	CH ₂ C≡CH	88
3.63	NO ₂	CH ₂ C≡CH	70
3.64	CF ₃	CH ₂ C≡CH	82
3.66	Cl	CH ₂ CH ₂ OH	80
3.67	NO ₂	CH ₂ CH ₂ OH	82
3.68	CF ₃	CH ₂ CH ₂ OH	80

Dans tous les cas, sous activation mécano-chimique, un produit unique a été formé, obtenu avec des rendements très bons à excellents (62 à 95 %), à l'état solide, sans utilisation de solvants et sans nécessité de purification sur colonne. Tous les produits ont été précipités en utilisant un volume optimal de mélange de solvants (DCM/Et₂O). La réaction fonctionne bien lorsque le substituant X de l'aldéhyde porte un groupe attracteur d'électrons. Lorsque X est un groupe donneur d'électron les produits de la réaction sont instables. La *N*-substitution de l'urée ne semble pas inhiber la réaction. Les 21 nouveaux produits linéaires de Biginelli ont été isolés et complètement caractérisés par les techniques spectroscopiques usuelles. L'analyse par diffraction des rayons X sur monocristaux de la molécule **3.61** a complété la caractérisation. Le tracé ORTEP de cette structure est présenté sur la Figure R.9, indiquant à l'état cristallin une distance N2-C2 non négligeable et supérieure à 5 Å. Nous pensons que c'est un élément important pour expliquer que l'atome d'azote ne peut pas attaquer le C-OH, car il n'y a pas

de rotations. La cyclisation à l'état solide (dans les conditions mécano-chimiques) pour obtenir le dérivé DHPM désiré est donc impossible.

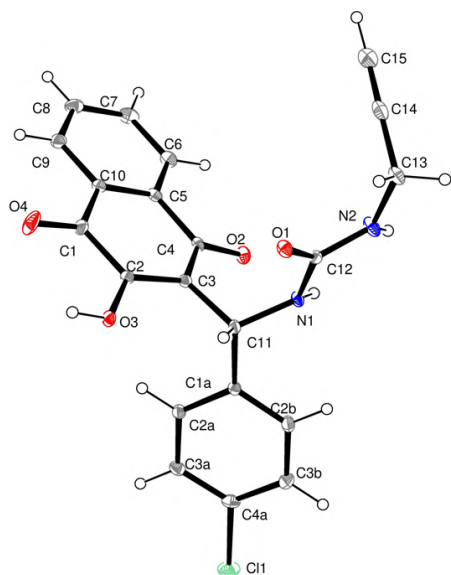


Figure R.9. La structure par diffraction de rayons-X de monocristaux de la molécule **3.61**.

Une étude par calcul DFT de la réaction de cyclisation indique que l'énergie d'activation de cette réaction est très élevée ($\Delta G = + 53$ kcal), même si le produit de Biginelli cyclisé semble thermodynamiquement plus stable que le produit linéaire [ΔG (linéaire \rightarrow cyclisé) = + 12 kcal]. (Schéma R.6). En parallèle, des études théoriques par DFT ont étayé nos résultats expérimentaux concernant le mécanisme proposé pour cette réaction de Biginelli spécifique impliquant la lawsone.

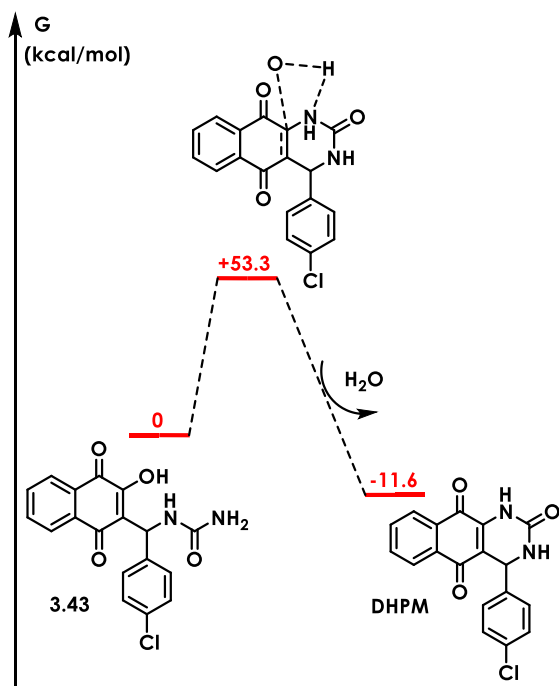


Schéma R.6. Chemin réactionnel de cyclisation du produit **3.43** calculé par DFT.

Le mécanisme que nous avons proposé est celui qui passe par l'intermédiaire de Knoevenagel.

La cyclisation spontanée étant impossible à l'état solide, nous avons tenté de cycliser en solution les produits linéaires de Biginelli isolés. Les composés **3.43** et **3.46** ont été choisis pour cela, afin de contrôler que la substitution de l'urée n'affectait pas l'étape de cyclisation en solution. Malgré toutes nos tentatives, nous n'avons jamais obtenu le produit dérivé cyclisé de type DHPM. Nous avons alors tenté d'activer la fonction énolique du motif lawsone en le faisant réagir avec le chloroformiate de *para*-nitrophényle. À partir de **3.46**, le dérivé cyclique **3.71** a alors été obtenu avec un rendement de 20 % après purification (Schéma R.7). Ce résultat pourra servir comme base d'étude plus approfondie pour synthétiser une nouvelle série de molécules cyclisées à partir de la série de produits linéaires de Biginelli.

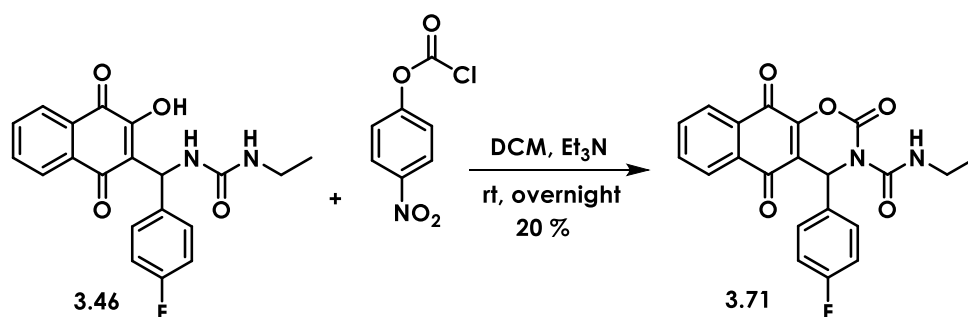


Schéma R.7. Cyclisation du produit **3.46** et formation du carbamate de lawsone **3.71**.

Les composés structurellement les plus proches aux produits linéaires de Biginelli sont les bases de Mannich de la lawsone. Ces composés présentent une activité prometteuse sur *L. pifanoi* et, dans une moindre mesure sur *P. falciparum* (Fig. R.10).

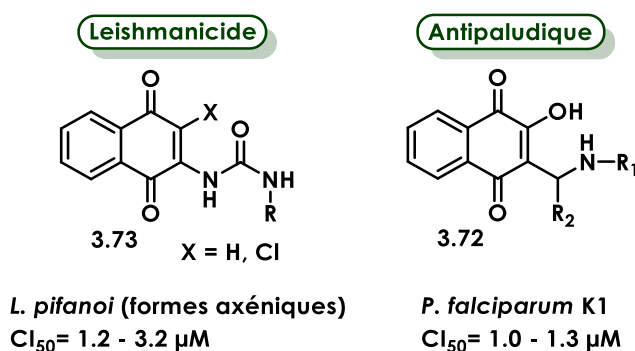


Figure R.10. Activités antiparasitaires de dérivés linéaires de la lawsone.

Tous les produits linéaires de Biginelli ont été évalués *in silico* par docking contre les deux cibles mitochondriales de *Plasmodium falciparum* : DHODH et bc1. Des résultats partiels sont présentés dans le tableau suivant (Tableau R.4). En général, beaucoup de molécules de la série ont présenté des scores très négatifs par rapport aux deux molécules de référence :

l'atovaquone et XCV. Cela indique que ces molécules pourraient avoir une bonne affinité sur les deux cibles : bc1 et DHODH.

Tableau R.4. Quelques résultats de docking de produits linéaires de Biginelli synthétisés.

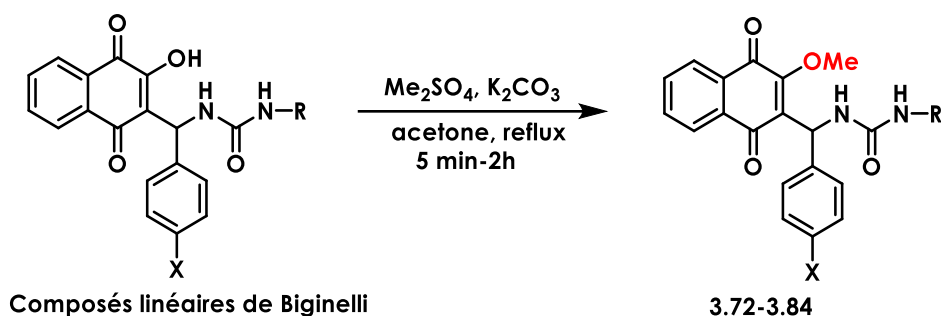
Molécule	Score de docking DHODH (kcal/mol)	Score de docking bc1 (kcal/mol)
3.43	-7.4	-8.8
3.46	-6.1	-9.1
3.47	-5.9	-8.9
3.55	-7.1	-9.9
3.57	-7.1	-7.3
3.60	-6.4	-6.1
3.66	-6.9	-9.3
3.67	-7.2	-4.7
Atovaquone	-	-11.3
XCV	-11.2	-

Après ce premier screening, toute la série de dérivés **3.43-3.68** a été soumise à une évaluation biologique principalement contre de *Plasmodium falciparum* (souches résistantes et sensibles à l'ART), *Mycobacterium tuberculosis* et *Leishmania donovani*. Malheureusement, aucune molécule n'a montré des valeurs de Cl_{50} *in vitro* inférieure à 10 μ M contre *P. falciparum* et contre les deux autres cibles.

Ceci nous a conduit à étudier la stabilité de ces composés. Les études effectuées en LC-MS en phase inverse, en fonction du temps et en présence d'une quantité catalytique d'acide, ont montré que les composés se décomposent en lawsone, aldéhyde et adduit de Michael. Nous estimons que la fonction énol pourrait fragiliser en milieu protique la liaison C-N, conduisant à éliminer l'urée. Donc, cette dégradation pourrait être responsable de la non-activité ou de la perte d'activité biologique observée.

Dans ce cadre, pour stabiliser ces structures, nous avons cherché à méthyler sélectivement la fonction énolique de ces dérivés linéaires. Plusieurs réactifs de méthylation ont été testés (méthylesulfonate de trifluorométhane, iodure de méthyle, fluorure de tétraméthylammonium, diméthylsulfate). Nous avons réussi à mettre au point un protocole de méthylation sélective en utilisant du diméthylsulfate dans de l'acétone à reflux, en présence d'un excès de carbonate de potassium. Les résultats sont résumés au tableau suivant.

Tableau R.5. Produits linéaires de Biginelli sélectivement méthylés.



Produit	X	R	Rend. (%)
3.71	F	Et	60
3.73	Cl	Et	73
3.74	Br	Et	65
3.75	I	Et	70
3.76	NO ₂	Et	42
3.77	CF ₃	Et	90
3.78	CH ₃	Et	70
3.79	OMe	Et	63
3.80	F	CH ₂ C≡CH	70
3.81	Cl	CH ₂ C≡CH	67
3.82	NO ₂	CH ₂ C≡CH	50
3.83	CF ₃	CH ₂ C≡CH	40
3.84	OMe	CH ₂ C≡CH	40

Treize produits méthylés sont obtenus en utilisant cette méthodologie. Des études de RMN 2D du produit **3.71** ont confirmé la sélectivité de la méthylation. Comme prévu, la méthylation a permis de stabiliser ce type de structures, même pour les molécules portant de groupes électro-donneurs. Les études *in silico* de la série méthylée de Biginelli ont montré que la méthylation ne modifie pas significativement les scores de docking avec les protéines mitochondriales bc1 et DHODH. Les résultats sont décrits dans le tableau R.6.

Tableau R.6. Evaluation *in vitro* et *in silico* de certains produits de Biginelli linéaires méthylés.

Composé	<i>P. falciparum</i> F32-ART Cl ₅₀ (μM)	<i>L. donovani</i> LV9 Intramacroph. Cl ₅₀ (μM)	IS	Score docking Pfbc1 (kcal/mol)	Score docking PfDHODH (kcal/mol)
3.72	2.8	2.1	5.7	-10.0	-9.1
3.75	4.5	4.5	22.5	-8.3	-9.1
3.77	4.8	1.5	68.5	nd	nd
3.80	5.0	1.3	76.3	-8.1	-6.7
3.81	10.0	1.4	69.4	-2.3	-6.3
3.83	6.0	2.1	46.5	nd	nd
Atovaquone	0.001	-	-	-11.3	nd
Miltéfosine	-	1.5	15.5	-	-

Tous les composés de la série O-méthylée ont une Cl₅₀ inférieure à 10 μM contre les souches de *P. falciparum* résistantes à l'artémisinine. Les composés **3.72**, **3.78** et **3.79** de la famille des N-éthylurées ont présenté des valeurs de Cl₅₀ comprises entre 2.8 μM et 3 μM, tandis que le dérivé N-propargylurée **3.80** a présenté une Cl₅₀ égale à 5 μM (Tableau R.6).

Surtout, l'ensemble de cette série s'est avérée active contre les amastigotes axéniques et intramacrophages de *L. donovani*. Sept (composés **3.72**, **3.76**, **3.77**, **3.79-3.81** et **3.83**) composés ont présenté des valeurs de Cl₅₀ (1.2-2.1 μM), du même ordre que le médicament de référence qui est la miltéfosine (Cl₅₀ = 1.5 μM) contre les formes intramacrophagiques du parasite. De plus, les indices de sélectivité sont au moins deux fois plus élevés que ceux de la miltéfosine (SI = 15.5) (Tableau R.6). L'activité de cette série contre *L. donovani* est donc remarquable.

4. Conclusion

Deux protocoles de réactions multicomposants impliquant la lawsone ont été développés, afin d'obtenir des dérivés de 1,4-naphtoquinones comme agents antiparasitaires et anti-infectieux. Des approches de chimie verte ont été appliquées afin de réduire les déchets et l'utilisation des solvants. Une série de naphtofuoroquinones diversement substituées à base de lawsone a été synthétisée pour la première fois, ainsi qu'une série de produits linéaires de Biginelli. Une nouvelle voie de synthèse a été mise au point pour l'obtention de composés tricycliques lawsone-carbamates. Cette voie peut encore être optimisée. Tous les composés synthétisés ont été évalués (ou sont en cours d'évaluation) essentiellement contre *Plasmodium falciparum*, *Leishmania donovani* et *Mycobacterium tuberculosis*. Une étude de docking impliquant une approche *in silico* sur deux cibles mitochondriales de *Plasmodium* a été également conduite.

Références

1. M. Cholewiński, M. Derda, and E. Hadaś. Parasitic diseases in humans transmitted by vectors. *Ann. Parasitol.*, **2015**, no. 3, pp. 137–157, doi: [10.17420/ap6103.01](https://doi.org/10.17420/ap6103.01).
2. <https://www.who.int/news-room/fact-sheets/detail/vector-borne-diseases>, page accessed 28.04.2023.
3. L. H. Miller, H. C. Ackerman, X. Su, and T. E. Wellems. Malaria biology and disease pathogenesis: insights for new treatments. *Nat Med*, **2013**, vol. 19, no. 2, pp. 156–167, doi: [10.1038/nm.3073](https://doi.org/10.1038/nm.3073).
4. <https://leishinforwho-cc55.es/essential-maps/>, page accessed 22.06.2023.
5. World Health Organization. World malaria Report **2020**, Geneva 2020.
6. Centers for Disease Control and Prevention. <https://www.cdc.gov/>, page accessed 23.06.2023.
7. H. Ledford. Malaria vaccine shows promise - now come tougher trials. *Nature*, **2021**, 593.
8. J. P. Daily. Malaria 2017: update on the clinical literature and management. *Curr. Infect. Dis. Rep.*, **2017**, vol. 19, no. 8, p. 28, doi: [10.1007/s11908-017-0583-8](https://doi.org/10.1007/s11908-017-0583-8).
9. World Health Organization. Guidelines for the treatment of Malaria, Third Edition. **2015**.
10. L. Paloque, A. P. Ramadani, O. Mercereau-Pujalon, J.-M. Augereau, and F. Benoit-Vical. *Plasmodium falciparum*: multifaceted resistance to artemisinins. *Malar. J.*, **2016**, vol. 15, no. 1, p. 149, doi: [10.1186/s12936-016-1206-9](https://doi.org/10.1186/s12936-016-1206-9).
11. B. Witkowski *et al.* Increased tolerance to artemisinin in *Plasmodium falciparum* is mediated by a quiescence mechanism. *Antimicrob. Agents Chemother.*, **2010**, vol. 54, no. 5, pp. 1872–1877, doi: [10.1128/AAC.01636-09](https://doi.org/10.1128/AAC.01636-09).
12. A. B. Vaidya and M. W. Mather. Mitochondrial evolution and functions in malaria parasites. *Annu. Rev. Microbiol.* **2009**, vol. 63, no. 1, pp. 249–267 doi: [10.1146/annurev.micro.091208.073424](https://doi.org/10.1146/annurev.micro.091208.073424).
13. T. J. Espino-Sanchez *et al.*, Direct tests of cytochrome c and c₁ functions in the electron transport chain of malaria parasites, *Proc. Natl. Acad. Sci. U.S.A.*, **2023**, vol. 120, no. 19, p. e2301047120, doi: [10.1073/pnas.2301047120](https://doi.org/10.1073/pnas.2301047120).
14. A. Singh, M. Maqbool, M. Mobashir, and N. Hoda, Dihydroorotate dehydrogenase: A drug target for the development of antimalarials, *Eur. J. Med. Chem.*, **2017**, vol. 125, pp. 640–651, doi: [10.1016/j.ejmech.2016.09.085](https://doi.org/10.1016/j.ejmech.2016.09.085).
15. D. Birth, W.-C. Kao, and C. Hunte, Structural analysis of atovaquone-inhibited cytochrome bc₁ complex reveals the molecular basis of antimalarial drug action, *Nat. Commun.*, **2014**, vol. 5, no. 1, p. 4029, doi: [10.1038/ncomms5029](https://doi.org/10.1038/ncomms5029).
16. I. K. Srivastava, J. M. Morrissey, E. Darrouzet, F. Daldal, and A. B. Vaidya, Resistance mutations reveal the atovaquone-binding domain of cytochrome b in malaria parasites, *Mol. Microbiol.*, **1999**, vol. 33, no. 4, pp. 704–711, doi: [10.1046/j.1365-2958.1999.01515.x](https://doi.org/10.1046/j.1365-2958.1999.01515.x).
17. https://www.who.int/health-topics/leishmaniasis#tab=tab_1, page accessed 22.06.2023.
18. S. Mann *et al.*, A review of leishmaniasis: current knowledge and future directions, *Curr. Trop. Med. Rep.*, **2021**, vol. 8, no. 2, pp. 121–132, doi: [10.1007/s40475-021-00232-7](https://doi.org/10.1007/s40475-021-00232-7).
19. D. Sereno, C. Maia, and K. Aït-Oudhia, Antimony resistance and environment: elusive links to explore during *Leishmania* life cycle, *Int. J. Parasitol. Drug*, **2012**, vol. 2, pp. 200–203, doi: [10.1016/j.ijpddr.2012.07.003](https://doi.org/10.1016/j.ijpddr.2012.07.003).
20. T. Müller, L. Johann, B. Jannack, M. Brückner, D. A. Lanfranchi, H. Bauer, C. Sanchez, V. Yardley, C. Deregnaucourt, J. Schrével, M. Lanzer, R. H. Schirmer, E. Davioud-Charvet, Glutathione reductase-catalyzed cascade of redox reactions to bioactivate potent antimalarial 1,4-naphthoquinones – A new strategy to combat malarial parasites. *J. Am. Chem. Soc.* **2011**, vol. 133, no. 30, pp. 11557–11571, doi: <https://doi.org/10.1021/ja201729z>.
21. T. E. Long, X. Lu, M. Galizzi, R. Docampo, J. Gut, and P. J. Rosenthal, Phosphonium lipocations as antiparasitic agents, *Bioorganic Med. Chem. Lett.*, **2012**, vol. 22, no. 8, pp. 2976–2979, doi: [10.1016/j.bmcl.2012.02.045](https://doi.org/10.1016/j.bmcl.2012.02.045).

22. A. Baramee, A. Coppin, M. Mortuaire, L. Pelinski, S. Tomavo, and J. Brocard, Synthesis and *in vitro* activities of ferrocenic aminohydroxynaphthoquinones against *Toxoplasma gondii* and *Plasmodium falciparum*, *Bioorganic Med. Chem.*, **2006**, vol. 14, no. 5, pp. 1294–1302, doi: [10.1016/j.bmc.2005.09.054](https://doi.org/10.1016/j.bmc.2005.09.054).
23. V. Sebastián-Pérez *et al.*, Naphthoquinone as a new chemical scaffold for leishmanicidal inhibitors of *Leishmania* GSK-3, *Biomedicines*, **2022**, vol. 10, no. 5, p. 1136, doi: [10.3390/biomedicines10051136](https://doi.org/10.3390/biomedicines10051136).
24. D. V. C. Mendonça *et al.*, Flau-A, a naphthoquinone derivative, is a promising therapeutic candidate against visceral leishmaniasis: a preliminary study, *Exp. Parasitol.*, **2022**, vol. 233, p. 108205, doi: [10.1016/j.exppara.2021.108205](https://doi.org/10.1016/j.exppara.2021.108205).
25. C. E. Pereyra, R. F. Dantas, S. B. Ferreira, L. P. Gomes, and F. P. Silva-Jr, The diverse mechanisms and anticancer potential of naphthoquinones, *Cancer Cell. Int.*, **2019**, vol. 19, no. 1, p. 207, doi: [10.1186/s12935-019-0925-8](https://doi.org/10.1186/s12935-019-0925-8).
26. P. Ravichandiran, S. Sheet, D. Premnath, A. R. Kim, and D. J. Yoo, 1,4-Naphthoquinone analogues: potent antibacterial agents and mode of action evaluation, *Molecules*, **2019**, vol. 24, no. 7, p. 1437, doi: [10.3390/molecules24071437](https://doi.org/10.3390/molecules24071437).
27. V. Giongo *et al.*, Antiviral potential of naphthoquinones derivatives encapsulated within liposomes, *Molecules*, **2021**, vol. 26, no. 21, p. 6440, doi: [10.3390/molecules26216440](https://doi.org/10.3390/molecules26216440).
28. A. Dömling, W. Wang, and K. Wang. Chemistry and biology of multicomponent reactions. *Chem. Rev.*, **2012**, vol. 112, no. 6, pp. 3083–3135, doi: [10.1021/cr100233r](https://doi.org/10.1021/cr100233r).
29. A. Strecker, Ueber die künstliche bildung der milchsäure und einen neuen, dem glycocoll homologen körper, *Ann. Chem. Pharm.*, **1850**, vol. 75, no. 1, pp. 27–45, doi: [10.1002/jlac.18500750103](https://doi.org/10.1002/jlac.18500750103).
30. C. Mannich and W. Krösche, Ueber ein kondensationsprodukt aus formaldehyd, ammoniak und antipyrin, *Arch. Pharm. Pharm. Med. Chem.*, **1912**, vol. 250, no. 1, pp. 647–667, doi: [10.1002/ardp.19122500151](https://doi.org/10.1002/ardp.19122500151).
31. P. Biginelli, Aldehyde-urea derivatives of aceto- and oxaloacetic Acids. *Gazz. Chim. Ital.*, **1893**, vol. 23, pp. 360-413.
32. M. Passerini, Three-component condensation (3CC) of carboxylic acids, c-isocyanides, and carbonyl compounds to afford α -acyloxycarboxamides, *Gazz. Chim. Ital.*, **1921**, vol. 51, pp. 126–129.
33. I. Ugi, R. Meyr, U. Fetzer and C. Steinbruckner, Versammlungsberichte, *Angew. Chem.*, **1959**, vol. 71, no. 11, pp. 373–388, doi: [10.1002/ange.19590711110](https://doi.org/10.1002/ange.19590711110)
34. T. F. Borgati, M. F. A. do Nascimento, J. F. Bernardino, L. C. O. Martins, A. G. Taranto, and A. B. de Oliveira, Synthesis, SAR, and docking studies disclose 2-arylfuran-1,4-naphthoquinones as *in vitro* antiplasmodial hits, *J. Trop. Med.*, **2017**, vol. 2017, pp. 1–11, doi: [10.1155/2017/7496934](https://doi.org/10.1155/2017/7496934).
35. M. O. F. Goulart *et al.*, Trypanocidal activity and redox potential of heterocyclic- and 2-hydroxy-naphthoquinones, *Bioorg. Med. Chem. Lett.*, **1997**, vol. 7, no. 15, pp. 2043–2048, doi: [10.1016/S0960-894X\(97\)00354-5](https://doi.org/10.1016/S0960-894X(97)00354-5).
36. A. Prateep *et al.*, Avicquinone B sensitizes anoikis in human lung cancer cells, *J. Biomed. Sci.*, **2018**, vol. 25, article no. 32, doi: [10.1186/s12929-018-0435-3](https://doi.org/10.1186/s12929-018-0435-3).
37. W. S. Jang *et al.* Naphthofuroquinone derivatives show strong antimycobacterial activities against drug-resistant *Mycobacteria*, *J. Chemother.*, **2017**, vol. 29, no. 6, pp. 338–343, doi: [10.1080/1120009X.2017.1296987](https://doi.org/10.1080/1120009X.2017.1296987).
38. W.-B. Kang, S. Nan'ya, T. Toru, and Y. Ueno, Regioselective addition reaction of lithium enolates to thio-substituted 1,4-naphthoquinones. Convenient synthesis of a naphthofuran-4,9-dione ring system, *Chem. Lett.*, **1988**, vol. 17, no. 8, pp. 1415–1418, doi: [10.1246/cl.1988.1415](https://doi.org/10.1246/cl.1988.1415).
39. Y. Rok Lee and B. So Kim, A facile method for the synthesis of dihydrofuranonaphthoquinones, furanonaphthoquinones, and benzofurano-

- naphthoquinones, *Syn. Comm.*, **2003**, vol. 33, no. 23, pp. 4123–4135, doi: [10.1081/SCC-120026354](https://doi.org/10.1081/SCC-120026354).
40. K. Kobayashi, T. Uneda, M. Kawakita, O. Morikawa, and H. Konishi, One-pot synthesis of naphtho[2,3-b]furan-4,9-diones by sequential coupling/ring closure reactions, *Tet. Lett.*, **1997**, vol. 38, no. 5, pp. 837–840, doi: [10.1016/S0040-4039\(96\)02462-8](https://doi.org/10.1016/S0040-4039(96)02462-8).
 41. M. B. Teimouri and H. R. Khavasi, One-pot three-component regioselective synthesis of linear naphtho[2,3-b]-furan-4,9-diones, *Tetrahedron*, **2007**, vol. 63, no. 41, pp. 10269–10275, doi: [10.1016/j.tet.2007.07.082](https://doi.org/10.1016/j.tet.2007.07.082).
 42. S. Jiménez-Alonso, J. Guasch, A. Estévez-Braun, I. Ratera, J. Veciana, and A. G. Ravelo, Electronic and cytotoxic properties of 2-amino-naphtho[2,3-b]furan-4,9-diones, *J. Org. Chem.*, **2011**, vol. 76, no. 6, pp. 1634–1643, doi: [10.1021/jo102233j](https://doi.org/10.1021/jo102233j).
 43. S. Oramas-Royo *et al.*, Design, synthesis, and biological evaluation of new embelin derivatives as CK2 inhibitors, *Bioorg. Chem.*, **2020**, vol. 95, p. 103520, doi: [10.1016/j.bioorg.2019.103520](https://doi.org/10.1016/j.bioorg.2019.103520).
 44. R. Kaur, S. Chaudhary, K. Kumar, M. K. Gupta, and R. K. Rawal, Recent synthetic and medicinal perspectives of dihydropyrimidinones: A review, *Eur. J. Med. Chem.*, **2017**, vol. 132, pp. 108–134, doi: [10.1016/j.ejmech.2017.03.025](https://doi.org/10.1016/j.ejmech.2017.03.025).
 45. N. October, N. D. Watermeyer, V. Yardley, T. J. Egan, K. Ncokazi, and K. Chibale, Reversed chloroquinones based on the 3,4-dihydropyrimidin-2(1H)-one scaffold: synthesis and evaluation for antimalarial, β -haematin inhibition, and cytotoxic activity, *ChemMedChem*, **2008**, vol. 3, no. 11, pp. 1649–1653, doi: [10.1002/cmdc.200800172](https://doi.org/10.1002/cmdc.200800172).
 46. A. N. Chiang *et al.*, Select pyrimidinones inhibit the propagation of the malarial parasite, *Plasmodium falciparum*, *Bioorg. Med. Chem.*, **2009**, vol. 17, no. 4, pp. 1527–1533, doi: [10.1016/j.bmc.2009.01.024](https://doi.org/10.1016/j.bmc.2009.01.024).
 47. K. R. Rogerio *et al.*, Synthesis and molecular modelling studies of pyrimidinones and pyrrolo[3,4-d]-pyrimidinodiones as new antiplasmodial compounds, *Mem. Inst. Oswaldo Cruz*, **2018**, vol. 113, no. 8, doi: [10.1590/0074-02760170452](https://doi.org/10.1590/0074-02760170452).
 48. B. Mohammadi-Ghalehbin *et al.*, Synthesis, antileishmanial activity and molecular docking study of new 3,4-dihydropyrimidinones/thiones, *Pharm. Chem. J.*, **2022**, vol. 55, no. 10, pp. 1050–1056, doi: [10.1007/s11094-021-02536-4](https://doi.org/10.1007/s11094-021-02536-4).
 49. M. Castro Jara *et al.*, Dihydropyrimidinones against multiresistant bacteria, *Front. Microbiol.*, **2022**, vol. 13, p. 743213, doi: [10.3389/fmicb.2022.743213](https://doi.org/10.3389/fmicb.2022.743213).
 50. V. Kamat, D. S. Reddy, and A. Kumar, Catalytic role in Biginelli reaction: synthesis and biological property studies of 2-oxo/thio-1,2,3,4-tetrahydropyrimidines, *Arch. Pharm.*, **2023**, vol. 356, no. 6, p. 2300008, doi: [10.1002/ardp.202300008](https://doi.org/10.1002/ardp.202300008).
 51. M. Puripat, R. Ramozzi, M. Hatanaka, W. Parasuk, V. Parasuk, and K. Morokuma, The Biginelli reaction is a urea-catalyzed organocatalytic multicomponent reaction, *J. Org. Chem.*, **2015**, vol. 80, no. 14, pp. 6959–6967, doi: [10.1021/acs.joc.5b00407](https://doi.org/10.1021/acs.joc.5b00407).
 52. W. Paengsri, N. Promsawan, and A. Baramée, Synthesis and evaluation of 2-hydroxy-1,4-naphthoquinone derivatives as potent antimalarial agents, *Chem. Pharm. Bull.*, **2021**, vol. 69, no. 3, pp. 253–257, doi: [10.1248/cpb.c20-00770](https://doi.org/10.1248/cpb.c20-00770).

CHAPTER 1

“General Introduction”

1.1 Vector-borne parasitic diseases in humans

Parasites belong to the oldest organisms living on earth. Their presence has even been confirmed in fossils millions of years old [1]. Parasitism is a type of antagonistic co-existence between two organisms, the parasite and its host, in which one derives benefits and the other suffers damage. Evolution through time permitted parasites to develop mechanism adaptations to ensure their survival and transmission. The host is used as a source of nutrients and as a living environment for the parasite. This kind of interaction between two organisms results in pathological states for the host. Epidemiologists estimate that $\frac{3}{4}$ of living organisms on the planet are getting infected by parasites [2].

Vector-borne diseases (VBDs) are illnesses caused by parasites, viruses, and bacteria transmitted by vectors to humans and/or animals. They account for more than 17% of all infectious diseases worldwide, causing more than 700.000 deaths annually [3]. They are common essentially in tropical and subtropical areas, affecting disproportionately the poorest populations.

The transmission of VBDs takes place mainly through blood-sucking by the infected vector which injects pathogens into human hosts during a blood meal, and later transmits it into a new host after the pathogen has been replicated. Once the vector becomes infectious, it is capable of pathogen transmission for the rest of its life during each blood meal. Nowadays, the increased distribution of VBDs is a result of numerous factors such as: an increase in international tourism, travel and trade, unplanned urbanization, immigration, import of food, lack of public awareness, and disregard of basic hygiene principles [2],[3]. Major outbreaks of vector-borne diseases have affected people all over the world as they claim lives and burden national health systems. Furthermore, sometimes they can cause chronic suffering to the victims, even disability leading to a potential social stigmatization of the patients and their families [3].

Despite all the economic, social and technological signs of progress during the last century, VBDs are still considered to be a serious health problem in societies in every part of the world. A non-exhaustive list of the most important vector-borne parasitic diseases is given below.

Table 1.1. Non-exhaustive list of vector-borne diseases caused by parasites. This table correlates every disease with the responsible types of parasites, the endemic zone, the vector and the number of cases reported by World Health Organization [3].

Disease	Parasite	Vector	Endemic zone	Cases number
Elephantiasis	<i>Wuchereria bancrofti</i> <i>Brugia spp.</i>	Mosquito	Africa, Asia, the Caribbean, the Middle East, Pacific Islands, South America	51 M (2018)
Malaria	<i>Plasmodium spp.</i>	Mosquito	Africa, South-East Asia, Latin America	247 M (2022)
Schistosomiasis	<i>Schistosoma spp.</i>	Aquatic snails	Africa, Asia, the Caribbean, South America, Corsica, Southeast Asia (China, Indonesia)	251 M (2021)
River blindness	<i>Onchocerca volvulus</i>	Blackflies	Africa, Brazil, Venezuela, Yemen	220 M (2017)
Leishmaniasis	<i>Leishmania spp.</i>	Sandflies	Africa, Brazil, Southeast Asia, Eastern Mediterranean, South Europe	700.000 - 1 M (2022)
Chagas disease	<i>Trypanosoma cruzi</i>	Triatome bugs	Central and South America	6 – 7 M (2022)
Sleeping disease	<i>Trypanosoma brucei</i>	Tsetse flies	Africa	700 (2021)

Among all vector-borne parasitic diseases listed above (elephantiasis, malaria, schistosomiasis, river blindness, leishmaniasis, Chagas and sleeping disease) this thesis is going to be focused on the elaboration and evaluation of new compounds designed to fight malaria and leishmaniasis which seem to be the most expanded in tropical and subtropical populations.

Besides, they seriously threaten the south European countries due to climate change as the vector can now expand to regions that were unsuitable for its survival before and they can benefit from extended periods of high temperatures for their replication [4].

1.2 Malaria

Malaria is a global health problem and one of the most life-threatening infectious diseases [5]. The World Health Organization (WHO) reported 247 million malaria cases globally in 2022, an increase of 2 million cases over the previous two years. Even while the number of cases decreased between 2000 and 2015 (245 million declined to 230 million across all endemic countries), they have surged since 2016, reaching a new yearly peak of 13 million cases going from 2019 to 2020, during the first year of the COVID-19 pandemic [6]. These additional cases were linked to malaria vital service disruption during the pandemic. In 2021, 84 countries were identified as malaria endemic, with the majority of them being situated in the world's southern

tropical and subtropical hemisphere. The countries with the most cases are concentrated in Africa and Latin America (Fig. 1.1).

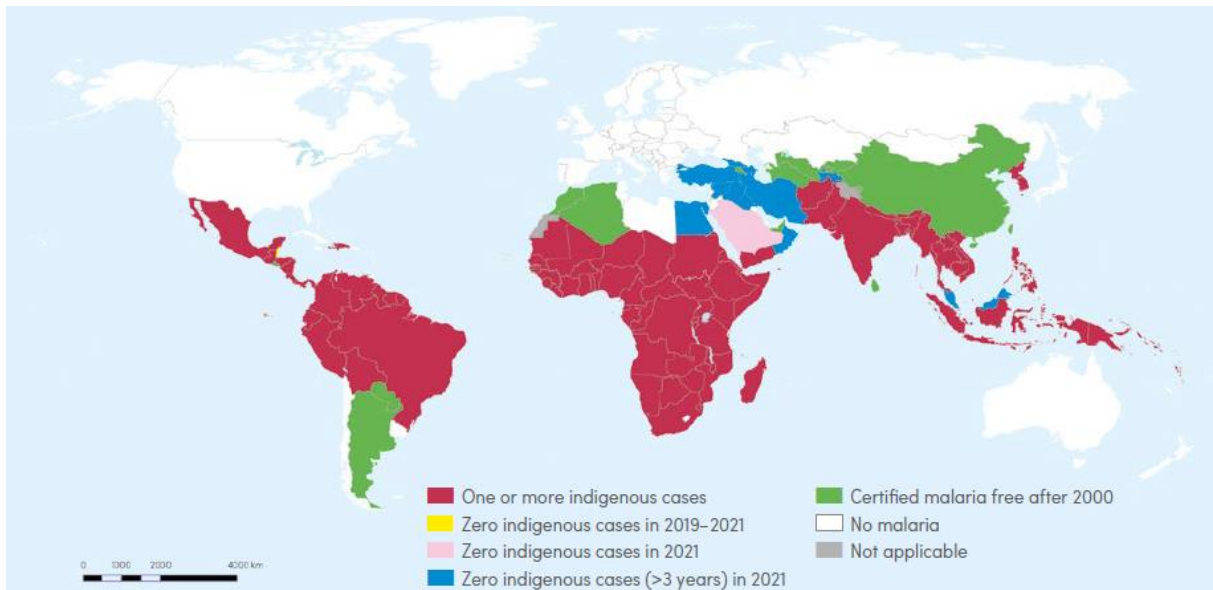


Figure 1.1. Malaria endemic countries in 2021 worldwide, all rights reserved to the authors of [6].

Malaria mortality rate has steadily decreased since 2000, from 897.000 deaths in 2000 to 577.000 deaths in 2015 and 568.000 deaths in 2019. However, malaria deaths escalated to 625.000 in 2020.

Interestingly, the percentage of overall malaria mortality among children under the age of five has decreased over the last two decades, from 87% in 2000 to 77% in 2015, and has remained stable since then.

The World Health Organization (WHO) establishes goals and provides constant funding for research projects with the goal of eliminating disease, improving patient quality of life, and reducing the social burden. Some of these are the Global Technical Strategy for Malaria 2016-2030 (GTS) and the Action and Investment to Fight Malaria 2013-2030 (AIM), which demonstrate the significance and urgency of this global health crisis [6].

1.2.1 Vector

Female *Anopheles* mosquitoes of 40 distinct species can operate as vectors, transmitting the disease to humans and mammals. Malaria-bearing *Anopheles* mosquitos are found all across the world [7].

1.2.2 Pathogen: *Plasmodium* spp.

The most common pathogens responsible for the disease in mammal hosts and subsequently in humans are the protozoan parasites of the *Plasmodium* genus. Six species

substantially menace human health namely *Plasmodium falciparum*, *P. vivax*, *P. ovale curtisi*, *P. ovale wallikeri*, *P. malariae* and *P. knowlesi*. Among them, *P. falciparum*, mostly found in all tropical regions, is widely regarded as the most lethal [8] while *P. vivax*, found almost everywhere, is the most widespread one as it can survive in extremely hot climate conditions [9]. *P. ovale* and *P. malariae* are far less prevalent pathogens while *P. knowlesi* has recently emerged as a significant cause of severe disease cases mostly localized in southern Asia [10].

Life cycle of *Plasmodium*

Malaria, like all VBDs, is transmitted through the bite of the parasite infected female mosquito *Anopheles spp.* During this blood meal, infected mosquitoes deliver *Plasmodium* sporozoites into the blood of the human host (Fig. 1.2, panel A). Within 30-60 minutes, sporozoites breach the sinusoidal barrier [11] and migrate to the host's liver where they invade the hepatocytes utilizing surface hepatocyte proteins [12]. While replicating in hepatocytes, sporozoites construct a particularly dense coat, resulting in the generation of a vacuole known as merozoite (Fig. 1.2, panel B). The merozoite develops and explodes over the next 10 days, eventually releasing 40,000 merozoites per hepatic cell into the blood hepatic stream [13]. Once in the bloodstream, unbound merozoites can engage with red blood cell surface receptors, subsequently binding and invading the erythrocytes (echinocytosis) [12].

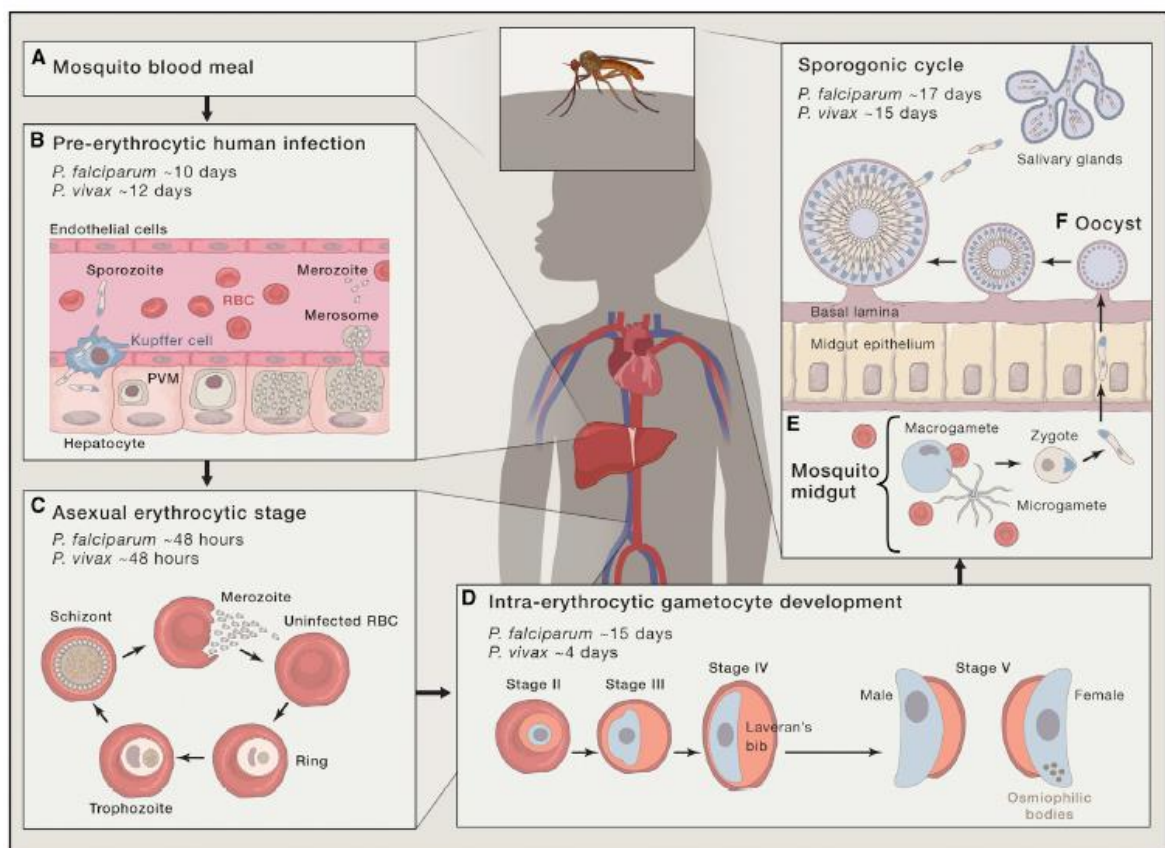


Figure 1.2. Life cycle of *Plasmodium falciparum*, all rights reserved to the authors of [12].

The asexual reproductive stage begins in the blood cells, which is associated to the disease's symptomatic stage (Fig. 1.2, panel C) [14]. Trophozoites mature into schizonts in a ring stage, causing the red blood cell to burst and new merozoites to be released into the bloodstream and infect other blood cells. The *Plasmodium* asexual replication cycle within erythrocytes lasts 36-72 hours, according to the parasite species [14]. Under certain circumstances, parasites can differentiate into mature gametocytes (Fig. 1.2, panel D) [15]. Gametocytes grow within the host's bone marrow over a span of 15 days, and once they are fully developed, they enter the peripheral circulation. Gametocytes gather in skin capillaries where they can be ingested by the subsequent mosquito vector during a subsequent blood meal [14]. The sporogonic cycle refers to the parasites' growth inside the mosquito, which occurs inside the insect's stomach. The resulting diploid zygote, created when the male and female gametes fuse (Fig. 1.2, panel E), grows into an ookinete and then leaves the gut through the epithelium as an oocyst. The oocysts go through cycles of replication, develop, burst, and release newly born sporozoites that make their way to the salivary glands of mosquitoes (Fig. 1.2, panel F) [16]. The new sporozoites can be inoculated in another human host and restart the cycle after 7-10 days.

1.2.3 Symptoms

The intense and synchronous proliferation of *Plasmodium* parasites into the red blood cells of the human host results in symptoms manifestation of malaria disease. Depending on the *Plasmodium* species, the first symptoms of the disease appear 4-8 days after the first infection. High fever (40 °C) can occur on a frequent basis, accompanied by shivering, severe headaches, diarrhea, vomiting, nausea, perspiration, and a fast temperature decrease and exhaustion [17]. Intense destruction of red blood cells eventually leads to hemolytic anemia, hepatitis, and hemoglobinuria. At that point, the symptoms worsen and include dyspnea, muscular and spine aches and pains and even neurological dysfunction due to micro thromboses in cerebral capillaries. Lack of treatment or resistance to drugs used can lead to malaria complications which include organ failure (spleen, kidney, and heart), severe anemia, respiratory distress and eventually death [18]. In addition, infection with *P. ovale*, *P. vivax*, or *P. malariae* can cause merozoite invasion of erythrocytes to be delayed for weeks, months, or even years due to the development of dormant liver-resident hypnozoites. Those forms have a substantially slower metabolism and are sporadically activated, resulting in malaria recurrence [14].

1.2.4 Malaria treatment: chemotherapy and drug resistance

The drugs currently used to fight against malaria can be classified into three main categories based on which stage of the *Plasmodium* life cycle they target. Drugs that impede *Plasmodium* spp. invasion or proliferation in the liver have a prophylactic activity. Drugs that can arrest the red blood cell proliferation stage are very effective and used to treat

symptomatic malaria. Finally, drugs that inhibit the development of gametocytes or their proliferation in the mosquito (including drugs that kill mosquitoes) are called transmission-blocking agents and they contribute to the prevention of resistance spread [14].

Nowadays, two drug treatments are recommended by WHO and Medicines for Malaria Venture (MMV) to combat malaria: chloroquine and artemisinin-based combination therapies (ACTs). Chloroquine (CQ) (Fig. 1.3, molecule **1.1**) was discovered in 1934, as a synthetic derivative of the natural product quinine (Fig. 1.3, molecule **1.2**). Ten years later, it was employed as an antimalarial agent and it was widely used since it was cheap, commercially available (Bayer), and effective against almost all *Plasmodium* species [19]. CQ (**1.1**) targets the erythrocyte cycle of the parasites, but it is devoid of significant activity against hepatic stages [20].

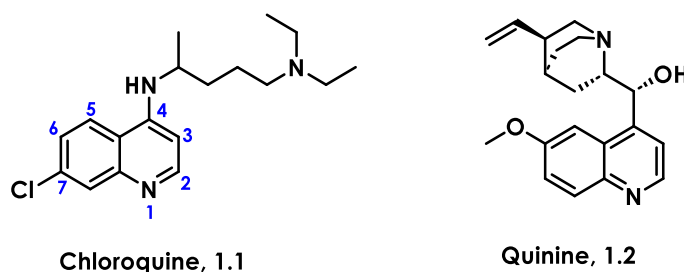


Figure 1.3. Structures of two historical antimalarials: chloroquine and quinine.

During the erythrocytic stage, into the acidic digestive vacuole of red blood cells, parasites need to digest the host's hemoglobin and utilize its amino acids as nutrients. During this digestion, the cofactor of hemoglobin, Fe(II)-heme is released. Fe(II)-heme is able to reduce the dioxygen to highly toxic hydroxyl radicals $\text{OH}\cdot$ (ROS). In order to avoid damage by ROS, the parasite subsequently crystallizes heme into redox-inactive hemozoin crystals, in which iron is in oxidation state (III), thus nontoxic [21]. The pharmacophore of CQ is the 7-chloro-4-aminoquinoline moiety (Fig. 1.3). CQ's mechanism of action is connected to its chemical structure: two basic nitrogen atoms and a plane aromatic moiety. The two basic nitrogen atoms of CQ have suitable pKa values, allowing CQ to efficiently accumulate into the acidic food vacuole of the parasite. As a result, CQ interacts with the Fe(II)-heme by pi-pi stacking thus preventing heme from biocrystallization to hemozoin. The parasite dies due to the increased load of toxic heme Fe(II)-heme complex [22].

CQ's extensive use resulted in parasite drug resistance in Southeast Asia, South America, and Africa, and it was spread all over the world. The emerging resistance resulted in its withdrawal from malaria treatment in 1960s [23].

Fortunately, artemisinin (ART), a natural product isolated from the leaves of a plant used in Chinese traditional medicine called *Artemisia annua*, was discovered ten years later (1971) by

Tu Youyou [24]. In 2015, she was awarded the Nobel Prize in Medicine for her contributions to the fight against malaria [25]. The pharmacophore of ART (Fig. 1.4, molecule **1.3**) is the peroxide bond contained in a 1,2,4-trioxane ring [26]. ART is effective against all *Plasmodium* species, including all strains resistant to the drugs in usage in those years [27]. However, solubility issues and a short half-life *in vivo* led to the development of a new generation of semi-synthetic ART derivatives by functionalization of the C-10 position (Fig. 1.4): artemether (**1.4**), artesunate (**1.5**), and artether (**1.6**), all of which are considered as prodrugs. Dihydroartemisinin (DHA) (**1.7**) is the generated active metabolite [28].

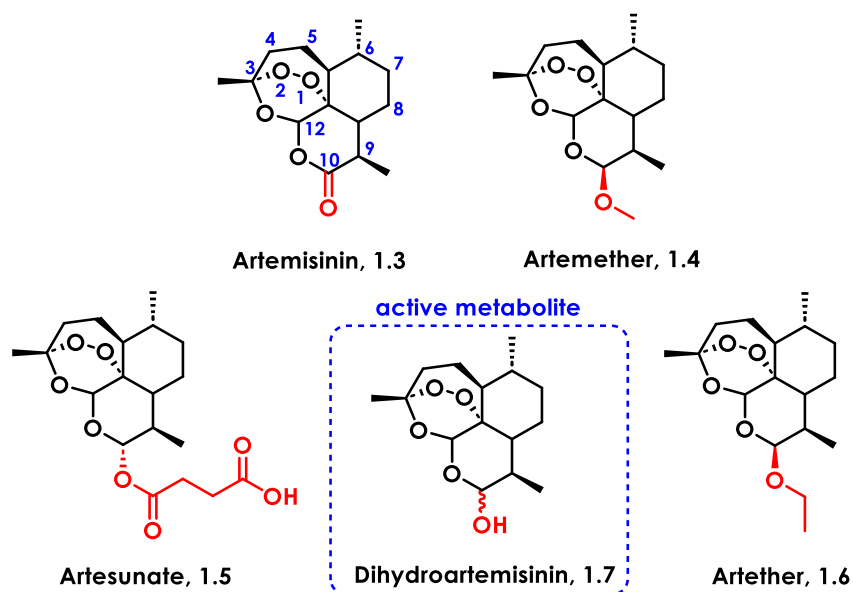
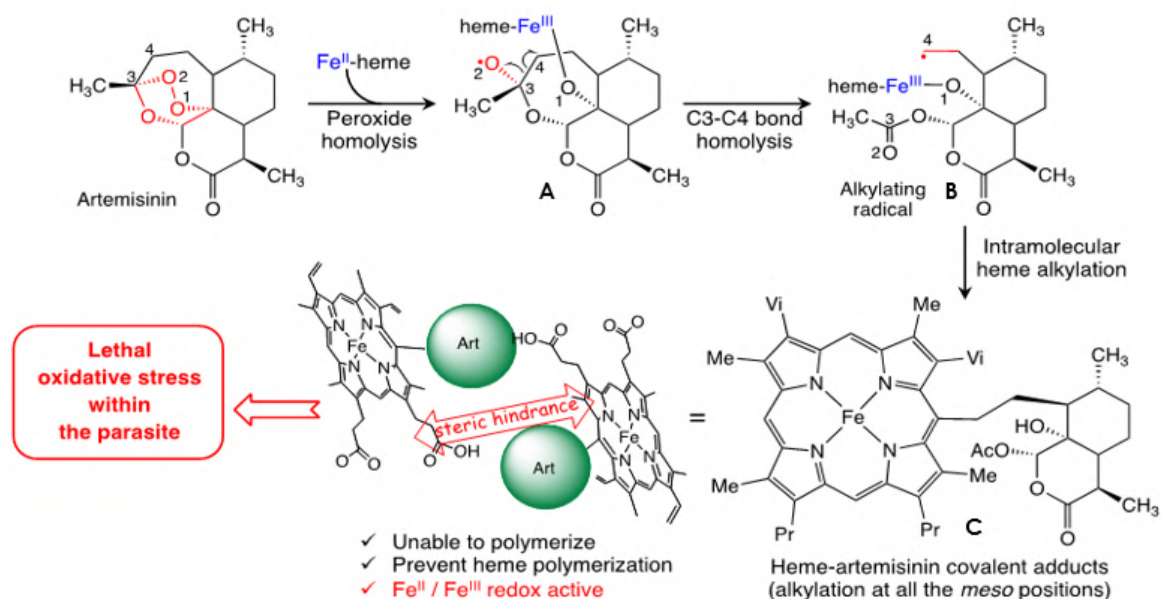


Figure 1.4. Structures of artemisinin and its derivatives.

The mechanism of action of ART has been extensively studied by our team and is associated to alkylation of heme to prevent hemozoin formation [29],[30]. In detail, ART's peroxide bond homolysis is promoted by a single electron transfer from the Fe(II)-heme (Scheme 1.1). This reductive activation generates an alkoxy radical **A**. This O-centered radical quickly rearranges to the alkyl radical **B** by homolytic cleavage of the adjacent C3-C4 bond. Intermediate **B** in turn alkylates intramolecularly all the *meso* carbons of the heme without regioselectivity, leading to the formation of heme-drug adducts **C**. These adducts are unable to interact to elongate the crystal any further due to steric hindrance (Scheme 1.1) due to the accumulated redox-active heme derivatives. As a result, preventing heme crystallization leads to lethal oxidative stress within the parasite and consequently to its death [31-34].



Scheme 1.1. ART as an heme-alkylating agent, all rights reserved to the authors of [35].

The current treatment recommended by the WHO and MMV is ART combination therapies (ACTs). This treatment is based on the co-administration of a fixed dose of two drugs: an artemisinin derivative (for its efficacy and short action) (Fig. 1.4) and a quinoline (e.g., amodiaquine (**1.8**), mefloquine (**1.9**), piperazine (**1.10**)) or another aromatic derivative (e.g., lumefantrine (**1.11**), pyrimethamine (**1.12**), pyronaridine (**1.13**), tafenoquine (**1.14**)) possessing different mechanisms of action and longer half-lives (Fig. 1.5) [27]. The ART derivatives rapidly slow down parasitemia and thus the symptoms manifestation. When ART is eliminated (1-2 hours), the remaining parasites are exposed to the long-lasting partner drugs well after the end of the usual 3-day course [35].

ACTs are currently the most effective available treatment. However, extensive use resulted in parasite resistance to ART, first observed in Cambodia in 2009 [36]. Resistance is now spreading over East Asia, Africa and south America [37],[38]. ART resistance is responsible for delayed parasitic clearance and increase in parasite recrudescence [39]. It has been shown that ART resistance mechanism involves a quiescent stage of *Plasmodium*: upon treatment, parasites stop their cell cycle and, after elimination of the drug, "awake" and continue their proliferation [40]. When the parasite enters the quiescent/dormant phase, it keeps a minimal metabolism and is, for example, able to regulate ART-induced oxidative damage [41].

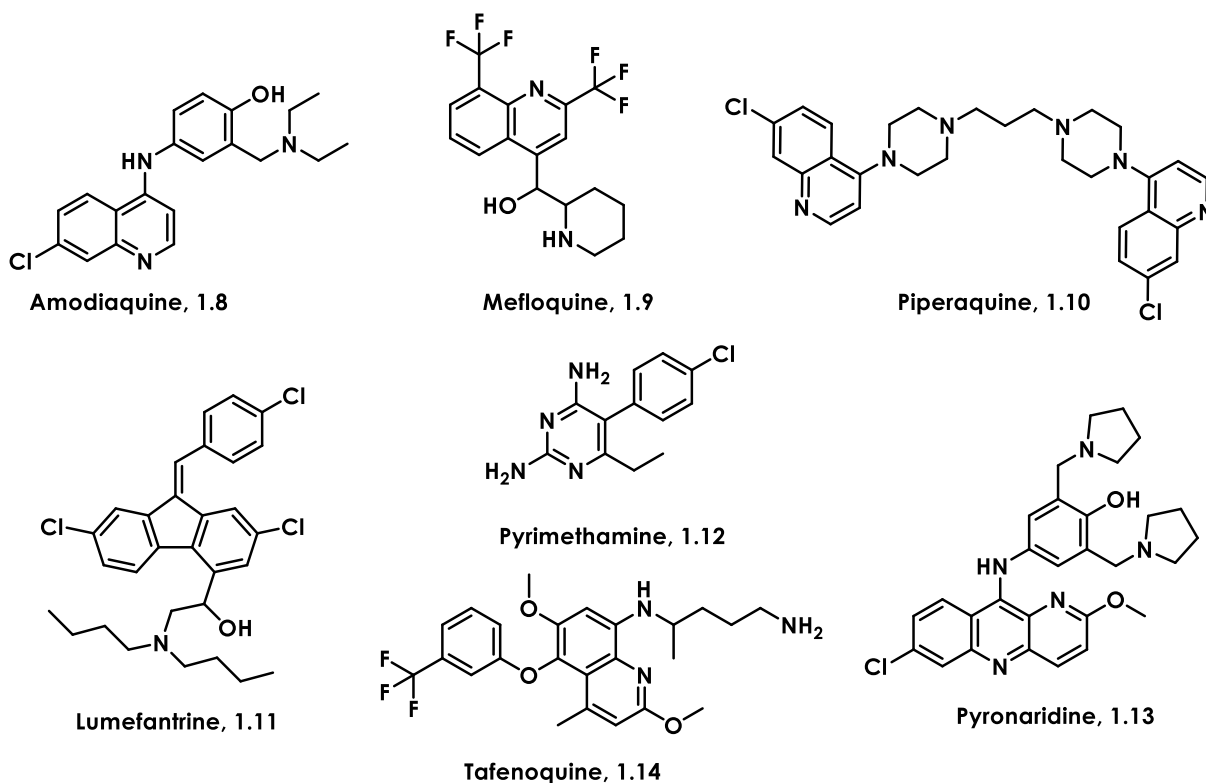


Figure 1.5. Partner drugs used with artemisinin derivatives as antimalarial treatments (ACTs).

Conversely, due to the quiescence, many parasite functions are slowed down or stopped and several parasite targets “disappear”. Consequently, ART resistant *Plasmodium* parasites are also multi-resistant to available drugs. There are currently no drugs efficient to target dormant parasites. It is thus important to develop novel antimalarial agents.

1.2.5 *Plasmodium* mitochondrial targets

In that respect, extensive attempts have been made to find new compounds with novel and selective modes of action in order to combat malaria. During the last two decades, there has been a surge of interest in two major categories of *Plasmodium* molecular targets: epigenetics [42] and mitochondrial [43],[44]. Epigenetics generally contribute to the regulation of gene expression resulting to *P. falciparum* phenotypic plasticity which in turn promotes its proliferation into the host [45]. While it is thought to be a novel antimalarial target, it will not be the focus of this thesis.

The *Plasmodium* mitochondrion was suggested as a potential antimalarial target in 1985 by Hudson *et al.*, focusing primarily on the electron transport chain (ETC), which has reduced function, when the pathogen is in mammalian erythrocytes [46]. ETC in *Plasmodium* is generally composed by three integral membrane enzyme complexes: complex II, III (or cytochrome bc 1) and IV [47]. While ETC remains active during *Plasmodium* asexual proliferation in the host, even into quiescent/dormant parasites, it does not contribute to ATP production, like in every other eukaryotic cell. Rather, ETC serves only one metabolic function: the regeneration of ubiquinone

(Q), which is required in turn as an electron acceptor for dihydroorotate dehydrogenase (DHODH), an essential enzyme for parasite's pyrimidine biosynthesis [48]. Thus, both biochemically related cytochrome bc1 (cyt bc1) [49] and DHODH [50] are considered to be two major druggable antimalarial targets against *Plasmodium*.

Cytochrome bc1 (cyt bc1) is one of the three primary respiratory enzyme complexes centered in *Plasmodium*'s inner mitochondrial membrane. It contains three subunits in its core catalytic domain: cytochrome c, cytochrome c1, and the Rieske Fe-S protein [51]. Cyt bc1 is essential for ETC mitochondrial function. Briefly, in the oxidative site (Q_o) ubiquinol (QH_2) is oxidized to ubiquinone (Q) and four protons are released into the intermembrane area. Ubiquinone (Q) is in turn reduced in the reductive site (Q_i), by using two protons from the matrix, to ubiquinol (QH_2) [49], [52]. Heme plays the role of electron transfer co-factor. Ubiquinone (Q) is then used by dihydroorotate dehydrogenase (DHODH) to generate orotate [48] (Fig. 1.6).

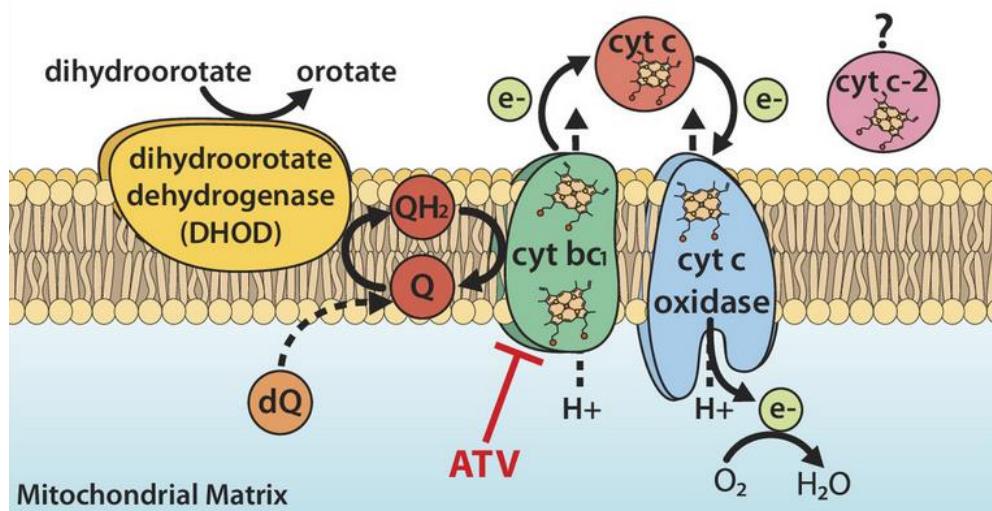


Figure 1.6. The electron transport chain in *P. falciparum* mitochondrion, all rights reserved to the authors of [49].

Cytochrome bc1 has been isolated and completely characterized by X-ray crystallography from mitochondria from various species, notably bovine [53], chicken [54], yeast [55], photosynthetic bacterium *Rhodobacter* [56], etc., with excellent resolutions. However, cyt bc1 crystallographic structure of *Plasmodium* is not yet reported in the literature.

Pyrimidines are used as precursors for DNA and RNA biosynthesis in every cell and are acquired either by *de novo* synthesis (from amino acids) or by salvaging preformed pyrimidine bases or nucleosides [57]. While both pathways are active in human hosts, *Plasmodium* lacks the pyrimidine salvage enzymes. DHODH catalyzes the fourth step of *Plasmodium*'s *de novo* pyrimidine biosynthesis. Dihydroorotate substrate is oxidized to orotate (Fig. 1.6) by using the Q co-enzyme (coQ), generated by cyt bc1, as a co-factor [48]. *Plasmodium*'s DHODH enzyme has been isolated and completely characterized by X-ray crystallography with excellent resolution [58].

Thus, inhibiting one or both mitochondrial targets, either cyt bc1 or DHODH, would compel the parasite to collapse either due to respiratory chain dysfunction or inability to biosynthesize the precursors for its DNA required for its proliferation.

1.2.6 Atovaquone: a bc1 inhibitor

Plasmodium's sensitivity in maintaining its mitochondrial membrane potential led to the development of the commercial drug Malarone (GlaxoSmithKline GSK) [27]. Malarone was marketed in the 2000s and proved to be very effective due to the combination of two drugs: atovaquone (**1.16**) and proguanil (**1.17**) (Fig. 1.7). Atovaquone (ATQ), a 2-hydroxy-1,4-naphthoquinone derivative, is a competitive inhibitor of the natural substrate ubiquinone (Q, **1.15**, Fig. 1.7) of cytochrome bc1 and serves as a competitive inhibitor in the Q_o site (Fig. 1.6), therefore blocking the mitochondrial ETC [59]. The second drug proguanil, when combined with atovaquone, has been shown to collapse the mitochondrial membrane potential, and thus lower the concentration of atovaquone below the effective dose [48]. Atovaquone/proguanil is still used today for medicinal malaria prophylaxis [60] and as an alternative treatment in chloroquine-resistant malaria cases [61]. However, reported mutations in the Q_o site of cyt bc1 resulted in parasite's resistance to atovaquone, reducing the drug's efficacy [62].

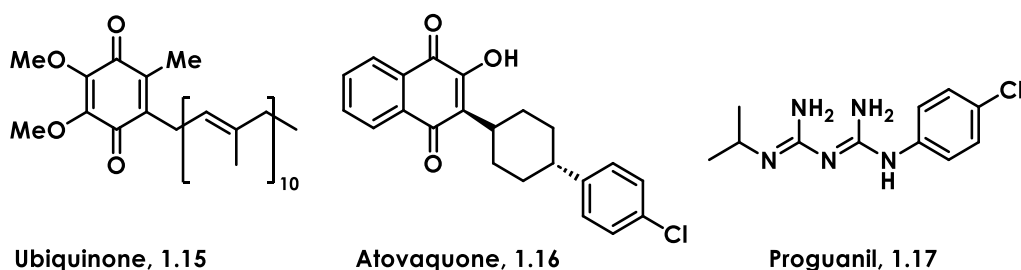


Figure 1.7. Structure of ubiquinone, atovaquone and proguanil.

1.3 Leishmaniasis

Leishmaniasis are a group of neglected tropical parasitic VBDs. This group of infectious diseases threaten more than 350 million of people around the globe (at risk of infection), in 98 countries with more than 12 million new cases reported by the WHO annually [63]. In general, tropical and subtropical countries, along with the southern European countries next to the Mediterranean basin are mainly affected by leishmaniasis (Fig. 1.8).

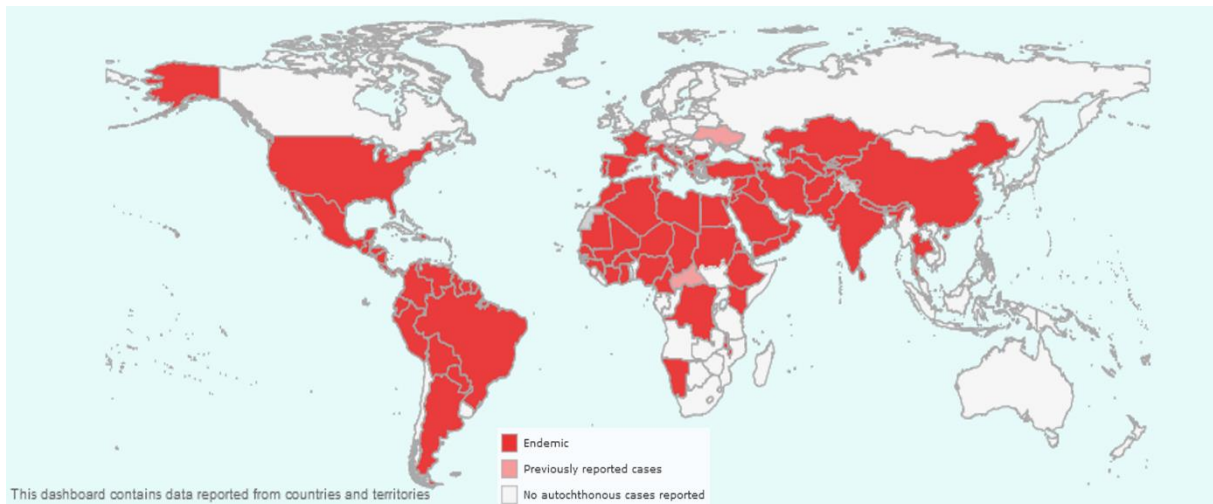


Figure 1.8. Leishmaniasis endemic countries (in red) in 2021 worldwide, reported by the WHO [63].

Leishmaniasis can be categorized in three types: visceral leishmaniasis (VL), cutaneous leishmaniasis (CL) and mucosal leishmaniasis (ML). VL is mostly known as kala-azar and is fatal in 95% of cases, if left untreated. The new annual cases are estimated around 50,000-90,000 worldwide, mostly concentrated in Brazil, East Africa and India. CL is the most common form of the disease and is mostly found in America, the Mediterranean countries and Asia. ML is most prevalent in Bolivia, Ethiopia, Brazil and Peru. Many new cases (600,000-1 million) of both CL and ML are reported to affect these regions annually [63].

Visceral leishmaniasis (VL) or kala-azar is the second most fatal tropical and subtropical disease after malaria and ranks seventh in terms of total number of years lost to premature death and years lost to disability [64],[65]. It affects the poorest populations (children and adults) with 20,000 to 30,000 deaths steadily reported each year, but only five to ten percent of patients eventually die because of complications or co-infections [66].

1.3.1 Vector

Phlebotomus and *Lutzomyia*, two of the approximately 100 genera of dipteran sandflies insects, can serve as vectors for the spread of this infectious disease. While *Lutzomyia* is primarily found in the New World (Central and South America), *Phlebotomus* is only found in the Old World (Europe, Asia, and Africa) [67]. They inhabit either woodlands and forests, or savannas and deserts [68].

1.3.2 Pathogen: *Leishmania* spp.

The protozoan parasites of the *Leishmania* genus, which can further be subdivided into the subgenera *Leishmania* and *Viannia*, depending on the parasite's development into the digestive tract of the sandfly vector, are the pathogens causing disease in mammal hosts. 22 out of about 30 species in total, can infect mammals and subsequently humans, namely, *L.*

donovani, *L. infantum*, *L. mexicana*, *L. tropica*, *L. major*, *L. aethiopica*, and *L. viannia* [69]. Each species has a distinct preference for a particular region. For instance, *L. donovani* (VL) is primarily a child-infecting pathogen that is widespread in East Africa (Sudan, Ethiopia, Somalia, and Kenya) and South Asia (Bangladesh, Nepal, and India) [70]. *L. infantum* (CL) is most frequently found in the Mediterranean basin, the Middle East, and Latin America [71].

Life cycle of *Leishmania* spp.

Leishmaniasis is transmitted to humans and mammals through the bite of the parasite-infected female phlebotomine sandflies. During this blood meal, the infected sandflies inject the *Leishmania* parasites into the mammal host through their proboscis. The parasites are in a metacyclic form, called promastigotes [2]. The promastigotes injected in the skin of the human host are quickly phagocytosed by resident macrophages and other types of mononuclear phagocytic cells. Inside these cells, they are subsequently transformed into tissue-stage amastigote forms (Fig. 1.9) and multiply by simple cell-division inside a formed vacuole [72]. The macrophage in turn gets destroyed after extensive parasite proliferation.

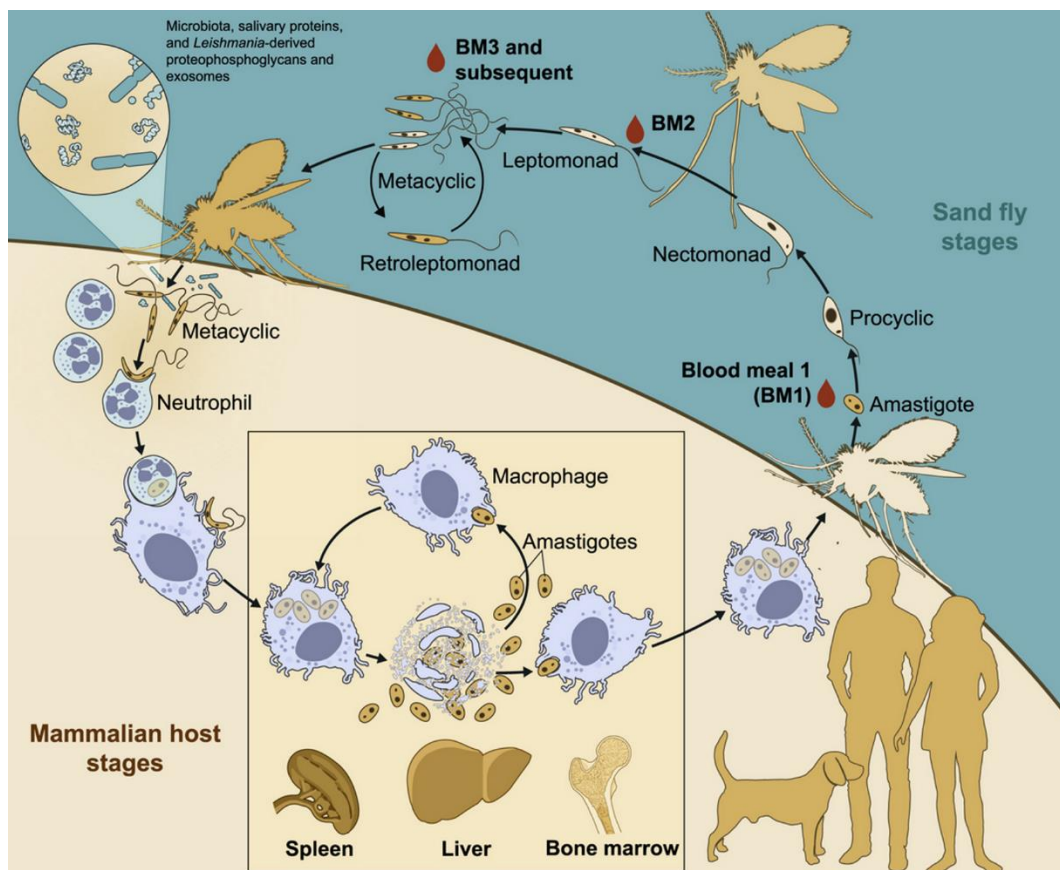


Figure 1.9. Life cycle of *Leishmania* spp., all rights reserved to the authors of [74].

The released amastigote forms can be phagocytosed by a nearby macrophage and travel the entire reticulo-endothelial system (spleen, liver, or bone marrow) via blood vessels.

Depending on the parasite species, the host, and other factors, the infection at this stage could result in symptoms manifestation of the disease (CL or VL) [73]. The infected tissues suffer severe damage. When another sandfly gets in contact with the corresponding infected tissue (lymphoid organs or blood parasitemia), gets in turn infected with free amastigotes. Amastigotes undergo numerous stages of modification before converting to procyclic promastigotes, and they then continue to proliferate in the insect's midgut [74]. After migrating to the salivary glands of the sandfly, they convert into contagious metacyclic promastigotes in order to restart the cycle during the following blood meal [75].

1.3.3 Symptoms

The disease could cause any symptoms, or it could be severe and potentially fatal for all three types. Cutaneous leishmaniasis or white leprosy (CL) is the most prevalent type. It can cause skin ulcers on various body parts, including the neck, face, and legs, which can grow over time and burst to leave an open wound. After a few months, the wound heals, and if there is no co-infection, there is no pain [2]. Mucosal leishmaniasis or espundia (ML) is much more persistent and exhibits nasal, oral or pharyngeal symptoms. If left untreated, it could lead to throat, nose and lips deformation [76]. Finally, visceral leishmaniasis or black fever (VL) symptoms include nausea, weight loss, fever, anemia and hepatosplenomegaly. 80-90% of untreated patients die within 1-2 years because of internal organs failure (e.g., spleen, liver) [77].

1.3.4 Leishmaniases treatment and drug resistance

The treatment should be adapted each time to the type of leishmaniasis and to the host. Generally speaking, pentavalent antimonial complexes, such as sodium stibogluconate (**1.18**) and meglumine antimoniate (**1.19**), have been used for more than 50 years as first line drugs [78](Fig. 1.10). The Sb(V) derivative acts as a pro-drug and is further modified into Sb(III) in the host's macrophages or into the parasite itself. Both Sb oxidation states lead to parasite killing by inhibiting either the glycolysis and other metabolic pathways or by acting as selective trypanothione reductase inhibitors [79],[80].

However, the extensive use of these drugs led quickly to emergence of parasite resistance [81]. In that respect, amphotericin B (amB, **1.20**) was then used as an alternative although it found to be toxic. AmB targets the binding of the promastigote to the host's macrophage [82]. Miltefosine (**1.21**) is the first oral treatment ever used against VL. While it is very efficient to decreasing the parasites proliferation into the host by interfering with the biosynthesis of phospholipids, its severe side effects and toxicity prevent it from being used as a first-line treatment [83]. Two other drugs used alone or in combination with others acting as parasite's mitochondrial inhibitors are paromomycin (**1.22**) [84] and pentamidine (**1.23**) (Fig. 1.10) [85].

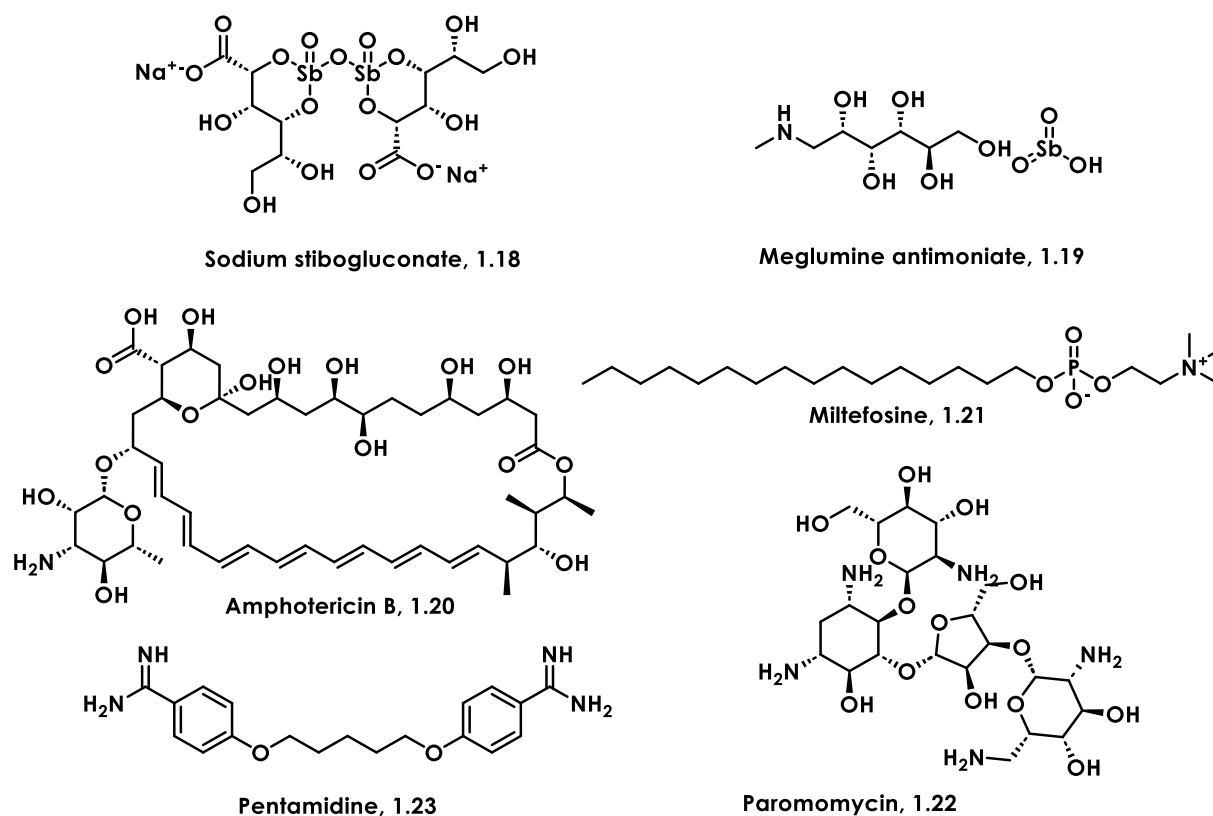


Figure 1.10. Drugs used against leishmaniasis.

Thus, there are major problems in terms of efficacy, toxicity and serious side effects of leishmaniasis chemotherapy. Therefore, more research should be done to discover new and safer leishmanicidal agents since there is currently no vaccine [69] for the disease.

1.4 Naphthoquinones and the lawsone scaffold

Quinones are natural products and play a crucial role in several living organisms including plants, animals, and microorganisms. Also, they can act as transporters of electrons in essential cellular biochemical pathways as for example the respiratory chain in mitochondria [86]. Quinones are fully conjugated cyclic diketones and they can be divided into three main categories based on the type of aromatic system associated to the quinone ring: benzoquinones (**1.24**) (benzene ring), naphthoquinones (**1.25**) (naphthalene ring), and anthraquinones (**1.26**) (anthracene ring) (Fig. 1.11).

It should be noted that the different positions of the two carbonyl groups 1,2 or 1,4 leads to different isomers with notably different physicochemical properties and consequently different pharmacological activities [87].

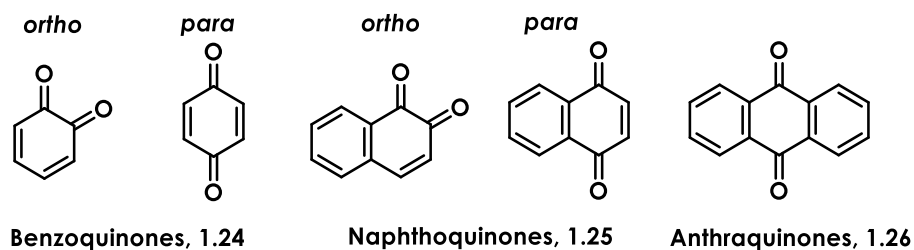


Figure 1.11. Basic cores of the quinone family.

Among all these categories, this thesis will be focused on the synthesis and biological evaluation of naphthoquinone derivatives. Naphthoquinones are widely distributed in nature [88] and they have been extensively studied both for their dyeing properties and pharmacological activities attributed to their redox potential [89]. Natural naphthoquinones have always been an inspiration for organic chemists aiming to synthesize novel bioactive molecules. In that respect, numerous synthetic 1,4-naphthoquinone derivatives have been reported for their antiplasmodial [90]–[92] (compounds **1.27-1.29**), leishmanicidal [93],[94] (compounds **1.30-1.31**), anticancer [87] (compound **1.32**), antibacterial [95] (compound **1.33**), antiviral [96] (compound **1.34**) activities (Fig. 1.12).

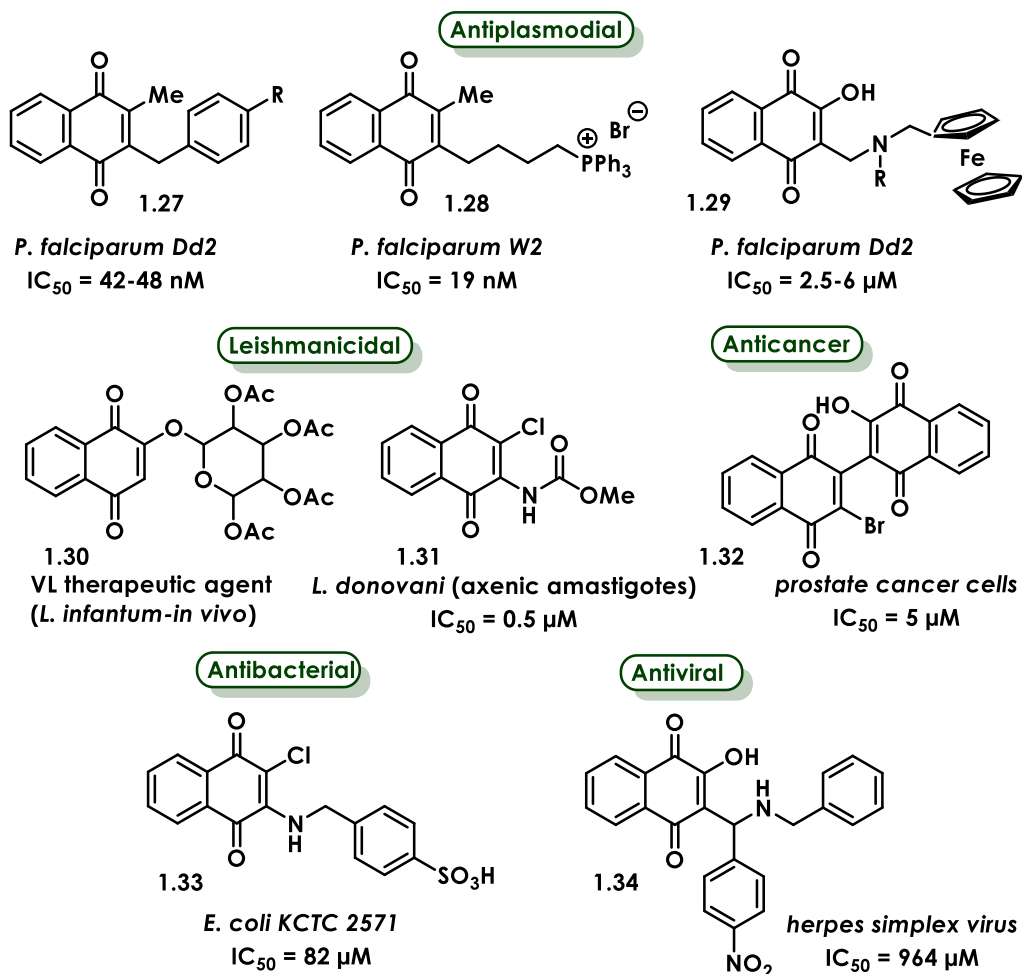


Figure 1.12. Examples of synthetic 1,4-naphthoquinones with various biological activities.

One of the simplest and most significant products of this family that can be used as starting material is 2-hydroxy-1,4-naphthoquinone also known as lawsone (**1.35**, Fig. 1.13) or hennotannic acid.

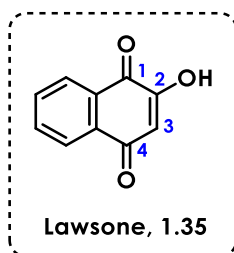


Figure 1.13. Lawsone (2-hydroxy-1,4-naphthoquinone) structure.

Originally isolated from the leaves of the henna plant (*Lawsonia* spp., Lythraceae), lawsone is a natural pigment called Nature Orange 6. In India, Africa, Egypt, and the Middle East, henna extracts have been used as a cosmetic dye for hair, fingernails and skin (tattoos, makeup) and as a commercial pigment (leather, silk, wool) since ancient times [97]. In addition, henna extracts have been extensively used in traditional medicine to treat infected wounds, headaches, fever, bronchitis, lumbago, syphilis, ophthalmia, sores and amenorrhea [98]. Henna is still cultivated and commercially used today, and there are even reports about its customary use in religious rituals [99].

Lawsone (**1.35**) can exist in three tautomeric forms in equilibrium theoretically: the most stable 1,4-naphthoquinone (**a**), the 1,2-naphthoquinone (**b**) and the least stable 1,2,4-naphthotriene (**c**) (Fig. 1.14) [100]. The intramolecular hydrogen bond formation between carbonyl C-1 and H-2 could explain the stability of **1.35 a**. The experimental pKa value of lawsone is reported to be 3.98 [100].

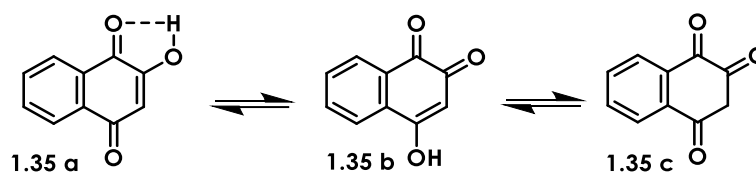


Figure 1.14. Tautomeric forms of lawsone.

This scaffold has been involved in various types of reactions [98], such as dimerizations, free radical alkylations, Michael and Mannich additions, C-3 and O-2 alkylations, etc., in order to access biologically active compounds. However, its involvement in multicomponent reactions in either its enol or keto form (active methylene) is not well established in the literature up to date.

1.5 Multicomponent reactions

Traditionally, organic syntheses rely on a sequence of reactions between two components following a linear synthetic scheme of adding steps in order to obtain a final product. Multicomponent reactions (MCRs), also known as tandem or domino reactions, are one-pot reactions employing more than two starting compounds and result in products that contain the majority of the starting compounds atoms [101](Fig. 1.15). Compared to the traditional total syntheses, they offer a plethora of benefits, including improved selectivity, safety, mild conditions, high bond forming index (multiple C-C, C-N, and C-O bond formations in just one synthetic transformation), atom economy, efficiency (one step synthesis vs sequential multistep synthesis), convergence, and sustainability (improved yields, shorter reaction times, and less waste production).

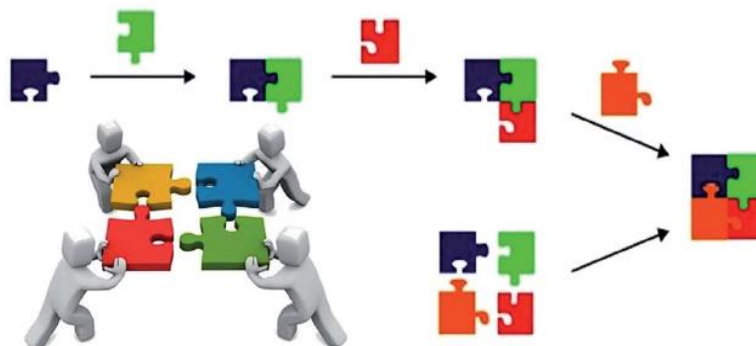


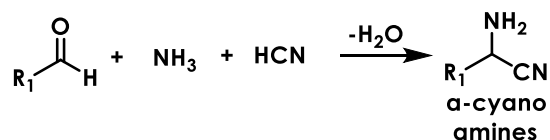
Figure 1.15. The concept of multicomponent reactions vs traditional linear synthesis, all rights reserved to the authors of [102].

1.5.1 The history of MCRs

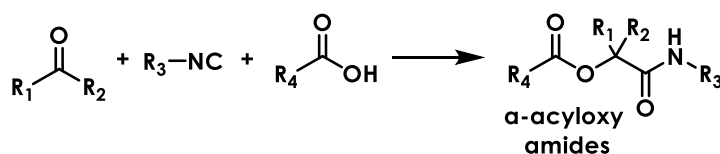
It would be possible that multicomponent reactions existed prior to life on this planet. Adenine, one of the DNA and RNA bases of all living creatures, is believed to be formed by five HCN molecules, each of which plays a crucial role [103]. Many MCRs are named reactions, well-known by the name of the researcher who first developed them. They could be divided in two main categories: isocyanide and carbonyl based. The first MCR ever discovered was by A. Strecker in 1850 [104]. It is a three-component condensation between ammonia, an aldehyde and hydrogen isocyanide leading to α -cyano amines, which can be consecutively hydrolyzed to amino acids (Scheme 1.2, reaction 1). This one-pot approach served as a starting point for further development of isocyanide based MCRs. Isocyanides are great candidates for MCRs because of their zwitterionic structure, which makes them susceptible to irreversible ring closure reactions, aromatization, and electrophilic addition [102]. In that respect, M. Passerini [105] reported the three-component reaction between ketones, isocyanides and carboxylic acids

to give α -acyloxy amides (Scheme 1.2, reaction 2). I. Ugi [106] developed the first four-component condensation between an amine, ketone or aldehyde, isocyanide and a carboxylic acid leading to bis-amides (Scheme 1.2, reaction 3). K. Groebke [107], C. Blackburn [108] and H. Bienaymé [109] worked towards the synthesis of imidazo-annulated pyridines, pyrazines and pyrimidines by using a three-component condensation between an aldehyde, an isocyanide and *ortho*-amino pyridine (Scheme 1.2, reaction 4).

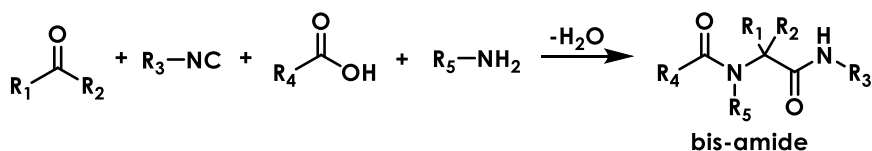
1. Strecker (1850)



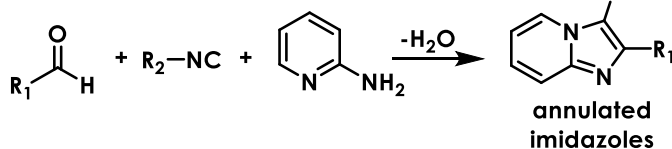
2. Passerini (1921)



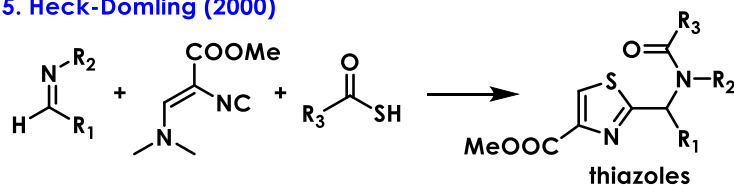
3. Ugi (1959)



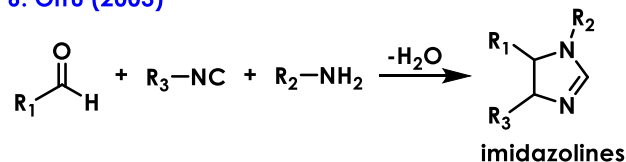
4. Groebke-Blackburn-Bienaymé (1998)



5. Heck-Domling (2000)



6. Orru (2003)

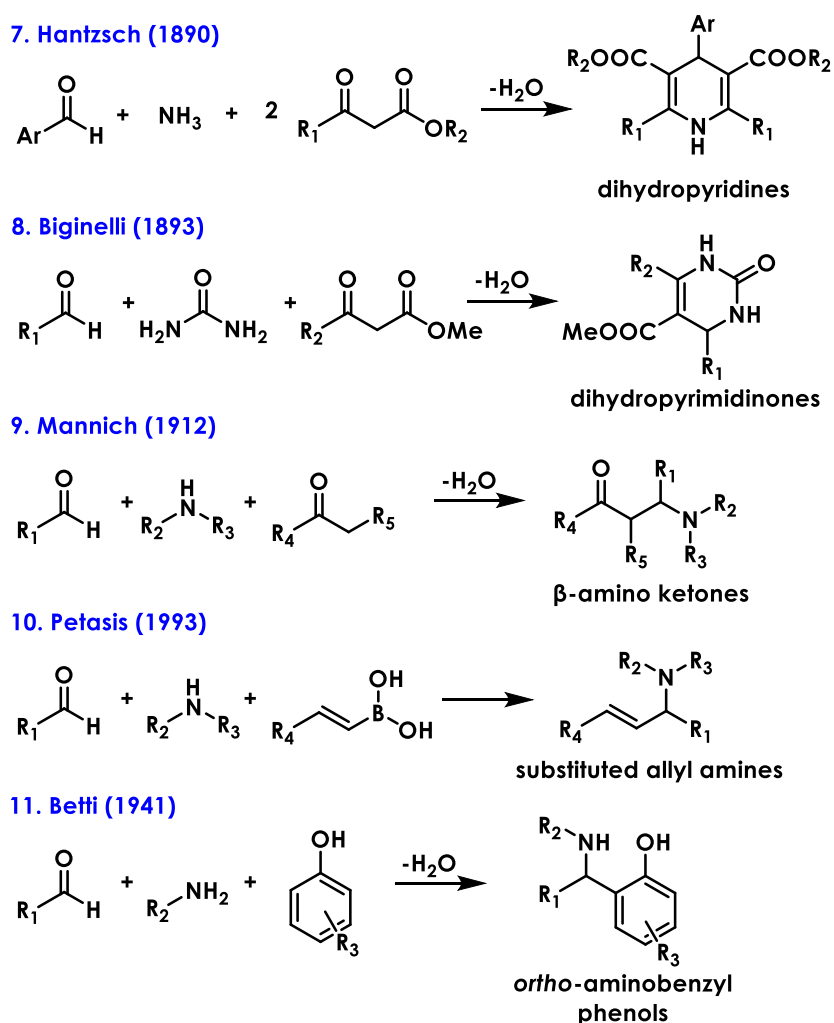


Scheme 1.2. Representative examples of isocyanide based MCRs.

S. Heck and A. Dömling [110] synthesized highly functionalized thiazoles by developing a one-pot reaction between an imine, an isocyanide and thio-carboxylic acid (Scheme 1.2, reaction 5). Orru and his research group [111] developed a three-component condensation between an aldehyde, an isocyanide and a primary amine leading to substituted imidazolines (Scheme

1.2, reaction 6). Every year, more and more MCRs are reported in the literature, but isocyanide-based MCRs are probably the most documented because they make it possible to synthesize a variety of scaffolds, including highly functionalized amides and any type of heterocycles.

The carbonyl based MCRs were found to be equally useful to access to a variety of scaffolds by employing an amino component. A. Hantzsch reported the first multicomponent reaction of this category in 1882 [112]. Symmetric dihydropyridines were synthesized by a three-component condensation of 2 equivalents of 1,3-diketone, an aromatic aldehyde, and ammonia (Scheme 1.3, reaction 7).



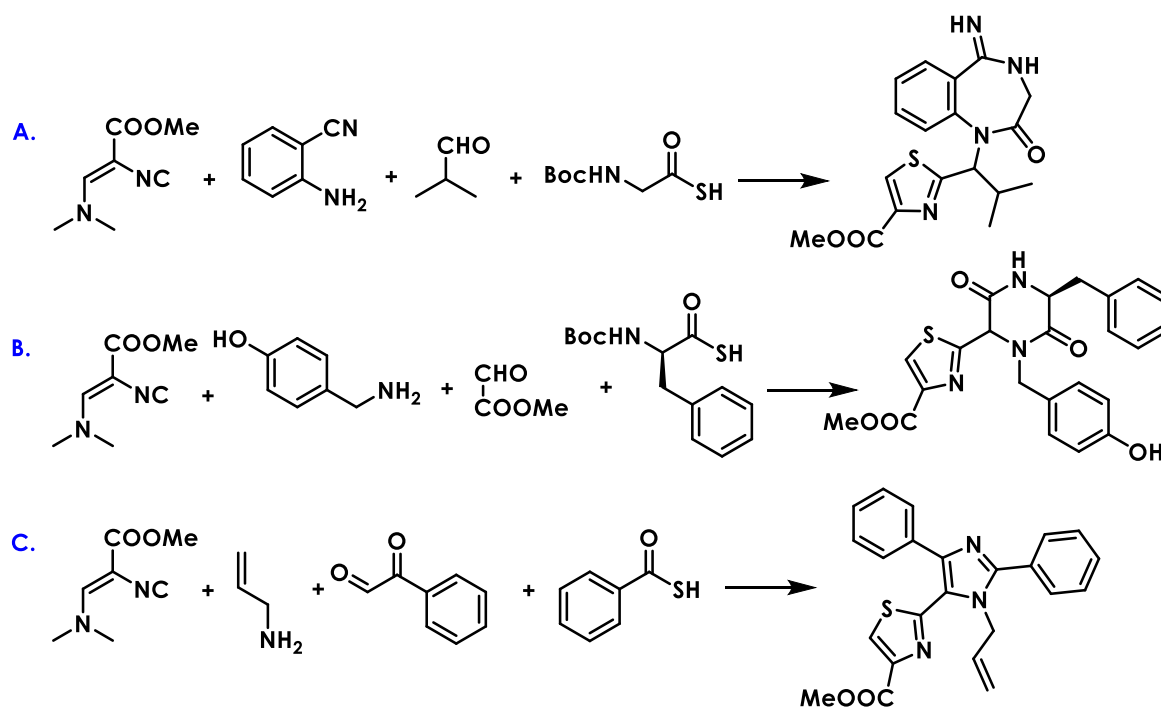
Scheme 1.3. Representative examples of carbonyl based MCRs.

A few years later, P. Biginelli [113] established a very efficient synthetic protocol to access to dihydropyrimidinone scaffolds using a three-component reaction between a urea, and aldehyde, and an active methylene compound (Scheme 1.3, reaction 8). C. Mannich [114] in turn developed a three-component condensation between an aldehyde, an amine (primary or secondary) and an α -methylene ketone to give β -amino substituted ketones (Scheme 1.3, reaction 9). Inspired by the Mannich reaction, A. Petasis [115] proposed an alternative

multicomponent reaction by replacing the α -methylene ketone component with a vinyl boronic acid to yield stereoselective tertiary allyl amines (Scheme 1.3, reaction 10). Last but not least, M. Betti and co-workers [116] reported the efficient synthesis of *ortho*-aminobenzyl phenols by developing accordingly a three-component condensation between an aldehyde, an amine and a phenol (Scheme 1.3, reaction 11). All these MCRs represent just a small example of all MCRs, including their variations, reported in the literature and their number is growing steadily. It is undeniable that MCRs enable fast and simple preparation of a sizable library of molecules (e.g., heterocycles) or critically important synthons (e.g., olefines) in a single step in a sustainable manner.

1.5.2 MCRs and Medicinal Chemistry

In recent years, a significant progress has been made in terms of identifying new druggable biological targets. The speed of these discoveries led to the development of combinatorial chemistry, as a useful tool for the generation of new drug-like molecules needed for structure-relationship studies (SARs) [117]. In that respect, the MCRs approach, permitting the generation of diverse compound libraries in a rather short period of time, has inevitably attracted massive interest in drug discovery. The unique features of MCRs make them excellent candidates to generate huge libraries of molecules by just varying the chemical nature of one component [118]. For example, the variation of a single component of Heck-Dömling reaction can lead to the generation of completely different heterocyclic systems [118] (Scheme 1.4). This fact could permit the acceleration of the hit assessment and thus the lead identification.



Scheme 1.4. Examples of different heterocycles generated by Heck-Dömling MCR.

Meanwhile, the onset of structure diversity could even result in the exploration and expansion of the chemical space, providing researchers with novel feasible small molecular weight bioactive compounds [119].

To conclude, MCRs have emerged as an efficient, green, and cost-effective alternative for multi-step synthesis of biologically active compounds. As a result, they could be a very useful tool in drug design and discovery, with a significant impact on each stage including lead discovery, lead optimization, and pre-clinical phase development.

1.6 Objectives

Malaria and leishmaniasis are two widely-spread infectious vector-borne diseases caused by parasites, affecting millions of people world-wide each year. While chemotherapy seems to be the only way to treat infected individuals, the emergence of parasite multidrug resistance has significantly reduced the efficacy of the majority of currently available drugs. This fact, along with serious secondary effects and toxicity issues of current treatments, leads the scientific community to search for new compounds. These compounds will be either able to target in a better and safer way already known biological pathways essential for parasite survival or exhibit activities to novel essential targets.

Atovaquone (ATQ), a 2-hydroxy-1,4-naphthoquinone/lawsone derivative, is a commercially available and FDA-approved antimalarial drug. Besides, as mentioned before, lawsone derivatives have also been reported to be promising leishmanicidal agents. In that respect, the research project of this thesis will first address the elaboration of novel focused libraries of lawsone derivatives, aiming to identify products active against parasitic diseases. These syntheses will preferably be carried out via multicomponent reactions (MCRs).

Thus, the synthetic goals are:

1st objective: Development of a new MCR methodology employing lawsone in isocyanide-based domino reaction under microwave conditions (Chapter II).

2nd objective: Development of a Biginelli MCR employing lawsone under mechanochemical activation (Chapter III).

Then, each family of compounds will be biologically evaluated *in vitro* against *P. falciparum*, *L. donovani* and other pathogens. The measured activities in the *P. falciparum* case will be compared to *in silico* docking of the molecules against two relevant targets of *Plasmodium* mitochondrion: cyt bc1 and DHODH.

1.7 References

1. M. K. Zapalski and B. L. M. Hubert, First fossil record of parasitism in Devonian calcareous sponges (stromatoporoids), *Parasitology*, **2011**, vol. 138, no. 1, pp. 132–138, doi: [10.1017/S0031182010001071](https://doi.org/10.1017/S0031182010001071).
2. C. Marcin, D. Monika, and H. Edward, Parasitic diseases in humans transmitted by vectors, *Ann. Parasitol.*, **2015**, no. 3, pp. 137–157, doi: [10.17420/ap6103.01](https://doi.org/10.17420/ap6103.01).
3. <https://www.who.int/news-room/fact-sheets/detail/vector-borne-diseases>, page accessed 28.04.2023.
4. W. Takken and H. van den Berg, Manual on prevention of establishment and control of mosquitoes of public health importance in the WHO European Region (with special reference to invasive mosquitoes), **2019**, WHO, Regional Office for Europe.
5. L. H. Miller, H. C. Ackerman, X. Su, and T. E. Wellems, Malaria biology and disease pathogenesis: insights for new treatments, *Nat. Med.*, **2013**, vol. 19, no. 2, pp. 156–167, doi: [10.1038/nm.3073](https://doi.org/10.1038/nm.3073).
6. WORLD MALARIA REPORT, **2022**, WHO.
7. S. Bhatt *et al.*, The effect of malaria control on *Plasmodium falciparum* in Africa between 2000 and 2015, *Nature*, **2015**, vol. 526, no. 7572, pp. 207–211, doi: [10.1038/nature15535](https://doi.org/10.1038/nature15535).
8. P. W. Gething *et al.*, Mapping *Plasmodium falciparum* mortality in Africa between 1990 and 2015, *N. Eng. J. Med.*, **2016**, vol. 375, no. 25, pp. 2435–2445, doi: [10.1056/NEJMoa1606701](https://doi.org/10.1056/NEJMoa1606701).
9. R. E. Howes *et al.*, Global epidemiology of *Plasmodium vivax*, *Am. J. Trop. Med. Hyg.*, **2016**, vol. 95, no. 6 Suppl, pp. 15–34, doi: [10.4269/ajtmh.16-0141](https://doi.org/10.4269/ajtmh.16-0141).
10. M. A. Ahmed and J. Cox-Singh, *Plasmodium knowlesi* - an emerging pathogen, *VOXS*, **2015**, vol. 10, no. S1, pp. 134–140, doi: [10.1111/voxs.12115](https://doi.org/10.1111/voxs.12115).
11. J. Tavares *et al.*, Role of host cell traversal by the malaria sporozoite during liver infection, *J. Exp. Med.*, **2013**, vol. 210, no. 5, pp. 905–915, doi: [10.1084/jem.20121130](https://doi.org/10.1084/jem.20121130).
12. A. F. Cowman, J. Healer, D. Marapana, and K. Marsh, Malaria: biology and disease, *Cell*, **2016**, vol. 167, no. 3, pp. 610–624, doi: [10.1016/j.cell.2016.07.055](https://doi.org/10.1016/j.cell.2016.07.055).
13. A. Sturm *et al.*, Manipulation of host hepatocytes by the malaria parasite for delivery into liver sinusoids, *Science*, **2006**, vol. 313, no. 5791, pp. 1287–1290, doi: [10.1126/science.1129720](https://doi.org/10.1126/science.1129720).
14. M. A. Phillips, J. N. Burrows, C. Manyando, R. H. Van Huijsduijnen, W. C. Van Voorhis, and T. N. C. Wells, Malaria, *Nat. Rev. Dis. Prim.*, **2017**, vol. 3, no. 1, p. 17050, doi: [10.1038/nrdp.2017.50](https://doi.org/10.1038/nrdp.2017.50).
15. D. A. Baker, Malaria gametocytogenesis, *Mol. Biochem. Parasitol.*, **2010**, vol. 172, no. 2, pp. 57–65, doi: [10.1016/j.molbiopara.2010.03.019](https://doi.org/10.1016/j.molbiopara.2010.03.019).
16. G. A. Josling and M. Llinás, Sexual development in *Plasmodium* parasites: knowing when it's time to commit, *Nat. Rev. Microbiol.*, **2015**, vol. 13, no. 9, pp. 573–587, doi: [10.1038/nrmicro3519](https://doi.org/10.1038/nrmicro3519).
17. A. Bartoloni and L. Zammarchi, Clinical aspects of uncomplicated and severe malaria, *Mediterr. J. Hematol. Infect. Dis.*, **2012**, vol. 4, no. 1, p. e2012026, doi: [10.4084/mjihid.2012.026](https://doi.org/10.4084/mjihid.2012.026).
18. S. O. Bittaye *et al.*, Clinical manifestations and outcomes of severe malaria in adult patients admitted to a tertiary hospital in the Gambia, *Malar. J.*, **2022**, vol. 21, no. 1, p. 270, doi: [10.1186/s12936-022-04294-4](https://doi.org/10.1186/s12936-022-04294-4).
19. F. Loeb, Activity of a new antimalarial agent, chloroquine (SN 7618): Statement approved by the board for coordination of malarial studies, *JAMA*, **1946**, vol. 130, no. 16, p. 1069, doi: [10.1001/jama.1946.02870160015006](https://doi.org/10.1001/jama.1946.02870160015006).
20. C. Coban, The host targeting effect of chloroquine in malaria, *Curr. Opin. Immunol.*, **2020**, vol. 66, pp. 98–107, doi: [10.1016/j.coi.2020.07.005](https://doi.org/10.1016/j.coi.2020.07.005).
21. S. E. Francis, D. J. Sullivan, and A. D. E. Goldberg, Hemoglobin metabolism in the malaria parasite *Plasmodium falciparum*, *Annu. Rev. Microbiol.*, **1997**, vol. 51, no. 1, pp. 97–123, doi: [10.1146/annurev.micro.51.1.97](https://doi.org/10.1146/annurev.micro.51.1.97).

22. M. Mushtaque Shahjahan, Reemergence of chloroquine (CQ) analogs as multi-targeting antimalarial agents: a review, *Eur. J. Med. Chem.*, **2015**, vol. 90, pp. 280–295, doi: [10.1016/j.ejmech.2014.11.022](https://doi.org/10.1016/j.ejmech.2014.11.022).
23. L. S. Ross and D. A. Fidock, Elucidating mechanisms of drug-resistant *Plasmodium falciparum*, *Cell Host & Microbe*, **2019**, vol. 26, no. 1, pp. 35–47, Jul. 2019, doi: [10.1016/j.chom.2019.06.001](https://doi.org/10.1016/j.chom.2019.06.001).
24. N. J. White, T. T. Hien, and F. H. Nosten, A brief history of Qinghaosu, *Trends Parasitol.*, **2015**, vol. 31, no. 12, pp. 607–610, doi: [10.1016/j.pt.2015.10.010](https://doi.org/10.1016/j.pt.2015.10.010).
25. <https://www.nobelprize.org/prizes/medicine/2015/summary/>, page accessed 21.07.2023.
26. C. Faurant, From bark to weed: the history of artemisinin, *Parasite*, **2011**, vol. 18, no. 3, pp. 215–218, doi: [10.1051/parasite/2011183215](https://doi.org/10.1051/parasite/2011183215).
27. E. G. Tse, M. Korsik, and M. H. Todd, The past, present and future of anti-malarial medicines, *Malar. J.*, **2019**, vol. 18, no. 1, p. 93, doi: [10.1186/s12936-019-2724-z](https://doi.org/10.1186/s12936-019-2724-z).
28. P. M. O'Neill, The therapeutic potential of semi-synthetic artemisinin and synthetic endoperoxide antimalarial agents, *Expert Opin. Investig. Drugs*, **2005**, vol. 14, no. 9, pp. 1117–1128, doi: [10.1517/13543784.14.9.1117](https://doi.org/10.1517/13543784.14.9.1117).
29. J. Wang *et al.*, Haem-activated promiscuous targeting of artemisinin in *Plasmodium falciparum*, *Nat. Commun.*, **2015**, vol. 6, no. 1, p. 10111, doi: [10.1038/ncomms10111](https://doi.org/10.1038/ncomms10111).
30. L. Tilley, J. Straimer, N. F. Gnädig, S. A. Ralph, and D. A. Fidock, Artemisinin action and resistance in *Plasmodium falciparum*, *Trends Parasitol.*, **2016**, vol. 32, no. 9, pp. 682–696, doi: [10.1016/j.pt.2016.05.010](https://doi.org/10.1016/j.pt.2016.05.010).
31. A. Robert, F. Benoit-Vical, C. Claparols, and B. Meunier, The antimalarial drug artemisinin alkylates heme in infected mice, *Proc. Natl. Acad. Sci. U.S.A.*, **2005**, vol. 102, no. 38, pp. 13676–13680, doi: [10.1073/pnas.0500972102](https://doi.org/10.1073/pnas.0500972102).
32. A. Robert, J. Cazelles, and B. Meunier, Characterization of the alkylation product of heme by the antimalarial drug artemisinin, *Angew. Chem. Int. Ed.*, **2001**, vol. 40, no. 10, pp. 1954–1957, doi: [10.1002/1521-3773\(20010518\)40:10<1954::AID-ANIE1954>3.0.CO;2-9](https://doi.org/10.1002/1521-3773(20010518)40:10<1954::AID-ANIE1954>3.0.CO;2-9).
33. S. A.-L. Laurent, A. Robert, and B. Meunier, C10-modified artemisinin derivatives: efficient heme-alkylating agents, *Angew. Chem. Int. Ed.*, **2005**, vol. 44, no. 14, pp. 2060–2063, doi: [10.1002/anie.200462556](https://doi.org/10.1002/anie.200462556).
34. B. Meunier and A. Robert, Heme as trigger and target for trioxane-containing antimalarial drugs, *Acc. Chem. Res.*, **2010**, vol. 43, no. 11, pp. 1444–1451, doi: [10.1021/ar100070k](https://doi.org/10.1021/ar100070k).
35. A. Robert, F. Benoit-Vical, Y. Liu, and B. Meunier, 2. Small Molecules: the past or the future in drug innovation?, in *Essential Metals in Medicine: Therapeutic Use and Toxicity of Metal Ions in the Clinic*, P. L. Carver, Ed., De Gruyter, **2019**, pp. 17–48. doi: [10.1515/9783110527872-002](https://doi.org/10.1515/9783110527872-002).
36. A. M. Dondorp *et al.*, Artemisinin resistance in *Plasmodium falciparum* Malaria, *N. Engl. J. Med.*, **2009**, vol. 361, no. 5, pp. 455–467, doi: [10.1056/NEJMoa0808859](https://doi.org/10.1056/NEJMoa0808859).
37. B. Balikagala *et al.*, Evidence of artemisinin-resistant malaria in Africa, *N. Engl. J. Med.*, **2021**, vol. 385, no. 13, pp. 1163–1171, doi: [10.1056/NEJMoa2101746](https://doi.org/10.1056/NEJMoa2101746).
38. L. C. Mathieu *et al.*, Kelch13 mutations in *Plasmodium falciparum* and risk of spreading in Amazon basin countries, *J. Antimicrob. Chemother.*, **2021**, vol. 76, no. 11, pp. 2854–2862, doi: [10.1093/jac/dkab264](https://doi.org/10.1093/jac/dkab264).
39. H. Noedl, Y. Se, K. Schaecher, B. L. Smith, D. Socheat, and M. M. Fukuda, Evidence of artemisinin-resistant malaria in western Cambodia, *N. Engl. J. Med.*, **2008**, vol. 359, no. 24, pp. 2619–2620, doi: [10.1056/NEJMc0805011](https://doi.org/10.1056/NEJMc0805011).
40. L. Paloque, A. P. Ramadani, O. Mercereau-Puijalon, J.-M. Augereau, and F. Benoit-Vical, *Plasmodium falciparum*: multifaceted resistance to artemisinins, *Malar. J.*, **2016**, vol. 15, no. 1, p. 149, doi: [10.1186/s12936-016-1206-9](https://doi.org/10.1186/s12936-016-1206-9).
41. B. Witkowski *et al.*, Increased tolerance to artemisinin in *Plasmodium falciparum* is mediated by a quiescence mechanism, *Antimicrob. Agents Chemother.*, **2010**, vol. 54, no. 5, pp. 1872–1877, doi: [10.1128/AAC.01636-09](https://doi.org/10.1128/AAC.01636-09).

42. A. Cortés, V. M. Crowley, A. Vaquero, and T. S. Voss, A view on the role of epigenetics in the biology of malaria parasites, *PLoS Pathog.*, **2012**, vol. 8, no. 12, p. e1002943, doi: [10.1371/journal.ppat.1002943](https://doi.org/10.1371/journal.ppat.1002943).
43. J. Krungkrai, The multiple roles of the mitochondrion of the malarial parasite, *Parasitology*, **2004**, vol. 129, no. 5, pp. 511–524, doi: [10.1017/S0031182004005888](https://doi.org/10.1017/S0031182004005888).
44. A. B. Vaidya and M. W. Mather, Mitochondrial evolution and functions in malaria parasites, *Annu. Rev. Microbiol.*, **2009**, vol. 63, no. 1, pp. 249–267, doi: [10.1146/annurev.micro.091208.073424](https://doi.org/10.1146/annurev.micro.091208.073424).
45. E. Gómez-Díaz *et al.*, Epigenetic regulation of *Plasmodium falciparum* clonally variant gene expression during development in *Anopheles gambiae*, *Sci. Rep.*, **2017**, vol. 7, no. 1, p. 40655, doi: [10.1038/srep40655](https://doi.org/10.1038/srep40655).
46. A. T. Hudson *et al.*, Novel anti-malarial hydroxynaphthoquinones with potent broad spectrum anti-protozoal activity, *Parasitology*, **1985**, vol. 90, no. 1, pp. 45–55, doi: [10.1017/S0031182000049003](https://doi.org/10.1017/S0031182000049003).
47. A. B. Vaidya and M. W. Mather, Mitochondrial evolution and functions in malaria parasites, *Annu. Rev. Microbiol.*, **2009**, vol. 63, no. 1, pp. 249–267, doi: [10.1146/annurev.micro.091208.073424](https://doi.org/10.1146/annurev.micro.091208.073424).
48. H. J. Painter, J. M. Morrissey, M. W. Mather, and A. B. Vaidya, Specific role of mitochondrial electron transport in blood-stage *Plasmodium falciparum*, *Nature*, **2007**, vol. 446, no. 7131, pp. 88–91, doi: [10.1038/nature05572](https://doi.org/10.1038/nature05572).
49. T. J. Espino-Sanchez *et al.*, Direct tests of cytochrome c and c₁ functions in the electron transport chain of malaria parasites, *Proc. Natl. Acad. Sci. U.S.A.*, **2023**, vol. 120, no. 19, p. e2301047120, doi: [10.1073/pnas.2301047120](https://doi.org/10.1073/pnas.2301047120).
50. A. Singh, M. Maqbool, M. Mobashir, and N. Hoda, Dihydroorotate dehydrogenase: A drug target for the development of antimalarials, *Eur. J. Med. Chem.*, **2017**, vol. 125, pp. 640–651, doi: [10.1016/j.ejmech.2016.09.085](https://doi.org/10.1016/j.ejmech.2016.09.085).
51. X. H. Yang and B. L. Trumpower, Protonmotive Q cycle pathway of electron transfer and energy transduction in the three-subunit ubiquinol-cytochrome c oxidoreductase complex of *Paracoccus denitrificans*, *J. Biol. Chem.*, **1988**, vol. 263, no. 24, pp. 11962–11970.
52. P. Mitchell, Possible molecular mechanisms of the protonmotive function of cytochrome systems, *J. Theor. Biol.*, **1976**, vol. 62, no. 2, pp. 327–367, doi: [10.1016/0022-5193\(76\)90124-7](https://doi.org/10.1016/0022-5193(76)90124-7).
53. D. Xia *et al.*, Crystal structure of the cytochrome bc₁ complex from bovine heart mitochondria, *Science*, **1997**, vol. 277, no. 5322, pp. 60–66, doi: [10.1126/science.277.5322.60](https://doi.org/10.1126/science.277.5322.60).
54. G.-F. Hao *et al.*, Computational discovery of picomolar Q_o site inhibitors of cytochrome bc₁ complex, *J. Am. Chem. Soc.*, **2012**, vol. 134, no. 27, pp. 11168–11176, doi: [10.1021/ja3001908](https://doi.org/10.1021/ja3001908).
55. S. R. N. Solmaz and C. Hunte, Structure of complex III with bound cytochrome c in reduced state and definition of a minimal core interface for electron transfer, *J. Biol. Chem.*, **2008**, vol. 283, no. 25, pp. 17542–17549, doi: [10.1074/jbc.M710126200](https://doi.org/10.1074/jbc.M710126200).
56. L. Esser, M. Elberry, F. Zhou, C.-A. Yu, L. Yu, and D. Xia, Inhibitor-complexed structures of the cytochrome bc₁ from the photosynthetic bacterium *Rhodobacter sphaeroides*, *J. Biol. Chem.*, **2008**, vol. 283, no. 5, pp. 2846–2857, doi: [10.1074/jbc.M708608200](https://doi.org/10.1074/jbc.M708608200).
57. M. A. Phillips and P. K. Rathod, *Plasmodium* dihydroorotate dehydrogenase: a promising target for novel anti-malarial chemotherapy, *IDDT*, **2010**, vol. 10, no. 3, pp. 226–239, doi: [10.2174/187152610791163336](https://doi.org/10.2174/187152610791163336).
58. D. E. Hurt, J. Widom, and J. Clardy, Structure of *Plasmodium falciparum* dihydroorotate dehydrogenase with a bound inhibitor, *Acta Crystallogr. D Biol. Crystallogr.*, **2006**, vol. 62, no. 3, pp. 312–323, doi: [10.1107/S0907444905042642](https://doi.org/10.1107/S0907444905042642).
59. D. Birth, W.-C. Kao, and C. Hunte, Structural analysis of atovaquone-inhibited cytochrome bc₁ complex reveals the molecular basis of antimalarial drug action, *Nat. Commun.*, **2014**, vol. 5, no. 1, p. 4029, doi: [10.1038/ncomms5029](https://doi.org/10.1038/ncomms5029).
60. D. G. Laloo and D. R. Hill, Preventing malaria in travellers, *BMJ*, **2008**, vol. 336, no. 7657, pp. 1362–1366, doi: [10.1136/bmj.a153](https://doi.org/10.1136/bmj.a153).

61. M. K. Laufer *et al.*, A longitudinal trial comparing chloroquine as monotherapy or in combination with artesunate, azithromycin or atovaquone-proguanil to treat malaria, *PLoS ONE*, **2012**, vol. 7, no. 8, p. e42284, doi: [10.1371/journal.pone.0042284](https://doi.org/10.1371/journal.pone.0042284).
62. I. K. Srivastava, J. M. Morrissey, E. Darrouzet, F. Daldal, and A. B. Vaidya, Resistance mutations reveal the atovaquone-binding domain of cytochrome b in malaria parasites, *Mol. Microbiol.*, **1999**, vol. 33, no. 4, pp. 704–711, doi: [10.1046/j.1365-2958.1999.01515.x](https://doi.org/10.1046/j.1365-2958.1999.01515.x).
63. <https://www.who.int/news-room/fact-sheets/detail/leishmaniasis>, page accessed 25.07.2023.
64. N. J. Kassebaum *et al.*, Global, regional, and national disability-adjusted life-years (DALYs) for 315 diseases and injuries and healthy life expectancy (HALE), 1990–2015: a systematic analysis for the global burden of disease study, *The Lancet*, **2016**, vol. 388, no. 10053, pp. 1603–1658, doi: [10.1016/S0140-6736\(16\)31460-X](https://doi.org/10.1016/S0140-6736(16)31460-X).
65. R. G. Wamai, J. Kahn, J. McGloin, and G. Ziaggi, Visceral leishmaniasis: a global overview, *J. Glob. Health. Sci.*, **2020**, vol. 2, no. 1, e3, doi: [10.35500/jghs.2020.2.e3](https://doi.org/10.35500/jghs.2020.2.e3).
66. https://www3.paho.org/hq/index.php?option=com_content&view=article&id=13648:leishmaniasis-fact-sheet-health-workers&Itemid=0&lang=en#_gsc.tab=0, page accessed 25.07.2023.
67. D. M. Pigott *et al.*, Global distribution maps of the leishmaniasis, *eLife*, **2014**, vol. 3, p. e02851 doi: [10.7554/eLife.02851](https://doi.org/10.7554/eLife.02851).
68. R. Killick-Kendrick, The biology and control of *Phlebotomine* sand flies, *Clin. Dermatol.*, **1999**, vol. 17, no. 3, pp. 279–289, doi: [10.1016/S0738-081X\(99\)00046-2](https://doi.org/10.1016/S0738-081X(99)00046-2).
69. S. Mann *et al.*, A review of leishmaniasis: current knowledge and future directions, *Curr. Trop. Med. Rep.*, **2021**, vol. 8, no. 2, pp. 121–132, doi: [10.1007/s40475-021-00232-7](https://doi.org/10.1007/s40475-021-00232-7).
70. C. Bern *et al.*, Loss of leishmanin skin test antigen sensitivity and potency in a longitudinal study of visceral leishmaniasis in Bangladesh, *Am. J. Trop. Med. Hyg.*, **2006**, vol. 75, no. 4, pp. 744–748.
71. B. E. McIlwee, S. E. Weis, and G. A. Hosler, Incidence of endemic human cutaneous leishmaniasis in the United States, *JAMA Dermatol.*, **2018**, vol. 154, no. 9, p. 1032, doi: [10.1001/jamadermatol.2018.2133](https://doi.org/10.1001/jamadermatol.2018.2133).
72. <https://www.cdc.gov/dpdx/leishmaniasis/index.html>, page accessed 30.07.2023.
73. K. J. Esch and C. A. Petersen, Transmission and epidemiology of zoonotic protozoal diseases of companion animals, *Clin. Microbiol. Rev.*, **2013**, vol. 26, no. 1, pp. 58–85, doi: [10.1128/CMR.00067-12](https://doi.org/10.1128/CMR.00067-12).
74. T. D. Serafim, E. Iniguez, and F. Oliveira, *Leishmania infantum*, *Trends Parasitol.*, **2020**, vol. 36, no. 1, pp. 80–81, doi: [10.1016/j.pt.2019.10.006](https://doi.org/10.1016/j.pt.2019.10.006).
75. D. E. Teixeira, M. Benchimol, J. C. F. Rodrigues, P. H. Crepaldi, P. F. P. Pimenta, and W. De Souza, The cell biology of *Leishmania*: how to teach using animations, *PLoS Pathog.*, **2013**, vol. 9, no. 10, p. e1003594, doi: [10.1371/journal.ppat.1003594](https://doi.org/10.1371/journal.ppat.1003594).
76. B. S. McGwire and A. R. Satoskar, Leishmaniasis: clinical syndromes and treatment, **2014**, *QJM*, vol. 107, no. 1, pp. 7–14, doi: [10.1093/qjmed/hct116](https://doi.org/10.1093/qjmed/hct116).
77. B. Monge-Maillo and R. López-Vélez, Therapeutic options for visceral leishmaniasis, *Drugs*, **2013**, vol. 73, no. 17, pp. 1863–1888, doi: [10.1007/s40265-013-0133-0](https://doi.org/10.1007/s40265-013-0133-0).
78. R. K. Singh, H. P. Pandey, and S. Sundar, Visceral leishmaniasis (kala-azar): challenges ahead, *Indian J. Med. Res.*, **2006**, vol. 123, no. 3, pp. 331–344.
79. K. El Fadili *et al.*, Role of the ABC transporter MRPA (PGPA) in antimony resistance in *Leishmania infantum* axenic and intracellular amastigotes, *Antimicrob. Agents Chemother.*, **2005**, vol. 49, no. 5, pp. 1988–1993, doi: [10.1128/AAC.49.5.1988-1993.2005](https://doi.org/10.1128/AAC.49.5.1988-1993.2005).
80. S. Wyllie, M. L. Cunningham, and A. H. Fairlamb, Dual action of antimonial drugs on thiol redox metabolism in the human pathogen *Leishmania donovani*, *J. Biol. Chem.*, **2004**, vol. 279, no. 38, pp. 39925–39932, doi: [10.1074/jbc.M405635200](https://doi.org/10.1074/jbc.M405635200).
81. D. Sereno, C. Maia, and K. Ait-Oudhia, Antimony resistance and environment: elusive links to explore during *Leishmania* life cycle, *Int. J. Parasitol. Drug*, **2012**, vol. 2, pp. 200–203, doi: [10.1016/j.ijpddr.2012.07.003](https://doi.org/10.1016/j.ijpddr.2012.07.003).

82. Y. D. Paila, B. Saha, and A. Chattopadhyay, Amphotericin B inhibits entry of *Leishmania donovani* into primary macrophages, *BBRC*, **2010**, vol. 399, no. 3, pp. 429–433, doi: [10.1016/j.bbrc.2010.07.099](https://doi.org/10.1016/j.bbrc.2010.07.099).
83. M. Rakotomanga, S. Blanc, K. Gaudin, P. Chaminade, and P. M. Loiseau, Miltefosine affects lipid metabolism in *Leishmania donovani* promastigotes, *Antimicrob. Agents Chemother.*, **2007**, vol. 51, no. 4, pp. 1425–1430, doi: [10.1128/AAC.01123-06](https://doi.org/10.1128/AAC.01123-06).
84. C. P. Thakur, T. P. Kanyok, A. K. Pandey, G. P. Sinha, C. Messick, and P. Olliaro, Treatment of visceral leishmaniasis with injectable paromomycin (aminosidine). An open-label randomized phase-II clinical study, *Trans. R. Soc. Trop. Med. Hyg.*, **2000**, vol. 94, no. 4, pp. 432–433, doi: [10.1016/S0035-9203\(00\)90131-7](https://doi.org/10.1016/S0035-9203(00)90131-7).
85. M. Basselin, F. Lawrence, and M. Robert-Gero, Pentamidine uptake in *Leishmania donovani* and *Leishmania amazonensis* promastigotes and axenic amastigotes, *Biochem. J.*, **1996**, vol. 315, no. 2, pp. 631–634, doi: [10.1042/bj3150631](https://doi.org/10.1042/bj3150631).
86. G. Powis, Free radical formation by antitumor quinones, *Free Radic. Biol. Med.*, **1989**, vol. 6, no. 1, pp. 63–101, doi: [10.1016/0891-5849\(89\)90162-7](https://doi.org/10.1016/0891-5849(89)90162-7).
87. C. E. Pereyra, R. F. Dantas, S. B. Ferreira, L. P. Gomes, and F. P. Silva-Jr, The diverse mechanisms and anticancer potential of naphthoquinones, *Cancer Cell. Int.*, **2019**, vol. 19, no. 1, p. 207, doi: [10.1186/s12935-019-0925-8](https://doi.org/10.1186/s12935-019-0925-8).
88. Y. Kumagai, Y. Shinkai, T. Miura, and A. K. Cho, The chemical biology of naphthoquinones and its environmental implications, *Annu. Rev. Pharmacol. Toxicol.*, **2012**, vol. 52, no. 1, pp. 221–247, doi: [10.1146/annurev-pharmtox-010611-134517](https://doi.org/10.1146/annurev-pharmtox-010611-134517).
89. L. I. López López, S. D. Nery Flores, S. Y. Silva Belmares, and A. Sáenz Galindo, Naphthoquinones: biological properties and synthesis of lawsone and derivatives - a structured review, *Vitae*, **2014**, vol. 21, no. 3, pp. 248–258, doi: [10.17533/udea.vitae.17322](https://doi.org/10.17533/udea.vitae.17322).
90. T. Müller, L. Johann, B. Jannack, M. Brückner, D. A. Lanfranchi, H. Bauer, C. Sanchez, V. Yardley, C. Deregnacourt, J. Schrével, M. Lanzer, R. H. Schirmer, E. Davioud-Charvet, Glutathione reductase-catalyzed cascade of redox reactions to bioactivate potent antimalarial 1,4-naphthoquinones – A new strategy to combat malarial parasites. *J. Am. Chem. Soc.* **2011**, vol. 133, no. 30, pp. 11557–11571, doi: <https://doi.org/10.1021/ja201729z>.
91. T. E. Long, X. Lu, M. Galizzi, R. Docampo, J. Gut, and P. J. Rosenthal, Phosphonium lipocations as antiparasitic agents, *Bioorganic Med. Chem. Lett.*, **2012**, vol. 22, no. 8, pp. 2976–2979, doi: [10.1016/j.bmcl.2012.02.045](https://doi.org/10.1016/j.bmcl.2012.02.045).
92. A. Baramee, A. Coppin, M. Mortuaire, L. Pelinski, S. Tomavo, and J. Brocard, Synthesis and *in vitro* activities of ferrocenic aminohydroxynaphthoquinones against *Toxoplasma gondii* and *Plasmodium falciparum*, *Bioorganic Med. Chem.*, **2006**, vol. 14, no. 5, pp. 1294–1302, doi: [10.1016/j.bmc.2005.09.054](https://doi.org/10.1016/j.bmc.2005.09.054).
93. V. Sebastián-Pérez *et al.*, Naphthoquinone as a new chemical scaffold for leishmanicidal inhibitors of *Leishmania* GSK-3, *Biomedicines*, **2022**, vol. 10, no. 5, p. 1136, doi: [10.3390/biomedicines10051136](https://doi.org/10.3390/biomedicines10051136).
94. D. V. C. Mendonça *et al.*, Flau-A, a naphthoquinone derivative, is a promising therapeutic candidate against visceral leishmaniasis: a preliminary study, *Exp. Parasitol.*, **2022**, vol. 233, p. 108205, doi: [10.1016/j.exppara.2021.108205](https://doi.org/10.1016/j.exppara.2021.108205).
95. P. Ravichandiran, S. Sheet, D. Premnath, A. R. Kim, and D. J. Yoo, 1,4-Naphthoquinone analogues: potent antibacterial agents and mode of action evaluation, *Molecules*, **2019**, vol. 24, no. 7, p. 1437, doi: [10.3390/molecules24071437](https://doi.org/10.3390/molecules24071437).
96. V. Giongo *et al.*, Antiviral potential of naphthoquinones derivatives encapsulated within liposomes, *Molecules*, **2021**, vol. 26, no. 21, p. 6440, doi: [10.3390/molecules26216440](https://doi.org/10.3390/molecules26216440).
97. K. N. Jallad and C. Espada-Jallad, Lead exposure from the use of *Lawsonia inermis* (Henna) in temporary paint-on-tattooing and hair dying, *Science of The Total Environment*, **2008**, vol. 397, no. 1–3, pp. 244–250, doi: [10.1016/j.scitotenv.2008.02.055](https://doi.org/10.1016/j.scitotenv.2008.02.055).
98. A. K. Jordão, M. D. Vargas, A. C. Pinto, F. D. C. Da Silva, and V. F. Ferreira, Lawsone in organic synthesis, *RSC Adv.*, **2015**, vol. 5, no. 83, pp. 67909–67943, doi: [10.1039/C5RA12785H](https://doi.org/10.1039/C5RA12785H).

99. A. Ashnagar, A. Shir, Isolation and characterization of 2-hydroxy-1,4-naphthoquinone (lawsone) from the powdered leaves of henna plant marketed in Ahwaz city of Iran, *Int. J. Chem. Tech. Res.*, **2011**, vol. 3, no. 4, pp. 1941-1944.
100. G. Lamoureux, A. L. Perez, M. Araya, and C. Agüero, Reactivity and structure of derivatives of 2-hydroxy-1,4-naphthoquinone (lawsone), *J. Phys. Org. Chem.*, **2008**, vol. 21, no. 12, pp. 1022–1028, doi: [10.1002/poc.1435](https://doi.org/10.1002/poc.1435).
101. I. Ugi, A. Dömling, and W. Hörl, Multicomponent reactions in organic chemistry, *Endeavour*, **1994**, vol. 18, no. 3, pp. 115–122, doi: [10.1016/S0160-9327\(05\)80086-9](https://doi.org/10.1016/S0160-9327(05)80086-9).
102. B. Török, C. Schäfer, and A. Kokel, Multicomponent reactions, *Heterogeneous Catalysis in Sustainable Synthesis*, Elsevier, **2022**, pp. 443–489. doi: [10.1016/B978-0-12-817825-6.00002-1](https://doi.org/10.1016/B978-0-12-817825-6.00002-1).
103. S. Drenkard, J. Ferris, and A. Eschenmoser, Chemie von-Aminonitrilen. Aziridin-2-carbonitril photochemische Bildung aus 2-aminopropennitril, *Helv. Chim. Acta*, **1990**, vol. 73, no. 5, pp. 1373–1390, doi: [10.1002/hlca.19900730524](https://doi.org/10.1002/hlca.19900730524).
104. A. Strecker, Ueber die künstliche bildung der milchsäure und einen neuen, dem glycocoll homologen körper, *Ann. Chem. Pharm.*, **1850**, vol. 75, no. 1, pp. 27–45, doi: [10.1002/jlac.18500750103](https://doi.org/10.1002/jlac.18500750103).
105. M. Passerini, Three-component condensation (3CC) of carboxylic acids, c-isocyanides, and carbonyl compounds to afford α -acyloxycarboxamides, *Gazz. Chim. Ital.*, **1921**, vol. 51, pp. 126–129.
106. I. Ugi, R. Meyr, U. Fetzer and C. Steinbruckner, Versammlungsberichte, *Angew. Chem.*, **1959**, vol. 71, no. 11, pp. 373–388, doi: [10.1002/ange.19590711110](https://doi.org/10.1002/ange.19590711110).
107. K. Groebke, L. Weber and F. Mehlin, Synthesis of imidazo[1,2-a] annulated pyridines, pyrazines and pyrimidines by a novel three-component condensation, *Synlett.*, **1998**, vol. 6, pp. 661-663, doi: [10.1055/s-1998-1721](https://doi.org/10.1055/s-1998-1721).
108. C. Blackburn, B. Guan, P. Fleming, K. Shiosaki, and S. Tsai, Parallel synthesis of 3-aminoimidazo[1,2-a]pyridines and pyrazines by a new three-component condensation, *Tet. Lett.*, **1998**, vol. 39, no. 22, pp. 3635–3638, doi: [10.1016/S0040-4039\(98\)00653-4](https://doi.org/10.1016/S0040-4039(98)00653-4).
109. H. Bienaymé and K. Bouzid, A new heterocyclic multicomponent reaction for the combinatorial synthesis of fused 3-aminoimidazoles, *Angew. Chem., Int. Ed. Engl.*, **1998**, vol. 37, no. 16, pp. 2234–2237, doi: [10.1002/\(SICI\)1521-3773\(19980904\)37:16<2234::AID-ANIE2234>3.0.CO;2-R](https://doi.org/10.1002/(SICI)1521-3773(19980904)37:16<2234::AID-ANIE2234>3.0.CO;2-R).
110. S. Heck and A. Domling, A versatile multi-component one-pot thiazole synthesis, *Synlett.*, **2000**, no. 03, pp. 424–426, doi: [10.1055/s-2000-6517](https://doi.org/10.1055/s-2000-6517).
111. R. S. Bon et al., Novel multicomponent reaction for the combinatorial synthesis of 2-imidazolines, *Org. Lett.*, **2003**, vol. 5, no. 20, pp. 3759–3762, doi: [10.1021/ol035521g](https://doi.org/10.1021/ol035521g).
112. A. Hantzsch, Ueber die synthese pyridinartiger verbindungen aus acetessigäther und aldehydammoniak, *Justus Liebigs Ann. Chem.*, **1882**, vol. 215, no. 1, pp. 1–82, doi: [10.1002/jlac.18822150102](https://doi.org/10.1002/jlac.18822150102).
113. P. Biginelli, Aldehyde-urea derivatives of aceto- and oxaloacetic Acids. *Gazz. Chim. Ital.*, **1893**, vol. 23, pp. 360-413.
114. C. Mannich and W. Krösche, Ueber ein kondensationsprodukt aus formaldehyd, ammoniak und antipyrin, *Arch. Pharm. Pharm. Med. Chem.*, **1912**, vol. 250, no. 1, pp. 647–667, doi: [10.1002/ardp.19122500151](https://doi.org/10.1002/ardp.19122500151).
115. N. A. Petasis and I. Akritopoulou, The boronic acid mannich reaction: a new method for the synthesis of geometrically pure allylamines, *Tet. Lett.*, **1993**, vol. 34, no. 4, pp. 583–586, doi: [10.1016/S0040-4039\(00\)61625-8](https://doi.org/10.1016/S0040-4039(00)61625-8).
116. C. Cardellicchio, M. A. M. Capozzi, and F. Naso, The Betti base: the awakening of a sleeping beauty, *Tetrahedron: Asymmetry*, **2010**, vol. 21, no. 5, pp. 507–517, doi: [10.1016/j.tetasy.2010.03.020](https://doi.org/10.1016/j.tetasy.2010.03.020).
117. M. J. Buskes, A. Coffin, D. M. Troast, R. Stein, and M.-J. Blanco, Accelerating drug discovery: synthesis of complex chemotypes via multicomponent reactions, *ACS Med. Chem. Lett.*, **2023**, vol. 14, no. 4, pp. 376–385, doi: [10.1021/acsmchemlett.3c00012](https://doi.org/10.1021/acsmchemlett.3c00012).

118. L. Weber, The application of multi-component reactions in drug discovery, *CMC*, **2002**, vol. 9, no. 23, pp. 2085–2093, doi: [10.2174/0929867023368719](https://doi.org/10.2174/0929867023368719).
119. A. Dömling, W. Wang, and K. Wang, Chemistry and biology of multicomponent reactions, *Chem. Rev.*, **2012**, vol. 112, no. 6, pp. 3083–3135, doi: [10.1021/cr100233r](https://doi.org/10.1021/cr100233r).

CHAPTER 2

**“Lawsonone in domino reaction
with aldehydes and alkyl-
isocyanides: synthetic
approaches and biological
activities”**

2.1 Introduction

In this chapter, the importance of the naphthofuroquinone scaffold will be emphasized, and many previous efforts toward its elaboration will be presented. The first synthetic approach to a multicomponent domino reaction between lawsone, various aldehydes, and alkyl isocyanides under microwave irradiation will be reported. This synthetic methodology leads to a series of naphthofuroquinones with fair yields. Meanwhile, direct condensation between lawsone and the corresponding isocyanide occurs when less electrophilic aldehydes are used, leading to the formation of naphthoenaminones. All series of obtained products will be biologically evaluated against *Plasmodium falciparum*, *Leishmania donovani* and other pathogens. The *in vitro* results will be reported along with an *in silico* study against both mitochondrial targets of *P. falciparum* cytochrome bc1 and DHODH enzyme.

2.1.1 Naphthofuroquinones and biological activities

Among naphthoquinones, there is one category called naphthofuroquinones (NFQs): a tricyclic 1,4- or 1,2-naphthoquinone bearing a fused furan ring. Compounds containing this type of scaffold were first identified and isolated from natural products. One of the first publications reporting naphthofuroquinones was published in the early 70s. Mathieson and Thomson while searching the different kinds of spinochrome pigments in different species of sea urchins, reported the identification of compounds responsible for their color (Fig. 2.1, molecule **2.1**) [1]. Tyler reported in 1988 that the lapacho tea, a natural herb that had been used for years [2] was found to contain biologically active compounds of the naphthofuroquinone family. Steinert *et al.* reported [3] in 1995 that substituted NFQs were the main quinone compounds in both methanolic and aqueous extracts of the inner bark of *Tabebuia avellanedae* (*Bignoniaceae*), which was used for the tea infusion (Fig. 2.1, molecules **2.2**, **2.3** and **2.4**). Thereupon, many different groups around the world have isolated NFQs from natural sources in order to discover, study, and confirm new potential biological properties. This research led to semi-synthetic and fully synthetic series of derivatives of the naphthofuroquinone family, allowing a further exploration of the spectrum of their potential biological activities.

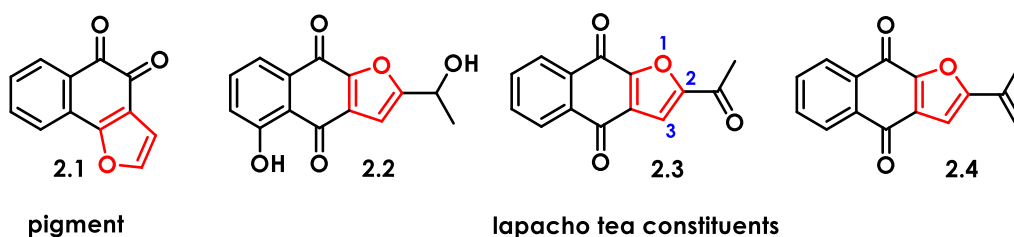


Figure 2.1. The first identified structures of naphthofuroquinones in natural products.

To begin with, compounds of the NFQ family have shown interesting antimicrobial activities. The synthetic compound DFC2 (Fig. 2.2, **2.5**) exhibited promising antimycobacterial activity ($IC_{50} = 0.5-0.9 \mu M$) against drug-resistant strains of *Mycobacterium tuberculosis*. This compound had lower cytotoxicity and better selectivity than the clinically used anti-tuberculosis drug isoniazid, but its mechanism of action remains unknown [4]. The natural compound N12D (Fig. 2.2, **2.6**) displayed an IC_{50} ($IC_{50} = 3-6 \mu M$) lower than oxacillin, which was used as reference drug, against drug-resistant strains of *Staphylococcus aureus*. Compound **2.6** (N12D) was able to penetrate bacteria biomembrane barriers and hence inhibited biofilms formation. Further studies proved that N12D mode of action was due to bacterial wall damage and disturbance of the gluconeogenesis pathway [5].

Many NFQ derivatives exhibited also anti-cancer properties. Some representative but not exhaustive examples can be cited. *Takano et al.* reported in 2009 [6] the synthesis of four series of naphthoquinones in order to evaluate them against different human tumor cell lines. Among all families of compounds, the NFQ family was found to be the most active and the one exhibiting tumor specificity by inducing early apoptotic markers. Several subsequent studies have shown that this simple NFQ motif was responsible for anti-tumoral activities. *Prateep et al.* [7] developed a research program focused on natural product Avicequinone-B (Fig. 2.2, **2.7**). This compound exhibited early (48 h) anti-proliferative activity ($IC_{50} = 4 \mu M$) in human lung cancer cells and was able to overcome cancer metastasis. More recently (2021), *Almeida et al.* reported a new synthetic antitumor NFQ (Fig. 2.2, CNFD, **2.8**) displaying anti-cancer activity against MCF-7 human breast adenocarcinoma cells ($IC_{50} = 0.98 \mu M$ for 48 h incubation). Very promising anti-tumoral effects were observed when CNFD was tested *in vivo* using a murine model [8].

Various studies focused on NFQ family have contributed to discovering enzyme inhibitory activities. For instance, the semi-synthetic avicequinone-C derivative **2.9**, (Fig. 2.2, **2.9**) displayed 22-fold more potent inhibitory activity of steroid 5 α -reductase ($IC_{50} = 0.20 \mu M$) than the natural avicequinone-C substrate ($IC_{50} = 4.5 \mu M$). The bioproduction of hormones linked to androgenic illnesses like prostate cancer and scalp hair loss may be balanced as a result of this enzyme inhibition [9]. Compound **2.10** displayed excellent inhibitory activity against various receptors of tyrosine kinases family (e.g., EGFR, VEGFR2, FGFR1 and PDGFRb). This activity was linked to antiangiogenic action [10].

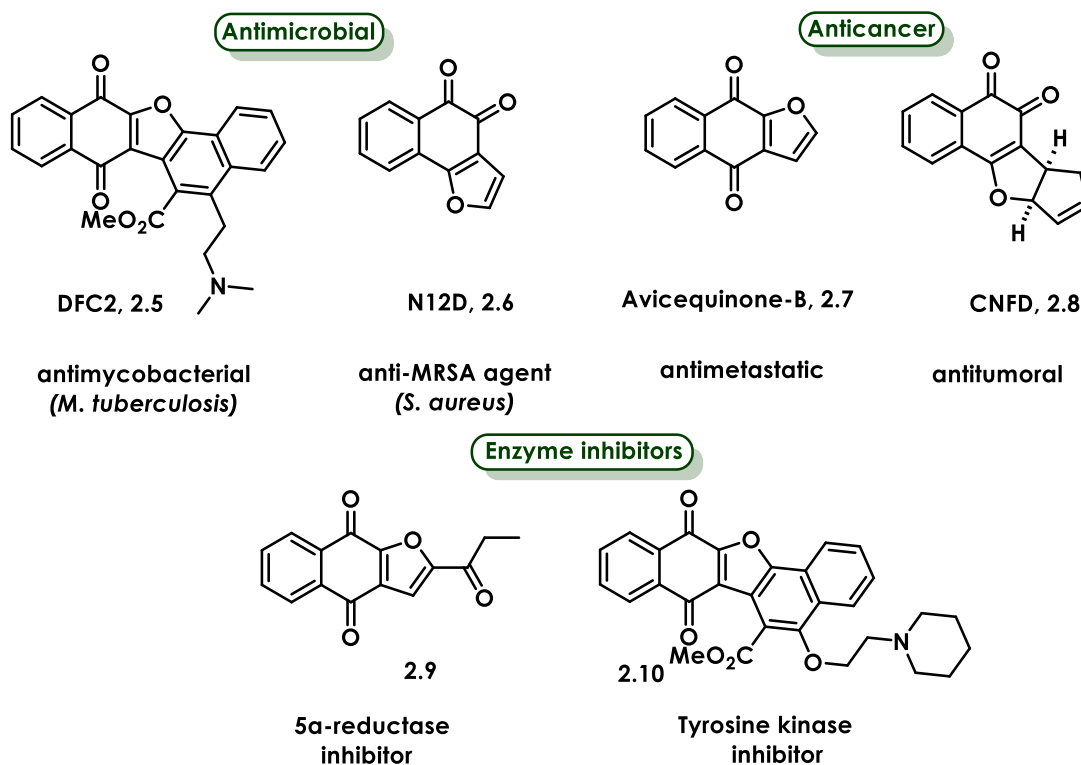


Figure 2.2. Examples of naphthofuroquinones exhibiting biological activities. MRSA stands for multidrug-resistant strains *S. aureus*.

Antiparasitic activities of NFQs

The antiparasitic activities of NFQs have been extensively investigated by many research groups. Again, some representative examples can be cited, without being exhaustive. Goulart *et al.* reported in 1997 [11] one of the first antiparasitic studies targeting the trypomastigote forms of *Trypanosoma cruzi*, parasite responsible for Chagas disease, and the observed activity was associated with the redox potentials of the tested compounds. *Ortho*-NFQs (N12D derivatives, Fig. 2.2) were able to eradicate the trypomastigote forms of *T. cruzi* remaining into experimentally infected mice blood (94-100% lysis at 0.20-0.50 mM after 24 h) (Fig. 2.3, **2.6** and **2.11a-b**). Later, Molfetta *et al.* [12] of the same research group, reported docking and molecular dynamic simulation studies suggesting that the activity of NFQs might be due to inhibition of human glutathione reductase (GR) or parasitic trypanothione reductase (TR). However, additional *in vitro* inhibitory tests should be carried out to support this hypothesis.

Exploiting the metabolic pathways that are essential for the parasite's survival in the host is one strategy to create targeted antileishmanial drugs. A well-established target used for rational drug design is the thiol-redox metabolism involving trypanothione and trypanothione reductase redox system, which is essential for *Leishmania* survival, giving rise to the development of parasite selective TR inhibitors [13]. Venkatesan *et al.* [14] conducted in 2010 a virtual screening of different families of tricyclic quinone derivatives against the TR of

Leishmania infantum, once its crystallographic structure was available, aiming to predict their possible binding mode in TR target. A majority of the molecules of the *ortho*- and *para*-NFQ series (Fig. 2.3, **2.7** and **2.12a-c**, **2.6** and **2.13a-b**) exhibited favorable binding interactions in the FAD binding domain of the active site of TR. The authors estimated that this binding could impede FAD orientation towards the active site of the enzyme, thus leading to TR inhibition. However, new series of NFQs should be synthesized and evaluated *in vitro* to confirm these *in silico* results and support this mode of action.

Last but not least, the antiplasmodial activity of NFQs was specially investigated and reported. For example, Durán-Lengua *et al.* reported [15] the synthesis and *in vitro* biological evaluation of a small library of furan-substituted NFQs. Among all synthesized compounds, **2.7** was found the most active of the series exhibiting an IC₅₀ value of 1.2 μM (SI = 47) against the Dd2 chloroquine (CQ) resistant *Plasmodium falciparum* strain, and an IC₅₀ value of 1.5 μM (SI = 38) against the 3D7 CQ-sensitive *P. falciparum* strain. This study revealed that potential alkyl-substitutions to the furan ring could be beneficial to the antiplasmodial activity. In 2017, Borgati *et al.* [16] synthesized 3 different series of naphthoquinones bearing various substituents to the furan ring. Among all 28 synthesized compounds, 16 were *ortho*- and *para*-NFQ, and all contributed to parasitemia reduction ranging between 45-90% at 25 μg/mL against the W2 CQ-resistant *P. falciparum*. In general, *para*-NFQs were found to be more effective than *ortho*-NFQs and *ortho*-NFQs were more cytotoxic (against Hep G2A16 cells) and less selective. Compounds **2.14** and **2.15** (Fig. 2.3) were the most potent of the series exhibiting the lowest IC₅₀ values, 11.7 μM and 18.8 μM respectively against *P. falciparum* (W2 strain), compared to an IC₅₀ of 0.28 μM for CQ which was used as reference drug. The *para*-NFQ derivatives displayed favorable binding energies when molecular docking was performed on *Plasmodium* enzyme targets, cytochrome bc1 and dihydroorotate dehydrogenase (DHODH) enzyme. The authors concluded that an aryl moiety or an alkyl group linked to the furan ring of NFQs had a positive effect on binding and thus on activities. The authors [16] suggested that further research should be conducted towards the discovery of novel active antiplasmodial molecules.

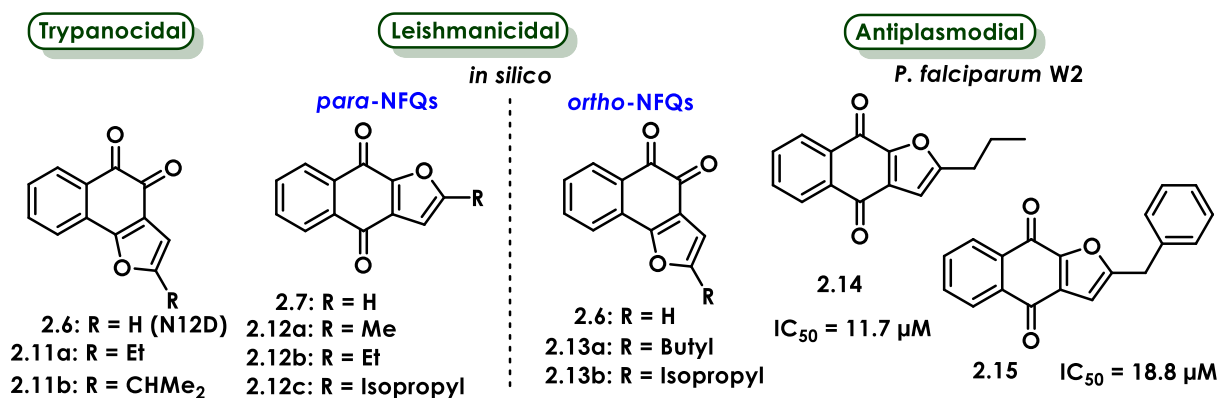
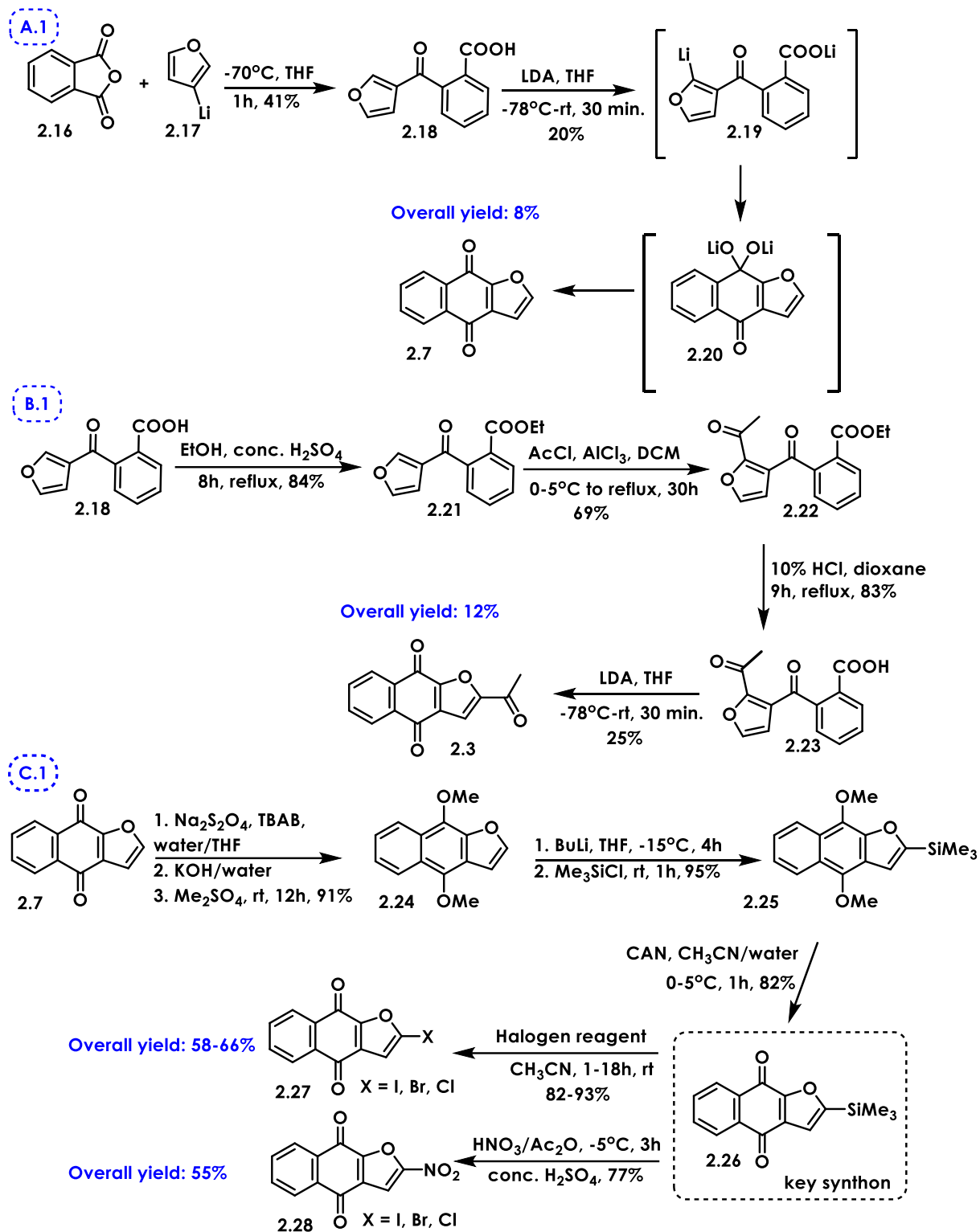


Figure 2.3. Antiparasitic activities of *ortho*- and *para*-naphthofuroquinones.

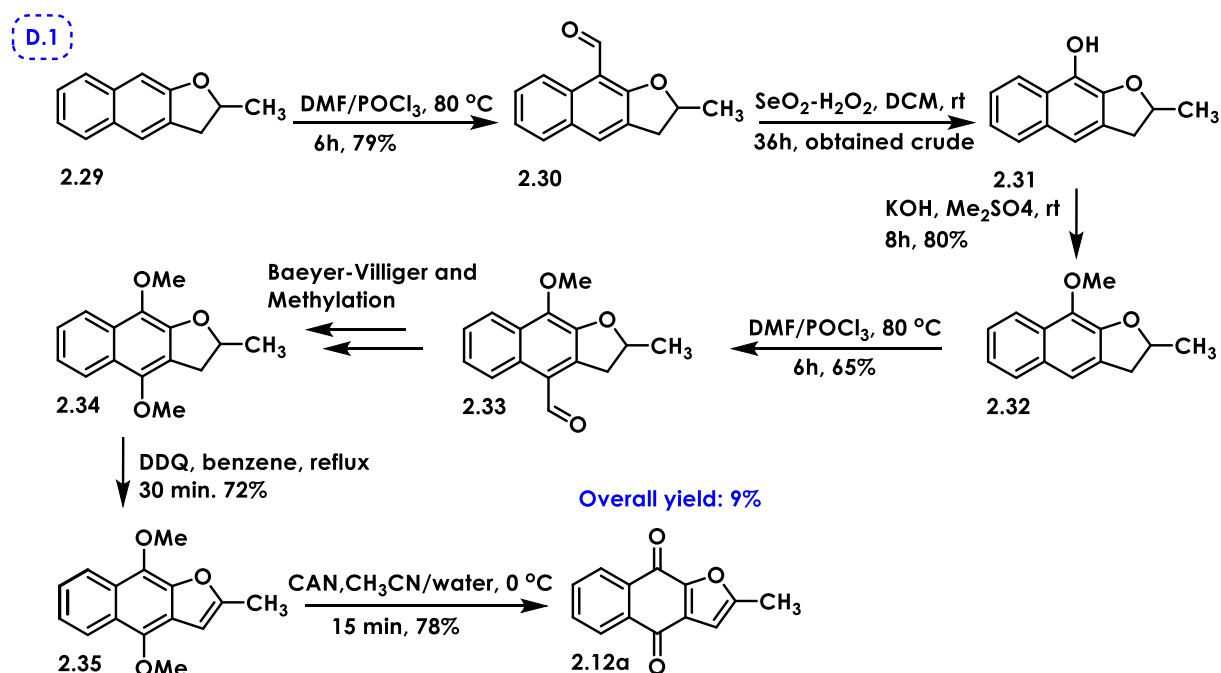
2.1.2 The synthetic procedures leading to naphthofuroquinones (NFQs)

Due to their potential as anti-infectious agents, NFQs have undergone a great deal of synthetic effort towards their elaboration. Some synthetic pathways have been proposed without considering lawsone functionalization.



Scheme 2.1. Towards NFQ elaboration without using lawsone functionalization (part I).

The first one was reported by Koyanagi *et al.* [17] in 1994 (Scheme 2.1, pathway A.1) using phthalic anhydride (**2.16**) inverse addition to 3-lithiofuran (**2.17**) previously prepared from the corresponding 3-bromofuran, leading to (3-furanoyl)benzoic acid (**2.18**). Treatment of **2.18** with an excess of LDA led to the target NFQ **2.7** via a dilithium salt intermediate **2.20**. This two-step synthesis initiated by a selective lithiation of **2.18** and subsequent rearrangement afforded **2.7** in 8% total yield. In an effort to address the issue of carbonyl substitution of the furan ring, the same research group proposed esterification of the benzoic acid **2.18** before acetylating in C-2 position, followed by the same cyclization procedure (Scheme 2.1, pathway B.1), thus leading to **2.3** with 12% overall yield [18]. For heteroatom furan functionalization, the same research group proposed the introduction of a trimethyl-silyl moiety at C-2, which could enable this position for electrophilic substitutions (Scheme 2.1, pathway C.1). Thus, **2.7** was submitted to Kraus and Man reductive methylation, leading to intermediate **2.24** with excellent yield. Treatment of **2.24** with butyl-lithium and chlorotrimethylsilane led to **2.25** which after oxidation provided the key synthon **2.26** [19]. The trimethyl-silyl group could be transformed into a halogen or a nitro group. In spite of high yields, this synthetic pathway requires linear multi-step synthesis, long reaction times, use of inert atmosphere and very sensitive chemicals, which makes this protocol hard to scale-up. In addition, furan C-2 substitution seemed very limited.

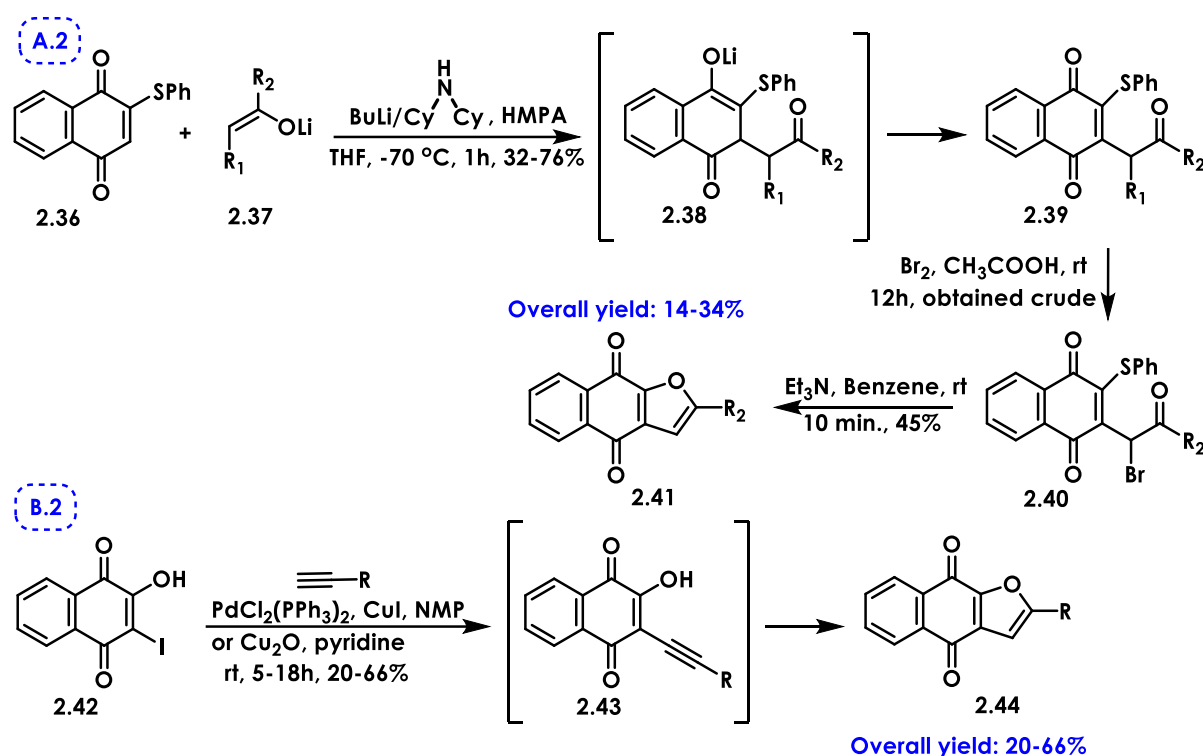


Scheme 2.2. Towards NFQ elaboration without using lawsone functionalization (part II).

The second synthetic strategy was not focused on the naphthofuran ring construction. Instead, it made use of conveniently already substituted dihydronaphthofurans as starting point (Scheme 2.2, pathway D.1) [20]. The starting compound **2.29** was first subjected to a Vilsmeier-Haack oxidation, followed by a Baeyer-Villiger reaction [21], giving rise to the phenolic

derivative **2.31** which was subsequently methylated. The methylated product **2.32** was subjected to the same series of reactions, leading to the *para*-dimethylated key intermediate **2.34** which, after dehydrogenation and oxidation, gave the target NFQ **2.12a** with 9% total yield. In addition, addressing the general scope of the reaction, the authors concluded that C-2 furan substituents other than carbon linear chains would probably not be tolerated.

Other synthetic approaches have been developed employing lawsone or its derivatives. One of the very first attempts on constructing the NFQ ring system was reported by Kang *et al.* in 1998 [22]. It involves regioselective addition of lithium enolates **2.37** in the presence of hazardous HMPA to thio-substituted lawsone derivatives **2.36** (Scheme 2.3, pathway A.2). This air-oxidation reaction led to intermediates **2.39** with low to good yields (32-76%).



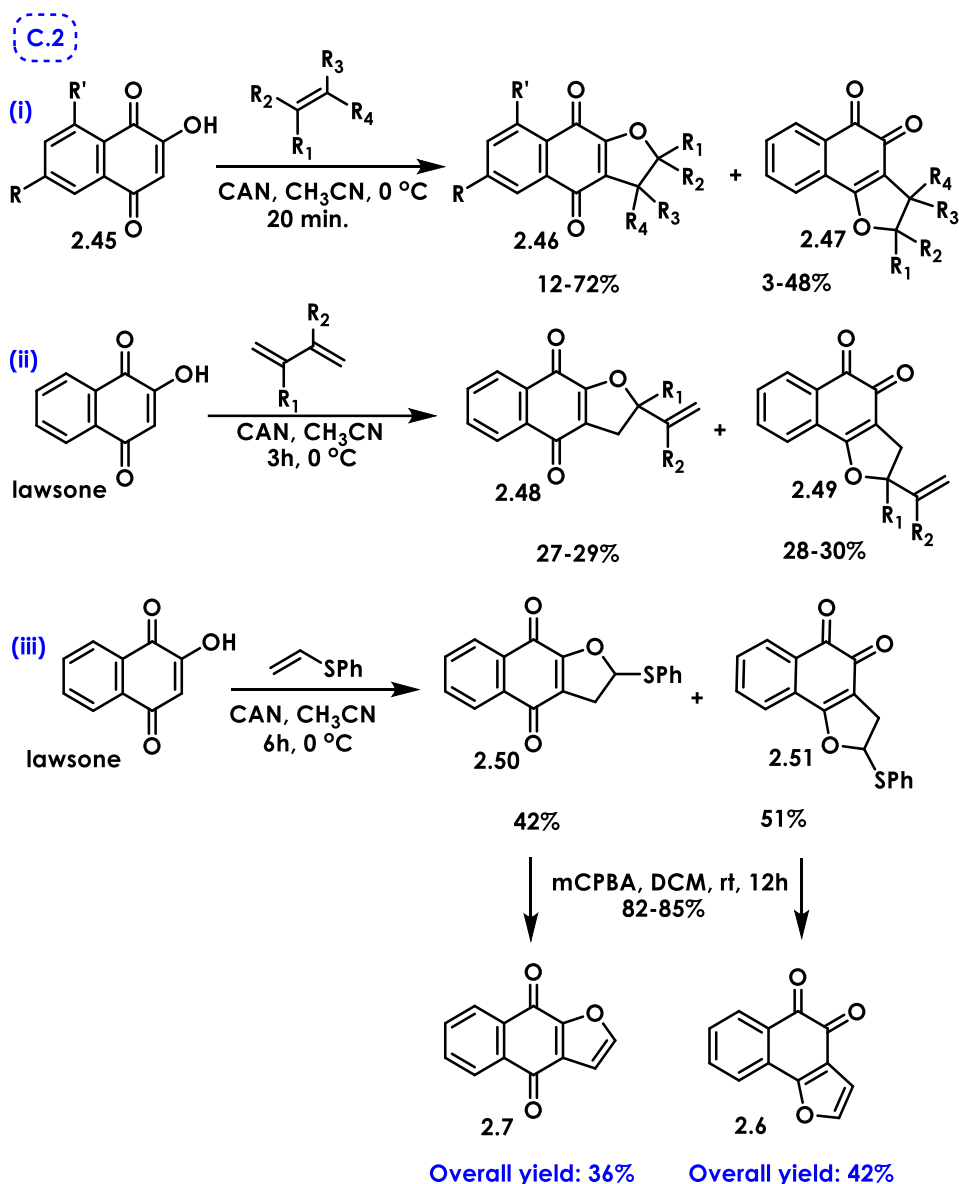
Scheme 2.3. Synthetic routes leading to NFQs, starting from lawsone derivatives (part I).

The transformation of **2.39** to target compounds **2.41** was successful after a two-steps procedure: bromination in acidic media followed by cyclization in the presence of Et₃N in benzene (45%), providing compounds **2.41** with total yields ranging between 14% and 34%. A.2 pathway was more efficient when R₂ = Ph, indicating that it could not be used as a broad procedure for a wide range of substrates, despite the advantage of the regioselectivity provided by the -SPh lawsone substituent of **2.36** used during the first oxidation step. Another one-pot strategy was based on using the transition metal-mediated hetero-annulation sequence reported by Kobayashi *et al.* [23]. 3-Iodolawsone (**3.42**) was submitted to a Sonogashira coupling with various terminal alkynes and led in one step to a small library of NFQs

2.44 (Scheme 2.3, pathway B.2). However, the authors could not avoid the competitive autoxidative coupling of terminal alkynes used as reagents. So, considerable amounts of 1,3-butadiynes $\text{CHC}\equiv\text{C}-\text{C}\equiv\text{CH}$ were formed as byproducts, explaining the low yields of the desired NFQs.

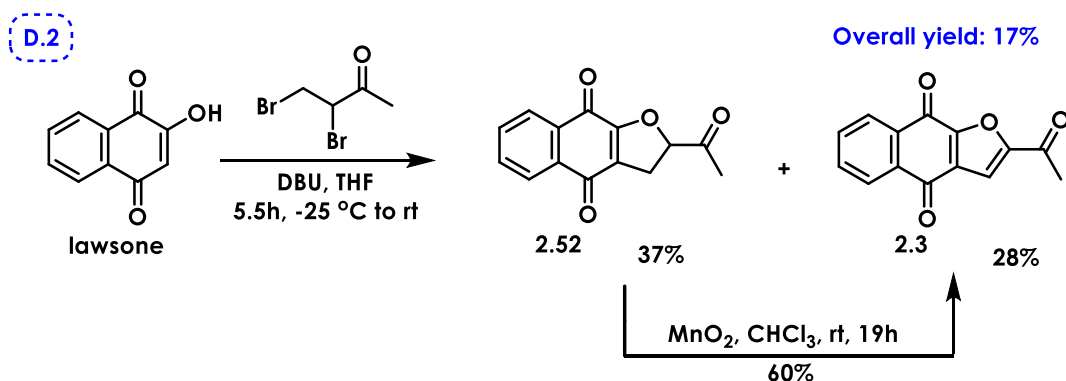
A very common synthetic strategy leading to NFQ structures is the [3+2] cycloadditions of 2-hydroxy-1,4-naphthoquinones (lawsone and lawsone derivatives) with various reagents mediated by ammonium cerium (IV) nitrate (CAN). Kobayashi *et. al* [24] reported this cycloaddition of lawsone derivatives with alkenes or phenylacetylene (Scheme 2.4, pathway C.2, i). However, the authors obtained a mixture of *ortho*- (**2.46**) and *para*-dihydronaphthoquinones (**2.47**) instead of the desired NFQ structures. The yields and product ratios were dependent on the substitution of the alkene involved. This was due to the stabilization of the generated naphthoquinone radical owing to CAN oxidation, and the stabilization ability of the carbocation intermediate. So, reactions with fully substituted alkenes were favored.

In 2000, Lee *et al.* reported [25] the use of 1,3-butadienes instead of alkenes. This reaction provided similar mixtures of the corresponding *ortho*- (**2.48**) and *para*-dihydronaphthoquinones (**2.49**) without increasing the yields. The single advantage of this approach was that it allowed a different spectrum of substitution on the dihydrofuran ring (Scheme 2.4, pathway C.2, ii). The same research group succeeded in ameliorating this protocol by replacing 1,3-butadienes with phenyl vinyl sulfides when carrying out this CAN mediated cycloaddition [26] (Scheme 2.4, pathway C.2, iii). In this case, lawsone conversion reached completion and led to the expected mixture of the corresponding *ortho*- (**2.48**) and *para*-dihydronaphthoquinones (**2.49**) which were separated and consecutively oxidized, leading to the target NFQ structures **2.7** and **2.6** with decent overall yields (36% and 42% respectively). In a follow-up work, the same procedure was applied to the synthesis of a series of angularly fused benzonaphthofuranoquinone derivatives [27]. To conclude, CAN-mediated cycloaddition reactions were not very effective at elaborating the target NFQ structures and they presented several limitations, including complex reaction mixtures and additional oxidation steps carried out under harsh conditions.



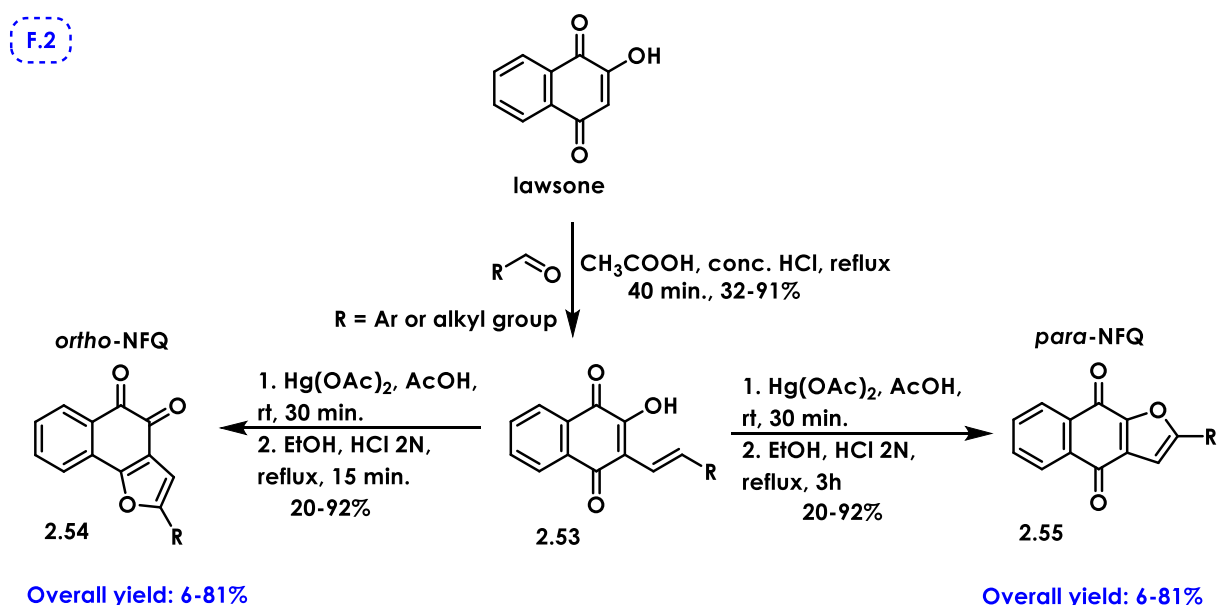
Scheme 2.4. Synthetic routes leading to NFQs, starting from lawsone derivatives (part II).

An alternative approach was proposed by Hagiwara *et al.* [28]. Lawsone was reacted with 3,4-dibromobutan-2-one and DBU excess in THF, leading to a mixture of 2-acyl dihydronaphthofuroquinone **2.52** and the desired *para*-NFQ **2.3** with 28% yield (Scheme 2.5, pathway D.2). The advantage of this methodology was the ability of efficient conversion of the undesired intermediate **2.52** into the target NFQ **2.3** by conventional oxidation using manganese dioxide.



Scheme 2.5. Synthetic routes leading to NFQs, starting from lawsone derivatives (part III).

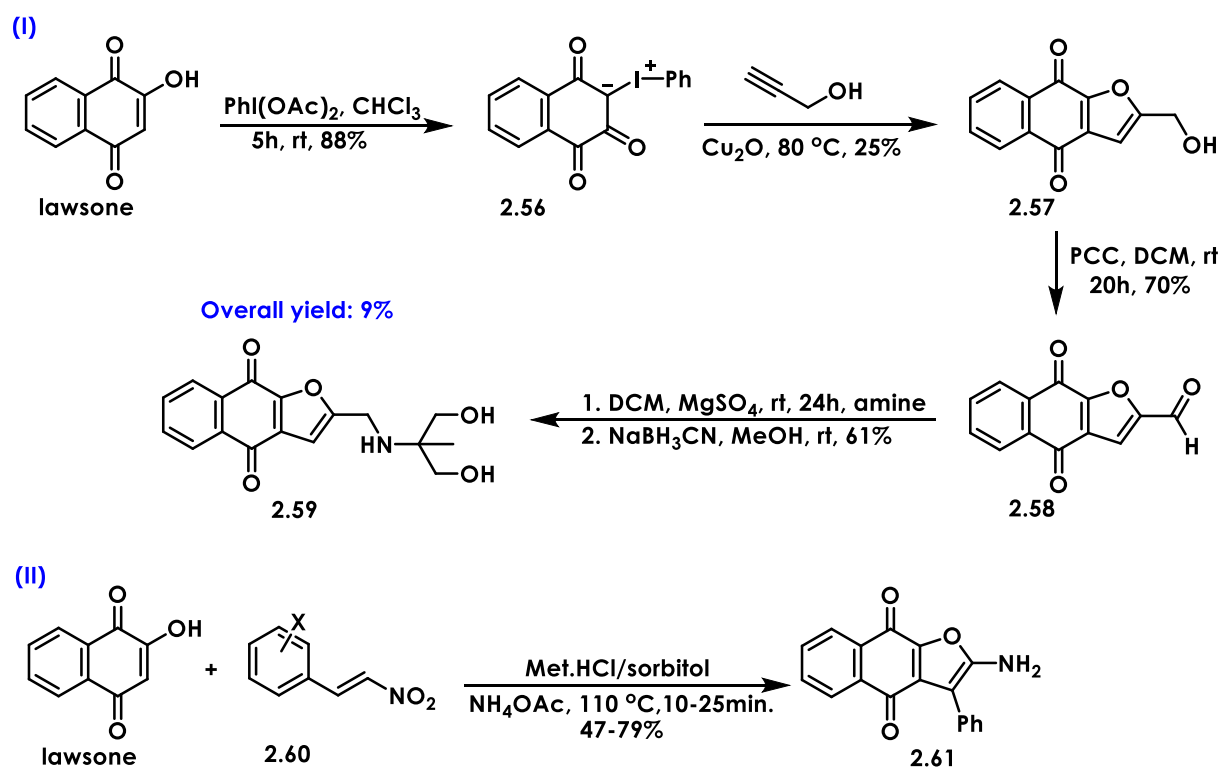
Finally, a more efficient two-step approach for the selective synthesis of a small library of C-2 alkyl- or aryl-substituted *ortho*- and *para*-NFQs was established by Borgati *et al.* in 2017 [16] (Scheme 2.6, pathway F.2). First, lawsone was submitted to an aldol condensation with allyl-aldehydes, producing crucial intermediate **2.53** in yields ranging between 32-91%. The desired naphthofuroquinones **2.54** and **2.55** were obtained after oxidative cyclization with Hg(OAc)₂. The formation of *ortho*- (**2.54**) or *para*-NFQ (**2.55**) could be favored by altering the reaction time in the second step. Products were isolated with fair overall yields. The kinetic product *ortho*-NFQ **2.54** formation was favored when the reaction mixture was exposed to HCl 2N for 15 minutes, while the thermodynamic products *para*-NFQ **2.55** were formed when the reaction mixture was treated with the same acidic solution for a longer period of time (3 h).



Scheme 2.6. Synthetic protocol towards a selective synthesis of a library of *ortho*- and *para*-NFQs.

Many efforts have been dedicated to the introduction of amino-substituents to the naphthofuroquinone structures for further functionalization of NFQs. Wu *et al.* [29] reported the treatment of lawsone with iodobenzene diacetate, leading to phenyl-iodonium intermediate

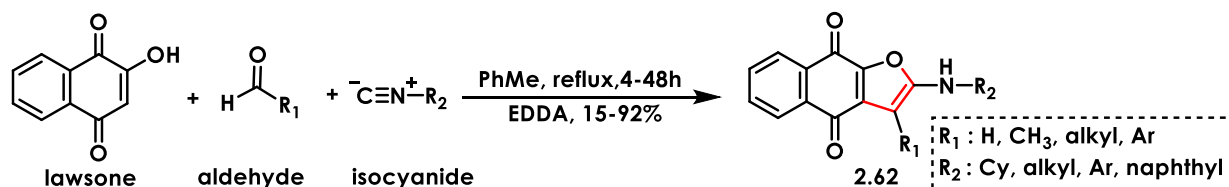
2.56 which was consecutively coupled with propargyl alcohol for ring closure (Scheme 2.7, pathway I). The resulting alcohol derivative **2.57** was further oxidized by pyridinium chloroformate and the obtained furanyl-aldehyde **2.58** was then submitted to reductive amination, to give 2-methylamino-substituted NFQ **2.59** with overall yield 9%. A short and direct synthesis by coupling the desired amino group to the NFQ structure in a deep eutectic mixture of sorbitol and metformin hydrochloride was also developed [30]. In that respect, lawsone was submitted to react with β -nitrostyrenes **2.60** and ammonium acetate leading to a series of 2-methylamino-NFQs **2.61** with yields ranging between 47-79% (Scheme 2.7, pathway II). Despite this one step green approach demanding shorter reaction times and affording acceptable yields of target products, amelioration of the reaction substrate scope is still needed, since the use of with β -nitrostyrenes allowed only the introduction of a C-3 phenyl substituent on the furan ring.



Scheme 2.7. Introducing amino substituents to NFQ structures.

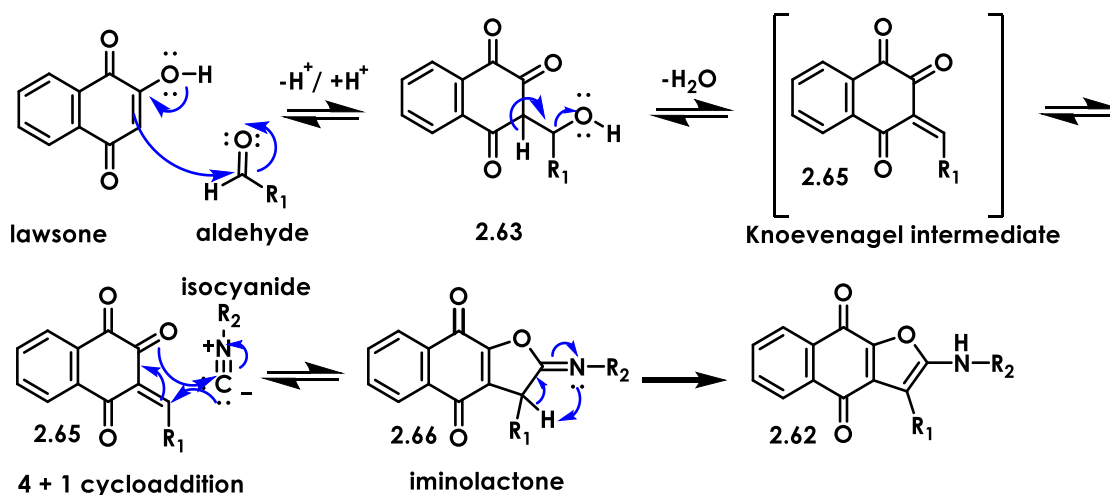
Teimuri *et al.* in 2007 reported the synthesis of 2-amino-3-alkyl/aryl-naphthofuroquinones via a one-pot multicomponent domino reaction (MCR) between 2-hydroxy-1,4-naphthoquinone (lawsone), isocyanides, and aldehydes, providing the advantage of forming three bonds (two C-C bonds and one C-O bond) in a single step via a [3+1+1] furan annulation strategy [31]. This MCR domino condensation was carried out in toluene, under reflux, and produced the desired 2-amino-NFQs **2.62** with yields varying between 40% and 60% in most cases (Scheme 2.8). This reaction seemed to tolerate both aliphatic and variously substituted aromatic aldehydes along with alkyl and aryl isocyanides. However, longer reaction times (up to 48 h)

were needed when reacting with aryl isocyanides. Aiming to make it both economically and environmentally friendly, the same reaction mixture was carried out in water. It provided similar results in shorter reaction times (2 h) and yields ranging between 60-75% [32]. However, the use of highly lipophilic aromatic isocyanides was not tolerated. Additionally, the use of ethylenediamine-*N,N'*-diacetic acid (EDDA) as a catalyst in refluxing toluene, resulted in reaction completion after only 30 min., with slightly better product yields (57-97%) [33].



Scheme 2.8. The multicomponent cascade reaction between lawsone, various aldehydes and isocyanides.

On a mechanistic point of view, the formation of 2-amino-NFQs **2.62** via this 3-component cascade reaction is initiated by a Knoevenagel condensation between lawsone and the corresponding aldehyde, producing the electron deficient conjugated enone intermediate **2.65**. Then, the electron-deficient heterodiene moiety of Knoevenagel adduct **2.65** reacts with the isocyanide via a [4+1] cycloaddition, to afford an iminolactone intermediate **2.66** which, after rearrangement, leads to the 2-amino-naphthofuroquinone **2.62** (Scheme 2.9).



Scheme 2.9. The proposed mechanism of domino multicomponent reaction between lawsone, an aldehyde and an isocyanide.

As the naphthofuroquinone family exhibits a very wide spectrum of biological activities, including antiparasitic ones, we intended to synthesize a focused library of variously substituted 2-amino-naphthofuroquinones. A multicomponent reaction methodology is the most efficient way compared to previously reported synthetic pathways towards NFQs.

2.2 Results and discussion

2.2.1 Chemistry – Synthesis

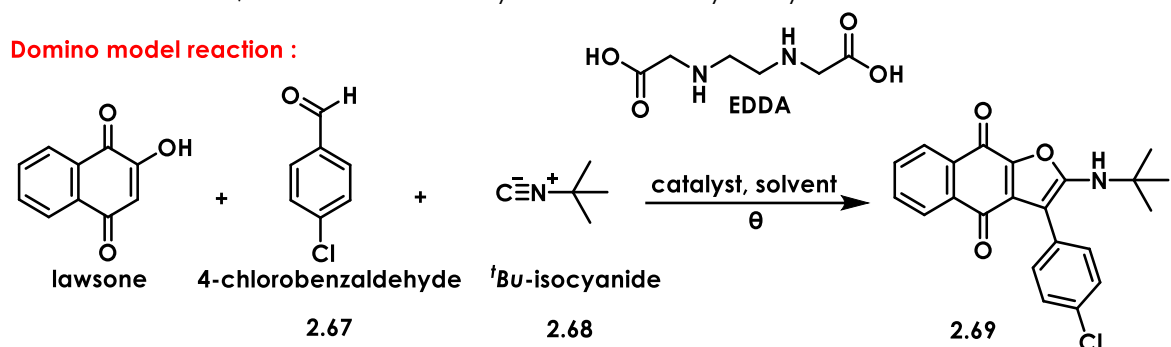
2.2.1.1. Reaction conditions for optimization studies

For this purpose, the reaction between lawsone, 4-chlorobenzaldehyde (or *para*-chlorobenzaldehyde) and *tert*-butyl isocyanide was studied as a model reaction (Table 2.1). 4-chlorobenzaldehyde was selected as a highly electrophilic aldehyde due to its electron withdrawing substituent and *tert*-butyl isocyanide belonged to the pool of hindered alkyl isocyanides that provided excellent results (over 80% yields) when this three-component reaction was first studied by Teimouri *et al* [31]. For every optimization experiment (0.4 mmol scale), the reaction mixture was controlled by thin layer chromatography (TLC) and stopped when no further evolution was observed. The solvent was removed by evaporation under reduced pressure. A sample of the crude residue was analyzed by ¹H NMR to calculate lawsone conversion and yield of expected product. Subsequently, the desired product **2.69** was obtained pure after medium pressure column chromatography on silica gel (40 g), using hexane/ethyl acetate (9:1) as eluent ("PuriFlash" system). The results are reported in Table 2.1.

First of all, the reaction was carried out according to the conditions reported by Teimouri *et al*. [31]. An equimolar mixture of the three component (lawsone/aldehyde/ isocyanide 1:1:1) was refluxed in toluene for 4 h without any catalyst (Table 2.1, entry 1). In our hands, the conversion of lawsone was 31 %, and the desired naphthofuroquinone **2.69** was isolated in 22% yield after chromatography. When the same reaction was carried out under the same conditions but with 10 mol% ethylenediamine-*N,N*-diacetic acid (EDDA) as a catalyst, both lawsone conversion and yield of **2.69** were doubled (Table 2.1, entry 2).

As the catalyst plays an important role, we then checked if it impacted the duration of the reaction. In that respect, the reaction was repeated and stopped after 2 h (Table 2.1, entry 2). However, the obtained results showed that after 2 h of reaction, lawsone conversion and isolated product yield were slightly, but not significantly, higher in the presence of EDDA (Table 2.1, entry 3). Conversely, when the reaction was repeated in refluxing toluene catalyzed by 10% mol EDDA with both *para*-chlorobenzaldehyde and *t*Bu-isocyanide in slight excess with respect to lawsone (1.2 equiv.), lawsone conversion reached 90% in 2 h (Table 2.1, entry 4). Although, these conditions resulted in a quite complicated reaction mixture, in comparison with all the previous attempts (Table 2.1, entries 1-3). The target 2-aminonaphthofuroquinone **2.69** was isolated with 30% yield, after two consecutive chromatographies.

Table 2.1. Optimization studies of experimental conditions for the model domino reaction between lawsone, 4-chlorobenzaldehyde and *tert*-butyl isocyanide.



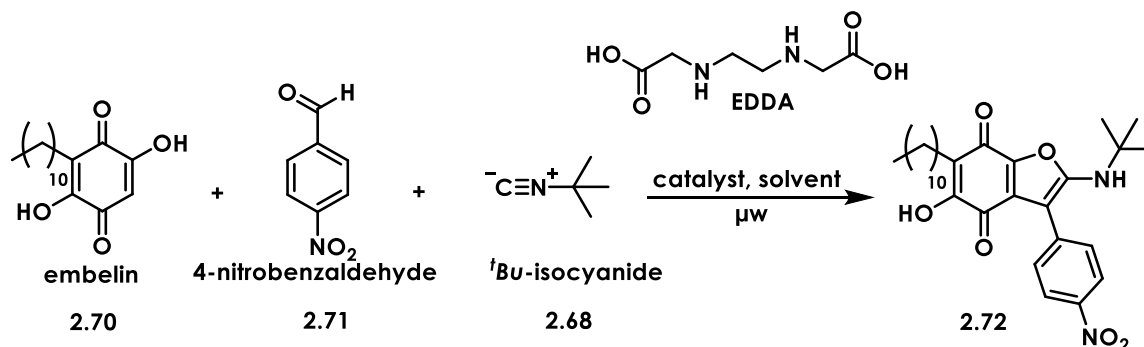
Entry	Method	Reaction time (min.)	Equiv. (lawsone/2.67/2.68)	Catalyst	Solvent	Lawsone conversion * (%)	Yield 2.69 ** (%)
1	Reflux	240	1:1:1	-	PhMe	31	22
2	Reflux	240	1:1:1	EDDA	PhMe	75	42
3	Reflux	120	1:1:1	EDDA	PhMe	34	26
4	Reflux	120	1:1.2:1.2	EDDA	PhMe	90	30
5	Irradiation (μw)	2 x 15	1:1:1	Et ₃ N	DCE	12	11
6	Irradiation (μw)	60	1:1:1	Et ₃ N	DCE	45	40
7	Irradiation (μw)	60	1:1:1	EDDA	DCE	60	59
8	Irradiation (μw)	2 x 60	1:1:1	EDDA	DCE	85	65
9	Irradiation (μw)	2 x 60	1:1.5:1	EDDA	DCE	100	66
10	Thermal activation	60	1:1:1	Et ₃ N	DCE	70	57
11	Thermal activation	60	1:1:1	EDDA	DCE	72	60
12	Thermal activation	60	1:1.5:1	EDDA	DCE	100	59

* Calculated on ¹H NMR spectrum of the crude mixture.

** Isolated yield, calculated on the starting amount of lawsone used.

Microwave-assisted (MWA) multicomponent reactions (MCRs) are one of the most effective methods for synthesizing biologically active heterocyclic molecules. These reactions are purposefully used to produce a variety of heterocycles as well as numerous point structure functionalization. High yields, shortened reaction times, selectivity, atom economy, and easier purification are the most highlighted advantages of microwave-assisted MCRs [34]. Such approach has recently been reported for the reaction between embelin (2,5-dihydroxy-3-undecyl-1,4-benzo-quinone, **2.70**), various aldehydes and isocyanides [35]. The authors conducted an optimization study between embelin (**2.70**), 4-nitrobenzaldehyde (**2.71**) and *tert*-butyl isocyanide (**2.68**) aiming to favor the first step of Knoevenagel condensation by varying all reaction conditions such as the solvent (ethanol, toluene, acetonitrile, 1,2-

dichloroethane), the catalyst (EDDA, triethylamine, proline), the temperature (150-180 °C), the reaction time (cycles of 15-30 min.) and the ratio of three reactants (Scheme 2.10). In their case, the best yield (70%) of target product **2.72** was obtained when an equimolar three-reactant mixture in 1,2-dichloroethane (DCE) was irradiated at 180 °C for 15 min under 10% mol EDDA catalysis. In addition, lawsone has never been reported to undergo such a reaction under microwave irradiation.



Scheme 2.10. Model reaction used for optimization studies under microwave irradiation of domino three-component reaction involving embelin [35].

An equimolar reaction mixture of lawsone, **2.67** and **2.68** in DCE was reacted under microwave irradiation (2 cycles x 15 min, at 160 °C, 6 bars, 300 W) in the presence of 10% mol Et_3N (Table 2.1, entry 5). Despite a low conversion of lawsone (12%), the expected product was easily isolated from the reaction mixture at 11% yield, meaning that the reaction was very selective. When the irradiation time was extended up to 60 min. (Table 2.1, entry 6), it provided better lawsone conversion (45%) and better isolated yield of **2.69** (45%). When the catalyst Et_3N was changed for EDDA (Table 2.1, entry 7), the reaction provided even more better lawsone conversion (60%) and isolated yield for **2.69** (59%). Afterwards, the irradiation time of the same equimolar mixture of lawsone, **2.67** and **2.68** in DCE, catalyzed by 10% mol EDDA was extended to 2 cycles x 60 min (Table 2.1, entry 8) leading to the best lawsone conversion (85%) and isolated yield (65%) of the desired 2-amino-naphthofuroquinone **2.69** reported until now. Finally, when reacting with 4-chlorobenzaldehyde in excess (1.5 equiv. vs 1 equiv. before) (Table 2.1, entry 9), full conversion of lawsone was achieved. However, the isolated yield of **2.69** did not increase significantly (66%). In fact, the isolation of **2.69** was problematic since the desired product was eluted very close to the unreacted aldehyde.

Finally, the reaction was thermally activated by using an Anton Paar apparatus Monowave 50. An equimolar reaction mixture of lawsone, **2.67** and **2.68** in DCE, catalyzed by 10% mol Et_3N , was heated for 1 h (182 °C, 15 bar) (Table 2.1, entry 10). For this reaction mixture, thermal activation provided better lawsone conversion (70%) in comparison to microwave irradiation (45%) (Table 2.1, entry 6), and consequently better yield of **2.69** (57% vs 40% under microwave irradiation). However, switching Et_3N to EDDA under the same reaction conditions did not significantly increase either lawsone conversion (up to 72%) or yield of **2.69** (60%) (Table 2.1,

entry 11). Moreover, the conversion of lawsone was complete in the presence of 4-chlorobenzaldehyde in excess (1.5 equiv.) (Table 2.1, entry 12). However, as observed before (Table 2.1, entry 9), the purification of the expected **2.69** was complicated and, consequently, its isolated yield as pure product was 59%. Again, a significant amount of the product was eluted as a mixture containing unreacted aldehyde.

Taking everything into consideration, model reaction activation under microwave irradiation and monowave heating conditions provided both better conversion of starting lawsone and better isolated yields of the product **2.69**, compared to conventional refluxing conditions. Indeed, the addition of 4-chlorobenzaldehyde in excess forced the Knoevenagel condensation and lawsone conversion was complete in every case. However, the excess of aldehyde resulted in making the isolation of the desired 2-amino-naphthofuroquinone **2.69** quite complicated and did not pillar atom economy, thus it could not be preferred as ideal reaction conditions. Surprisingly, EDDA catalysis provided better selectivity and yields under microwave irradiation, which was not the case under thermal activation as EDDA and Et₃N catalysis made no difference.

As a conclusion, the most efficient reaction conditions in terms of reaction time, atom economy, solvent use, catalysis, and purification convenience were those depicted in entry 7, Table 2.1: microwave irradiation of an equimolar reaction mixture (lawsone/4-chlorobenzaldehyde/*tert*-butyl isocyanide 1:1:1) in 1,2-dichloroethane for 1 h, catalyzed by 10 mol% ethylenediamine-*N,N*-diacetic acid.

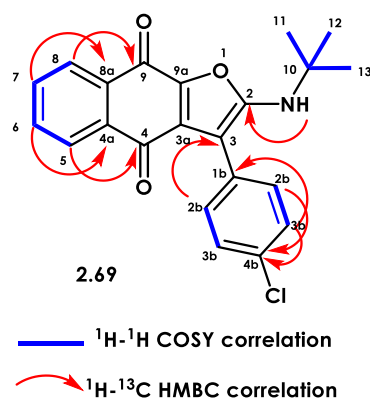
2.2.1.2. Structure characterization of model compound **2.69**

The chemical structure of compound **2.69** was unambiguously determined by NMR analyses in CDCl₃ at 298K (¹H, ¹³C, COSY and HMBC). All ¹H and ¹³C signals were assigned based on chemical shifts (δ , ppm), spin-spin coupling constants, splitting patterns and signal intensities. The ¹H and ¹³C assignments of **2.69** are summarized in Table 2.2. ¹H NMR spectrum exhibited all expected signals (δ , ppm) for all different protons of naphthoquinone ring system as well as the aromatic protons of 4-chlorophenyl moiety and the alkyl protons of *tert*-butyl substituent (Table 2.2). The characteristic proton NH, was detected at 4.82 ppm as a singlet. Concerning the naphthoquinone ring: H-5 and H-8 signals appeared as doublet of doublets at 8.02 ppm and 8.17 ppm respectively and H-6 and H-7 appeared as triplet of doublets at 7.61 ppm and 7.69 ppm respectively. For the 4-chlorophenyl moiety, the 2 magnetically equivalent protons H-2b could be distinguished from 2 magnetically equivalent protons H-3b by COSY. The methyl groups of protons H-11, H-12, and H-13 of *tert*-butyl substituent of **2.69** appeared at 1.50 ppm (9H).

The ¹³C resonance data revealed 18 resonances in total corresponding to all differently hybridized carbons of molecule **2.69** (Table 2.2). All four sp² carbons belonging to the basic

scaffold of naphthoquinone ring C-5, C-6, C-7 and C-8 were found at 126.6 ppm, 132.5 ppm, 133.9 ppm and 126.3 ppm respectively, while all quaternary carbons provided less intense but unambiguous signals in the aromatic region: C-4a at 133.3 ppm and C-8a at 133.2 ppm (Table 2.2). In addition, the attribution of both carbonyl groups C-4 and C-9 was based on a detailed NMR study previously performed by Borgati *et al.* [36]. As in their case, the HMBC correlation between H-3 and C-4 allowed unambiguous assignment of C-4. Similarly, carbonyl C-9 and C-4 were detected at 169.6 ppm and 182.0 ppm, respectively. Concerning the furan ring structure, C-9a, C-3a, C-3 and C-2 were detected at 144.2 ppm, 130.4 ppm, 130.4 ppm and 159.4 ppm, respectively. A downfield signal at 54.3 ppm was attributed to the quaternary C-10, while all -CH₃ groups (C-11, C-12, C-13) appeared as a very intense unique signal at 30.2 ppm (Table 2.2).

Table 2.2. ¹H and ¹³C NMR data assignments of compound **2.69** in CDCl₃ at 298K, at 400 MHz and 101 MHz respectively.



¹ H and/or ¹³ C numbering *	¹ H chemical shift (ppm)	¹³ C chemical shift (ppm)
C-2	-	159.4
C-9a	-	144.2
C-9	-	169.6
C-8a	-	133.2
CH-8	8.17 (dd, <i>J</i> =7.6 Hz, <i>J</i> =1.0 Hz)	126.3
CH-7	7.69 (td, <i>J</i> =7.6 Hz, <i>J</i> =1.0 Hz)	133.9
CH-6	7.61 (td, <i>J</i> =7.5 Hz, <i>J</i> =1.3 Hz)	132.5
CH-5	8.02 (dd, <i>J</i> =7.5 Hz, <i>J</i> =1.3 Hz)	126.6
C-4a	-	133.3
C-4	-	182.0
C-3a	-	130.4
C-3	-	99.1
C-1a	-	133.4
CH-2b	7.44 (m)	130.9
CH-3b	7.47 (m)	129.3
C-4b	-	133.7
CH-3b	7.47 (m)	129.3
CH-2b	7.44 (m)	130.9
NH	4.82 (s)	-
C-10	-	54.3
CH ₃ -11,12,13	1.50 (s)	30.2

* IUPAC rules are used for ¹H and ¹³C numbering of **2.69**.

COSY correlations revealed the neighboring pair of protons H-5/H-6, H-6/H-7, H-7/H-8 and H-2b/H-3b of the 4-chlorophenyl ring. Among all HMBC correlations presented in Table 2.2, the correlation between NH and C-2 provides an unambiguous proof of the furan cyclization, along with the correlation between H-2b and C-3. In addition, the HMBC correlations between H-5 and C-4 on one hand, and H-8 and C-9 on the other hand, provided extra proofs of the assignment of carbonyl groups of the *para*-naphthofuroquinone **2.69**.

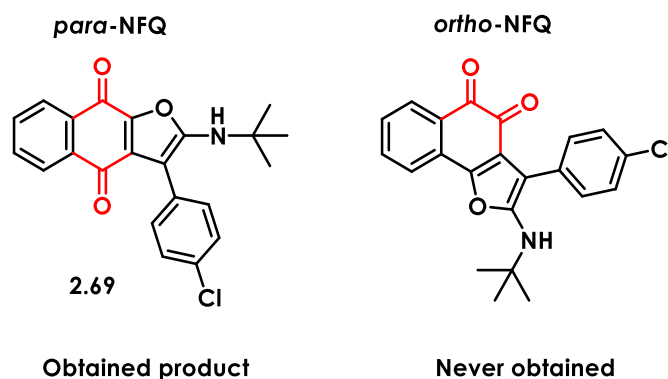


Figure 2.4. *Para*-naphthoquinone **2.69** was selectively obtained.

Compound **2.69** was recrystallized in methylene chloride (DCM). X-ray diffraction spectroscopy (Mo-K radiation) was used to analyze the resulting single crystals, which appeared as deep violet platelets (Fig. 2.5). This molecule crystallized in the $P2_1/n$ space group. All atoms of all three rings (furan and naphthoquinone) of NFQ moiety shared the same plane. In addition, the quaternary carbon atom of the *tert*-butyl group (C-10) was found practically coplanar with the furan ring system (C-6b/C-1/C-3/C-2), while the *para*-chlorophenyl aromatic ring displayed a dihedral angle of 44.2° with the furan ring. This result suggests that diversifying the C-3 and C-2 substituents of the furan ring could play a role to optimize interaction of molecule **2.69** with the binding site of the target bc1 and/or DHODH of *P. falciparum*, since C-2 and C-3 may be two structural points offering interactions extension and exploration of the cavity into the binding site. Moreover, it should be mentioned that the distance between both oxygen atoms O2 and O1 could favorize a potential metal coordination as the dihedral angle (O-1/ C-2/N-1/C-10) was measured having the value of 16.3° .

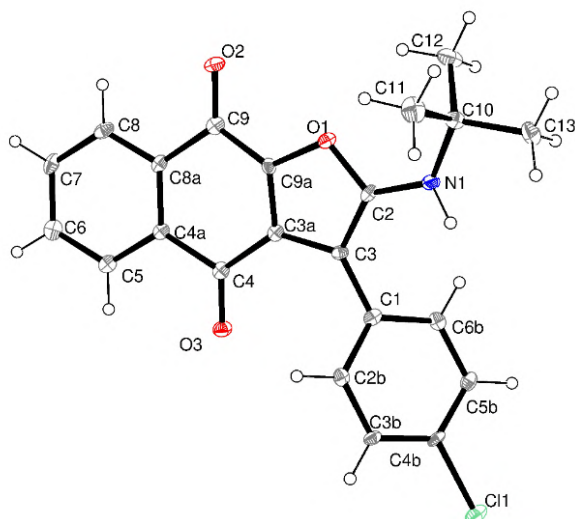


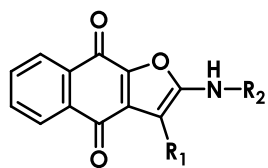
Figure 2.5. X-ray structure of compound **2.69**.

2.2.1.3. Substrate scope for domino multicomponent reaction

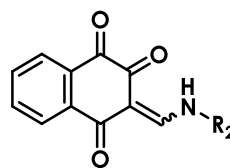
Having in hand the optimal reaction conditions to obtain compound **2.69** in good yield and selectivity (entry 7, Table 2.1, Scheme 2.11), the substrate scope of this reaction was then further explored by modifying both aldehyde and isocyanide reactants. A whole library of various aldehydes was selected to undergo this multicomponent reaction (variously substituted benzaldehydes bearing electron-donating and electron-withdrawing groups, aldehydes bearing heteroaromatic rings and heterocyclic motifs and *N*-substituted piperidine carbaldehydes). Concerning the isocyanide component, three commercially available alkyl-isocyanides were selected to take part to this domino reaction: *tert*-butyl-, butyl- and cyclohexyl-isocyanides. Among them, *tert*-butyl isocyanide was chosen to react with lawsone and the whole above-mentioned library of aldehydes while the two other isocyanides were reacted with a representative example of each aldehyde category, namely 4-chlorobenzaldehyde, 3,4,5-trimethoxy benzaldehyde, *N*-methyl indazole-5-carbaldehyde, 2-nitrofuraldehyde, and *N*-benzyl-4-piperidine carboxaldehyde, in order to provide the first series of 2-amino-naphthofuroquinones for an initial screening. The obtained results are summarized in Table 2.3 and Scheme 2.11.

The reaction between lawsone, *tert*-butyl isocyanide and a variety of aldehydes was carried out in DCE, and monitored by thin layer chromatography (TLC). It was stopped when lawsone completely disappeared. The solvent was removed by evaporation under reduced pressure and the crude reaction mixture was analysed by ¹H NMR to determine aldehyde conversion. Afterwards, all products were isolated by column chromatography on silica gel, using appropriate mixtures of organic eluents (see Experimental Part). As a reminder, 60% conversion of *para*-chlorobenzaldehyde led to 59% yield of **2.69** meaning that the three-component

Table 2.3. Structures and isolated yields of the whole list of products obtained by domino multicomponent reaction between lawsone, aldehydes and isocyanides.

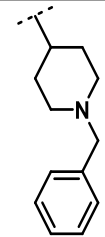
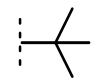
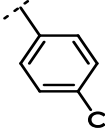
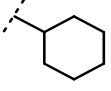
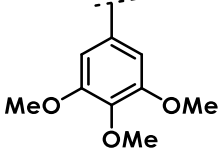
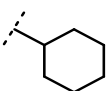
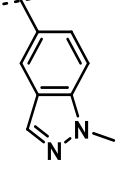
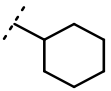
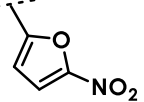
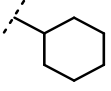
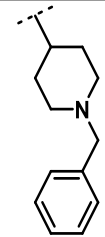
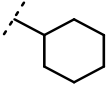
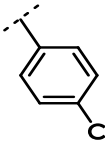
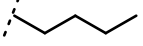
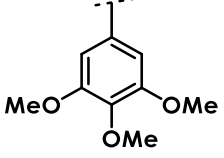
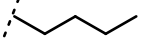
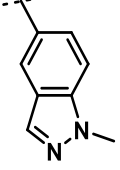
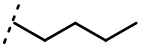
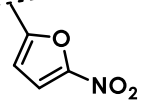
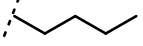


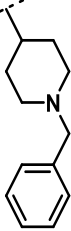
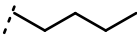
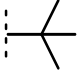
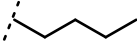
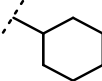
2.69-2.90



2.91-2.93

Entry	Products	R ₁	R ₂	Aldehyde conversion * (%)	Isolated yields ** (%)
1	2.69 2.91			60	59 traces
2	2.73 2.91			30	30 20
3	2.74 2.91			60	55 nd
4	2.75 2.91			45	25 nd
5	2.76 2.91			30	30 40
6	2.77 2.91			80	35 nd
7	2.78 2.91			20	19 traces
8	2.79 2.91			95	52 nd

9	2.80 2.91			91	53 nd
10	2.81 2.92			50	46 nd
11	2.82 2.92			45	42 nd
12	2.83 2.92			40	40 nd
13	2.84 2.92			54	12 nd
14	2.85 2.92			60	45 nd
15	2.86 2.93			55	55 traces
16	2.87 2.93			45	40 nd
17	2.88 2.93			30	nd 50
18	2.89 2.93			10	8 nd

19	2.90 2.93			35	30 nd
20	2.91	-		-	40
21	2.92	-		-	50
22	2.93	-		-	nd

* Calculated based on ¹H NMR spectrum of the crude mixture.

** Calculated based on the starting amount of lawsone used.

nd stands for non-detected.

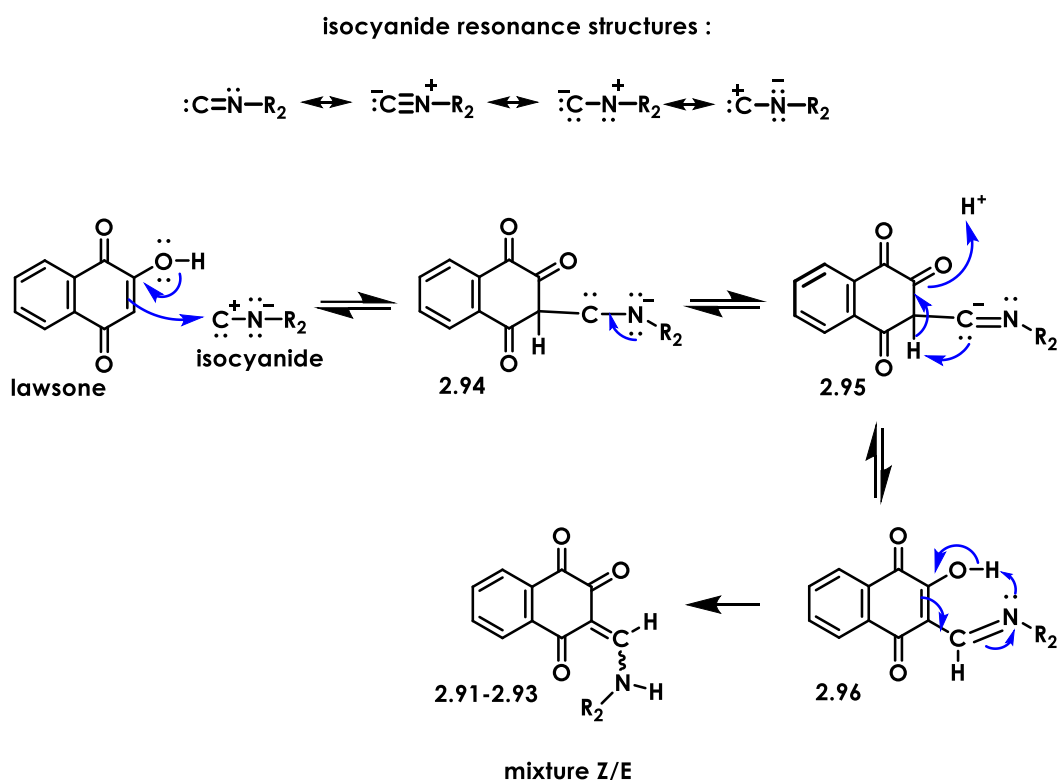
When *tert*-butyl isocyanide was replaced by cyclohexyl isocyanide and the multicomponent reaction was repeated with every corresponding aldehyde, the NFQ derivatives **2.81**, **2.82**, **2.83**, and **2.85** were obtained with yields ranging between 42 and 46% and excellent selectivity (Table 2.3, entries 10-12 and 14). The enaminone side product **2.92** was observed only in the crude reaction mixture of entry 12 (estimated yield 20%). However, its isolation was impossible because it was unstable during the purification procedure. The reaction between cyclohexyl isocyanide, lawsone and 2-nitrofur aldehyde provided a sluggish mixture and the desired domino adduct **2.84** was collected with low yield (12%) (Table 2.3, entry 13).

Finally, each representative example of the aldehyde library was chosen to react with lawsone and *n*-butyl isocyanide. Reactions involving aromatic aldehydes provided the best yields of the corresponding NFQs **2.86** and **2.87** (55% and 40%, respectively, Table 2.3, entries 15-16). No side product was detected. In contrast, when *N*-methyl-5-indazole carbaldehyde was used, the formation of the NFQ **2.88** was observed in the reaction mixture (low estimated yield) (Table 2.3, entry 17). Unfortunately, all purification or recrystallization efforts failed. The compound seemed to be unstable on silica gel column. On the other hand, the enaminone **2.93** was isolated instead with 50% yield (Z/E ratio = 1:1) (Table 2.3, entry 17). *N*-benzyl piperidine carbaldehyde did not offer high conversion (35%) and NFQ **2.90** was obtained with 30% yield (Table 2.3, entry 19). Unfortunately, the reaction between lawsone, *n*-butyl isocyanide and 4-nitrofur aldehyde was sluggish, leading to only 8% yield of target NFQ **2.89** (Table 2.3, entry 18).

To summarize, the substrate scope of the reaction between lawsone, aldehydes and isocyanides was proved to be very broad. This reaction could tolerate aromatic aldehydes with

electron donating and electron withdrawing groups, and aldehydes bearing heterocycles and heteroaromatic rings. Among them, 2-nitrofuraldehyde provided the most sluggish reaction mixtures and thus the lowest yields, most probably because of solubility issues. In addition, a side reaction was observed between lawsone and the corresponding isocyanide when less reactive (less electrophilic) aldehydes were used as reactants (especially *N*-methyl-5-indazole carbaldehyde). The resulting products of this two-component reaction possessing an enaminone structure were never reported before. The obtained enaminones were found to be *E/Z* mixtures of two isomers in 1:1 ratio (complete 2D NMR study is reported in this Chapter). This reaction activated under microwave irradiation allowed the selective synthesis of a series of 19 novel *para*-naphthofuroquinones and lawsone enaminone derivatives with low to fair yields but in a single step. All three alkyl-isocyanides used were equivalently well tolerated under these reaction conditions. Reactions with cyclohexyl and *n*-butyl isocyanide were extremely selective comparing to *tert*-butyl isocyanide.

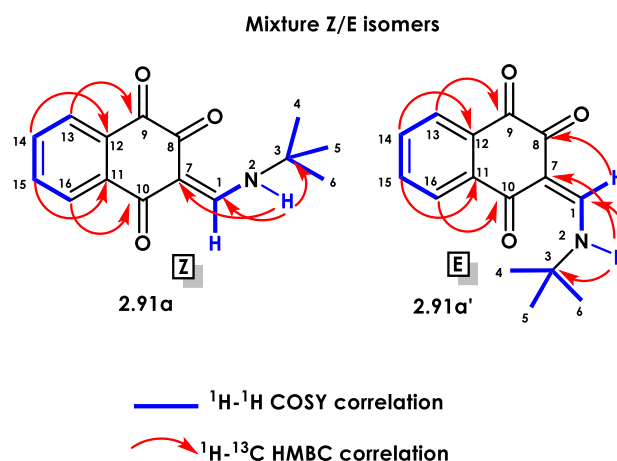
A proposed mechanism for the formation of enaminone products is depicted in Scheme 2.12. The deprotonation of the OH of the enol form of the lawsone reagent (attached to C-2) initiates the nucleophilic attack on the LUMO (*) orbital of the terminal electrophilic carbon atom of the isocyanide, resulting in intermediate **2.94**. After that, the electron-rich nitrogen transfers its free electron pair by forming a double bond with the nucleophilic carbon, generating the **2.95** keto-intermediate. This carbon of **2.95** in turn deprotonates the neighboring C-3 to yield the **2.96** enol-intermediate. The double bond changes position and gets attached directly to the naphthoquinone ring as a result of intramolecular reorganization, leading to the enaminone products **2.91-2.93**.



Scheme 2.12. Proposed mechanism of two-component reaction between lawsone and isocyanides.

Enaminone derivatives **2.91** and **2.92** were fully characterized by a full pack of NMR studies (^1H , ^{13}C , COSY and HMBC). Both compounds were found to be a mixture of isomers E and Z in a 1:1 ratio. All the ^1H and ^{13}C signals were assigned based on chemical shifts, spin-spin coupling constants, splitting patterns and signal intensities. ^1H and ^{13}C chemical shifts of **2.91a/2.91a'** are presented in Table 2.4. ^1H NMR spectras of lawsone enaminone derivatives with aromatic amines have been recently reported by Olyaei *et al* [37]. In our case, consistently with Olyaei's study, two characteristic downfield signals corresponding to amino NH protons of **2.91a** mixture appeared at 12.07 ppm and 12.22 ppm for **2.91a** (Z isomer) and **2.91a'** (E isomer), respectively. The alkene proton H-1 appeared at 8.55 ppm for **2.91a** (Z isomer) and 8.67 ppm for **2.91a'** (E isomer) as a doublet. The integrals of these two signals allowed the quantitative determination of each isomer (almost 50:50). NH and H-1 were proved to be neighbour protons based on extra evidence provided by COSY correlations. All aromatic protons of the naphthoquinone structure were found in the expected aromatic region between 7.80-8.27 ppm, most of them as multiplets.

Concerning ^{13}C NMR signals, the three carbonyl groups of the cyclohexanetrione scaffold were attributed as follows: C-9 at 181.7 ppm for **2.91a** (Z isomer) and 182.0 ppm for **2.91a'** (E isomer), C-8 at 176.8 ppm for **2.91a** and 177.5 ppm for **2.91a'**, C-10 at 184.5 ppm for **2.91a** and 181.9 ppm for **2.91a'**.

Table 2.4. ^1H and ^{13}C NMR data assignments of **2.91a/2.91a'** in CDCl_3 at 298K.

^1H and/or ^{13}C numbering	^1H chemical shift, ppm		^{13}C chemical shift, ppm	
	2.91a	2.91a'	2.91a	2.91a'
C-7	-	-	108.6	109.3
C-8	-	-	176.8	177.5
C-9	-	-	181.7	182.0
C-12	-	-	132.3	132.3
CH-13	8.18 (m)	8.19 (m)	128.3	127.7
CH-14	7.72 (td, $J=7.6$ Hz, 1.5 Hz)	7.72 (td, $J=7.6$ Hz, 1.5 Hz)	133.3	133.4
CH-15	7.84 (m)	7.82 (m)	135.6	135.4
CH-16	8.16 (m)	8.27 (m)	126.5	127.3
C-11	-	-	134.5	136.3
C-10	-	-	184.5	181.9
CH-1	8.55 (d, $J=1.5$ Hz)	8.67 (d, $J=1.5$ Hz)	157.9	157.4
NH	12.07 (bs)	12.22 (bs)	-	-
C-3	-	-	56.5	56.5
CH ₃ -4,5,6	1.52 (s)	1.52 (s)	29.6	29.6

* IUPAC numbering is not used here. For the sake of clarity, chemical shifts are reported starting by the naphthoquinone ring (C-7 to C-10), followed by the alkene chain.

The keto form of these naphthoquinone derivatives was confirmed by comparing it to its enol form which would display an expected C–OH signal around 156–160 ppm (Figure 2.6, C-2 of 3-alkenyl-2-hydroxy naphthoquinones) [38]. Thus, C-8 of **2.91a/2.91a'** was unambiguously attributed to a carbonyl group (Figure 2.6, C-8 of naphthoenaminones, Table 2.4). In addition, the enedione sequence C-1/C-7/C-8 and C-1/C-7/C-10 was confirmed by attributing C-7 at 108.6 ppm for **2.91a** and 109.3 ppm for **2.91a'** and C-1 at 157.9 ppm for **2.91a** and 157.4 ppm for **2.91a'**. This result provided strong evidence of the keto form of this derivative. In fact, in the enol form, C-7 should be found downfield shifted by $\Delta\delta = 8\text{--}12$ ppm (Figure 2.6, C-3 was found at 118 ppm and C-1a at 135 ppm on 3-alkenyl-2-hydroxy naphthoquinones structures). A significant difference between E and Z isomers was assessed by HMBC correlations. In fact, H-

1 was correlated to C-8 for **2.91a'** (E isomer) but not for **2.91a** (Z isomer). The assignment for the mixture **2.92a/2.92a'** was carried out by analogy.

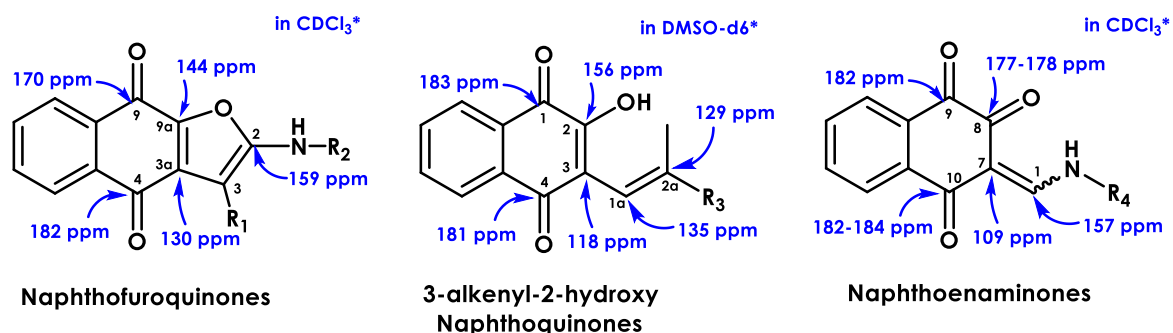


Figure 2.6. Comparative study of ^{13}C NMR chemical shifts for three different naphthoquinone derivatives: naphthofuroquinones, 3-alkenyl-2-hydroxy-naphtho-quinones and naphthoenaminones.

2.3 Biological and *in silico* evaluation of the synthesized series

All synthesized products were biologically evaluated *in vitro* against *Plasmodium falciparum*, *Leishmania donovani*, *Mycobacterium tuberculosis*, *Staphylococcus aureus*, and *Pseudomonas aeruginosa*. The chemosensitivity tests against *P. falciparum* were conducted by our own team under the supervision of Dr. Françoise-Benoit Vical (UPR 8241 CNRS LCC and Inserm ERL 1289). The biological evaluation against *L. donovani* was conducted at the Faculty of Pharmacy of the University of Paris-Saclay under the supervision of Prof. Philippe M. Loiseau ("Chémotherapies antiparasitaires: Biomolécules, conception, Isolement, Synthèse", UMR 8076 CNRS BioCIS). The antimicrobial evaluation against *M. tuberculosis*, *S. aureus* and *P. aeruginosa* was conducted at the Lazzaro Spallanzani Institute of the Department of Biology and Biotechnology of the University of Pavia (Italy) under the supervision of Prof. Maria Rosalia Pasca.

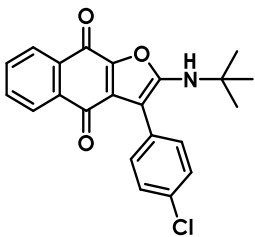
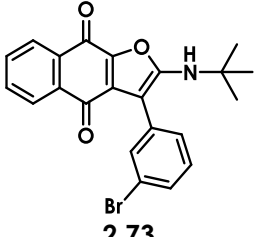
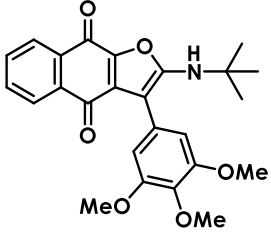
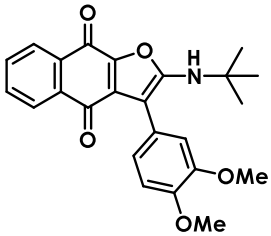
As a complement of antimalarial evaluation *in vitro*, docking studies were also conducted by Dr. Alfonso T. Garcia-Sosa at the Institute of Chemistry, Department of Molecular Technology of University of Tartu (Estonia). In this study, the docking of each new compound in the potential mitochondrial targets of *P. falciparum*, namely cytochrome bc1 and dihydroorotate dehydrogenase (DHODH), was carried out. The binding site was determined and the evaluation of molecules interactions with the binding site was associated to their docking scores.

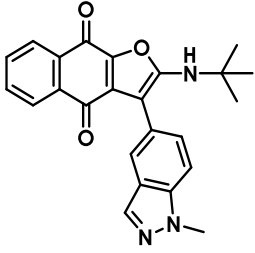
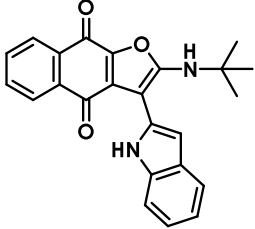
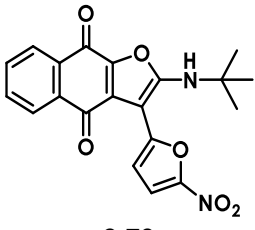
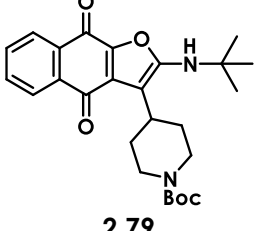
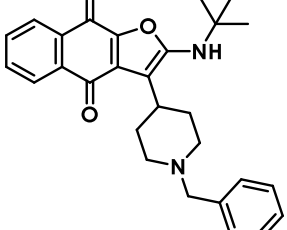
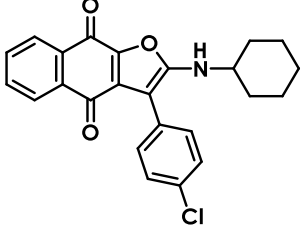
2.3.1 Activities against *P. falciparum* and *in silico* studies

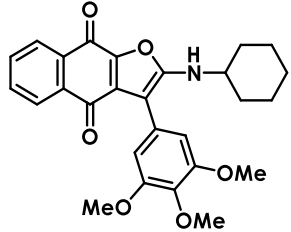
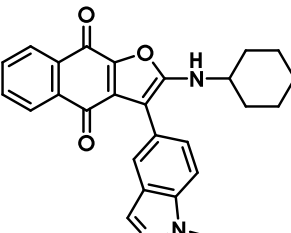
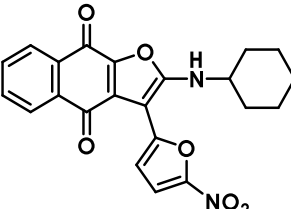
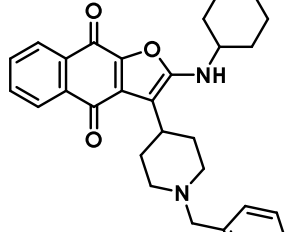
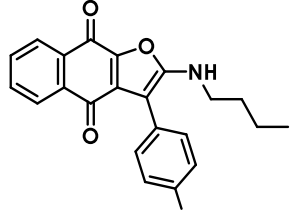
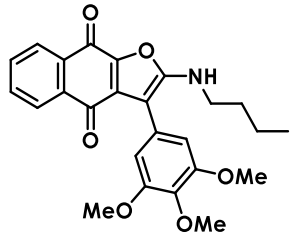
The antiplasmodial activity was evaluated against the F32-ART strain of *P. falciparum*. This strain is artemisinin resistant; it has been selected in our laboratory after 144 intermittent and increasing doses of the drug. The antiplasmodial activity at two doses (1 μM and 10 μM , in

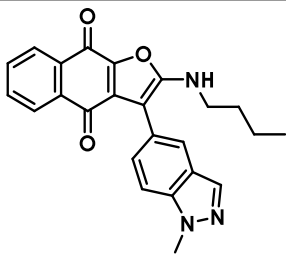
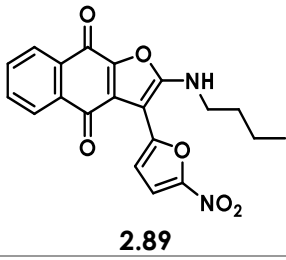
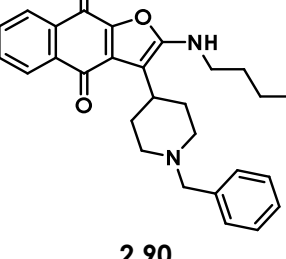
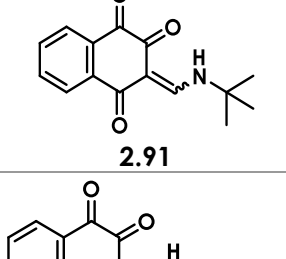
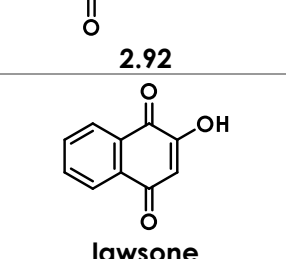
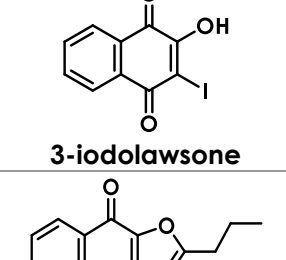
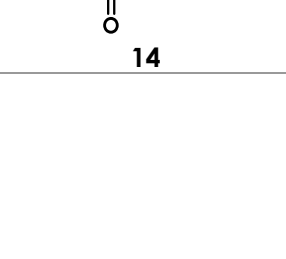

triplicate) was, first, established using the SYBR Green I Dye-Based Fluorescence Assay. For molecules able to inhibit more than 50% of parasite growth at 10 μM , the precise IC_{50} values were then determined [39],[40]. The molecules exhibiting the best antiplasmodial activities were tested on Vero cells to determine their cytotoxicity CC_{50} . Their selectivity index (SI) was calculated as the ratio of cytotoxicity to activity $\text{CC}_{50}/\text{IC}_{50}$. Both elementary synthons lawsone and 3-iodolawsone and the reference drug atovaquone were evaluated for comparison. The obtained results are summarized in Table 2.5.

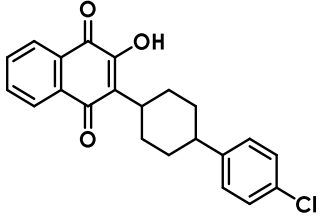
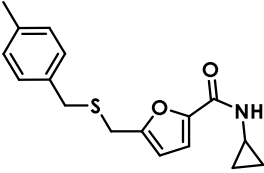
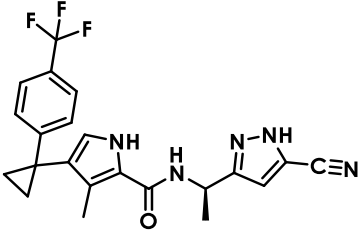
Table 2.5. Antiplasmodial activity and predicted docking scores of naphthofuroquinone and naphthoenaminone series.

Entry	Compound	<i>P. falciparum</i> F32-ART IC_{50} (μM)	CC_{50} (μM)	SI	Docking score Pfbc1 (kcal/mol)	Docking score PfdHODH (kcal/mol)
1	 2.69	>10	-	-	-9.7	-6.8
2	 2.73	>10	-	-	-7.1	-7.7
3	 2.74	>10	-	-	0.0	-7.0
4	 2.75	>10	-	-	-9.2	-8.3

5	 <p>2.76</p>	>10	-	-	0.0	-6.8
6	 <p>2.77</p>	>10	-	-	-3.5	-6.9
7	 <p>2.78</p>	>10	-	-	-3.5	-7.3
8	 <p>2.79</p>	>10	-	-	-8.9	-9.4
9	 <p>2.80</p>	2.5	86	34	-12.2	-11.0
10	 <p>2.81</p>	11.0	50	4.5	-9.5	-8.2

11	 <p style="text-align: center;">2.82</p>	6.0	>100	16	-8.8	-9.0
12	 <p style="text-align: center;">2.83</p>	10.0	-	-	-2.6	-6.3
13	 <p style="text-align: center;">2.84</p>	>10	-	-	-10.0	-7.3
14	 <p style="text-align: center;">2.85</p>	3.6	36	10	-6.4	-9.3
15	 <p style="text-align: center;">2.86</p>	>10	-	-	-11.2	-11.1
16	 <p style="text-align: center;">2.87</p>	9.0	>100	>10	-10.4	-9.2

17	 <p>2.88</p>	not tested	-	-	-	-
18	 <p>2.89</p>	>10	-	-	-10.5	-9.0
19	 <p>2.90</p>	4.0	24	6	-10.8	-9.3
20	 <p>2.91</p>	1.4	>50	>36	$\alpha = -7.2$ $\alpha' = -7.0$	$\alpha = -7.0$ $\alpha' = -7.0$
21	 <p>2.92</p>	1.9	>50	>26	$\alpha = -7.5$ $\alpha' = -7.3$	$\alpha = -7.1$ $\alpha' = -7.5$
22	 <p>lawsone</p>	>10	-	-	-6.5	-6.6
23	 <p>3-iodolawsone</p>	>50	-	-	-6.9	-7.1
24	 <p>14</p>	11.7	-	-	-8.7	-8.7

25	 atovaquone	0.001	6	6000	-12.1	-10.7
26	 MMV007571	1	-	-	-8.6	-7.3
27	 XCV	0.073	-	-	-	-11.2

* CC₅₀ = cytotoxicity assay, SI = CC₅₀/IC₅₀.

Three pools of molecules can be distinguished depending on their isocyanide scaffold (namely, *tert*-butyl, cyclohexyl and *n*-butyl). Among NFQs issued from *tert*-butyl isocyanide (entries 1-9, Table 2.5), only compound **2.80** carrying a (1-benzyl-piperidin-4-yl) substituent attached to C-3 exhibited an IC₅₀ value lower than 10 μM (IC₅₀ = 2.5 μM) and a very good selectivity index (SI = 34).

Concerning the NFQs synthesized from cyclohexyl isocyanide, four out of five compounds (**2.81-2.85**, entries 10-14, Table 2.5) exhibited IC₅₀ values ranging between 3.6 and 11 μM, with the most potent being NFQ **2.85** (entry 11, Table 2.5). This compound has a particular interest as it is substituted by two amino groups: an exocyclic (*N*-cyclohexyl) at C-2 and an endocyclic (*N*-substituted piperidinyl ring) attached to C-3 of the furan ring. Compound **2.85** exhibited promising results in cytotoxicity assay (CC₅₀ = 36 μM) and sequentially a selectivity index value SI = 10.

Comparing all molecules of this series (**2.81-2.85**, entries 10-14, Table 2.5), it appeared that having an heteroaromatic substituent at C-3 of the naphthofuran ring (e.g., 2-nitrofurane : compound **2.84**, or *N*-methyl-5-indazole : compound **2.83**) or an aromatic ring bearing an electron-withdrawing group (compound **2.81**) resulted in values of IC₅₀ ≥ 10 μM, meaning that this type of substituents are deleterious for the antiplasmodial activity. However, a trimethoxy-substituted (strong electron-donating effect) aromatic ring attached to C-3 of the furan ring (Table 2.5, entry 11, compound **2.82**) provided more encouraging results, with IC₅₀ = 6 μM and SI = 16.

Among NFQ issued from *n*-butyl isocyanide (Table 2.5, entries 15-19), compounds **2.87** (Table 2.5, entry 16) and **2.90** (Table 2.5, entry 19) exhibited IC₅₀ values lower than 10 μM. Compound **2.90**, having the same C-3 furan substituent as **2.85** (entry 11, Table 2.5) of cyclohexyl series of molecules exhibited the lowest IC₅₀ value at 4 μM. However, **2.90** is less compelling than compound **2.85** due to its higher cytotoxicity (CC₅₀ = 24 μM) and subsequently weak selectivity index (SI = 6). Therefore, among all *n*-butyl NFQ derivatives, compound **2.87** could be more pharmacologically promising as it exhibits an IC₅₀ in the same range as **2.90** but displays a considerably lower cytotoxicity value (SI > 100 μM).

In the enamino naphthoquinone series, both **2.91** and **2.92** (Table 25, entries 20 and 21) exhibited the lowest IC₅₀ values of the whole series described in this chapter. In fact, **2.91** and **2.92** exhibited IC₅₀ values at 1.4 μM and 1.9 μM, respectively, far below, lawsone and 3-iodolawsone (IC₅₀ > 10 and 50 μM, respectively, Table 2.5, entries 22 and 23). In addition, **2.91** and **2.92** have a low cytotoxicity (CC₅₀ > 50 μM) and, consequently, very encouraging selectivity indexes (SI > 36 for **2.91** and SI > 26 for **2.92**).

It should be noted that, to the best of our knowledge, this is the first time that the activity of a naphthoenaminone systems with a dione function has been evaluated against *P. falciparum*. These molecules retain the 1,4-naphthoquinone scaffold of atovaquone, but the 2-hydroxy group is replaced by a ketone group. The 2-hydroxyl functionality of atovaquone has been considered to be critical for interaction with the bc1 complex, and it is supposed that this interaction is impaired in atovaquone-resistant *Plasmodium* [41]. While nothing is reported concerning enamino derivatives with antiparasitic activities similar naphtho-enaminone structures have been reported to act as moderate antitumoral agents against Ehrlich ascites carcinoma (EAC) cells *in vitro* [42] in a dose-dependent manner. However, bulky (aromatic and piperidiny) amino-substituents decreased the antitumoral activity and affected the cytotoxicity values.

When everything is taken into account, 6 out of 19 compounds of the 2-amino-naphthofuroquinone family were found to be 2- to 5-fold more effective against *P. falciparum* artemisinin resistant strains than the parent derivative **2.14** reported by Borgati *et al.* [16] which exhibited an IC₅₀ value at 11.7 μM against *P. falciparum* chloroquine resistant strains. Compound **2.14** did not bear any substituent at C-3 of the furan ring and did not contain any amino group attached at C-2. The *N*-benzyl piperidiny substituent at C-3 resulted in positive pharmacomodulation because, whatever the amino-substituent at C-2 was, the IC₅₀ values of all molecules containing a *N*-benzyl piperidiny substituent at C-3 (**2.80**, **2.85**, and **2.90**) were found lower than 10 μM. As for the naphthoenaminone derivatives **2.91** and **2.92**, the modification of the enol form of 2-hydroxy function to a carbonyl group could be an interesting way to set up new hits that could overcome *Plasmodium* atovaquone resistance (Figure 2.7).

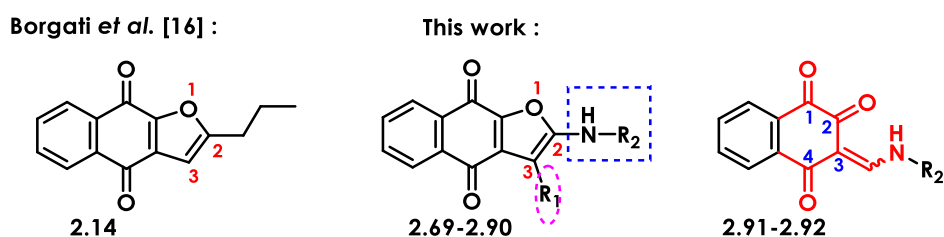


Figure 2.7. This work contributed into varying the furan substitution of NFQ derivatives aiming to obtain active antiparasitic compounds.

In general, when discussing the structures of NFQ derivatives, a C-2 substitution of the furan ring with a flexible alkyl amino group could be recommended, while a C-3 substitution with aromatic or heteroaromatic rings would not be recommended, unless it has a *N*-benzyl piperidinyl substituent. However, more data should be collected in order to pave a way towards more active compounds against *P. falciparum* (Fig. 2.7). In addition, the amino substituent of naphthoenaminone derivatives could be further explored in order to get bioactive molecules against quiescent *Plasmodium*.

Docking studies

Molecular docking studies were conducted against both mitochondrial targets anticipated to interact with all molecules mentioned in this chapter: bc1 cytochrome and DHODH of *Plasmodium falciparum* in order to support the explanation of the observed biological activities. First, as far as bc1 target is concerned, the interactions between all molecules and the *P. falciparum* target bc1 were determined using the AlphaFold2-modeled structure of the cytochrome enzyme Q7HP03 [43]. The X-ray structure of the complex of atovaquone bound in the catalytic Qo site of bc1 in *Saccharomyces cerevisiae* was extracted from Protein Data Bank (PDB: 4PD4) [44]. Its good resolution was suitable for docking studies (3.04 Å). The predicted protein structure's local quality metrics were all rated as being very good. This means that all amino acid residues near to the binding site region (the central groove inside the α -helices, next to Tyr 263) exhibited a low position error, according to per-residue confidence scores (pLDDT) and predicted alignment error (PEA). So, the final predicted model used for docking of bc1 enzyme was highly confident (Fig. 2.8) [45].

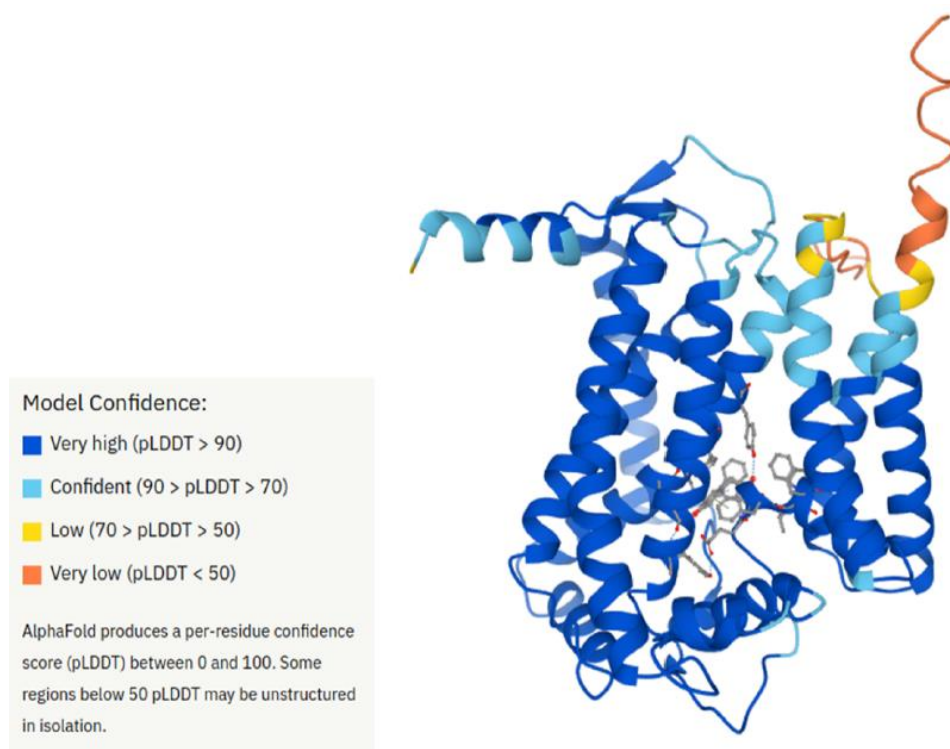


Figure 2.8. Model confidence for bc1 target used for docking studies. The binding site is depicted in stick representation.

For the second target dihydroorotate dehydrogenase (DHODH), the target preparation was much easier. The X-ray crystal structure of *P. falciparum* DHODH bound with DSM782 (or XCV) was available in PDB (PDB: 7L01) with a resolution well adapted for docking studies (1.60 Å) [46],[47]. All docking scores of this library of compounds are presented along, with the biological activities against *P. falciparum* ART resistant strain in Table 2.5. Atovaquone was used as positive control for docking against bc1 (Table 2.5, entry 25), MMV007571 against both bc1 and DHODH (Table 2.5, entry 26) [48],[49] and XCV (Table 2.5, entry 27) against DHODH, as its inhibitor [50].

Into the bc1 binding site, atovaquone (ATQ) was found to bind in two distinct orientations, both flipped and unflipped, with primarily hydrophobic interactions stabilizing its pose (docking score = -12.1 kcal/mol). The non-ionized pose of atovaquone was imposed during the determination of the binding site box. A hydrogen bond was imposed between ATQ's -OH and His 242. The naphthoquinone ring, for example, offered hydrophobic interactions with Ile 258, His 242, and Met 133 amino acid residues, while its 4-(*para*-chlorophenyl)cyclohexyl moiety provided hydrophobic interactions with Ile 141, Phe 267, and Tyr 268. The aromatic ring also allowed for pi-pi stacking with Phe 264. MMV007571 was found to bind at the same part of the bc1 cavity compared to ATQ, exhibiting a similar interaction map and docking score (docking score = -8.6 kcal/mol). Its binding pose was stabilized by strong hydrophobic interactions with the majority of the amino acid residues located into the binding site, namely Glu 261, His 242, Ile 258 and Val 140 (Fig. 2.9).

Into the DHODH binding site, XCV was found to interact with almost every amino acid residue of the cavity. Its binding pose was stabilized by using substantial hydrogen bonds formed by two amino groups of XCV structure with His 185 and by the carbonyl group of XCV structure with Arg 265 residue (docking score = -11.2 kcal/mol). Besides, the rest of the structure provided strong Van der Waals interactions with Lys 229, Phe 227, Glu 182 and Phe 188 residues. However, when ATQ was subjected to interact with DHODH binding site, no matter its excellent binding score (-10.7 kcal/mol), the compound was not able to bind deep enough into the cavity. As a result, the naphthoquinone ring is partially outside of the cavity (Fig. 2.10).

Lawsone and 3-iodolawsone (Table 2.5, entries 23-24) exhibited almost the same docking scores against both mitochondrial targets bc1 and DHODH, meaning that C-3 substitution with a bulky group (e.g. halogen iodine) would not be expected to affect the binding affinity. However, comparing to ATQ and XCV, lawsone and its 3-iodo derivative were found to bind just at the entrance of the cavity, explaining their low docking scores and their deceiving *in vitro* activity.

Molecule **2.80** (Table 2.5, entry 9) of the *tert*-butyl series of the NFQ series exhibited the best docking scores (≤ -11 kcal/mol) against both bc1 and DHODH targets, values which were comparable to both positive controls atovaquone and XCV. These results align well with its reported biological activity since **2.80** had the lowest IC₅₀ value among all NFQs synthesized herein. Compound **2.80** was found to bind into bc1 target flipped while presenting less intense hydrophobic interactions compared to ATQ. The naphthoquinone ring exhibited hydrophobic interactions with Phe 267 and Tyr 268 residues while partially was situated outside of the binding site. However, the *N*-benzyl piperidinyll moiety significantly contributed to binding by extending the hydrophobic interactions of this molecule with Glu 137, Met 133, Ile 141 and Glu 261 residues, showing the importance of furan C-3 substitution to cavity exploration into bc1. The amino C-2 furan substituent equally offered extension of hydrophobic interactions with the key amino acid residue Glu 261. In DHODH **2.80** was found to bind at the same part of the cavity as ATQ but less deep than the natural ligand XCV. Again, an important part of the NFQ ring was found to be solvent exposed and the bulky 2-amino substituent was found too big to enter the cavity due to steric hindrance. However, the naphthoquinone ring of **2.80** exhibited important hydrophobic interactions with the key amino acid residues Phe 188, Leu 187, just like in XCV case. The C-3 furan substituent was found to play an important role in the exploration of the cavity as it offered strong hydrophobic interactions with Gly 535, Tyr 168 and Met 536.

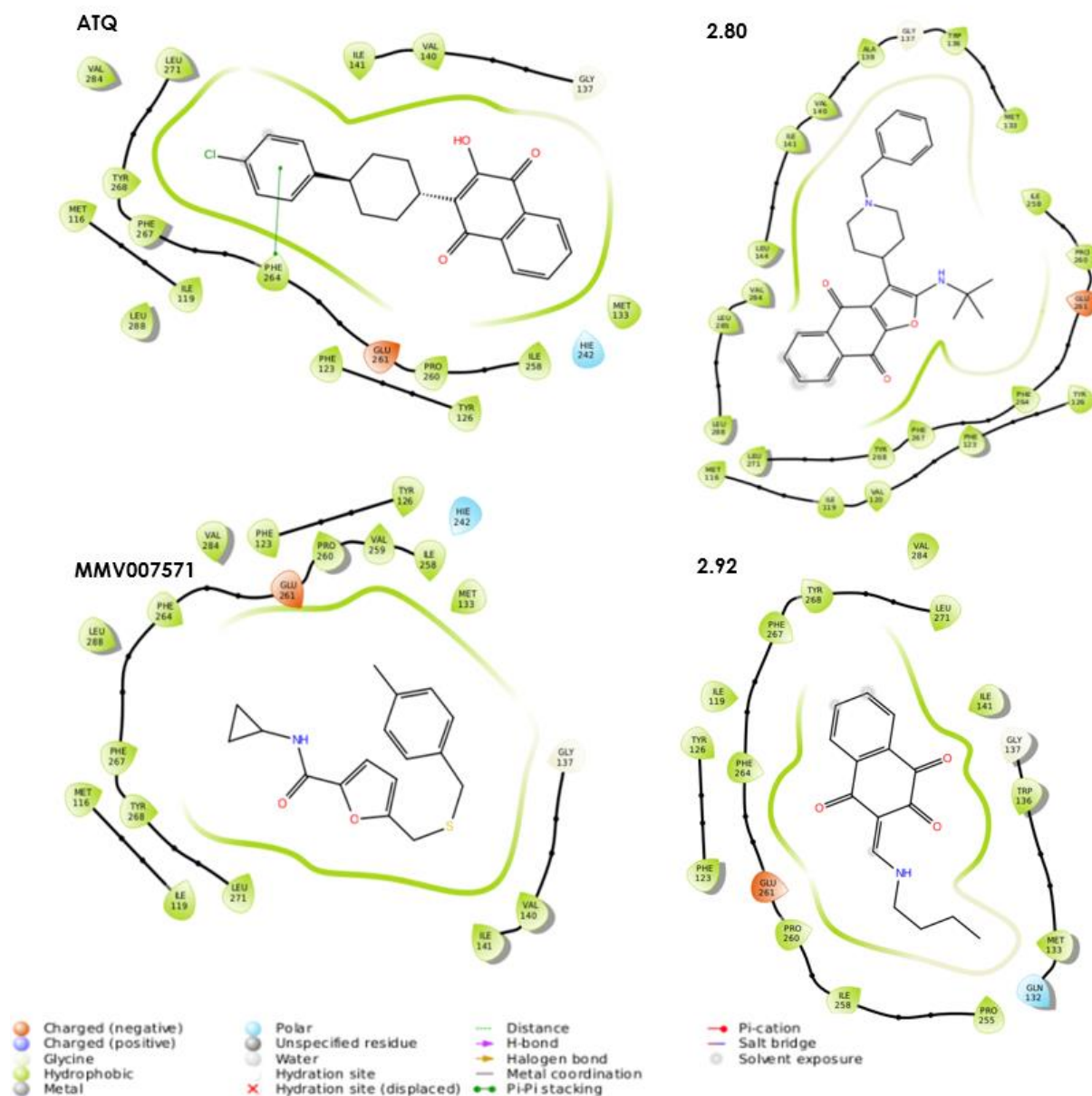


Figure 2.9. Binding modes and interactions for selected compounds in the binding site of bc1.

All amino-cyclohexyl NFQ derivatives (**2.81-2.85**, Table 2.5, entries 10-14) except **2.83** exhibited very favorable docking binding scores with both *P. falciparum* bc1 complex and DHODH. This result could support the proposal that the C-3 furan substituent should not bear an heteroaromatic ring, since it contributes to interactions inhibition with both bc1 and DHODH binding sites. Compound **2.85** (Table 2.5, entry 14) could probably bind to DHODH rather than bc1 complex; in fact, it exhibited a low docking score against bc1 (-6.4 kcal/mol), compared to atovaquone (-12.1 kcal/mol). Finally, all *n*-butyl NFQ derivatives showed favorable docking scores against both targets probably because the *n*-butyl chain provided with very strong hydrophobic interactions with amino acids of the enzyme sites. Compound **2.90** (Table 2.5, entry 19), which exhibited the lower IC₅₀ value among all *n*-butyl NFQs, displayed favorable docking poses against both mitochondrial targets and good (≤ -9 kcal/mol) docking scores.

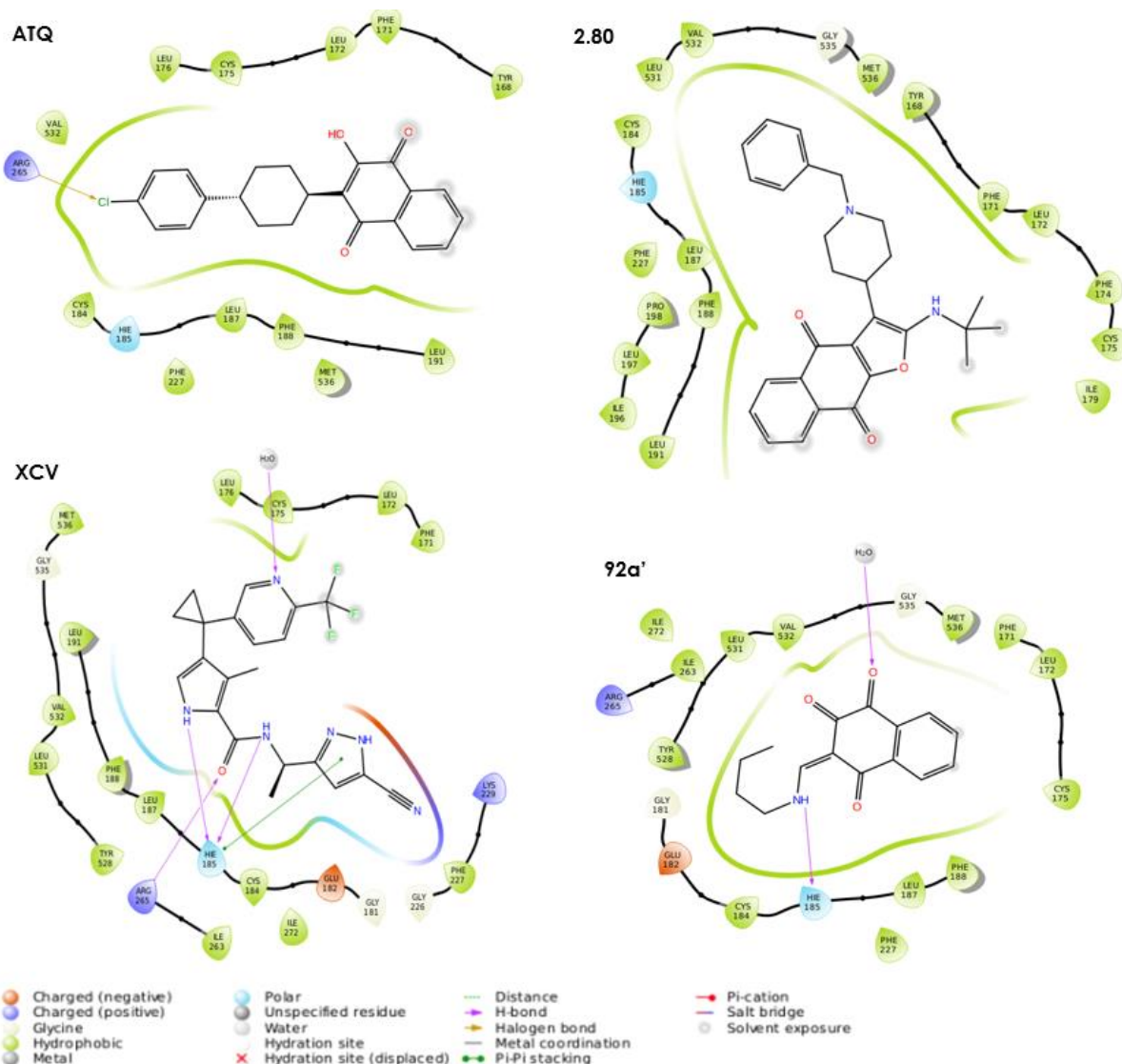


Figure 2.10. Binding modes and interactions for selected compounds in the binding site of DHODH.

In the enaminone series (compounds **2.91-2.92**, Table 2.5, entries 20–21), the E and Z isomers of each compound exhibited similar binding scores against both targets. For instance, compound **2.92a'** was found to bind at the same part of the cavity of bc1 mitochondrial target, just like ATQ. The naphthoquinone ring of the compound was however flipped and had a different orientation. It exhibited strong hydrophobic interactions with Phe 264, Ile 141, Gly 137 and Trp 136 residues while the linear amino substituent contributed to the expansion of hydrophobic interactions with Pro 255, Gln 132, Ile 258 and Met 133. Similar results were obtained when **2.92a'** was docked against DHODH target. The compound was located at the same part of the binding site compared with XCV. With improved predicted docking scores at the hydrated binding site compared to the non-hydrated, compound **2.92a'** in particular was predicted to make effective use of bridging water molecules [51] in the DHODH binding site. That was found to be the case of natural DHODH inhibitor XCV (Fig. 2.10). The naphthoquinone

ring contributed to binding pose stability with strong hydrophobic interactions with two key amino acid residues Leu 187 and Phe 188. The linear amino substituent extended the hydrophobic interactions with Glu 181, Glu 182 and Cys 184 and the NH group contributed with a hydrogen bond formation with the neighbor amino acid His 185 in DHODH.

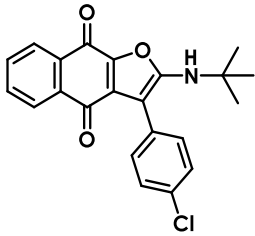
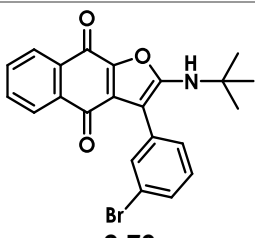
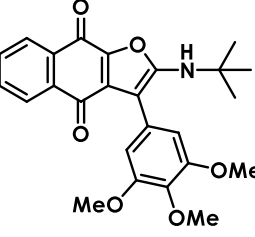
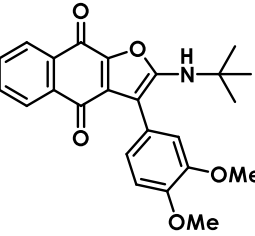
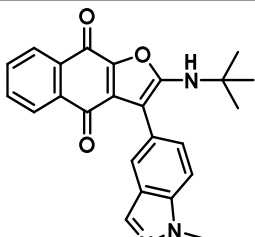
Swiss-ADME [52] was used to calculate the ADME properties of all compounds. Each compound of the series met Lipinski's rule of five for bioavailability, and the majority additionally satisfied the lead-likeness according to the Ghose, Veber, Egan, and Muegge filters [53]. PAINS warning [54] was inevitable due to the naphthoquinone scaffold.

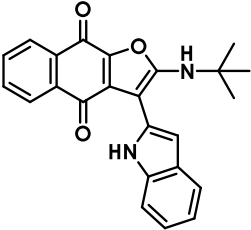
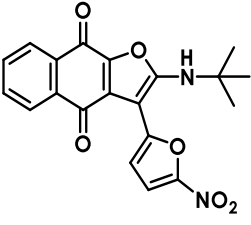
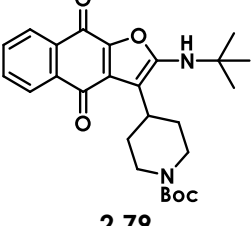
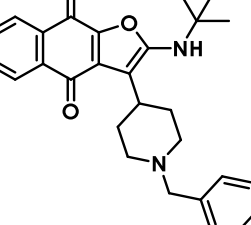
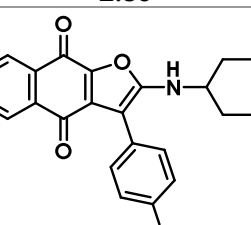
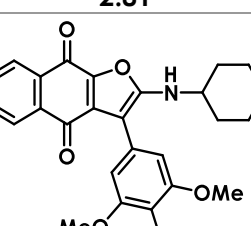
After taking everything into account, the favorable multitarget binding of these compounds and their drug-likeness could provide further inspiration regarding the synthesis of novel (variously substituted) naphthofuroquinone and naphthoenaminone series as potential antiplasmodial hits.

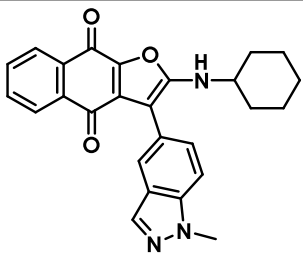
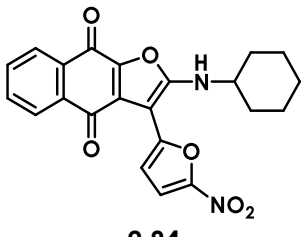
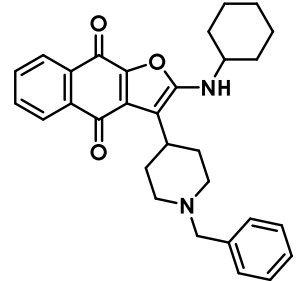
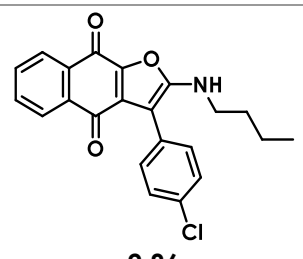
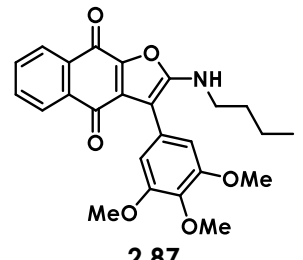
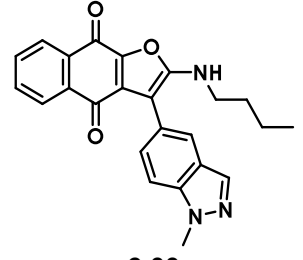
2.3.2 Activities against *L. donovani*

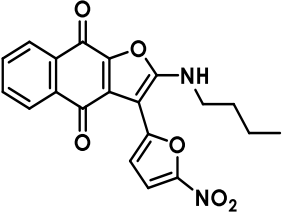
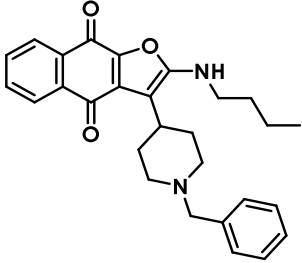
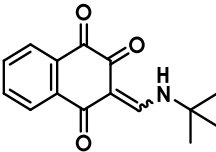
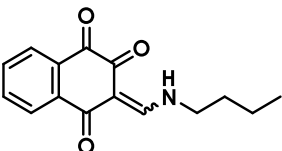
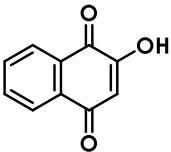
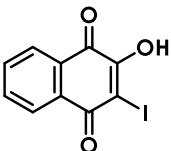
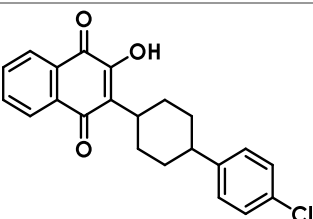
The antileishmanial activity of synthesized series was assessed *in vitro* against *L. donovani* LV9 axenic amastigotes and intramacrophage amastigotes forms. Shortly, SYBR Green method first established the leishmanicidal activity against *L. donovani* axenic amastigotes forms [55]. The compounds exhibiting IC₅₀ values lower than 10 μ M were further evaluated against intramacrophage amastigote forms. Cytotoxicity was evaluated on RAW 264.7 macrophages using the resazurin method [56]. The cytotoxicity determination method was then used to choose the appropriate compound doses for further investigation on the *L. donovani* intramacrophage amastigote model. Macrophages were infected with *L. donovani* axenic amastigotes with 10 parasites per macrophage. The percentage of infected macrophages was about 80%, and the mean number of amastigotes per infected macrophage was 4 to 5 in the untreated controls [55]. The impact of the compounds is expressed as a percentage of inhibition of parasite growth, as assessed by the SYBR Green incorporation technique. Results are reported as IC₅₀ values. Miltefosine was used as reference drug. The obtained results are summarized in Table 2.6.

Table 2.6. Leishmanicidal activity of the whole series synthesized herein against *L. donovani* LV9 axenic amastigote and intramacrophage amastigote forms.

Entry	Compound	<i>L. donovani</i> axenic amastigotes IC ₅₀ ± SD (μM)	<i>L. donovani</i> intramacrophage amastigotes IC ₅₀ (μM)	CC ₅₀ (μM)	SI
1	 2.69	> 100	-	-	-
2	 2.73	50.9 ± 4.4	-	-	-
3	 2.74	> 100	-	-	-
4	 2.75	49.3 ± 5.3	-	-	-
5	 2.76	> 100	-	-	-

6	 <p>2.77</p>	29.3 ± 4.2	-	-	-
7	 <p>2.78</p>	> 100	-	-	-
8	 <p>2.79</p>	12.3 ± 2.2	7.0	49.2	7.1
9	 <p>2.80</p>	46.7 ± 2.8	-	-	-
10	 <p>2.81</p>	7.0 ± 2.6	9.4	54.2	5.8
11	 <p>2.82</p>	54.3 ± 4.2	-	-	-

12	 <p>2.83</p>	46.7 ± 2.8	-	-	-
13	 <p>2.84</p>	> 100	-	-	-
14	 <p>2.85</p>	45.3 ± 5.9	-	-	-
15	 <p>2.86</p>	45.3 ± 3.8	-	-	-
16	 <p>2.87</p>	44.2 ± 1.8	-	-	-
17	 <p>2.88</p>	not tested	-	-	-

18	 <p>2.89</p>	> 100	-	-	-
19	 <p>2.90</p>	> 100	-	-	-
20	 <p>2.91</p>	3.0 ± 0.3	3.5	> 100	> 28.5
21	 <p>2.92</p>	3.6 ± 0.2	6.3	46.5	7.3
22	 <p>lawsone</p>	4.4 ± 0.5	6.3	44	7
23	 <p>3-iodolawsone</p>	5.2 ± 0.6	13.2	56.2	4.3
24	 <p>atovaquone</p>	5.1 ± 0.4	11.1	44	4.0
25	Miltefosine	3.0 ± 0.2	1.5	22.6	15.5

* CC_{50} = cytotoxicity assay, $SI = CC_{50}/IC_{50}$. CC_{50} was evaluated against macrophage RAW 264.7 mouse monocyte cell lines.

Among all *tert*-butyl series of NFQ derivatives (entries 1-9, Table 2.6) only compound **2.79** (entry 8, Table 2.6) carrying a *N*-Boc piperidinyl substituent attached to C-3, exhibited an IC₅₀ value lower than 10 μM (IC₅₀ = 7.0 μM) against *L. donovani* intramacrophage amastigote forms. With a cytotoxicity value at CC₅₀ = 49.2 μM, this compound exhibited an acceptable selectivity index of 7. Most molecules of the *tert*-butyl family such as **2.73**, **2.75**, **2.77** and **2.80** exhibited inhibitions against *L. donovani* axenic amastigote forms with IC₅₀ values in the range 29-51 μM which did not justify further investigation on the intramacrophage parasites.

Concerning the cyclohexyl series of NFQs, compound **2.81** (Table 2.6, entry 10) exhibited promising IC₅₀ values against both axenic amastigote (IC₅₀ = 7.0 μM) and intramacrophage (IC₅₀ = 9.4 μM) forms. This molecule exhibited a CC₅₀ value on macrophages at 54 μM, thus attributing it a SI close to 6. However, in general, derivatives of the *n*-butyl series cases (molecules **2.86** and **2.87**, entries 15 and 16 respectively) the compounds were found to have IC₅₀ values higher than 40 μM against axenic forms, values which did not justify further exploration.

Despite all results obtained for the NFQ series, lawsone (entry 22, Table 2.6), 3-iodolawsone (entry 23) and both naphthoenaminones **2.91-2.92** (entries 20-21, Table 2.6) and atovaquone (entry 24, Table 2.6) were found active against both *L. donovani* forms axenic and intramacrophage amastigotes. They exhibited IC₅₀ values comparable to miltefosine during the first screen. Remarkably, compound **2.91** was found to be the most active, with the same IC₅₀ value as miltefosine against axenic amastigote forms (IC₅₀ = 3.0 μM) (entries 20 and 25, Table 2.6, for **2.91** and miltefosine, respectively). Against intramacrophage amastigote forms, the activity of **2.91** was also comparable to that of miltefosine (IC₅₀ = 3.5 μM and 1.5 μM for **2.91** and miltefosine, respectively). Noteworthy, the selectivity of **2.91** for *L. donovani* with respect to macrophages, was SI > 28, twice the value of the clinically used miltefosine. Compound **2.92** displayed a similar pharmacological profile as lawsone (IC₅₀ = 6.3 μM) against macrophage amastigote forms and reasonable selectivity index (SI = 7.3 μM).

Thus, the naphthoenaminone derivatives could be promising as leishmanicidal agents. These results indicate that substitution of lawsone at C-3 by enamines or other kind of substituents may significantly decrease the cytotoxicity of the compounds and, consequently, improve their leishmanicidal selectivity. So, this series deserves further investigation. Both **2.91** and **2.92** should undergo *in vivo* evaluation against *L. donovani* /BALB /c mouse model.

2.3.3 Activities against other pathogens

Activities against various microorganisms

The antimycobacterial activity (MIC_{90}) of the synthesized series was assessed *in vitro* against *M. tuberculosis* H37Rv using the resazurin reduction microplate assay method [56]. Mycobacterial cultures were established for each compound at two different concentrations. Cultures without containing any compound and any inoculum were prepared and used as negative controls. Mycobacterial viability was evaluated after 24 h of incubation with resazurin and was measured by cytofluorometry. The impact of the potential drugs is expressed as a percentage of decrease in *M. tuberculosis* growth and is reported as an IC_{50} value, calculated from experimental MIC ($\mu\text{g/mL}$). Streptomycin was used as the positive control ($IC_{50} = 0.4 \mu\text{M}$).

The antibacterial activity against *S. aureus* ATCC25923 and *P. aeruginosa* PAO1 was evaluated by determining MICs in Mueller-Hinton Broth II cation adjusted by the 2-fold microdilution method. The microtiter plates were incubated at 37 °C for 24 hours, and growth was measured using the resazurin method [56]. The MIC was defined as the lowest drug concentration that prevented the color change from blue to pink, which indicated bacterial growth. Ciprofloxacin ($IC_{50} = 3 \mu\text{M}$) was used as positive control against *S. aureus* and against *P. aeruginosa* ($IC_{50} = 0.5 \mu\text{M}$). Some representative results are presented in Fig. 2.11.

The majority of compounds of this library exhibited IC_{50} values higher than 150 μM against *M. tuberculosis*. Among all tested compounds, three compounds bearing the *N*-benzyl piperidinyl motif displayed modest antitubercular activities (**2.80**, **2.85** and **2.90**, Fig. 2.11). Compound **2.80** had an IC_{50} value of 9 μM and compounds **2.81**, **2.84**, **2.85** and **2.90** exhibited IC_{50} values in the range 18-39 μM , while the reference drug streptomycin displayed $IC_{50} = 0.4 \mu\text{M}$ in the same conditions. So, further tuning of the substitution pattern of the NFQ scaffold should be done to improve activity. It would be recommended to start by fusing an aromatic ring, imitating molecule DFC2 (**2.5**, Fig. 2.2) aiming to enhance any potential antimycobacterial activities.

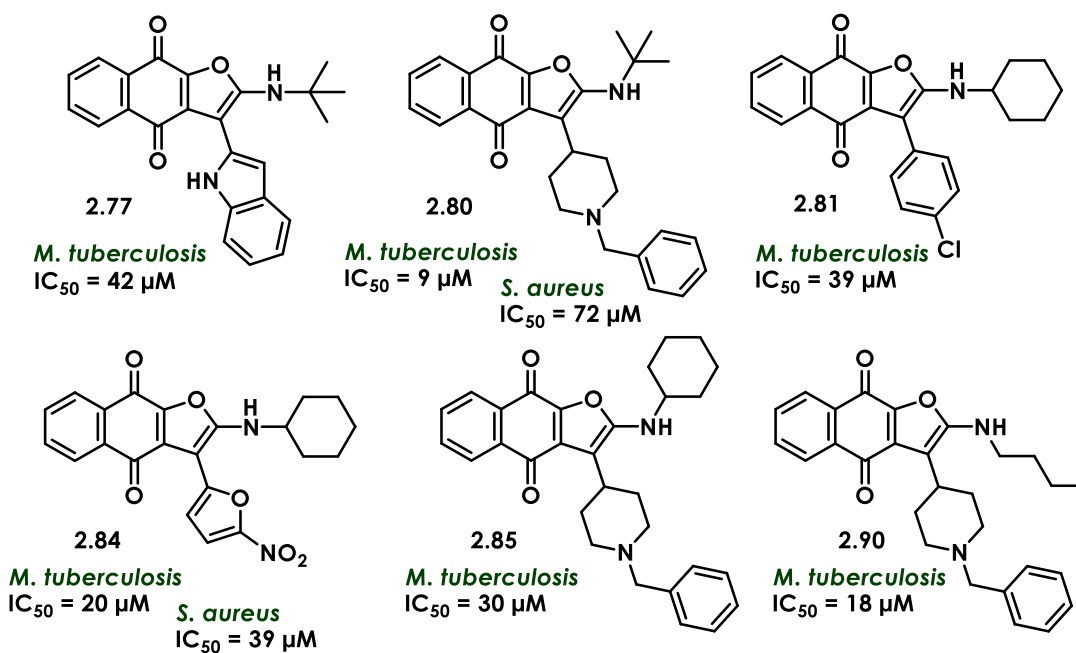


Figure 2.11. Representative examples of NFQs and their antimicrobial activities.

Unfortunately, the whole series described herein was found to be inactive against *P. aeruginosa* PAO1 as they exhibited IC_{50} values higher than $150 \mu M$, while the reference drug ciprofloxacin exhibited IC_{50} equal to $0.5 \mu M$. Two compounds exhibited moderate antibacterial activities against *S. aureus* ATCC25923 with IC_{50} values below $150 \mu M$. Compounds **2.80** and **2.84** (Fig. 2.11) exhibited IC_{50} values equal to $72 \mu M$ and $39 \mu M$, respectively. However, further studies should be done in order to reach to a safe conclusion concerning how the structural modification of amino-NFQs could potentially enhance the antibacterial activity of these compounds.

2.4 Conclusion and Perspectives

Chemistry-Synthesis

A multicomponent domino reaction involving lawsone, various aldehydes, and alkyl-isocyanides was established and optimized using microwave irradiation. This protocol was used to synthesize a novel series of 19 variously substituted 3-amino-naphthofuroquinone derivatives with yields ranging between 19% and 59% (compounds **2.69-2.90**). In parallel, two naphthoenaminones (compounds **2.91** and **2.92**) were isolated as a *Z/E* mixture (50/50) as a result of the two-component direct condensation between lawsone and the corresponding commercially available isocyanides, with yields of 40% and 50%, respectively. Neither these naphthoenaminone structures had been reported before, either this way of synthesizing them.

As a next step, the reaction should be further studied under thermal activation in order to evaluate the substrate scope and especially if it could provide less complicated reaction mixtures and shorter reaction times.

In some cases, while aldehyde's conversion was very high, the yields of NFQs were low to good because of solubility and purification problems. In that respect, efforts should be oriented towards finding the appropriate purification conditions in order to favor the isolation of the target 3-amino-naphthofuroquinone with high purity. A recrystallization of the desired product could be also an option in a scale-up model, when the reaction mixture is enriched to the target NFQ.

Concerning the substrate scope of the multicomponent domino reaction, the reaction was found to tolerate a wide spectrum of aldehyde reactant (aromatic aldehydes bearing either an electron donating or an electron withdrawing group, heteroaromatic aldehydes and *N*-piperidinyl carbaldehydes). However, only three commercially available alkyl isocyanides were used (*tert*-butyl, butyl and cyclohexyl isocyanides). Thus, developing a larger and more variable isocyanide library could be a priority in order to add further points to the chemical space exploration.

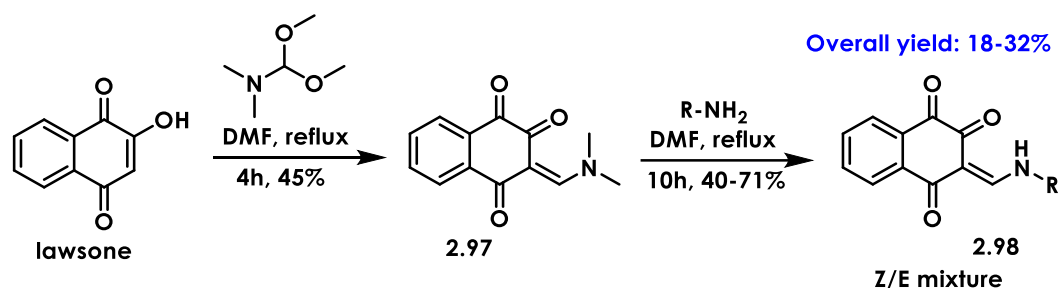
In this regard, many studies have been dedicated to developing new libraries of isocyanides for use in MCRs. Thanks to the group of Prof. Dömling ongoing projects, libraries with a wide structural diversity are now accessible [57]. This group recently reported the synthesis of a library of isocyanides, based on formamide dehydration. Isocyanides are obtained in high yields, with increasing safety, scalability, and significantly reducing chemical waste (Scheme 2.13). This methodology allows the synthesis of cyclic, acyclic, aliphatic, bulky, aromatic, amino-acid derived isocyanides substituted with a great variety of functional groups such as halogens, boronic esters, ethers, esters, hydroxy, polyamines and tertiary amines. In addition, this method can be applied to optically active substrates. As far as heterocycles containing isocyanide scaffolds are concerned, the authors observed that these products were unstable, but they should be generated *in situ* [58].



Scheme 2.13. General synthesis of variously substituted isocyanides.

Finally, a study should be carried out in order to further optimize the unusual formation of naphthoenaminones issued from the condensation of lawsone and the used alkyl-isocyanide. Besides, more synthetic methodologies should be established, giving the access to this type of structures. To the best of our knowledge, there is only one publication mentioning the synthesis

of naphthoenaminone derivatives in two steps starting from lawsone (Scheme 2.14). The methodology is based on reaction of lawsone with *N,N*-dimethylformamide dimethyl acetal, providing intermediate **2.97**. Reaction of **2.97** with a primary or a secondary amine can lead to the target compounds **2.98** with total yields ranging between 18-32% [42]. This could be a starting point for further development and exploration of the substrate scope.



Scheme 2.14. Reported synthesis of naphthoenaminone derivatives.

Biological activities

Among the NFQ family, compounds **2.80**, **2.85** and **2.90**, bearing the *N*-benzyl piperidinyl substituent attached to C-3 of the furan ring were found to have the lowest IC_{50} values (2.5 - 4.0 μ M) against the *P. falciparum* ART resistant strain F32-ART, and acceptable selectivity index values (in the range 6-34) (Fig. 2.12). Derivative **2.79**, bearing a *N*-Boc piperidinyl substituent at C-3 of the furan ring, exhibited the lowest IC_{50} value (7.0 μ M) against *L. donovani* amastigote forms of this NFQ series (Fig. 2.12).

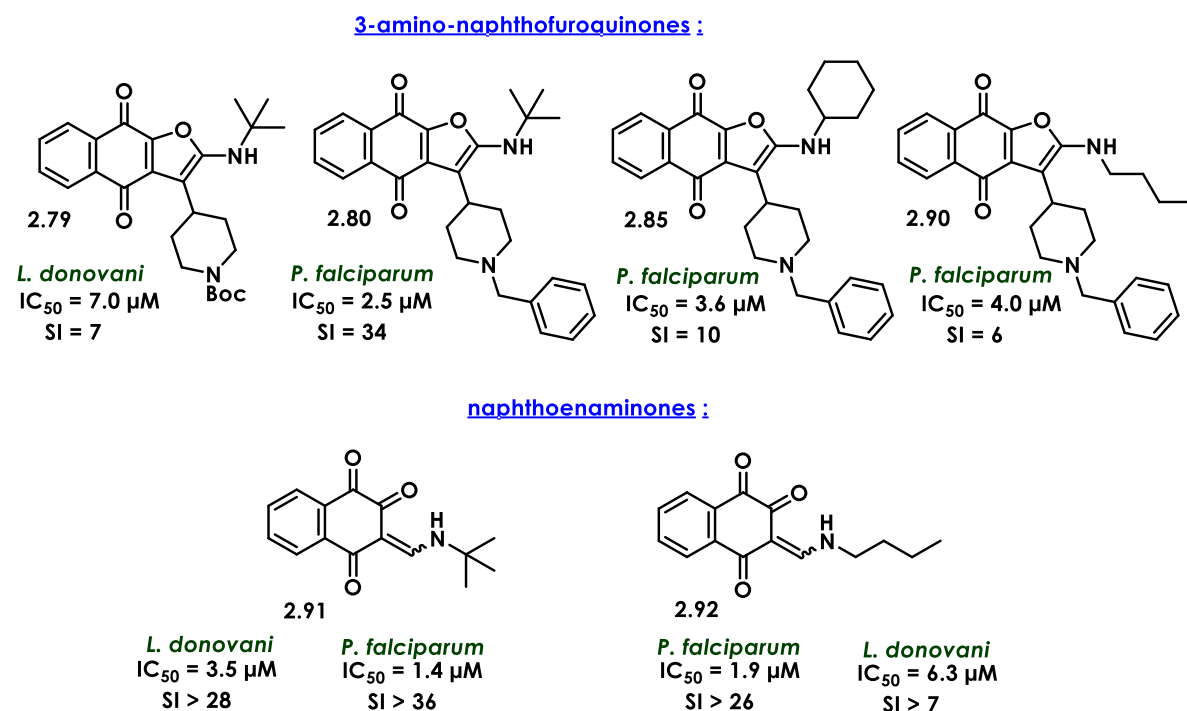


Figure 2.12. Antiparasitic activity. Selected compounds exhibiting the smallest IC_{50} values against *P. falciparum* and *L. donovani*.

Based on the observed activities, substitution at C-3 by a *N*-piperidinyl group afforded encouraging antiparasitic activities. As a next step, the piperidinyl group could be changed for a cyclohexyl-Ar in order to mimic the atovaquone structure. Compounds like **2.79**, bearing the *N*-Boc piperidinyl motif could also be used as the starting point of a new series. *N*-Boc piperidinyl could be used as a linker, after *N*-deprotection allowing further structure modification by coupling with other reagents in order to generate a novel 3-amino-naphthofuroquinone library. Besides, alkyl C-2 amino substituents (isopropyl, monoterpenes, etc.) should be preferred in order to improve the interaction in DHODH and bc1 cavities, and to achieve better antiparasitic activities.

Finally, a very large and synthetically feasible 3-amino-naphthoquinone series could be designed as a next step by varying either the aldehyde and isocyanide counterparts. This series could be docked against both *P. falciparum* mitochondrial targets cytochrome bc1 and DHODH. In interface with the obtained docking scores, we then could prioritize the synthesis of the compounds exhibiting the most promising interactions with both binding sites.

2.5 Experimental part

2.5.1 Materials and methods

Reagents and solvents were purchased from Sigma Aldrich, TCI, Alfa Aesar and Fluorochem and used as received. Microwave irradiation reactions were performed in a CEM Discover SP Microwave Model 909150 / SN: DC 9208 apparatus. The A monowave 50 thermic reactor was from Anton Paar. Thin layer chromatography (TLC) was performed on silica gel 60 F254 plates (Merck). The compounds and the reaction mixtures were visualized on the TLC plates by irradiation with UV light.

For Flash Column Chromatography, a PuriFlash XS520Plus system was used with PF-30SIHP-JP-F0040 columns. When PE/A* is mentioned in the Experimental Part, A* stands for the mixture of solvents DCM/AcOEt (8:2).

¹H and ¹³C NMR spectra were recorded on a Bruker Avance I 300 MHz (300 MHz for ¹H and 75 MHz for ¹³C), or a Bruker Avance III Nanobay 400 MHz (400.0 MHz for ¹H and 101 MHz for ¹³C), or a Bruker Avance 600 MHz (600 MHz for ¹H and 151 MHz for ¹³C) equipped with a 5 mm triple resonance inverse Z-gradient probe (TBI ¹H, ³¹P, BB). NMR samples were prepared by dissolving 10-20 mg of each compound in 600 μL of CDCl₃ or DMSO-*d*₆. Chemical shifts (δ) for ¹H and ¹³C are relative to TMS as external standard, using ¹H (residual) or ¹³C chemical shifts of the solvent (δ = 7.26 ppm for CDCl₃ and 2.50 ppm for DMSO-*d*₆). Coupling constants (*J*) are given in Hz. All ¹H and ¹³C signals were assigned on the basis of chemical shifts, spin-spin coupling constants, splitting patterns, and signal intensities, by using ¹H-¹H COSY45, ¹H-¹³C HSQC, and ¹H-¹³C HMBC

experiments. Gradient-enhanced ^1H COSY45 was performed by including 8 scans per increment. ^1H - ^{13}C correlation spectra using a gradient-enhanced HSQC sequence (delay was optimised for $^1J_{\text{CH}}$ of 145 Hz) was obtained with 16 scans per increment. Gradient-enhanced HMBC experiment was performed allowing 62.5 ms for long-range coupling evolution (64 scans). Typically, 2048 t_2 data points were collected for 256 t_1 increments.

High resolution mass spectrometry (HRMS) analyses were carried out on an XevoG2QTof (Waters) using electrospray ionization (ESI).

The X-ray diffraction analysis of a single crystal was collected on a Bruker Kapa Apex II diffractometer equipped with a 30 W air-cooled microfocus source using MoK α radiation ($\lambda = 0.71073 \text{ \AA}$). The SHELXS-97 software was used to analyze the structure.

Melting points were determined using a Stuart SMP3 apparatus and the obtained values are not corrected. UV-visible spectra of selected compounds (CH_2Cl_2 solutions at 0.01 or 0.02 mg/mL) were recorded in solution, from 200 to 800 nm on a Cary 3500 spectrophotometer. Infrared spectra of selected compounds as powders, were measured using the Perkin Elmer Frontier MIR/FIR spectrometer.

2.5.2 Synthetic protocols

Microwave irradiation procedure

A suspension of lawsone (0.4 mmol) in 1,2-dichloroethane (7 mL) was charged with the corresponding aldehyde (0.4 mmol), isocyanide (0.4 mmol) and 10 mol% of EDDA. The reaction mixture was then stirred and irradiated (200 W, 7 bar) for 1-4 h at 160°C until completion of the reaction (monitored by TLC). The solvent was removed under vacuum and the residue was diluted in DCM. The organic phase was washed with 5 wt% NaHCO_3 aqueous solution, water and brine. The organic layer was dried over Na_2SO_4 , filtered, and evaporated under reduced pressure. The obtained products were then purified by flash column chromatography (FCC).

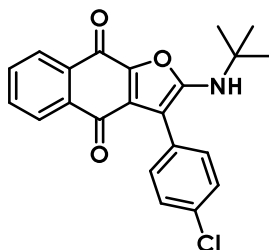
Conventional procedure

A mixture of lawsone (0.6 mmol) in toluene (10 mL) was charged with the corresponding aldehyde (0.6 mmol), isocyanide (0.6 mmol) and 10 mol% of EDDA. The resulting suspension was stirred under reflux overnight until completion of the reaction (monitored by TLC). The solvent was removed under vacuum evaporation and the residue was diluted in DCM. The organic phase was then washed with 5 wt% NaHCO_3 aqueous solution NaHCO_3 , water, and

brine. The organic layer was dried over Na₂SO₄, filtered, and evaporated under reduced pressure. The obtained crude products were then purified by FCC.

2.5.3 Compounds characterization

2-(*tert*-butylamino)-3-(4-chlorophenyl)naphtho[2,3-*b*]furan-4,9-dione (**2.69**)



The compound was synthesized by following the above-mentioned microwave procedure (0.23 mmol of lawsone). Reaction time 2 cycles x 60 min. Aldehyde conversion 70%. FCC with Hex/AcOEt (9:1) to yield 50 mg (59%) of product (violet solid, m.p. 237-239 °C).

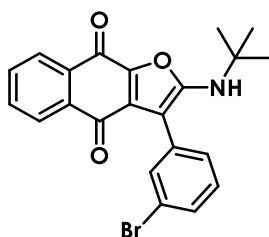
R_f (Hex/AcOEt 9:1) = 0.18.

¹H NMR (400 MHz, CDCl₃) δ 8.17 (dd, *J* = 7.6, 1.0 Hz, 1H), 8.02 (dd, *J* = 7.6, 1.0 Hz, 1H), 7.69 (td, *J* = 7.5, 1.3 Hz, 1H), 7.61 (td, *J* = 7.5, 1.3 Hz, 1H), 7.49 – 7.34 (m, 4H), 4.82 (s, 1H), 1.50 (s, 9H).

¹³C NMR (101 MHz, CDCl₃) δ 182.0 (C=O), 169.6 (C=O), 159.4 (C), 144.2 (C), 133.9 (CH), 133.7 (C), 133.4 (C), 133.3 (C), 132.5 (CH), 130.9 (2 x CH), 130.4 (C), 129.3 (2 x CH), 128.8 (C), 126.6 (CH), 126.3 (CH), 99.1 (C), 54.3 (C), 30.2 (3 x CH₃).

HRMS calculated for C₂₂H₁₉ClNO₃ + [M+H]⁺ = 380.1053 found 380.1058.

3-(3-bromophenyl)-2-(*tert*-butylamino)naphtho[2,3-*b*]furan-4,9-dione (**2.73**)



The compound was synthesized by following the above-mentioned microwave procedure (0.4 mmol of lawsone). Reaction time 4 cycles x 60 min. Aldehyde conversion 30%. FCC with cyclohex/AcOEt (9:1) to yield 50 mg (30%) of the product as a violet solid (m.p. 193-194 °C).

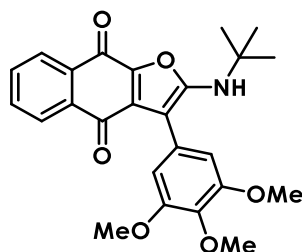
R_f (cyclohex/AcOEt 9:1) = 0.26.

^1H NMR (400 MHz, CDCl_3) δ 8.14 (dd, $J = 7.6, 0.9$ Hz, 1H), 8.01 (dd, $J = 7.6, 0.9$ Hz, 1H), 7.68 (td, $J = 7.5, 1.4$ Hz, 1H), 7.60 (dt, $J = 7.5, 1.4$ Hz, 2H), 7.46 (ddd, $J = 7.9, 1.9, 1.1$ Hz, 1H), 7.42 – 7.36 (m, 1H), 7.30 (t, $J = 7.9$ Hz, 1H), 4.86 (s, 1H), 1.50 (s, 9H).

^{13}C NMR (101 MHz, CDCl_3) δ 181.7 (C=O), 169.6 (C=O), 159.4 (C), 144.1 (C), 133.8 (CH), 133.2 (C), 132.5 (C), 132.4 (CH), 132.4 (CH), 130.8 (CH), 130.4 (CH), 130.3 (C), 128.1 (CH), 126.5 (CH), 126.2 (CH), 122.9 (C), 98.7 (C), 54.2 (C), 30.1 (3 x CH_3).

HRMS calculated for $\text{C}_{22}\text{H}_{19}\text{BrNO}_3 + [\text{M}+\text{H}]^+ = 424.0548$ found 424.0548.

2-(tert-butylamino)-3-(3,4,5-trimethoxyphenyl)naphtho[2,3-b]furan-4,9-dione (**2.74**)



The compound was synthesized by following the above-mentioned microwave procedure (0.3 mmol of lawsone). Reaction time 2 cycles x 60 min. Aldehyde conversion 60%. FCC with Hex/AcOEt (7:3) to yield 66 mg (55%) of the product as a violet solid (m.p. 218–220 °C).

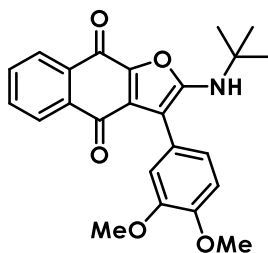
R_f (Hex/AcOEt 7:3) = 0.23.

^1H NMR (400 MHz, CDCl_3) δ 8.15 (dd, $J = 7.6, 1.0$ Hz, 1H), 8.02 (dd, $J = 7.6, 1.0$ Hz, 1H), 7.67 (td, $J = 7.5, 1.3$ Hz, 1H), 7.59 (td, $J = 7.5, 1.3$ Hz, 1H), 6.72 (s, 2H), 4.98 (s, 1H), 3.90 (s, 3H), 3.89 (s, 6H), 1.50 (s, 9H).

^{13}C NMR (101 MHz, CDCl_3) δ 181.9 (C=O), 169.4 (C=O), 159.6 (C), 153.6 (C), 144.0 (C), 137.7 (C), 133.8 (CH), 133.4 (2C), 132.3 (CH), 130.4 (C), 126.5 (CH), 126.1 (CH), 125.6 (C), 106.7 (CH), 100.5 (C), 61.0 (CH_3), 56.4 (2 x CH_3), 54.1 (C), 30.2 (3 x CH_3).

HRMS calculated for $\text{C}_{25}\text{H}_{26}\text{NO}_6 + [\text{M}+\text{H}]^+ = 436.1760$ found 436.1761.

2-(tert-butylamino)-3-(3,4-dimethoxyphenyl)naphtho[2,3-b]furan-4,9-dione (**2.75**)



The compound was synthesized by following the above-mentioned microwave general procedure (0.4 mmol of lawsone). Reaction time 2 cycles x 60 min. Aldehyde conversion 45%.

FCC with petroleum ether (PE)/AcOEt (8:2) to yield 35 mg (25%) of the product as a violet solid (m.p. 226-228 °C).

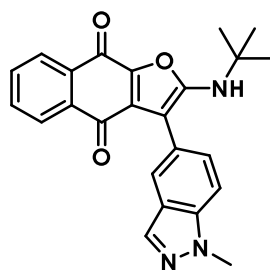
R_f (Hex/AcOEt 8:2) = 0.17.

¹H NMR (400 MHz, CDCl₃) δ 8.16 (dd, *J* = 7.6, 0.9 Hz, 1H), 8.03 (dd, *J* = 7.6, 0.9 Hz, 1H), 7.68 (td, *J* = 7.5, 1.4 Hz, 1H), 7.59 (td, *J* = 7.5, 1.4 Hz, 1H), 7.06 (d, *J* = 1.9 Hz, 1H), 7.03 – 6.92 (m, 2H), 4.93 (s, 1H), 3.93 (s, 6H), 1.49 (s, 9H).

¹³C NMR (101 MHz, CDCl₃) δ 182.0 (C=O), 169.3 (C=O), 159.7 (C), 149.3 (C), 148.8 (C), 143.9 (C), 133.8 (CH), 133.5 (C), 133.4 (C), 132.3 (CH), 130.6 (C), 126.5 (CH), 126.2 (CH), 122.7 (C), 121.5 (CH), 113.3 (CH), 111.6 (CH), 100.6 (C), 56.2 (CH₃), 56.1 (CH₃), 54.1 (C), 30.2 (3 x CH₃).

HRMS calculated for C₂₄H₂₄NO₅ + [M+H]⁺ = 406.1654 found 406.1655.

2-(tert-butylamino)-3-(1-methyl-1H-indazol-5-yl)naphtho[2,3-b]furan-4,9-dione (**2.76**)



The compound was synthesized by following the above-mentioned alternative conventional procedure (0.5 mmol of lawsone). Reaction time 48 h. Aldehyde conversion 30%. FCC with PE/A* (5:5) and then PE/A* (4:6) to yield 60 mg (30%) of the product as a blue-violet solid (m.p. 219-221 °C).

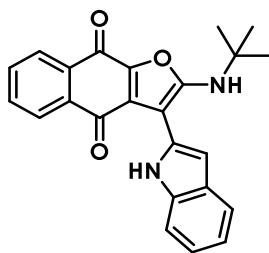
R_f (PE/A 4:6) = 0.32.

¹H NMR (400 MHz, CDCl₃) δ 8.13 (dd, *J* = 7.6, 1.1 Hz, 1H), 7.99 – 7.90 (m, 2H), 7.75 (d, *J* = 0.8 Hz, 1H), 7.66 (td, *J* = 7.5, 1.3 Hz, 1H), 7.56 (td, *J* = 7.5, 1.3 Hz, 1H), 7.49 – 7.40 (m, 2H), 5.11 (s, 1H), 4.04 (s, 3H), 1.50 (s, 9H).

¹³C NMR (101 MHz, CDCl₃) δ 182.0 (C=O), 169.0 (C=O), 159.8 (C), 143.8 (C), 139.3 (C), 133.7 (CH), 133.5 (C), 133.3 (C), 132.9 (CH), 132.2 (CH), 130.8 (C), 128.6 (CH), 126.4 (CH), 126.1 (CH), 124.3 (C), 122.3 (C), 121.6 (CH), 109.4 (CH), 100.7 (C), 54.1 (C), 35.6 (CH₃), 30.1 (3 x CH₃).

HRMS calculated for C₂₄H₂₂N₃O₃ + [M+H]⁺ = 400.1661 found 400.1659.

2-(*tert*-butylamino)-3-(1*H*-indol-2-yl)naphtho[2,3-*b*]furan-4,9-dione (**2.77**)



The compound was synthesized by following the above-mentioned microwave procedure (0.4 mmol of lawsone). Reaction time 2 cycles x 60 min. Aldehyde conversion 80%. FCC with cyclohexane/AcOEt (9:1) to yield 50 mg (35%) of the product as a blue solid (m.p. 219-220 °C).

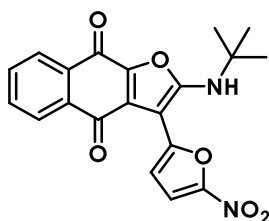
R_f (cyclohexane/AcOEt 9:1) = 0.24.

¹H NMR (400 MHz, CDCl₃) δ 11.37 (s, 1H), 8.14 (dd, *J* = 7.6, 1.3 Hz, 2H), 7.70 (td, *J* = 7.5, 1.4 Hz, 1H), 7.63 (td, *J* = 7.5, 1.4 Hz, 1H), 7.55 (d, *J* = 7.8 Hz, 1H), 7.50 (dd, *J* = 8.1, 0.6 Hz, 1H), 7.24 – 7.18 (m, 1H), 7.13 – 7.06 (m, 1H), 6.40 (d, *J* = 1.4 Hz, 1H), 5.46 (s, 1H), 1.63 (s, 9H).

¹³C NMR (101 MHz, CDCl₃) δ 183.6 (C=O), 168.9 (C=O), 159.4 (C), 143.7 (C), 135.4 (C), 134.4 (CH), 133.2 (C), 132.9 (C), 132.4 (CH), 129.5 (C), 128.8 (C), 128.6 (C), 127.1 (CH), 126.2 (CH), 122.5 (CH), 120.3 (CH), 119.8 (CH), 111.4 (CH), 97.5 (CH), 93.5 (C), 54.7 (C), 30.1 (3 x CH₃).

HRMS calculated for C₂₄H₂₁N₂O₃ + [M+H]⁺ = 385.1552 found 385.1553.

2-(*tert*-butylamino)-3-(5-nitrofuran-2-yl)naphtho[2,3-*b*]furan-4,9-dione (**2.78**)



The compound was synthesized by following the above-mentioned microwave procedure (0.4 mmol of lawsone). Reaction time 2 cycles x 60 min. Aldehyde conversion 20%. FCC with PE/DCM (4:6) to yield 45 mg (19%) of the product as a purple solid (m.p. 274-276 °C).

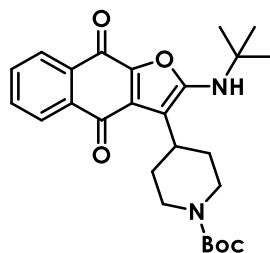
R_f (PE/DCM 3:7) = 0.21.

¹H NMR (400 MHz, CDCl₃) δ 8.16 (dd, *J* = 14.5, 7.2 Hz, 2H), 7.77 – 7.64 (m, 3H), 7.48 (d, *J* = 3.9 Hz, 1H), 6.97 (s, 1H), 1.63 (s, 9H).

¹³C NMR (151 MHz, DMSO-*d*₆, 100 °C) δ 180.0 (C=O), 168.7 (C=O), 159.6 (C), 149.8 (C), 143.4 (C), 133.7 (CH), 132.5 (CH), 132.1 (C), 131.8 (C), 127.6 (C), 125.9 (CH), 125.1 (CH), 123.5 (C), 114.7 (CH), 110.8 (CH), 87.4 (C), 54.0 (C), 28.8 (3 x CH₃).

HRMS calculated for $C_{20}H_{17}N_2O_6$ + $[M+H]^+$ = 381.1087 found 381.1090.

tert-butyl 4-(2-(*tert*-butylamino)-4,9-dioxo-4,9-dihydronaphtho[2,3-*b*]furan-3-yl)piperidine-1-carboxylate (**2.79**)



The compound was synthesized by following the above-mentioned microwave procedure (0.4 mmol of lawsone). Reaction time 2 cycles x 60 min. Aldehyde conversion 95%. FCC with PE/AcOEt (8:2) to yield 95 mg (52%) of the product as a violet oil.

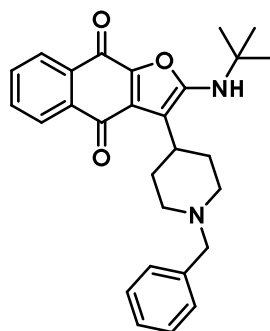
R_f (PE/AcOEt 8:2) = 0.22.

1H NMR (400 MHz, $CDCl_3$) δ 8.15 – 8.09 (m, 1H), 8.04 (d, J = 8.8 Hz, 1H), 7.67 (td, J = 7.5, 1.5 Hz, 1H), 7.61 (td, J = 7.5, 1.5 Hz, 1H), 4.24 (s, 2H), 2.99 (tt, J = 12.4, 3.6 Hz, 1H), 2.80 (t, J = 11.9 Hz, 2H), 1.95 (qd, J = 12.7, 4.3 Hz, 2H), 1.68 – 1.61 (m, 2H), 1.50 (s, 9H), 1.46 (s, 9H).

^{13}C NMR (101 MHz, $CDCl_3$) δ 182.6 (C=O), 169.7 (C=O), 158.5 (C), 155.1 (C), 144.5 (C), 133.7 (CH), 133.3 (C), 133.2 (C), 132.4 (CH), 131.3 (C), 126.5 (CH), 126.1 (CH), 105.2 (C), 79.7 (C), 60.5 (C), 54.3 (C), 32.5 (2 x CH_2), 30.4 (3 x CH_3), 30.2 (2 x CH_2), 28.6 (3 x CH_3).

HRMS calculated for $C_{26}H_{33}N_2O_5$ + $[M+H]^+$ = 453.2389 found 453.2383.

3-(1-benzylpiperidin-4-yl)-2-(*tert*-butylamino)naphtho[2,3-*b*]furan-4,9-dione (**2.80**)



The compound was synthesized by following the above-mentioned microwave procedure (0.3 mmol of lawsone). Reaction time 1 cycle x 60 min. Aldehyde conversion 91%. FCC with DCM/MeOH/ Et_3N (98:2:1) to yield 70 mg (53%) of the product as a violet solid (m.p. 168-170 °C).

R_f (DCM/MeOH/ Et_3N 98:2:1) = 0.35.

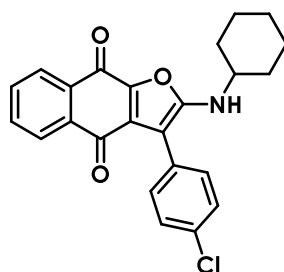
^1H NMR (400 MHz, CDCl_3) δ 8.15 (dd, $J = 7.6, 1.0$ Hz, 1H), 8.07 (dd, $J = 7.6, 1.0$ Hz, 1H), 7.68 (td, $J = 7.5, 1.4$ Hz, 1H), 7.62 (td, $J = 7.5, 1.4$ Hz, 1H), 7.43 – 7.29 (m, 5H), 4.64 (s, 1H), 3.62 (s, 2H), 3.05 (d, $J = 10.2$ Hz, 3H), 2.18 – 2.07 (m, 4H), 1.72 (d, $J = 12.6$ Hz, 2H), 1.47 (s, 9H).

^{13}C NMR (101 MHz, CDCl_3) δ 184.1 (C=O), 183.0 (C=O), 169.2 (C), 158.9 (C), 133.7 (CH), 133.6 (C), 133.3 (C), 132.2 (CH), 131.5 (C), 129.5 (CH), 128.4 (2 x CH), 127.3 (CH), 126.4 (2 x CH), 126.1 (CH), 63.4 (CH_2), 54.3 (C), 54.2 (2 x CH_2), 32.0 (2 x CH_2), 30.4 (3 x CH_3), 29.8 (CH).

IR (cm^{-1}): 1183 (C-O), 1201 (C-N), 1396 and 1460 (CH_3), 1532 (ArH), 1558 (ArH), 1560 (ArH), 1631 (C=O), 1634 (ArH), 1672 (C=O), 3316 (N-H).

HRMS calculated for $\text{C}_{28}\text{H}_{31}\text{N}_2\text{O}_3 + [\text{M}+\text{H}]^+ = 443.2335$ found 443.2333.

3-(4-chlorophenyl)-2-(cyclohexylamino)naphtho[2,3-b]furan-4,9-dione (**2.81**)



The compound was synthesized by following the above-mentioned microwave procedure (0.4 mmol of lawsone). Reaction time 2 cycles x 60 min. Aldehyde conversion 50%. FCC with PE/AcOEt (9:1) to yield 74 mg (46%) of the product as a violet solid (m.p. 187-189 °C).

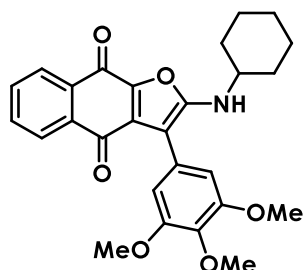
R_f (PE/AcOEt 9:1) = 0.33.

^1H NMR (400 MHz, CDCl_3) δ 8.16 (dd, $J = 7.6, 1.0$ Hz, 1H), 8.01 (dd, $J = 7.6, 1.0$ Hz, 1H), 7.68 (td, $J = 7.5, 1.3$ Hz, 1H), 7.60 (td, $J = 7.5, 1.3$ Hz, 1H), 7.47 – 7.33 (m, 4H), 4.82 (d, $J = 8.3$ Hz, 1H), 3.82 (ddd, $J = 10.3, 8.2, 4.0$ Hz, 1H), 2.13 – 2.01 (m, 2H), 1.82 – 1.70 (m, 2H), 1.70 – 1.59 (m, 2H), 1.42 (tt, $J = 18.3, 4.7$ Hz, 2H), 1.32 – 1.17 (m, 2H).

^{13}C NMR (101 MHz, CDCl_3) δ 182.0 (C=O), 169.5 (C=O), 159.1 (C), 143.5 (C), 133.9 (CH), 133.6 (C), 133.4 (C), 133.2 (C), 132.4 (C), 131.1 (C), 130.8 (2 x CH), 129.2 (2 x CH), 128.7 (C), 126.6 (CH), 126.3 (CH), 97.6 (C), 52.5 (CH), 34.0 (2 x CH_2), 25.4 (CH_2), 24.8 (2 x CH_2).

HRMS calculated for $\text{C}_{24}\text{H}_{21}\text{ClNO}_3 + [\text{M}+\text{H}]^+ = 406.1210$ found 406.1206.

2-(cyclohexylamino)-3-(3,4,5-trimethoxyphenyl)naphtho[2,3-b]furan-4,9-dione (**2.82**)



The compound was synthesized by following the above-mentioned microwave procedure (0.4 mmol of lawsone). Reaction time 2 cycles x 60 min. Aldehyde conversion 45%. The crude product was purified by FCC with cyclohex/AcOEt (8:2) to yield 77 mg (42%) of the product as a blue solid (m.p. 163-165 °C).

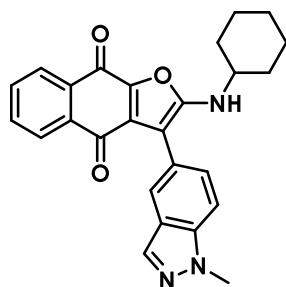
R_f (cyclohex/AcOEt 8:2) = 0.25.

¹H NMR (400 MHz, CDCl₃) δ 8.15 (dd, *J* = 7.6, 1.0 Hz, 1H), 8.02 (dd, *J* = 7.6, 1.0 Hz, 1H), 7.68 (td, *J* = 7.5, 1.3 Hz, 1H), 7.59 (td, *J* = 7.5, 1.3 Hz, 1H), 6.73 (s, 2H), 4.94 (d, *J* = 8.5 Hz, 1H), 3.90 (s, 3H), 3.89 (s, 6H), 2.08 (dd, *J* = 12.1, 3.0 Hz, 2H), 1.80 – 1.70 (m, 2H), 1.69 – 1.59 (m, 1H), 1.50 – 1.36 (m, 2H), 1.33 – 1.12 (m, 4H).

¹³C NMR (101 MHz, CDCl₃) δ 182.0 (C=O), 169.3 (C=O), 159.3 (2C), 153.6 (C), 143.3 (C), 137.7 (C), 133.8 (CH), 133.4 (C), 133.3 (C), 132.3 (CH), 131.1 (C), 126.5 (CH), 126.2 (CH), 125.5 (C), 106.8 (2 x CH), 99.0 (C), 61.0 (CH₃), 56.4 (2 x CH₃), 52.4 (CH), 34.0 (2 x CH₂), 25.4 (CH₂), 24.8 (2 x CH₂).

HRMS calculated for C₂₇H₂₈NO₆ + [M+H]⁺ = 462.1917 found 462.1917.

2-(cyclohexylamino)-3-(1-methyl-1H-indazol-5-yl)naphtho[2,3-b]furan-4,9-dione (**2.83**)



The compound was synthesized by following the above-mentioned alternative conventional procedure (0.5 mmol of lawsone). Reaction time 24 h. Aldehyde conversion 40%. The crude product was purified by FCC with PE/A* (5:5) and then PE/A* (4:6) to yield 85 mg (40%) of the product as a blue-violet solid (m.p. 158-160 °C).

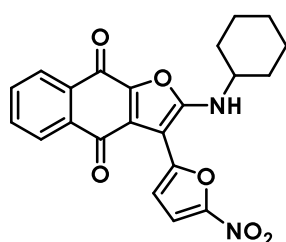
R_f (PE/A 5:5) = 0.13.

^1H NMR (400 MHz, CDCl_3) δ 8.15 (dd, $J = 7.6, 0.9$ Hz, 1H), 8.01 – 7.93 (m, 2H), 7.76 (s, 1H), 7.67 (td, $J = 7.5, 1.3$ Hz, 1H), 7.58 (td, $J = 7.5, 1.3$ Hz, 1H), 7.48 (dt, $J = 17.5, 5.1$ Hz, 2H), 5.09 (d, $J = 8.4$ Hz, 1H), 4.06 (s, 3H), 3.93 – 3.78 (m, 1H), 2.13 – 2.00 (m, 2H), 1.83 – 1.69 (m, 4H), 1.32 – 1.07 (m, 4H).

^{13}C NMR (101 MHz, CDCl_3) δ 182.1 (C=O), 169.0 (C=O), 159.5 (C), 143.1 (C), 139.3 (C), 133.8 (CH), 133.6 (C), 133.2 (C), 132.9 (CH), 132.2 (CH), 131.5 (C), 128.7 (CH), 126.4 (CH), 126.2 (CH), 124.3 (C), 122.3 (C), 121.6 (CH), 109.4 (CH), 99.2 (C), 52.5 (CH), 35.7 (CH_3), 34.0 (2 x CH_2), 25.4 (CH_2), 24.9 (2 x CH_2).

HRMS calculated for $\text{C}_{26}\text{H}_{24}\text{N}_3\text{O}_3$ + $[\text{M}+\text{H}]^+ = 426.1818$ found 426.1809.

2-(cyclohexylamino)-3-(5-nitrofuran-2-yl)naphtho[2,3-b]furan-4,9-dione **(2.84)**



The compound was synthesized by following the above-mentioned microwave procedure (0.4 mmol of lawsone). Reaction time 2 cycles x 60 min. Aldehyde conversion 54%. FCC with PE/DCM (2:8) to yield 25 mg (12%) of the product as a purple solid (m.p. 163-165 °C).

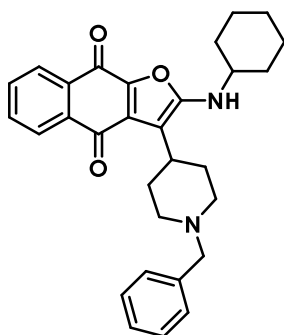
R_f (PE/AcOEt 3:7) = 0.21.

^1H NMR (400 MHz, CDCl_3) δ 8.20 (d, $J = 3.8$ Hz, 1H), 8.18 – 8.12 (m, 1H), 7.78 – 7.67 (m, 2H), 7.49 (d, $J = 4.0$ Hz, 1H), 7.38 (d, $J = 3.8$ Hz, 1H), 7.07 (d, $J = 4.5$ Hz, 1H), 3.81 (dddd, $J = 14.5, 10.5, 8.3, 4.0$ Hz, 1H), 2.01 – 1.91 (m, 2H), 1.88 – 1.74 (m, 4H), 1.72 – 1.61 (m, 2H), 1.54 (dd, $J = 13.7, 6.0$ Hz, 2H).

^{13}C NMR (151 MHz, DMSO-d_6 , 100 °C) δ 180.1 (C=O), 175.8 (C=O), 159.4 (C), 149.6 (C), 147.9 (C), 142.7 (C), 137.9 (C), 133.7 (CH), 132.5 (CH), 132.1 (C), 125.1 (CH), 125.8 (CH), 125.1 (CH), 114.7 (CH), 111.0 (CH), 85.9 (C), 52.7 (CH), 31.8 (2 x CH_2), 24.5 (CH_2), 23.2 (2 x CH_2).

HRMS calculated for $\text{C}_{22}\text{H}_{19}\text{N}_2\text{O}_6$ + $[\text{M}+\text{H}]^+ = 407.1243$ found 407.1243.

3-(1-benzylpiperidin-4-yl)-2-(cyclohexylamino)naphtho[2,3-b]furan-4,9-dione (**2.85**)



The compound was synthesized by following the above-mentioned microwave procedure (0.4 mmol of lawsone). Reaction time 2 cycles x 60 min. Aldehyde conversion 60%. FCC with DCM/MeOH (98:2) and then DCM/MeOH (95:5) to yield 84 mg (45%) of the product as a blue-violet solid (m.p. 221-223 °C).

R_f (DCM/MeOH 98:2) = 0.11.

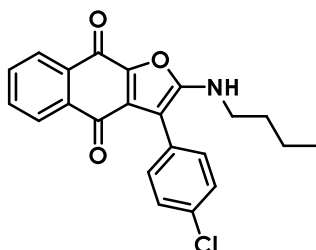
¹H NMR (400 MHz, CDCl₃) δ 8.12 (dd, *J* = 7.6, 1.0 Hz, 1H), 8.02 (dd, *J* = 7.6, 1.0 Hz, 1H), 7.65 (td, *J* = 7.5, 1.4 Hz, 1H), 7.57 (td, *J* = 7.5, 1.4 Hz, 1H), 7.37 – 7.26 (m, 5H), 5.27 – 5.16 (m, 1H), 3.87 – 3.72 (m, 1H), 3.56 (s, 2H), 3.31 – 3.18 (m, 1H), 3.02 (d, *J* = 11.1 Hz, 2H), 2.15 (dd, *J* = 15.0, 7.3 Hz, 2H), 2.08 – 1.92 (m, 4H), 1.80 – 1.59 (m, 4H), 1.48 – 1.35 (m, 2H), 1.34 – 1.11 (m, H).

¹³C NMR (101 MHz, CDCl₃) δ 183.4 (C=O), 168.4 (C=O), 159.1 (C), 142.5 (C), 137.7 (C), 133.8 (C), 133.8 (CH), 133.2 (C), 132.3 (C), 131.9 (CH), 129.6 (2 x CH), 128.4 (2 x CH), 127.4 (CH), 126.3 (CH), 126.1 (CH), 102.5 (C), 63.5 (2 x CH₂), 54.1 (CH₂), 52.9 (CH), 34.1 (2 x CH₂), 30.8 (CH), 29.7 (2 x CH₂), 25.5 (CH₂), 25.0 (2 x CH₂).

IR (cm⁻¹): 1098 (C-O), 1220 (C-N), 1453 (CH₂), 1468 (CH₂), 1528 (ArH), 1562 (ArH), 1579 (ArH), 1637 (C=O), 1638 (ArH), 1675 (C=O), 3277 (N-H).

HRMS calculated for C₃₀H₃₃N₂O₃ + [M+H]⁺ = 469.2491 found 469.2486.

2-(butylamino)-3-(4-chlorophenyl)naphtho[2,3-b]furan-4,9-dione (**2.86**)



The compound was synthesized by following the above-mentioned microwave procedure (0.4 mmol of lawsone). Reaction time 3 cycles x 60 min. Aldehyde conversion 55%. FCC with Hex/AcOEt (85:15) to yield 84 mg (55%) of the product as a violet solid (m.p. 167-169 °C).

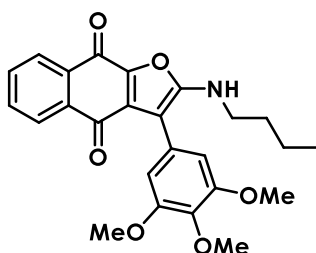
R_f (Hex/AcOEt 8:2) = 0.30.

¹H NMR (400 MHz, CDCl₃) δ 8.18 – 8.14 (m, 1H), 8.02 (d, J = 8.6 Hz, 1H), 7.69 (td, J = 7.5, 1.4 Hz, 1H), 7.61 (td, J = 7.5, 1.4 Hz, 1H), 7.42 (s, 4H), 4.93 (t, J = 5.9 Hz, 1H), 3.52 (td, J = 7.1, 6.1 Hz, 2H), 1.73 – 1.52 (m, 3H), 1.46 – 1.37 (m, 2H), 0.96 (t, J = 7.3 Hz, 3H).

¹³C NMR (101 MHz, CDCl₃) δ 182.00 (C=O), 169.6 (C=O), 159.7 (C), 143.4 (C), 133.9 (CH), 133.6 (C), 133.3 (C), 133.2 (C), 132.5 (CH), 131.1 (C), 130.8 (2 x CH), 129.2 (2 x CH), 128.7 (C), 126.6 (CH), 126.3 (CH), 97.4 (C), 43.3 (CH₂), 32.3 (CH₂), 20.1 (CH₂), 13.9 (CH₃).

HRMS calculated for C₂₂H₁₉ClNO₃ + [M+H]⁺ = 380.1053 found 380.1061.

2-(butylamino)-3-(3,4,5-trimethoxyphenyl)naphtho[2,3-b]furan-4,9-dione (**2.87**)



The compound was synthesized by following the above-mentioned microwave procedure (0.4 mmol of lawsone). Reaction time 4 cycles x 60 min. Aldehyde conversion 45%. FCC with Hex/AcOEt (7:3) to yield 69 mg (40%) of the product as a dark blue oil.

R_f (Hex/AcOEt 7:3) = 0.21.

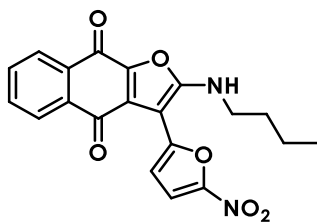
¹H NMR (400 MHz, CDCl₃) δ 8.16 (dd, J = 7.6, 0.9 Hz, 1H), 8.03 (dd, J = 7.6, 0.9 Hz, 1H), 7.68 (td, J = 7.5, 1.4 Hz, 1H), 7.60 (td, J = 7.5, 1.4 Hz, 1H), 6.73 (s, 2H), 5.05 (t, J = 5.9 Hz, 1H), 3.91 (s, 3H), 3.90 (s, 6H), 3.52 (dd, J = 13.2, 7.0 Hz, 2H), 1.64 (dt, J = 19.8, 7.5 Hz, 2H), 1.41 (dq, J = 14.6, 7.4 Hz, 2H), 0.96 (t, J = 7.4 Hz, 3H).

¹³C NMR (101 MHz, CDCl₃) δ 182.0 (C=O), 169.4 (C=O), 160.0 (C), 153.6 (2 x C), 143.3 (C), 137.7 (C), 133.8 (CH), 133.4 (C), 133.3 (C), 132.3 (CH), 131.2 (C), 126.6 (CH), 126.2 (CH), 125.5 (C), 106.8 (2 x CH), 98.8 (C), 61.0 (CH₃), 56.4 (2 x CH₃), 43.2 (CH₂), 32.3 (CH₂), 20.1 (CH₂), 13.8 (CH₃).

IR (cm⁻¹): 1124 (C-O), 1412 (CH₂), 1355 and 1454 (CH₃), 1539 (ArH), 1584 (C=O), 1600 (C=O), 3323 (N-H).

HRMS calculated for C₂₅H₂₆NO₆ + [M+H]⁺ = 436.1760 found 436.1759.

2-(butylamino)-3-(5-nitrofuran-2-yl)naphtho[2,3-b]furan-4,9-dione (**2.89**)



The compound was synthesized by following the above-mentioned microwave procedure (0.4 mmol of lawsone). Reaction time 2 cycles x 60 min. Aldehyde conversion 10%. FCC with PE/DCM (3:7) to yield 16 mg (8%) of the product as a purple oil.

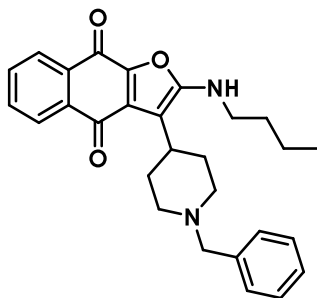
R_f (PE/DCM 3:7) = 0.12.

¹H NMR (400 MHz, CDCl₃) δ 8.20 – 8.09 (m, 2H), 7.72 (dq, J = 14.5, 7.5, 1.1 Hz, 3H), 7.48 (d, J = 4.0 Hz, 1H), 6.76 (t, J = 6.6 Hz, 1H), 3.72 (dd, J = 12.9, 6.9 Hz, 2H), 1.85 – 1.72 (m, 2H), 1.42 – 1.29 (m, 2H), 1.03 (t, J = 7.3 Hz, 3H).

¹³C NMR (151 MHz, DMSO-d₆, 100 °C) δ 180.1 (C=O), 168.5 (C=O), 160.2 (C), 149.6 (C), 142.5 (C), 133.7 (CH), 132.4 (CH), 132.1 (C), 131.9 (C), 128.6 (C), 125.8 (CH), 125.1 (CH), 124.0 (C), 114.8 (CH), 111.1 (CH), 85.6 (C), 42.2 (CH₂), 30.7 (CH₂), 18.8 (CH₂), 12.9 (CH₃).

HRMS calculated for C₂₀H₁₅N₂O₆⁻ [M-H]⁻ = 379.0930 found 379.0923.

3-(1-benzylpiperidin-4-yl)-2-(butylamino)naphtho[2,3-b]furan-4,9-dione (**2.90**)



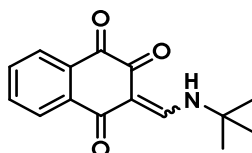
The compound was synthesized by following the above-mentioned microwave procedure (0.4 mmol of lawsone). Reaction time 2 cycles x 60 min. Aldehyde conversion 35%. FCC with DCM/MeOH (99:1) and then DCM/MeOH (97:3) to yield 45 mg (30%) of the product as a blue-violet oil. R_f (DCM/MeOH 97:3) = 0.22.

¹H NMR (300 MHz, CDCl₃) δ 8.15 – 8.09 (m, 1H), 8.03 (dd, J = 7.5, 1.2 Hz, 1H), 7.66 (td, J = 7.5, 1.5 Hz, 1H), 7.58 (td, J = 7.5, 1.5 Hz, 1H), 7.37 – 7.27 (m, 5H), 5.08 (s, 1H), 3.57 (s, 2H), 3.49 (dd, J = 13.1, 7.0 Hz, 2H), 3.23 (tt, J = 12.2, 3.9 Hz, 1H), 3.02 (d, J = 11.3 Hz, 2H), 2.14 (t, J = 10.9 Hz, 2H), 1.97 (qd, J = 12.4, 3.2 Hz, 2H), 1.79 – 1.67 (m, 2H), 1.67 – 1.57 (m, 2H), 1.41 (dq, J = 14.4, 7.3 Hz, 2H), 0.96 (t, J = 7.3 Hz, 3H).

^{13}C NMR (101 MHz, CDCl_3) δ 183.4 (C=O), 168.4 (C=O), 159.7 (C), 142.5 (C), 137.8 (C), 133.8 (C), 133.8 (CH), 133.2 (C), 132.3 (C), 132.0 (CH), 129.6 (2 x CH), 128.4 (2 x CH), 127.4 (CH), 126.3 (CH), 126.1 (CH), 102.2 (C), 63.5 (CH_2), 54.1 (2 x CH_2), 43.6 (2 x CH_2), 32.4 (CH_2), 30.9 (CH_2), 30.0 (CH), 20.1 (CH_2), 13.9 (CH_3).

HRMS calculated for $\text{C}_{28}\text{H}_{31}\text{N}_2\text{O}_3$ + $[\text{M}+\text{H}]^+$ = 443.2335 found 443.2334.

3-((*tert*-butylamino)methylene)naphthalene-1,2,4(3H)-trione (**2.91**)



The compound was synthesized by following the above-mentioned microwave procedure (0.4 mmol of lawsone). Reaction time 2 cycles x 60 min. Aldehyde conversion 30%. FCC with Hex/AcOEt (7:3) and then Hex/AcOEt (1:1) to yield 40 mg (40 %) of the product as a yellow solid (m.p. 169 °C decomposition).

R_f (Hex/AcOEt 1:1) = 0.42.

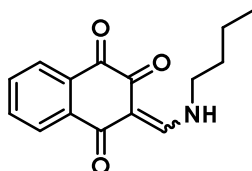
^1H NMR (300 MHz, CDCl_3) δ 12.17 (s, 1H), 12.04 (s, 1H), 8.65 (d, J = 14.9 Hz, 1H), 8.54 (d, J = 15.0 Hz, 1H), 8.29 – 8.21 (m, 1H), 8.16 (ddt, J = 7.2, 2.8, 1.4 Hz, 1H), 7.77 (td, J = 7.6, 1.5 Hz, 1H), 7.68 (tdd, J = 7.6, 6.2, 1.5 Hz, 1H), 1.49 (s, 9H).

^{13}C NMR (75 MHz, CDCl_3) δ 181.7 (C=O), 181.6 (C=O), 177.7 (C=O), 157.7 (CH), 157.2 (CH), 135.1 (CH), 134.9 (CH), 134.2 (C), 133.1 (CH), 133.0 (CH), 132.9 (C), 128.1 (CH), 127.6 (CH), 127.1 (CH), 126.6 (CH), 109.6 (C), 109.0 (C), 56.1 (C), 56.0 (C), 29.6 (3 x CH_3).

IR (cm^{-1}): 1348 and 1428 (CH_3), 1561 (ArH), 1562 (ArH), 1594 (C=O), 1611 (C=O), 1659 (C=O), 1668 (ArH).

HRMS calculated for $\text{C}_{15}\text{H}_{16}\text{NO}_3$ + $[\text{M}+\text{H}]^+$ = 258.1130 found 258.1132.

3-((butylamino)methylene)naphthalene-1,2,4(3H)-trione (**2.92**)



The compound was synthesized by following the above-mentioned alternative procedure (0.5 mmol of lawsone). Reaction time 24 h. Aldehyde conversion 22%. FCC with PE/A* (5:5) and then PE/A* (4:6) to yield 129 mg (50%) of the product as a yellow solid (m.p. 159 °C, decomposition).

R_f (PE/A 4:6) = 0.20.

¹H NMR (400 MHz, CDCl₃) δ 11.72 (s, 1H), 11.58 (s, 1H), 8.54 (d, J = 14.5 Hz, 1H), 8.42 (d, J = 14.5 Hz, 1H), 8.20 (d, J = 7.7 Hz, 1H), 8.15 – 8.08 (m, 1H), 7.75 (t, J = 7.5 Hz, 1H), 7.67 (t, J = 7.5 Hz, 1H), 3.58 (dq, J = 13.8, 6.7 Hz, 2H), 1.78 – 1.64 (m, 2H), 1.42 (dq, J = 14.7, 7.4 Hz, 2H), 0.95 (td, J = 7.2, 2.6 Hz, 3H).

¹³C NMR (75 MHz, CDCl₃) δ 181.6 (C=O), 181.5 (C=O), 177.8 (C=O), 162.0 (CH), 161.5 (CH), 135.1 (CH), 134.9 (CH), 134.1 (C), 133.2 (CH), 133.1 (CH), 132.8 (C), 128.1 (CH), 127.7 (CH), 127.2 (CH), 126.7 (CH), 109.8 (C), 109.2 (C), 51.1 (CH₂), 32.1 (CH₂), 19.7 (CH₂), 13.6 (CH₃).

HRMS calculated for C₁₅H₁₆NO₃ + [M+H]⁺ = 258.1130 found 258.1134.

2.5.4 Computational and docking experiments

The AlphaFold2 predicted structure of the protein bc1 of *Plasmodium falciparum* was downloaded from the European Bioinformatics Institute website and preprocessed with PrepWizard [Schrödinger LLC. 2021] to add hydrogens, minimize structure, and resolve ionization states and clashes. The binding site was specified in analogy to structure 4pd4 from the PDB.

The X-ray crystal protein structure (7I01, Resolution = 1.60 Å) for *Pf* DHOHD was downloaded from PDB and preprocessed with PrepWiz [Schrödinger LLC. 2021] both with and without water molecules. Co-factors (flavin mononucleotide (FMN) and orotic acid (ORO)) were kept in the structure. The co-crystallized natural ligand DSM782 (N-(1-(5-cyano-1H-pyrazol-3-yl)ethyl)-3-methyl-4-(1-(6-(trifluoromethyl)pyridin-3-yl)cyclopropyl)-1H-pyrrole-2-carboxamide, XCV) was also extracted and re-docked (self-dock) for comparison and used as positive control.

All compounds were imported as SMILES or drawn; energy minimized with Maestro [Schrödinger LLC. 2021], and then processed with LigPrep [Schrödinger LLC. 2021] for assigning tautomers, and ionization states around pH 7 +/- 2. The synthesized compounds and known inhibitors were used as controls. Molecules were docked into the binding site of bc1 using Glide XP [Schrödinger LLC. 2021], including aromatic hydrogens as donors, halogen acceptors, and other settings.

The input file is provided below:

FORCEFIELD OPLS_2005

GRID_CENTER -1.9900714545454548, 7.686090977272727, 9.326240250000001

GRIDFILE glide-grid_AF-Q7_2.zip

HBOND_ACCEP_HALO True

HBOND_DONOR_AROMH True

INNERBOX 12, 12, 12

OUTERBOX 29.189783718905936, 29.189783718905936, 29.189783718905936

RECEP_FILE glide-grid_AF-Q7_2.maegz

Molecules were also docked into the binding site of DHODH, as defined by the co-crystallized ligand inhibitor XCV, in several runs using both the crystallographic waters as well as without them.

The input file is provided below:

EPIK_PENALTIES False

EXPANDED_SAMPLING True

FORCEFIELD OPLS_2005

GRIDFILE glide-grid_4_nowats.zip

HBOND_ACCEP_HALO True

HBOND_DONOR_AROMH True

INCLUDE_INPUT_RINGS True

LIGANDFILE todock.sdf

POSTDOCK_XP_DELE 0.5

PRECISION XP

WRITE_XP_DESC False

2.6 References

1. J. W. Mathieson and R. H. Thomson, Naturally occurring quinones. Part XVIII. New spinochromes from *Diadema antillarum*, *Spatangus purpureus*, and *Temnopleurus toreumaticus*, *J. Chem. Soc., C*, **1971**, p. 153-160, doi: [10.1039/j39710000153](https://doi.org/10.1039/j39710000153).
2. V. E. Tyler, *The new honest herbal: A sensible guide to the use of herbs and related remedies*, **1988**, 2nd ed. Philadelphia, Pa: Stickley.
3. J. Steinert, H. Khalaf, and M. Rimpler, HPLC separation and determination of naphtho[2,3-b]furan-4,9-diones and related compounds in extracts of *Tabebuia avellanedae* (Bignoniaceae), *J. Chromatogr. A*, **1995**, vol. 693, no. 2, pp. 281–287, doi: [10.1016/0021-9673\(94\)01128-2](https://doi.org/10.1016/0021-9673(94)01128-2).
4. W. S. Jang *et al.* Naphthofuroquinone derivatives show strong antimycobacterial activities against drug-resistant *Mycobacteria*, *J. Chemother.*, **2017**, vol. 29, no. 6, pp. 338–343, doi: [10.1080/1120009X.2017.1296987](https://doi.org/10.1080/1120009X.2017.1296987).
5. S.-C. Yang *et al.*, Naphtho[1,2-b]furan-4,5-dione is a potent anti-MRSA agent against planktonic, biofilm and intracellular bacteria, *Future Microbiol.*, **2017**, vol. 12, no. 12, pp. 1059–1073, doi: [10.2217/fmb-2017-0044](https://doi.org/10.2217/fmb-2017-0044).
6. A. Takano *et al.*, Tumor-specific cytotoxicity and type of cell death induced by naphtho[2,3-b]furan-4,9-diones and related compounds in human tumor cell Lines: relationship to electronic structure, *Anticancer Res.*, **2009**, vol. 29, pp. 455–464.
7. A. Prateep *et al.*, Avicequinone B sensitizes anoikis in human lung cancer cells, *J. Biomed. Sci.*, **2018**, vol. 25, article no. 32, doi: [10.1186/s12929-018-0435-3](https://doi.org/10.1186/s12929-018-0435-3).
8. P. D. O. De Almeida *et al.* A new synthetic antitumor naphthoquinone induces ROS-mediated apoptosis with activation of the JNK and p38 signaling pathways, *Chem. Biol. Interact.*, **2021**, vol. 343, article no. 109444, doi: [10.1016/j.cbi.2021.109444](https://doi.org/10.1016/j.cbi.2021.109444).
9. W. Karnsomwan, P. Netcharoensirisuk, T. Rungrotmongkol, W. De-Eknamkul, and S. Chamni, Synthesis, biological evaluation and molecular docking of Avicequinone C analogues as potential steroid 5 α -reductase inhibitors, *Chem. Pharm. Bull.*, **2017**, vol. 65, no. 3, pp. 253–260, doi: [10.1248/cpb.c16-00727](https://doi.org/10.1248/cpb.c16-00727).
10. K.-I. Lee *et al.*, Naphthofuroquinone derivatives: inhibition of receptor tyrosine kinases, *Bioorg. Med. Chem. Lett.*, **2006**, vol. 16, no. 3, pp. 737–742, doi: [10.1016/j.bmcl.2005.08.115](https://doi.org/10.1016/j.bmcl.2005.08.115).
11. M. O. F. Goulart *et al.*, Trypanocidal activity and redox potential of heterocyclic- and 2-hydroxy-naphthoquinones, *Bioorg. Med. Chem. Lett.*, **1997**, vol. 7, no. 15, pp. 2043–2048, doi: [10.1016/S0960-894X\(97\)00354-5](https://doi.org/10.1016/S0960-894X(97)00354-5).
12. F. A. De Molfetta, R. F. De Freitas, A. B. F. Da Silva, and C. A. Montanari, Docking and molecular dynamics simulation of quinone compounds with trypanocidal activity, *J. Mol. Model.*, **2009**, vol. 15, no. 10, pp. 1175–1184, doi: [10.1007/s00894-009-0468-3](https://doi.org/10.1007/s00894-009-0468-3).
13. A. K. Shukla, B. K. Singh, S. Patra, and V. K. Dubey, Rational approaches for drug designing against *Leishmaniasis*, *Appl. Biochem. Biotechnol.*, **2010**, vol. 160, no. 8, pp. 2208–2218, doi: [10.1007/s12010-009-8764-z](https://doi.org/10.1007/s12010-009-8764-z).
14. S. K. Venkatesan, A. K. Shukla, and V. K. Dubey, Molecular docking studies of selected tricyclic and quinone derivatives on trypanothione reductase of *Leishmania infantum*, *J. Comput. Chem.*, **2010**, pp. 2463-2475, doi: [10.1002/jcc.21538](https://doi.org/10.1002/jcc.21538).
15. M. Duran Lengua *et al.*, Synthetic alkyl substituted quinones oxidize membrane proteins and arrest *Plasmodium falciparum* growth *in vitro*, *Afr. J. Pharm. Pharmacol.*, **2015**, vol. 9, no. 23, pp. 595–602, doi: [10.5897/AJPP2014.4257](https://doi.org/10.5897/AJPP2014.4257).
16. T. F. Borgati, M. F. A. do Nascimento, J. F. Bernardino, L. C. O. Martins, A. G. Taranto, and A. B. de Oliveira, Synthesis, SAR, and docking studies disclose 2-arylfuran-1,4-naphthoquinones as *in vitro* antiplasmodial hits, *J. Trop. Med.*, **2017**, vol. 2017, pp. 1–11, doi: [10.1155/2017/7496934](https://doi.org/10.1155/2017/7496934).
17. J. Koyanagi, K. Yamamoto, K. Nakayama, and A. Tanaka, A short-step synthesis of naphtho[2,3-b]furan-4,9-dione, *J. Heterocycl. Chem.*, **1994**, vol. 31, no. 5, pp. 1303–1304, doi: [10.1002/jhet.5570310534](https://doi.org/10.1002/jhet.5570310534).

18. J. Koyanagi, K. Yamamoto, K. Nakayama, and A. Tanaka, A facile synthesis of 2-acetylnaphtho[2,3-b]furan-4,9-dione, *J. Heterocycl. Chem.*, **1995**, vol. 32, no. 4, pp. 1289–1291, doi: [10.1002/jhet.5570320432](https://doi.org/10.1002/jhet.5570320432).
19. J. Koyanagi, K. Yamamoto, K. Nakayama, and A. Tanaka, A new synthetic route to 2-substituted naphtho[2,3-b]furan-4,9-dione, *J. Heterocycl. Chem.*, **1997**, vol. 34, no. 2, pp. 407–412, doi: [10.1002/jhet.5570340209](https://doi.org/10.1002/jhet.5570340209).
20. H. M. Godbole, A. A. Ranade, A. R. Joseph, and M. V. Paradkar, Novel synthesis of linear furonaphthoquinones, *Syn. Comm.*, **2000**, vol. 30, no. 16, pp. 2951–2960, doi: [10.1080/00397910008087445](https://doi.org/10.1080/00397910008087445).
21. L. Syper, The Baeyer-Villiger oxidation of aromatic aldehydes and ketones with hydrogen peroxide catalyzed by selenium compounds. A convenient method for the preparation of phenols, *Synthesis*, **1989**, vol. 1989, no. 03, pp. 167–172, doi: [10.1055/s-1989-27183](https://doi.org/10.1055/s-1989-27183).
22. W.-B. Kang, S. Nan'ya, T. Toru, and Y. Ueno, Regioselective addition reaction of lithium enolates to thio-substituted 1,4-naphthoquinones. Convenient synthesis of a naphthofuran-4,9-dione ring system, *Chem. Lett.*, **1988**, vol. 17, no. 8, pp. 1415–1418, doi: [10.1246/cl.1988.1415](https://doi.org/10.1246/cl.1988.1415).
23. K. Kobayashi, T. Uneda, M. Kawakita, O. Morikawa, and H. Konishi, One-pot synthesis of naphtho[2,3-b]furan-4,9-diones by sequential coupling/ring closure reactions, *Tet. Lett.*, **1997**, vol. 38, no. 5, pp. 837–840, doi: [10.1016/S0040-4039\(96\)02462-8](https://doi.org/10.1016/S0040-4039(96)02462-8).
24. K. Kobayashi *et al.*, One-step synthesis of naphthofurandione, benzofurandione, and phenalenofuranone derivatives by the CAN-mediated cycloaddition, *BCSJ*, **1998**, vol. 71, no. 7, pp. 1691–1697, doi: [10.1246/bcsj.71.1691](https://doi.org/10.1246/bcsj.71.1691).
25. Y. R. Lee, B. S. Kim, and D. H. Kim, Ceric ammonium nitrate (CAN)-mediated oxidative cycloaddition of 1,3-dicarbonyls to conjugated compounds. Efficient synthesis of dihydrofurans, dihydrofurocoumarins, dihydrofuroquinolines, dihydrofurophenalenones, and furonaphthoquinone natural products, *Tetrahedron*, **2000**, vol. 56, no. 45, pp. 8845–8853, doi: [10.1016/S0040-4020\(00\)00839-5](https://doi.org/10.1016/S0040-4020(00)00839-5).
26. Y. Rok Lee, B. So Kim, Y. Ug Jung, W. Soo Koh, J. Soon Cha, and N. Woo Kim, Facile synthesis of avicequinone-B natural product, *Syn. Comm.*, **2002**, vol. 32, no. 20, pp. 3099–3105, doi: [10.1081/SCC-120013719](https://doi.org/10.1081/SCC-120013719).
27. Y. Rok Lee and B. So Kim, A facile method for the synthesis of dihydrofuranonaphthoquinones, furanonaphthoquinones, and benzofuranonaphthoquinones, *Syn. Comm.*, **2003**, vol. 33, no. 23, pp. 4123–4135, doi: [10.1081/SCC-120026354](https://doi.org/10.1081/SCC-120026354).
28. H. Hagiwara, K. Sato, D. Nishino, T. Hoshi, T. Suzuki, and M. Ando, Domino Michael-O-alkylation reaction: one-pot synthesis of 2,4-diacylhydrofuran derivatives and its application to antitumor naphthofuran synthesis, *J. Chem. Soc. Perkin Trans. 1*, **2001**, no. 22, pp. 2946–2957, doi: [10.1039/b107180g](https://doi.org/10.1039/b107180g).
29. C. Wu, R. K. Johnson, M. R. Mattern, J. C. Wong, and D. G. I. Kingston, Synthesis of furanonaphthoquinones with hydroxyamino side chains, *J. Nat. Prod.*, **1999**, vol. 62, no. 7, pp. 963–968, doi: [10.1021/np9900019](https://doi.org/10.1021/np9900019).
30. K. Rad-Moghadam, S. A. R. Mousazadeh Hassani, and S. Toorchi Roudsari, The deep eutectic melt of sorbitol and metformin hydrochloride: synthesis of 3-substituted 2-aminonaphtho[2,3-b]furan-4,9-diones and their photophysical properties, *RSC Adv.*, **2016**, vol. 6, no. 16, pp. 13152–13159, doi: [10.1039/C5RA19619A](https://doi.org/10.1039/C5RA19619A).
31. M. B. Teimouri and H. R. Khavasi, One-pot three-component regioselective synthesis of linear naphtho[2,3-b]-furan-4,9-diones, *Tetrahedron*, **2007**, vol. 63, no. 41, pp. 10269–10275, doi: [10.1016/j.tet.2007.07.082](https://doi.org/10.1016/j.tet.2007.07.082).
32. M. B. Teimouri and R. Bazhrang, An efficient three-component reaction involving [3+1+1] furannulation leading to furanonaphthoquinones in water, *Monatsh. Chem.*, **2008**, vol. 139, no. 8, pp. 957–961, doi: [10.1007/s00706-007-0846-4](https://doi.org/10.1007/s00706-007-0846-4).

33. S. Jiménez-Alonso, J. Guasch, A. Estévez-Braun, I. Ratera, J. Veciana, and A. G. Ravelo, Electronic and cytotoxic properties of 2-amino-naphtho[2,3-b]furan-4,9-diones, *J. Org. Chem.*, **2011**, vol. 76, no. 6, pp. 1634–1643, doi: [10.1021/jo102233j](https://doi.org/10.1021/jo102233j).
34. S. Gulati, S. E. John, and N. Shankaraiah, Microwave-assisted multicomponent reactions in heterocyclic chemistry and mechanistic aspects, *Beilstein J. Org. Chem.*, **2021**, vol. 17, pp. 819–865, doi: [10.3762/bjoc.17.71](https://doi.org/10.3762/bjoc.17.71).
35. S. Oramas-Royo *et al.*, Design, synthesis, and biological evaluation of new embelin derivatives as CK2 inhibitors, *Bioorg. Chem.*, **2020**, vol. 95, p. 103520, doi: [10.1016/j.bioorg.2019.103520](https://doi.org/10.1016/j.bioorg.2019.103520).
36. T. Borgati, J. De Souza, and A. De Oliveira, A complete and unambiguous ¹H and ¹³C NMR signals assignment of *para*-naphthoquinones, *ortho*- and *para*-furanonaphthoquinones, *J. Braz. Chem. Soc.*, **2019**, doi: [10.21577/0103-5053.20190009](https://doi.org/10.21577/0103-5053.20190009).
37. A. Olyaei, A. Mohamadi, and N. Rahmani, Green synthesis of new lawsone enamines and their *Z/E* (C-C)-isomerization induced by organic solvent, *RSC Adv.*, **2021**, vol. 11, no. 21, pp. 12990–12994, doi: [10.1039/D1RA01858B](https://doi.org/10.1039/D1RA01858B).
38. A. L. Perez, G. Lamoureux, and B. Y. Zhen-Wu, Synthesis of 2-hydroxy-3-substituted naphthoquinones using the Heck reaction, *Tet. Lett.*, **2007**, vol. 48, no. 23, pp. 3995–3998, doi: [10.1016/j.tetlet.2007.04.033](https://doi.org/10.1016/j.tetlet.2007.04.033).
39. T. Reyser *et al.*, Alkoxyamines designed as potential drugs against *Plasmodium* and *Schistosoma* parasites, *Molecules*, **2020**, vol. 25, no. 17, p. 3838, doi: [10.3390/molecules25173838](https://doi.org/10.3390/molecules25173838).
40. M. Oujii *et al.*, Hybrid gold(I) NHC-artemether complexes to target *Falciparum* malaria parasites, *Molecules*, **2020**, vol. 25, no. 12, p. 2817, doi: [10.3390/molecules25122817](https://doi.org/10.3390/molecules25122817).
41. A. B. Vaidya and M. W. Mather, Atovaquone resistance in malaria parasites, *Drug Resist. Updat.*, **2000**, vol. 3, no. 5, pp. 283–287, doi: [10.1054/drup.2000.0157](https://doi.org/10.1054/drup.2000.0157).
42. W. S. Hamama, A. E.-D. E. Hassanien, and H. H. Zoorob, Adaptable access for naphthoquinone annulation: bioactivity and molecular modeling evaluations, *J. Heterocyclic Chem.*, **2017**, vol. 54, no. 6, pp. 3273–3281, doi: [10.1002/jhet.2947](https://doi.org/10.1002/jhet.2947).
43. About the malaria box | Medicines for Malaria Venture <https://www.mmv.org/mmv-open/malaria-box/aboutmalaria-box.2020>, page accessed 16.11.2020.
44. D. Birth, W.-C. Kao, and C. Hunte, Structural analysis of atovaquone-inhibited cytochrome bc1 complex reveals the molecular basis of antimalarial drug action, *Nat. Commun.*, **2014**, vol. 5, no. 1, p. 4029, doi: [10.1038/ncomms5029](https://doi.org/10.1038/ncomms5029).
45. M. Varadi *et al.*, AlphaFold protein structure database: massively expanding the structural coverage of protein-sequence space with high-accuracy models, *Nucleic Acids Res.*, **2022**, vol. 50, no. D1, pp. D439–D444, doi: [10.1093/nar/gkab1061](https://doi.org/10.1093/nar/gkab1061).
46. D. E. Hurt, J. Widom, and J. Clardy, Structure of *Plasmodium falciparum* dihydroorotate dehydrogenase with a bound inhibitor, *Acta Crystallogr. D Biol. Crystallogr.*, **2006**, vol. 62, no. 3, pp. 312–323, doi: [10.1107/S0907444905042642](https://doi.org/10.1107/S0907444905042642).
47. X. Deng, D. Matthews, P. K. Rathod, and M. A. Phillips, The X-ray structure of *Plasmodium falciparum* dihydroorotate dehydrogenase bound to a potent and selective *N*-phenylbenzamide inhibitor reveals novel binding-site interactions, *Acta Crystallogr. F Struct. Biol. Commun.*, **2015**, vol. 71, no. 5, pp. 553–559, doi: [10.1107/S2053230X15000989](https://doi.org/10.1107/S2053230X15000989).
48. B. K. Dickerman *et al.*, Identification of inhibitors that dually target the new permeability pathway and dihydroorotate dehydrogenase in the blood stage of *Plasmodium falciparum*, *Sci. Rep.*, **2016**, vol. 6, no. 1, p. 37502, doi: [10.1038/srep37502](https://doi.org/10.1038/srep37502).
49. R. Rawat and S. M. Verma, An exclusive computational insight toward molecular mechanism of MMV007571, a multitarget inhibitor of *Plasmodium falciparum*, *J. Biomol. Struct. Dyn.*, **2020**, vol. 38, no. 18, pp. 5362–5373, doi: [10.1080/07391102.2019.1700165](https://doi.org/10.1080/07391102.2019.1700165).
50. M. J. Palmer *et al.*, Potent antimalarials with development potential identified by structure-guided computational optimization of a pyrrole-based dihydroorotate dehydrogenase

- inhibitor series, *J. Med. Chem.*, **2021**, vol. 64, no. 9, pp. 6085–6136, doi: [10.1021/acs.jmedchem.1c00173](https://doi.org/10.1021/acs.jmedchem.1c00173).
51. A. T. García-Sosa, Hydration properties of ligands and drugs in protein binding sites: tightly-bound, bridging water molecules and their effects and consequences on molecular design strategies, *J. Chem. Inf. Model.*, **2013**, vol. 53, no. 6, pp. 1388–1405, doi: [10.1021/ci3005786](https://doi.org/10.1021/ci3005786).
52. <http://www.swissadme.ch/index.php>, page accessed 12.12.2021.
53. C. Hetényi, U. Maran, A. T. García-Sosa, and M. Karelson, Structure-based calculation of drug efficiency indices, *J. Bioinform.*, **2007**, vol. 23, no. 20, pp. 2678–2685, doi: [10.1093/bioinformatics/btm431](https://doi.org/10.1093/bioinformatics/btm431).
54. J. L. Dahlin and M. A. Walters, How to triage PAINS-full research, *Assay Drug. Dev. Technol.*, **2016**, vol. 14, no. 3, pp. 168–174, doi: [10.1089/adt.2015.674](https://doi.org/10.1089/adt.2015.674).
55. S. Pomel *et al.*, An adamantamine derivative as a drug candidate for the treatment of visceral leishmaniasis, *J. Antimicrob. Chemother.*, **2021**, vol. 76, no. 10, pp. 2640–2650, doi: [10.1093/jac/dkab226](https://doi.org/10.1093/jac/dkab226).
56. J.-C. Palomino, A. Martin, M. Camacho, H. Guerra, J. Swings, and F. Portaels, Resazurin microtiter assay plate: simple and inexpensive method for detection of drug resistance in *Mycobacterium tuberculosis*, *J. Antimicrob. Chemother.*, **2002**, vol. 46, no. 8, pp. 2720–2722, doi: [10.1128/AAC.46.8.2720-2722.2002](https://doi.org/10.1128/AAC.46.8.2720-2722.2002).
57. P. Patil, M. Ahmadian-Moghaddam, and A. Dömling, Isocyanide 2.0, *Green Chem.*, **2020**, vol. 22, no. 20, pp. 6902–6911, doi: [10.1039/D0GC02722G](https://doi.org/10.1039/D0GC02722G).
58. C. G. Neochoritis, S. Stotani, B. Mishra, and A. Dömling, Efficient isocyanide-less isocyanide-based multicomponent reactions, *Org. Lett.*, **2015**, vol. 17, no. 8, pp. 2002–2005, doi: [10.1021/acs.orglett.5b00759](https://doi.org/10.1021/acs.orglett.5b00759).

CHAPTER 3

“Lawsonone in Biginelli reaction with aldehydes and (alkyl)ureas: synthetic approaches and biological activities”

3.1 Introduction

In this chapter, many attempts will be presented concerning the synthesis of derivatives containing the 3,4-dihydropyrimidinone scaffold (DHPM). This scaffold can be easily accessed via a Biginelli three-component reaction between a urea, an aldehyde and lawsone, contributing as the active methylene substrate. The importance of this structure will be emphasized, regarding its contribution to a variety of biological activities. The developed synthetic methodology used herein, leads to a series of non-cyclized DHPM compounds never reported before, that we named Biginelli-linear products. Their stability will be discussed and optimized. The biological activity of obtained products will be evaluated against *Plasmodium falciparum*, *Leishmania donovani* and other pathogens. The *in vitro* results are reported, along with an *in silico* study against the two mitochondrial targets of *P. falciparum*: cytochrome bc1 and dihydroorotate dehydrogenase (DHODH).

3.1.1 3,4-Dihydropyrimidinones exhibit diverse biological activities

Heterocyclic compounds have been the focus of significant attention for their diverse synthetic potential and intriguing pharmacological activities. Pyrimidine, a key heterocyclic moiety, is one such compound. The pyrimidine scaffold is essential to life as it forms part of vitamins such as riboflavin (**3.1**), thiamine (**3.2**), and folic acid (**3.3**) and is a vital building block for DNA, as it is incorporated into the bases thymine (**3.4**), cytosine (**3.5**), and uracil (**3.6**) (Fig. 3.1, panel A) [1]. As a result, drugs that incorporate the pyrimidine ring, may possess excellent pharmacological properties. Analogues of this essential six membered heterocyclic 1,3-dinitrogen fragment are also bioactive compounds, among them the 3,4-dihydropyrimidinones (DHPMs) (Fig. 3.1, panel B).

A quite extensive study has been conducted during the last two decades in order to elaborate 3,4-dihydropyrimidinone derivatives aiming to enhance antiplasmodial activity and reverse drug resistance of *Plasmodium*. October *et al.* [2] reported the synthesis of DHPM hybrids with chloroquine (CQ) linked via an amide bond generated by a terminal diamine.

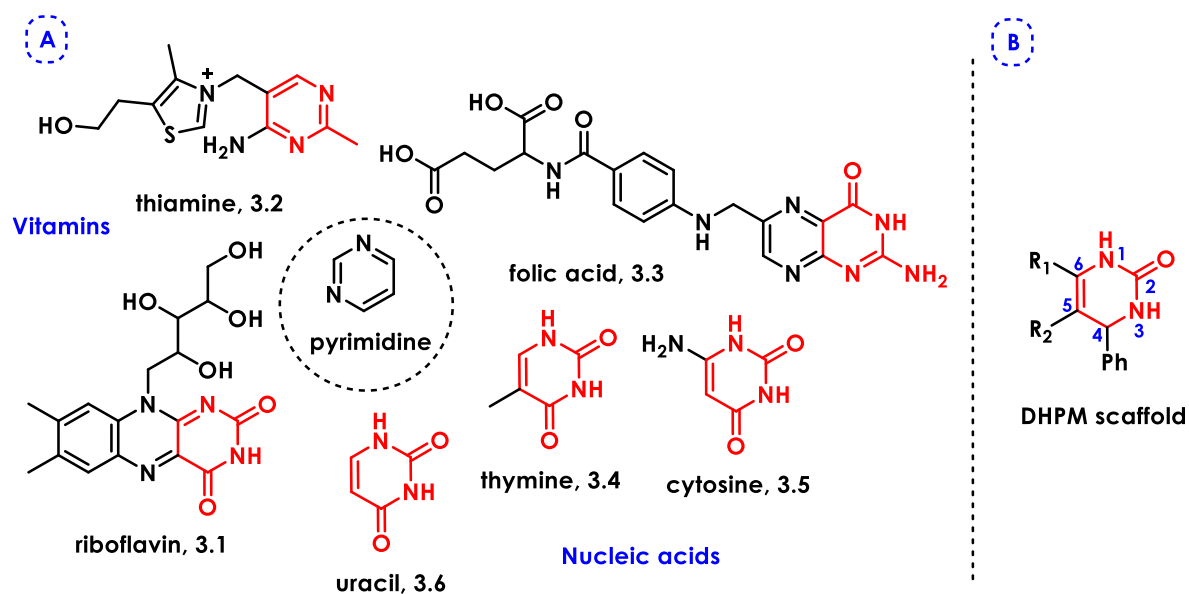


Figure 3.1. Pyrimidine is an essential scaffold for living organisms as a building block of vitamins and DNA bases.

The most active hybrid of the series (molecule **3.7**, Fig. 3.2) exhibited an IC₅₀ value in the range 16-51 nM against *P. falciparum* 3D7 CQ-sensitive strains with a therapeutic index (TI) over 300. In addition, **3.7** displayed a low IC₅₀ value in the range 2-9 nM against CQ-resistant strain K1 of *Plasmodium falciparum*, with a satisfactory therapeutic index higher than 2000. As the majority of hybrids of the same family were found to be more potent against CQ-resistant strains than CQ itself, the authors asserted that it could be due to DHPM moiety introduction. Due to the presence of a 4-amino-7-chloroquinoline in **3.7**, the proposed mechanism of action of this molecule was probably β -hematin inhibition.

Moreover, several DHPM derivatives without 4-aminoquinoline moiety (**3.8-3.10**) were found active against CQ-resistant strains, suggesting the value of the DHPM moiety to inhibit the *P. falciparum* asexual blood stage proliferation [3]. Nine compounds exhibited IC₅₀ values in the range 30 nM-1.8 μ M. Molecules **3.8** (IC₅₀ = 30 nM), **3.9** (IC₅₀ = 200 nM) and **3.10** (IC₅₀ = 300 nM) depicted in Fig. 3.2 are characteristic examples of the above-mentioned structures. However, it was not mentioned if they were capable to reverse parasite resistance. The same research group reported some years later other DHPM-CQ hybrids with both moieties being attached together through a triazole linker. Nonetheless, the switch of the linker and/or the removal of C-6 aryl substituent decreased the antiplasmodial activity [4], [5]. The most interesting compound of this series was **3.11** (Fig. 3.2) that exhibited low parasitemia inhibition (35%) at 1 μ M against asexual stages of *P. falciparum*. Rodrigues Rogerio *et al.* reported the synthesis of a series of 3,4-dihydropyrimidinone derivatives [6]. Three out of nine compounds exhibited IC₅₀ values varying between 1.8 μ M and 3.2 μ M, with the most potent being compound **3.12** (Fig. 3.2), when evaluated *in vitro* against *P. falciparum* W2 CQ-resistant strains. The same compound was evaluated *in vivo* using *P. berghei* infected mice and presented 60% of

parasitemia reduction after eight days of oral treatment at the daily dose of 30 mg/kg. This work clearly suggested the importance of mono *para*-substituted aryl group at C-6 of 3,4-dihydropyrimidinone ring for antiplasmodial activity, since differently positioned aryl substituents (*ortho*, *meta* and multi-substitution) resulted in IC₅₀ values higher than 20 μM.

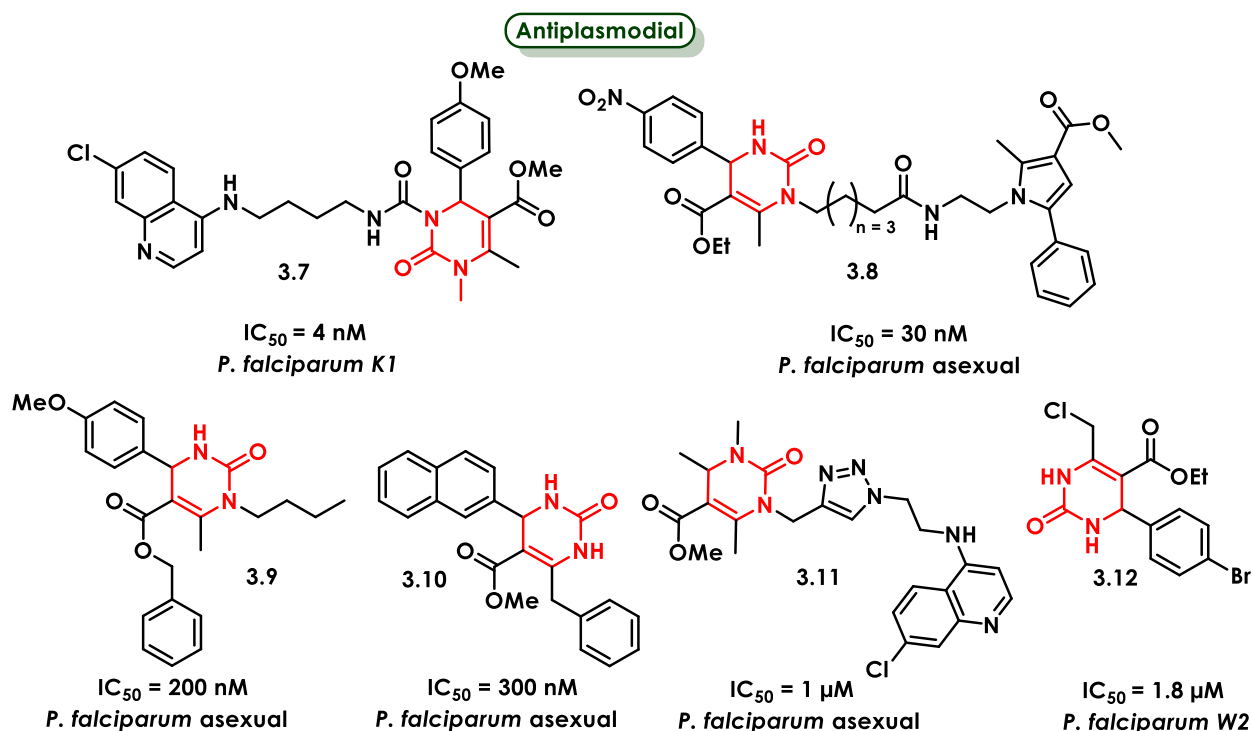


Figure 3.2. 3,4-dihydropyrimidinone derivatives as antiplasmodial agents.

In contrast, there are few studies in the literature reporting the leishmanicidal activity of DHPM derivatives. Compound **3.13** (Fig. 3.3) exhibited an IC₅₀ value of 23 μM *in vitro* against *L. donovani* amastigotes; however, further *in vivo* evaluation against intracardially infected Syrian golden hamsters (*Mesocricetus auratus*) was very promising [7]. This molecule diminished parasitemia up to 93% (at 50 mg/kg) in infected hamsters in a dose dependent manner, selectively targeting the parasites and not the host cells. Its mechanism of action was related to parasite mitochondrial membrane dysfunction and was confirmed by inhibition of the pteridine reductase I (PTR1) enzyme. Compound **3.14** (Fig. 3.3) exhibited an IC₅₀ value in the same range as **3.13** (IC₅₀ = 25 μM) *in vitro* against *L. major* promastigotes [8]. The interaction of **3.14** with PTR1 studied *in silico*, indicated that **3.14** exhibited favorable interactions and binding poses with the proposed target. However, as the authors pointed out, more research is needed before compound **3.14** can be considered a potent leishmanicidal agent.

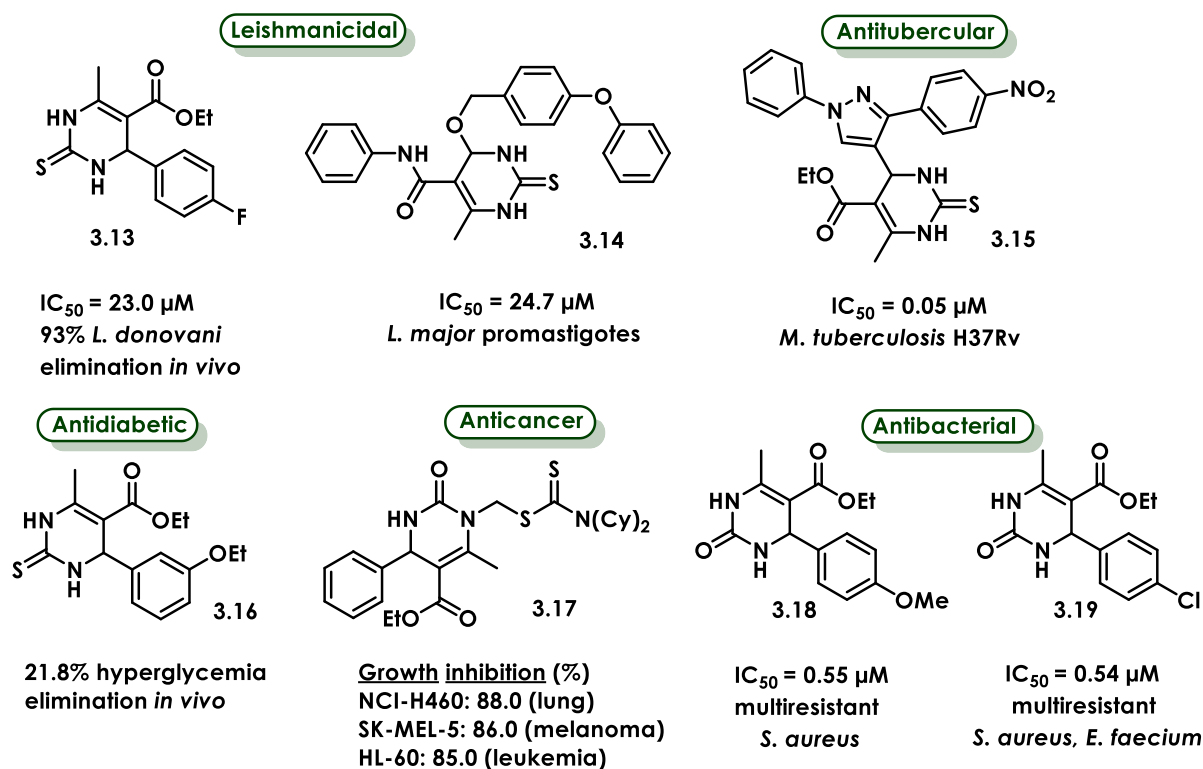


Figure 3.3. 3,4-Dihydropyrimidinone derivatives with various biological activities.

In addition, the DHPM scaffold has been accounted for antitubercular activities. **3.15** (Fig. 3.3) exhibited potent activities ($IC_{50} = 0.05 \mu M$) and excellent selectivity index ($SI > 500$), even better than the reference drug isoniazid ($IC_{50} = 0.22 \mu M$) upon *in vitro* evaluation against *M. tuberculosis* H37Rv [9]. The authors demonstrated that the DHPM-pyrazolyl fragment was essential for the biological activity.

Very recently, a series of 3,4-dihydropyrimidinone derivatives was evaluated *in vivo* against male type 2 diabetic rats [10]. The obtained results were quite promising as molecule **3.16** (Fig. 3.3) was able to inhibit hyperglycemia in a dose dependent manner (22% at 50 mg/kg after 7 days), while the referenced drug (gliclazide) presented 48% anti-hyperglycemic activity *in vivo* under the same conditions. However, the mechanism of action is yet unknown.

Furthermore, the cytotoxic activity of DHPM derivatives has been evaluated. Such an example is compound **3.17** (Fig. 3.3) exhibiting compelling activities against multiple cancer cell lines [11]. Compound **3.17** inhibited the growth of NCI-H460, SK-MEL-5, and HL-60 (TB) cancer cell lines by 88%, 86%, and 85%, respectively, at 10 μM concentration, without cytotoxicity to normal cells. Further enzyme inhibition assays demonstrated that the activity of this compound could be associated with the inhibition of cell signaling pathway factors such as mTOR ($IC_{50} = 0.64 \mu M$) and VEGFR-2 ($IC_{50} = 1.97 \mu M$), suggesting a pro-apoptotic activity and cell cycle arrest at G2/M phase.

The antibacterial properties of 3,4-dihydropyrimidinones have also been reported. For example, compounds **3.18** and **3.19** (Fig. 3.3) displayed remarkable activities against multidrug resistant hospital isolates bacteria (from patients) [12]. **3.18** exhibited an IC₅₀ value of 0.55 μM against multi-resistant *S. aureus* and **3.19** a fairly comparable value against both *S. aureus* and *E. faecium* while maintaining cell viability.

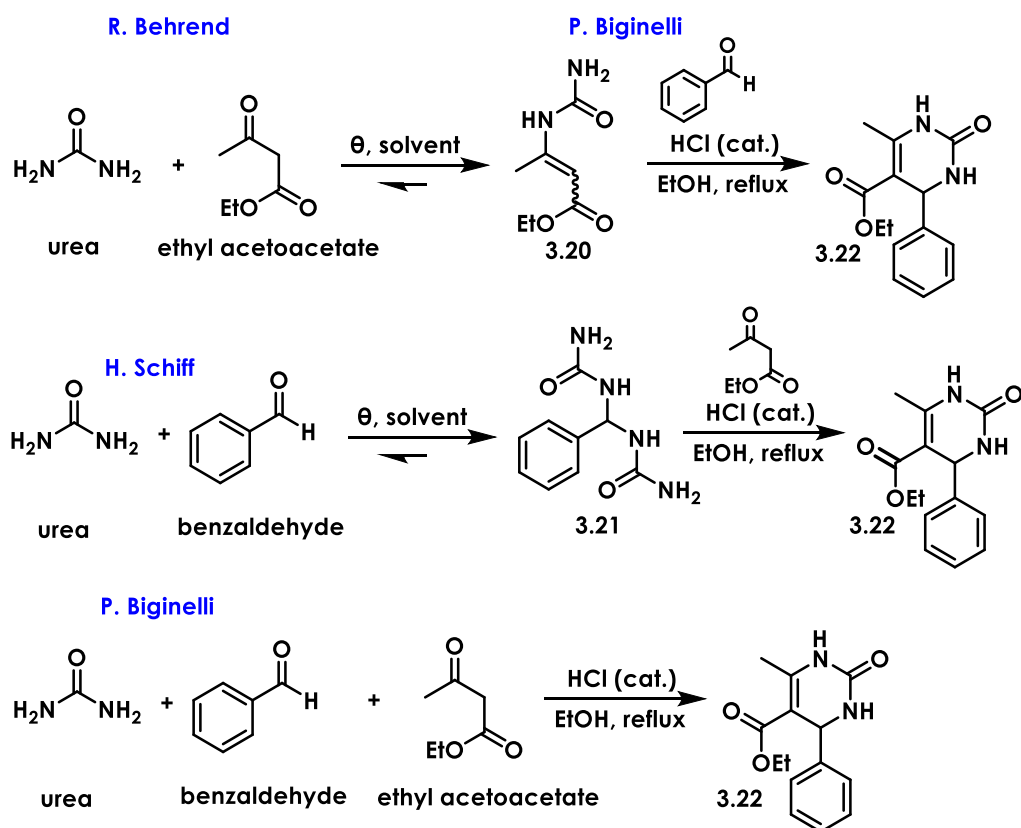
To summarize, molecules containing the DHPM scaffold own an extremely broad range of biological activities [1].

3.1.2 One step synthesis of 3,4-dihydropyrimidinones: The Biginelli reaction

Even if the synthesis of DHPM-1,4-naphthoquinone hybrids remains challenging, many efforts have been made to synthesize the 3,4-dihydro-pyrimidinone (DHPM) scaffold efficiently. The Biginelli reaction, instigated by Pietro Biginelli in 1893 [13], is one of the most extensively used multicomponent reactions for the synthesis of heterocyclic compounds. It is a three-component condensation reaction between an aldehyde, an active methylene compound and a (thio)urea, under acidic catalysis.

Discovery

P. Biginelli combined the results obtained from earlier studies by R. Behrend [14] and H. Schiff [15] to develop a multicomponent one-pot protocol. Behrend investigated the reaction between urea and ethyl acetoacetate providing the ethyl β-carbamido adduct **3.20**. Schiff reported the reaction of urea with benzaldehyde providing the benzal-bisurea (**3.21**) (Scheme 3.1). Some years later, Biginelli observed that the same heterocyclic DHPM product **3.22** was synthesized when **3.20** was allowed to react with benzaldehyde and when **3.21** was submitted to reaction with ethyl acetoacetate under the same experimental conditions. This would mean that both **3.20** and **3.21** formations were reversible, and the reaction between all three resulting compounds in solution (urea, ethyl acetoacetate, and benzaldehyde) leads to the same DHPM adduct regardless of the order in which they are added together.

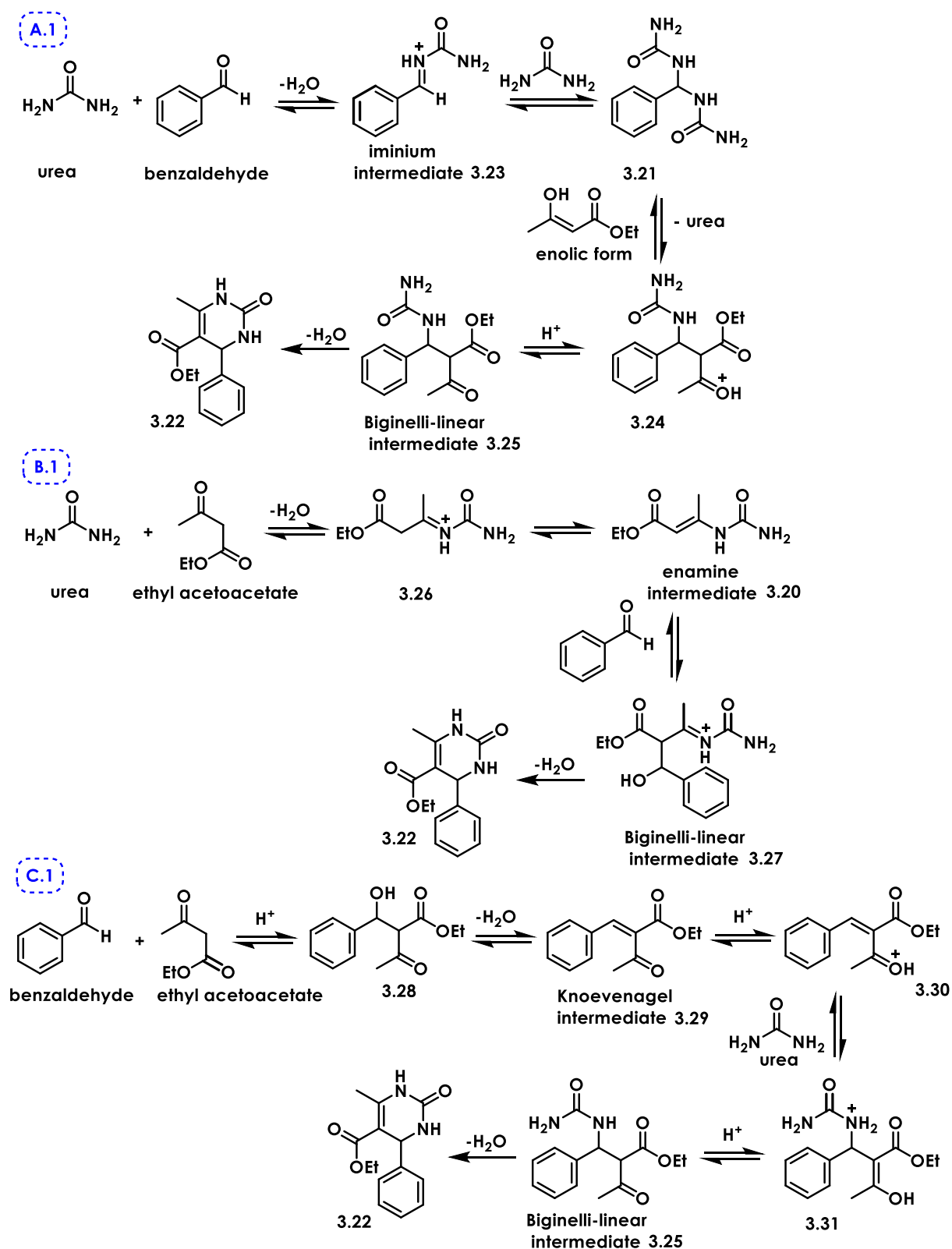


Scheme 3.1. The discovery of the three-component Biginelli reaction.

Mechanistic studies

The mechanism of this simple-to-handle reaction has been a debate for many generations of chemists worldwide. Biginelli proved that there were four possible ways to synthesize the target DHPM scaffold: i) a three-component reaction between urea, benzaldehyde and ethyl acetoacetate, ii) reaction between benzal-bisurea (**3.21**, Scheme 3.1) and ethyl acetoacetate, iii) reaction between ethyl β -carbamidocrotonate (**3.20**) and benzaldehyde and consequently iv) reaction between the Knoevenagel intermediate (formed by benzaldehyde and ethyl acetoacetate) and urea. Many research groups have conducted numerous studies to propose and validate the mechanistic pathway of this multicomponent condensation.

The first explanation was proposed by Folkers and Johnson [16] in 1933, when they synthesized all expected intermediates and involved them in the reaction with the third component. All the four potential combinations mentioned above (i-iv) were investigated. Their extended study resulted in three possible reaction pathways (Scheme 3.2, A.1-C.1).

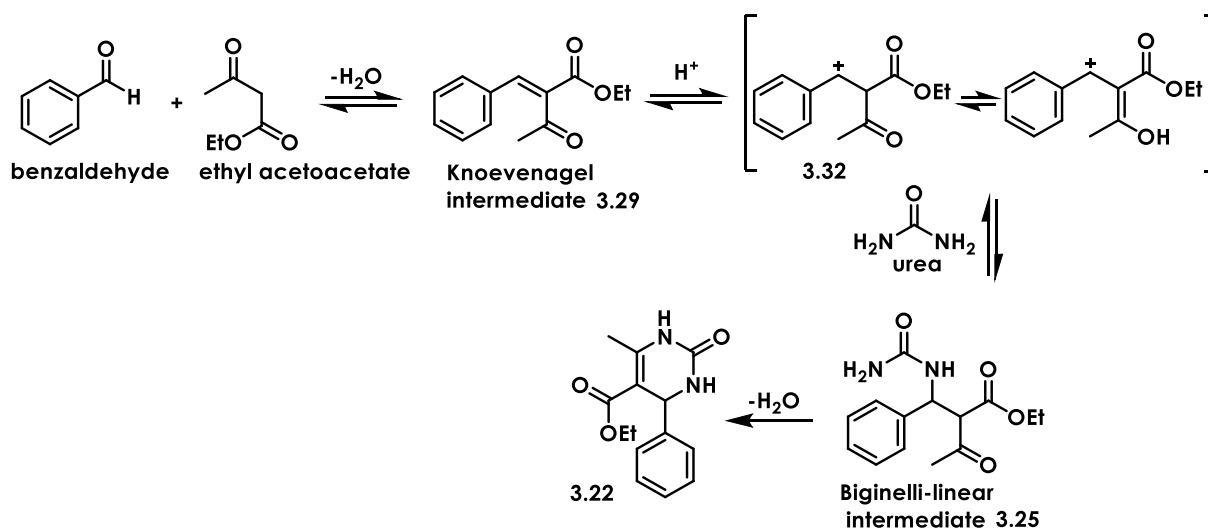


Scheme 3.2. The first mechanisms proposed for the Biginelli reaction in 1933 by Folkers and Johnson.

Briefly, the synthesis of benzal-bisurea **3.21** intermediate followed by its reaction with the enolic form of ethyl acetoacetate resulted in the formation of the desired DHPM, passing through an uncharged Biginelli-linear intermediate **3.25**, which was never isolated (Scheme 3.2, pathway A.1). Similarly, the reaction of urea with ethyl acetoacetate led to the enamine

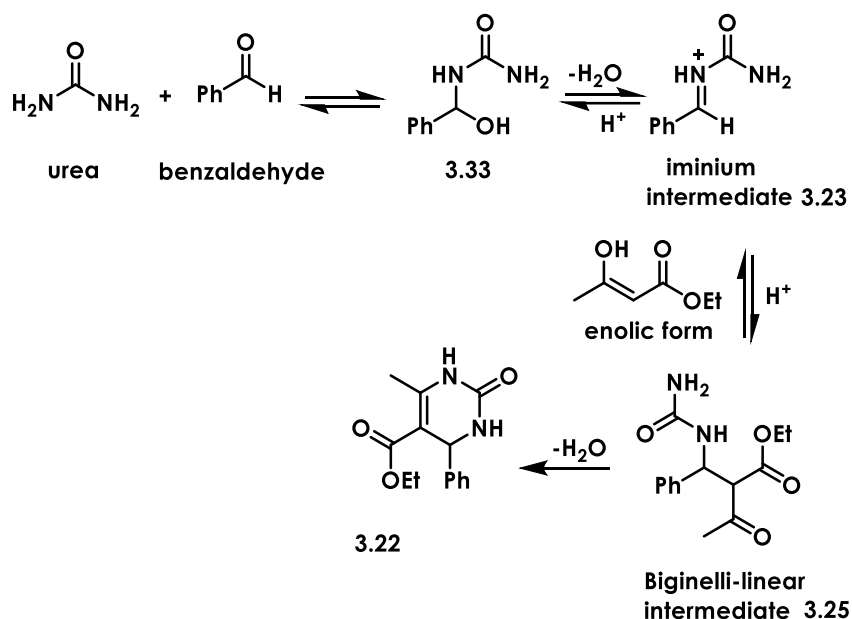
intermediate **3.20**, which afforded the DHPM derivative after condensation with benzaldehyde (Scheme 3.2, pathway B.1). Finally, a third combination was benzaldehyde reacting with ethyl acetoacetate to provide the Knoevenagel intermediate **3.29**, which led to the same DHPM **3.22**, but with lower yields, via a **3.25** Biginelli-linear intermediate (Scheme 3.2, pathway C.1). The authors emphasized the need for acidic catalysis (without acid, the reaction did not yield the desired DHPM) and the fact that urea was probably reacting first either with benzaldehyde or ethyl acetoacetate, meaning that the C.1 pathway did not seem probable.

In contrast, the work of Sweet and Fissekis [17] strongly supported an initial stage involving an acid-catalyzed aldol condensation between the aldehyde and ethyl acetoacetate (Scheme 3.3). This hypothesis was supported by the formation of a carbenium intermediate **3.32** which was subsequently attacked by urea, leading to the Biginelli-linear intermediate **3.25**. This intermediate led after intramolecular cyclization to DHPM **3.22**. This cyclization was suggested to be the rate-determining step (RDS) of the reaction. In addition, the authors suggested that the ability of the already synthesized Knoevenagel compounds to form DHPMs after reaction with urea, strongly supports their proposed mechanism.



Scheme 3.3. Mechanism focused on Knoevenagel intermediate proposed for the Biginelli reaction in 1973 by Sweet and Fissekis.

However, Kappe [18] investigated the mechanism of Biginelli condensation in CD_3OH under slightly acidic catalysis (HCl), to monitor the formation of any type of intermediate by $^1\text{H}/^{13}\text{C}$ NMR spectroscopy. This follow-up work completely rejected both the Knoevenagel (Scheme 3.2, pathway C.1) and enamine (Scheme 3.2, pathway B.1) pathways. All experimental data were in favor of a mechanism involving an iminium **3.23** as the key intermediate which, after reaction with ethyl acetoacetate, led to **3.22** DHPM formation (Scheme 3.4). The author suggested that passing from the iminium intermediate to the Biginelli-linear **3.25** was the rate-determining step.

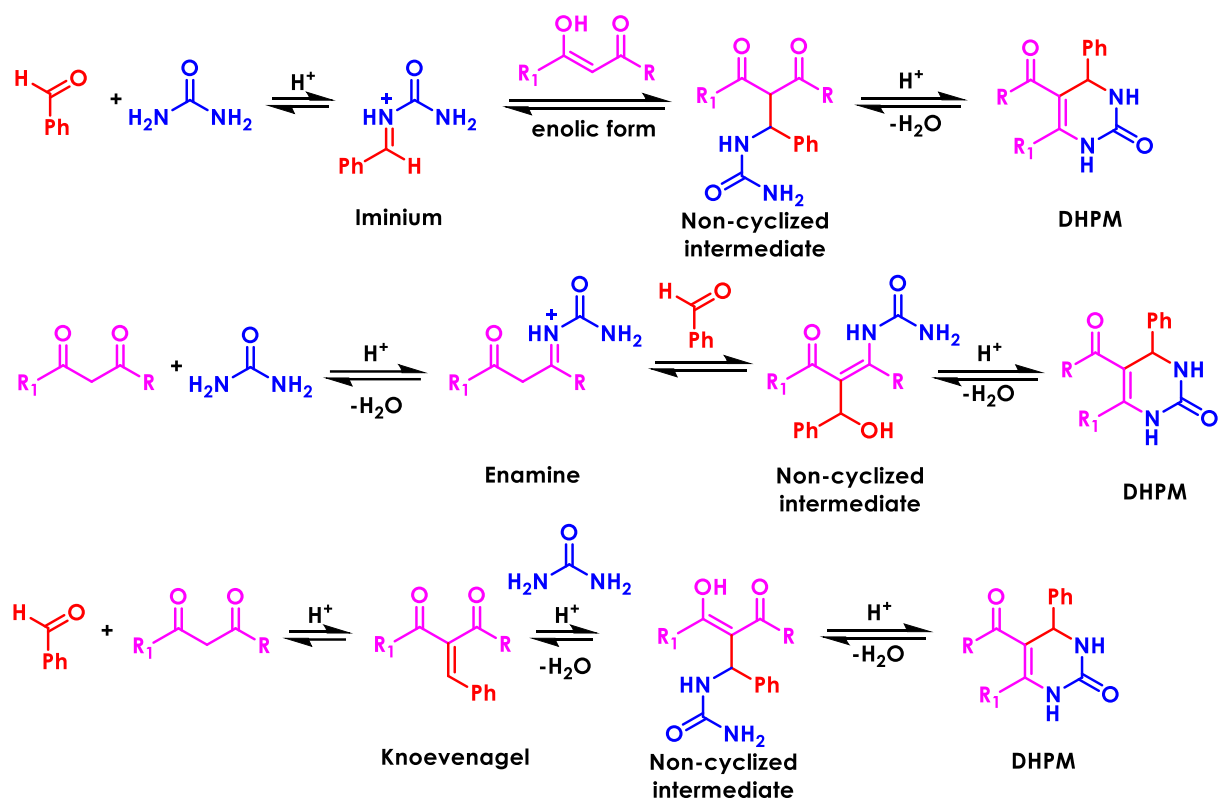


Scheme 3.4. Mechanism proposed by Kappe: the iminium route of the Biginelli reaction.

Experimental tandem MS experiments (ESI-MS/MS) and Density Functional Theory (DFT) calculations [19] carried out by De Souza *et al.* supported Kappe's conclusions. This work demonstrated that the iminium mechanism for the Biginelli reaction is the most kinetically and thermodynamically favorable. In addition, various precursors and intermediates related to the iminium mechanism were detected using ESI-MS. The so-called Knoevenagel mechanism seemed to be the slowest and least favorable among the three.

Additional calculations employing the Artificial Force Induced Reaction method (AFIR) by Puripat *et al.* [20] were applied to search for all potential mechanistic pathways for the Biginelli reaction. The authors concluded that 1) a second urea molecule could be beneficial catalyzing nearly every step of the reaction; 2) the substitution pattern of the aryl ring of the aldehyde has little impact on the reaction; and 3) the rate-determining step (RDS) is the C-N bond formation during the final intramolecular cyclization step for iminium and enamine intermediates mechanisms, and the C-O bond cleavage for the Knoevenagel intermediate mechanism.

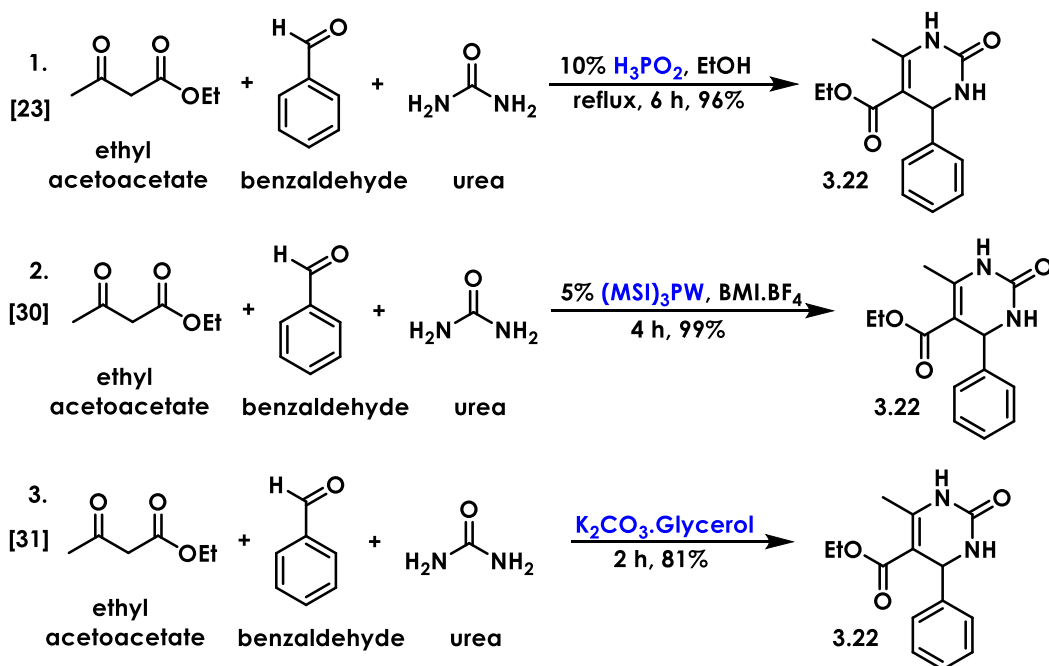
To sum up, over the years, three mechanisms have been proposed for this cascade reaction, each is characterized by the formation of a specific intermediate: enamine, iminium, or Knoevenagel (summarized in Scheme 3.5). Although all three mechanisms remain theoretically feasible, the RDS can vary significantly depending on the reaction conditions, the nature and substitution of the reactants and acid catalysts.



Scheme 3.5. Summary of all three proposed mechanisms for the Biginelli reaction.

Catalysts

Catalysts have an important impact in the Biginelli reaction. Their role has been extensively studied, optimized, and varied over the years. A vast spectrum of catalysts has been used in order to improve the yields of DHPMs [21]. Numerous acid catalysts such as hydrochloric acid (HCl) [13], sulfuric acid (H₂SO₄) [22], hypophosphorous acid (H₃PO₂) [23], *p*-toluene sulfonic acid (*p*-TSA) [24], Lewis acids (gallium (II) halides) [25], transition metal halides (CuCl₂) [26], chiral phosphoric acids [27], etc. have been used, aiming to reduce both reaction time and chemical waste. Bipiperazine-metal complexes [28], nanocatalysts such as ZnO nanoparticles [29], ionic liquids [30], deep eutectic solvents [31], enzymes [32], photocatalysts [33] and even bioorganic waste [34] have been reported to catalyze the Biginelli reaction providing excellent yields, depending on the substrates used. However, this topic is still under intense investigation aiming to develop greener, more efficient and less energy consuming synthetic technologies.



Scheme 3.6. Some examples of catalysts used in the Biginelli reaction (1) hypophosphorous acid, (2) protic metal containing ionic liquid, (3) deep eutectic solvent medium.

Substrate scope

The Biginelli reaction has been used extensively because of the rich structural variety of DHPM structures that can be obtained [35] (Fig. 3.4), which are dependent on its three building blocks, namely an aldehyde, urea, and an active methylene compound. The aldehydes range from commercially available aliphatic, aromatic, heterocyclic, heteroaromatic, and organometallic derivatives to sugars. Various mono- or di-substituted ureas or thioureas with different aromatic, alkyl, benzyl, and heterocyclic groups are well tolerated. As far as the active methylene compounds are concerned, linear or cyclic 1,3-dicarbonyl compounds bearing aryl, alkyl and heterocyclic rings have been reported to participate in the Biginelli reaction. Nevertheless, the literature does not provide strong evidence of 1,4-naphthoquinones involvement as Biginelli substrates.

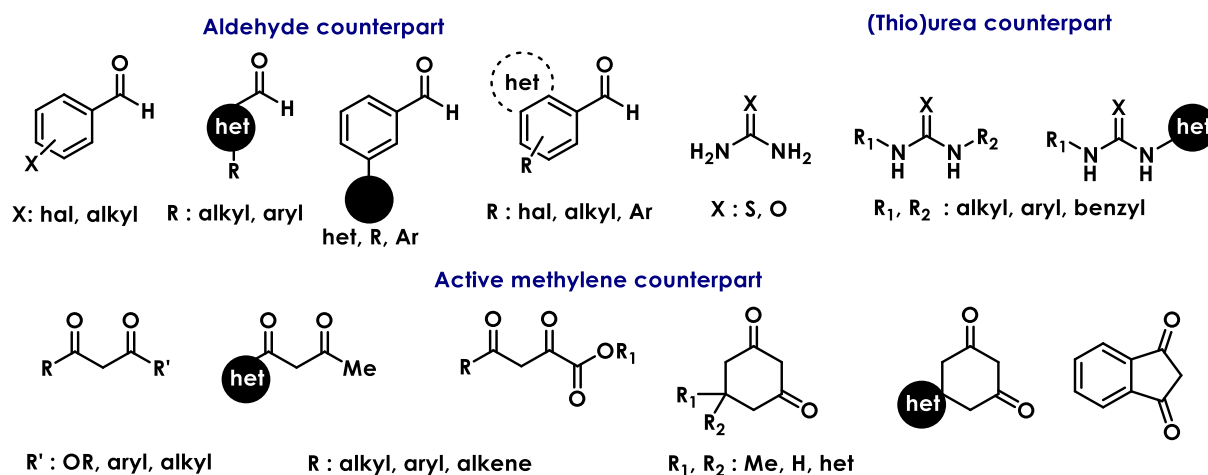
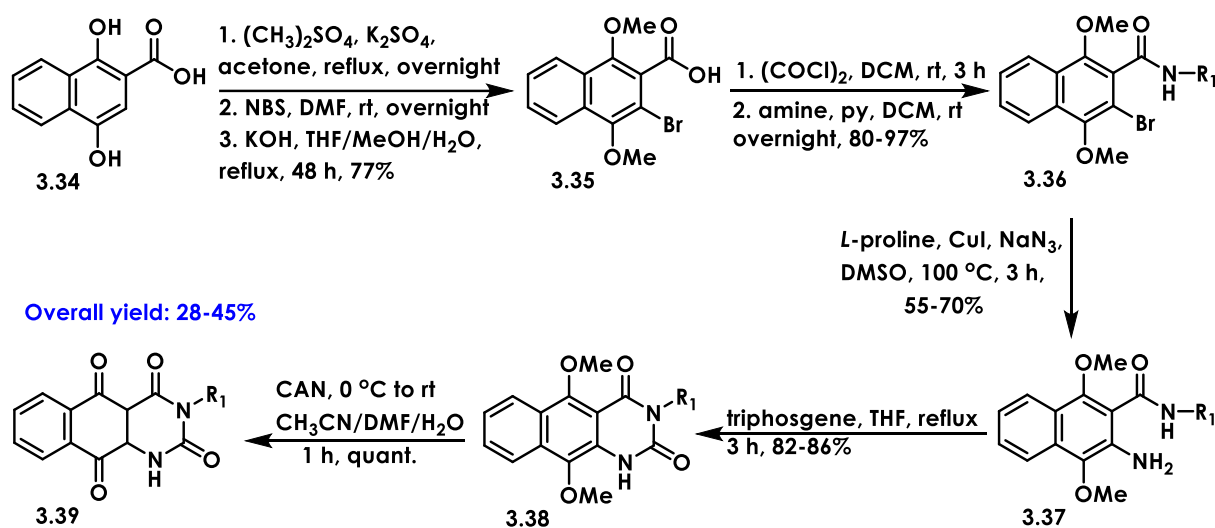


Figure 3.4. The wide substrate scope of the Biginelli reaction.

3.1.3 Multi-step synthesis of fused 3,4-dihydropyrimidinone-1,4-naphtho-quinones

Despite several references to bioactive fused pyrimidinone based heterocyclic derivatives [36], examples of naphtho-DHPM hybrids or derivatives are scarce. This could be due to their complicated synthesis. Aiming to access a library of 1,4-naphthoquinone pyrimidinone-fused hybrids Kim *et al.* established a multistep synthetic protocol [37] (Scheme 3.7).



Scheme 3.7. Multistep synthesis of naphthoquinone-pyrimidinone derivatives.

The commercially available 1,4-dihydroxy-2-naphthoic acid (**3.34**) was first subjected to total methylation (both phenol and acid functional groups), using dimethyl sulfate under reflux conditions. The resulting methyl ester was then brominated by *N*-bromosuccinimide (NBS) and subsequently hydrolyzed under basic protic conditions, resulting in a dimethylated carboxylic acid **3.35**. The acid function was activated via oxalyl chloride and allowed to react with a series of variously substituted primary amines, leading to intermediate amides **3.36**, with yields ranging between 80% and 97%. Amination of the bromo-substituted aromatic carbon of **3.36** allowed

ring closure to provide **3.38** intermediate with very good yields (82-86%). Finally, the desired fused pyrimidine-1,4-naphthoquinone derivatives **3.39** were obtained after oxidation by ceric ammonium nitrate (CAN), with overall yields between 28% and 45% (5 steps).

Despite the good overall yields provided for the synthesis of the target hybrid compounds **3.39**, the reaction times are quite long, and they require the careful use of chemicals like triphosgene, toxic and highly flammable oxalyl chloride, and corrosive CAN reagent.

So, as the DHPM family exhibits a very wide spectrum of biological activities, including antiparasitic ones, we intended to synthesize a focused library of DHPM-naphthoquinone derivatives via a multicomponent Biginelli reaction methodology. In that respect, the reaction between lawsone, benzaldehydes and (alkyl)ureas was investigated.

3.2 Results and discussion (Part I)

After taking into consideration the pharmacological importance of the DHPM scaffold and the possibility of synthesis by one-step multicomponent Biginelli reaction, we aimed to synthesize a series of fused heterocyclic naphthoquinones DHPM-NFQ hybrids potentially active against *P. falciparum*, *L. donovani*, and other pathogens.

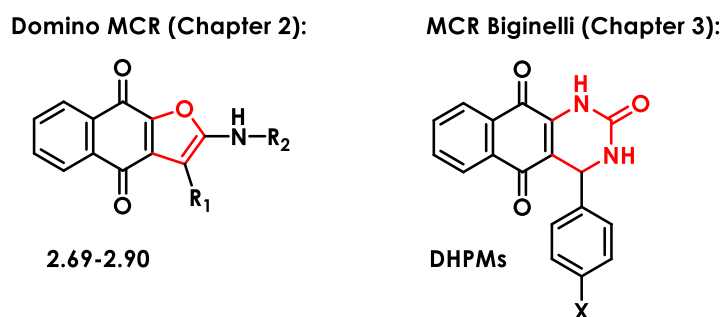


Figure 3.5. Fused heterocyclic naphthoquinones.

3.2.1 Chemistry – Synthesis

3.2.1.1 Reaction conditions optimization studies

First of all, the reaction between lawsone, 4-chlorobenzaldehyde (or *para*-chlorobenzaldehyde) (**3.40**) and urea (**3.41**) was investigated as a model reaction to establish an efficient synthetic protocol (Table 3.1). The reaction was carried out under conventional conditions (acidic catalysis in common protic solvents), and also in ionic liquids (ILs) and deep eutectic solvents (DES). Different activation methods of the reaction were also investigated, such as microwave irradiation and mechanochemical activation.

For every optimization experiment, the reaction mixture was collected after completion (lawsone consumption) and adequately treated to remove the solvents (if necessary) and catalysts. A sample of the crude residue was analyzed by ^1H NMR spectroscopy to evaluate both the aldehyde conversion and products yield. Surprisingly, the expected cyclized DHPM product **3.42** was never obtained. The products of this reaction were found to be a non-cyclized Biginelli compound **3.43** and a Michael adduct **3.44**. **3.43** is a three-component linear product of the Biginelli reaction. **3.44** is the two-component product issued from direct aldol condensation between 1 equiv. of 4-chlorobenzaldehyde and 2 equiv. of lawsone probably via the formation of the Knoevenagel intermediate. The results are summarized in Table 3.1.

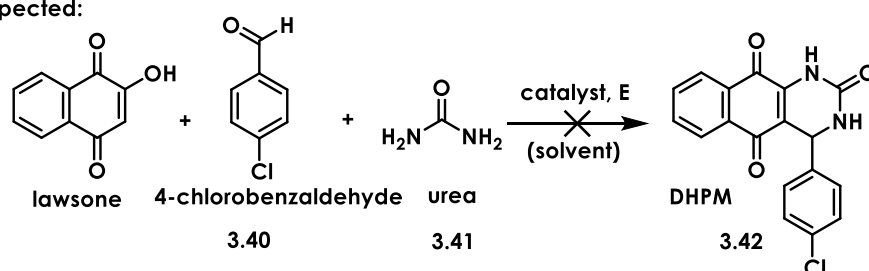
First, initial efforts were inspired by Patel's *et al.* recently reported protocol for the synthesis of DHPMs [38]. The authors reported the same reaction between lawsone, 4-chlorobenzaldehyde, and urea catalyzed by 0.5% zinc acetate ($\text{Zn}(\text{OAc})_2$) in ethanol (EtOH) at room temperature, providing DHPM **3.42** in excellent yield (93%).

However, in our hands, while this protocol was repeated (Table 3.1, entry 1) many times, the formation of DHPM was not observed. Instead, the Michael adduct **3.44** was collected in 45% yield after precipitation, matching very well with aldehyde conversion (50%), indicating that the reaction was selective.

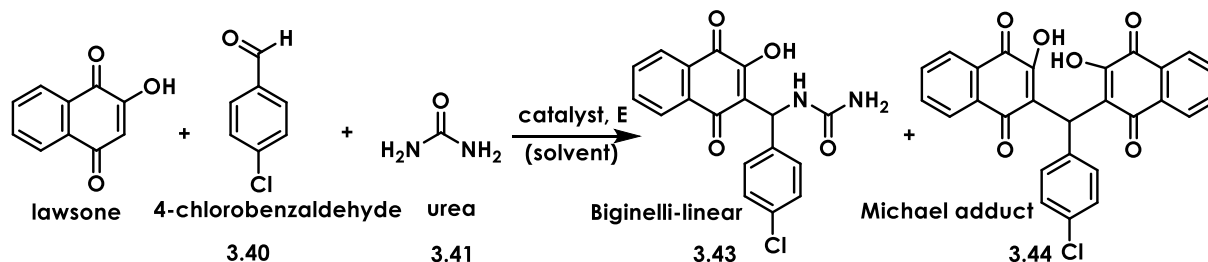
Table 3.1. Optimization studies of experimental conditions for the model Biginelli reaction between lawsone, 4-chlorobenzaldehyde and urea.

Biginelli model reaction :

What was expected:



What was delivered:



Entry	Activation method	Temperature (°C)	Reaction time (min.)	Equiv. (lawsone/ 3.40/3.41)	Catalyst	Solvent	3.40 conversion * (%)	Yield 3.43 ** (%)	Yield 3.44 ** (%)
1	solution	rt	overnight	1:1:1	0.5% Zn(OAc) ₂	EtOH	50	-	45
2	reflux	80	overnight	1.2:1.2:1	10% H ₃ PO ₂	EtOH	50	35	15
3	IL	80	120	1:1:1	IL	[HNMP]HSO ₄	60	traces	47
4	IL	80	300	1:1:1	IL	BMI.NTF ₂	84	traces	46
5	DES	80	60	1:2:1	DES	Choline chloride/Urea	40	20	30
6	DES	70	60	1:1:1	DES	Choline chloride/ Chloroacetic acid	35	-	30
7	irradiation (μw)	160	2 x 60	1.2:1.2:1	10% H ₃ PO ₂	EtOH	2	traces	-
8	irradiation (μw)	160	60	1:1:1	20% p-TSA	CH ₃ CN	8	5	-
9	Mechanochemistry MM400 (30 Hz)	-	2 x 40	1:1:1	10% H ₃ PO ₂	-	50	30	-
10	Mechanochemistry MM400 (30 Hz)	-	2 x 40	1:1:1	20% p-TSA	-	50	45	-
11	Mechanochemistry MM400 (30 Hz)	-	2 x 40	1:1:1.5	20% p-TSA	-	70	55	-
12	Mechanochemistry P7 (800 rpm)	-	2 x 40	1:1:1.5	20% p-TSA	-	95	90	-

*Calculated based on ¹H NMR spectrum of the crude mixture after work up.

** Isolated yield, calculated based on the starting amount of lawsone used.

No traces of any Biginelli products (**3.42** and **3.43**) were found when the crude reaction mixture was analyzed by ¹H NMR and mass spectroscopy. When the amount of catalyst was increased up to 20%, no significant changes were observed. Patel's protocol [38] was repeated several times because it was one of the few that used lawsone as an active methylene compound in the Biginelli reaction. In our hands, the cyclized DHPM was never obtained, as mentioned before. After reviewing carefully their work, we can notice that the NMR characterization of some of the reported DHMP compounds was either incomplete or ambiguous. We suppose that the authors possibly did not report the exact experimental protocol.

When the model reaction mixture was heated under reflux in EtOH and catalyzed by 10 mol% hypophosphorous acid (H₃PO₂) [23] with both lawsone and *para*-chlorobenzaldehyde in slight excess (1.2 equiv. of each with respect to urea) (Table 3.1, entry 2), no DHPM was formed either. Biginelli-linear **3.43** was isolated from the reaction mixture as the major product with 35% yield, while Michael's adduct **3.44** formation was evident (isolated with 15% yield). Variation of the catalyst (CuCl₂, HCl, H₂SO₄, *p*-TSA, CH₃COOH, L-Tyr, silica) and/or excess of reactants did not change the result of the reaction in solution.

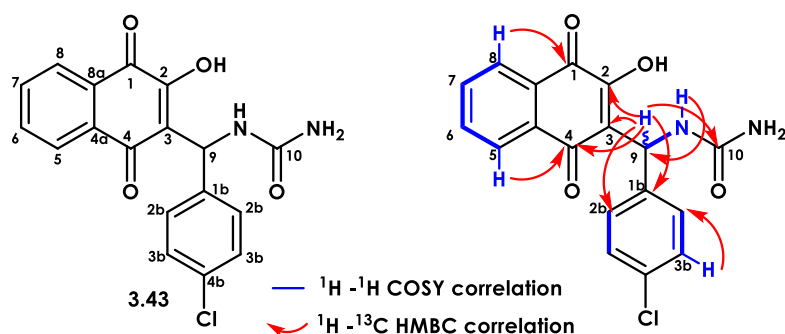
Faced to this failure, our attention was turned to ILs and DES, because such media have been reported to be beneficial in Biginelli reaction catalysis and activation. Ionic liquids have been reported to stabilize some reactive intermediates in the Biginelli reaction [39]. DES were chosen because they have similar physicochemical properties to ionic liquids and are more eco-compatible and easier to synthesize [40],[41]. Among various ionic liquids, homemade 1-methyl-2-pyrrolidonium hydrogen sulfate {[HNMP]HSO₄} [42] and commercially available 1-butyl-3-methylimidazolium bis(trifluoromethane-sulfonyl)imide {BMI.NTF₂} [30] were tested. Reaction in these IL media (Table 3.1, entries 3 and 4) did not afford any Biginelli-type compounds. Instead, Michael adduct **3.44** was found to be the major product, obtained in 46-47% yield in these cases. This protocol using {[HNMP]HSO₄}, reported by Patil *et al.* [42] was repeated multiple times, because it is one of the very rare protocols involving lawsone in the Biginelli reaction. Sonication activation of the reaction was also tested as an alternative (same conditions as entry 3). The reaction mixture ended up by solidification as described by the authors [42]. However, in our hands, the obtained solid corresponded to the Michael adduct **3.44** and not to the desired DHPM as they claimed. Then, two DES media were chosen and prepared according to the literature. When the reaction was carried out in choline chloride/urea [43], the Biginelli-linear compound **3.43** was obtained in 20% yield (Table 3.1, entry 5), along with **3.44** (30%). However, when choline chloride/chloroacetic acid [44] was used as the reaction medium (Table 3.1, entry 6), only compound **3.44** was obtained in 30% yield.

The reaction was also tested under microwave irradiation (Table 3.1, entries 7 and 8). Under these conditions, only 2% and 8% of aldehyde conversion and only traces or <5% of compound **3.43** were detected in the reaction mixtures. Faced to these disappointing results, many modifications including catalyst (CH₃COOH, *p*-TSA, H₃PO₂), temperature (80-180 °C), reaction time, and solvent (EtOH, CH₃CN, IL) were carried out. These attempts failed to improve the reaction outcome and yield, leading always to compound **3.43** with a maximum yield of 5%, among unreacted starting materials.

Finally, the reaction was activated using mechanochemical means. When operating an equimolar mixture of all three components with 10% H₃PO₂ as the catalyst, in a vibratory ball mill (MM400) at a frequency of 30 Hz for two successive runs of 40 min each, compound **3.43** was obtained in 30% yield along with unreacted starting compounds (Table 3.1, entry 9). Modification of the catalyst for *p*-TSA (20%) [45] increased the yield of **3.43** up to 45% (Table 3.1, entry 10). Moreover, when urea was in excess (1.5 equiv. with respect to lawsone) the yield of **3.43** was improved up to 55% (Table 3.1, entry 11). The Biginelli-linear product **3.43** was obtained pure by precipitation in a minimum volume of the mixture DCM/Et₂O (1:2). Importantly, when operating with the planetary ball mill Pulverisette 7 (P7) instead of the vibratory mill MM440, compound **3.43** was obtained in an excellent 90% yield (Table 3.1, entry 12) and purification occurred by simply washing with water to remove the urea excess and catalyst. Remarkably, under mechanochemical activation, the Michael adduct **3.44** was never formed, and the Biginelli-linear compound **3.43** was, in all cases, the unique product of this multicomponent reaction, proving its selectivity.

3.2.1.2 Structure characterization of model compound **3.43**

The chemical structure of compound **3.43** was unambiguously attributed thanks to ¹H, ¹³C NMR and 2D ¹H-¹H correlated spectroscopy (COSY) and ¹H-¹³C heteronuclear multiple bond correlation (HMBC) NMR analyses in DMSO-*d*₆ at 298K. All ¹H and ¹³C signals were assigned based on chemical shifts (δ, ppm), spin-spin coupling constants, splitting patterns and signal intensities. The ¹H and ¹³C assignments of **3.43** are summarized in Table 3.2. The ¹H NMR spectrum exhibited all expected signals (δ, ppm) for all different protons of naphthoquinone ring system as well as the aromatic protons of 4-chlorophenyl moiety. The characteristic proton H-9 was found at 6.40 ppm as a doublet, coupled with its neighbor NH proton which was detected at 6.82 ppm. The ¹³C resonance data exhibited 16 signals in total, that were non-ambiguously assigned. The ¹³C-¹H HMBC experiment showed correlation between H-9 and NH, C-2, C-3, C-4 and C-10 allowing to unambiguously assign the peaks at 155.8 ppm and 158.0 ppm to C-2 and C-10, respectively.

Table 3.2. ^1H and ^{13}C NMR data assignments of compound **3.43** in DMSO- d_6 at 298K.

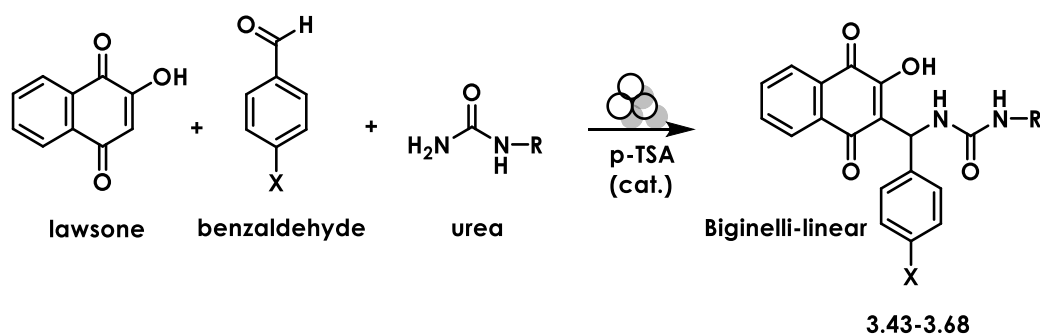
$^1\text{H}/^{13}\text{C}$ numbering	^1H chemical shift (ppm)	^{13}C chemical shift (ppm)
C-1	-	181.3
C-2	-	155.8
C-3	-	122.6
C-4	-	184.1
C-4a	-	130.8
CH-5	7.80 (m)	125.8
CH-6	8.03 (m)	134.8
CH-7	7.90 (m)	133.4
CH-8	7.94 (dd, $J = 7.6, 1.4$ Hz)	125.7
C-8a	-	130.1
CH-9	6.40 (d, $J = 9.8$ Hz)	46.3
C-10	-	158.0
NH	6.82 (d, $J = 9.8$ Hz)	-
NH ₂	5.88 (bs)	-
C-1b	-	141.8
CH-2b	7.32 (m)	127.7
CH-3b	7.32 (m)	128.0
C-4b	-	131.8

* ^1H and ^{13}C numbering of **3.43** do not follow IUPAC rules.

3.2.1.3 Substrate scope for the mechanochemically activated Biginelli-type reaction

After establishing the optimal reaction conditions (Table 3.1, entry 12) to obtain compound **3.43**, the substrate scope of this Biginelli-type reaction was explored. Lawsone was submitted to reaction with various *para*-substituted benzaldehydes, bearing either electron donating or electron withdrawing substituents, and *N*-alkylated urea derivatives, namely *N*-ethyl, *N*-butyl, *N*-propargylurea and 2-hydroxyethyl urea. A ratio 1:1:1.5 of the three reactants lawsone/benzaldehyde/urea was operated in a planetary ball mill (P7), catalyzed by 20 mol% *p*-TSA, while the number of runs was optimized for each case (reported in the Experimental Part). The obtained results are summarized in Table 3.3.

Table 3.3. Structures and isolated yields of products obtained by this Biginelli-type reaction between lawsone, benzaldehydes and *N*-alkylureas.



Entry	Product	X	R	Yield * (%)
1	3.43	Cl	H	90
2	3.45	OMe	H	60**
3	3.46	F	CH ₂ CH ₃	63
4	3.47	Cl	CH ₂ CH ₃	62
5	3.48	Br	CH ₂ CH ₃	70
6	3.49	I	CH ₂ CH ₃	70
7	3.50	NO ₂	CH ₂ CH ₃	85
8	3.51	CF ₃	CH ₂ CH ₃	90
9	3.52	CH ₃	CH ₂ CH ₃	70
10	3.53	OMe	CH ₂ CH ₃	60**
11	3.54	F	CH ₂ CH ₂ CH ₂ CH ₃	81
12	3.55	Cl	CH ₂ CH ₂ CH ₂ CH ₃	85
13	3.56	Br	CH ₂ CH ₂ CH ₂ CH ₃	95
14	3.57	NO ₂	CH ₂ CH ₂ CH ₂ CH ₃	90
15	3.58	CF ₃	CH ₂ CH ₂ CH ₂ CH ₃	80
16	3.59	OMe	CH ₂ CH ₂ CH ₂ CH ₃	70**
17	3.60	F	CH ₂ C≡CH	83
18	3.61	Cl	CH ₂ C≡CH	73
19	3.62	Br	CH ₂ C≡CH	88
20	3.63	NO ₂	CH ₂ C≡CH	70
21	3.64	CF ₃	CH ₂ C≡CH	82
22	3.65	OMe	CH ₂ C≡CH	70**
23	3.66	Cl	CH ₂ CH ₂ OH	80
24	3.67	NO ₂	CH ₂ CH ₂ OH	82
25	3.68	CF ₃	CH ₂ CH ₂ OH	80

* Isolated yield of target compound.

** Non purified ¹H NMR estimated yields.

Every reaction mixture was controlled by thin-layer chromatography (TLC) after every run, and it was stopped when both lawsone and benzaldehyde were fully consumed or when there was no more evolution. The obtained residue was washed with water to remove urea excess and catalyst. The crude reaction mixture was then analyzed by ¹H NMR. All products were purified by crystallization in a minimum volume of a mixture of organic solvents, DCM/Et₂O in the majority of cases. No column chromatography was necessary for purifications of any reaction mixture mentioned herein.

The reaction between lawsone, *N*-ethylurea, and a variety of *para*-substituted aldehydes was first studied. In all cases where the benzaldehyde was substituted with a halogen atom (Table 3.3, entries 3-6) or a methyl group (Table 3.3, entry 9), the non-cyclized products **3.46-3.49** and **3.52** were obtained in 62-70% yields, along with unreacted starting compounds. When *p*-nitrobenzaldehyde or *p*-trifluoromethyl benzaldehyde were used, the yields of the expected products **3.50** and **3.51** increased up to 85% and 90%, respectively (Table 3.3, entries 6 and 7, respectively). No side products were obtained. So, the selectivity of the reaction providing Biginelli-linear derivatives was higher than 95%.

When *N*-ethylurea was changed to *N*-butylurea, the conversion of both starting materials in deficit (benzaldehyde and lawsone) reached completion. All target compounds **3.54-3.58** (Table 3.3, entries 11-15) were obtained with yields ranging between 80% and 95%. Once more, a unique major product was identified, and no side products were formed.

Similar results were obtained when *N*-propynylurea/*N*-propargylurea was subjected to this Biginelli-type reaction with lawsone and various *para*-substituted benzaldehydes. The corresponding products **3.60-3.64** (Table 3.3, entries 17-21) were obtained after crystallization, with yields ranging between 70% and 88%. Finally, 2-hydroxyethylurea was also chosen to undergo this three-component reaction. The expected products **3.66-3.68** (Table 3.3, entries 23-25) were obtained in 80%-82% yield, no matter the *para*-substituent of the benzaldehyde used, namely -Cl, -NO₂ or -CF₃.

3.2.1.4 X-ray diffraction analysis of compound 3.61

Among all the compounds mentioned above, single crystals of **3.61**, suitable for analysis by X-ray diffraction were obtained. Crystallization was achieved in a mixture of dichloromethane and methanol (3:1). The obtained single crystals appeared as yellow platelets, and exhibited a triclinic P-1 space group under Mo-K α radiation ($\lambda = 0.71073 \text{ \AA}$). Inspection of the structure indicated dihedral angles of 19.7° for O-3/O-2/C-3/C-11, 9.2° for C-2/C-3/C-11/N-1, 83.6° for C-4/C-3/C-11/N-1, and 79.5° for C-3/C-11/N-1/C-12, meaning that the three components of the molecule (urea, naphthoquinone, and 4-chlorophenyl rings) did not share planarity. All hydrogen bonds, N-1/H-1, N-2/H-2, O-3/H-3, and C-11/H-11, had consistent values. Finally, it is worth mentioning the long distance between the remote atoms N-2/C-2 ($d = 5.3 \text{ \AA}$) and N-2/O-3 ($d = 5.8 \text{ \AA}$). This could potentially explain the non-formation of the cyclized Biginelli DHPM when using lawsone (Fig. 3.6).

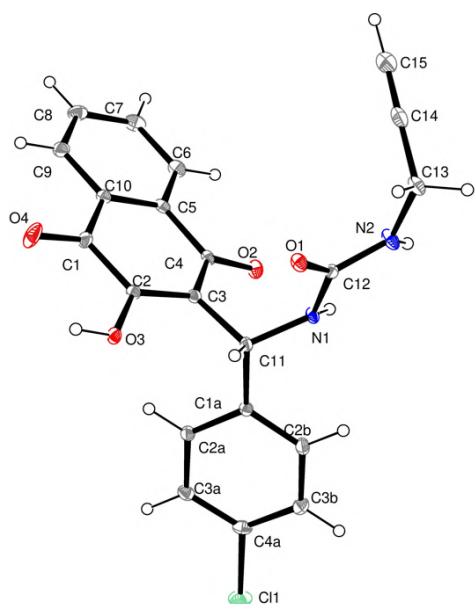


Figure 3.6. X-ray structure of compound **3.61**.

3.2.1.5 The reaction with *p*-anisaldehyde / *p*-OMe benzaldehyde

As mentioned in the Table 3.3 (entries 2,10,16 and 22), when the reaction was carried out with *p*-anisaldehyde, no matter the urea component used, a complicated mixture was obtained. ¹H NMR of all crude mixtures indicated the formation of the Biginelli-linear compounds **3.45**, **3.53**, **3.59** and **3.65**, (estimated yield between 60% and 70%), along with the Michael adduct and other unidentified compounds. All attempts for isolation by crystallization or flash column chromatography failed. So, all reaction mixtures were subjected to semi-preparative reversed phase HPLC. All reaction mixtures exhibited the same analytical profile.

The treatment of compound **3.65** (Table 3.3, entry 22) is presented herein as an example. When the crude reaction mixture of **3.65** was analyzed by LC-MS (gradient of water/acetonitrile, 0.1 vol% formic acid), the data collected (Fig. 3.7, panel A) were in agreement with what was observed after the ¹H NMR analysis. The Biginelli-linear **3.65** was found to be the major product (70%, eluted at *t* = 6.1 min) along with three other peaks at *t* = 4.4, 5.3 and 7.7 min. The product eluted at *t* = 7.7 min was identified by coupled LC/MS to be the Michael adduct (**3.69**) (25% by ¹H NMR) (*m/z* = 466.5). The other two peaks remained unidentified as they did not correspond to any starting compound, potential intermediate of the Biginelli reaction or the DHPM itself. The product **3.65** was successfully isolated from the reaction mixture (Fig. 3.7, panel B). However, when the isolated fraction was analyzed again after 30 min, under the same experimental conditions (Fig. 3.7, panel C), the formation of two new peaks at *t* = 4.4 and 5.2 min was evident. Interestingly, the same purified collected fraction had a different profile after 2 h (Fig. 3.7, panel D). In fact, the Michael adduct **3.69** was

reformed and the obtained chromatogram was similar to the one corresponding to the crude mixture before purification (Fig. 3.7, panel A).

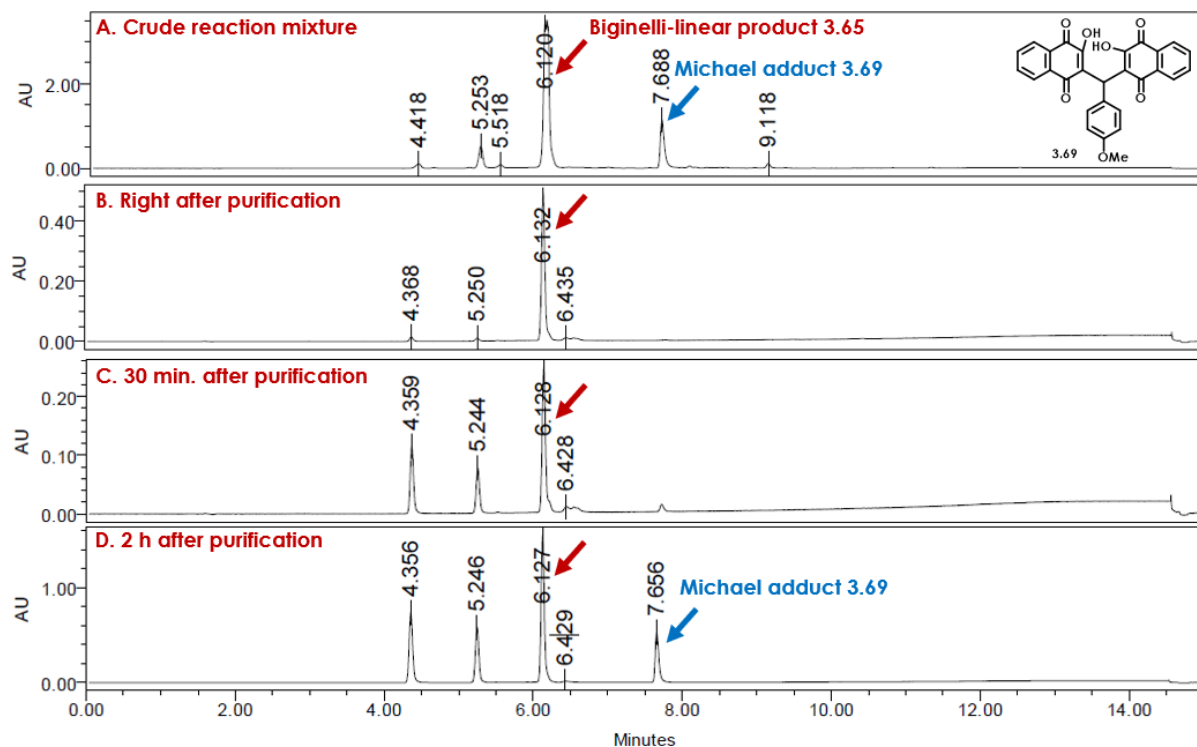


Figure 3.7. HPLC reversed phase (column C-18) chromatograms (A-D) for compound **3.65** by using a gradient of H₂O+0.1% HCOOH/ CH₃CN+0.1% HCOOH as the mobile phase and detection at 254 nm.

It was supposed that the formation of the Michael product was induced by the presence of acid under the HPLC conditions. So, the same semi-prep. reversed phase purification was repeated for a newly synthesized reaction mixture of compound **3.65** by using gradient of water/acetonitrile containing 0.1% of diethylamine (DEA). The Biginelli-linear **3.65** was found to be the major product (80%, eluted at $t = 3.2$ min.) along with two other peaks at $t = 3.0$, and 0.9 min. The product eluted at $t = 3.0$ min was identified by coupled LC/MS to be the Michael adduct **3.69** ($m/z = 466.5$) (Fig. 3.8, panel A). The other two peaks remained unidentified as they did not correspond to any starting compound or intermediates, peaks reported in acidic media (Fig. 3.7, panel A), potential intermediate of the Biginelli reaction or the DHPM itself. Compound **3.65** was successfully isolated (Fig. 3.8, panel B) and remained stable for a longer period of time (at least 24 h) (Fig. 3.8, panel C). The Michael adduct **3.65** was isolated as pure product with 25% yield by recrystallization.

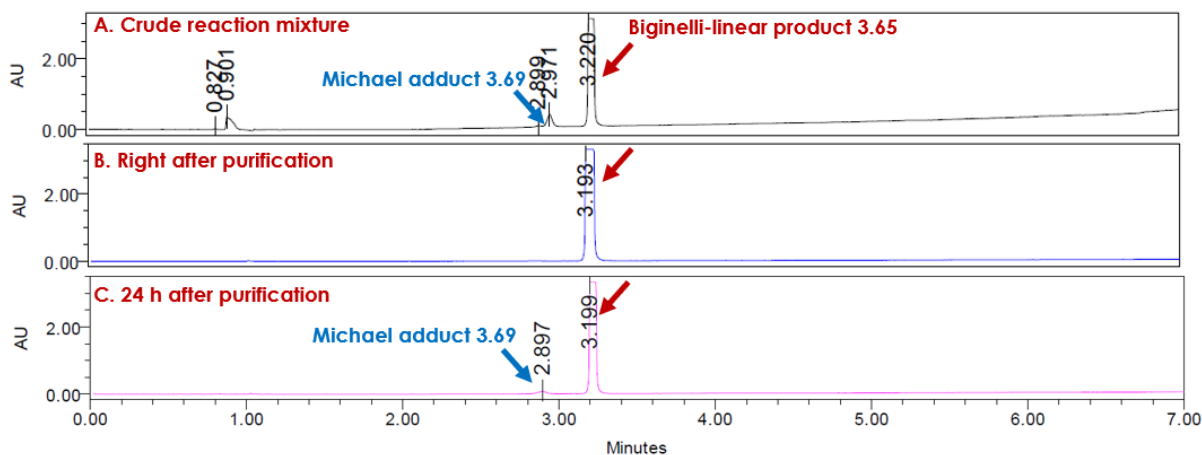


Figure 3.8. HPLC reversed phase (column C-18) chromatograms (A-D) for compound **3.65** by using a gradient of H₂O+0.1% DEA / CH₃CN+0.1% DEA as the mobile phase and detection at 254 nm.

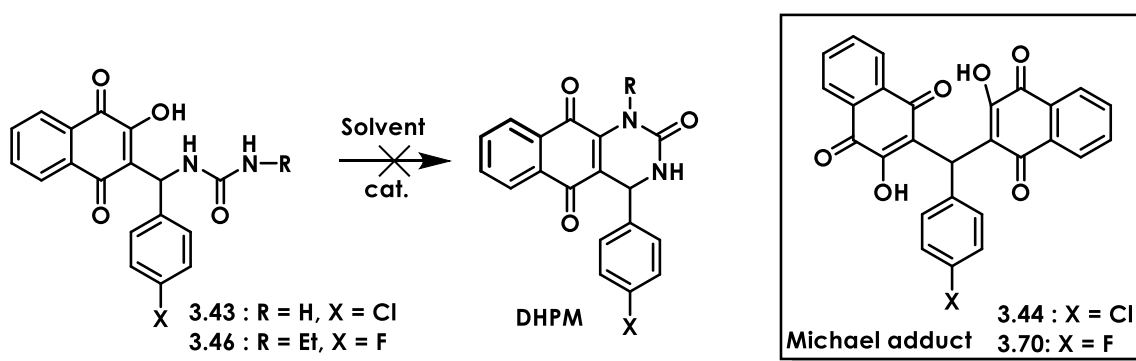
After taking all experimental data into consideration, two main products were synthesized under all tested experimental conditions: the so-called Biginelli-linear product and its corresponding Michael adduct. To the best of our knowledge, it is the first time that a Biginelli-linear compound was isolated, which until now was supposed to be an intermediate of the classical Biginelli reaction. It is also important to point out that this is the single compound issued from the mechanochemical reactions performed.

In addition, it should be noticed that the Biginelli-linear compound was not stable under acidic conditions and was transformed to the Michael adduct. This reaction probably involves reversible equilibrium reactions affording the Knoevenagel intermediate. This Knoevenagel intermediate could be formed either directly from the reaction between lawsone and the corresponding aldehyde, either by decomposition of reactive intermediates, allowing it to react with a second equiv. of lawsone, leading to the stable Michael adduct.

3.2.1.6 Cyclization attempts of Biginelli-linear **3.43** and **3.46** in solution

As spontaneous cyclization of Biginelli-linear products was found to be challenging in solid state, many attempts of cyclization were carried out in solution, to benefit from bond rotations. Both compounds **3.43** and **3.46** were chosen to undergo the cyclization studies in order to control that urea substitution was not affecting the cyclization step. For compound **3.46**, attempts are summarized in Table 3.4, while for compound **3.43** three attempts have been made, namely in EtOH, {[HNMP]HSO₄} (IL medium) and choline chloride/chloroacetic acid (DES medium).

Table 3.4. Cyclization attempts of Biginelli-linear compounds 3.43 and 3.46.



Entry	Activation method	Temperature (°C)	Reaction time (min.)	Catalyst	Solvent	Yield of Michael (%)
1	solution	rt	overnight	0.5% Zn(OAc) ₂	EtOH	-
2	IL	80	60	IL	[HNMP]HSO ₄	40-45
3	DES	70	180	DES	Choline chloride/ Chloroacetic acid	<5
4	irradiation (μw)	160	30	CH ₃ COOH	CH ₃ COOH (glacial)	<5
5	Eaton's reagent	rt	180	Eaton's reagent	MeSO ₃ H	-

When compounds **3.43** and **3.46** were introduced in EtOH (protic conditions), catalyzed by Zn(OAc)₂ [38] (Table 3.4, entry 1), no reaction was observed, even with long reaction times (overnight), and the starting compounds were recovered unchanged. When compounds **3.43** and **3.46** were introduced in the homemade IL medium {[HNMP]HSO₄} [42], no cyclization was observed either (Table 3.4, entry 2). The corresponding Michael adducts **3.44** and **3.70** were isolated as major products with 40% and 43% yield, respectively, after crushing the reaction mixture into ice and collecting the precipitates, as indicated in the literature [42].

Cyclization attempts in the homemade DES medium choline chloride/chloroacetic acid [44] afforded less than 5% of Michael adducts **3.44** and **3.70** (estimated by ¹H NMR analysis of the crude mixture) among unreacted starting compounds (Table 3.4, entry 3). No DHPM formation was observed. Harsh cyclization conditions such as microwave irradiation in glacial acetic acid applied to **3.46**, provided a very complicated and quite unstable reaction mixture (Table 3.4, entry 4). The starting **3.46** was entirely decomposed, while the corresponding Michael adduct **3.70** was detected in the crude reaction mixture with less than 5% estimated yield. Finally, the same reaction catalyzed by Eaton's reagent [46] (phosphorus pentoxide P₂O₅ in methanesulfonic acid ratio 1/10) afforded an unstable reaction mixture in which no product

could be identified after numerous purification efforts and spectroscopic analyses (Table 3.4, entry 5). Nonetheless, for these two latter attempts (unstable reaction mixtures) the decomposition of the starting Biginelli-linear compound was obvious as all three counterparts (lawsone, urea, benzaldehyde) were identified in the reaction mixtures by ^1H NMR and mass spectroscopy analyses.

3.2.1.7 Theoretical studies

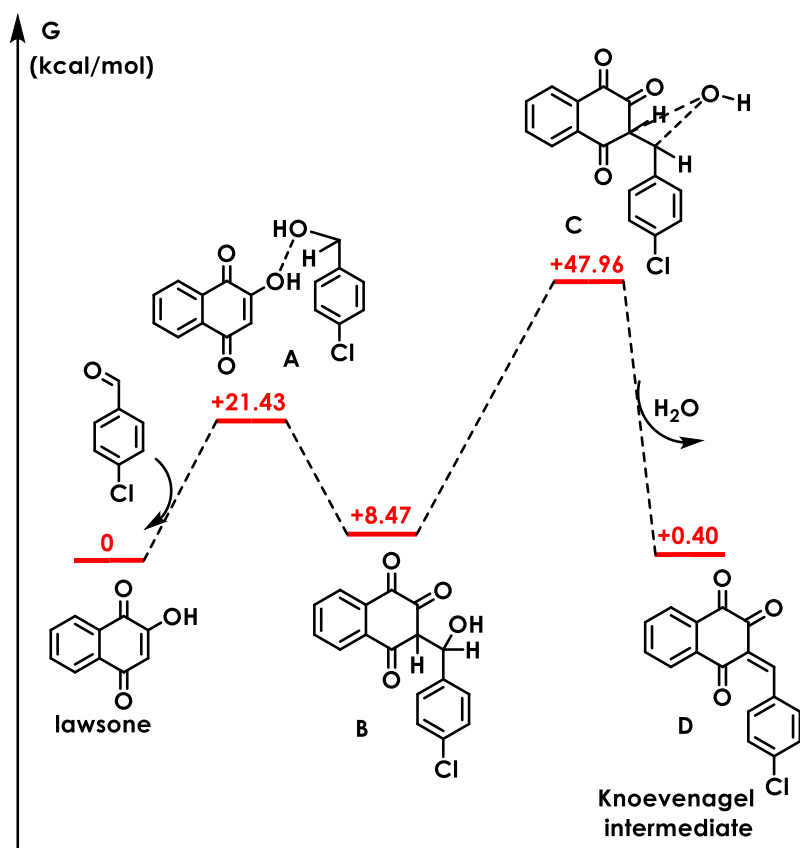
Without aiming to undergo an extensive theoretical study concerning all possible mechanisms of this reaction and all potential intermediates that could be in equilibrium, and taking into account the Michael formation, we wished to explain the experimental results by using a preliminary (density functional theory) DFT modeling [47–49]. This study was conducted by Dr. Jean-Marc Sotiropoulos and Prof. Philippe Carbonnière at the « Institut des Sciences Analytiques et de Physico-Chimie pour l'Environnement et les Matériaux » (CNRS-IPREM), of Université de Pau et des pays de l'Adour (UMR 5254), in France.

The results of DFT calculations in the gas and/or liquid phases (protic solvent) cannot be immediately transferred to solid state issues. Nonetheless, these results may provide valid insights into the energies involved in the process as well as the activation energy gaps. It is essential to note that the Biginelli-linear compound could not be cyclized by any experimental means via mechanochemical activation.

In comparison to conventional reaction conditions, mechanochemical reactions can produce unexpected products or product ratios. As an example, Gonnet *et al.* studied the elucidation of the Diels-Alder reaction kinetics between diphenylfulvene and maleimide [50a]. Later, based on DFT calculations, Sakai, Gonnet *et al.* reported the origin of mechanochemical selectivity in a Diels-Alder model reaction. They concluded that application of a mechanical force can result in lowering the activation barrier on one pathway (endo-type), but not on the other (exo-type) [50b].

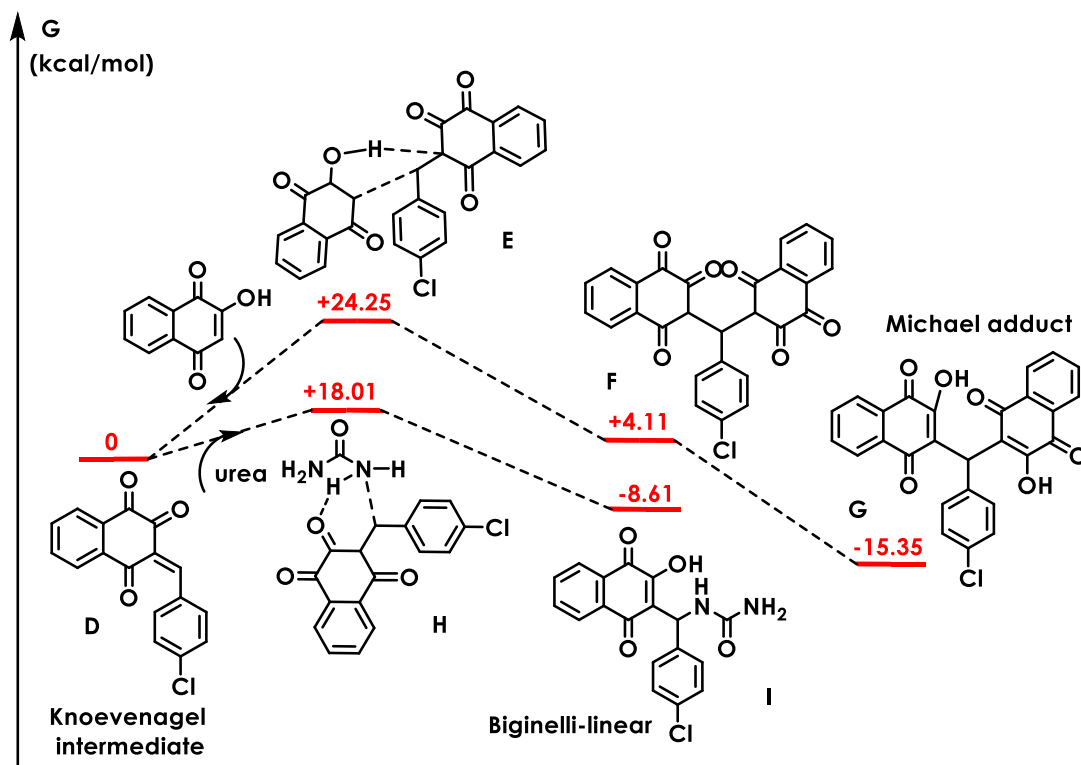
During our study, the initial step of the reaction was considered to be the addition of lawsone to the benzaldehyde. Both *para*-substituted benzaldehydes bearing either an electron withdrawing (4-chlorobenzaldehyde) or an electron donating group (*p*-OMe benzaldehyde) were studied and demonstrated similar energy profiles, no matter the type of the substituent. A preliminary DFT modeling in gas phase, using the B3LYP functional coupled with a 6-31+G(d,p) Gaussian basis set and accounting for dispersion (D3), when using *p*-chlorobenzaldehyde, displayed the energy profile depicted into scheme 3.8. The nucleophilic attack of lawsone to the carbonyl group of the aldehyde, led to an initial hydrated intermediate **B** with rapid kinetics (driving force step). The calculated activation energy for **B** formation was found to be $\Delta G = 21.43$ kcal/mol (20.96 kcal/mol for *p*-OMe) while the energy

level of the intermediate itself was placed at 8.47 kcal/mol (9.78 kcal/mol for *p*-OMe). Slow dehydration of **B** (rate determining step) demanded the respectable amount of 39.49 kcal/mol (39.27 kcal/mol for *p*-anisaldehyde) as activation energy, passing through the very reactive intermediate **C**, placed at 47.96 kcal/mol (49.05 kcal/mol for *p*-OMe), which was subsequently transformed into the stable expected Knoevenagel intermediate **D** (Scheme 3.8).



Scheme 3.8. DFT calculations of the Knoevenagel intermediate pathway.

Two potential reaction pathways can emerge starting from Knoevenagel intermediate **D** (Scheme 3.9). The first pathway involves its reaction with another equiv. of lawsone with an activation energy $\Delta G = 24.25$ kcal/mol (27.79 kcal/mol for *p*-OMe). This leads to the formation of a significantly stable tri-ketone Michael derivative **F** placed at 4.11 kcal/mol (6.48 kcal/mol for *p*-OMe) which converts to the far more stable enol form **G** placed at -15.35 kcal/mol (-12.67 kcal/mol for *p*-OMe) (driving force step). The second pathway involves the reaction between **D** and urea. In this case, the expected Biginelli-linear product **I** can be formed, placed at -8.61 kcal/mol (5.11 kcal/mol for *p*-OMe). The calculated activation energy for **I** formation was found to be $\Delta G = 18.01$ kcal/mol (20.11 kcal/mol for *p*-OMe).



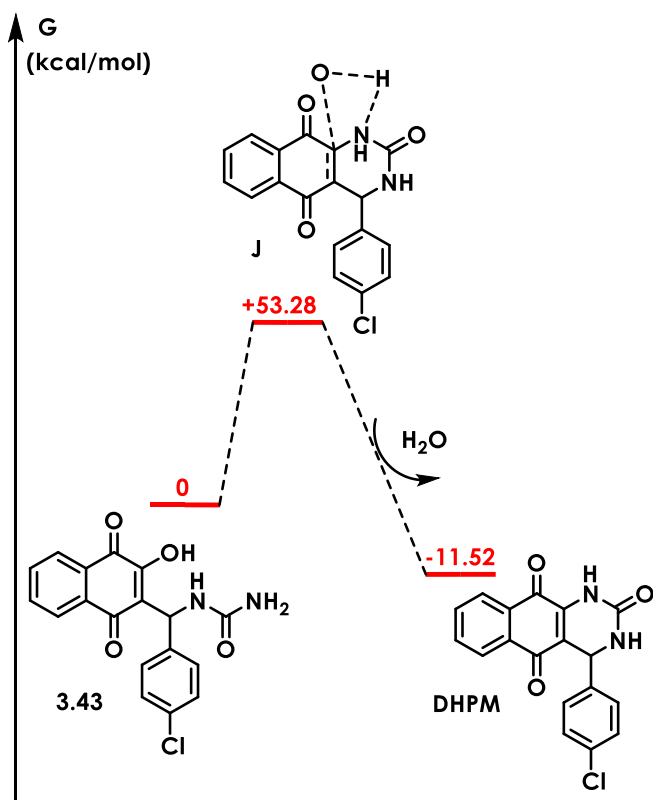
Scheme 3.9. DFT calculations for Michael adduct formation and Biginelli-linear product via Knoevenagel intermediate.

Afterwards, the DFT calculations were repeated taking into account the effect of ethanol (protic conditions) as solvent, by using the conductor-like polarizable continuum model (C-PCM) [51]. The obtained results were similar to the model used in gas phase, explained above. The protic polar solvent (EtOH) was also considered in this study and did not seem to significantly modify neither the energy barrier responsible for Michael adduct formation ($\Delta G = 25.0$ kcal/mol) nor the energy activation barrier responsible for Biginelli-linear product formation ($\Delta G = 20.0$ kcal/mol). These findings are in agreement with all the obtained experimental data.

To conclude, the proposed mechanism for the Biginelli reaction between 2-hydroxy-1,4-naphthoquinone (lawsone), *para*-substituted benzaldehydes, bearing either an electron donating or an electron withdrawing group, and urea could support a mechanism via the Knoevenagel intermediate formation. Two potential pathways could be in competition in solution (protic solvents, ILs, DES): lawsone or urea addition to the Knoevenagel intermediate. The lawsone addition, leading to the Michael adduct, seems to be less energetically favored than the three-component reaction (urea addition) even if the Michael adduct is much more stable than the Biginelli-linear product. Finally, it seems that Biginelli-linear products bearing benzyl substituents at C-3 with electron donating groups (4-OMe) are in general significantly less thermodynamically stable when comparing them to benzyl substituents at C-3 with electron withdrawing groups (4-Cl). Compound's **3.43** lowest energy (4-Cl) was estimated to be equal to -8.61 kcal/mol, while compound's **3.45** lowest energy (4-OMe) was placed at +5.11 kcal/mol.

Energy profile for the cyclization of Biginelli-linear to DHPM derivative

The cyclization step of the model Biginelli-linear **3.43** to the desired DHPM final product was also evaluated using the same DFT model in gas phase (Scheme 3.10). The activation energy for this cyclization was found to be $\Delta G = 53.28$ kcal/mol ($\Delta G = 53.48$ kcal/mol for *p*-OMe).

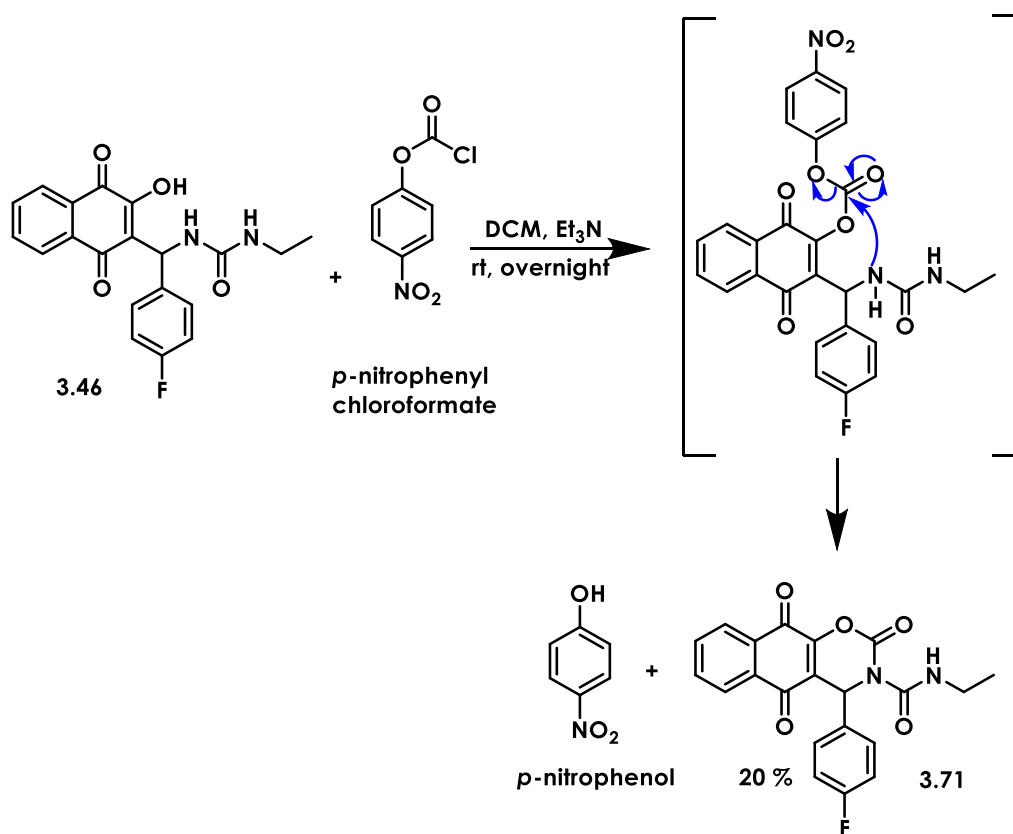


Scheme 3.10. DFT calculations for cyclization pathway of **3.43**.

Even if the cyclized desired DHPM product was significantly more thermodynamically stable than the non-cyclized linear molecule **3.43**, placed at -11.52 kcal/mol (-12.34 kcal/mol for *p*-OMe), it is needed to overcome a huge energy barrier at + 53 kcal. Thus, this intramolecular condensation is not favorable. In addition, the DFT model suggested that the structure of Biginelli-linear products carries restrictions. In fact, the calculated structure of **3.43** aligned with the obtained X-ray structure of **3.61** derivative. Indeed, the amido substituent of **3.43** (and **3.61**) at C-3 is located very far and opposite to carbon C-2 which is supposed to attack. As a result, even if we can consider that by mechanochemical friction we can transfer energy to the Biginelli-linear derivative, the amount is not enough for the cyclization to take place, even if the cyclized structure is thermodynamically favored (-11.52 kcal/mol).

3.2.1.8 Cyclization of Biginelli-linear **3.46** via activation of the 2-hydroxy function

Taking into account all the previous failed cyclization attempts, new methodologies needed to be elaborated focusing on the activation of the enol functional group of the Biginelli-linear derivatives. *Para*-nitrophenyl chloroformate was selected for the 2-hydroxy activation, a well-known methodology used in nucleoside synthesis. In that respect, *N*-ethylurea substituted derivative **3.46** was chosen to react with *para*-nitrophenyl chloroformate in pyridine at room temperature [52]. As no product formation was observed, the reaction was repeated under reflux in pyridine for 2 h. The latter led to an unstable reaction mixture due to the decomposition of the starting compound (evidenced by ¹H NMR and mass spectroscopy). Neither the corresponding DHPM, nor the expected carbonate ester was formed. After a few more attempts, compound **3.46** was submitted to reaction with *para*-nitrophenyl chloroformate in dry dichloromethane (DCM) with excess of Et₃N, at ambient temperature, overnight [53]. Gratifyingly, the cyclized derivative **3.71** was obtained in 20% yield after semi-prep. reversed phase HPLC purification (scheme 3.11).

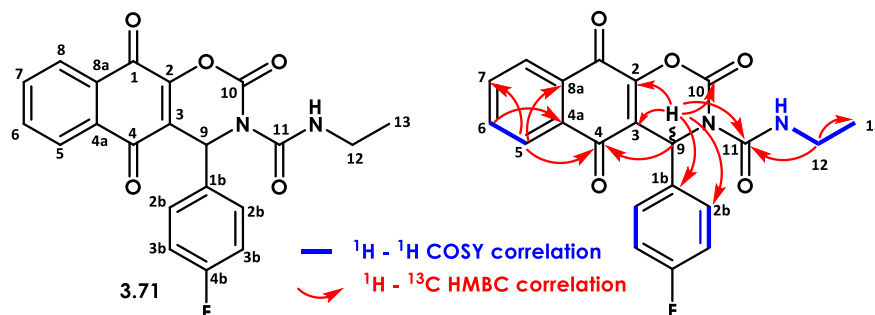


Scheme 3.11. Cyclization of **3.46** into the naphtho-carbamate **3.71**.

To the best of our knowledge, it is the first time that an ureido-bearing 1,4-naphthoquinone carbamate is synthesized, paving the way for further developments of this synthetic approach.

The structure of compound **3.71** was confirmed by 2D-NMR analyses at 298 K in CDCl₃. All ¹H and ¹³C signals were assigned based on the chemical shifts, spin-spin coupling constants, splitting patterns, and signal intensities by using ¹H-¹H COSY, ¹H-¹³C HSQC, and ¹H-¹³C HMBC experiments. The ¹H and ¹³C chemical shifts of **3.71** are given in Table 3.5.

Table 3.5. ¹H and ¹³C NMR data assignments of compound **3.71** in CDCl₃ at 298K.



¹ H/ ¹³ C numbering	¹ H chemical shift (ppm)	¹³ C chemical shift (ppm)
C-1		176.3
C-2		147.6
C-3		123.3
C-4		180.9
C-4a		131.3
CH-5	8.05 (m)	127.0
CH-6	7.79 (m)	135.0
CH-7	7.90 (m)	134.6
CH-8	8.17 (m)	127.1
C-8a		131.3
CH-9	6.84 (s)	52.6
C-1b		134.0
CH-2b	7.44 (m)	129.5 (d, J = 8.0 Hz)
CH-3b	7.03 (m)	116.3 (d, J = 21.0 Hz)
C-4b		163.0 (d, J = 248.0 Hz)
C-10		148.5
C-11		151.3
NH	8.41 (t, J = 5.6 Hz)	
CH-12	α= 3.33 (m) b=3.37 (m)	36.3
CH-13	1.17 (t, J = 7.3 Hz)	14.7

* ¹H and ¹³C numbering of **3.71** do not follow IUPAC rules.

The ¹H NMR spectrum revealed some significant features: the NH showed up as a broad triplet at 8.41 ppm, indicating a coupling to the nearby CH₂ group, as demonstrated by the COSY experiment, while H-9 was found at 6.84 as a sharp singlet, indicating that it had no neighbor protons. The rigidity of the structure caused the protons H_a-12 and H_b-12 to appear as diastereotopic, and they demonstrated coupling with both their neighbors CH₃ and NH. For each type of carbon, the ¹³C resonance data revealed a total of 19 signals, their attribution enabled the non-ambiguous structure identification of **3.71**.

The signals at 176.3 ppm and 180.9 ppm were attributed to the two carbonyl groups of the naphthoquinone ring, while the urea carbon C-11 resonated at 151.3 ppm. The newly formed carbamate carbonyl C-10 signal appeared at 148.5 ppm. The ^{13}C - ^1H HMBC experiment contributed to the identification of all long-range couplings between protons and carbons. In addition, the correlation of H-9 with all carbons C-2, C-3, C-4, C-10, C-1b, C-2b, C-3b, and C-11 as well as the revelation of the relevantly different dislocated chemical shifts values for H-9 and C-9 between **3.71** (H-9 at 6.84 ppm and C-9 at 52.6 ppm) and starting compound **3.46** (H-9 at 6.54 ppm and C-9 at 49.0 ppm) permitted the unambiguous structure confirmation of the cyclized naphtho-carbamate derivative **3.71**.

3.3 Biological and *in silico* evaluation of the Biginelli-linear series

Although the Biginelli-linear series was not intended to be our objective, the biological activities of these new molecules were investigated. Related compounds, 2-hydroxy-1,4-naphthoquinone derivatives bearing C-3 substituted amino moieties, particularly known as lawsone Mannich bases, have been reported in the literature (Fig. 3.9, compounds **3.72**), and their antiplasmodial activities against *P. falciparum* CQ-sensitive (3D-7) and CQ-resistant (RKL-2) and multidrug resistant (K1) strains were evaluated [54],[55]. The most promising among them retained IC_{50} values between 1.0 μM and 1.3 μM , better than CQ which was used as reference. However, the mechanism of action of these compounds was not known. The ethyl-amino substituent at C-3 was found to be an important feature for the observed activity, while the better combination of the side chains R_1 and R_2 is still under investigation [56].

In addition, similar naphthoquinone derivatives with a urea moiety have recently been reported to exhibit leishmanicidal activities with IC_{50} values between 1.2 μM and 3.2 μM against *L. pifanoi* axenic amastigote forms, and selectivity index values ranging between 2.3 and 3.3 [57] (Fig. 3.9, compounds **3.73**). Their IC_{50} values were comparable to the parent MBC-132 (IC_{50} = 0.5 μM and SI = 5.1) (Fig. 3.8), a well-known *L. donovani* GSK-3s inhibitor. However, their proposed mechanism of action, namely inhibition of glutathione reductase GSK-3, was not proved.

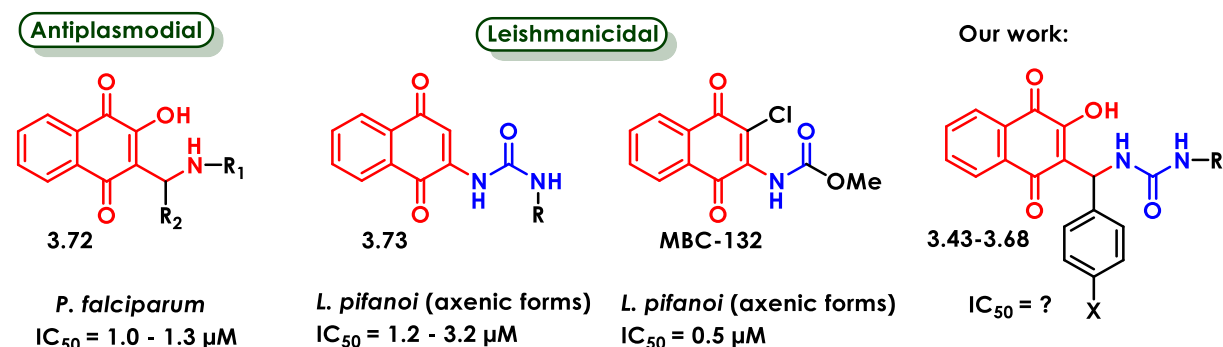


Figure 3.9. Lawsone Mannich bases and their antiparasitic activities.

3.3.1 *In silico* evaluation against mitochondrial targets of *P. falciparum*

The *in silico* evaluation of the following synthesized series was conducted by me during my internship (2 months) in the Institute of Chemistry, Department of Molecular Technology (Tartu, 50411, Estonia) while supervised by Dr Alfonso Garcia-Sosa. The Biginelli-linear series was first submitted to an *in silico* screening against both mitochondrial targets of *P. falciparum* bc1 and DHODH in order to verify if there could be any potential interactions between them. For bc1 target, the cytochrome enzyme Q7HP03, isolated from the X-ray complex structure of atovaquone in the catalytic Qo site of bc1 in *Saccharomyces cerevisiae* (PDB: 4PD4) was used [58]. As it did not belong to *P. falciparum* parasite, it was AlphaFold2 modeled. The final predicted model used for docking of bc1 was highly confident (See Chapter 2 for more details). For DHODH target, the X-ray crystal structure of the enzyme bound with XCV of *P. falciparum* was available in PDB (PDB: 7L01) with very good resolution and was used as such [59] (See Chapter 2 for more details).

Atovaquone (ATQ) was used as positive control for docking against bc1 (Table 3.6, entry 22) and XCV (Table 3.6, entry 23) against DHODH, as its inhibitor. Both ATQ and XCV were used exactly as found into the binding site of the corresponding mitochondrial target without generating extra ionization forms and isomers after auto-docking. The most favorable binding pose of the naphthoquinone structure for ATQ and all molecules of the series was found to be its ionized tautomeric form presented in Fig. 3.10. The ligand-protein system was completely free to reach the most energetically favorable pose, without imposing any restrictions. During this study, water molecules were completely removed before docking for both targets. The interactions of ATQ were similar to those of MMV007571 (See Chapter 2) in both targets. The naphthoquinone ring of ATQ and the whole series of molecules was found to bind in its tautomeric form to both targets (Table 3.6).

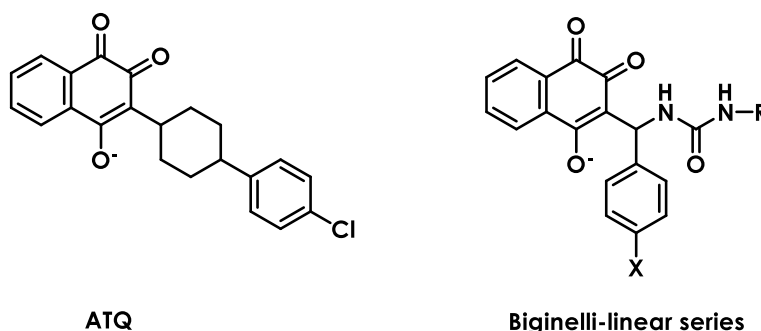
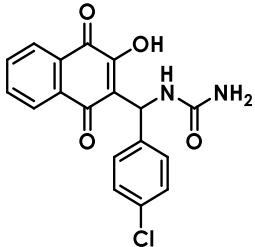
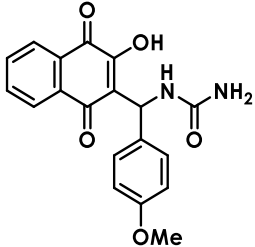
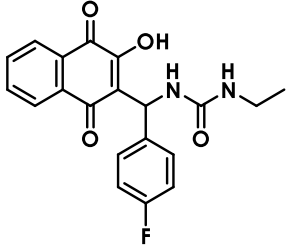
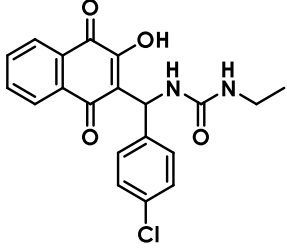


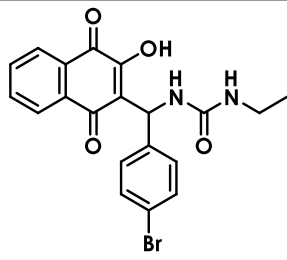
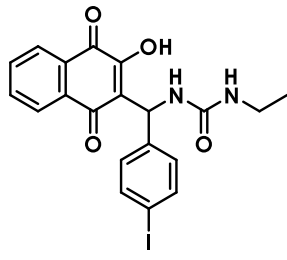
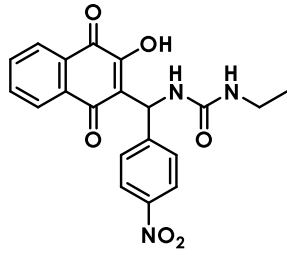
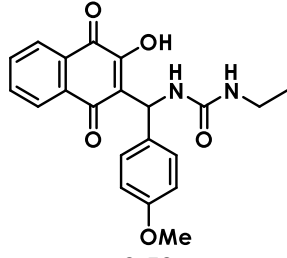
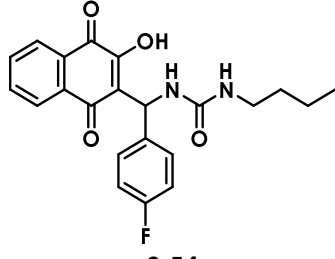
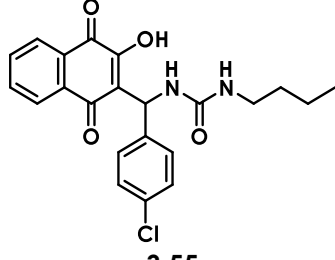
Figure 3.10. Optimal structure found for binding into the bc1 binding site.

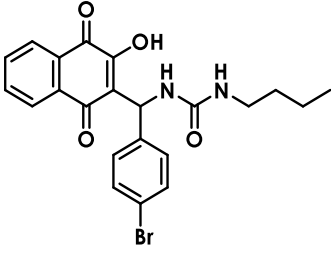
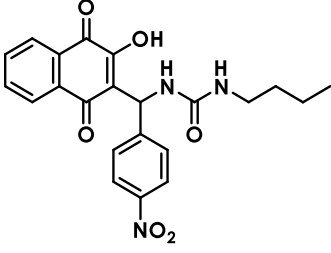
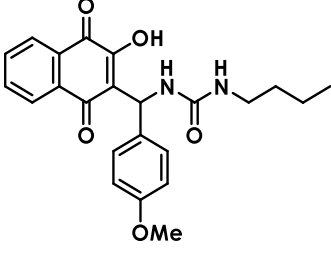
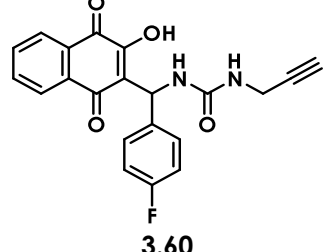
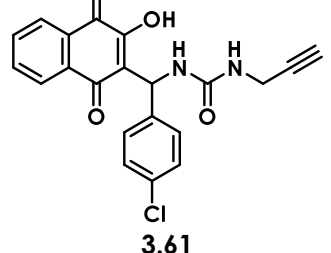
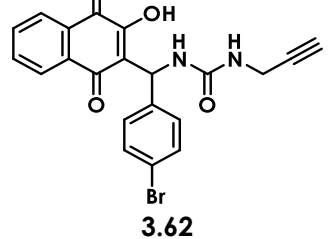
Into bc1, precisely, the naphthoquinone ring of ATQ exhibited strong hydrophobic interactions with Met 133, Ile 141 and Ile 258. The cyclohexyl moiety contributed to strong hydrophobic interactions with Ile 141 and Phe 264, while the *para*-chlorobenzyl substituent was placed out of the binding site (solvent exposed). In DHODH binding site, XCV formed substantial

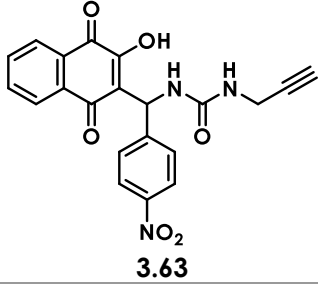
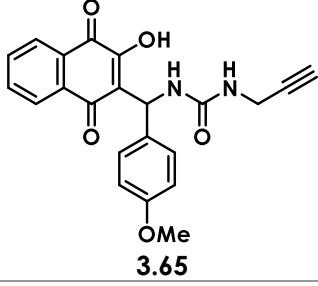
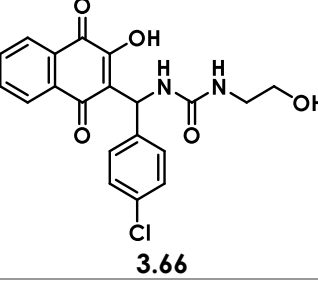
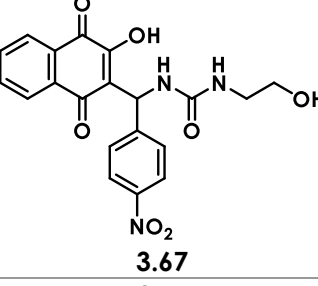
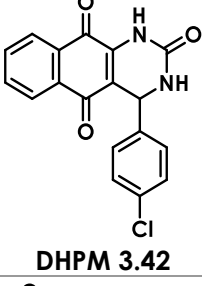
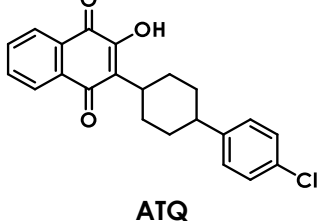
hydrogen bonds with Arg 265 and His 185 and displayed strong polar interactions with Cys 184 and His 185. However, the CF₃ substituent was placed out of the binding site (solvent exposed). All docking scores of this library of compounds are presented in Table 3.6.

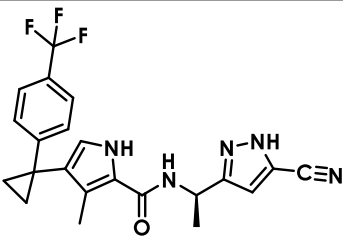
Table 3.6. *In silico* evaluation of Biginelli-linear series: predicted docking scores of compounds against bc1 and DHODH mitochondrial targets of *P. falciparum*.

Entry	Compound	Docking score <i>Pfbc1</i> (kcal/mol)	Docking score <i>PfDHODH</i> (kcal/mol)
1	 <p style="text-align: center;">3.43</p>	-8.8	-7.4
2	 <p style="text-align: center;">3.45</p>	-9.1	-5.2
3	 <p style="text-align: center;">3.46</p>	-9.1	-6.1
4	 <p style="text-align: center;">3.47</p>	-9.0	-5.9

5	 <p style="text-align: center;">3.48</p>	-6.7	-4.9
6	 <p style="text-align: center;">3.49</p>	-5.6	-8.6
7	 <p style="text-align: center;">3.50</p>	-8.7	-6.4
8	 <p style="text-align: center;">3.53</p>	-9.4	-6.0
9	 <p style="text-align: center;">3.54</p>	-6.7	-6.8
10	 <p style="text-align: center;">3.55</p>	-10.0	-7.1

11	 <p style="text-align: center;">3.56</p>	-9.0	-7.0
12	 <p style="text-align: center;">3.57</p>	-7.3	-7.1
13	 <p style="text-align: center;">3.59</p>	-8.0	-6.9
14	 <p style="text-align: center;">3.60</p>	-6.1	-6.4
15	 <p style="text-align: center;">3.61</p>	-2.7	-6.6
16	 <p style="text-align: center;">3.62</p>	-6.9	-7.0

17	 <p style="text-align: center;">3.63</p>	-3.1	-5.8
18	 <p style="text-align: center;">3.65</p>	-5.8	-5.9
19	 <p style="text-align: center;">3.66</p>	-9.3	-6.9
20	 <p style="text-align: center;">3.67</p>	-4.7	-7.2
21	 <p style="text-align: center;">DHPM 3.42</p>	-8.2	-10.1
22	 <p style="text-align: center;">ATQ</p>	-11.3	-

23	 <p style="text-align: center;">XCV</p>	-	-11.2
----	---	---	-------

A generated library of decoys [60],[61] that was downloaded from Maestro Schrodinger was used to assess the obtained docking scores. The naphthoquinone derivatives with the highest docking scores (more negative) out of the entire set of molecules were re-docked with this library of 1000 drug-like molecules (decoys). The most active compounds of all naphthoquinone families for the bc1 target were ranked in the top 10%, passing the decoys test. The most active compounds of all naphthoquinone families for DHODH received a 19% top score, which was also acceptable. ATQ and XCV were both ranked even higher, belonging to less than top 5% of all molecules tested. This proves that the docking methodology used was reliable and did not produce any false positives.

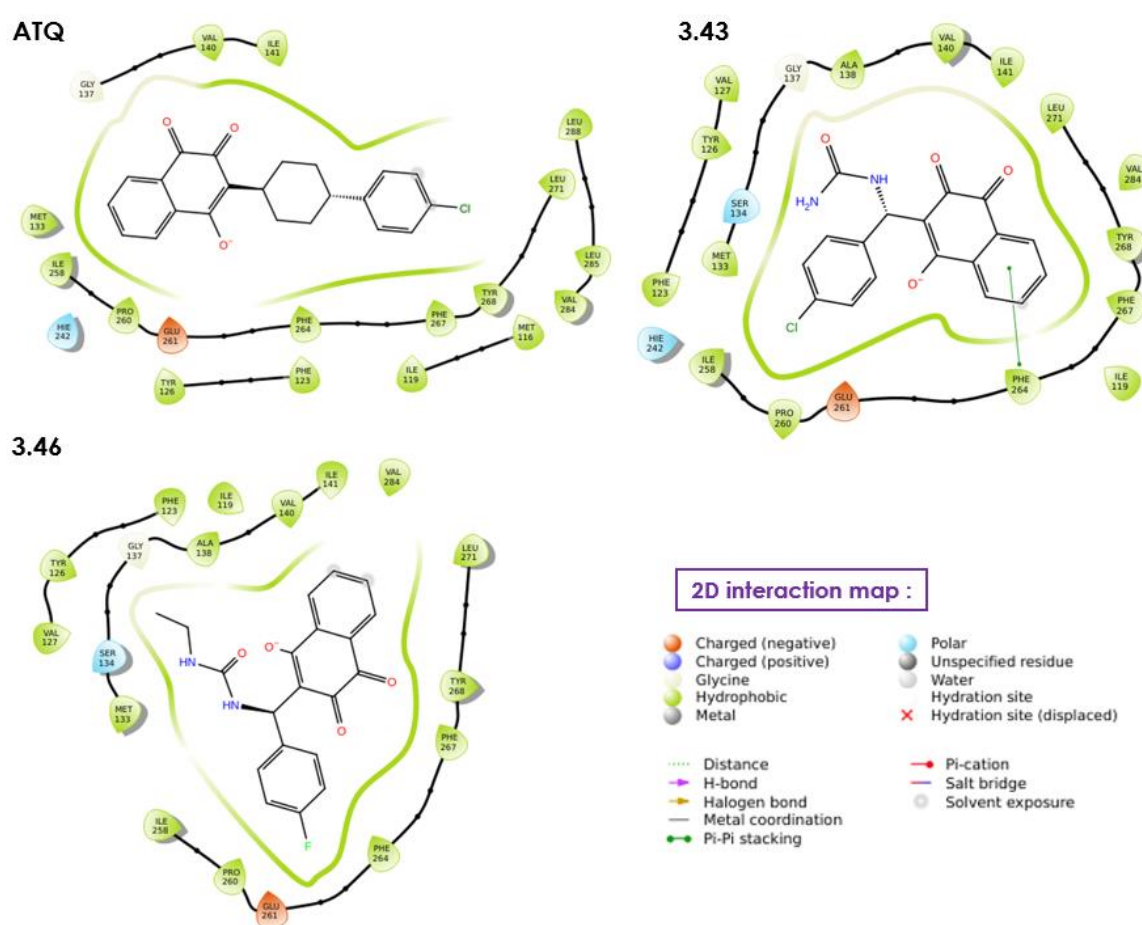
All 2-hydroxy-1,4-naphthoquinone derivatives were docked into the binding site of bc1 and DHODH, and their anticipated interactions revealed comparable binding modes and interaction partners as compared to the known inhibitors ATQ and XCV. In addition, the whole series of molecules was found capable to enter the binding site, even in cases when the docking scores were not quite favorable. Five families of molecules can be distinguished, characterized by the urea side chain substitution: urea (no substituent), ethyl, butyl, propynyl/propargyl and 2-hydroxyethyl urea-naphthoquinone derivatives.

o **P. falciparum cyt bc1 mitochondrial target:**

Generally speaking, against bc1 target, all except propargyl urea derivatives (Table 3.6, entries 14-18) bearing a 4-halogen substituted phenyl ring at C-3 exhibited the higher (more negative) docking scores. This can be accounted for the naphthoquinone ring's numerous potent hydrophobic and pi-pi stacking interactions with the bc1 binding site. For example, compounds **3.43** (urea derivative), **3.46** (ethyl urea derivative) and **3.66** (2-hydroxyethyl urea derivative) (Fig. 3.11) exhibited comparable docking scores (Table 3.6, entries 1, 3 and 19, respectively) and quite similar binding poses to atovaquone at the same position of the cavity and very strong hydrophobic interactions with the bc1 target.

However, it should be noted that the naphthoquinone ring of these three derivatives had a different orientation in comparison to ATQ while entering the binding site. This orientation favored an extra pi-pi stacking of the naphthoquinone ring of compound **3.43** and **3.66** with Phe 264 residue (Fig. 3.11). In addition, for compound **3.66**, the terminal hydroxy group is able to form a hydrogen bond with Leu 271.

The butyl-urea derivative **3.55** (Table 3.6, entry 10) exhibited the best (-10 kcal/mol) docking score of the whole series against bc1. This result was consistent with the fact that **3.55** exhibited a very similar binding pose to that of ATQ and it entered into the binding site having the same orientation. That permitted strong hydrophobic interactions with all neighbor amino acid residues and pi-pi stacking interactions with Phe 264 and Tyr 126 (Fig. 3.11).



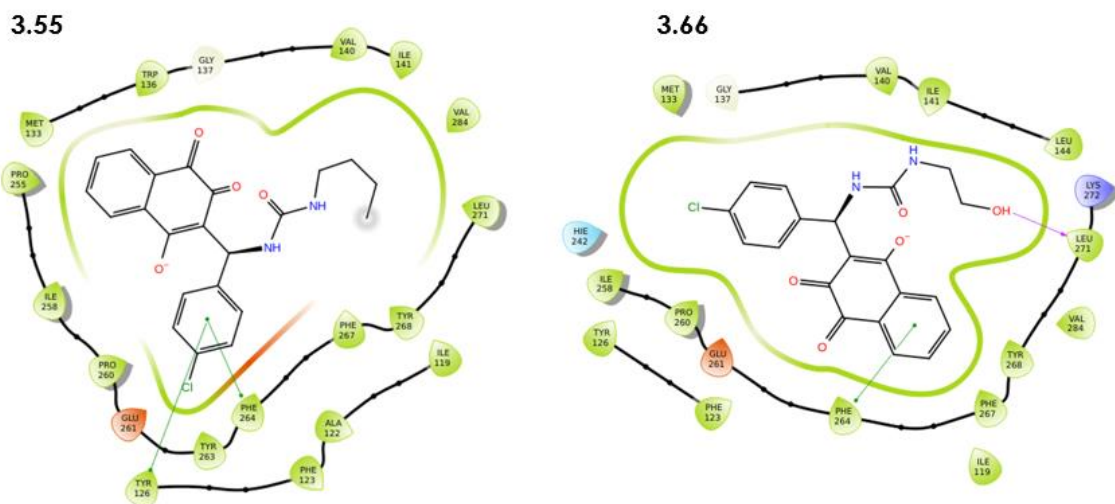


Figure 3.11. Binding modes and interactions for selected compounds in the binding site of bc1.

The desired DHPM structure was also evaluated *in silico*. Compound **3.42** (Table 3.6, entry 21) exhibited an acceptable docking score (-8.2 kcal/mol) against bc1 mitochondrial target of *P. falciparum*. **3.42** had the same orientation as atovaquone while entering the binding site and displayed a similar binding pose. The 3,4-dihydropyrimidinone ring offered an extra pi-pi stacking with Tyr 268, in addition to a variety of strong hydrophobic interactions with all amino acid residues (Fig. 3.12).

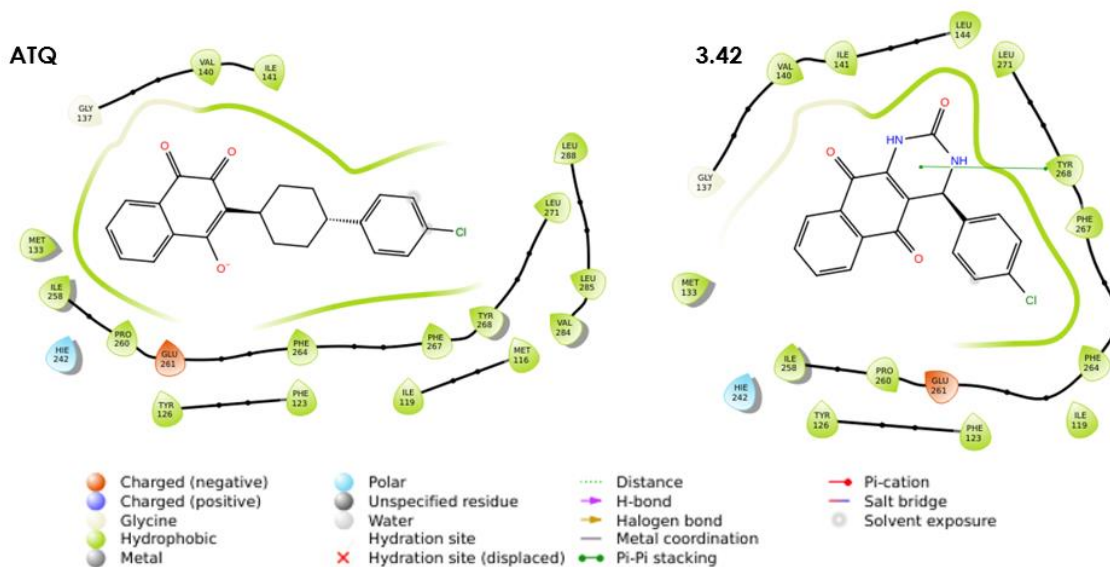


Figure 3.12. Binding modes and interactions for compound **3.42**, compared to atovaquone in the binding site of bc1.

- **P. falciparum DHODH mitochondrial target:**

Generally speaking, against DHODH target, the butyl-urea series of Biginelli-linear derivatives **3.54-3.59** (Table 3.6, entries 9-13) presented the most promising (more negative) docking scores compared to the other families of molecules. Concurrently, the *para*-phenyl substituent seemed not to play a crucial role for this family of compounds as its modification made no difference regarding the obtained docking scores. A similar trend was observed for the 2-hydroxyethyl urea family of Biginelli-linear compounds **3.66-3.67** (Table 3.6, entries 19-20) as well as for the 4-halogen phenyl substituted **3.60-3.62** of propargyl-urea family (Table 3.6, entries 14-16).

This can be accounted for the naphthoquinone ring's numerous potent hydrophobic interactions and hydrogen bond formations with the corresponding residues into the DHODH binding site. For example, compounds **3.43** (urea derivative), **3.46** (ethyl-urea) and **3.55** (butyl-urea) (Fig. 3.13) exhibited comparable docking scores (Table 3.6, entries 1, 3 and 10, respectively) and were all located at the same part of DHODH binding site. However, it was another part of the cavity, right next to XCV's binding site. Conspicuously, the naphthoquinone ring seemed to play a crucial role in binding and it exhibited strong hydrophobic interactions with His 185, Arg 265, Phe 227 and Tyr 168 residues (molecule **3.43**, Fig. 3.13).

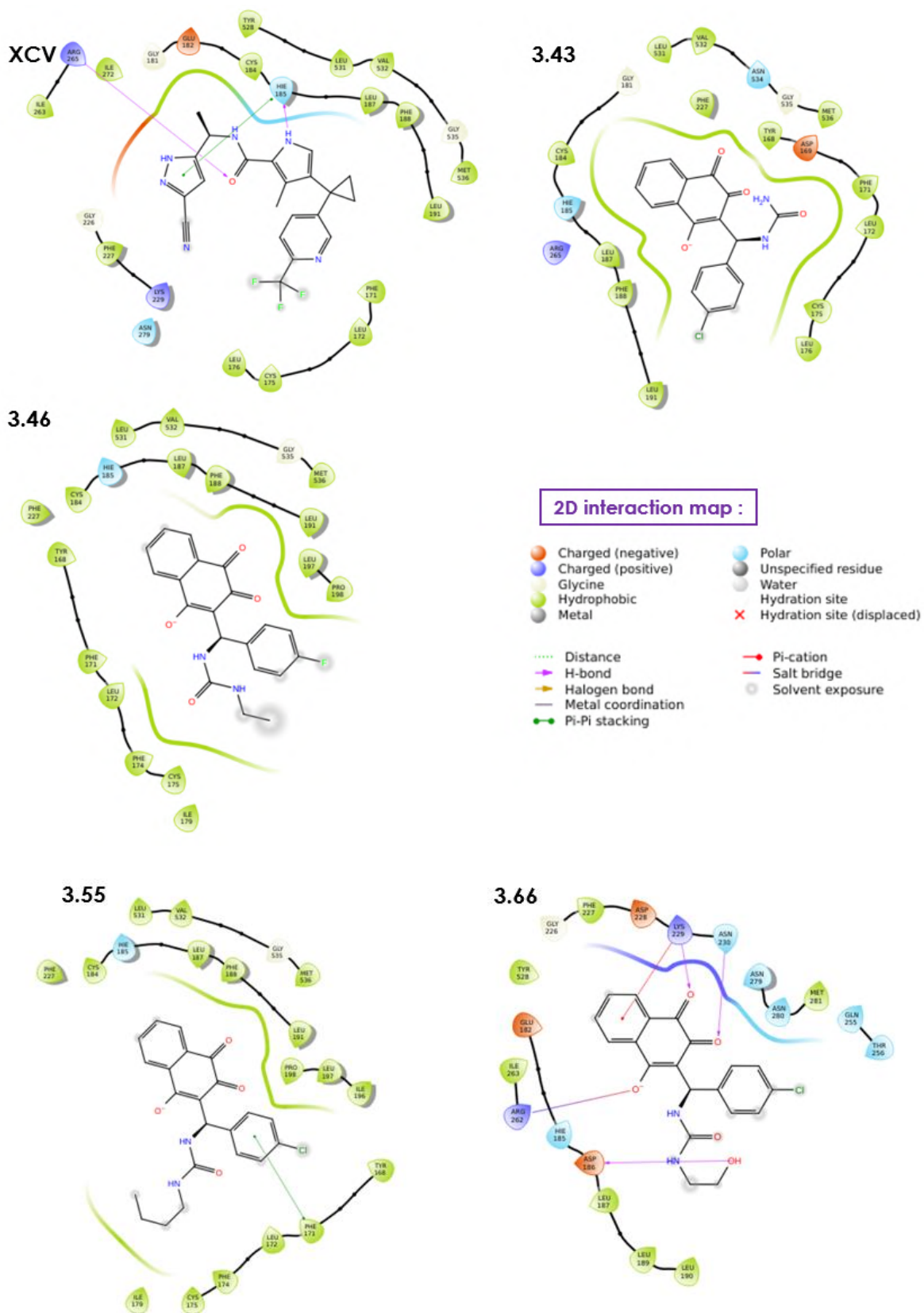


Figure 3.13. Binding modes and interactions for selected compounds in the binding site of DHODH.

Withal, a small part of the molecule (4-Cl phenyl substituent) was found exposed to the solvent. Urea substitution either with ethyl (**3.46**, Figure 3.11) or butyl (**3.55**, Fig. 3.13) side chains seemed to push further the molecule to the exterior of the binding site. As a result, a part of the hydrophobic interactions of the naphthoquinone rings of the structures was lost.

Only the derivatives of 2-hydroxyethyl urea appeared to have a nearly identical position in the binding site than XCV, the inhibitor of DHODH. For instance, **3.66** demonstrated comparable interactions with XCV and explored the binding site deeper. The naphthoquinone ring of compound **3.66** contributed significant van der Waals interactions with Asp 228, Lys 229, Asn 230, and other nearby amino acid residues, as well as pi-pi stacking with Lys 229. Along with two additional hydrogen bonds that two carbonyl groups of the lawsone scaffold formed with Lys 229 and Asn 230, the terminal hydroxy group formed a long-range hydrogen bond with Asp 186 to further stabilize this pose (Fig. 3.13).

The desired DHPM structure was evaluated against DHODH. Compound **3.42** (Table 3.6, entry 21) exhibited an excellent docking score (-10.0 kcal/mol) against DHODH mitochondrial target of *P. falciparum*, even better than the whole Biginelli-linear series (docking scores around -7.0 kcal/mol). **3.42** found to share the major part of XCV's binding site. The naphthoquinone ring offered both hydrophobic and van der Waals interactions with His 185, Cys 184 and Leu 531. The 3,4-dihydropyrimidinone ring contributed to additional hydrophobic interactions with the other part of the cavity (Fig. 3.14).

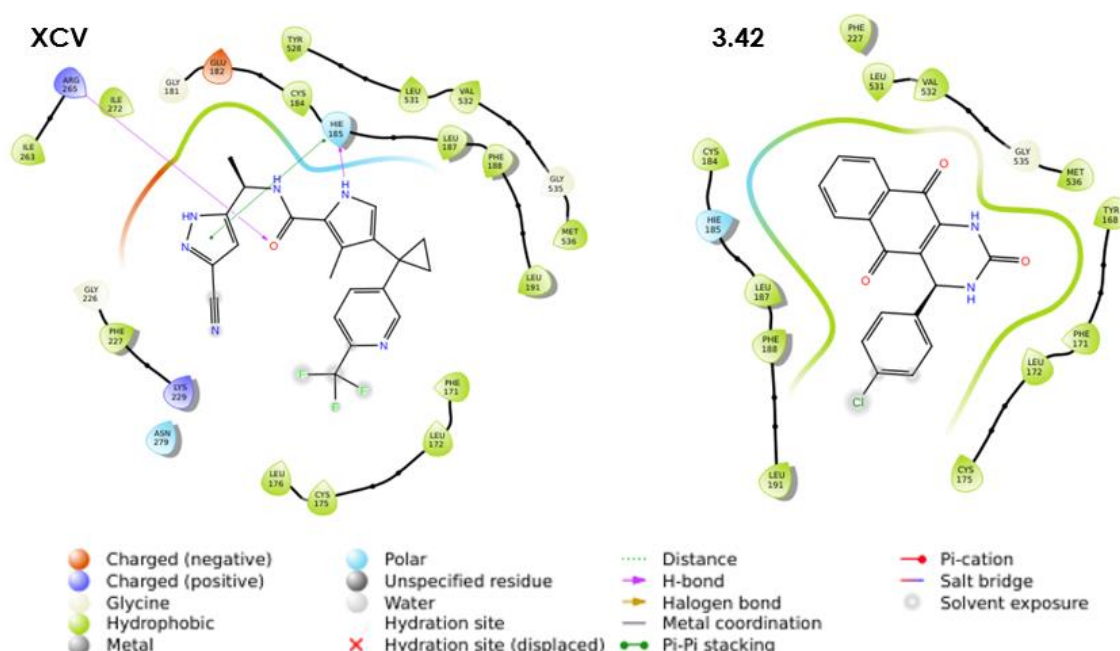


Figure 3.14. Binding modes and interactions for compound **3.42**, compared to XCV in the binding site of DHODH.

To sum up, this unique series of Biginelli-linear naphthoquinone derivatives could work as cytochrome bc1 inhibitors as the whole series, except for propargyl-urea naphthoquinone

derivatives, exhibited comparable docking scores to the reference drug ATQ. For DHODH, among all families of compounds, the 2-hydroxyethyl-urea naphthoquinone derivatives were able to share a similar binding map with XCV. Finally, a potential cyclized DHPM family of naphthoquinones could act both as bc1 and DHODH inhibitors, targeting both mitochondrial targets at the same time.

Consequently, all Biginelli-linear series were worth being biologically evaluated against *P. falciparum*, *L. donovani* and other pathogens in order to further investigate their potential as anti-infectious agents.

3.3.2 Biological evaluation of Biginelli-linear series

Activities against *P. falciparum*

The promising docking scores obtained for the majority of the Biginelli-linear series against both *P. falciparum* mitochondrial targets bc1 and DHODH encouraged a further *in vitro* evaluation. The antiplasmodial activity of the synthesized series was evaluated by our own team (see Chapter 2) at three doses (0.1 μM , 1 μM and 10 μM) against the artemisinin resistant strain of *P. falciparum* F32-ART. Unfortunately, the whole series of Biginelli-linear compounds **3.43-3.68**, along with all isolated Michael adducts **3.44** and **3.69** exhibited IC_{50} values higher than 10 μM . Thus, they are considered inactive against *P. falciparum*. The carbamate derivative **3.71** will be biologically evaluated against *P. falciparum* in the near future.

Activities against *L. donovani*

The antileishmanial activity of synthesized series was evaluated *in vitro* against *L. donovani* LV9 axenic amastigote and intramacrophage amastigote forms (see Chapter 2 for methodology). The majority of the series of Biginelli-linear compounds along with isolated Michael adducts **3.44** and **3.69** exhibited IC_{50} values higher than 15 μM against both forms of *Leishmania* parasites. Miltefosine was used as the reference drug and exhibited the IC_{50} values of 3.0 μM and 1.5 μM against axenic amastigotes and intramacrophage amastigotes, respectively (SI = 15.5). Three compounds (**3.51**, **3.67** and **3.68**) of the Biginelli-linear library exhibited IC_{50} values less than 16 μM and 4 μM against axenic and intramacrophage amastigotes, respectively (Fig. 3.15). Compounds **3.51** and **3.68** bearing a *para*-trifluoromethylphenyl substituent exhibited IC_{50} values equal to 4 μM and 9.6 μM against *L. donovani* axenic amastigotes, respectively. The same compounds had even better IC_{50} values against intramacrophage amastigotes, namely 1.6 μM for **3.51** and 3.2 μM for **3.68**. **3.51** exhibited an excellent selectivity index (SI = 64), meaning that it was 4-fold times safer than miltefosine and equally active. Compound **3.68** had a selectivity index (SI = 14.3) comparable to miltefosine. Finally, compound **3.67** exhibited an IC_{50} value of 15.8 μM and 2.4 μM against

axenic and intramacrophage amastigotes, respectively (SI = 12.8). However, further studies are required before any conclusions can be drawn about the pharmacophore of this class of compounds and what would be the right combination of side chains (urea substitution) and phenyl substituent.

Biginelli-linear lawsone derivatives:

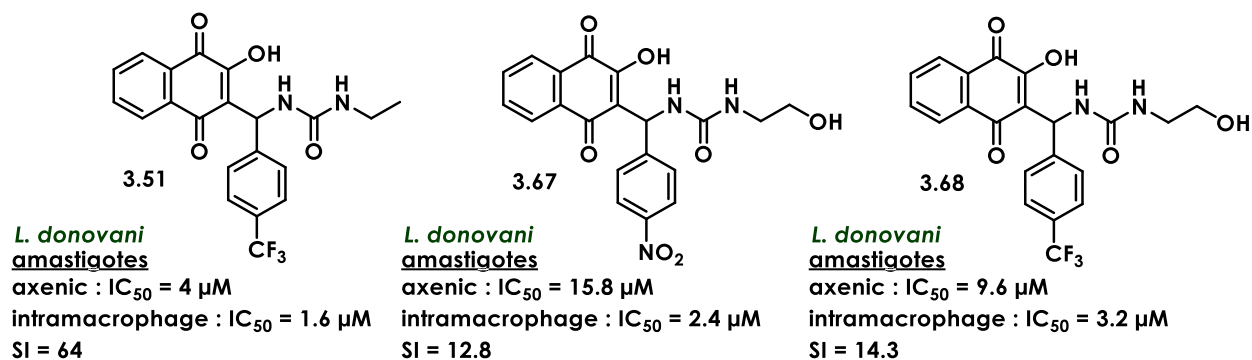


Figure 3.15. The most active compounds of the Biginelli-linear series against *L. donovani*.

The biological evaluation of the carbamate derivative **3.71** against *L. donovani* LV9 axenic amastigotes forms is currently in progress.

Activities against *M. tuberculosis*

The antimycobacterial activity (MIC₉₀) of the synthesized series was evaluated *in vitro* against *M. tuberculosis* H37Rv (see Chapter 2 for methodology). Unfortunately, the whole series of Biginelli-linear compounds **3.43-3.68**, along with all isolated Michael adducts **3.44** and **3.69** exhibited IC₅₀ values higher than 100 μM. Thus, they are considered inactive against *M. tuberculosis*. In addition, the carbamate naphthoquinone derivative **3.71** exhibited an IC₅₀ value higher than 81 μM after a preliminary screening against *M. abscessus* ATCC-19977. Compared to bedaquiline which was used as reference drug and had an IC₅₀ at 3.6 μM, **3.71** was therefore considered inactive. As a result, there was no further *in vitro* evaluation against *M. tuberculosis* H37Rv.

Antimicrobial activities

A potential antibacterial activity was investigated against various Gram-positive and Gram-negative bacteria such as *E. coli* ATCC-25922, *S. aureus* ATCC-29213, *K. pneumoniae* BAA-1705, *A. baumannii* BAA-1605, and *P. aeruginosa* ATCC-27853. This evaluation was carried out at the Division of Microbiology, Central Drug Research Institute, under the supervision of Dr Sidharth Chopra (CSIR-CDRI, Lucknow 226031, Uttar Pradesh, India). All tests and MIC determinations were carried out according to already established protocols [62]. Levofloxacin was used as a reference drug for the whole screening against all above mentioned bacterial strains.

Unfortunately, almost the entire series of Biginelli-linear compounds **3.43-3.68**, along with all isolated Michael adducts **3.44** and **3.69** exhibited IC_{50} values higher than 160 μM . Thus, they are considered inactive against all bacteria. Only Biginelli-linear derivative **3.49** bearing an ethyl-urea side chain and a *para*-iodophenyl substituent exhibited the lowest IC_{50} at 34 μM against *S. aureus*, while the reference drug levofloxacin displayed an IC_{50} equal to 0.35 μM .

Overall, it was discovered that the Biginelli-linear series was ineffective against almost all examined pathogens. Taking into account the problems with stability in solution, and disappointing biological activities *in vitro*, the lack of activity of these compounds may be caused by their decomposition into the cell media during the *in vitro* tests. Since docking revealed that they could bind to both DHODH and bc1 mitochondrial targets of *P. falciparum*, a method for stabilizing these structures was worth being developed.

3.4 Results and discussion (Part II)

The first part of the chapter demonstrated that the Biginelli-linear compounds exhibited stability problems in aqueous slightly acidic and less in basic conditions. Their decomposition leads to Michael adducts formation and starting compounds.

That may be the main reason why these compounds did not exhibit any interesting biological activities. The enol form of these compounds could be responsible for this aqueous instability. Therefore, in parallel to cyclization studies (Part I), our interest was also focused on deactivating the enol function of lawsone moiety, by alkylating the 2-hydroxy group.

The methyl group is the smallest existing alkyl group, a well-known and high-impact substituent that has the potential to gently produce small changes in terms of molecular weight, lipophilicity, and possibly biological activity without significantly altering the binding properties of the Biginelli-linear series [63].

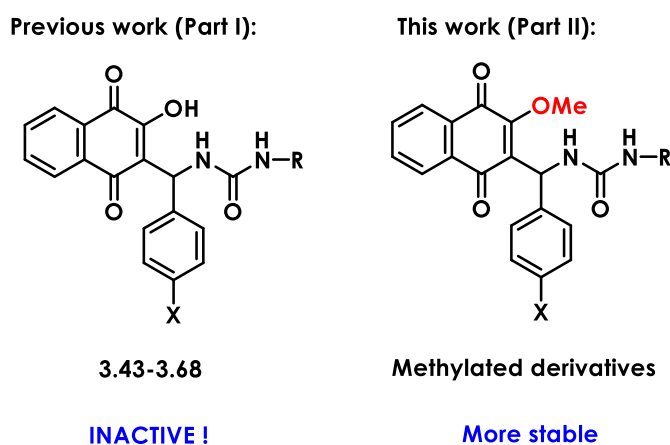


Figure 3.16. Blocking the enol function of lawsone moiety of Biginelli-linear series by methylation.

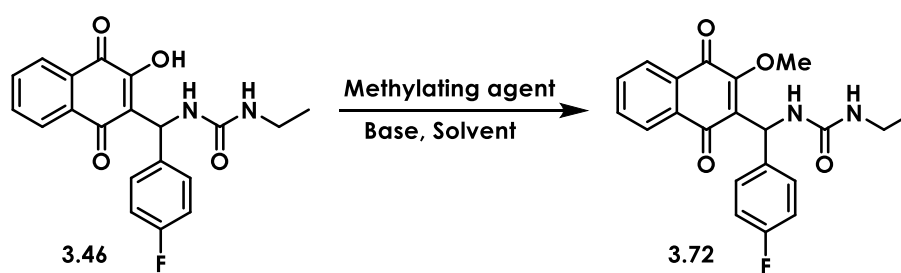
3.4.1 Chemistry – Synthesis of O-methylated Biginelli-linear compounds

3.4.1.1 Reaction conditions for optimization studies

Given that the Biginelli-linear products had three potential positions that could be methylated (2-OH and both NH of the urea scaffold), an effective and selective methylation protocol had to be established in order to prevent multiple methylated side products. Compound **3.46** was chosen for all methylation studies. All attempts were made in solution, by varying both the methylating agent and the base required for 2-OH deprotonation-activation. All reactions were controlled by TLC and stopped when they were complete or there was no more evolution. Afterwards, the crude reaction mixtures were collected after a rapid aqueous treatment (work up), analyzed by ^1H NMR and mass spectrometry. The results are summarized in Table 3.7.

Cheng *et al.* [64] made extensive use of the rather unusual methylating agent tetramethylammonium fluoride (TMAF) in their attempts to find a way for chemoselective methylations of aromatic and heteroaromatic amides, amines, phenols, and alcohols. Their control experiments demonstrated that TMAF could provide the methyl transfer source and fluoride itself could act as the required base. The authors came to the conclusion that using toluene as a solvent could be beneficial for the purification process because the excess of TMAF used in the reaction as well as the byproduct Me_3NHf could be easily removed by precipitation in toluene once the reaction was complete.

Table 3.7. Selective methylation attempts of Biginelli-linear compound **3.46**.



Entry	Methylating agent	Base	Solvent	Temperature (°C)	Reaction time (h)	Yield * (%)
1	Me_4NF	-	PhMe	100	3	-
2	Me_4NF	py	PhMe	100	3	-
3	MeI	NaH	DMF	0-40	overnight	traces
4	TfOMe	<i>n</i> -BuLi	THF	-78	4	-
5	TfOMe	<i>n</i> -BuLi	THF	0	4	traces
6	Me_2SO_4	K_2CO_3	acetone	reflux	0.5	60 **

* Estimated yield based on ^1H NMR analysis of the crude mixture. ** Isolated yield.

However, when this methylation protocol was repeated for **3.46** (Table 3.7, entry 1), only decomposition of the starting compound was observed. Nothing was changed by the addition of 1 eq. of pyridine (Table 3.7, entry 2).

The same outcome was obtained when the methylating agent was changed for methyl iodide (MeI) in the presence of NaH in DMF [2], (Table 3.7, entry 3). Moreover, traces of the expected O-methylated product were found among other poly-methylated products, after extracting the crude reaction mixture in AcOEt. This methodology was not further optimized because the reaction was very sluggish and thus might favor the formation of undesirable byproducts.

A variation of Evans protocol was also tested aiming to selectively methylate **3.46** [65]. **3.46** was subjected to react with methyl triflate in THF, activated by n-BuLi at very low temperature in order to impede the decomposition of starting materials (Table 3.7, entry 4). Under these conditions, no reaction was observed at -78 °C and the starting compound was fully recovered. When the same reaction was repeated at 0 °C for 4 hours, only traces of the desired product **3.72** along with unreacted **3.46**, were found in the crude reaction mixture, controlled by ¹H NMR and mass spectroscopy (Table 3.7, entry 5). A complex reaction mixture was produced by varying the temperature (between rt and 50 °C) and the reaction time (6 hours and overnight), but this did not increase the yield of the desired O-methylated **3.72** because a part of the initial **3.46** was decomposed.

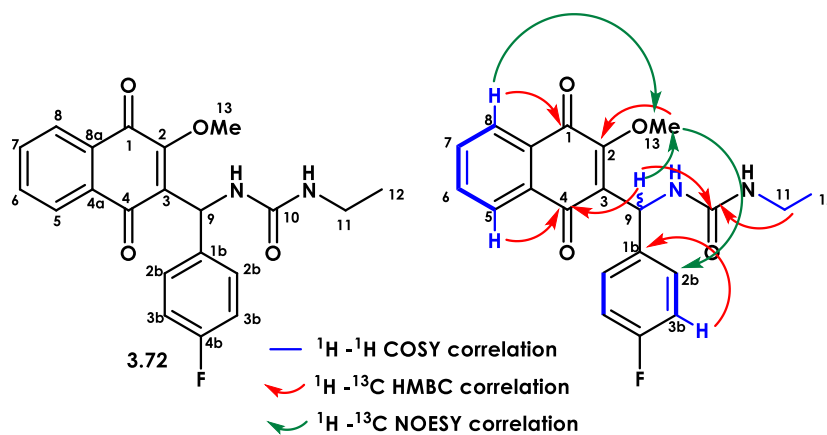
After a thorough search in the literature regarding naphthoquinones and their reactions, only one very old methylation protocol was found to be well adapted for lawsone (and other families of quinones), developed by Rao *et al.* [66]. The authors subjected lawsone to react with 1.8 equiv. of dimethyl sulfate (Me₂SO₄) and 6.3 equiv. potassium carbonate (K₂CO₃) in anhydrous refluxing acetone for 3 hours. Then, 2-methoxy-1,4-naphthoquinone was isolated (83% yield) after recrystallization in benzene. The same methodology was followed for the selective methylation of the Biginelli-linear **3.46**. Indeed, reaction of **3.46** with the same ratio of Me₂SO₄ (1.8 equiv.) and K₂CO₃ (6.3 equiv.) to the one reported by Rao *et al.* led to the mono-methylated product **3.72** after 30 min of reaction (Table 3.7, entry 6). The reaction was monitored by TLC and was stopped when the starting **3.46** was fully consumed. While the mono-methylated product was the major product of this reaction, however traces of potential N-methylated products were detected in the crude reaction mixture (estimated yield of byproducts 20%). Finally, the desired **3.72** was isolated with 60% yield from the reaction mixture by filtration, and was recrystallized in DCM.

3.4.1.2 Structure characterization of monomethylated compound **3.72**

The chemical structure of compound **3.72** was unambiguously determined by using a full pack of ¹H, ¹³C NMR and 2D ¹H-¹H homonuclear correlated spectroscopy (COSY) and nuclear

Overhauser enhancement spectroscopy (NOESY) and ^1H - ^{13}C heteronuclear multiple bond correlation (HMBC) NMR analyses in CDCl_3 at 298 K. All ^1H and ^{13}C signals were assigned based on chemical shifts (δ , ppm), spin-spin coupling constants, splitting patterns and signal intensities. The ^1H and ^{13}C assignments of **3.72** are summarized in Table 3.8.

Table 3.8. ^1H and ^{13}C NMR data assignments of compound **3.72** in CDCl_3 at 298 K.



$^1\text{H}/^{13}\text{C}$ numbering	^1H chemical shift (ppm)	^{13}C chemical shift (ppm)
C-1	-	181.6
C-2	-	157.3
C-3	-	131.9
C-4	-	186.1
C-4a	-	131.8
CH-5	8.00 (m)	126.3
CH-6	7.74 (m)	134.2
CH-7	7.73 (dd, $J = 5.8, 3.3$ Hz)	133.8
CH-8	8.06 (m)	126.4
C-8a	-	131.4
CH-9	6.63 (bs)	48.5
C-10	-	157.2
CH ₂ -11	3.26 (q, $J = 7.2$ Hz)	35.6
CH ₃ -12	1.16 (t, $J = 7.2$ Hz)	15.4
CH ₃ -13	4.26 (s)	62.0
NH	6.82 (d, $J = 10.1$ Hz)	-
NHt	5.88 (bs)	-
C-1b	-	163.5 (d, $J = 2.7$ Hz)
CH-2b	7.38 (m)	127.9 (d, $J = 8.2$ Hz)
CH-3b	7.00 (m)	115.4 (d, $J = 21.2$ Hz)
C-4b	-	161.9 (d, $J = 246.0$ Hz)

* ^1H and ^{13}C numbering of **3.72** do not follow IUPAC rules.

¹H NMR spectrum exhibited all expected signals (δ , ppm) for all different protons of naphthoquinone ring system as well as the aromatic protons of 4-fluorophenyl moiety. The desired methyl group protons H-13 was found at 4.26 ppm as a singlet. H-9 was found at 6.63 ppm coupled with its neighbor proton NH which was found at 6.82 ppm. The ¹³C resonance data revealed 19 signals in total, allowing the non-ambiguous structure identification of **3.72**. The methyl group resonated at 62.0 ppm. Finally, the ¹³C-¹H HMBC experiment permitted to identify of all long-range couplings. The experiment showed correlation between H-9 and carbonyl group C-4, and between methyl protons H-13 and C-2. Meanwhile, the ¹³C-¹H NOESY experiment further confirmed that the methylation occurred at O-2 and not in another position existing in equilibrium as methyl protons H-13 were correlated to C-8, C-9 and C-2b.

3.4.1.3 Synthesis of a small library of O-methylated Biginelli-linear derivatives

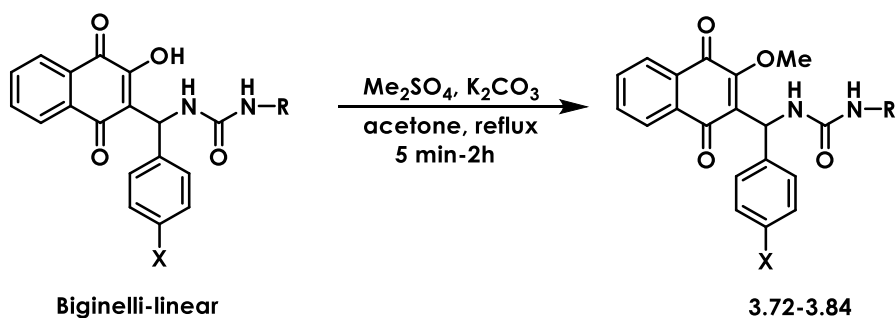
Since this protocol provided both selectivity and acceptable yield, it was used for the methylation of selected products of the Biginelli-linear series. Every reaction mixture was monitored by TLC, and it was stopped when the starting compound was fully consumed or there was no more evolution. The crude reaction mixtures were analyzed by ¹H NMR spectroscopy to verify if any secondary products were formed. The reaction mixtures were filtered to remove K₂CO₃ excess, and medium pressure flash column chromatography (PuriFlash) was used to separate the desired O-methylated product from the crude filtrate. Many attempts were made in order to improve the green character of this step. In principle, crystallization was a good way to purify the target compound. However, recrystallization could not be used as a general purification method as in many recrystallized compounds an amount of dimethyl sulfate was present (10-15%). For that reason, the method used for the purification of all final compounds was by medium pressure flash column chromatography. All the results are summarized in Table 3.9.

All *N*-ethyl substituted Biginelli-linear derivatives were methylated. The *N*-ethyl compounds bearing a 4-halogen or methyl substituted phenyl ring attached to C-3 led to the corresponding methylated derivatives **3.72-3.75** and **3.78** with yields ranging between 60% and 73% (Table 3.9, entries 1-4 and 7, respectively). The methylation was complete for all compounds **3.72**, **3.73**, **3.78**, **3.73** and **3.75** in 15 min-90 min. The mono-methylation of the *p*-nitrophenyl derivative **3.76** was sluggish with a 42% yield at 90 min. The quite opposite was observed for *para*-trifluoromethyl derivative which were complete in 5 min., with an excellent 90% yield.

Afterwards, selected *N*-propargyl substituted Biginelli-linear derivatives were subjected to selective methylation. Contrary to the *N*-ethyl series, these reactions needed generally more than 1 h to reach completion, because of delocalization of the electrons of the enol function of the lawsone moiety. In terms of yields, the *para*-halogen phenyl substituted derivatives **3.80**

and **3.81** (Table 3.9, entries 9-10) were obtained in the same range as the corresponding *N*-ethyl ones 70% and 67%, respectively. Compounds **3.82** and **3.83** bearing strong electron withdrawing groups such as NO₂ (Table 3.9, entry 11) and CF₃ (Table 3.9, entry 12) were obtained with lower 50% and 40% yields, respectively.

Table 3.9. Selective methylation of selective Biginelli-linear products.



Entry	Product	X	R	Reaction time (min.)	Yield (%)
1	3.72	F	CH ₂ CH ₃	60	60
2	3.73	Cl	CH ₂ CH ₃	60	73
3	3.74	Br	CH ₂ CH ₃	15	65
4	3.75	I	CH ₂ CH ₃	15	70
5	3.76	NO ₂	CH ₂ CH ₃	90	42
6	3.77	CF ₃	CH ₂ CH ₃	5	90
7	3.78	CH ₃	CH ₂ CH ₃	60	70
8	3.79	OMe	CH ₂ CH ₃	60	63
9	3.80	F	CH ₂ C≡CH	90	70
10	3.81	Cl	CH ₂ C≡CH	90	67
11	3.82	NO ₂	CH ₂ C≡CH	120	50
12	3.83	CF ₃	CH ₂ C≡CH	90	40
13	3.84	OMe	CH ₂ C≡CH	45	40

* Isolated yield after FCC purification.

Even though the main product of these reactions was the desired mono-methylated one, the reaction was quite sluggish and was stopped before it was fully completed, to prevent the formation of unwanted *N*-methylated byproducts, explaining the low yields for these two cases.

As already mentioned before (Part I, Chapter 3), the purification of the Biginelli-linear derivatives bearing a *para*-methoxy (*p*-OMe) phenyl substituted system, was difficult. In that respect, the crude reaction mixture was used as such for the subsequent methylation. All crude reaction mixtures containing *p*-OMe phenyl substituted Biginelli-linear derivatives underwent ¹H NMR and mass spectroscopic analyses, which revealed that they are 55–65% enriched with the desired Biginelli-linear methylated product. The desired products **3.79** and **3.84** were easily isolated after flash column chromatography with 63% and 40% yield, respectively. It should be noted that the methylated compounds were found to be stable while passing through a silica gel column under usual purification conditions.

All O-methylated Biginelli-linear derivatives were stable both as powders and in solution at room temperature and light exposition for two months. Decomposition of the solids was seen only at temperatures higher than 180 °C. The hypothesis of blocking the enol function of lawsone moiety of Biginelli-linear derivatives by methylation was thus proven to be correct and resulted in the synthesis of much more stable molecules.

3.5 Biological and *in silico* evaluation of the O-methylated series

All O-methylated products were biologically evaluated against *P. falciparum*, *L. donovani*, *M. tuberculosis*, Gram positive and negative bacteria and other pathogens. In addition, all compounds were *in silico* evaluated against two mitochondrial targets of *P. falciparum*: cytochrome bc1 and dihydroorotate dehydrogenase (DHODH) enzyme by docking each molecule to both binding sites of the targets. The binding site was determined and the evaluation of molecules interactions with the binding site was associated to their docking scores.

3.5.1 Activities against *P. falciparum* *in vitro* and *in silico* studies

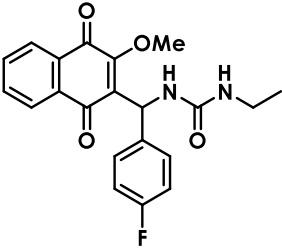
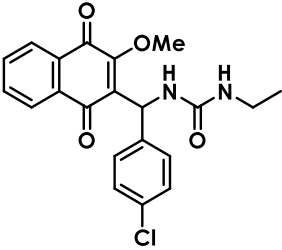
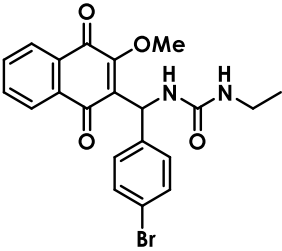
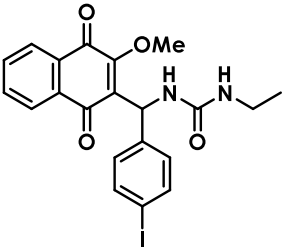
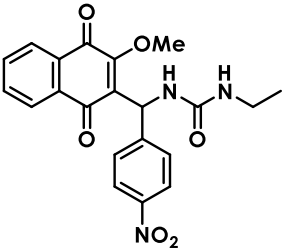
The antiplasmodial activity of the –OMe series was assessed against the F32-ART strain of *P. falciparum*, at two doses (1 μM and 10 μM) (see Chapter 2). The precise IC₅₀ values of the compounds were then determined using a chemosensitivity experiment for molecules inhibiting more than 50% of parasite growth at 10 μM. Atovaquone (ATQ) and DHA were used as reference drugs. The obtained *in vitro* results are summarized in Table 3.10.

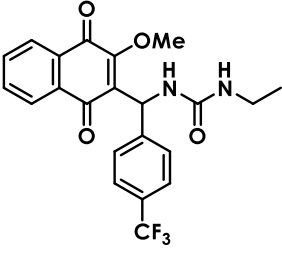
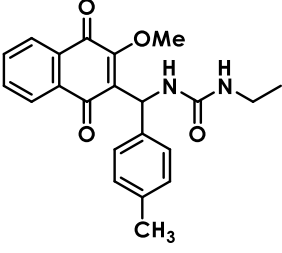
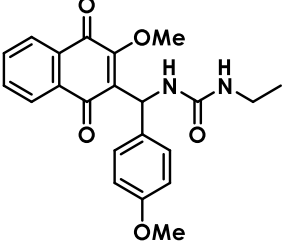
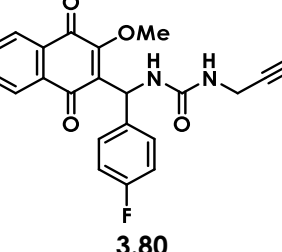
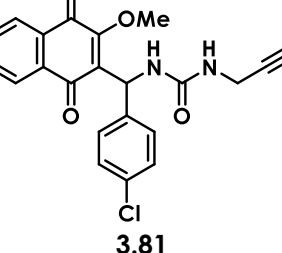
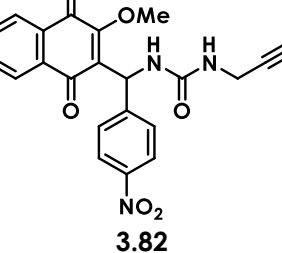
Blocking the enol function of lawsone moiety of Biginelli-linear derivatives by methylation, led to IC₅₀ values lower than 10 μM against *P. falciparum* for the whole series of methylated compounds. More precisely, two families of methylated Biginelli-linear compounds can be distinguished: the *N*-ethyl and *N*-propargyl urea substituted derivatives.

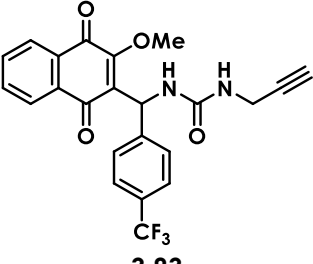
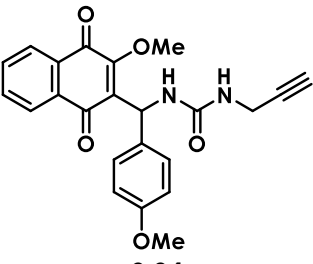
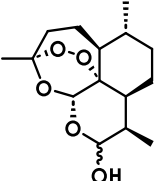
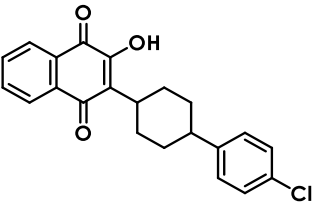
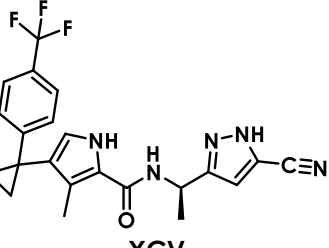
Among *N*-ethyl-urea family of methylated Biginelli-linear compounds, compound **3.72** (Table 3.10, entry 1), containing a *para*-fluorophenyl moiety exhibited the lowest IC₅₀ value (IC₅₀

= 2.8 μM) of the whole *N*-ethyl urea substituted family and of the entire methylated series in general.

Table 3.10. Antiplasmodial activity and predicted docking scores of methylated Biginelli-linear series.

Entry	Compound	<i>P. falciparum</i> F32-ART IC ₅₀ (μM)	Inhibition (%) at 1 μM	Docking score Pfbc1 (kcal/mol)	Docking score PfdHODH (kcal/mol)
1	 3.72	2.8	14	-10.0	-9.1
2	 3.73	5.5	6	-8.9	-8.7
3	 3.74	5.5	3	-8.9	-6.4
4	 3.75	4.5	14	-8.3	-9.1
5	 3.76	4.0	15	-8.1	-7.5

6	 <p style="text-align: center;">3.77</p>	4.8	15	nd	nd
7	 <p style="text-align: center;">3.78</p>	3.0	25	nd	nd
8	 <p style="text-align: center;">3.79</p>	3.0	17	-7.3	-6.5
9	 <p style="text-align: center;">3.80</p>	5.0	9	-8.1	-6.7
10	 <p style="text-align: center;">3.81</p>	10.0	15	-2.7	-6.3
11	 <p style="text-align: center;">3.82</p>	10.0	3	-8.2	-6.2

12	 <p style="text-align: center;">3.83</p>	6.0	0	nd	nd
13	 <p style="text-align: center;">3.84</p>	5.0	21	-9.4	-6.5
14	 <p style="text-align: center;">DHA</p>	0.003	95	nd	nd
15	 <p style="text-align: center;">ATQ</p>	0.001	85	-11.3	nd
16	 <p style="text-align: center;">XCV</p>	nd	nd	nd	-11.2

* nd stands for non-determined.

However, when fluorine was substituted with another halogen (Table 3.10, entries 2-4, molecules **3.73-3.75**) or a strong electron withdrawing group (Table 3.10, entries 5-6, molecules **3.76-3.77**) the IC₅₀ values were higher, ranging from 4.0 to 5.5 μM. Conversely, when fluorine was changed for an electron donating group with an inductive (Table 3.10, entry 7, molecule **3.78**) or mesomeric effect (Table 3.10, entry 8, molecule **3.79**), the IC₅₀ values remained almost the same to 3.0 μM for both **3.78** and **3.79**, when compared to **3.72**.

Concerning the *N*-propargyl urea family of methylated Biginelli-linear compounds, the fluoro-containing derivatives **3.80** (Table 3.10, entry 9) and **3.83** (Table 3.10, entry 12) exhibited the lowest IC₅₀ value of the family, found at 5.0 μM for **3.80** and 6.0 μM for **3.83**. Compound **3.84**

(Table 3.10, entry 13), which contained an electron donating group with a mesomeric effect, namely *para*-methoxyphenyl, had an IC₅₀ value of 5.0 μM, which was very similar to the IC₅₀ values of the fluoro-containing derivatives **3.80** and **3.83**. Adversely, compounds containing a *para*-chloro (Table 3.10, entry 10, molecule **3.81**) or *para*-nitrophenyl (Table 3.10, entry 11, molecule **3.82**) moieties exhibited the highest IC₅₀ values of the series equal to 10.0 μM for both compounds. For the whole series of tested compounds, inhibition of parasitemia at 1 μM did not exceed 20%.

In silico screening

The methylated Biginelli-linear series was submitted to an *in silico* screening against both mitochondrial targets of *P. falciparum* bc1 and DHODH in order to check their potential interactions with these two targets (See Chapter 3 – Part I for more details). Atovaquone (ATQ) was used as positive control for docking against bc1 (Table 3.10, entry 14), and XCV (Table 3.10, entry 15) against DHODH. All docking scores of this library of compounds are presented in Table 3.10.

When tested *in silico*, compound **3.72** (Table 3.10, entry 1, IC₅₀ = 2.6 μM) exhibited the best (more negative) docking scores against both mitochondrial targets bc1 and DHODH. Concerning bc1 target, selective methylation allowed **3.72** to interact with the bc1 binding site by binding a little deeper into the cavity and being rotated compared to ATQ (Fig. 3.17). **3.72**'s naphthoquinone ring exhibited hydrophobic interactions with His 242, Ile 258, Pro 260 and Met 133, as seen in ATQ binding as well. While the OMe group only provided light hydrophobic interactions with neighbor amino residues in the binding site, it forced the naphthoquinone ring to flip and fit better to the cavity of bc1 compared to the non-methylated **3.46** (Fig. 3.11). The same orientation in binding was retained no matter the *p*-phenyl substituent of the methylated *N*-ethyl urea substituted compounds. For instance, compound **3.79** (Table 3.10, entry 8) bearing an electron donating group exhibited similar binding poses to **3.72** in *P. falciparum* bc1 binding site (Fig. 3.17). The naphthoquinone ring of **3.79** exhibited strong hydrophobic interactions with all key-amino acid residues of bc1 such as ATQ and offered an additional strong hydrogen bond between carbonyl C-4 and Glu 261.

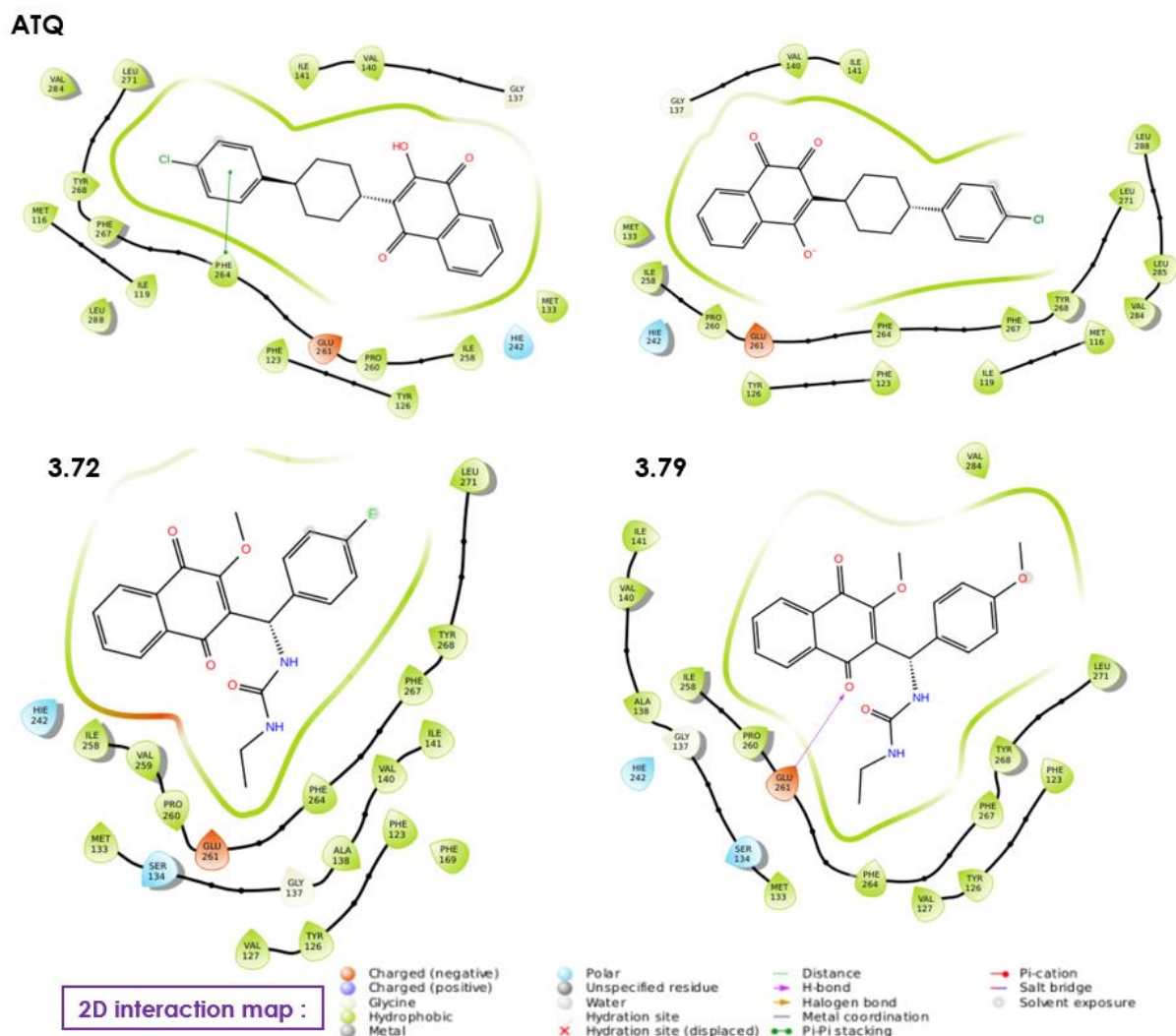


Figure 3.17. Binding modes and interactions for compound **3.72** and **3.79**, compared to ATQ in the binding site of bc1.

Concerning DHODH target, selective methylation allowed compound **3.72** to interact with the binding site slightly deeper than the inhibitor XCV. While methylation had no effect on the binding mode of **3.72** when compared to non-methylated **3.46** (Fig. 3.13), it did extend the hydrophobic interactions of the naphthoquinone ring with Asp 169 (Fig. 3.18). The *N*-ethyl urea and *para*-fluorophenyl substituents, on the other hand, were placed outside of the binding site. In contrast to the bc1 target, where other *para*-phenyl substituents of methylated *N*-ethyl urea derivatives had no effect on the orientation of the corresponding compound into the binding site, it was critical in DHODH. For example, compound **3.79** (Table 3.10, entry 8) with a *p*-OMe phenyl substituent (Fig. 3.18) had a very different interaction map with DHODH compared to XCV (Fig. 3.18), as **3.79** was only partially in contact with the binding site. Furthermore, unlike in the case of **3.72**, the naphthoquinone ring of **3.79** did not provide any hydrophobic interactions with the binding site but exhibited very strong Van der Waals and polar interactions with Asn 239, Lys 229, and Asp 226 as long as a hydrogen bond with Lys 229 residue. In addition, urea's carbonyl group provided a strong hydrogen bond with Asn 230, which added stability. Even

though the *N*-ethyl-urea substituent was found to be rotated in comparison to **3.72**, it was still found to be outside of the binding site.

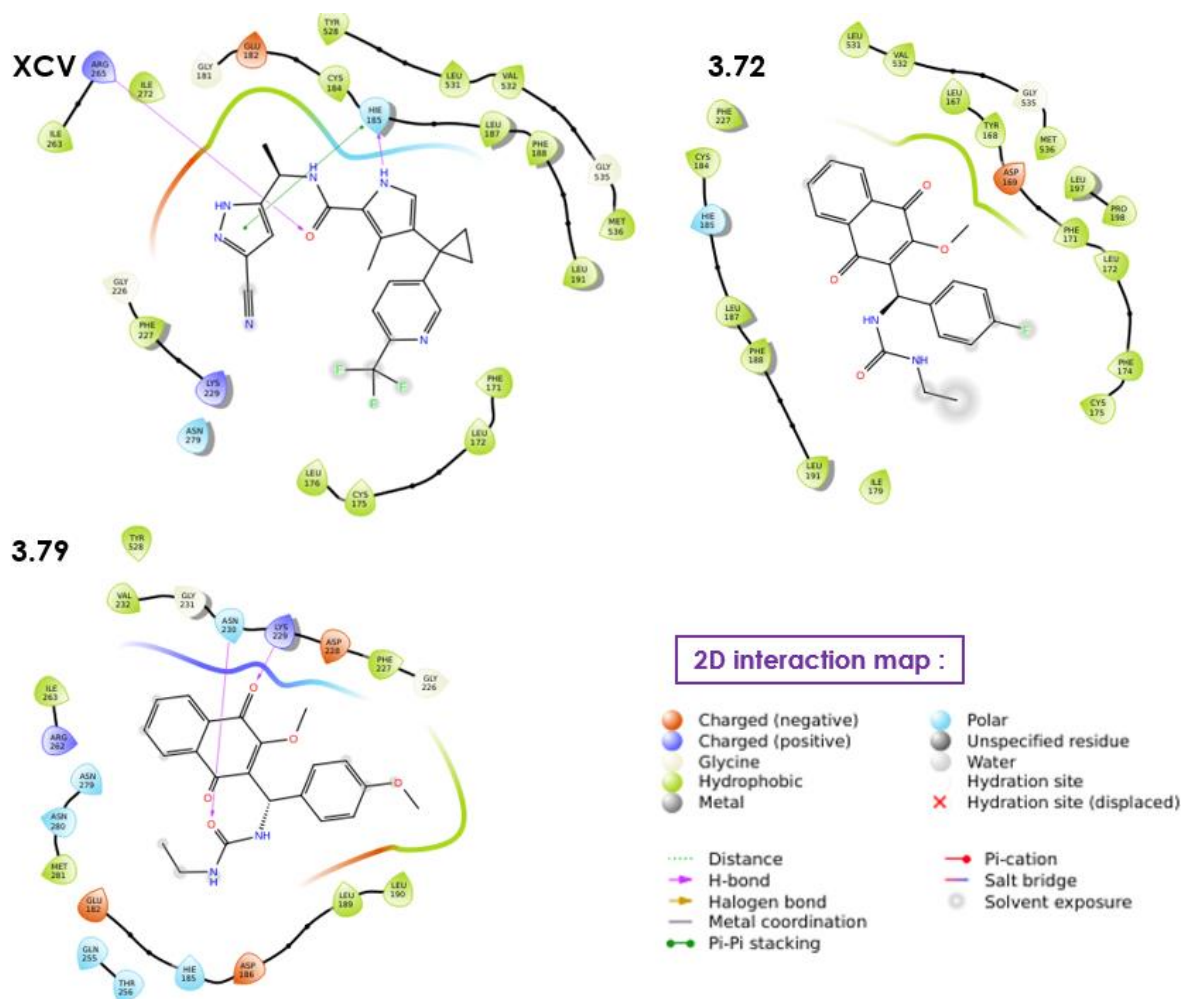


Figure 3.18. Binding modes and interactions for compound **3.72** and **3.79**, compared to XCV in the binding site of DHODH of *P. falciparum*.

A preliminary docking study of some putative fully methylated Biginelli-linear derivatives was also conducted for comparison purposes. In fact, when the Biginelli-linear compounds were fully methylated, they ended up losing binding affinity with both *P. falciparum* mitochondrial targets due to steric hindrance. Their docking scores were found to be significantly lower when compared to the unmethylated and selectively *O*-methylated series. For instance, the fully methylated derivative of **3.72** (Fig. 3.19, panel A) was forced to flip in order to fit into the bc1 binding site.

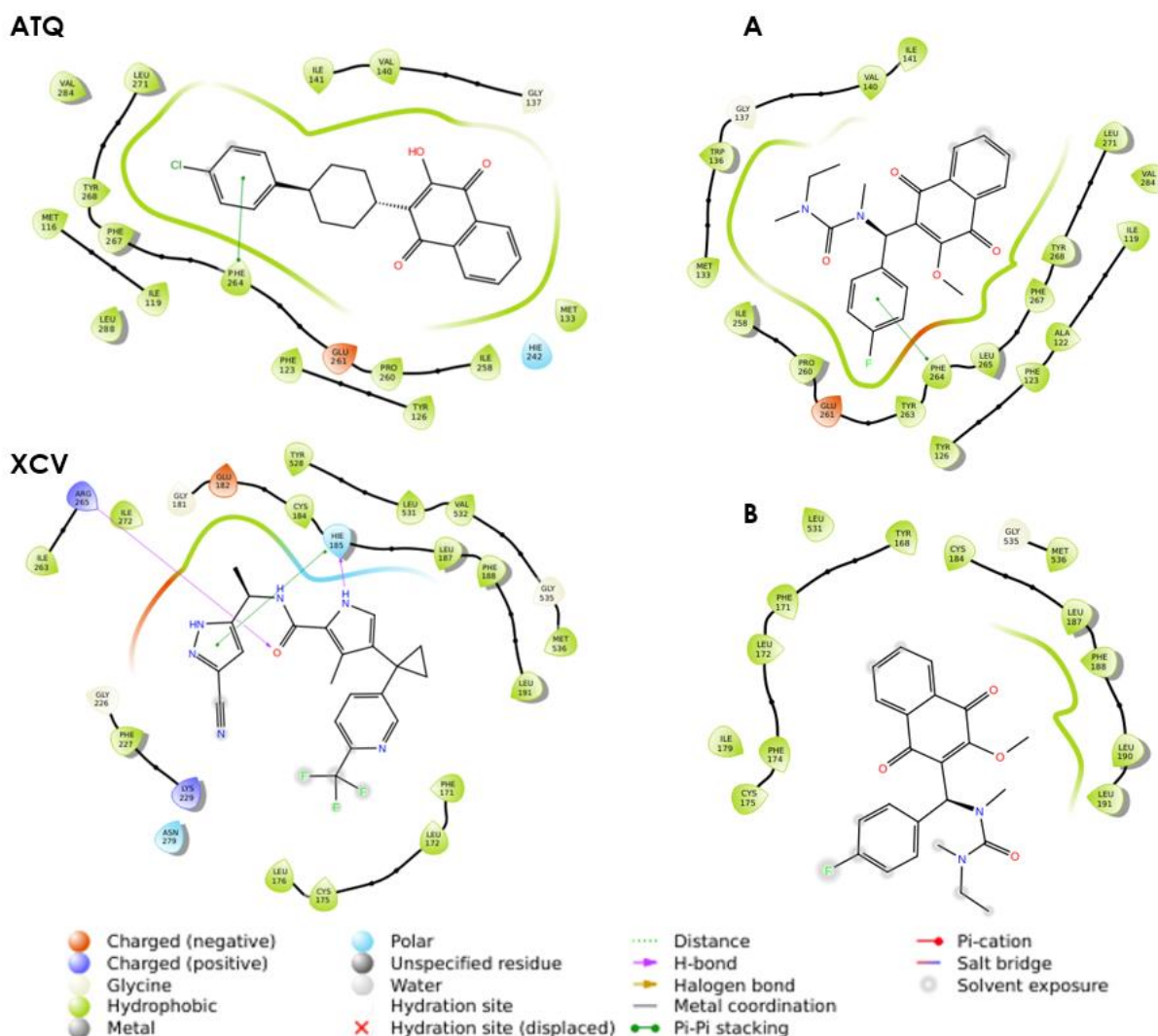


Figure 3.19. Binding modes and interactions for a fully methylated Biginelli-linear derivative in both bc1 (panel A) and DHODH (panel B) targets.

As a result, an important part of the naphthoquinone ring could no longer participate in hydrophobic interactions, explaining the relatively low (less negative) docking score of -6.4 kcal/mol against bc1, compared to -10.0 kcal/mol prior to full methylation (Table 3.10, entry 1, molecule **3.72**). The situation was even worse for binding to DHODH. The fully methylated derivative of **3.72** (Fig. 3.19, panel B) did not appear to change orientation as it approached the binding side, but almost the entire structure was unable to enter the cavity, explaining the obtained docking score of -5.2 kcal/mol compared to -9.2 kcal/mol prior to full methylation (Table 3.10, entry 1, molecule **3.72**).

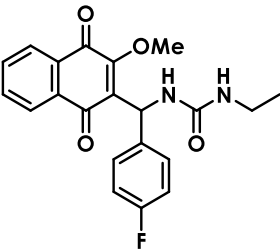
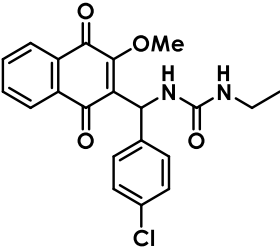
In conclusion, while the unmethylated Biginelli-linear parent molecules were found to be inactive against *P. falciparum*, the entire series of selectively *O*-methylated Biginelli-linear compounds exhibited IC_{50} values lower than $10 \mu\text{M}$. Among them, compound **3.72** had the lowest IC_{50} value at $2.8 \mu\text{M}$ and the deepest docking scores against both *P. falciparum* mitochondrial targets bc1 and DHODH. In addition, 10 out of the 13 compounds exhibited IC_{50} values lower than $5 \mu\text{M}$. In comparison to the *N*-propargyl family of compounds, it appears that

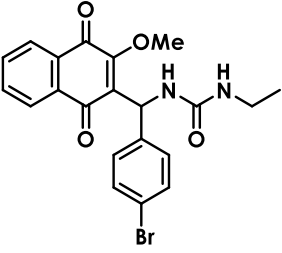
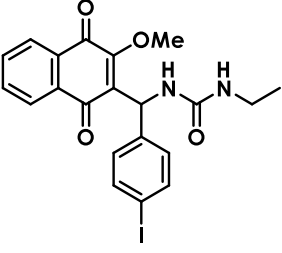
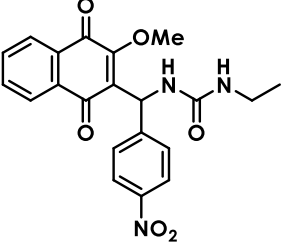
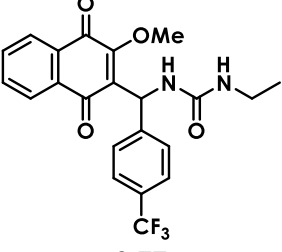
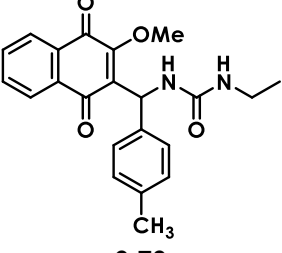
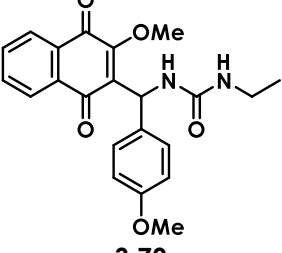
N-ethyl substitution of the urea moiety provided better activities. Besides, N-ethyl should be the longest carbon chain attached to urea moiety because longer carbon chains could prevent the molecules to enter both bc1 and DHODH binding sites. As for the *para*-phenyl substituent could be either F among all electron withdrawing groups or OMe from electron donating groups. These findings were consistent with previously published work, and further substituent modulation is required to achieve better activities. Finally, additional docking studies indicated that the majority of these compounds may act as both bc1 and DHODH inhibitors of *P. falciparum*, thereby targeting both mechanisms simultaneously. This could be considered a benefit when developing compounds to combat multi-drug resistance.

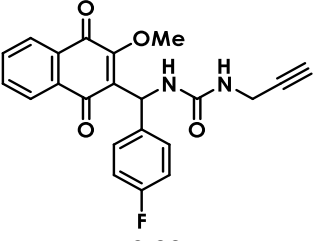
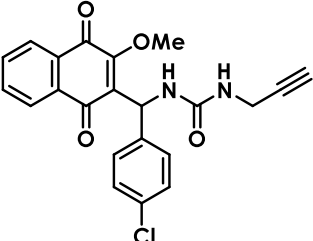
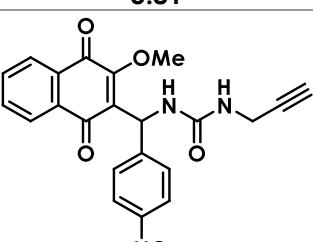
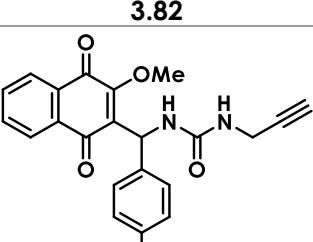
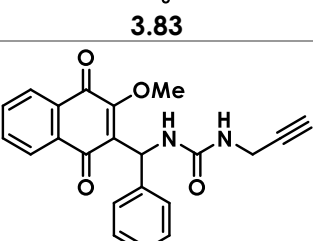
3.5.2 Activities against *L. donovani*

The leishmanicidal activity of synthesized series was assessed *in vitro* against *L. donovani* LV9 axenic amastigotes and intramacrophage amastigotes forms (see Chapter 2 for methodology). Shortly, first the leishmanicidal activity against *L. donovani* axenic amastigotes forms was evaluated. The compounds exhibiting IC₅₀ values lower than 10 μM were further evaluated against intramacrophage amastigote forms. Cytotoxicity was evaluated on RAW 264.7 macrophages. Miltefosine was used as reference drug. The obtained results are summarized in Table 3.11.

Table 3.11. Leishmanicidal activity of O-methylated Biginelli-linear series.

Entry	Compound	<i>L. donovani</i> axenic amastigotes IC ₅₀ ± SD (μM)	<i>L. donovani</i> intramacrophage amastigotes IC ₅₀ (μM)	CC ₅₀ (μM)	SI
1	 3.72	4.2 ± 1.5	2.1	12.2	5.7
2	 3.73	5.0 ± 1.3	7.5	> 100	13.4

3	 <p>3.74</p>	5.4 ± 0.6	7.0	> 100	14.3
4	 <p>3.75</p>	1.6 ± 0.2	4.5	> 100	22.5
5	 <p>3.76</p>	2.9 ± 0.2	1.2	> 100	82
6	 <p>3.77</p>	2.7 ± 0.3	1.5	> 100	68.5
7	 <p>3.78</p>	7.5 ± 2.7	8.9	> 100	11.3
8	 <p>3.79</p>	5.5 ± 0.9	1.5	> 100	67.1

9	 3.80	2.6 ± 0.3	1.3	> 100	76.3
10	 3.81	4.1 ± 1.2	1.4	> 100	69.4
11	 3.82	5.9 ± 0.5	7.2	> 100	13.4
12	 3.83	3.0 ± 0.2	2.1	> 100	46.5
13	 3.84	5.5 ± 1.1	> 100	> 100	nd
14	Miltefosine	3.0	1.5	-	15.5

*nd stands for non-determined.

The whole series of 13 novel O-methylated Biginelli-linear derivatives **3.72-3.84** was found to be active (IC_{50} values lower than $10 \mu M$) against both amastigotes forms, axenic and intramacrophage, of *L. donovani* in contrast to the non-methylated series (Chapter 3, Part I).

Among the N-ethyl urea family of compounds, the derivatives bearing a *para*-phenyl substituted moiety with strong electron withdrawing groups such as NO_2 for **3.76** (Table 3.11,

entry 5) and CF₃ for **3.77** (Table 3.11, entry 6) exhibited excellent IC₅₀ values (1.2 μM and 1.5 μM, respectively) against intramacrophage amastigote forms, very similar to miltefosine (IC₅₀ = 1.5 μM). In addition, they were found to be at least 4-fold times more selective (SI = 82 for **3.76** and 68.5 for **3.77**) than the reference drug (SI = 15.5). Among all (*para*)halogen-phenyl substituted derivatives, the *para*-fluorophenyl compound **3.72** (Table 3.11, entry 1) exhibited an IC₅₀ value equal to 2.1 μM against intramacrophage amastigotes, similar to **3.76** and **3.77**, and a SI 2.5-fold times lower (SI = 5.7) than miltefosine (Table 3.11, entry 14). However, when the halogen substituent was modified to Cl or Br (compounds **3.73** and **3.74**, Table 3.11, entries 2-3) the IC₅₀ values increased up to 7.5 μM and 7.0 μM, respectively, while the SI were found to be very similar (SI = 13.4 and 14.3, respectively). Compound **3.75** (Table 3.11, entry 4) exhibited an IC₅₀ value at 4.5 μM against intramacrophage amastigotes and a SI of 22.5. Surprisingly, among the *N*-ethyl urea derivatives bearing a *para*-phenyl substituted moiety with electron donating groups **3.78** and **3.79** (Table 3.11, entries 7-8), compound **3.79** exhibited an excellent IC₅₀ and SI value at 1.5 μM and 67.1, respectively, compared to miltefosine. However, the change of OMe group of **3.79** for Me (compound **3.78**) led to a significant decrease concerning both the activity (IC₅₀ = 8.9 μM) and selectivity (SI = 11.3) values.

Among the *N*-propargyl urea family of compounds, the *para*-halogen phenyl substituted derivatives **3.80-3.81** (Table 3.11, entries 9-10) and the CF₃ substituted derivative **3.83** (Table 3.11, entry 12) exhibited similar IC₅₀ values 1.3 μM, 1.4 μM and 2.1 μM, respectively. The SI for these compounds ranged between 46.5-76.3, meaning that all three compounds were at least 3-fold times more selective than miltefosine, used as reference (SI = 15.5). Compound **3.82** (Table 3.11, entry 11) exhibited an IC₅₀ value at 7.2 μM and SI equal to 13.4. Finally, compound **3.84** (Table 3.11, entry 13) exhibited a very promising IC₅₀ value of 5.5 μM against axenic amastigotes, but was found to be inactive against intramacrophage amastigote forms.

To sum up, the entire *O*-methylated series of the Biginelli-linear derivatives was found to be active (IC₅₀ lower than 10 μM) against both axenic and intramacrophage amastigote forms of *L. donovani*, which was not the case for the previous non-methylated compounds. In comparison to the reference drug miltefosine, 11 out of 13 compounds were found to be at least 2-fold times more selective, indicating that the series is not toxic to the host cells. However, further studies need to be done in order to understand the factors that could influence the leishmanicidal activity as obviously the electronic effects are not sufficient. That could help to reach a safe conclusion concerning the optimum combination of urea and phenyl substituents of this series of compounds.

3.5.3 Activities against various microorganisms

A potential antimicrobial activity was investigated against various Gram-positive and Gram-negative bacteria such as *E. coli* ATCC-25922, *S. aureus* ATCC-29213, *K. pneumoniae* BAA-1705, *A. baumannii* BAA-1605, and *P. aeruginosa* ATCC-27853. Levofloxacin was used as a reference

drug for the whole screening against all above mentioned bacterial strains. The antimycobacterial activity (MIC_{90}) of the synthesized series was assessed *in vitro* against *M. tuberculosis* H37Rv. Streptomycin was used as positive control (see Chapter 3-Part I for methodology).

The entire series was found to be inactive against bacteria *E. coli*, *K. pneumoniae*, *A. baumannii* and *P. aeruginosa* with IC_{50} values higher than 100 μM , in comparison to levofloxacin which exhibited IC_{50} values ranging from 0.04 to 11.1 μM , depending on the bacterial strain. The activities of **3.72-3.84** were only moderate against *M. tuberculosis* and *S. aureus*. Four out of the thirteen compounds were found to be interesting against *M. tuberculosis* with IC_{50} values lower than 100 μM . Compound **3.75** (Fig. 3.20), belonging to *N*-ethyl substituted family of methylated Biginelli-linear derivatives, exhibited the lowest IC_{50} value (20.4 μM), nevertheless 20-fold times higher than that of streptomycin ($IC_{50} = 0.43 \mu M$). Compounds **3.81** and **3.83** (Fig. 3.20) of *N*-propargyl urea substituted family exhibited IC_{50} values of 48.9 μM and 45.2 μM , respectively, 40-fold higher than streptomycin. This preliminary activity screening did not encourage further cytotoxicity evaluation.

Five of the thirteen compounds exhibited IC_{50} values lower than 100 μM against *S. aureus*, while IC_{50} value of the reference drug levofloxacin was 0.35 μM . Compound **3.75**, exhibited the lowest IC_{50} value (65.3 μM), nonetheless 60-fold higher than that of levofloxacin. The remaining four compounds **3.72**, **3.74**, **3.80**, and **3.81** had IC_{50} values ranging from 72.2 to 83.7 μM . This preliminary activity screening did not justify further cytotoxicity investigation. However, more results are required to provide reliable conclusions about structure-relationship for this type of molecules.

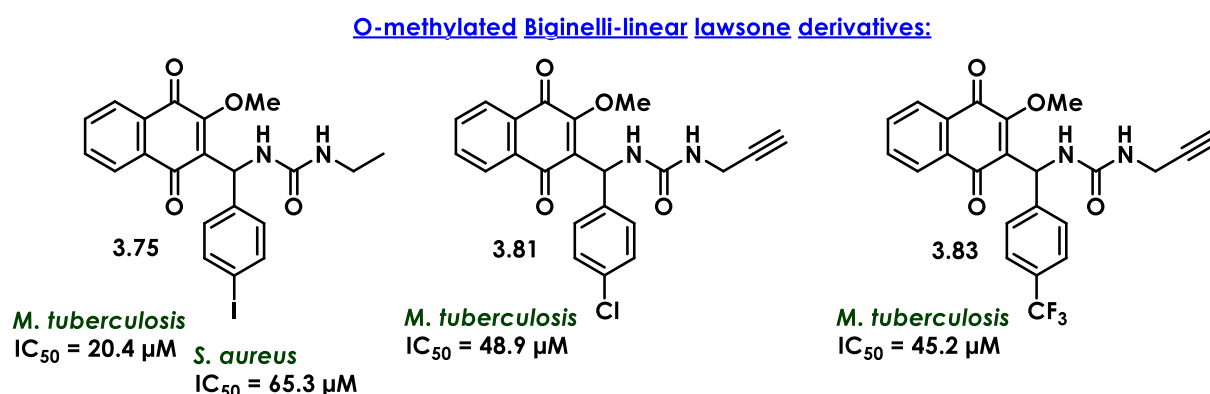


Figure 3.20. Selected examples of methylated Biginelli-linear compounds with antimicrobial activities.

3.6 Conclusion and Perspectives

Chemistry-Synthesis

A multicomponent Biginelli reaction involving lawsone, various *para*-substituted benzaldehydes and (alkyl)ureas was extensively studied under various conditions namely, protic solvents, ILs, DES and in solid state. The expected 3,4-dihydropyrimidone products (DHPMs) were never obtained. While the reaction in solution (or ILs or DES) provided the corresponding two-component Michael adducts issued from the aldol condensation between 2 equiv. of lawsone and 1 equiv. of benzaldehyde, in solid state the three-component reaction was favored instead. The optimal three-component reaction under mechanochemical activation afforded a series of 21 novel Biginelli-linear lawsone derivatives **3.43-3.68** with yields ranging between 60% and 90%, without needing column chromatography purification. Noteworthy, such Biginelli-linear compounds were never isolated before as they were supposed to be intermediates of the classic Biginelli reaction.

In that respect, many efforts were made in order to cyclize compounds **3.43** and **3.46** in solution. Surprisingly, the desired DHPM products were never obtained and the corresponding Michael adducts were again isolated as major products, indicating a mechanism passing through the formation of the Knoevenagel intermediate. Our proposed mechanistic pathway was supported by DFT studies. Besides, further cyclization attempts by activating the 2-hydroxy function of **3.46** led to the unique carbamate lawsone derivative **3.71**. This was also the first ever reported synthesis of a naphtho-carbamate bearing a urea moiety.

On the other hand, in order to avoid the instability and decomposition of these compounds in acidic aqueous solution, important for *in vitro* tests, a selective O-methylation of the enol function of Biginelli-linear derivatives was established. 13 selectively methylated products of the Biginelli-linear series **3.72-3.84** were efficiently obtained with yields ranging between 40% and 90%. The compounds were found to be stable in solution, confirming our hypothesis.

As a next step, the cyclization step leading to the carbamate formation should be optimized and the substrate scope of this reaction should be studied in order to pave the way for the synthesis of a small library of variously substituted naphtho-carbamates bearing a (alkyl)urea scaffold.

In addition, the Biginelli reaction involving lawsone should be further explored. More catalysts and conditions should be screened aiming to obtain the desired DHPM products both in solution and in solid state. Besides, this study could be further extended to other 1,3-diketone scaffolds, possessing an active methylene function, such as dimedone and/or syncarpic acid.

Finally, computational DFT calculations could be used in solid state by using our obtained X-ray data of isolated Biginelli-linear compounds in order to better understand the mechanism and the limits of this three-component reaction under mechanochemical conditions.

Biological activities

The entire Biginelli-linear series **3.43-3.68** (enol system) was found to be inactive against *P. falciparum*, *L. donovani* and other pathogens probably due to compounds' instability under *in vitro* conditions. However, that was not the case for the selectively O-methylated analogues **3.72-3.84**.

The entire methylated series exhibited $IC_{50} \leq 10 \mu M$ against *P. falciparum* ART-resistant strains. Compounds **3.72**, **3.78**, and **3.79** of the *N*-ethyl urea family exhibited IC_{50} values ranging between $2.8 \mu M$ and $3 \mu M$, while the *N*-propargyl urea derivative **3.80** exhibited an IC_{50} equal to $5 \mu M$ (Fig. 3.21).

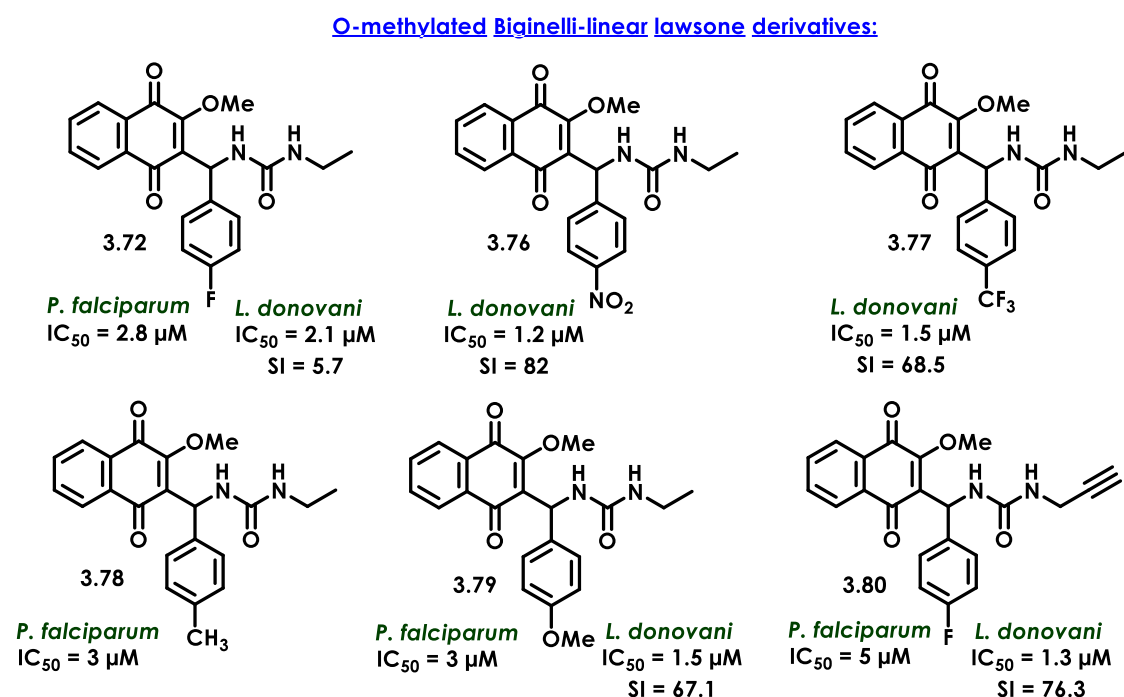


Figure 3.21. Antiparasitic activity. Selected compounds exhibiting the smallest IC_{50} values against *P. falciparum* and *L. donovani* intramacrophage amastigote forms.

Concerning the activities against *L. donovani*, the whole O-methylated series of Biginelli-linear compounds was found to be active against both axenic and intramacrophage amastigotes of the parasite. Seven (compounds **3.72**, **3.76**, **3.77**, **3.79-3.81** and **3.83**) (Fig. 3.21) out of thirteen compounds in total exhibited IC_{50} values ($1.2-2.1 \mu M$) in the same range with the reference drug miltefosine ($IC_{50} = 1.5 \mu M$) against intramacrophage amastigotes. Interestingly, the selectivity indexes were found to be at least 2-fold times higher than that of miltefosine (SI = 15.5) (Fig. 3.21). This first screening could be a great start to design and synthesize more efficient leishmanicidal agents. However, further studies are needed in order to understand

which factors (substitution pattern, lipophilicity, electron effects, etc.) influence both the activity and cytotoxicity.

As a next step, the efficiency of a one-pot two-step reaction should be tested. In that way, knowing the fragility of the enol function, a two-step approach might lead directly to novel O-methylated derivatives, thus enhancing the substrate scope.

The role of the O-alkyl group for these series should be further examined. Replacing it by longer linear or conjugated carbon chains and aromatic substrates could provide further insights concerning activity. Also, the side alkynes (such as molecule **3.80**) could be subjected in click reactions with azides in order to generate a new library of 1,2,3-triazole-naphthoquinone conjugates, as such derivatives have already been reported for their antiparasitic activities [67-69].

Last but not least, the stability of Biginelli-linear and methylated Biginelli-linear molecules *in vitro* should be examined. A good starting point for this could be to introduce these compounds in different ionic and buffer solutions (acid, basic and neutral) at 37 °C and control their degradation profile by LC-MS and/or UV-vis.

The mode of action of the most promising compounds in both terms of activity and selectivity of the O-methylated series should be investigated and proved.

3.7 Experimental Part

3.7.1 Materials and methods

Reagents and solvents were purchased from Sigma Aldrich, TCI, Alfa Aesar and Fluorochem and used as received. Microwave irradiation reactions were performed in a CEM Discover SP Microwave Model 909150 / SN: DC 9208 apparatus. Mechanochemical reactions were performed by using a Retsch Mixer Mill MM400 with 10 mL zirconium oxide jar with 5.8 g of zirconium oxide balls (2 balls, 5 mm diameter each) and a Fritsch Planetary Micro Mill PULVERISETTE 7 with 20 mL zirconium oxide jar with 14.7 g of zirconium oxide balls (5 balls, 10 mm diameter each). Thin layer chromatography (TLC) was performed on silica gel 60 F254 plates (Merck

Purifications by medium-pressure chromatography were carried out using a PuriFlash XS520Plus system with PF-30SIHP-JP-F0040 columns.

The HPLC analysis was conducted by using the following system: detector 2998 and a binary pump Waters 2545 in combination with a C18 column (XBridge 5 μ m 150mm x 19 mm). Water with 0.1% HCOOH and CH₃CN with 0.1% HCOOH (or 0.1% DEA) were employed as solvents A and B with a flow rate of 20 mL/min. The elution was followed by UV detection at 260 nm.

^1H and ^{13}C NMR spectra for the reported compounds were recorded on a Bruker Avance I 300 MHz (300 MHz for ^1H and 75 MHz for ^{13}C), or a Bruker Avance III Nanobay 400 MHz (400.0 MHz for ^1H and 101 MHz for ^{13}C), or a Bruker Avance 600 MHz (600 MHz for ^1H and 151 MHz for ^{13}C) equipped with a 5 mm triple resonance inverse Z-gradient probe (TBI ^1H , ^{31}P , BB). NMR samples were prepared by dissolving 10–20 mg of each compound in 600 μL of CDCl_3 or $\text{DMSO-}d_6$. Chemical shifts (δ) for ^1H and ^{13}C are relative to TMS as external standard, using ^1H (residual) or ^{13}C chemical shifts of the solvent ($\delta = 7.26$ ppm for CDCl_3 , 3.31 ppm for MeOD, and 2.50 ppm for $\text{DMSO-}d_6$). TMS was used as external reference for ^1H and ^{13}C NMR spectras while CFCl_3 for ^{19}F spectras. All ^1H and ^{13}C signals were assigned on the basis of chemical shifts, spin-spin coupling constants, splitting patterns, and signal intensities, and by using $^1\text{H-}^1\text{H}$ COSY45, $^1\text{H-}^{13}\text{C}$ HSQC, and $^1\text{H-}^{13}\text{C}$ HMBC experiments. Gradient-enhanced ^1H COSY45 was performed by including 8 scans for per increment. $^1\text{H-}^{13}\text{C}$ correlation spectra using a gradient-enhanced HSQC sequence (delay was optimised for $^1J_{\text{CH}}$ of 145 Hz) was obtained with 16 scans per increment. Gradient-enhanced HMBC experiment was performed allowing 62.5 ms for long-range coupling evolution (64 scans were accumulated). Typically, 2048 t_2 data points were collected for 256 t_1 increments.

High resolution mass spectrometry (HRMS) analyses were carried out on a XevoG2QTof equipment (Waters) using electrospray ionization (ESI).

The X-ray diffraction of single crystals was collected on a Bruker Kapa Apex II diffractometer equipped with a 30 W air-cooled microfocus source using MoK α radiation ($\lambda = 0.71073$ Å). The SHELXS-97 software was used to analyze the structures.

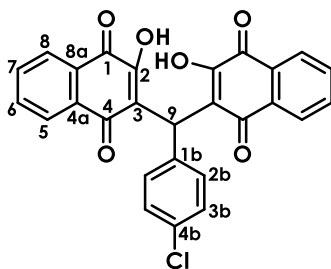
Melting points were determined using a Stuart SMP3 apparatus and the obtained values are not corrected. UV-visible spectra of selected compounds (CH_2Cl_2 solutions at 0.01 or 0.02 mg/mL) were recorded from 200 to 800 nm on Cary 3500 spectrophotometers (see supporting information). Infrared spectra of selected compounds were measured using the Perkin Elmer Frontier MIR/FIR spectrometer and reported in the experimental part. The samples were used as such (powders).

3.7.2 Synthetic protocols and compounds characterization

Synthesis of Michael adduct 3.44

A mixture of lawsone (1.5 mmol), urea (1.5 mmol) and 4-chlorobenzaldehyde (1.5 mmol) in 2 mL ionic liquid $[\text{HNMP}]^+[\text{HSO}_4]^-$ media was stirred at 80 °C for 30 min, until it turned into a red solid. Then, iced water was added and the resulting suspension stayed under vigorous stirring for 10 min. The red solid was isolated by filtration and washed with excess of water. Afterwards, the crude product was purified by recrystallization in EtOH to afford 332 mg of **3.44** as a yellow-orange solid (yield 47%, mp 180–182 °C).

3,3'-((4-chlorophenyl)methylene)bis(2-hydroxynaphthalene-1,4-dione), (**3.44**)



R_f (Hex/AcOEt 1:1) = 0.12.

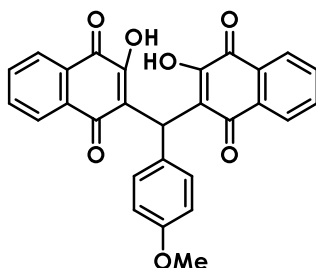
¹H NMR (400 MHz, CDCl₃) δ 8.10 (dd, *J* = 7.6, 1.5 Hz, 4H, H5 and H6), 7.76 (td, *J* = 7.6, 1.5 Hz, 2H, H8), 7.70 (td, *J* = 7.6, 1.5 Hz, 2H, H7), 7.23 (m, 4H, H2b and H3b), 6.15 (s, 1H, H9), 3.49 (s, 2H, OH).

¹³C NMR (101 MHz, CDCl₃) δ 184.5 (2 x C=O, C4), 181.4 (2 x C=O, C1), 154.6 (2 x C-OH, C2), 137.1 (C, C1b), 135.3 (2 x CH, C6), 133.4 (2 x CH, C7), 132.9 (2 x C, C4a), 132.6 (C-Cl, C4b), 129.8 (2 x CH, C5), 129.6 (2 x C, C8a), 128.5 (2 x CH, C8), 127.4 (2 x CH, C3b), 126.5 (2 x CH, C2b), 122.3 (2 x C, C3), 37.6 (CH, C9).

HRMS calculated for C₂₇H₁₄O₆Cl⁻ [M - H]⁻ = 469.0479; found 469.0481.

Characterization of Michael adduct 3.69 (isolated out of the crude reaction mixture of **3.65**)

3,3'-((4-methoxyphenyl)methylene)bis(2-hydroxynaphthalene-1,4-dione), (**3.69**)



Yellow solid (mp 222–223 °C).

R_f (AcOEt) = 0.12.

¹H NMR (DMSO, 300 MHz) δ 3.69 (s, 3H), 5.94 (s, 1H), 6.75 (d, 2H, *J* = 8.7 Hz), 7.14 (d, 2H, 8.7 Hz), 7.77 (dt, 2H, *J* = 7.5, 1.5 Hz), 7.82 (dt, 2H, *J* = 7.5, 1.5 Hz), 7.92 (dd, 2H, *J* = 7.5, 1.5 Hz), 7.98 (dd, 2H, *J* = 7.5, 1.5 Hz).

¹³C NMR (DMSO-*d*₆, 75 MHz) δ 183.7 (2 x C=O), 181.3 (2 x C=O), 157.3 (2 x C-OH), 155.9 (2 x C), 134.7 (2 x CH), 133.2 (2 x CH), 132.7 (2 x C), 132.2 (2 x C), 129.9 (2 x CH), 129.4 (2 x CH), 126.1 (2 x CH), 125.6 (2 x C), 113.1 (2 x CH), 54.9 (C), 37.3 (CH).

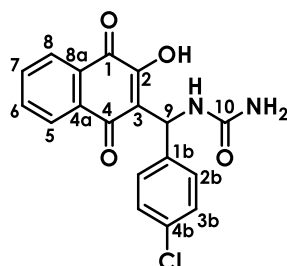
HRMS calculated for $C_{28}H_{17}O_7$ [$M - H$] $^-$ = 465.0974; found 465.0984.

General synthetic protocol for the mechanochemical synthesis of Biginelli-type linear lawsone derivatives

Lawsone (1.0 equiv, 2.2 mmol), 4-substituted-benzaldehyde (1.0 equiv, 2.2 mmol), urea or *N*-alkylated urea (1.5 equiv, 3.3 mmol) and *p*-toluenesulfonic acid (pTSA) (0.2 equiv, 0.44 mmol) were added in a 20 mL zirconium oxide jar with 14.7 g of zirconium oxide balls (5 balls, 10 mm diameter each). The reaction was operated in a planetary ball milling Pulverisette 7 at 800 rpm (2 cycles x 40-60 min, 1 x pause 10 min). Afterwards, the reaction mixture was either scratched out of the jars either recovered by dissolving it in MeOH. If needed, the solvent was removed under vacuum. The collected residue was dissolved in dichloromethane. The organic phase was washed with water and brine. The organic layers were collected, dried over Na_2SO_4 , filtered, and evaporated under reduced pressure. The obtained crude products were then purified by crystallization in dichloromethane/diethyl ether or dichloromethane/methanol. The products were isolated as solids after filtration and washing with Et_2O .

Biginelli-linear lawsone derivatives characterization

3-[[4'-chlorophenyl]methylurea]-2-hydroxynaphthalene-1,4-dione, **(3.43)**



The compound was synthesized by following the above-mentioned general procedure (2.2 mmol of lawsone scale). Ball milling for 2 cycles x 40 min. The crude product was purified by crystallization in DCM/ Et_2O to yield 710 mg (90%) of the target product as a yellow solid (mp 137–139 °C).

R_f (DCM/MeOH 9:1) = 0.11.

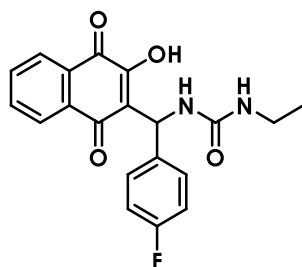
1H NMR (400 MHz, DMSO) δ 8.03 – 7.99 (m, 1H, H6), 7.94 (dd, J = 7.6, 1.4 Hz, 1H, H8), 7.87 – 7.83 (m, 1H, H7), 7.83 – 7.78 (m, 1H, H5), 7.36 – 7.29 (m, 4H, H2b and H3b), 6.81 (d, J = 9.8 Hz, 1H, NH), 6.40 (d, J = 9.8 Hz, 1H, H9), 5.90 (bs, 2H, NH_2).

^{13}C NMR (75 MHz, DMSO) δ 184.1 (C=O, C4), 181.3 (C=O, C1), 158.0 (NH-C=O, C10), 155.8 (C-OH, C2), 141.8 (C, C1b), 134.8 (CH, C6), 133.4 (CH, C7), 131.8 (C-Cl, C4b), 130.8 (C, C4a), 130.1

(C, C8a), 128.0 (2 x CH, C3b), 127.7 (2 x CH, C2b), 125.8 (CH, C5), 125.7 (CH, C8), 122.6 (C, C3), 46.3 (CH, C9).

HRMS calculated for $C_{18}H_{12}N_2O_4Cl$ $[M - H]^- = 355.0486$; found 355.0486.

3-[(4'-fluorophenyl)methyl-(N'-ethyl)-urea]-2-hydroxynaphthalene-1,4-dione, (**3.46**)



The compound was synthesized by following the above-mentioned general procedure (1.5 mmol of lawsone scale). Ball milling for 2 cycles x 60 min. The crude product was purified by crystallization in DCM to yield 350 mg (63%) of the target product as a yellow solid (mp 172–174 °C).

Rf (Hex/AcOEt 1:1) = 0.11.

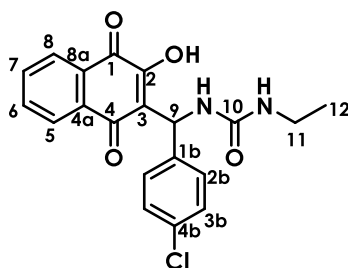
1H NMR (400 MHz, MeOD) δ 8.04 (tt, $J = 7.4, 1.0$ Hz, 2H), 7.77 (td, $J = 7.5, 1.5$ Hz, 1H), 7.73 (td, $J = 7.5, 1.5$ Hz, 1H), 7.45 – 7.38 (m, 2H), 7.04 – 6.96 (m, 2H), 6.54 (s, 1H), 3.16 (q, $J = 7.2$ Hz, 2H), 1.10 (t, $J = 7.2$ Hz, 3H).

^{13}C NMR (101 MHz, MeOD) δ 186.0 (C=O), 182.7 (C=O), 163.2 (d, $J = 244.4$ Hz, C-F), 160.3 (NH-C=O), 156.9 (C-OH), 139.3 (d, $J = 3.0$ Hz, C), 135.7 (CH), 134.3 (CH), 133.8 (C), 131.5 (C), 129.2 (CH), 129.1 (CH), 127.1 (d, $J = 25.3$ Hz, 2 x CH), 123.9 (C), 115.8 (d, $J = 22.2$ Hz, 2 x CH), 49.0 (CH), 35.8 (CH₂), 15.7 (CH₃).

^{19}F NMR (376 MHz, MeOD) δ -118.61 (m, $J = 9.5$ Hz).

HRMS calculated for $C_{20}H_{18}N_2O_4F^+$ $[M + H]^+ = 369.1251$; found 369.1245, for $C_{20}H_{17}N_2O_4NaF^+$ $[M + Na]^+ = 391.1070$; found 391.1064.

3-[(4'-chlorophenyl)methyl-(N'-ethyl)-urea]-2-hydroxynaphthalene-1,4-dione, (**3.47**)



The compound was synthesized by following the above-mentioned general procedure (1.5 mmol of lawsone scale). Ball milling for 2 cycles x 40 min. The crude product was purified by crystallization in DCM/MeOH/Et₂O to yield 358 mg (62%) of the target product as a yellow solid (mp 168–170 °C).

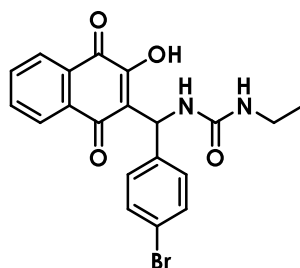
R_f (Hex/AcOEt 3:7) = 0.10.

¹H NMR (300 MHz, MeOD) δ 8.04 (td, *J* = 7.5, 2.2 Hz, 2H, H5 and H6), 7.75 (dtd, *J* = 7.5, 1.7 Hz, 2H, H7 and H8), 7.42 – 7.33 (m, 2H, H2b), 7.31 – 7.19 (m, 2H, H3b), 6.55 (s, 1H, H9), 3.16 (q, *J* = 7.2 Hz, 2H, H11), 1.10 (t, *J* = 7.2 Hz, 3H, H12).

¹³C NMR (75 MHz, MeOD) δ 186.0 (C=O, C4), 182.6 (C=O, C1), 160.2 (NH-C=O, C10), 156.9 (C-OH, C2), 142.1 (C, C1b), 135.8 (CH, C6), 134.3 (CH, C7), 133.7 (C, C4a), 133.5 (C-Cl, C4b), 131.5 (C, C8a), 129.3 (2 x CH, C2b), 128.9 (2 x CH, C3b), 127.2 (CH, C5), 127.0 (CH, C8), 123.7 (C, C3), 48.9 (CH, C9), 35.8 (CH₂, C11), 15.7 (CH₃, C12).

HRMS calculated for C₂₀H₁₈N₂O₄Cl⁺ [M + H]⁺ = 385.0955; found 385.0949, for C₂₀H₁₇N₂O₄NaCl + [M + Na]⁺ = 407.0775; found 407.0769.

3-[(4'-bromophenyl)methyl-(*N*'-ethyl)-urea]-2-hydroxynaphthalene-1,4-dione, (**3.48**)



The compound was synthesized by following the above-mentioned general procedure (1.3 mmol of lawsone scale). Ball milling for 2 cycles x 50 min. The crude product was purified by crystallization in DCM/Et₂O to yield 391 mg (70%) of the target product as a yellow solid (mp 187–189 °C).

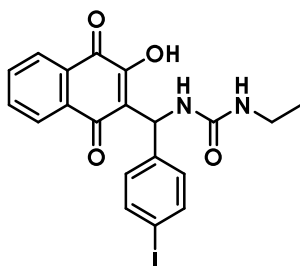
R_f (Hex/AcOEt 3:7) = 0.10.

¹H NMR (300 MHz, MeOD) δ 8.07 – 7.98 (m, 2H), 7.75 (dd, *J* = 7.5, 1.6 Hz, 2H), 7.46 – 7.38 (m, 2H), 7.35 – 7.28 (m, 2H), 6.53 (s, 1H), 3.16 (q, *J* = 7.2 Hz, 2H), 1.10 (t, *J* = 7.2 Hz, 3H).

¹³C NMR (101 MHz, DMSO) δ 184.2 (C=O), 181.3 (C=O), 157.2 (NH-C=O), 155.8 (C-OH), 142.3 (C), 134.8 (CH), 133.4 (CH), 131.7 (C), 130.8 (2 x CH), 130.1 (C), 128.1 (2 x CH), 125.8 (C), 125.7 (C), 122.5 (C-Br), 119.3 (C), 46.4 (CH), 34.1 (CH₂), 15.6 (CH₃).

HRMS calculated for C₂₀H₁₈N₂O₄Br⁺ [M + H]⁺ = 429.0450; found 429.0446, for C₂₀H₁₇N₂O₄NaBr + [M + Na]⁺ = 451.0269; found 451.0264 with consistent isotopic profile.

3-[[4'-iodophenyl)methyl-(N'-ethyl)-urea]-2-hydroxynaphthalene-1,4-dione, (3.49)



The compound was synthesized by following the above-mentioned general procedure (1.3 mmol of lawsone scale). Ball milling for 2 cycles x 50 min. The crude product was purified by crystallization in DCM/Et₂O to yield 433 mg (70%) of the target product as a yellow solid (mp 186–188 °C).

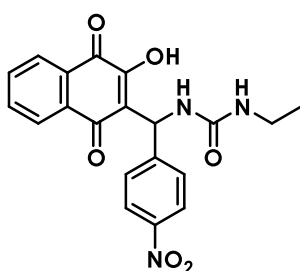
R_f (Hex/AcOEt 1:9) = 0.29.

¹H NMR (400 MHz, MeOD) δ 8.07 – 8.00 (m, 2H), 7.77 (td, *J* = 7.5, 1.6 Hz, 1H), 7.72 (td, *J* = 7.5, 1.6 Hz, 1H), 7.64 – 7.58 (m, 2H), 7.22 – 7.14 (m, 2H), 6.52 (s, 1H), 3.16 (q, *J* = 7.2 Hz, 2H), 1.09 (t, *J* = 7.2 Hz, 3H).

¹³C NMR (101 MHz, MeOD) δ 185.9 (C=O), 182.6 (C=O), 160.2 (NH-C=O), 157.1 (C-OH), 143.3 (C), 138.4 (2 x CH), 135.8 (CH), 134.3 (CH), 133.8 (C), 131.6 (C), 129.5 (2 x CH), 127.2 (C), 127.0 (C), 123.6 (C), 92.5 (C-I), 49.1 (CH), 35.8 (CH₂), 15.7 (CH₃).

HRMS calculated for C₂₀H₁₈N₂O₄⁺ [M + H]⁺ = 477.0311; found 477.0315, for C₂₀H₁₇N₂O₄NaI⁺ [M + Na]⁺ = 499.0131; found 499.0133.

3-[[4'-nitrophenyl)methyl-(N'-ethyl)-urea]-2-hydroxynaphthalene-1,4-dione, (3.50)



The compound was synthesized by following the above-mentioned general procedure (1.5 mmol of lawsone scale). Ball milling for 2 cycles x 50 min. The crude product was purified by crystallization in DCM/Et₂O to yield 504 mg (85%) of the target product as a yellow-orange solid (mp 183–185 °C).

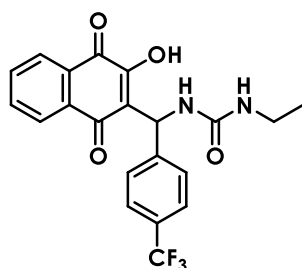
R_f (Hex/AcOEt 3:7) = 0.09.

^1H NMR (400 MHz, MeOD) δ 8.19 – 8.13 (m, 2H), 8.06 (dd, J = 7.5, 1.4 Hz, 1H), 8.02 (dd, J = 7.5, 1.4 Hz, 1H), 7.81 – 7.71 (m, 2H), 7.66 – 7.61 (m, 2H), 6.67 (s, 1H), 3.17 (q, J = 7.2 Hz, 2H), 1.11 (t, J = 7.2 Hz, 3H).

^{13}C NMR (101 MHz, MeOD) δ 185.8 (C=O), 182.5 (C=O), 160.1 (C), 157.5 (NH-C=O), 151.3 (C-OH), 148.2 (C), 135.8 (CH), 134.4 (CH), 133.7 (C), 131.6 (C), 128.3 (2 x CH), 127.2 (CH), 127.1 (CH), 124.4 (2 x CH), 123.0 (C), 49.1 (CH), 35.8 (CH₂), 15.7 (CH₃).

HRMS calculated for C₂₀H₁₈N₃O₆⁺ [M + H]⁺ = 396.1196; found 396.1193, for C₂₀H₁₇N₃O₆Na⁺ [M + Na]⁺ = 418.1015; found 418.1009.

3-[(4'-trifluoromethylphenyl)methyl-(N'-ethyl)-urea]-2-hydroxynaphthalene-1,4-dione, **(3.51)**



The compound was synthesized by following the above-mentioned general procedure (1.0 mmol of lawsone scale). Ball milling for 1 cycle x 45 min. The crude product was purified by crystallization in DCM/MeOH/Et₂O to yield 376 mg (90%) of the target product as a yellow solid (mp 166–168 °C).

R_f (Hex/AcOEt 1:1) = 0.08.

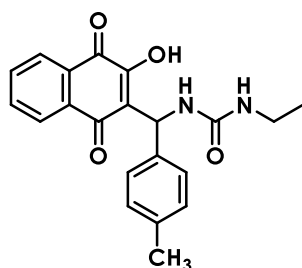
^1H NMR (400 MHz, DMSO) δ 8.04 – 7.99 (m, 1H), 7.96 – 7.91 (m, 1H), 7.82 (dtd, J = 17.8, 7.5, 1.5 Hz, 2H), 7.65 (d, J = 8.7 Hz, 2H), 7.55 – 7.48 (m, 2H), 6.75 (d, J = 9.7 Hz, 1H), 6.53 (m, 2H), 3.08 – 2.95 (m, 2H), 0.99 (t, J = 7.2 Hz, 3H).

^{13}C NMR (101 MHz, DMSO) δ 184.1 (C=O), 181.3 (C=O), 157.3 (NH-C=O), 156.0 (C-OH), 147.7 (C), 134.8 (CH), 133.4 (CH), 131.7 (C), 130.2 (C), 127.0 (d, J = 33.3 Hz, C), 126.6 (2 x CH), 125.9 (CH), 125.7 (CH), 124.9 (q, J = 3.9 Hz, 2 x CH), 124.4 (q, J = 272.7 Hz, CF₃), 122.3 (C), 46.7 (CH), 34.1 (CH₂), 15.5 (CH₃).

^{19}F NMR (282 MHz, DMSO) δ -60.69.

HRMS calculated for C₂₁H₁₈N₂O₄F₃⁺ [M + H]⁺ = 419.1219; found 419.1219 with consistent isotopic profile.

3-[(4'-tolyl)methyl-(N'-ethyl)-urea]-2-hydroxynaphthalene-1,4-dione, (3.52)



The compound was synthesized by following the above-mentioned general procedure (2.0 mmol of lawsone scale). Ball milling for 2 cycles x 60 min. The crude product was purified by crystallization in DCM to yield 510 mg (70%) of the target product as a yellow solid (mp 175–177 °C).

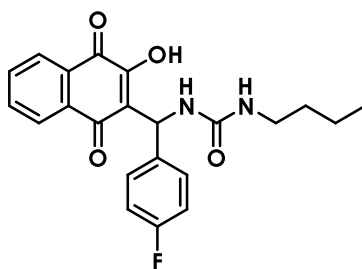
R_f (AcOEt) = 0.21.

¹H NMR (300 MHz, MeOD) δ 8.02 (t, *J* = 7.5 Hz, 2H), 7.79 – 7.66 (m, 2H), 7.28 (d, *J* = 8.1 Hz, 2H), 7.08 (d, *J* = 8.1 Hz, 2H), 6.52 (s, 1H), 3.16 (q, *J* = 7.2 Hz, 2H), 2.27 (s, 3H), 1.10 (t, *J* = 7.2 Hz, 3H).

¹³C NMR (101 MHz, MeOD) δ 186.1 (C=O), 182.7 (C=O), 160.4 (NH-C=O), 156.5 (C-OH), 140.1 (C), 137.5 (C), 135.7 (CH), 134.3 (CH), 133.8 (C), 131.5 (C), 129.9 (2 x CH), 127.2 (2 x CH), 127.2 (CH), 126.9 (CH), 124.4 (C), 49.3 (CH), 35.8 (CH₂), 21.0 (PhCH₃), 15.7 (CH₃).

HRMS calculated for C₂₁H₂₁N₂O₄⁺ [M+H]⁺ = 365.1501; found 365.1499, for C₂₁H₂₀N₂O₄Na⁺ [M + Na]⁺ = 387.1321; found 387.1320.

3-[(4'-fluorophenyl)methyl-(N'-butyl)-urea]-2-hydroxynaphthalene-1,4-dione, (3.54)



The compound was synthesized by following the above-mentioned general procedure (1.4 mmol of lawsone scale). Ball milling for 2 cycles x 50 min. The crude product was purified by crystallization in DCM to yield 450 mg (81%) of the target product as a yellow solid (mp 172–174 °C).

R_f (Hex/AcOEt 3:7) = 0.12.

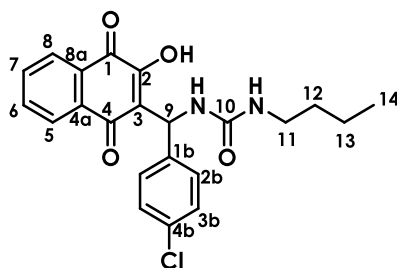
¹H NMR (400 MHz, MeOD) δ 8.04 (ddd, *J* = 8.9, 7.4, 1.8 Hz, 2H), 7.75 (dtd, *J* = 19.6, 7.4, 1.5 Hz, 2H), 7.42 (dd, *J* = 8.6, 5.3 Hz, 2H), 7.03 – 6.95 (m, 2H), 6.54 (s, 1H), 3.12 (t, *J* = 7.0 Hz, 2H), 1.50 – 1.41 (m, 2H), 1.41 – 1.29 (m, 2H), 0.92 (t, *J* = 7.3 Hz, 3H).

^{13}C NMR (101 MHz, MeOD) δ 185.9 (C=O), 182.7 (C=O), 163.2 (d, J = 244.4 Hz, C-F), 160.4 (NH-C=O), 157.1 (C-OH), 139.3 (d, J = 3.0 Hz, C), 135.7 (CH), 134.3 (CH), 133.9 (C), 131.6 (C), 129.2 (CH), 129.1 (CH), 127.1 (d, J = 24.2 Hz, 2 x CH), 123.9 (C), 115.8 (d, J = 22.2 Hz, 2 x CH), 49.0 (CH), 40.7 (CH₂), 33.4 (CH₂), 21.0 (CH₂), 14.1 (CH₃).

^{19}F NMR (282 MHz, DMSO) δ -117.01.

HRMS calculated for C₂₂H₂₂N₂O₄F⁺ [M+H]⁺=397.1564; found 397.1564, for C₂₂H₂₁N₂O₄FNa⁺ [M + Na]⁺ = 419.1383; found 419.1379.

3-[(4'-chlorophenyl)methyl-(N'-butyl)-urea]-2-hydroxynaphthalene-1,4-dione, (**3.55**)



The compound was synthesized by following the above-mentioned general procedure (1.5 mmol of lawsone scale). Ball milling for 2 cycles x 45 min. The crude product was purified by crystallization in DCM/Et₂O to yield 526 mg (85%) of the target product as a yellow solid (mp 160–162 °C).

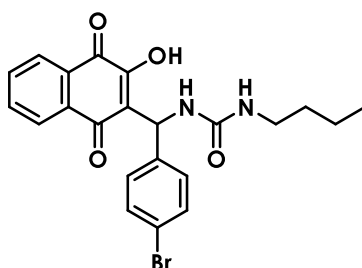
R_f (Hex/AcOEt 3:7) = 0.16.

^1H NMR (400 MHz, MeOD) δ 8.09 – 7.98 (m, 2H, H5 and H6), 7.77 (td, J = 7.5, 1.6 Hz, 1H, H8), 7.72 (td, J = 7.5, 1.6 Hz, 1H, H7), 7.41 – 7.36 (m, 2H, H2b), 7.29 – 7.24 (m, 2H, H3b), 6.54 (s, 1H, H9), 3.13 (t, J = 7.0 Hz, 2H, H11), 1.49 – 1.41 (m, 2H, H12), 1.40 – 1.29 (m, 2H, H13), 0.92 (t, J = 7.3 Hz, 3H, H14).

^{13}C NMR (101 MHz, DMSO) δ 184.1 (C=O, C4), 181.3 (C=O, C1), 157.4 (NH-C=O, C10), 155.9 (C-OH, C2), 141.9 (C, C1b), 134.7 (CH, C6), 133.4 (CH, C7), 131.8 (C, C4a), 130.8 (C-Cl, C4b), 130.1 (C, C8a), 128.0 (2 x CH, C2b), 127.7 (2 x CH, C3b), 125.8 (CH, C5), 125.7 (CH, C8), 122.5 (C3), 46.4 (CH₂, C11), 39.7 (CH, C9), 32.0 (CH₂, C12), 19.5 (CH₂, C13), 13.7 (CH₃, C14).

HRMS calculated for C₂₂H₂₂N₂O₄Cl⁺ [M+H]⁺=413.1268; found 413.1268, for C₂₂H₂₁N₂O₄ClNa⁺ [M + Na]⁺ = 435.1088; found 435.1085.

3-[(4'-bromophenyl)methyl-(N'-butyl)-urea]-2-hydroxynaphthalene-1,4-dione, (**3.56**)



The compound was synthesized by following the above-mentioned general procedure (1.3 mmol of lawsone scale). Ball milling for 1 cycle x 60 min. The crude product was purified by crystallization in DCM/Et₂O to yield 564 mg (95%) of the target product as a yellow solid (mp 165–167 °C).

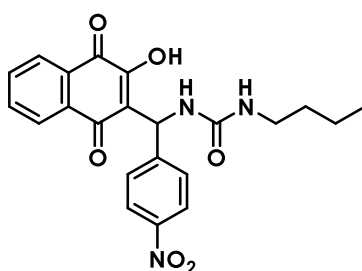
R_f (Hex/AcOEt 3:7) = 0.11.

¹H NMR (400 MHz, MeOD) δ 8.08 – 8.00 (m, 2H), 7.78 (td, *J* = 7.5, 1.6 Hz, 1H), 7.73 (td, *J* = 7.5, 1.6 Hz, 1H), 7.45 – 7.39 (m, 2H), 7.36 – 7.29 (m, 2H), 6.53 (s, 1H), 3.13 (t, *J* = 7.0 Hz, 2H), 1.51 – 1.41 (m, 2H), 1.39 – 1.27 (m, 2H), 0.92 (t, *J* = 7.3 Hz, 3H).

¹³C NMR (101 MHz, MeOD) δ 186.0 (C=O), 182.6 (C=O), 160.4 (NH-C=O), 156.9 (C-OH), 142.7 (C), 135.8 (CH), 134.3 (CH), 133.8 (C), 132.3 (2 x CH), 131.6 (C), 129.3 (2 x CH), 127.2 (CH), 127.0 (CH), 123.6 (C-Br), 121.4 (C), 49.1 (CH), 40.7 (CH₂), 33.4 (CH₂), 21.0 (CH₂), 14.1 (CH₃).

HRMS calculated for C₂₂H₂₂N₂O₄Br⁺ [M+H]⁺=457.0763; found 457.0764, for C₂₂H₂₁N₂O₄BrNa⁺ [M + Na]⁺ = 479.0582; found 479.0586.

3-[(4'-nitrophenyl)methyl-(N'-butyl)-urea]-2-hydroxynaphthalene-1,4-dione, (**3.57**)



The compound was synthesized by following the above-mentioned general procedure (1.4 mmol of lawsone scale). Ball milling for 1 cycle x 50 min. The crude product was purified by crystallization in DCM/Et₂O to yield 534 mg (90%) of the target product as a yellow-orange solid (mp 175–177 °C).

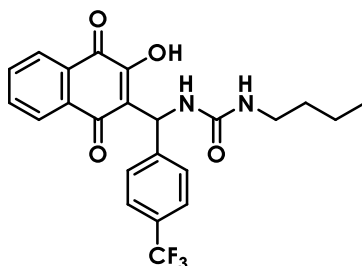
R_f (Hex/AcOEt 3:7) = 0.12.

^1H NMR (400 MHz, MeOD) δ 8.21 – 8.13 (m, 2H), 8.07 (dd, $J = 7.1, 1.7$ Hz, 1H), 8.05 – 7.98 (m, 1H), 7.76 (dtd, $J = 17.6, 7.5, 1.4$ Hz, 2H), 7.68 – 7.58 (m, 2H), 6.67 (s, 1H), 3.14 (t, $J = 7.0$ Hz, 2H), 1.52 – 1.42 (m, 2H), 1.40 – 1.30 (m, 2H), 0.92 (t, $J = 7.3$ Hz, 3H).

^{13}C NMR (101 MHz, MeOD) δ 185.7 (C=O), 182.6 (C=O), 160.3 (C), 157.7 (NH-C=O), 151.4 (C-OH), 148.2 (C), 135.8 (CH), 134.4 (CH), 133.8 (C), 131.6 (C), 128.3 (2 x CH), 127.2 (CH), 127.1 (CH), 124.4 (2 x CH), 123.0 (C), 49.2 (CH), 40.8 (CH₂), 33.4 (CH₂), 21.0 (CH₂), 14.1 (CH₃).

HRMS calculated for C₂₂H₂₂N₃O₆⁺ [M+H]⁺ = 424.1509; found 424.1511, for C₂₂H₂₁N₃O₆Na⁺ [M + Na]⁺ = 446.1328; found 443.1328.

3-[(4'-trifluoromethylphenyl)methyl-(N'-butyl)-urea]-2-hydroxynaphthalene-1,4-dione, **(3.58)**



The compound was synthesized by following the above-mentioned general procedure (2.0 mmol of lawsone scale). Ball milling for 2 cycles x 60 min. The crude product was purified by crystallization in cold Et₂O to yield 714 mg (80%) of the target product as a yellow solid (mp 156–158 °C).

R_f (Hex/AcOEt 1:1) = 0.24.

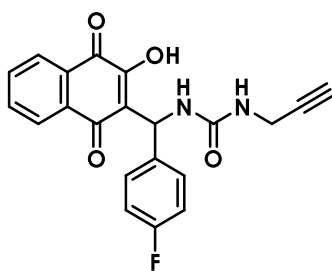
^1H NMR (400 MHz, MeOD) δ 8.04 (ddd, $J = 12.4, 7.4, 1.8$ Hz, 2H), 7.81 – 7.70 (m, 2H), 7.58 (s, 4H), 6.64 (s, 1H), 3.14 (t, $J = 7.0$ Hz, 2H), 1.51 – 1.41 (m, 2H), 1.41 – 1.30 (m, 2H), 0.92 (t, $J = 7.3$ Hz, 3H).

^{13}C NMR (101 MHz, MeOD) δ 185.9 (C=O), 182.6 (C=O), 160.4 (NH-C=O), 157.2 (C-OH), 148.0 (C), 135.8 (CH), 134.4 (CH), 133.7 (C), 131.6 (C), 130.0 (d, $J = 34.1$ Hz, C), 127.8 (2 x CH), 127.3 (CH), 127.0 (CH), 126.1 (q, $J = 4.0$ Hz, 2 x CH), 125.7 (q, $J = 271.7$ Hz, CF₃), 123.4 (C), 49.2 (CH), 40.7 (CH₂), 33.4 (CH₂), 21.0 (CH₂), 14.1 (CH₃).

^{19}F NMR (282 MHz, MeOD) δ -63.87.

HRMS calculated for C₂₃H₂₀N₂O₄F₃⁻ [M - H]⁻ = 445.1375; found 445.1377.

3-[[4'-fluorophenyl)methyl-(N'-propargyl)-urea]-2-hydroxynaphthalene-1,4-dione, (**3.60**)



The compound was synthesized by following the above-mentioned general procedure (1.4 mmol of lawsone scale). Ball milling for 2 cycles x 50 min. The crude product was purified by crystallization in DCM to yield 440 mg (83%) of the target product as an olive-colored solid (mp 180–182 °C).

R_f (Hex/AcOEt 3:7) = 0.18.

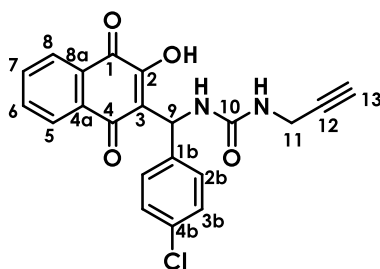
^1H NMR (400 MHz, MeOD) δ 8.04 (tt, J = 7.7, 1.2 Hz, 2H), 7.75 (dtd, J = 18.9, 7.5, 1.6 Hz, 2H), 7.45 – 7.38 (m, 2H), 7.04 – 6.96 (m, 2H), 6.55 (s, 1H), 3.91 (t, J = 2.3 Hz, 2H), 2.53 (t, J = 2.5 Hz, 1H).

^{13}C NMR (101 MHz, MeOD) δ 186.0 (C=O), 182.6 (C=O), 163.2 (d, J = 244.4 Hz, C-F), 159.7 (NH-C=O), 156.7 (C-OH), 139.0 (d, J = 3.0 Hz, C), 135.8 (CH), 134.3 (CH), 133.7 (C), 131.5 (C), 129.2 (CH), 129.1 (CH), 127.1 (d, J = 26.3 Hz, 2 x CH), 123.7 (C), 115.8 (d, J = 21.2 Hz, 2 x CH), 81.7 (C), 71.9 (CH), 49.1 (CH), 30.3 (CH₂).

^{19}F NMR (376 MHz, MeOD) δ -118.51.

HRMS calculated for C₂₁H₁₆N₂O₄F + [M + H]⁺ = 379.1094; found 379.1095.

3-[[4'-chlorophenyl)methyl-(N'-propargyl)-urea]-2-hydroxynaphthalene-1,4-dione, (**3.61**)



The compound was synthesized by following the above-mentioned general procedure (1.5 mmol of lawsone scale). Ball milling for 2 cycles x 40 min. The crude product was purified by crystallization in DCM to yield 432 mg (73%) of the target product as a yellow solid (mp 180–182 °C).

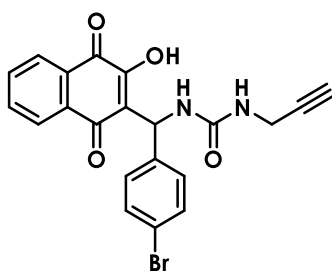
R_f (Hex/AcOEt 3:7) = 0.16.

^1H NMR (400 MHz, MeOD) δ 8.03 (ddd, $J = 8.8, 7.5, 1.6$ Hz, 2H, H5 and H6), 7.74 (dtd, $J = 18.7, 7.5, 1.6$ Hz, 2H, H7 and H8), 7.42 – 7.33 (m, 2H, H2b), 7.31 – 7.22 (m, 2H, H3b), 6.55 (s, 1H, H9), 3.91 (t, $J = 2.3$ Hz, 2H, H11), 2.53 (t, $J = 2.5$ Hz, 1H, H13).

^{13}C NMR (101 MHz, MeOD) δ 185.9 (C=O, C4), 182.5 (C=O, C1), 159.7 (NH-C=O, C10), 157.0 (C-OH, C2), 141.9 (C, C1b), 135.8 (CH, C6), 134.3 (CH, C7), 133.7 (C, C4a), 133.6 (C-Cl, C4b), 131.5 (C, C8a), 129.3 (2 x CH, C3b), 128.9 (2 x CH, C2b), 127.2 (CH, C5), 127.0 (CH, C8), 123.5 (C, C3), 81.7 (C, C12), 71.9 (CH, C13), 49.0 (CH, C9), 30.3 (CH₂, C11).

HRMS calculated for C₂₁H₁₆N₂O₄Cl + [M+H]⁺ = 395.0799; found 395.0798.

3-[(4'-bromophenyl)methyl-(N'-propargyl)-urea]-2-hydroxynaphthalene-1,4-dione, (**3.62**)



The compound was synthesized by following the above-mentioned general procedure (2.0 mmol of lawsone scale). Ball milling for 2 cycles x 60 min. The crude product was purified by crystallization in DCM/Et₂O to yield 770 mg (88%) of the target product as a yellow solid (mp 176–178 °C).

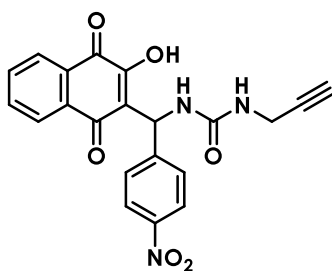
R_f (Hex/AcOEt 3:7) = 0.20.

^1H NMR (300 MHz, DMSO) δ 11.82 (bs, 1H), 8.03 – 7.99 (m, 1H), 7.98 – 7.91 (m, 1H), 7.82 (dtd, $J = 7.5, 1.6$ Hz, 2H), 7.50 – 7.43 (m, 2H), 7.29 – 7.20 (m, 2H), 6.94 – 6.83 (m, 2H), 6.41 (d, $J = 9.9$ Hz, 1H), 3.81 (dt, $J = 5.4, 2.7$ Hz, 2H), 3.06 (t, $J = 2.5$ Hz, 1H).

^{13}C NMR (101 MHz, MeOD) δ 185.9 (C=O), 182.5 (C=O), 159.7 (NH-C=O), 156.9 (C-OH), 142.4 (C), 135.8 (CH), 134.4 (CH), 133.7 (C), 132.3 (2 x CH), 131.5 (C), 129.3 (2 x CH), 127.3 (CH), 127.0 (CH), 123.4 (C), 121.5 (C-Br), 81.7 (C), 71.9 (CH), 49.1 (CH) 30.3 (CH₂).

HRMS calculated for C₂₁H₁₆N₂O₄Br + [M+H]⁺ = 439.0293; found 439.0288.

3-[[4'-nitrophenyl)methyl-(N'-propargyl)-urea]-2-hydroxynaphthalene-1,4-dione, **(3.63)**



The compound was synthesized by following the above-mentioned general procedure (1.4 mmol of lawsone scale). Ball milling for 2 cycles x 40 min. The crude product was purified by crystallization in DCM/Et₂O to yield 398 mg (70%) of the target product as a brownish solid (mp 170–172 °C).

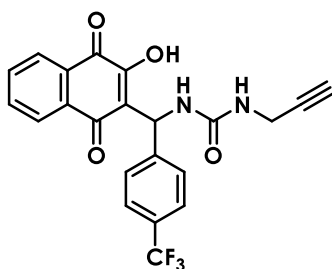
R_f (Hex/AcOEt 3:7) = 0.14.

¹H NMR (400 MHz, MeOD) δ 11.88 (bs, 1H), 8.22 – 8.12 (m, 2H), 8.09 – 8.05 (m, 1H), 8.05 – 7.99 (m, 1H), 7.81 – 7.71 (m, 2H), 7.65 – 7.60 (m, 2H), 6.68 (s, 1H), 3.93 (dd, J = 3.7, 2.5 Hz, 2H), 2.55 (t, J = 2.5 Hz, 1H).

¹³C NMR (101 MHz, MeOD) δ 185.8 (C=O), 182.4 (C=O), 159.6 (NH-C=O C), 157.2 (C-OH), 151.0 (C), 148.2 (C), 135.8 (CH), 134.5 (CH), 133.6 (C), 131.6 (C), 128.3 (2 x CH), 127.3 (CH), 127.1 (CH), 124.4 (2 x CH), 122.8 (C), 81.6 (C), 72.0 (CH), 49.2 (CH), 30.3 (CH₂).

HRMS calculated for C₂₁H₁₆N₃O₆⁺ [M+H]⁺ = 406.1039; found 406.1037.

3-[[4'-trifluoromethylphenyl)methyl-(N'-propargyl)-urea]-2-hydroxynaphthalene-1,4-dione, **(3.64)**



The compound was synthesized by following the above-mentioned general procedure (1.0 mmol of lawsone scale). Ball milling for 2 cycles x 40 min. The crude product was purified by crystallization in DCM to yield 351 mg (82%) of the target product as a yellow solid (mp 169–171 °C).

R_f (Hex/AcOEt 7:3) = 0.06.

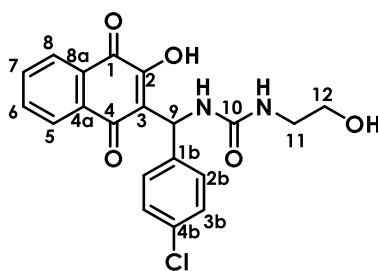
¹H NMR (400 MHz, DMSO) δ 8.03 – 8.00 (m, 1H), 7.95 – 7.92 (m, 1H), 7.82 (dtd, J = 18.3, 7.5, 1.6 Hz, 2H), 7.65 (d, J = 8.0 Hz, 2H), 7.51 (dd, J = 8.0, 0.9 Hz, 2H), 6.96 (d, J = 9.2 Hz, 1H), 6.92 (t, J = 5.6 Hz, 1H), 6.52 (d, J = 9.2 Hz, 1H), 3.85 – 3.80 (m, 2H), 3.07 (t, J = 2.5 Hz, 1H).

^{13}C NMR (101 MHz, DMSO) δ 184.0 (C=O), 181.3 (C=O), 156.9 (NH-C=O), 156.3 (C-OH), 147.4 (C), 134.7 (CH), 133.4 (CH), 131.8 (C), 130.2 (C), 127.1 (d, J = 39.4 Hz, C), 126.5 (2 x CH), 125.9 (CH), 125.7 (CH), 125.0 (q, J = 3.0 Hz, 2 x CH), 124.4 (q, J = 231.7 Hz, CF_3), 121.9 (C), 82.2 (C), 72.8 (CH), 46.8 (CH), 28.8 (CH_2).

^{19}F NMR (376 MHz, DMSO) δ -60.73.

HRMS calculated for $\text{C}_{22}\text{H}_{14}\text{N}_2\text{O}_4\text{F}_3^-$ [M-H] $^-$ = 427.0906; found 427.0902.

3-[[4'-chlorophenyl)methyl-(N-2-hydroxyethyl)-urea]-2-hydroxynaphthalene-1,4-dione, **(3.66)**



The compound was synthesized by following the above-mentioned general procedure (1.4 mmol of lawsone scale). Ball milling for 2 cycles x 50 min. The crude product was purified by crystallization in DCM/MeOH/Et₂O to yield 449 mg (80%) of the target product as a yellow-orange solid (mp 85-87 °C).

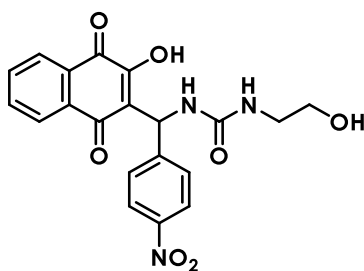
R_f (Hex/AcOEt 3:7) = 0.08.

^1H NMR (300 MHz, MeOD) δ 8.05 – 7.95 (m, 2H, H5 and H6), 7.72 (dtd, J = 7.5, 1.6 Hz, 2H, H7 and H8), 7.43 – 7.35 (m, 2H, H2b), 7.30 – 7.23 (m, 2H, H3b), 6.56 (s, 1H, H9), 3.58 (t, J = 5.6 Hz, 2H, H11), 3.26 (t, J = 5.6 Hz, 2H, H12).

^{13}C NMR (101 MHz, MeOD) δ 185.9 (C=O, C4), 182.5 (C=O, C1), 160.5 (NH-C=O, C10), 156.8 (C-OH, C2), 142.0 (C, C1b), 135.8 (CH, C6), 134.3 (CH, C7), 133.7 (C, C4a), 133.5 (C-Cl, C4b), 131.5 (C, C8a), 129.2 (2 x CH, C2b), 128.9 (2 x CH, C3b), 127.2 (CH, C5), 127.0 (CH, C8), 123.7 (C, C3), 62.6 (CH_2 , C12), 49.0 (CH, C9), 43.5 (CH_2 , C11).

HRMS calculated for $\text{C}_{20}\text{H}_{16}\text{N}_2\text{O}_5\text{Cl}^-$ [M-H] $^-$ = 399.0748; found 399.0750.

3-[(4'-nitrophenyl)methyl-(N-2-hydroxyethyl)-urea]-2-hydroxynaphthalene-1,4-dione, **(3.67)**



The compound was synthesized by following the above-mentioned general procedure (1.4 mmol of lawsone scale). Ball milling for 2 cycles x 50 min. The crude product was purified by crystallization in DCM/MeOH/Et₂O to yield 472 mg (82%) of the target product as a yellow solid (mp 184–186 °C).

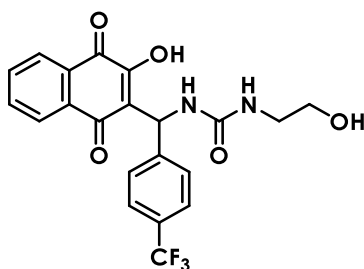
R_f (Hex/AcOEt 3:7) = 0.08.

¹H NMR (400 MHz, DMSO) δ 8.16 (d, *J* = 8.7 Hz, 2H), 8.02 (d, *J* = 7.0 Hz, 1H), 7.94 (d, *J* = 7.0 Hz, 1H), 7.89 – 7.77 (m, 2H), 7.56 (d, *J* = 8.7 Hz, 2H), 6.94 (d, *J* = 9.4 Hz, 1H), 6.69 (bs, 1H), 6.55 (d, *J* = 9.4 Hz, 1H), 3.42 – 3.33 (m, 2H), 3.09 (t, *J* = 5.1 Hz, 2H).

¹³C NMR (101 MHz, DMSO) δ 183.9 (C=O), 181.2 (C=O), 157.5 (NH-C=O), 156.2 (C-OH), 151.0 (C), 146.1 (C), 134.8 (CH), 133.4 (CH), 131.7 (C), 130.1 (C), 127.0 (2 x CH), 125.9 (C), 125.7 (C), 123.3 (2 x CH), 121.9 (C), 60.7 (CH₂), 46.7 (CH), 42.3 (CH₂).

HRMS calcd for C₂₀H₁₈N₃O₇ + [M+H]⁺ = 412.1145; found 412.1141.

3-[(4'-trifluoromethylphenyl)methyl-(N-2-hydroxyethyl)-urea]-2-hydroxynaphthalene-1,4-dione, **(3.68)**



The compound was synthesized by following the above-mentioned general procedure (2.0 mmol of lawsone scale). Ball milling for 2 cycles x 60 min. The crude product was purified by crystallization in DCM to yield 690 mg (80%) of the target product as a yellow solid (mp 167–169 °C).

R_f (AcOEt) = 0.05.

^1H NMR (300 MHz, DMSO) δ 11.82 (bs, 1H), 8.06 – 7.99 (m, 1H), 7.94 (dd, J = 7.5, 1.6 Hz, 1H), 7.83 (dtd, J = 7.4, 1.6 Hz, 2H), 7.65 (d, J = 8.4 Hz, 2H), 7.51 (d, J = 8.4 Hz, 2H), 6.91 (d, J = 9.0 Hz, 1H), 6.69 (t, J = 6.1 Hz, 1H), 6.52 (d, J = 9.0 Hz, 1H), 3.48 – 3.25 (m, 2H), 3.09 (m, 2H).

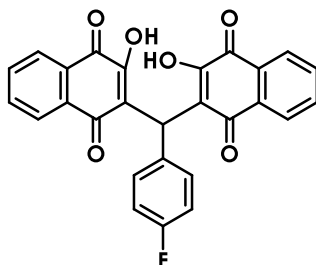
^{13}C NMR (75 MHz, DMSO) δ 184.0 (C=O), 181.3 (C=O), 157.5 (NH-C=O), 156.1 (C-OH), 147.8 (C), 134.7 (CH), 13.4 (CH), 131.8 (C), 130.2 (C), 127.0 (d, J = 31.5 Hz, C), 126.6 (2 x CH), 125.9 (CH), 125.7 (CH), 125.0 (q, J = 3.8 Hz, 2 x CH), 124.8 (q, J = 272.1 Hz, CF_3), 122.3 (C), 60.7 (CH_2), 46.7 (CH), 42.2 (CH_2).

HRMS calculated for $\text{C}_{21}\text{H}_{16}\text{N}_2\text{O}_5\text{F}_3^-$ $[\text{M}-\text{H}]^-$ = 433.1011; found 433.1020.

Synthesis of Michael adduct **3.70**

Compound **3.43** (1.3 mmol) was added in 3 mL ionic liquid $[\text{HNMP}]^+[\text{HSO}_4]^-$ media and was stirred at 80 °C for 60 min, until it turned into a brown solid. Then, iced water was added and the resulting suspension stayed under vigorous stirring for 10 min. The red solid was isolated by filtration and washed with excess of water. Afterwards, the crude product was purified by recrystallization in EtOH and washed with cold (0 °C) Et_2O to afford 238 mg of **3.70** as an orange solid (yield 40%, mp 202–204 °C).

3,3'-((4-fluorophenyl)methylene)bis(2-hydroxynaphthalene-1,4-dione), (**3.70**)



R_f (Hex/AcOEt 1:1) = 0.11.

^1H NMR (400 MHz, DMSO) δ 8.00 – 7.96 (m, 2H), 7.94 – 7.91 (m, 2H), 7.80 (dtd, J = 18.9, 7.4, 1.5 Hz, 4H), 7.29 – 7.22 (m, 2H), 7.04 – 6.95 (m, 2H), 5.98 (s, 1H).

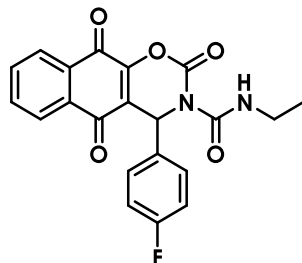
^{13}C NMR (101 MHz, DMSO) δ 183.5 (2 x C), 181.3 (2 x C), 160.5 (d, J = 243.8 Hz, C-F), 156.6 (2 x C), 137.0 (d, J = 3.1 Hz, C), 134.6 (2 x CH), 133.1 (2 x CH), 132.2 (2 x C), 129.9 (2 x C), 129.8 (d, J = 8.2 Hz, 2 x CH), 126.0 (2 x CH), 125.6 (2 x CH), 123.0 (2 x C), 114.2 (d, J = 21.4 Hz, 2 x CH), 36.94 (CH).

HRMS calculated for $\text{C}_{27}\text{H}_{15}\text{O}_6\text{F}^-$ $[\text{M}-\text{H}]^-$ = 453.0774; found 453.0781.

Cyclization: Synthesis of lawsone carbamate **3.71**

Et₃N (1.75 mmol, 2.2 equiv) was added dropwise in a suspension of linear Biginelli compound **3.46** (0.80 mmol, 1 equiv) in 10 mL anhydrous DCM under inert argon atmosphere. To the providing red solution, a solution of *para*-nitrophenyl chloroformate (0.9 mmol, 1.1 equiv) in 5 mL anhydrous DCM was added dropwise. Bubbling was observed during the addition at this step. The reaction stayed under stirring at rt, overnight under inert argon atmosphere. The end of the reaction was controlled by TLC. The solvent was then removed under pressure and the residue was dissolved in AcOEt. The organic phase was then washed successively with 5% aqueous solution of citric acid, water and brine. The organic phase was collected, dehydrated by Na₂SO₄, filtered and condensated until dry. The crude product was first purified by PuriFlash column chromatography by using Hex/AcOEt (8:2) followed by Hex/AcOEt (7:3) as isocratic systems of eluents. The product was obtained pure after a second semi-prep HPLC purification (the byproduct *p*-nitrophenol has the same R_f and was 90% pure after the first attempt) by using a C18 column and a gradient system of 0.1% HCOOH.H₂O/ 0.1% HCOOH.CH₃CN as eluent at 20% yield as yellow oil.

N-Ethyl-4-(*p*-fluorophenyl)-2,9,10-trioxo-3,4-dihydro-10*H*,9*H*,2*H*-1-oxa-3-azaanthracene-3-carboxamide, (**3.71**)



R_f (Hex/AcOEt 8:2) = 0.20.

¹H NMR (400 MHz, CDCl₃) δ 8.41 (t, *J* = 5.6 Hz, 1H), 8.20 – 8.13 (m, 1H), 8.08 – 8.01 (m, 1H), 7.81 – 7.73 (m, 2H), 7.49 – 7.40 (m, 2H), 7.08 – 6.98 (m, 2H), 6.84 (s, 1H), 3.42 – 3.22 (m, 2H), 1.17 (t, *J* = 7.3 Hz, 3H).

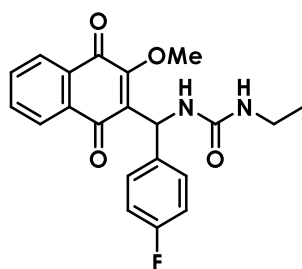
¹³C NMR (101 MHz, CDCl₃) δ 180.9 (C=O), 176.3 (C=O), 163.0 (d, *J* = 248.0 Hz, C-F), 151.3 (NH-C=O), 148.5 (N-(C=O)-O), 147.5 (C-O), 135.0 (CH), 134.6 (CH), 134.0 (C), 131.3 (C), 130.7 (C), 129.5 (d, *J* = 8.0 Hz, 2 x CH), 127.1 (CH), 127.0 (CH), 123.3 (C), 116.3 (d, *J* = 21.0 Hz, 2 x CH), 52.6 (CH), 36.3 (CH₂), 14.7 (CH₃).

HRMS calculated for C₂₁H₁₅N₂O₅F⁻ [M - H]⁻ = 394.0965; found 399.0969.

General synthetic protocol for selective methylation of Biginelli-type linear lawsone derivatives

A solution of the corresponding Biginelli-linear derivative (1.0 equiv, 0.5 mmol) in anhydrous acetone (5 mL) at 30 °C was charged with potassium carbonate (6.3 equiv, 3.2 mmol) and the color changed immediately from yellow to deep red. After 5 min. of stirring, the reaction mixture was charged with dimethyl sulfate (2.0 equiv, 1.0 mmol) and the system was set on reflux. Afterwards, the reaction mixture was allowed to cool to room temperature and the potassium carbonate excess was filtered out. The providing white solid was thoroughly washed with 50 mL of acetone. The filtrate was collected and the solvent was evaporated under reduced pressure. The obtained crude products were then purified by PuriFlash column chromatography by using Hex/AcOEt as gradient and/or isocratic systems of eluents, while silica gel columns were used as static phase. The desired methylated products were obtained pure with good yields.

3-[(4'-fluorophenyl)methyl-(N'-ethyl)-urea]-2-methoxynaphthalene-1,4-dione, (**3.72**)



The compound was synthesized by following the above-mentioned general procedure (0.22 mmol of starting compound scale). Reaction time 60 min. The crude product was purified by crystallization in 3 mL DCM to yield 50 mg (60%) of the target product as a yellow solid (mp 186–188 °C decomposition).

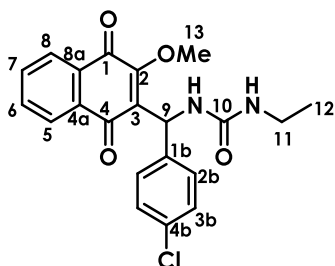
R_f (Hex/AcOEt 7:3) = 0.10.

$^1\text{H NMR}$ (300 MHz, CDCl_3) δ 8.08 – 8.01 (m, 1H), 8.01 – 7.94 (m, 1H), 7.71 (dd, $J = 5.8, 3.3$ Hz, 2H), 7.39 – 7.33 (m, 2H), 6.97 (s, 2H), 6.61 (s, 1H), 6.19 (s, 1H), 4.23 (s, 3H), 3.24 (q, $J = 7.2$ Hz, 2H), 1.14 (t, $J = 7.2$ Hz, 3H).

$^{13}\text{C NMR}$ (101 MHz, CDCl_3) δ 186.1 (C=O), 181.6 (C=O), 163.6 (d, $J = 2.7$ Hz, C), 161.9 (d, $J = 246.0$ Hz, C-F), 157.3 (C-OMe), 157.1 (NH-C=O), 134.2 (CH), 133.8 (CH), 131.9 (C), 131.8 (C), 131.4 (C), 127.9 (d, $J = 8.2$ Hz, 2 x CH), 126.4 (CH), 126.3 (CH), 115.4 (d, $J = 21.2$ Hz, 2 x CH), 62.0 (OCH₃), 48.5 (CH), 35.6 (CH₂), 15.4 (CH₃).

HRMS calculated for $\text{C}_{21}\text{H}_{20}\text{N}_2\text{O}_4\text{F}^+$ $[\text{M}+\text{H}]^+ = 383.1407$; found 383.1411.

3-[(4'-chlorophenyl)methyl-(N'-ethyl)-urea]-2-methoxynaphthalene-1,4-dione, **(3.73)**



The compound was synthesized by following the above-mentioned general procedure (0.31 mmol of starting compound scale). Reaction time 60 min. The crude product was purified by PuriFlash FCC with Hex/AcOEt (7:3) and then with Hex/AcOEt (6:4) to yield 90 mg (73%) of the target product as a yellow solid (mp 213–125 °C decomposition).

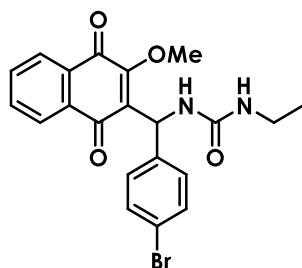
R_f (Hex/AcOEt 6:4) = 0.17.

¹H NMR (400 MHz, CDCl₃) δ 8.02 (dd, *J* = 5.8, 3.3 Hz, 1H, H5), 7.95 (dd, *J* = 5.8, 3.3 Hz, 1H, H6), 7.72 – 7.65 (m, 2H, H7 and H8), 7.31 (d, *J* = 8.6 Hz, 2H, H2b), 7.23 (d, *J* = 8.6 Hz, 2H, H3b), 6.62 (d, *J* = 10.1 Hz, 1H, H9), 6.24 (d, *J* = 10.1 Hz, 1H, NH), 4.70 (t, *J* = 5.5 Hz, 1H, NHEt), 4.22 (s, 3H, H13), 3.23 (q, *J* = 7.2 Hz, 2H, H11), 1.12 (t, *J* = 7.2 Hz, 3H, H12).

¹³C NMR (101 MHz, CDCl₃) δ 186.0 (C=O, C4), 181.7 (C=O, C1), 157.5 (C-OMe, C2), 157.4 (NH-C=O, C10), 139.7 (C, C1b), 134.3 (CH, C6), 133.8 (CH, C7), 132.9 (C, C4a), 132.2 (C-Cl, C4b), 131.8 (C, C8a), 131.5 (C, C3), 128.7 (2 x CH, C3b), 127.7 (2 x CH, C2b), 126.5 (CH, C5), 126.3 (CH, C8), 62.1 (OCH₃, C13), 48.5 (CH, C9), 35.6 (CH₂, C11), 15.4 (CH₃, C12).

HRMS calculated for C₂₁H₂₀N₂O₄Cl⁺ [M+H]⁺ = 399.1112; found 399.1112.

3-[(4'-bromophenyl)methyl-(N'-ethyl)-urea]-2-methoxynaphthalene-1,4-dione, **(3.74)**



The compound was synthesized by following the above-mentioned general procedure (0.23 mmol of starting compound scale). Reaction time 15 min. The crude product was purified by PuriFlash FCC with gradient eluent Hex/AcOEt (6:4) to Hex/AcOEt (3:7) to yield 66 mg (65%) of the target product as a yellow solid (mp 220–222 °C decomposition).

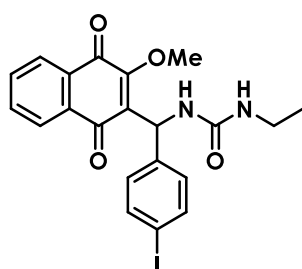
R_f (Hex/AcOEt 3:7) = 0.26.

^1H NMR (400 MHz, CDCl_3) δ 8.06 – 8.00 (m, 1H), 7.98 – 7.93 (m, 1H), 7.73 – 7.66 (m, 2H), 7.43 – 7.36 (m, 2H), 7.29 – 7.22 (m, 2H), 6.60 (d, $J = 10.1$ Hz, 1H), 6.19 (d, $J = 10.1$ Hz, 1H), 4.58 (t, $J = 5.5$ Hz, 1H), 4.23 (s, 3H), 3.23 (q, $J = 7.2$ Hz, 2H), 1.13 (t, $J = 7.2$ Hz, 3H).

^{13}C NMR (101 MHz, CDCl_3) δ 186.0 (C=O), 181.7 (C=O), 157.5 (C-OMe), 157.3 (NH-C=O), 140.2 (C), 134.3 (CH), 133.9 (CH), 132.1 (C-Br), 131.9 (C), 131.7 (2 x CH), 131.5 (C), 128.1 (2 x CH), 126.5 (CH), 126.4 (CH), 121.1 (C), 62.1 (OCH₃), 48.6 (CH), 35.6 (CH₂), 15.5 (CH₃).

HRMS calculated for $\text{C}_{21}\text{H}_{20}\text{N}_2\text{O}_4\text{Br}^+$ $[\text{M}+\text{H}]^+ = 443.0606$; found 443.0597.

3-[[4'-iodophenyl)methyl-(N'-ethyl)-urea]-2-methoxynaphthalene-1,4-dione, (**3.75**)



The compound was synthesized by following the above-mentioned general procedure (0.31 mmol of starting compound scale). Reaction time 15 min. The crude product was purified by PuriFlash FCC with gradient eluent Hex/AcOEt (7:3) to Hex/AcOEt (3:7) to yield 108 mg (70%) of the target product as a yellow solid (mp 217–219 °C decomposition).

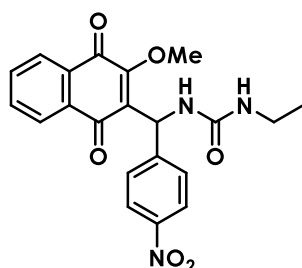
R_f (Hex/AcOEt 6:4) = 0.17.

^1H NMR (300 MHz, CDCl_3) δ 8.08 – 8.02 (m, 1H), 8.02 – 7.93 (m, 1H), 7.73 – 7.65 (m, 2H), 7.63 – 7.57 (m, 2H), 7.13 (d, $J = 7.8$ Hz, 2H), 6.59 (d, $J = 9.7$ Hz, 1H), 6.14 (d, $J = 9.7$ Hz, 1H), 4.23 (s, 3H), 3.23 (q, $J = 7.2$ Hz, 2H), 1.13 (t, $J = 7.2$ Hz, 3H).

^{13}C NMR (101 MHz, CDCl_3) δ 186.0 (C=O), 181.7 (C=O), 157.5 (C-OMe), 157.3 (NH-C=O), 140.9 (C), 137.6 (2 x CH), 134.3 (CH), 133.9 (CH), 132.0 (C), 131.8 (C), 131.5 (C), 128.3 (2 x CH), 126.5 (CH), 126.4 (CH), 92.7 (C-I), 62.2 (OCH₃), 48.7 (CH), 35.6 (CH₂), 15.5 (CH₃).

HRMS calculated for $\text{C}_{21}\text{H}_{20}\text{N}_2\text{O}_4\text{I}^+$ $[\text{M}+\text{H}]^+ = 491.0468$; found 491.0460.

3-[[4'-nitrophenyl)methyl-(N'-ethyl)-urea]-2-methoxynaphthalene-1,4-dione, **(3.76)**



The compound was synthesized by following the above-mentioned general procedure (0.30 mmol of starting compound scale). Reaction time 90 min. The crude product was purified by PuriFlash FCC with Hex/AcOEt (6:4) and Hex/AcOEt (3:7) to yield 52 mg (42%) of the target product as a yellow-orange solid (mp 212–214 °C decomposition).

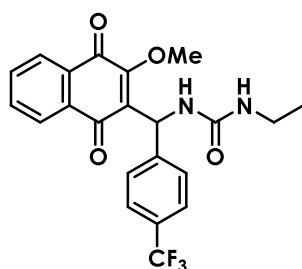
R_f (Hex/AcOEt 1:1) = 0.16.

¹H NMR (300 MHz, CDCl₃) δ 8.18 – 8.11 (m, 2H), 8.08 – 8.01 (m, 1H), 7.99 – 7.93 (m, 1H), 7.76 – 7.68 (m, 2H), 7.58 – 7.53 (m, 2H), 6.76 (d, *J* = 10.0 Hz, 1H), 6.19 (d, *J* = 10.0 Hz, 1H), 4.54 (t, *J* = 5.6 Hz, 1H), 4.29 (s, 3H), 3.26 (q, *J* = 7.2 Hz, 2H), 1.15 (t, *J* = 7.2 Hz, 3H).

¹³C NMR (75 MHz, CDCl₃) δ 185.9 (C=O), 181.5 (C=O), 157.7 (C-OMe), 157.1 (NH-C=O), 148.8 (C), 147.1 (C-NO₂), 134.5 (CH), 134.1 (CH), 131.7 (C), 131.5 (C), 131.0 (C), 127.1 (2 x CH), 126.7 (CH), 126.4 (CH), 123.9 (2 x CH), 62.4 (OCH₃), 48.7 (CH), 35.7 (CH₂), 15.5 (CH₃).

HRMS calculated for C₂₁H₂₀N₃O₆ [M+H]⁺ = 410.1352; found 410.1345.

3-[[4'-trifluoromethylphenyl)methyl-(N'-ethyl)-urea]-2-methoxynaphthalene-1,4-dione, **(3.77)**



The compound was synthesized by following the above-mentioned general procedure (0.15 mmol of starting compound scale). Reaction time 5 min. The crude product was purified by PuriFlash FCC with Hex/AcOEt (6:4) and Hex/AcOEt (1:1) to yield 54 mg (90%) of the target product as an orange solid (mp 206–208 °C decomposition).

R_f (Hex/AcOEt 1:1) = 0.28.

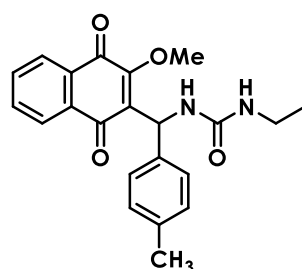
^1H NMR (400 MHz, CDCl_3) δ 8.06 – 8.00 (m, 1H), 7.97 – 7.91 (m, 1H), 7.72 – 7.64 (m, 2H), 7.55 – 7.46 (m, 4H), 6.72 (d, J = 10.0 Hz, 1H), 6.30 (d, J = 10.0 Hz, 1H), 4.75 (t, J = 5.5 Hz, 1H), 4.24 (s, 3H), 3.30 – 3.18 (m, 2H), 1.13 (t, J = 7.2 Hz, 3H).

^{13}C NMR (101 MHz, CDCl_3) δ 185.9 (C=O), 181.6 (C=O), 157.6 (C-OMe), 157.4 (NH-C=O), 145.2 (C), 134.4 (CH), 133.9 (CH), 131.8 (C), 131.5 (C), 129.4 (d, J = 32.6 Hz, C), 128.5 (q, J = 163.2 Hz, CF_3), 126.6 (2 x CH), 126.5 (CH), 126.3 (CH), 125.6 (q, J = 3.9 Hz, 2 x CH), 122.9 (C), 62.2 (OCH₃), 48.7 (CH), 35.6 (CH₂), 15.5 (CH₃).

^{19}F NMR (376 MHz, CDCl_3) δ -62.5.

HRMS calculated for $\text{C}_{22}\text{H}_{20}\text{N}_2\text{O}_4\text{F}_3$ $[\text{M}+\text{H}]^+$ = 433.1375; found 433.1379.

3-[(4'-methylphenyl)methyl-(N'-ethyl)-urea]-2-methoxynaphthalene-1,4-dione, (**3.78**)



The compound was synthesized by following the above-mentioned general procedure (0.41 mmol of starting compound scale). Reaction time 60 min. The crude product was purified by PuriFlash FCC with Hex/AcOEt (6:4) and Hex/AcOEt (1:1) to yield 109 mg (70%) of the target product as a yellow solid (mp 217–219 °C decomposition).

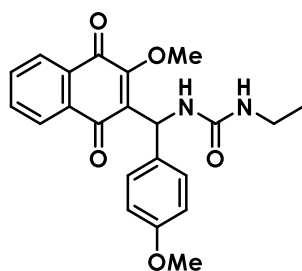
R_f (Hex/AcOEt 6:4) = 0.23.

^1H NMR (400 MHz, CDCl_3) δ 8.04 – 7.99 (m, 1H), 7.99 – 7.94 (m, 1H), 7.69 – 7.65 (m, 2H), 7.31 – 7.25 (m, 2H), 7.08 (d, J = 7.8 Hz, 2H), 6.60 (d, J = 10.2 Hz, 1H), 6.21 (d, J = 10.2 Hz, 1H), 4.64 (t, J = 5.6 Hz, 1H), 4.20 (s, 3H), 3.22 (q, J = 7.3, 2H), 2.28 (s, 3H), 1.12 (t, J = 7.3 Hz, 3H).

^{13}C NMR (101 MHz, CDCl_3) δ 186.1 (C=O), 181.8 (C=O), 157.5 (C-OMe), 157.4 (NH-C=O), 137.9 (C), 136.8 (C), 134.2 (CH), 133.7 (CH), 133.0 (C), 132.0 (C), 131.5 (C), 129.3 (2 x CH), 126.4 (CH), 126.3 (CH), 126.2 (2 x CH), 62.0 (OCH₃), 48.9 (CH), 35.6 (CH₂), 21.1 (CH₃), 15.5 (CH₃).

HRMS calculated for $\text{C}_{22}\text{H}_{23}\text{N}_2\text{O}_4$ $[\text{M}+\text{H}]^+$ = 379.1658; found 379.1653.

3-[(4'-methoxyphenyl)methyl-(N'-ethyl)-urea]-2-methoxynaphthalene-1,4-dione, **(3.79)**



The compound was synthesized by following the above-mentioned general procedure (0.26 mmol of starting compound scale). Reaction time 60 min. The crude product was recrystallized in 5 mL DCM to yield 66 mg (63%) of the pure target product as a yellow solid (mp 213–215 °C decomposition), after filtration.

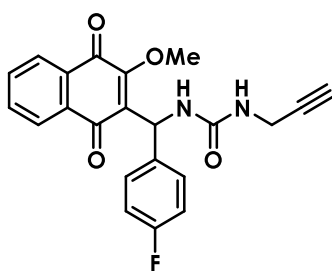
R_f (Hex/AcOEt 1:1) = 0.20.

¹H NMR (400 MHz, MeOD) δ 8.06 – 7.96 (m, 2H), 7.79 – 7.73 (m, 2H), 7.32 – 7.22 (m, 2H), 6.91 – 6.79 (m, 2H), 6.52 (s, 1H), 4.14 (s, 3H), 3.75 (s, 3H), 3.16 (q, J = 7.2 Hz, 2H), 1.09 (t, J = 7.2 Hz, 3H).

¹³C NMR (101 MHz, MeOD) δ 186.4 (C=O), 182.9 (C=O), 160.2 (C-OMe), 159.1 (NH-C=O), 135.3 (CH), 134.8 (CH), 134.4 (C), 134.3 (C), 133.1 (C), 132.9 (C), 128.4 (2 x CH), 127.1 (CH), 127.0 (CH), 123.7 (C), 114.8 (2 x CH), 62.1 (OCH₃), 55.7 (OCH₃), 49.1 (CH), 35.8 (CH₂), 15.7 (CH₃).

HRMS calculated for C₂₂H₂₃N₂O₅ [M+H]⁺ = 395.1607; found 395.1608.

3-[(4'-fluoromethylphenyl)methyl-(N'-propargyl)-urea]-2-methoxynaphthalene-1,4-dione, **(3.80)**



The compound was synthesized by following the above-mentioned general procedure (0.32 mmol of starting compound scale). Reaction time 90 min. The crude product was purified by PuriFlash FCC with Hex/AcOEt (7:3) and Hex/AcOEt (6:4) to yield 88 mg (70%) of the pure target product as a yellow solid (mp 196–198 °C decomposition).

R_f (Hex/AcOEt 6:4) = 0.30.

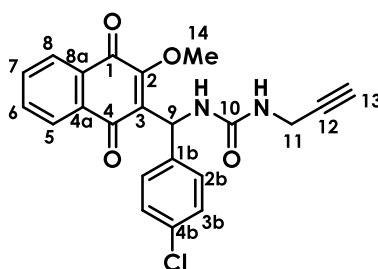
^1H NMR (400 MHz, CDCl_3) δ 8.06 – 8.00 (m, 1H), 8.00 – 7.95 (m, 1H), 7.70 (dd, $J = 5.7, 3.3$ Hz, 2H), 7.39 – 7.30 (m, 2H), 7.01 – 6.92 (m, 2H), 6.62 (d, $J = 10.1$ Hz, 1H), 6.36 (d, $J = 10.1$ Hz, 1H), 4.80 (t, $J = 5.5$ Hz, 1H), 4.23 (s, 3H), 4.01 (ddd, $J = 5.5, 2.6, 0.8$ Hz, 2H), 2.21 (t, $J = 2.5$ Hz, 1H).

^{13}C NMR (101 MHz, CDCl_3) δ 186.0 (C=O), 181.7 (C=O), 162.1 (d, $J = 252.5$ Hz, C-F), 157.4 (C-OMe), 156.7 (NH-C=O), 136.5 (d, $J = 3.0$ Hz, C), 134.4 (CH), 133.9 (CH), 132.0 (C), 131.9 (C), 131.5 (C), 128.1 (CH), 128.0 (CH), 126.5 (d, $J = 14.1$ Hz, 2 x CH), 115.5 (d, $J = 21.2$ Hz, 2 x CH), 80.5 (C), 71.6 (CH), 62.1 (OCH₃), 48.7 (CH), 30.4 (CH₂).

^{19}F NMR (376 MHz, CDCl_3) δ -115.6 (m, F).

HRMS calculated for $\text{C}_{22}\text{H}_{18}\text{N}_2\text{O}_4\text{F}$ $[\text{M}+\text{H}]^+ = 393.1251$; found 393.1248.

3-[[4'-chloromethylphenyl)methyl-(*N*'-propargyl)-urea]-2-methoxynaphthalene-1,4-dione, (3.81)



The compound was synthesized by following the above-mentioned general procedure (0.30 mmol of starting compound scale). Reaction time 90 min. The crude product was purified by PuriFlash FCC with Hex/AcOEt (7:3) and Hex/AcOEt (6:4) to yield 82 mg (67%) of the pure target product as a yellow solid (mp 210–212 °C decomposition).

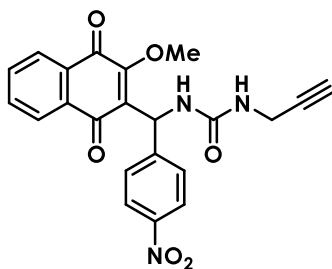
R_f (Hex/AcOEt 7:3) = 0.17.

^1H NMR (400 MHz, CDCl_3) δ 8.06 – 8.00 (m, 1H, H5), 7.98 – 7.93 (m, 1H, H6), 7.72 – 7.66 (m, 2H, H7 and H8), 7.34 – 7.29 (m, 2H, H2b), 7.25 – 7.22 (m, 2H, H3b), 6.62 (d, $J = 10.0$ Hz, 1H, H9), 6.38 (d, $J = 10.0$ Hz, 1H, NH), 4.88 (t, $J = 5.5$ Hz, 1H, NHR), 4.23 (s, 3H, H14), 4.01 (ddd, $J = 5.5, 2.6, 0.8$ Hz, 2H, H11), 2.21 (t, $J = 2.5$ Hz, 1H, H13).

^{13}C NMR (101 MHz, CDCl_3) δ 185.9 (C=O, C4), 181.7 (C=O, C1), 157.5 (C-OMe, C2), 156.7 (NH-C=O, C10), 139.4 (C, C1b), 134.4 (CH, C6), 133.9 (CH, C7), 133.1 (C, C4a), 131.8 (C-Cl, C4b), 131.7 (C, C8a), 131.5 (C, C3), 128.8 (2 x CH, C3b), 127.7 (2 x CH, C2b), 126.6 (CH, C5), 126.4 (CH, C8), 80.5 (C, C12), 71.6 (CH, C13), 62.2 (OCH₃, C14), 48.7 (CH, C9), 30.4 (CH₂, C11).

HRMS calculated for $\text{C}_{22}\text{H}_{18}\text{N}_2\text{O}_4\text{Cl}$ $[\text{M}+\text{H}]^+ = 409.0955$; found 409.0958.

3-[(4'-nitromethylphenyl)methyl-(N'-propargyl)-urea]-2-methoxynaphthalene-1,4-dione, **(3.82)**



The compound was synthesized by following the above-mentioned general procedure (0.37 mmol of starting compound scale). Reaction time 120 min. The crude product was purified by PuriFlash FCC with Hex/AcOEt (7:3) and Hex/AcOEt (1:1), both isocratic, to yield 78 mg (50%) of the pure target product as a yellow solid (mp 206–208 °C decomposition).

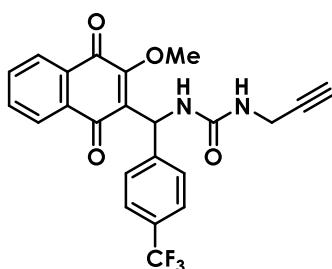
R_f (Hex/AcOEt 6:4) = 0.25.

¹H NMR (400 MHz, CDCl₃) δ 8.16 – 8.11 (m, 2H), 8.08 – 8.01 (m, 1H), 7.98 – 7.93 (m, 1H), 7.75 – 7.69 (m, 2H), 7.59 – 7.52 (m, 2H), 6.76 (d, *J* = 9.9 Hz, 1H), 6.41 (d, *J* = 9.9 Hz, 1H), 4.91 (t, *J* = 5.6 Hz, 1H), 4.29 (s, 3H), 4.03 (ddd, *J* = 5.6, 2.5, 1.1 Hz, 2H), 2.23 (t, *J* = 2.5 Hz, 1H).

¹³C NMR (101 MHz, CDCl₃) δ 185.8 (C=O), 181.5 (C=O), 157.6 (C-OMe), 156.6 (NH-C=O), 148.5 (C), 147.2 (C-NO₂), 134.6 (CH), 134.1 (CH), 131.6 (C), 131.5 (C), 130.6 (C), 127.2 (2 x CH), 126.7 (CH), 126.4 (CH), 123.9 (2 x CH), 80.3 (C), 71.8 (CH), 62.4 (OCH₃), 48.8 (CH), 30.5 (CH₂).

HRMS calculated for C₂₂H₁₈N₃O₆ [M+H]⁺ = 420.1196; found 420.1193.

3-[(4'-trifluoromethylphenyl)methyl-(N'-propargyl)-urea]-2-methoxynaphthalene-1,4-dione, **(3.83)**



The compound was synthesized by following the above-mentioned general procedure (0.23 mmol of starting compound scale). Reaction time 90 min. The crude product was purified by PuriFlash FCC with Hex/AcOEt (7:3) and Hex/AcOEt (6:4), both isocratic, to yield 41 mg (40%) of the pure target product as a yellow solid (mp 218–220 °C decomposition).

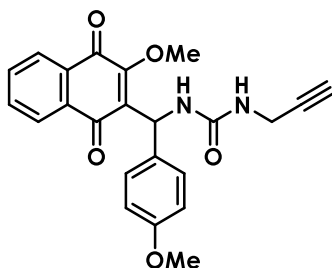
R_f (Hex/AcOEt 7:3) = 0.15.

^1H NMR (400 MHz, CDCl_3) δ 8.07 – 8.02 (m, 1H), 8.00 – 7.95 (m, 1H), 7.74 – 7.68 (m, 2H), 7.58 – 7.47 (m, 4H), 6.71 (d, $J = 10.0$ Hz, 1H), 6.35 (d, $J = 10.0$ Hz, 1H), 4.75 (t, $J = 5.6$ Hz, 1H), 4.27 (s, 3H), 4.02 (ddd, $J = 5.6, 2.6, 0.8$ Hz, 2H), 2.23 (t, $J = 2.6$ Hz, 1H).

^{13}C NMR (101 MHz, DMSO) δ 184.4 (C=O), 181.0 (C=O), 158.1 (NH-C=O), 156.8 (C-OMe), 146.7 (C), 134.3 (CH), 134.0 (CH), 131.5 (C), 130.7 (C), 127.3 (d, $J = 32.3$ Hz, C), 126.5 (2 x CH), 126.0 (CH), 125.6 (CH), 127.4 (q, $J = 255.5$ Hz, CF_3), 125.1 (q, $J = 3.9$ Hz, 2 x CH), 122.9 (C), 82.1 (C), 72.9 (CH), 61.5 (OCH_3), 46.9 (CH), 28.8 (CH_2).

HRMS calculated for $\text{C}_{23}\text{H}_{18}\text{N}_2\text{O}_4\text{F}_3$ $[\text{M}+\text{H}]^+ = 443.1219$; found 443.1215.

3-[[4'-methoxymethylphenyl)methyl-(N'-propargyl)-urea]-2-methoxynaphthalene-1,4-dione,
(3.84)



The compound was synthesized by following the above-mentioned general procedure (0.51 mmol of starting compound scale). Reaction time 45 min. The crude product was purified by PuriFlash FCC with Hex/AcOEt (7:3) and Hex/AcOEt (6:4), both isocratic, to yield 80 mg (40%) of the pure target product as a yellow solid (mp 209–211 °C decomposition).

R_f (Hex/AcOEt 6:4) = 0.31.

^1H NMR (400 MHz, CDCl_3) δ 8.05 – 8.00 (m, 1H), 8.00 – 7.96 (m, 1H), 7.72 – 7.66 (m, 2H), 7.33 – 7.28 (m, 2H), 6.86 – 6.79 (m, 2H), 6.57 (d, $J = 10.2$ Hz, 1H), 6.29 (d, $J = 10.2$ Hz, 1H), 4.69 (t, $J = 5.6$ Hz, 1H), 4.22 (s, 3H), 4.01 (ddd, $J = 5.6, 2.6, 1.1$ Hz, 2H), 3.75 (s, 3H), 2.21 (t, $J = 2.6$ Hz, 1H).

^{13}C NMR (101 MHz, CDCl_3) δ 186.1 (C=O), 181.8 (C=O), 158.9 (NH-C=O), 157.3 (C), 156.7 (C-OMe), 134.3 (CH), 133.8 (CH), 132.7 (C), 132.5 (C), 132.0 (C), 131.5 (C), 127.6 (2 x CH), 126.4 (CH), 126.4 (CH), 114.1 (2 x CH), 81.7 (CH), 71.5 (CH), 62.1 (OCH_3), 55.4 (OCH_3), 48.9 (CH), 30.4 (CH_2).

HRMS calculated for $\text{C}_{23}\text{H}_{20}\text{N}_2\text{O}_5\text{Na}$ $[\text{M}+\text{Na}]^+ = 427.1270$; found 427.1269.

3.7.3 Docking experiments

The AlphaFold2 predicted structure of the protein bc1 of *Plasmodium falciparum* was downloaded from the European Bioinformatics Institute website and preprocessed with PrepWizard and treated and minimized as already described in Chapter 2 (Experimental Part) FORCEFIELD OPLS_2005.

The X-ray crystal protein structure for *Plasmodium* DHODH was downloaded from PDB (7L01), preprocessed and minimized as already described in Chapter 2 (Experimental Part) FORCEFIELD OPLS_2005.

The binding sites for both receptors were generated as described in Chapter 2 (Experimental Part).

All molecules were docked into the binding site of both targets DHODH, in several runs using both the crystallographic waters as well as without them. The docking scores reported in this chapter's tables are without waters.

Ligand preparation (LigPrep)

All compounds were imported as drawn and energy minimized with Maestro [Schrödinger LLC, 2021].

FORCEFIELD OPLS_2005

GENERATE POSSIBLE STATES pH 7 ± 2 True

EPIK PENALTIES False

INCLUDE ORIGINAL STATE True

DESALT True

GENERATE TAUTOMERS True

GENERATE STEREOISOMERS True (15 per ligand max.)

Docking (GlideDock)

FORCEFIELD OPLS_2005

SCALING FACTOR 0.80

PARTIAL CHARGE CUTOFF 0.15

PRECISION XP True

LIGAND SAMPLING FLEXIBLE True
INPUT RING CONFORMATION True
EPIK PENALTIES True
EXPANDED SAMPLING True
DISTANCE DEPENDENT DIELECTRIC CONSTANT 4.0
MAX NUMBER OF MINIMIZATION STEPS 100
H BOND HALOGEN ACCEPTOR True
H BOND AROMATIC DONOR True
RMS 0.5
MAX ATOMIC DISPLACEMENT 1.3 Å

3.8 References

1. R. Kaur, S. Chaudhary, K. Kumar, M. K. Gupta, and R. K. Rawal, Recent synthetic and medicinal perspectives of dihydropyrimidinones: A review, *Eur. J. Med. Chem.*, **2017**, vol. 132, pp. 108–134, doi: [10.1016/j.ejmech.2017.03.025](https://doi.org/10.1016/j.ejmech.2017.03.025).
2. N. October, N. D. Watermeyer, V. Yardley, T. J. Egan, K. Ncokazi, and K. Chibale, Reversed chloroquines based on the 3,4-dihydropyrimidin-2(1H)-one scaffold: synthesis and evaluation for antimalarial, β -haematin inhibition, and cytotoxic activity, *ChemMedChem*, **2008**, vol. 3, no. 11, pp. 1649–1653, doi: [10.1002/cmdc.200800172](https://doi.org/10.1002/cmdc.200800172).
3. A. N. Chiang *et al.*, Select pyrimidinones inhibit the propagation of the malarial parasite, *Plasmodium falciparum*, *Bioorg. Med. Chem.*, **2009**, vol. 17, no. 4, pp. 1527–1533, doi: [10.1016/j.bmc.2009.01.024](https://doi.org/10.1016/j.bmc.2009.01.024).
4. R. A. Adigun, F. P. Malan, M. O. Balogun, and N. October, Rational optimization of dihydropyrimidinone-quinoline hybrids as *Plasmodium falciparum* glutathione reductase inhibitors, *ChemMedChem*, **2022**, vol. 17, no. 10, doi: [10.1002/cmdc.202200034](https://doi.org/10.1002/cmdc.202200034).
5. R. A. Adigun, F. P. Malan, M. O. Balogun, and N. October, Design, synthesis, and in silico-in vitro antimalarial evaluation of 1,2,3-triazole-linked dihydropyrimidinone quinoline hybrids, *Struct. Chem.*, **2023**, doi: [10.1007/s11224-023-02142-y](https://doi.org/10.1007/s11224-023-02142-y).
6. K. R. Rogerio *et al.*, Synthesis and molecular modelling studies of pyrimidinones and pyrrolo[3,4-d]-pyrimidinodiones as new antiplasmodial compounds, *Mem. Inst. Oswaldo Cruz*, **2018**, vol. 113, no. 8, doi: [10.1590/0074-02760170452](https://doi.org/10.1590/0074-02760170452).
7. N. Singh *et al.*, An orally effective dihydropyrimidinone (DHPM) analogue induces apoptosis-like cell death in clinical isolates of *Leishmania donovani* overexpressing pteridine reductase 1, *Parasitol. Res.*, **2009**, vol. 105, no. 5, pp. 1317–1325, doi: [10.1007/s00436-009-1557-z](https://doi.org/10.1007/s00436-009-1557-z).
8. B. Mohammadi-Ghalehbin *et al.*, Synthesis, antileishmanial activity and molecular docking study of new 3,4-dihydropyrimidinones/thiones, *Pharm. Chem. J.*, **2022**, vol. 55, no. 10, pp. 1050–1056, doi: [10.1007/s11094-021-02536-4](https://doi.org/10.1007/s11094-021-02536-4).

9. A. R. Trivedi, V. R. Bhuvra, B. H. Dholariya, D. K. Dodiya, V. B. Kataria, and V. H. Shah, Novel dihydropyrimidines as a potential new class of antitubercular agents, *Bioorg. Med. Chem. Lett.*, **2010**, vol. 20, no. 20, pp. 6100–6102, doi: [10.1016/j.bmcl.2010.08.046](https://doi.org/10.1016/j.bmcl.2010.08.046).
10. K. M. Bairagi *et al.*, Chemistry, anti-diabetic activity and structural analysis of substituted dihydropyrimidine analogues, *J. Mol. Struct.*, **2021**, vol. 1227, p. 129412, doi: [10.1016/j.molstruc.2020.129412](https://doi.org/10.1016/j.molstruc.2020.129412).
11. A. S. Mostafa and K. B. Selim, Synthesis and anticancer activity of new dihydropyrimidinone derivatives, *Eur. J. Med. Chem.*, **2018**, vol. 156, pp. 304–315, doi: [10.1016/j.ejmech.2018.07.004](https://doi.org/10.1016/j.ejmech.2018.07.004).
12. M. Castro Jara *et al.*, Dihydropyrimidinones against multiresistant bacteria, *Front. Microbiol.*, **2022**, vol. 13, p. 743213, doi: [10.3389/fmicb.2022.743213](https://doi.org/10.3389/fmicb.2022.743213).
13. P. Biginelli, Aldehyde-urea derivatives of aceto- and oxaloacetic acids. *Gazz. Chim. Ital.*, **1893**, vol. 23, pp. 360-413.
14. R. Behrend, *Ann. Chem. Pharm.* **1879**, vol. 209, p. 5.
15. H. Schiff, Ueber acrolein-harnstoff, *Ber. Dtsch. Chem. Ges.*, **1882**, vol. 15, no. 1, pp. 1393–1397, doi: [10.1002/cber.188201501300](https://doi.org/10.1002/cber.188201501300).
16. K. Folkers, T. B. Johnson, Researches on pyrimidines. CXXXVI. The mechanism of formation of tetrahydropyrimidines by the Biginelli reaction, *J. Am. Chem. Soc.*, **1933**, vol. 55, pp. 3784–3791.
17. F. S. Sweet, J. D. Fissekis, Synthesis of 3,4-dihydro-2 (1H)-pyrimidinones and the mechanism of the Biginelli reaction, *J. Am. Chem. Soc.*, **1973**, vol. 95, pp. 8741–8749.
18. C. O. Kappe, A reexamination of the mechanism of the Biginelli dihydropyrimidine synthesis. Support for an *N*-acyliminium ion intermediate, *J. Org. Chem.*, **1997**, vol. 62, no. 21, pp. 7201–7204, doi: [10.1021/jo971010u](https://doi.org/10.1021/jo971010u).
19. R. O. M. A. De Souza *et al.*, The Three-component Biginelli reaction: a combined experimental and theoretical mechanistic investigation, *Chem. Eur. J.*, **2009**, vol. 15, no. 38, pp. 9799–9804, doi: [10.1002/chem.200900470](https://doi.org/10.1002/chem.200900470).
20. M. Puripat, R. Ramozzi, M. Hatanaka, W. Parasuk, V. Parasuk, and K. Morokuma, The Biginelli reaction is a urea-catalyzed organocatalytic multicomponent reaction, *J. Org. Chem.*, **2015**, vol. 80, no. 14, pp. 6959–6967, doi: [10.1021/acs.joc.5b00407](https://doi.org/10.1021/acs.joc.5b00407).
21. V. Kamat, D. S. Reddy, and A. Kumar, Catalytic role in Biginelli reaction: synthesis and biological property studies of 2-oxo/thioxo-1,2,3,4-tetrahydropyrimidines, *Arch. Pharm.*, **2023**, vol. 356, no. 6, p. 2300008, doi: [10.1002/ardp.202300008](https://doi.org/10.1002/ardp.202300008).
22. K. Malani, S. S. Thakkar, M. C. Thakur, A. Ray, and H. Doshi, Synthesis, characterization and in silico designing of diethyl-3-methyl-5-(6-methyl-2-thioxo-4-phenyl-1,2,3,4-tetrahydropyrimidine-5-carboxamido) thiophene-2,4-dicarboxylate derivative as anti-proliferative and anti-microbial agents, *Bioorg. Chem.*, **2016**, vol. 68, pp. 265–274, doi: [10.1016/j.bioorg.2016.09.001](https://doi.org/10.1016/j.bioorg.2016.09.001).
23. Z. Moutaoukil, C. Ronco, and R. Benhida, One-pot synthesis of dihydropyrimidines via eco-friendly phosphorus derivatives catalysis, *J. Saudi Chem. Soc.*, **2022**, vol. 26, no. 1, p. 101398, doi: [10.1016/j.jscs.2021.101398](https://doi.org/10.1016/j.jscs.2021.101398).
24. R. Chikhale *et al.*, Development of selective DprE1 inhibitors: design, synthesis, crystal structure and antitubercular activity of benzothiazolylpyrimidine-5-carboxamides, *Eur. J. Med. Chem.*, **2015**, vol. 96, pp. 30–46, doi: [10.1016/j.ejmech.2015.04.011](https://doi.org/10.1016/j.ejmech.2015.04.011).
25. H. Yuan, K. Zhang, J. Xia, X. Hu, and S. Yuan, Gallium (III) chloride-catalyzed synthesis of 3,4-dihydropyrimidinones for Biginelli reaction under solvent-free conditions, *Cogent Chem.*, **2017**, vol. 3, no. 1, p. 1318692, doi: [10.1080/23312009.2017.1318692](https://doi.org/10.1080/23312009.2017.1318692).
26. N. Jankovic, Z. Bugarcic, and S. Markovic, Double catalytic effect of (PhNH₃)₂CuCl₄ in a novel, highly efficient synthesis of 2-oxo and thioxo-1,2,3,4-tetra-hydropyrimidines, *J. Serb. Chem. Soc.*, **2015**, vol. 80, no. 5, pp. 595–604, doi: [10.2298/JSC141028011J](https://doi.org/10.2298/JSC141028011J).
27. X. Hu, R. Zhang, J. Xie, Z. Zhou, and Z. Shan, Synthesis of a novel sterically hindered chiral cyclic phosphoric acid derived from l-tartaric acid and application to the asymmetric

- catalytic Biginelli reaction, *Tetrahedron: Asymmetry*, **2017**, vol. 28, no. 1, pp. 69–74, doi: [10.1016/j.tetasy.2016.11.014](https://doi.org/10.1016/j.tetasy.2016.11.014).
28. X. Zhang, X. Gu, Y. Gao, S. Nie, and H. Lu, $(C_5H_6N_4O)(C_5H_5N_4O)_3(C_5H_4N_4O)[Bi_2Cl_{11}]Cl_2$ as a simple and efficient catalyst in Biginelli reaction: organometal as a catalyst in Biginelli reaction, *Appl. Organometal. Chem.*, **2017**, vol. 31, no. 4, p. e3590, doi: [10.1002/aoc.3590](https://doi.org/10.1002/aoc.3590).
 29. T. Raj *et al.*, Solvent-less mechanochemical approach to the synthesis of pyrimidine derivatives, *ACS Sustainable Chem. Eng.*, **2017**, vol. 5, no. 2, pp. 1468–1475, doi: [10.1021/acssuschemeng.6b02030](https://doi.org/10.1021/acssuschemeng.6b02030).
 30. H. G. O. Alvim *et al.*, Ionic liquid effect over the Biginelli reaction under homogeneous and heterogeneous catalysis, *ACS Catal.*, **2013**, vol. 3, no. 7, pp. 1420–1430, doi: [10.1021/cs400291t](https://doi.org/10.1021/cs400291t).
 31. N. S. Pawar, P. N. Patil, and R. N. Pachpande, An efficient synthesis and antibacterial activity of some novel 3,4-dihydropyrimidin-2-(1H)-ones, *ECSOC-25*, MDPI, **2021**, p. 37. doi: [10.3390/ecsoc-25-11720](https://doi.org/10.3390/ecsoc-25-11720).
 32. S. Chidambaram, A. A.-F. Mostafa, A. Abdulrahman Al-Askar, S. R. M. Sayed, S. Radhakrishnan, and I. Akbar, Green catalyst Cu(II)-enzyme-mediated eco-friendly synthesis of 2-pyrimidinamines as potential larvicides against *Culex quinquefasciatus* mosquito and toxicity investigation against non-target aquatic species, *Bioorg. Chem.*, **2021**, vol. 109, p. 104697, doi: [10.1016/j.bioorg.2021.104697](https://doi.org/10.1016/j.bioorg.2021.104697).
 33. F. Mohamadpour, Carbazole-based photocatalyst (4CzIPN) for novel donor-acceptor (D-A) fluorophore-catalyzed visible-light-induced photosynthesis of 3,4-dihydropyrimidin-2-(1H)-ones/thiones via a proton-coupled electron transfer (PCET) process, *RSC Adv.*, **2023**, vol. 13, no. 4, pp. 2514–2522, doi: [10.1039/D2RA07064B](https://doi.org/10.1039/D2RA07064B).
 34. S. A. Jagatap, V. S. Patil, G. P. Sadawarte and J. D. Rajput, Bio-waste curd water as a greener protocol for the synthesis of Biginelli products at ambient temperature, *J. Chem. Edu. Res. Prac.*, **2021**, vol. 5, no. 2, pp. 91-94.
 35. H. Nagarajiah, A. Mukhopadhyay, and J. N. Moorthy, Biginelli reaction: an overview, *Tet. Lett.*, **2016**, vol. 57, no. 47, pp. 5135–5149, doi: [10.1016/j.tetlet.2016.09.047](https://doi.org/10.1016/j.tetlet.2016.09.047).
 36. P. Seboletswe, P. Awolade, and P. Singh, Recent developments on the synthesis and biological activities of fused pyrimidinone derivatives, *ChemMedChem*, **2021**, vol. 16, no. 13, pp. 2050–2067, doi: [10.1002/cmdc.202100083](https://doi.org/10.1002/cmdc.202100083).
 37. K. Kim, D. Kim, H. Lee, T. H. Lee, K.-Y. Kim, and H. Kim, New pyrimidinone-fused 1,4-naphthoquinone derivatives inhibit the growth of drug resistant oral bacteria, *Biomedicines*, **2020**, vol. 8, no. 6, p. 160, doi: [10.3390/biomedicines8060160](https://doi.org/10.3390/biomedicines8060160).
 38. P. N. Patel, N. C. Patel, and D. H. Desai, Synthesis of novel disperse dyes with dihydropyrimidinone scaffold: development of multicomponent protocol, *Russ. J. Org. Chem.*, **2022**, vol. 58, no. 4, pp. 536–540, doi: [10.1134/S1070428022040108](https://doi.org/10.1134/S1070428022040108).
 39. L. M. Ramos *et al.*, The Biginelli reaction with an imidazolium-tagged recyclable iron catalyst: kinetics, mechanism, and antitumoral Activity, *Chem. Eur. J.*, **2013**, vol. 19, no. 13, pp. 4156–4168, doi: [10.1002/chem.201204314](https://doi.org/10.1002/chem.201204314).
 40. P. Liu, J.-W. Hao, L.-P. Mo, and Z.-H. Zhang, Recent advances in the application of deep eutectic solvents as sustainable media as well as catalysts in organic reactions, *RSC Adv.*, **2015**, vol. 5, no. 60, pp. 48675–48704, doi: [10.1039/C5RA05746A](https://doi.org/10.1039/C5RA05746A).
 41. D. A. Alonso, A. Baeza, R. Chinchilla, G. Guillena, I. M. Pastor, and D. J. Ramón, Deep Eutectic Solvents: the organic reaction medium of the century, *Eur. J. Org. Chem.*, **2016**, vol. 2016, no. 4, pp. 612–632, doi: [10.1002/ejoc.201501197](https://doi.org/10.1002/ejoc.201501197).
 42. S. R. Patil, A. S. Choudhary, V. S. Patil, and N. Sekar, Synthesis, optical properties, dyeing study of dihydropyrimidones (DHPMs) skeleton: green and regioselectivity of novel Biginelli scaffold from lawsone, *Fibers Polym.*, **2015**, vol. 16, no. 11, pp. 2349–2358, doi: [10.1007/s12221-015-5233-x](https://doi.org/10.1007/s12221-015-5233-x).

43. S. Lakshmanan, D. Govindaraj, N. Ramalakshmi, and S. A. Antony, Synthesis, molecular docking, DFT calculations and cytotoxicity activity of benzo[g]quinazoline derivatives in choline chloride-urea, *Journal of Molecular Structure*, **2017**, vol. 1150, pp. 88–95, doi: [10.1016/j.molstruc.2017.08.082](https://doi.org/10.1016/j.molstruc.2017.08.082).
44. A. R. Momeni, H. A. Samimi, H. Vaezzadeh, Eutectic mixture choline chloride–chloroacetic acid: a new and efficient catalyst for synthesis of 3,4-dihydropyrimidin-2-ones, *Chem. Methodol.*, **2018**, vol. 4, pp. 253–261.
45. A. K. Bose, S. Pednekar, S. N. Ganguly, G. Chakraborty, and M. S. Manhas, A simplified green chemistry approach to the Biginelli reaction using 'Grindstone Chemistry', *Tet. Lett.*, **2004**, vol. 45, no. 45, pp. 8351–8353, doi: [10.1016/j.tetlet.2004.09.064](https://doi.org/10.1016/j.tetlet.2004.09.064).
46. A. Borse, M. Patil, N. Patil, and R. Shinde, A green, expeditious, one-pot synthesis of 3,4-dihydropyrimidin-2(1H)-ones using a mixture of phosphorus pentoxide-methanesulfonic acid at ambient temperature, *ISRN Org. Chem.*, **2012**, pp. 1–6, doi: [10.5402/2012/415645](https://doi.org/10.5402/2012/415645).
47. A. D. Becke, Density-functional exchange-energy approximation with correct asymptotic behavior, *Phys. Rev. A*, **1988**, vol. 38, no. 6, pp. 3098–3100, doi: [10.1103/PhysRevA.38.3098](https://doi.org/10.1103/PhysRevA.38.3098).
48. A. D. Becke, Density-functional thermochemistry. III. The role of exact exchange, *J. Chem. Phys.*, **1993**, vol. 98, no. 7, pp. 5648–5652, doi: [10.1063/1.464913](https://doi.org/10.1063/1.464913).
49. S. Grimme, Semiempirical GGA-type density functional constructed with a long-range dispersion correction, *J. Comput. Chem.*, **2006**, vol. 27, no. 15, pp. 1787–1799, doi: [10.1002/jcc.20495](https://doi.org/10.1002/jcc.20495).
50. (a) L. Gonnet *et al.*, Elucidation of the Diels–Alder reaction kinetics between diphenylfulvene and maleimide by mechanochemistry and in solution, *ACS Sustainable Chem. Eng.*, **2021**, vol. 9, no. 12, pp. 4453–4462, doi: [10.1021/acssuschemeng.0c08314](https://doi.org/10.1021/acssuschemeng.0c08314). (b) W. Sakai, L. Gonnet, N. Haruta, T. Sato, and M. Baron, Origin of stereoselectivity in a mechanochemical reaction of diphenylfulvene and maleimide, *J. Phys. Chem. A*, **2023**, vol. 127, no. 28, pp. 5790–5794, doi: [10.1021/acs.jpca.3c01332](https://doi.org/10.1021/acs.jpca.3c01332).
51. M. Cossi, N. Rega, G. Scalmani, and V. Barone, Energies, structures, and electronic properties of molecules in solution with the C-PCM solvation model, *J. Comput. Chem.*, **2003**, vol. 24, no. 6, pp. 669–681, doi: [10.1002/jcc.10189](https://doi.org/10.1002/jcc.10189).
52. R. L. Letsinger and K. K. Ogilvie, Use of p-nitrophenyl chloroformate in blocking hydroxyl groups in nucleosides, *J. Org. Chem.*, **1967**, vol. 32, no. 2, pp. 296–300, doi: [10.1021/jo01288a011](https://doi.org/10.1021/jo01288a011).
53. Z. Zhang, K. Tanabe, H. Hatta, and S. Nishimoto, Bioreduction activated prodrugs of camptothecin: molecular design, synthesis, activation mechanism and hypoxia selective cytotoxicity, *Org. Biomol. Chem.*, **2005**, vol. 3, no. 10, p. 1905, doi: [10.1039/b502813b](https://doi.org/10.1039/b502813b).
54. D. Sharma, D. Chetia, and M. Rudrapal, Design, synthesis and antimalarial activity of some new 2-hydroxy-1,4-naphthoquinone-4-hydroxyaniline hybrid Mannich bases, *Asian J. Chem.*, **2016**, vol. 28, no. 4, pp. 782–788, doi: [10.14233/ajchem.2016.19478](https://doi.org/10.14233/ajchem.2016.19478), and references therein.
55. M. Arundhati, C. Dipak, and R. Mithun, Synthesis and antimalarial activity of Lawsone Mannich base derivatives, *IJPER*, **2018**, vol. 52, no. 3, pp. 472–479, doi: [10.5530/ijper.52.3.55](https://doi.org/10.5530/ijper.52.3.55), and references therein.
56. W. Paengsri, N. Promsawan, and A. Baramee, Synthesis and evaluation of 2-hydroxy-1,4-naphthoquinone derivatives as potent antimalarial agents, *Chem. Pharm. Bull.*, **2021**, vol. 69, no. 3, pp. 253–257, doi: [10.1248/cpb.c20-00770](https://doi.org/10.1248/cpb.c20-00770).
57. V. Sebastián-Pérez *et al.*, Naphthoquinone as a new chemical scaffold for leishmanicidal inhibitors of *Leishmania* GSK-3, *Biomedicines*, **2022**, vol. 10, no. 5, p. 1136, doi: [10.3390/biomedicines10051136](https://doi.org/10.3390/biomedicines10051136).
58. D. Birth, W.-C. Kao, and C. Hunte, Structural analysis of atovaquone-inhibited cytochrome bc1 complex reveals the molecular basis of antimalarial drug action, *Nat. Commun.*, **2014**, vol. 5, no. 1, p. 4029, doi: [10.1038/ncomms5029](https://doi.org/10.1038/ncomms5029).

59. D. E. Hurt, J. Widom, and J. Clardy, Structure of *Plasmodium falciparum* dihydroorotate dehydrogenase with a bound inhibitor, *Acta Crystallogr. D Biol. Crystallogr.*, **2006**, vol. 62, no. 3, pp. 312–323, doi: [10.1107/S0907444905042642](https://doi.org/10.1107/S0907444905042642).
60. R. A. Friesner *et al.*, Glide: A new approach for rapid, accurate docking and scoring. 1. Method and assessment of docking accuracy, *J. Med. Chem.*, **2004**, vol. 47, no. 7, pp. 1739–1749, doi: [10.1021/jm0306430](https://doi.org/10.1021/jm0306430).
61. T. A. Halgren *et al.*, Glide: A new approach for rapid, accurate docking and scoring. 2. Enrichment factors in database screening, *J. Med. Chem.*, **2004**, vol. 47, no. 7, pp. 1750–1759, doi: [10.1021/jm030644s](https://doi.org/10.1021/jm030644s).
62. CLSI. CLSI Document M100-S21; Performance standards for antimicrobial susceptibility testing, twenty-first informational supplement; clinical and laboratory standards institute: **2011**, Wayne, PA, USA.
63. S. Sun and J. Fu, Methyl-containing pharmaceuticals: Methylation in drug design, *Bioorg. Med. Chem. Lett.*, **2018**, vol. 28, no. 20, pp. 3283–3289, doi: [10.1016/j.bmcl.2018.09.016](https://doi.org/10.1016/j.bmcl.2018.09.016).
64. H.-G. Cheng, M. Pu, G. Kundu, and F. Schoenebeck, Selective methylation of amides, *N*-heterocycles, thiols, and alcohols with tetramethylammonium fluoride, *Org. Lett.*, **2020**, vol. 22, no. 1, pp. 331–334, doi: [10.1021/acs.orglett.9b04400](https://doi.org/10.1021/acs.orglett.9b04400).
65. D. A. Evans, A. M. Ratz, B. E. Huff, and G. S. Sheppard, Mild alcohol methylation procedure for the synthesis of polyoxygenated natural products. Applications to the synthesis of Ionomycin A, *Tet. Lett.*, **1994**, vol. 35, no. 39, pp. 7171–7172, doi: [10.1016/0040-4039\(94\)85352-5](https://doi.org/10.1016/0040-4039(94)85352-5).
66. G. S. K. Rao, K. V. Rao, and T. R. Seshadri, A note on the formation of quinones by oxidative demethylation and the effect of methylating agents on them, *Proc. Indian Acad. Sci.*, **1948**, vol. 27, no. 4, p. 245, doi: [10.1007/BF03171012](https://doi.org/10.1007/BF03171012).
67. Oramas-Royo *et al.*, Synthesis and antiplasmodial activity of 1,2,3-triazole-naphthoquinone conjugates, *Molecules*, **2019**, vol. 24, no. 21, p. 3917, doi: [10.3390/molecules24213917](https://doi.org/10.3390/molecules24213917).
68. R. M. Costa Souza *et al.*, Biological activity of 1,2,3-triazole-2-amino-1,4-naphthoquinone derivatives and their evaluation as therapeutic strategy for malaria control, *Eur. J. Med. Chem.*, **2023**, vol. 255, p. 115400, , doi: [10.1016/j.ejmech.2023.115400](https://doi.org/10.1016/j.ejmech.2023.115400).
69. T. T. Guimarães *et al.*, Potent naphthoquinones against antimony-sensitive and -resistant *Leishmania* parasites: Synthesis of novel α - and nor- α -lapachone-based 1,2,3-triazoles by copper-catalyzed azide–alkyne cycloaddition, *Eur. J. Med. Chem.*, **2013**, vol. 63, pp. 523–530, doi: [10.1016/j.ejmech.2013.02.038](https://doi.org/10.1016/j.ejmech.2013.02.038).

“General Conclusion”

4.1 General Conclusion

This thesis was focused on the design and synthesis of novel naphthoquinone derivatives as potential antiparasitic agents. In that respect, commercially available 2-hydroxy-naphthoquinone (lawsone) was employed in multicomponent reactions aiming to provide new 1,4-naphthoquinone families in one step.

First, a multicomponent domino reaction using lawsone, aldehydes, and alkyl-isocyanides was established and optimized under microwave irradiation. The reaction tolerated very well a very wide substrate scope of aldehydes. A novel series of 19 3-amino-naphthofuroquinone derivatives was obtained with yields ranging from 19% to 59%. In parallel, the direct two-component condensation between lawsone and alkyl isocyanides led to two naphthoenaminone compounds never reported before, isolated as a Z/E mixture, with yields between 40% and 50%. Thus, our first synthetic objective was successfully accomplished.

The second synthetic objective was focused in a multicomponent Biginelli reaction involving lawsone, *para*-substituted benzaldehydes, and (alkyl)ureas. The reaction was studied under various conditions including protic solvents, ionic liquids (ILs), deep eutectic solvents (DES), and in the solid state (mechanochemical activation). The classic 3,4-dihydropyrimidone Biginelli products (DHPMs) were never obtained.

In solution, ILs, and DES, the reaction predominantly yielded two-component Michael adducts resulting from the aldol condensation between lawsone and benzaldehyde. However, a remarkable shift occurred in the solid state, favoring the three-component reaction. Mechanochemical activation, led to the synthesis of 21 novel Biginelli-linear lawsone derivatives with good yields ranging from 60% to 90%. All cyclisation efforts (in solution, by grinding) failed to afford the desired DHPM derivatives. This outcome made us to investigate the mechanistic pathway of this reaction leading to the Biginelli-linear compounds which were initially considered to be intermediates of the classic Biginelli reaction. We suggested that lawsone reacts first with the aldehyde, affording a Knoevenagel intermediate which is further attacked by the (alkyl)urea.

Finally, selected Biginelli-linear compounds were selectively methylated affording 13 novel compounds with yields ranging from 40% to 90%. These methylated derivatives were found to be stable in solution, in contrast with their precursors.

In essence, this work did not only unveiled novel synthetic pathways and compounds but also provided valuable insights into the mechanistic intricacies of the Biginelli reaction,

contributing to the advancement of organic chemistry and offering potential solutions for enhancing the chemical space of the naphthoquinone family.

Among all the synthesized compounds mentioned herein, the naphthofuroquinones, obtained through the domino reaction, exhibited the highest IC_{50} values against both *Plasmodium falciparum* ART-resistant strains (IC_{50} values 2.5-10 μ M) and *L. donovani* intramacrophage amastigotes. These results agree with the reported results in the literature. However, the two novel naphthoenaminone compounds were active against both parasites and exhibited very good selectivity indexes.

The Biginelli-linear family of compounds was found to be inactive against every pathogen. The more stable O-methylated derivatives exhibited the lowest IC_{50} values among all families of compounds mentioned herein. The O-methylated Biginelli-linear series had IC_{50} values ranging from 2.8 μ M to 10 μ M against *Plasmodium falciparum* ART-resistant strains. This family of compounds was found to be very promising against *L. donovani* intramacrophage amastigotes and had IC_{50} values ranging between 1.5 μ M and 10 μ M and very good selectivity indexes (SI 5.7-82), in the majority of cases better than the reference drug miltefosine (IC_{50} = 1.5 μ M and SI = 15.5).

ANNEXES

1. Crystallographic data for compound 2.69

Table A1: Crystallographic Data of compound **2.69**

$C_{22}H_{18}ClNO_3$	
$M_r = 379.82$	$D_x = 1.361 \text{ Mg m}^{-3}$
Monoclinic, $P2_1/n$	
Hall symbol: -P 2yn	Mo K α radiation, $\lambda = 0.71073 \text{ \AA}$
$a = 12.024 (3) \text{ \AA}$	Cell parameters from 2329 reflections
$b = 13.290 (3) \text{ \AA}$	$\theta = 2.3\text{--}25.0^\circ$
$c = 12.093 (3) \text{ \AA}$	$\mu = 0.23 \text{ mm}^{-1}$
$\beta = 106.410 (7)^\circ$	$T = 100 \text{ K}$
$V = 1853.6 (8) \text{ \AA}^3$	Platelet, purple
$Z = 4$	$0.15 \times 0.08 \times 0.02 \text{ mm}$
$F(000) = 792$	

Table A2: Data collection

Bruker Kappa APEX II diffractometer	1726 reflections with $I > 2\sigma(I)$
Radiation source: fine-focus sealed tube	$R_{\text{int}} = 0.214$
Graphite monochromator	$\theta_{\text{max}} = 25.1^\circ$, $\theta_{\text{min}} = 2.1^\circ$
ω - ϕ scans	$h = -13 \text{ } 14$
Absorption correction: multi-scan [c.f. r.h. blessing, acta cryst. (1995), a51, 33-38]	$k = -15 \text{ } 15$
$T_{\text{min}} = 0.619$, $T_{\text{max}} = 0.745$	$l = -14 \text{ } 14$
30237 measured reflections	Standard reflections: 0
3298 independent reflections	

Table A3: Refinement

Refinement on F^2	
Least-squares matrix: full	Hydrogen site location: mixed

$R[F^2 > 2\sigma(F^2)] = \underline{0.072}$	<u>H atoms treated by a mixture of independent and constrained refinement</u>
$wR(F^2) = \underline{0.131}$	$w = 1/[\sigma^2(F_o^2) + (0.0439P)^2]$ where $P = (F_o^2 + 2F_c^2)/3$
$S = \underline{1.05}$	$(\Delta/\sigma)_{\max} = \underline{0.003}$
<u>3298</u> reflections	$\Delta\rho_{\max} = \underline{0.30} \text{ e } \text{\AA}^{-3}$
<u>250</u> parameters	$\Delta\rho_{\min} = \underline{-0.35} \text{ e } \text{\AA}^{-3}$
<u>0</u> restraints	Extinction correction: <u>none</u>

Table A4: Fractional atomic coordinates and isotropic or equivalent isotropic displacement parameters (\AA^2)

	x	y	z	$U_{\text{iso}}^*/U_{\text{eq}}$
C1	0.6627 (3)	0.3403 (2)	0.2385 (3)	0.0180 (9)
C2	0.8746 (3)	0.2953 (3)	0.2663 (3)	0.0166 (9)
C2B	0.5713 (3)	0.3148 (3)	0.2838 (3)	0.0186 (10)
H2B	0.588857	0.290713	0.360812	0.022*
C3	0.7844 (3)	0.3340 (2)	0.3056 (3)	0.0163 (9)
C3A	0.8409 (3)	0.3652 (3)	0.4200 (3)	0.0166 (9)
C3B	0.4570 (3)	0.3233 (3)	0.2206 (3)	0.0187 (9)
H3B	0.396526	0.305861	0.253430	0.022*
C4	0.7954 (4)	0.4095 (3)	0.5108 (3)	0.0180 (9)
C4A	0.8852 (3)	0.4305 (3)	0.6234 (3)	0.0170 (9)
C4B	0.4320 (3)	0.3576 (3)	0.1084 (3)	0.0171 (9)
C5	0.8478 (4)	0.4643 (3)	0.7153 (3)	0.0222 (10)
H5	0.767422	0.473253	0.706528	0.027*
C5B	0.5182 (3)	0.3821 (3)	0.0593 (3)	0.0208 (10)
H5B	0.499327	0.404239	-0.018459	0.025*
C6	0.9283 (4)	0.4850 (3)	0.8203 (3)	0.0268 (11)
H6	0.902575	0.506584	0.883803	0.032*
C6B	0.6333 (3)	0.3743 (3)	0.1241 (3)	0.0200 (10)
H6B	0.692983	0.392326	0.090515	0.024*
C7	1.0453 (4)	0.4743 (3)	0.8330 (3)	0.0239 (10)
H7	1.099856	0.490817	0.904291	0.029*

C8	1.0833 (4)	0.4398 (3)	0.7422 (3)	0.0232 (10)
H8	1.163988	0.431756	0.751668	0.028*
C8A	1.0039 (3)	0.4166 (3)	0.6368 (3)	0.0173 (9)
C9	1.0478 (4)	0.3733 (3)	0.5425 (3)	0.0188 (9)
C9A	0.9577 (3)	0.3488 (3)	0.4422 (3)	0.0168 (9)
C10	0.9638 (3)	0.1904 (3)	0.1371 (3)	0.0227 (10)
C11	0.9866 (4)	0.0963 (3)	0.2120 (3)	0.0377 (12)
H11A	1.022274	0.115292	0.292489	0.057*
H11B	1.038990	0.051435	0.186125	0.057*
H11C	0.913155	0.061455	0.205438	0.057*
C12	1.0741 (4)	0.2512 (3)	0.1512 (4)	0.0345 (12)
H12A	1.056429	0.311770	0.103225	0.052*
H12B	1.131203	0.210376	0.127421	0.052*
H12C	1.105793	0.270686	0.232234	0.052*
C13	0.9151 (4)	0.1611 (3)	0.0108 (3)	0.0301 (11)
H13A	0.843550	0.122456	0.000801	0.045*
H13B	0.972059	0.120031	-0.012933	0.045*
H13C	0.898411	0.222048	-0.036667	0.045*
N1	0.8709 (3)	0.2526 (2)	0.1642 (3)	0.0222 (8)
H1	0.796 (3)	0.235 (3)	0.126 (3)	0.027*
O1	0.9792 (2)	0.30454 (17)	0.3465 (2)	0.0198 (7)
O2	1.1529 (2)	0.36154 (18)	0.5533 (2)	0.0240 (7)
O3	0.6930 (2)	0.42649 (18)	0.4989 (2)	0.0225 (7)
Cl1	0.28725 (9)	0.36933 (8)	0.02686 (9)	0.0307 (3)

Table A5: Atomic displacement parameters (\AA^2)

	U^{11}	U^{22}	U^{33}	U^{12}	U^{13}	U^{23}
C1	0.019 (3)	0.010 (2)	0.023 (2)	-0.0005 (18)	0.002 (2)	-0.0043 (17)
C2	0.018 (3)	0.011 (2)	0.017 (2)	-0.0013 (18)	-0.001 (2)	0.0002 (17)
C2B	0.024 (3)	0.013 (2)	0.019 (2)	-0.002 (2)	0.007 (2)	-0.0049 (17)
C3	0.014 (3)	0.014 (2)	0.020 (2)	-0.0016 (18)	0.004 (2)	0.0003 (17)
C3A	0.020 (3)	0.010 (2)	0.019 (2)	0.0001 (19)	0.0042 (19)	0.0034 (18)

C3B	0.013 (3)	0.019 (2)	0.022 (2)	-0.0020 (18)	0.001 (2)	-0.0057 (18)
C4	0.023 (3)	0.010 (2)	0.021 (2)	0.001 (2)	0.005 (2)	0.0057 (17)
C4A	0.019 (3)	0.010 (2)	0.020 (2)	0.0015 (18)	0.003 (2)	0.0027 (17)
C4B	0.013 (2)	0.012 (2)	0.021 (2)	0.0007 (18)	-0.0039 (19)	-0.0066 (18)
C5	0.022 (3)	0.018 (2)	0.024 (2)	-0.0004 (19)	0.003 (2)	0.0000 (19)
C5B	0.024 (3)	0.017 (2)	0.019 (2)	0.002 (2)	0.000 (2)	0.0000 (17)
C6	0.032 (3)	0.021 (2)	0.026 (3)	0.000 (2)	0.006 (2)	-0.0001 (19)
C6B	0.025 (3)	0.015 (2)	0.021 (2)	-0.002 (2)	0.009 (2)	0.0004 (18)
C7	0.030 (3)	0.019 (2)	0.017 (2)	0.002 (2)	-0.002 (2)	-0.0026 (18)
C8	0.018 (3)	0.018 (2)	0.029 (3)	0.0027 (19)	0.000 (2)	0.0072 (19)
C8A	0.021 (3)	0.010 (2)	0.018 (2)	-0.0028 (19)	0.001 (2)	0.0046 (17)
C9	0.023 (3)	0.009 (2)	0.024 (2)	-0.001 (2)	0.005 (2)	0.0039 (18)
C9A	0.020 (3)	0.017 (2)	0.015 (2)	0.0019 (19)	0.006 (2)	-0.0021 (17)
C10	0.022 (3)	0.020 (2)	0.028 (2)	-0.002 (2)	0.009 (2)	-0.0037 (18)
C11	0.047 (3)	0.029 (3)	0.038 (3)	0.008 (2)	0.014 (3)	0.000 (2)
C12	0.026 (3)	0.034 (3)	0.048 (3)	-0.007 (2)	0.019 (2)	-0.014 (2)
C13	0.038 (3)	0.030 (3)	0.027 (2)	-0.002 (2)	0.016 (2)	-0.006 (2)
N1	0.015 (2)	0.028 (2)	0.022 (2)	-0.0011 (17)	0.0040 (17)	-0.0077 (16)
O1	0.0159 (17)	0.0193 (14)	0.0218 (15)	0.0014 (13)	0.0014 (14)	-0.0016 (12)
O2	0.0147 (18)	0.0260 (16)	0.0290 (16)	0.0006 (14)	0.0026 (14)	0.0030 (13)
O3	0.0177 (19)	0.0234 (15)	0.0254 (16)	0.0020 (13)	0.0045 (14)	-0.0038 (12)
Cl1	0.0202 (7)	0.0336 (6)	0.0314 (6)	0.0039 (5)	-0.0041 (5)	-0.0022 (5)

Table A6: Geometric parameters (Å, °)

C1—C2B	1.402 (5)	C6—H6	0.9500
C1—C6B	1.402 (5)	C6B—H6B	0.9500
C1—C3	1.462 (5)	C7—C8	1.382 (5)
C2—N1	1.349 (4)	C7—H7	0.9500
C2—O1	1.360 (4)	C8—C8A	1.394 (5)
C2—C3	1.398 (5)	C8—H8	0.9500
C2B—C3B	1.375 (5)	C8A—C9	1.500 (5)
C2B—H2B	0.9500	C9—O2	1.243 (4)

C3—C3A	1.421 (5)	C9—C9A	1.418 (5)
C3A—C9A	1.371 (5)	C9A—O1	1.385 (4)
C3A—C4	1.481 (5)	C10—N1	1.498 (5)
C3B—C4B	1.382 (5)	C10—C12	1.521 (5)
C3B—H3B	0.9500	C10—C11	1.523 (5)
C4—O3	1.220 (4)	C10—C13	1.523 (5)
C4—C4A	1.505 (5)	C11—H11A	0.9800
C4A—C5	1.385 (5)	C11—H11B	0.9800
C4A—C8A	1.403 (5)	C11—H11C	0.9800
C4B—C5B	1.372 (5)	C12—H12A	0.9800
C4B—C11	1.748 (4)	C12—H12B	0.9800
C5—C6	1.389 (5)	C12—H12C	0.9800
C5—H5	0.9500	C13—H13A	0.9800
C5B—C6B	1.388 (5)	C13—H13B	0.9800
C5B—H5B	0.9500	C13—H13C	0.9800
C6—C7	1.378 (6)	N1—H1	0.92 (4)
C2B—C1—C6B	117.2 (4)	C8—C7—H7	119.9
C2B—C1—C3	122.8 (3)	C7—C8—C8A	120.3 (4)
C6B—C1—C3	120.0 (4)	C7—C8—H8	119.8
N1—C2—O1	118.4 (3)	C8A—C8—H8	119.8
N1—C2—C3	129.6 (4)	C8—C8A—C4A	119.2 (3)
O1—C2—C3	112.0 (3)	C8—C8A—C9	118.9 (4)
C3B—C2B—C1	122.2 (4)	C4A—C8A—C9	121.9 (3)
C3B—C2B—H2B	118.9	O2—C9—C9A	124.7 (3)
C1—C2B—H2B	118.9	O2—C9—C8A	122.3 (4)
C2—C3—C3A	103.6 (3)	C9A—C9—C8A	113.0 (3)
C2—C3—C1	125.7 (3)	C3A—C9A—O1	109.1 (3)
C3A—C3—C1	130.7 (3)	C3A—C9A—C9	128.6 (3)
C9A—C3A—C3	109.0 (3)	O1—C9A—C9	122.3 (3)
C9A—C3A—C4	119.4 (3)	N1—C10—C12	111.3 (3)
C3—C3A—C4	131.6 (4)	N1—C10—C11	110.0 (3)
C2B—C3B—C4B	118.6 (4)	C12—C10—C11	111.4 (3)

C2B—C3B—H3B	120.7	N1—C10—C13	105.1 (3)
C4B—C3B—H3B	120.7	C12—C10—C13	109.0 (3)
O3—C4—C3A	124.0 (4)	C11—C10—C13	109.9 (3)
O3—C4—C4A	121.0 (3)	C10—C11—H11A	109.5
C3A—C4—C4A	115.1 (4)	C10—C11—H11B	109.5
C5—C4A—C8A	120.0 (4)	H11A—C11—H11B	109.5
C5—C4A—C4	118.2 (4)	C10—C11—H11C	109.5
C8A—C4A—C4	121.8 (3)	H11A—C11—H11C	109.5
C5B—C4B—C3B	121.5 (4)	H11B—C11—H11C	109.5
C5B—C4B—C11	119.2 (3)	C10—C12—H12A	109.5
C3B—C4B—C11	119.3 (3)	C10—C12—H12B	109.5
C4A—C5—C6	119.8 (4)	H12A—C12—H12B	109.5
C4A—C5—H5	120.1	C10—C12—H12C	109.5
C6—C5—H5	120.1	H12A—C12—H12C	109.5
C4B—C5B—C6B	119.5 (3)	H12B—C12—H12C	109.5
C4B—C5B—H5B	120.2	C10—C13—H13A	109.5
C6B—C5B—H5B	120.2	C10—C13—H13B	109.5
C7—C6—C5	120.5 (4)	H13A—C13—H13B	109.5
C7—C6—H6	119.8	C10—C13—H13C	109.5
C5—C6—H6	119.8	H13A—C13—H13C	109.5
C5B—C6B—C1	121.0 (4)	H13B—C13—H13C	109.5
C5B—C6B—H6B	119.5	C2—N1—C10	126.8 (3)
C1—C6B—H6B	119.5	C2—N1—H1	109 (2)
C6—C7—C8	120.1 (4)	C10—N1—H1	116 (2)
C6—C7—H7	119.9	C2—O1—C9A	106.3 (3)

Table A7: Hydrogen-bond geometry (Å, °)

D—H···A	D—H	H···A	D···A	D—H···A
N1—H1···O2 ⁱ	0.92 (4)	2.13 (4)	2.997 (4)	157 (3)
C12—H12B···O3 ⁱⁱ	0.98	2.63	3.535 (5)	153
C12—H12C···O1	0.98	2.37	2.984 (5)	120
C13—H13A···O2 ⁱ	0.98	2.55	3.348 (5)	138

C13—H13A···O3 ⁱⁱⁱ	0.98	2.64	3.367 (5)	131
N1—H1···O2 ⁱ	0.92 (4)	2.13 (4)	2.997 (4)	157 (3)
C12—H12B···O3 ⁱⁱ	0.98	2.63	3.535 (5)	153
C12—H12C···O1	0.98	2.37	2.984 (5)	120
C13—H13A···O2 ⁱ	0.98	2.55	3.348 (5)	138
C13—H13A···O3 ⁱⁱⁱ	0.98	2.64	3.367 (5)	131

Symmetry codes: (i) $x-1/2, -y+1/2, z-1/2$; (ii) $x+1/2, -y+1/2, z-1/2$; (iii) $-x+3/2, y-1/2, -z+1/2$.

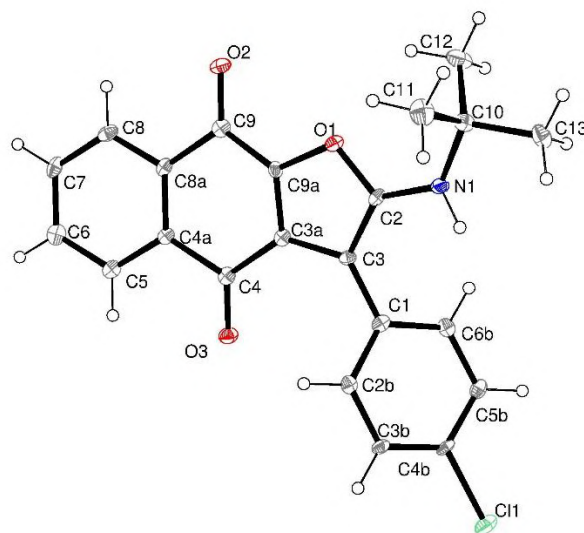


Figure A1: Crystallographic structure of compound **2.69**

2. Crystallographic data for compound **3.61**

Table A8: Crystallographic data for compound **3.61**

$C_{21}H_{15}ClN_2O_4$	$F(000) = 408$
$M_r = 394.80$	
Triclinic, P-1	$D_x = 1.412 \text{ Mg m}^{-3}$
Hall symbol: -P 1	
$a = 9.5285 (15) \text{ \AA}$	Mo K α radiation, $\lambda = 0.71073 \text{ \AA}$

$b = 10.8463 (17) \text{ \AA}$	Cell parameters from <u>9921</u> reflections
$c = 10.9208 (16) \text{ \AA}$	$\theta = 2.5\text{--}36.9^\circ$
$\alpha = 94.939 (9)^\circ$	$\mu = 0.24 \text{ mm}^{-1}$
$\beta = 113.931 (8)^\circ$	$T = 100 \text{ K}$
$\gamma = 110.838 (8)^\circ$	<u>Block, yellow</u>
$V = 928.4 (3) \text{ \AA}^3$	<u>0.18</u> × <u>0.10</u> × <u>0.04</u> mm
$Z = 2$	

Table A9: Data collection

<u>Bruker Kappa APEX II</u> diffractometer	<u>3423</u> reflections with $I > 2\sigma(I)$
Radiation source: <u>fine-focus sealed tube</u>	$R_{\text{int}} = 0.056$
<u>Graphite</u> monochromator	$\theta_{\text{max}} = 26.4^\circ$, $\theta_{\text{min}} = 2.1^\circ$
ω - ϕ scans	$h = -11 \text{ } 11$
Absorption correction: <u>multi-scan</u> [c.f. r.h. blessing, <i>acta cryst.</i> (1995), a51, 33-38]	$k = -13 \text{ } 13$
$T_{\text{min}} = 0.715$, $T_{\text{max}} = 0.743$	$l = -13 \text{ } 13$
<u>39871</u> measured reflections	Standard reflections: <u>0</u>
<u>3787</u> independent reflections	

Table A10: Refinement

Refinement on F^2	
Least-squares matrix: <u>full</u>	Hydrogen site location: <u>mixed</u>
$R[F^2 > 2\sigma(F^2)] = 0.035$	<u>H atoms treated by a mixture of independent and constrained refinement</u>
$wR(F^2) = 0.094$	$w = 1/[\sigma^2(F_o^2) + (0.0353P)^2 + 0.7665P]$ where $P = (F_o^2 + 2F_c^2)/3$
$S = 1.04$	$(\Delta/\sigma)_{\text{max}} = 0.001$
<u>3787</u> reflections	$\Delta\rho_{\text{max}} = 0.37 \text{ e \AA}^{-3}$
<u>259</u> parameters	$\Delta\rho_{\text{min}} = -0.36 \text{ e \AA}^{-3}$
<u>0</u> restraints	Extinction correction: <u>none</u>

Table A11: Fractional atomic coordinates and isotropic or equivalent isotropic displacement parameters (\AA^2)

	x	y	z	$U_{\text{iso}}^*/U_{\text{eq}}$
C1	0.3609 (2)	0.02555 (15)	0.66677 (17)	0.0198 (3)
C1A	0.23661 (17)	0.41456 (14)	0.67006 (15)	0.0144 (3)
C2	0.26302 (18)	0.11018 (14)	0.63711 (15)	0.0146 (3)
C2A	0.28821 (18)	0.39958 (15)	0.80487 (15)	0.0170 (3)
H2A	0.311460	0.323348	0.824861	0.020*
C2B	0.2024 (2)	0.52667 (16)	0.64309 (16)	0.0221 (3)
H2B	0.165706	0.537336	0.551427	0.026*
C3	0.31583 (18)	0.22860 (14)	0.60102 (14)	0.0143 (3)
C3A	0.30604 (19)	0.49471 (16)	0.91028 (16)	0.0200 (3)
H3A	0.340146	0.483567	1.001701	0.024*
C3B	0.2207 (2)	0.62329 (17)	0.74746 (18)	0.0255 (4)
H3B	0.197475	0.699683	0.728155	0.031*
C4	0.48788 (18)	0.28985 (14)	0.61690 (14)	0.0152 (3)
C4A	0.2734 (2)	0.60568 (16)	0.88002 (16)	0.0214 (3)
C5	0.58968 (18)	0.20848 (15)	0.64490 (14)	0.0162 (3)
C6	0.74895 (19)	0.26095 (16)	0.65075 (16)	0.0219 (3)
H6	0.793074	0.348431	0.635773	0.026*
C7	0.8434 (2)	0.18490 (18)	0.67863 (18)	0.0263 (4)
H7	0.951875	0.220730	0.681819	0.032*
C8	0.7817 (2)	0.05743 (18)	0.70184 (17)	0.0244 (3)
H8	0.847850	0.006794	0.721574	0.029*
C9	0.6228 (2)	0.00428 (16)	0.69611 (16)	0.0206 (3)
H9	0.579389	-0.083127	0.711441	0.025*
C10	0.52745 (18)	0.07983 (15)	0.66773 (15)	0.0163 (3)
C11	0.20248 (18)	0.30243 (14)	0.55341 (14)	0.0143 (3)
H11	0.083392	0.232258	0.519429	0.017*
C12	0.11935 (18)	0.26723 (14)	0.30524 (15)	0.0149 (3)
C13	0.0812 (2)	0.23991 (16)	0.06734 (16)	0.0220 (3)
H13A	0.052177	0.295479	0.002098	0.026*

H13B	-0.025638	0.160747	0.046118	0.026*
C14	0.1942 (2)	0.18894 (17)	0.04345 (17)	0.0265 (4)
C15	0.2841 (3)	0.1478 (2)	0.0222 (2)	0.0393 (5)
H15	0.349 (3)	0.109 (2)	0.004 (2)	0.047*
N1	0.20678 (15)	0.35434 (12)	0.43586 (12)	0.0153 (3)
N2	0.15434 (17)	0.32243 (13)	0.20854 (13)	0.0228 (3)
O1	0.01213 (13)	0.14886 (10)	0.27472 (11)	0.0189 (2)
O2	0.54967 (13)	0.40855 (10)	0.61017 (11)	0.0204 (2)
O3	0.12003 (13)	0.06443 (10)	0.64617 (11)	0.0175 (2)
O4	0.29957 (18)	-0.08393 (13)	0.68741 (18)	0.0427 (4)
Cl1	0.30280 (6)	0.72832 (5)	1.01386 (4)	0.03234 (13)
H1	0.299320	0.424210	0.454280	0.016 (4)*
H2	0.240808	0.402761	0.236869	0.027 (5)*
H3	0.097110	-0.008350	0.666970	0.049 (7)*

Table A12: Atomic displacement parameters (\AA^2)

	U^{11}	U^{22}	U^{33}	U^{12}	U^{13}	U^{23}
C1	0.0230 (8)	0.0160 (7)	0.0266 (8)	0.0095 (6)	0.0154 (7)	0.0098 (6)
C1A	0.0137 (6)	0.0130 (6)	0.0157 (7)	0.0041 (5)	0.0076 (6)	0.0040 (5)
C2	0.0138 (6)	0.0144 (7)	0.0150 (7)	0.0047 (5)	0.0075 (6)	0.0034 (5)
C2A	0.0172 (7)	0.0186 (7)	0.0169 (7)	0.0086 (6)	0.0084 (6)	0.0066 (6)
C2B	0.0327 (9)	0.0198 (7)	0.0178 (7)	0.0136 (7)	0.0129 (7)	0.0085 (6)
C3	0.0166 (7)	0.0128 (7)	0.0140 (7)	0.0056 (6)	0.0081 (6)	0.0036 (5)
C3A	0.0184 (7)	0.0271 (8)	0.0148 (7)	0.0102 (6)	0.0078 (6)	0.0049 (6)
C3B	0.0379 (9)	0.0193 (8)	0.0271 (8)	0.0168 (7)	0.0179 (7)	0.0089 (7)
C4	0.0176 (7)	0.0142 (7)	0.0112 (6)	0.0038 (6)	0.0072 (6)	0.0028 (5)
C4A	0.0212 (8)	0.0215 (8)	0.0194 (7)	0.0075 (6)	0.0103 (6)	-0.0011 (6)
C5	0.0159 (7)	0.0176 (7)	0.0120 (6)	0.0042 (6)	0.0069 (6)	0.0017 (5)
C6	0.0181 (7)	0.0227 (8)	0.0211 (8)	0.0043 (6)	0.0099 (6)	0.0041 (6)
C7	0.0162 (7)	0.0340 (9)	0.0264 (8)	0.0082 (7)	0.0111 (7)	0.0033 (7)
C8	0.0216 (8)	0.0331 (9)	0.0204 (8)	0.0167 (7)	0.0079 (6)	0.0032 (7)
C9	0.0226 (8)	0.0214 (8)	0.0184 (7)	0.0109 (6)	0.0092 (6)	0.0042 (6)

C10	0.0174 (7)	0.0168 (7)	0.0149 (7)	0.0067 (6)	0.0086 (6)	0.0028 (5)
C11	0.0169 (7)	0.0132 (6)	0.0136 (7)	0.0056 (5)	0.0081 (6)	0.0054 (5)
C12	0.0159 (7)	0.0143 (7)	0.0167 (7)	0.0076 (6)	0.0084 (6)	0.0056 (5)
C13	0.0244 (8)	0.0228 (8)	0.0154 (7)	0.0055 (6)	0.0100 (6)	0.0053 (6)
C14	0.0326 (9)	0.0263 (8)	0.0190 (8)	0.0084 (7)	0.0137 (7)	0.0097 (6)
C15	0.0527 (12)	0.0508 (12)	0.0378 (11)	0.0323 (11)	0.0311 (10)	0.0232 (9)
N1	0.0178 (6)	0.0118 (6)	0.0151 (6)	0.0032 (5)	0.0091 (5)	0.0052 (5)
N2	0.0269 (7)	0.0155 (6)	0.0168 (6)	-0.0018 (5)	0.0115 (6)	0.0028 (5)
O1	0.0197 (5)	0.0148 (5)	0.0192 (5)	0.0022 (4)	0.0108 (4)	0.0048 (4)
O2	0.0193 (5)	0.0143 (5)	0.0240 (6)	0.0022 (4)	0.0109 (5)	0.0071 (4)
O3	0.0168 (5)	0.0146 (5)	0.0260 (6)	0.0065 (4)	0.0136 (4)	0.0105 (4)
O4	0.0432 (8)	0.0293 (7)	0.0906 (12)	0.0251 (6)	0.0499 (8)	0.0403 (7)
C11	0.0392 (3)	0.0333 (2)	0.0249 (2)	0.01861 (19)	0.01478 (19)	-0.00284 (17)

Table A13: Geometric parameters (Å, °)

C1—O4	1.2090 (19)	C6—C7	1.390 (2)
C1—C10	1.478 (2)	C6—H6	0.9500
C1—C2	1.494 (2)	C7—C8	1.387 (3)
C1A—C2B	1.392 (2)	C7—H7	0.9500
C1A—C2A	1.395 (2)	C8—C9	1.387 (2)
C1A—C11	1.5243 (19)	C8—H8	0.9500
C2—O3	1.3226 (17)	C9—C10	1.393 (2)
C2—C3	1.359 (2)	C9—H9	0.9500
C2A—C3A	1.389 (2)	C11—N1	1.4551 (17)
C2A—H2A	0.9500	C11—H11	1.0000
C2B—C3B	1.390 (2)	C12—O1	1.2329 (17)
C2B—H2B	0.9500	C12—N2	1.3554 (19)
C3—C4	1.461 (2)	C12—N1	1.3658 (19)
C3—C11	1.520 (2)	C13—N2	1.453 (2)
C3A—C4A	1.381 (2)	C13—C14	1.469 (2)
C3A—H3A	0.9500	C13—H13A	0.9900
C3B—C4A	1.382 (2)	C13—H13B	0.9900
C3B—H3B	0.9500	C14—C15	1.185 (3)

C4—O2	1.2336 (18)	C15—H15	0.93 (2)
C4—C5	1.493 (2)	N1—H1	0.8641 (12)
C4A—C11	1.7471 (16)	N2—O3	5.8051 (18)
C5—C6	1.390 (2)	N2—H2	0.8774 (13)
C5—C10	1.397 (2)	O3—H3	0.8191 (10)
O4—C1—C10	123.43 (14)	C9—C8—C7	119.70 (15)
O4—C1—C2	118.54 (14)	C9—C8—H8	120.2
C10—C1—C2	118.02 (13)	C7—C8—H8	120.2
C2B—C1A—C2A	118.54 (13)	C8—C9—C10	119.57 (15)
C2B—C1A—C11	121.32 (13)	C8—C9—H9	120.2
C2A—C1A—C11	119.88 (12)	C10—C9—H9	120.2
O3—C2—C3	120.66 (13)	C9—C10—C5	120.85 (14)
O3—C2—C1	117.10 (12)	C9—C10—C1	119.60 (13)
C3—C2—C1	122.23 (13)	C5—C10—C1	119.51 (13)
C3A—C2A—C1A	120.86 (14)	N1—C11—C3	112.29 (12)
C3A—C2A—H2A	119.6	N1—C11—C1A	111.12 (11)
C1A—C2A—H2A	119.6	C3—C11—C1A	113.62 (11)
C3B—C2B—C1A	121.37 (14)	N1—C11—H11	106.4
C3B—C2B—H2B	119.3	C3—C11—H11	106.4
C1A—C2B—H2B	119.3	C1A—C11—H11	106.4
C2—C3—C4	119.32 (13)	O1—C12—N2	121.76 (13)
C2—C3—C11	120.83 (13)	O1—C12—N1	123.41 (13)
C4—C3—C11	119.73 (12)	N2—C12—N1	114.79 (12)
C4A—C3A—C2A	118.94 (14)	N2—C13—C14	113.73 (14)
C4A—C3A—H3A	120.5	N2—C13—H13A	108.8
C2A—C3A—H3A	120.5	C14—C13—H13A	108.8
C4A—C3B—C2B	118.47 (14)	N2—C13—H13B	108.8
C4A—C3B—H3B	120.8	C14—C13—H13B	108.8
C2B—C3B—H3B	120.8	H13A—C13—H13B	107.7
O2—C4—C3	120.34 (13)	C15—C14—C13	179.05 (18)
O2—C4—C5	120.36 (13)	C14—C15—H15	176.0 (15)
C3—C4—C5	119.28 (12)	C12—N1—C11	120.22 (12)

C3A—C4A—C3B	121.82 (14)	C12—N1—H1	116.63 (13)
C3A—C4A—Cl1	118.92 (12)	C11—N1—H1	115.77 (12)
C3B—C4A—Cl1	119.25 (12)	C12—N2—C13	121.29 (12)
C6—C5—C10	119.20 (14)	C12—N2—O3	11.26 (8)
C6—C5—C4	120.27 (13)	C13—N2—O3	120.59 (9)
C10—C5—C4	120.52 (13)	C12—N2—H2	118.38 (13)
C5—C6—C7	119.73 (15)	C13—N2—H2	118.60 (13)
C5—C6—H6	120.1	O3—N2—H2	114.94 (9)
C7—C6—H6	120.1	C2—O3—N2	60.54 (8)
C8—C7—C6	120.95 (15)	C2—O3—H3	114.04 (11)
C8—C7—H7	119.5	N2—O3—H3	144.89 (9)
C6—C7—H7	119.5		

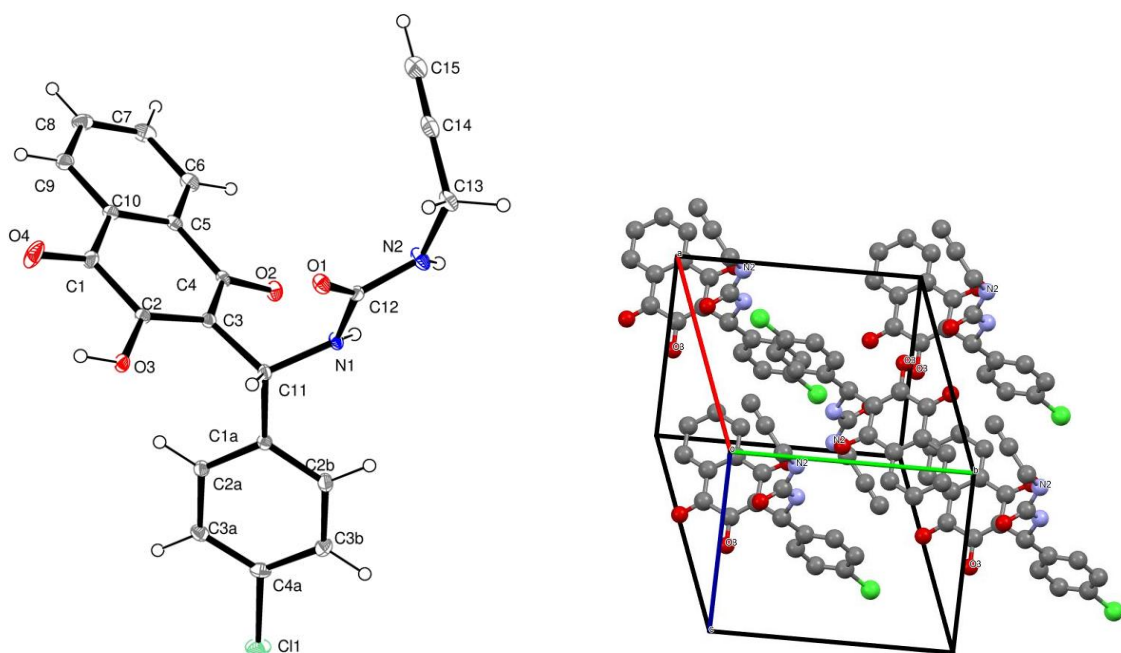
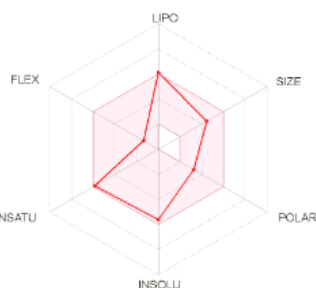
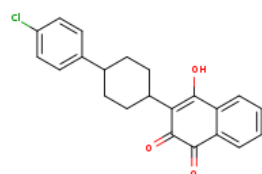


Figure A2: Crystallographic structure and crystal lattice of compound **3.61**.

3. ADME properties for synthesized compounds (generated by SwissADME)

Atovaquone (for comparison)



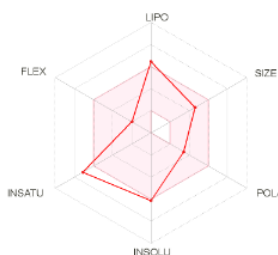
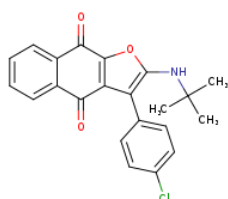
SMILES Clc1ccc(cc1)C1CCC(CC1)C1=C(O)c2c(C(=O)C1=O)cccc2

Physicochemical Properties	
Formula	C22H19ClO3
Molecular weight	366.84 g/mol
Num. heavy atoms	26
Num. arom. heavy atoms	12
Fraction Csp3	0.27
Num. rotatable bonds	2
Num. H-bond acceptors	3
Num. H-bond donors	1
Molar Refractivity	102.61
TPSA	54.37 Å²
Lipophilicity	
Log $P_{o/w}$ (iLOGP)	2.98
Log $P_{o/w}$ (XLOGP3)	5.23
Log $P_{o/w}$ (WLOGP)	5.35
Log $P_{o/w}$ (MLOGP)	3.28
Log $P_{o/w}$ (SILICOS-IT)	5.19
Consensus Log $P_{o/w}$	4.41

Water Solubility	
Log S (ESOL)	-5.62
Solubility	8.82e-04 mg/ml ; 2.41e-06 mol/l
Class	Moderately soluble
Log S (Ali)	-6.12
Solubility	2.78e-04 mg/ml ; 7.58e-07 mol/l
Class	Poorly soluble
Log S (SILICOS-IT)	-6.97
Solubility	3.97e-05 mg/ml ; 1.08e-07 mol/l
Class	Poorly soluble
Pharmacokinetics	
GI absorption	High
BBB permeant	Yes
P-gp substrate	No
CYP1A2 inhibitor	Yes
CYP2C19 inhibitor	Yes
CYP2C9 inhibitor	Yes
CYP2D6 inhibitor	No
CYP3A4 inhibitor	Yes
Log K_p (skin permeation)	-4.82 cm/s
Druglikeness	
Lipinski	Yes; 0 violation
Ghose	Yes
Veber	Yes
Egan	Yes
Muegge	No; 1 violation: XLOGP3>5
Bioavailability Score	0.85
Medicinal Chemistry	
PAINS	2 alerts: imine_one_A, quinone_D
Brenk	1 alert: diketo_group
Leadlikeness	No; 2 violations: MW>350, XLOGP3>3.5
Synthetic accessibility	4.07

3.1 Naphthofuroquinones

Compound 2.69

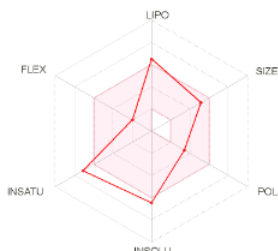
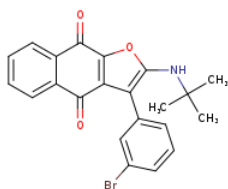


SMILES Cc1ccc(cc1)c1c(oc2c1C(=O)c1ccccc1C2=O)NC(C)(C)C

Physicochemical Properties	
Formula	C ₂₂ H ₁₈ ClNO ₃
Molecular weight	379.84 g/mol
Num. heavy atoms	27
Num. arom. heavy atoms	17
Fraction Csp ³	0.18
Num. rotatable bonds	3
Num. H-bond acceptors	3
Num. H-bond donors	1
Molar Refractivity	106.23
TPSA	59.31 Å ²
Lipophilicity	
Log <i>P</i> _{o/w} (ILOGP)	3.36
Log <i>P</i> _{o/w} (XLOGP3)	5.82
Log <i>P</i> _{o/w} (WLOGP)	5.40
Log <i>P</i> _{o/w} (MLOGP)	2.99
Log <i>P</i> _{o/w} (SILICOS-IT)	5.66
Consensus Log <i>P</i> _{o/w}	4.65

Water Solubility	
Log S (ESOL)	-6.13
Solubility	2.82e-04 mg/ml ; 7.42e-07 mol/l
Class	Poorly soluble
Log S (Ali)	-6.84
Solubility	5.54e-05 mg/ml ; 1.46e-07 mol/l
Class	Poorly soluble
Log S (SILICOS-IT)	-8.79
Solubility	6.16e-07 mg/ml ; 1.62e-09 mol/l
Class	Poorly soluble
Pharmacokinetics	
GI absorption	High
BBB permeant	Yes
P-gp substrate	No
CYP1A2 inhibitor	Yes
CYP2C19 inhibitor	Yes
CYP2C9 inhibitor	Yes
CYP2D6 inhibitor	No
CYP3A4 inhibitor	Yes
Log <i>K</i> _p (skin permeation)	-4.48 cm/s
Druglikeness	
Lipinski	Yes; 0 violation
Ghose	Yes
Veber	Yes
Egan	Yes
Muegge	No; 1 violation: XLOGP3>5
Bioavailability Score	0.55
Medicinal Chemistry	
PAINS	1 alert: quinone_A
Brenk	0 alert
Leadlikeness	No; 2 violations: MW>350, XLOGP3>3.5
Synthetic accessibility	3.80

Compound 2.73

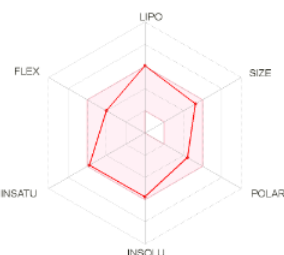
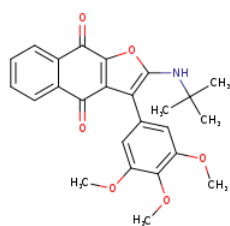


SMILES Brc1ccc(c1)c1c(oc2c1C(=O)c1ccccc1C2=O)NC(C)(C)C

Physicochemical Properties	
Formula	C ₂₂ H ₁₈ BrNO ₃
Molecular weight	424.29 g/mol
Num. heavy atoms	27
Num. arom. heavy atoms	17
Fraction Csp ³	0.18
Num. rotatable bonds	3
Num. H-bond acceptors	3
Num. H-bond donors	1
Molar Refractivity	108.92
TPSA	59.31 Å ²
Lipophilicity	
Log <i>P</i> _{o/w} (ILOGP)	3.45
Log <i>P</i> _{o/w} (XLOGP3)	5.89
Log <i>P</i> _{o/w} (WLOGP)	5.50
Log <i>P</i> _{o/w} (MLOGP)	3.10
Log <i>P</i> _{o/w} (SILICOS-IT)	5.70
Consensus Log <i>P</i> _{o/w}	4.73

Water Solubility	
Log S (ESOL)	-6.45
Solubility	1.51e-04 mg/ml ; 3.55e-07 mol/l
Class	Poorly soluble
Log S (Ali)	-6.91
Solubility	5.23e-05 mg/ml ; 1.23e-07 mol/l
Class	Poorly soluble
Log S (SILICOS-IT)	-8.99
Solubility	4.36e-07 mg/ml ; 1.03e-09 mol/l
Class	Poorly soluble
Pharmacokinetics	
GI absorption	High
BBB permeant	No
P-gp substrate	No
CYP1A2 inhibitor	Yes
CYP2C19 inhibitor	Yes
CYP2C9 inhibitor	Yes
CYP2D6 inhibitor	No
CYP3A4 inhibitor	No
Log <i>K</i> _p (skin permeation)	-4.71 cm/s
Druglikeness	
Lipinski	Yes; 0 violation
Ghose	Yes
Veber	Yes
Egan	Yes
Muegge	No; 1 violation: XLOGP3>5
Bioavailability Score	0.55
Medicinal Chemistry	
PAINS	1 alert: quinone_A
Brenk	0 alert
Leadlikeness	No; 2 violations: MW>350, XLOGP3>3.5
Synthetic accessibility	3.85

Compound 2.74

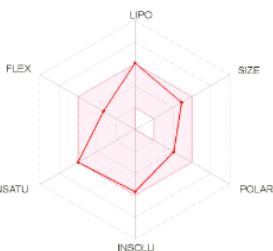
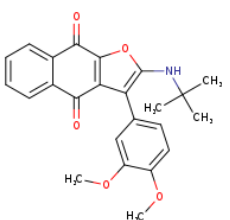


SMILES COC1cc(cc(c1OC)OC)c1c(cc2c1C(=O)c1ccccc1C2=O)NC(C)(C)C

Physicochemical Properties	
Formula	C25H25NO6
Molecular weight	435.47 g/mol
Num. heavy atoms	32
Num. arom. heavy atoms	17
Fraction Csp3	0.28
Num. rotatable bonds	6
Num. H-bond acceptors	6
Num. H-bond donors	1
Molar Refractivity	120.69
TPSA	87.00 Å ²
Lipophilicity	
Log P_{ow} (ILOGP)	3.79
Log P_{ow} (XLOGP3)	5.11
Log P_{ow} (WLOGP)	4.77
Log P_{ow} (MLOGP)	1.50
Log P_{ow} (SILICOS-IT)	5.23
Consensus Log P_{ow}	4.08

Water Solubility	
Log S (ESOL)	-5.76
Solubility	7.63e-04 mg/ml ; 1.75e-06 mol/l
Class	Moderately soluble
Log S (Ali)	-6.68
Solubility	9.08e-05 mg/ml ; 2.09e-07 mol/l
Class	Poorly soluble
Log S (SILICOS-IT)	-8.51
Solubility	1.35e-06 mg/ml ; 3.10e-09 mol/l
Class	Poorly soluble
Pharmacokinetics	
GI absorption	High
BBB permeant	No
P-gp substrate	No
CYP1A2 inhibitor	No
CYP2C19 inhibitor	Yes
CYP2C9 inhibitor	Yes
CYP2D6 inhibitor	No
CYP3A4 inhibitor	Yes
Log K_p (skin permeation)	-5.33 cm/s
Druglikeness	
Lipinski	Yes; 0 violation
Ghose	Yes
Veber	Yes
Egan	Yes
Muegge	No; 1 violation: XLOGP3>5
Bioavailability Score	0.55
Medicinal Chemistry	
PAINS	1 alert: quinone_A
Brenk	0 alert
Leadlikeness	No; 2 violations: MW>350, XLOGP3>3.5
Synthetic accessibility	4.20

Compound 2.75

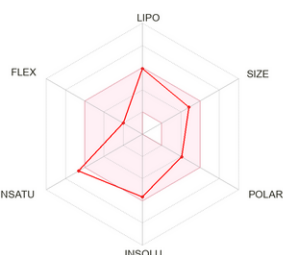
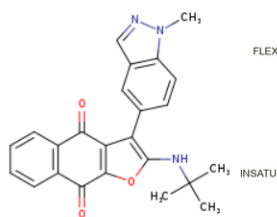


SMILES COC1cc(ccc1OC)c1c(cc2c1C(=O)c1ccccc1C2=O)NC(C)(C)C

Physicochemical Properties	
Formula	C24H23NO5
Molecular weight	405.44 g/mol
Num. heavy atoms	30
Num. arom. heavy atoms	17
Fraction Csp3	0.25
Num. rotatable bonds	5
Num. H-bond acceptors	5
Num. H-bond donors	1
Molar Refractivity	114.20
TPSA	77.77 Å ²
Lipophilicity	
Log P_{ow} (ILOGP)	3.61
Log P_{ow} (XLOGP3)	5.14
Log P_{ow} (WLOGP)	4.76
Log P_{ow} (MLOGP)	1.83
Log P_{ow} (SILICOS-IT)	5.15
Consensus Log P_{ow}	4.10

Water Solubility	
Log S (ESOL)	-5.68
Solubility	8.45e-04 mg/ml ; 2.08e-06 mol/l
Class	Moderately soluble
Log S (Ali)	-6.52
Solubility	1.23e-04 mg/ml ; 3.03e-07 mol/l
Class	Poorly soluble
Log S (SILICOS-IT)	-8.41
Solubility	1.58e-06 mg/ml ; 3.91e-09 mol/l
Class	Poorly soluble
Pharmacokinetics	
GI absorption	High
BBB permeant	No
P-gp substrate	No
CYP1A2 inhibitor	Yes
CYP2C19 inhibitor	Yes
CYP2C9 inhibitor	Yes
CYP2D6 inhibitor	No
CYP3A4 inhibitor	Yes
Log K_p (skin permeation)	-5.12 cm/s
Druglikeness	
Lipinski	Yes; 0 violation
Ghose	Yes
Veber	Yes
Egan	Yes
Muegge	No; 1 violation: XLOGP3>5
Bioavailability Score	0.55
Medicinal Chemistry	
PAINS	1 alert: quinone_A
Brenk	0 alert
Leadlikeness	No; 2 violations: MW>350, XLOGP3>3.5
Synthetic accessibility	4.04

Compound 2.76

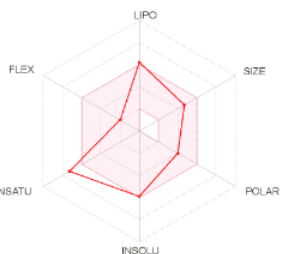
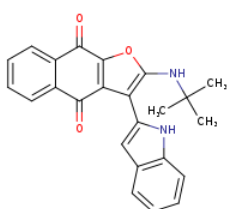


SMILES O=C1c2c(c(cc2C(=O)c2c1cccc2)NC(C)(C)C)c1ccc2c(c1)cnn2C

Physicochemical Properties	
Formula	C24H21N3O3
Molecular weight	399.44 g/mol
Num. heavy atoms	30
Num. arom. heavy atoms	20
Fraction Csp3	0.21
Num. rotatable bonds	3
Num. H-bond acceptors	4
Num. H-bond donors	1
Molar Refractivity	115.77
TPSA	77.13 Å ²
Lipophilicity	
Log <i>P</i> _{ow} (iLOGP)	3.12
Log <i>P</i> _{ow} (XLOGP3)	4.84
Log <i>P</i> _{ow} (WLOGP)	4.63
Log <i>P</i> _{ow} (MLOGP)	2.23
Log <i>P</i> _{ow} (SILICOS-IT)	4.47
Consensus Log <i>P</i> _{ow}	3.86

Water Solubility	
Log S (ESOL)	-5.66
Solubility	8.72e-04 mg/ml ; 2.18e-06 mol/l
Class	Moderately soluble
Log S (Ali)	-6.19
Solubility	2.56e-04 mg/ml ; 6.41e-07 mol/l
Class	Poorly soluble
Log S (SILICOS-IT)	-8.23
Solubility	2.33e-06 mg/ml ; 5.83e-09 mol/l
Class	Poorly soluble
Pharmacokinetics	
GI absorption	High
BBB permeant	No
P-gp substrate	Yes
CYP1A2 inhibitor	Yes
CYP2C19 inhibitor	Yes
CYP2C9 inhibitor	Yes
CYP2D6 inhibitor	No
CYP3A4 inhibitor	Yes
Log <i>K</i> _p (skin permeation)	-5.30 cm/s
Druglikeness	
Lipinski	Yes; 0 violation
Ghose	Yes
Weber	Yes
Egan	Yes
Muegge	Yes
Bioavailability Score	0.55
Medicinal Chemistry	
PAINS	1 alert: quinone_A
Brenk	0 alert
Leadlikeness	No; 2 violations: MW>350, XLOGP3>3.5
Synthetic accessibility	3.87

Compound 2.77

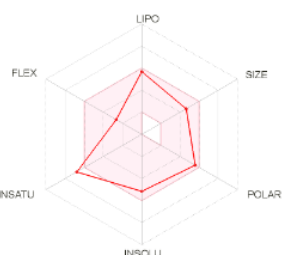
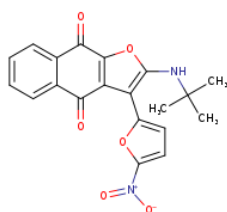


SMILES O=C1c2c(cc2c2cc3c([nH]2)cccc3)NC(C)(C)C(=O)c2c1cccc2

Physicochemical Properties	
Formula	C24H20N2O3
Molecular weight	384.43 g/mol
Num. heavy atoms	29
Num. arom. heavy atoms	20
Fraction Csp3	0.17
Num. rotatable bonds	3
Num. H-bond acceptors	3
Num. H-bond donors	2
Molar Refractivity	113.07
TPSA	75.10 Å ²
Lipophilicity	
Log <i>P</i> _{ow} (iLOGP)	3.31
Log <i>P</i> _{ow} (XLOGP3)	5.36
Log <i>P</i> _{ow} (WLOGP)	5.22
Log <i>P</i> _{ow} (MLOGP)	2.23
Log <i>P</i> _{ow} (SILICOS-IT)	5.57
Consensus Log <i>P</i> _{ow}	4.34

Water Solubility	
Log S (ESOL)	-5.91
Solubility	4.70e-04 mg/ml ; 1.22e-06 mol/l
Class	Moderately soluble
Log S (Ali)	-6.69
Solubility	7.84e-05 mg/ml ; 2.04e-07 mol/l
Class	Poorly soluble
Log S (SILICOS-IT)	-9.06
Solubility	3.37e-07 mg/ml ; 8.77e-10 mol/l
Class	Poorly soluble
Pharmacokinetics	
GI absorption	High
BBB permeant	No
P-gp substrate	Yes
CYP1A2 inhibitor	Yes
CYP2C19 inhibitor	Yes
CYP2C9 inhibitor	Yes
CYP2D6 inhibitor	No
CYP3A4 inhibitor	Yes
Log <i>K</i> _p (skin permeation)	-4.84 cm/s
Druglikeness	
Lipinski	Yes; 0 violation
Ghose	Yes
Weber	Yes
Egan	Yes
Muegge	No; 1 violation: XLOGP3>5
Bioavailability Score	0.55
Medicinal Chemistry	
PAINS	1 alert: quinone_A
Brenk	0 alert
Leadlikeness	No; 2 violations: MW>350, XLOGP3>3.5
Synthetic accessibility	3.93

Compound 2.78



SMILES O=C1c2c(c(oc2C(=O)c2c1cccc2)NC(C)(C)C)ccc(O1)[N+](=O)[O-]

Physicochemical Properties

Formula	C20H16N2O6
Molecular weight	380.35 g/mol
Num. heavy atoms	28
Num. arom. heavy atoms	16
Fraction Csp3	0.20
Num. rotatable bonds	4
Num. H-bond acceptors	6
Num. H-bond donors	1
Molar Refractivity	102.30
TPSA	118.27 Å²

Lipophilicity

Log $P_{o/w}$ (ILOGP)	2.31
Log $P_{o/w}$ (XLOGP3)	4.46
Log $P_{o/w}$ (WLOGP)	4.24
Log $P_{o/w}$ (MLOGP)	1.17
Log $P_{o/w}$ (SILICOS-IT)	2.24
Consensus Log $P_{o/w}$	2.88

Water Solubility

Log S (ESOL)	-5.17
Solubility	2.59e-03 mg/ml ; 6.81e-06 mol/l
Class	Moderately soluble
Log S (Ali)	-6.66
Solubility	8.26e-05 mg/ml ; 2.17e-07 mol/l
Class	Poorly soluble
Log S (SILICOS-IT)	-6.77
Solubility	6.49e-05 mg/ml ; 1.71e-07 mol/l
Class	Poorly soluble

Pharmacokinetics

GI absorption	High
BBB permeant	No
P-gp substrate	No
CYP1A2 inhibitor	Yes
CYP2C19 inhibitor	Yes
CYP2C9 inhibitor	Yes
CYP2D6 inhibitor	No
CYP3A4 inhibitor	Yes
Log K_p (skin permeation)	-5.45 cm/s

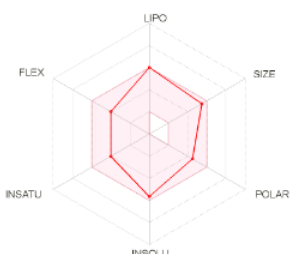
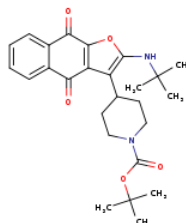
Druglikeness

Lipinski	Yes; 0 violation
Ghose	Yes
Veber	Yes
Egan	Yes
Muegge	Yes
Bioavailability Score	0.55

Medicinal Chemistry

PAINS	1 alert: quinone_A
Brenk	2 alerts: nitro_group, oxygen-nitrogen_single_bond
Leadlikeness	No; 2 violations: MW>350, XLOGP3>3.5
Synthetic accessibility	4.02

Compound 2.79



SMILES O=C(N1CCC(CC1)c1c(oc2c1C(=O)c1cccc1C2=O)NC(C)(C)OC(C)(C)C

Physicochemical Properties

Formula	C26H32N2O5
Molecular weight	452.54 g/mol
Num. heavy atoms	33
Num. arom. heavy atoms	11
Fraction Csp3	0.50
Num. rotatable bonds	6
Num. H-bond acceptors	5
Num. H-bond donors	1
Molar Refractivity	130.42
TPSA	88.85 Å²

Lipophilicity

Log $P_{o/w}$ (ILOGP)	4.21
Log $P_{o/w}$ (XLOGP3)	4.99
Log $P_{o/w}$ (WLOGP)	4.81
Log $P_{o/w}$ (MLOGP)	2.27
Log $P_{o/w}$ (SILICOS-IT)	4.48
Consensus Log $P_{o/w}$	4.15

Water Solubility

Log S (ESOL)	-5.64
Solubility	1.04e-03 mg/ml ; 2.29e-06 mol/l
Class	Moderately soluble
Log S (Ali)	-6.60
Solubility	1.15e-04 mg/ml ; 2.54e-07 mol/l
Class	Poorly soluble
Log S (SILICOS-IT)	-6.99
Solubility	4.68e-05 mg/ml ; 1.04e-07 mol/l
Class	Poorly soluble

Pharmacokinetics

GI absorption	High
BBB permeant	No
P-gp substrate	Yes
CYP1A2 inhibitor	No
CYP2C19 inhibitor	Yes
CYP2C9 inhibitor	Yes
CYP2D6 inhibitor	No
CYP3A4 inhibitor	Yes
Log K_p (skin permeation)	-5.52 cm/s

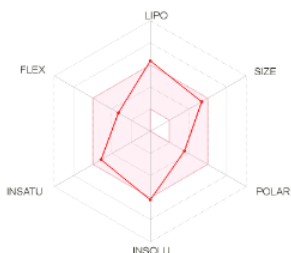
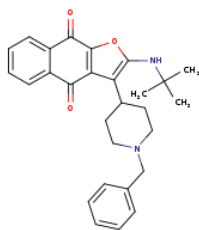
Druglikeness

Lipinski	Yes; 0 violation
Ghose	No; 1 violation: MR>130
Veber	Yes
Egan	Yes
Muegge	Yes
Bioavailability Score	0.55

Medicinal Chemistry

PAINS	1 alert: quinone_A
Brenk	0 alert
Leadlikeness	No; 2 violations: MW>350, XLOGP3>3.5
Synthetic accessibility	4.37

Compound 2.80

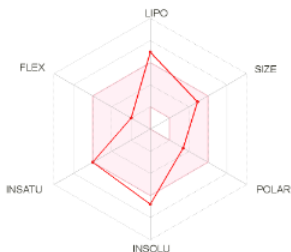
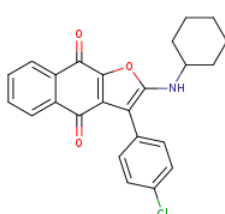


SMILES O=C1c2c(C3CCN(CC3)C)cccc2)c(=O)c2c1cccc2)NC(C)(C)C

Physicochemical Properties	
Formula	C ₂₈ H ₃₀ N ₂ O ₃
Molecular weight	442.55 g/mol
Num. heavy atoms	33
Num. arom. heavy atoms	17
Fraction Csp ³	0.36
Num. rotatable bonds	5
Num. H-bond acceptors	4
Num. H-bond donors	1
Molar Refractivity	133.96
TPSA	62.55 Å ²
Lipophilicity	
Log <i>P</i> _{o/w} (ILOGP)	3.90
Log <i>P</i> _{o/w} (XLOGP3)	5.64
Log <i>P</i> _{o/w} (WLOGP)	4.92
Log <i>P</i> _{o/w} (MLOGP)	2.92
Log <i>P</i> _{o/w} (SILICOS-IT)	5.57
Consensus Log <i>P</i> _{o/w}	4.59

Water Solubility	
Log S (ESOL)	-6.19
Solubility	2.87e-04 mg/ml ; 6.48e-07 mol/l
Class	Poorly soluble
Log S (Ali)	-6.72
Solubility	8.48e-05 mg/ml ; 1.92e-07 mol/l
Class	Poorly soluble
Log S (SILICOS-IT)	-9.02
Solubility	4.26e-07 mg/ml ; 9.62e-10 mol/l
Class	Poorly soluble
Pharmacokinetics	
GI absorption	High
BBB permeant	Yes
P-gp substrate	Yes
CYP1A2 inhibitor	No
CYP2C19 inhibitor	Yes
CYP2C9 inhibitor	Yes
CYP2D6 inhibitor	No
CYP3A4 inhibitor	Yes
Log <i>K</i> _p (skin permeation)	-5.00 cm/s
Druglikeness	
Lipinski	Yes; 0 violation
Ghose	No; 1 violation: MR>130
Veber	Yes
Egan	Yes
Muegge	No; 1 violation: XLOGP3>5
Bioavailability Score	0.55
Medicinal Chemistry	
PAINS	1 alert: quinone_A
Brenk	0 alert
Leadlikeness	No; 2 violations: MW>350, XLOGP3>3.5
Synthetic accessibility	4.64

Compound 2.81

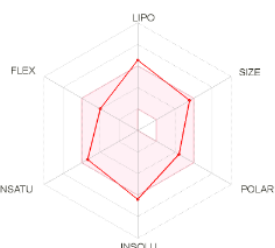
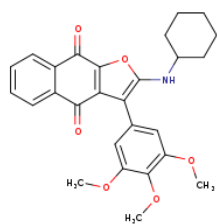


SMILES Clc1ccc(cc1)c1c(NC2CCCC2)oc2c1C(=O)c1cccc1C2=O

Physicochemical Properties	
Formula	C ₂₄ H ₂₀ ClNO ₃
Molecular weight	405.87 g/mol
Num. heavy atoms	29
Num. arom. heavy atoms	17
Fraction Csp ³	0.25
Num. rotatable bonds	3
Num. H-bond acceptors	3
Num. H-bond donors	1
Molar Refractivity	113.69
TPSA	59.31 Å ²
Lipophilicity	
Log <i>P</i> _{o/w} (ILOGP)	3.63
Log <i>P</i> _{o/w} (XLOGP3)	6.65
Log <i>P</i> _{o/w} (WLOGP)	5.93
Log <i>P</i> _{o/w} (MLOGP)	3.41
Log <i>P</i> _{o/w} (SILICOS-IT)	5.97
Consensus Log <i>P</i> _{o/w}	5.12

Water Solubility	
Log S (ESOL)	-6.78
Solubility	6.71e-05 mg/ml ; 1.65e-07 mol/l
Class	Poorly soluble
Log S (Ali)	-7.70
Solubility	8.15e-06 mg/ml ; 2.01e-08 mol/l
Class	Poorly soluble
Log S (SILICOS-IT)	-8.99
Solubility	4.11e-07 mg/ml ; 1.01e-09 mol/l
Class	Poorly soluble
Pharmacokinetics	
GI absorption	High
BBB permeant	No
P-gp substrate	Yes
CYP1A2 inhibitor	Yes
CYP2C19 inhibitor	Yes
CYP2C9 inhibitor	Yes
CYP2D6 inhibitor	No
CYP3A4 inhibitor	No
Log <i>K</i> _p (skin permeation)	-4.05 cm/s
Druglikeness	
Lipinski	Yes; 0 violation
Ghose	No; 1 violation: WLOGP>5.6
Veber	Yes
Egan	No; 1 violation: WLOGP>5.88
Muegge	No; 1 violation: XLOGP3>5
Bioavailability Score	0.55
Medicinal Chemistry	
PAINS	1 alert: quinone_A
Brenk	0 alert
Leadlikeness	No; 2 violations: MW>350, XLOGP3>3.5
Synthetic accessibility	3.89

Compound 2.82

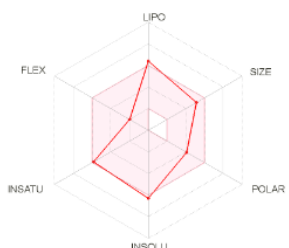
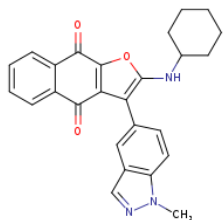


SMILES COc1cc(cc1OC)OC1c1c(NC2CCCC2)oc2c1C(=O)c1cccc1C2=O

Physicochemical Properties	
Formula	C27H27NO6
Molecular weight	461.51 g/mol
Num. heavy atoms	34
Num. arom. heavy atoms	17
Fraction Csp3	0.33
Num. rotatable bonds	6
Num. H-bond acceptors	6
Num. H-bond donors	1
Molar Refractivity	128.15
TPSA	87.00 Å²
Lipophilicity	
Log P_{ow} (ILOGP)	3.97
Log P_{ow} (XLOGP3)	5.93
Log P_{ow} (WLOGP)	5.30
Log P_{ow} (MLOGP)	1.91
Log P_{ow} (SILICOS-IT)	5.51
Consensus Log P_{ow}	4.52

Water Solubility	
Log S (ESOL)	-6.41
Solubility	1.79e-04 mg/ml ; 3.88e-07 mol/l
Class	Poorly soluble
Log S (Ali)	-7.53
Solubility	1.36e-05 mg/ml ; 2.94e-08 mol/l
Class	Poorly soluble
Log S (SILICOS-IT)	-8.71
Solubility	9.02e-07 mg/ml ; 1.95e-09 mol/l
Class	Poorly soluble
Pharmacokinetics	
GI absorption	High
BBB permeant	No
P-gp substrate	Yes
CYP1A2 inhibitor	No
CYP2C19 inhibitor	Yes
CYP2C9 inhibitor	Yes
CYP2D6 inhibitor	No
CYP3A4 inhibitor	No
Log K_p (skin permeation)	-4.90 cm/s
Druglikeness	
Lipinski	Yes; 0 violation
Ghose	Yes
Weber	Yes
Egan	Yes
Muegge	No; 1 violation: XLOGP3>5
Bioavailability Score	0.55
Medicinal Chemistry	
PAINS	1 alert: quinone_A
Brenk	0 alert
Leadlikeness	No; 2 violations: MW>350, XLOGP3>3.5
Synthetic accessibility	4.31

Compound 2.83

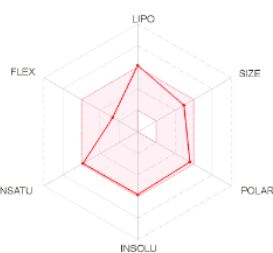
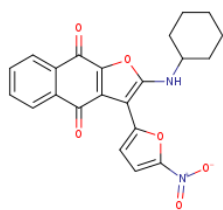


SMILES O=C1c2c(c(oc2C(=O)c1cccc2)NC1CCCC1)c1ccc2c(c1)cnn2C

Physicochemical Properties	
Formula	C26H23N3O3
Molecular weight	425.48 g/mol
Num. heavy atoms	32
Num. arom. heavy atoms	20
Fraction Csp3	0.27
Num. rotatable bonds	3
Num. H-bond acceptors	4
Num. H-bond donors	1
Molar Refractivity	123.23
TPSA	77.13 Å²
Lipophilicity	
Log P_{ow} (ILOGP)	3.34
Log P_{ow} (XLOGP3)	5.67
Log P_{ow} (WLOGP)	5.16
Log P_{ow} (MLOGP)	2.64
Log P_{ow} (SILICOS-IT)	4.75
Consensus Log P_{ow}	4.31

Water Solubility	
Log S (ESOL)	-6.31
Solubility	2.06e-04 mg/ml ; 4.85e-07 mol/l
Class	Poorly soluble
Log S (Ali)	-7.05
Solubility	3.75e-05 mg/ml ; 8.82e-08 mol/l
Class	Poorly soluble
Log S (SILICOS-IT)	-8.44
Solubility	1.56e-06 mg/ml ; 3.66e-09 mol/l
Class	Poorly soluble
Pharmacokinetics	
GI absorption	High
BBB permeant	No
P-gp substrate	Yes
CYP1A2 inhibitor	Yes
CYP2C19 inhibitor	Yes
CYP2C9 inhibitor	Yes
CYP2D6 inhibitor	No
CYP3A4 inhibitor	No
Log K_p (skin permeation)	-4.87 cm/s
Druglikeness	
Lipinski	Yes; 0 violation
Ghose	Yes
Weber	Yes
Egan	Yes
Muegge	No; 1 violation: XLOGP3>5
Bioavailability Score	0.55
Medicinal Chemistry	
PAINS	1 alert: quinone_A
Brenk	0 alert
Leadlikeness	No; 2 violations: MW>350, XLOGP3>3.5
Synthetic accessibility	4.00

Compound 2.84

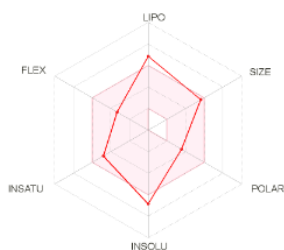
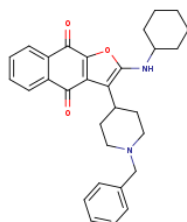


SMILES [O-][N+](=O)c1ccc(o1)c1c(NC2CCCC2)oc2c1C(=O)c1ccccc1C2=O

Physicochemical Properties	
Formula	C22H18N2O6
Molecular weight	406.39 g/mol
Num. heavy atoms	30
Num. arom. heavy atoms	16
Fraction Csp3	0.27
Num. rotatable bonds	4
Num. H-bond acceptors	6
Num. H-bond donors	1
Molar Refractivity	109.77
TPSA	118.27 Å²
Lipophilicity	
Log P_{ow} (iLOGP)	2.76
Log P_{ow} (XLOGP3)	5.28
Log P_{ow} (WLOGP)	4.78
Log P_{ow} (MLOGP)	1.61
Log P_{ow} (SILICOS-IT)	2.54
Consensus Log P_{ow}	3.39

Water Solubility	
Log S (ESOL)	-5.82
Solubility	6.20e-04 mg/ml ; 1.53e-06 mol/l
Class	Moderately soluble
Log S (Ali)	-7.51
Solubility	1.24e-05 mg/ml ; 3.06e-08 mol/l
Class	Poorly soluble
Log S (SILICOS-IT)	-6.97
Solubility	4.33e-05 mg/ml ; 1.07e-07 mol/l
Class	Poorly soluble
Pharmacokinetics	
GI absorption	Low
BBB permeant	No
P-gp substrate	No
CYP1A2 inhibitor	Yes
CYP2C19 inhibitor	Yes
CYP2C9 inhibitor	Yes
CYP2D6 inhibitor	No
CYP3A4 inhibitor	Yes
Log K_p (skin permeation)	-5.03 cm/s
Druglikeness	
Lipinski	Yes; 0 violation
Ghose	Yes
Veber	Yes
Egan	Yes
Muegge	No; 1 violation: XLOGP3>5
Bioavailability Score	0.55
Medicinal Chemistry	
PAINS	1 alert: quinone_A
Brenk	2 alerts: nitro_group, oxygen-nitrogen_single_bond
Leadlikeness	No; 2 violations: MW>350, XLOGP3>3.5
Synthetic accessibility	4.11

Compound 2.85

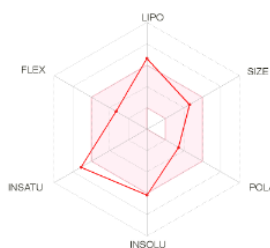
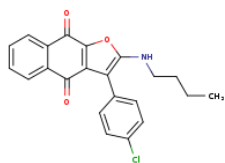


SMILES O=C1c2c(C3CCN(CC3)C3CCCC3)c(oc2C(=O)c2c1cccc2)NC1CCC1

Physicochemical Properties	
Formula	C30H32N2O3
Molecular weight	468.59 g/mol
Num. heavy atoms	35
Num. arom. heavy atoms	17
Fraction Csp3	0.40
Num. rotatable bonds	5
Num. H-bond acceptors	4
Num. H-bond donors	1
Molar Refractivity	141.43
TPSA	62.55 Å²
Lipophilicity	
Log P_{ow} (iLOGP)	4.11
Log P_{ow} (XLOGP3)	6.47
Log P_{ow} (WLOGP)	5.46
Log P_{ow} (MLOGP)	3.30
Log P_{ow} (SILICOS-IT)	5.83
Consensus Log P_{ow}	5.03

Water Solubility	
Log S (ESOL)	-6.85
Solubility	6.61e-05 mg/ml ; 1.41e-07 mol/l
Class	Poorly soluble
Log S (Ali)	-7.58
Solubility	1.24e-05 mg/ml ; 2.64e-08 mol/l
Class	Poorly soluble
Log S (SILICOS-IT)	-9.22
Solubility	2.85e-07 mg/ml ; 6.08e-10 mol/l
Class	Poorly soluble
Pharmacokinetics	
GI absorption	High
BBB permeant	No
P-gp substrate	Yes
CYP1A2 inhibitor	No
CYP2C19 inhibitor	Yes
CYP2C9 inhibitor	Yes
CYP2D6 inhibitor	Yes
CYP3A4 inhibitor	Yes
Log K_p (skin permeation)	-4.56 cm/s
Druglikeness	
Lipinski	Yes; 0 violation
Ghose	No; 1 violation: MR>130
Veber	Yes
Egan	Yes
Muegge	No; 1 violation: XLOGP3>5
Bioavailability Score	0.55
Medicinal Chemistry	
PAINS	1 alert: quinone_A
Brenk	0 alert
Leadlikeness	No; 2 violations: MW>350, XLOGP3>3.5
Synthetic accessibility	4.81

Compound 2.86

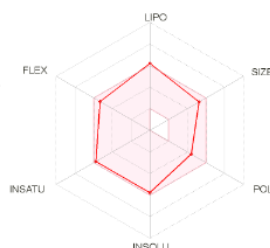
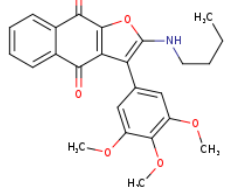


SMILES CCCCNc1oc2c(c1c1ccc(cc1)Cl)C(=O)c1c(C2=O)cccc1

Physicochemical Properties	
Formula	C ₂₂ H ₁₈ ClNO ₃
Molecular weight	379.84 g/mol
Num. heavy atoms	27
Num. arom. heavy atoms	17
Fraction Csp ³	0.18
Num. rotatable bonds	5
Num. H-bond acceptors	3
Num. H-bond donors	1
Molar Refractivity	106.19
TPSA	59.31 Å ²
Lipophilicity	
Log <i>P</i> _{ow} (iLOGP)	3.50
Log <i>P</i> _{ow} (XLOGP3)	6.09
Log <i>P</i> _{ow} (WLOGP)	5.40
Log <i>P</i> _{ow} (MLOGP)	2.99
Log <i>P</i> _{ow} (SILICOS-IT)	5.99
Consensus Log <i>P</i> _{ow}	4.79

Water Solubility	
Log S (ESOL)	-6.17
Solubility	2.58e-04 mg/ml ; 6.80e-07 mol/l
Class	Poorly soluble
Log S (Ali)	-7.12
Solubility	2.91e-05 mg/ml ; 7.65e-08 mol/l
Class	Poorly soluble
Log S (SILICOS-IT)	-9.18
Solubility	2.50e-07 mg/ml ; 6.59e-10 mol/l
Class	Poorly soluble
Pharmacokinetics	
GI absorption	High
BBB permeant	Yes
P-gp substrate	No
CYP1A2 inhibitor	Yes
CYP2C19 inhibitor	Yes
CYP2C9 inhibitor	Yes
CYP2D6 inhibitor	No
CYP3A4 inhibitor	Yes
Log <i>K</i> _p (skin permeation)	-4.29 cm/s
Druglikeness	
Lipinski	Yes; 0 violation
Ghose	Yes
Veber	Yes
Egan	Yes
Muegge	No; 1 violation: XLOGP3>5
Bioavailability Score	0.55
Medicinal Chemistry	
PAINS	1 alert: quinone_A
Brenk	0 alert
Leadlikeness	No; 2 violations: MW>350, XLOGP3>3.5
Synthetic accessibility	3.77

Compound 2.87

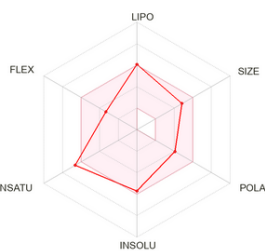
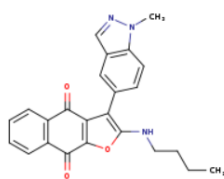


SMILES CCCCNc1oc2c(c1c1cc(OC)c(c1)OC)OC(C(=O)c1c(C2=O)cccc1

Physicochemical Properties	
Formula	C ₂₅ H ₂₅ NO ₆
Molecular weight	435.47 g/mol
Num. heavy atoms	32
Num. arom. heavy atoms	17
Fraction Csp ³	0.28
Num. rotatable bonds	8
Num. H-bond acceptors	6
Num. H-bond donors	1
Molar Refractivity	120.65
TPSA	87.00 Å ²
Lipophilicity	
Log <i>P</i> _{ow} (iLOGP)	3.93
Log <i>P</i> _{ow} (XLOGP3)	5.37
Log <i>P</i> _{ow} (WLOGP)	4.77
Log <i>P</i> _{ow} (MLOGP)	1.50
Log <i>P</i> _{ow} (SILICOS-IT)	5.56
Consensus Log <i>P</i> _{ow}	4.23

Water Solubility	
Log S (ESOL)	-5.79
Solubility	7.09e-04 mg/ml ; 1.63e-06 mol/l
Class	Moderately soluble
Log S (Ali)	-6.95
Solubility	4.88e-05 mg/ml ; 1.12e-07 mol/l
Class	Poorly soluble
Log S (SILICOS-IT)	-8.90
Solubility	5.48e-07 mg/ml ; 1.26e-09 mol/l
Class	Poorly soluble
Pharmacokinetics	
GI absorption	High
BBB permeant	No
P-gp substrate	No
CYP1A2 inhibitor	No
CYP2C19 inhibitor	Yes
CYP2C9 inhibitor	Yes
CYP2D6 inhibitor	No
CYP3A4 inhibitor	Yes
Log <i>K</i> _p (skin permeation)	-5.14 cm/s
Druglikeness	
Lipinski	Yes; 0 violation
Ghose	Yes
Veber	Yes
Egan	Yes
Muegge	No; 1 violation: XLOGP3>5
Bioavailability Score	0.55
Medicinal Chemistry	
PAINS	1 alert: quinone_A
Brenk	0 alert
Leadlikeness	No; 3 violations: MW>350, Rotors>7, XLOGP3>3.5
Synthetic accessibility	4.18

Compound 2.88

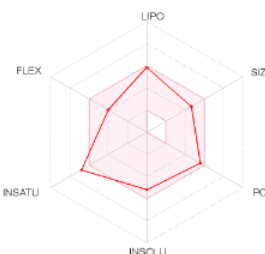
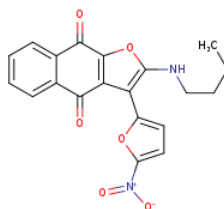


SMILES CCCCNc1oc2c(c1c1ccc3c(c1)cnn3C)C(=O)c1c(C2=O)ccc1

Physicochemical Properties	
Formula	C ₂₄ H ₂₁ N ₃ O ₃
Molecular weight	399.44 g/mol
Num. heavy atoms	30
Num. arom. heavy atoms	20
Fraction Csp ³	0.21
Num. rotatable bonds	5
Num. H-bond acceptors	4
Num. H-bond donors	1
Molar Refractivity	115.73
TPSA	77.13 Å ²
Lipophilicity	
Log <i>P</i> _{o/w} (iLOGP)	3.24
Log <i>P</i> _{o/w} (XLOGP3)	5.11
Log <i>P</i> _{o/w} (WLOGP)	4.63
Log <i>P</i> _{o/w} (MLOGP)	2.23
Log <i>P</i> _{o/w} (SILICOS-IT)	4.80
Consensus Log <i>P</i> _{o/w}	4.00

Water Solubility	
Log S (ESOL)	-5.70
Solubility	7.99e-04 mg/ml ; 2.00e-06 mol/l
Class	Moderately soluble
Log S (Ali)	-6.47
Solubility	1.34e-04 mg/ml ; 3.36e-07 mol/l
Class	Poorly soluble
Log S (SILICOS-IT)	-8.62
Solubility	9.47e-07 mg/ml ; 2.37e-09 mol/l
Class	Poorly soluble
Pharmacokinetics	
GI absorption	High
BBB permeant	No
P-gp substrate	Yes
CYP1A2 inhibitor	Yes
CYP2C19 inhibitor	Yes
CYP2C9 inhibitor	Yes
CYP2D6 inhibitor	No
CYP3A4 inhibitor	Yes
Log <i>K</i> _p (skin permeation)	-5.11 cm/s
Druglikeness	
Lipinski	Yes; 0 violation
Ghose	Yes
Weber	Yes
Egan	Yes
Muegge	No; 1 violation: XLOGP3>5
Bioavailability Score	0.55
Medicinal Chemistry	
PAINS	1 alert: quinone_A
Brenk	0 alert
Leadlikeness	No; 2 violations: MW>350, XLOGP3>3.5
Synthetic accessibility	3.87

Compound 2.89

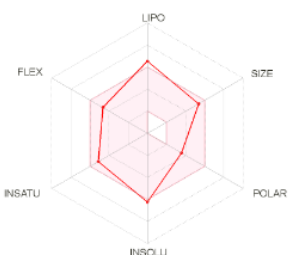
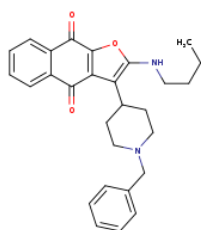


SMILES CCCCNc1oc2c(c1c1ccc(o1)[N+](=O)[O-])C(=O)c1c(C2=O)cccc1

Physicochemical Properties	
Formula	C ₂₀ H ₁₆ N ₂ O ₆
Molecular weight	380.35 g/mol
Num. heavy atoms	28
Num. arom. heavy atoms	16
Fraction Csp ³	0.20
Num. rotatable bonds	6
Num. H-bond acceptors	6
Num. H-bond donors	1
Molar Refractivity	102.27
TPSA	118.27 Å ²
Lipophilicity	
Log <i>P</i> _{o/w} (iLOGP)	2.48
Log <i>P</i> _{o/w} (XLOGP3)	4.72
Log <i>P</i> _{o/w} (WLOGP)	4.24
Log <i>P</i> _{o/w} (MLOGP)	1.17
Log <i>P</i> _{o/w} (SILICOS-IT)	2.56
Consensus Log <i>P</i> _{o/w}	3.03

Water Solubility	
Log S (ESOL)	-5.20
Solubility	2.41e-03 mg/ml ; 6.33e-06 mol/l
Class	Moderately soluble
Log S (Ali)	-6.93
Solubility	4.44e-05 mg/ml ; 1.17e-07 mol/l
Class	Poorly soluble
Log S (SILICOS-IT)	-7.16
Solubility	2.64e-05 mg/ml ; 6.93e-08 mol/l
Class	Poorly soluble
Pharmacokinetics	
GI absorption	High
BBB permeant	No
P-gp substrate	No
CYP1A2 inhibitor	Yes
CYP2C19 inhibitor	Yes
CYP2C9 inhibitor	Yes
CYP2D6 inhibitor	No
CYP3A4 inhibitor	Yes
Log <i>K</i> _p (skin permeation)	-5.27 cm/s
Druglikeness	
Lipinski	Yes; 0 violation
Ghose	Yes
Weber	Yes
Egan	Yes
Muegge	Yes
Bioavailability Score	0.55
Medicinal Chemistry	
PAINS	1 alert: quinone_A
Brenk	2 alerts: nitro_group, oxygen-nitrogen_single_bond
Leadlikeness	No; 2 violations: MW>350, XLOGP3>3.5
Synthetic accessibility	3.99

Compound 2.90



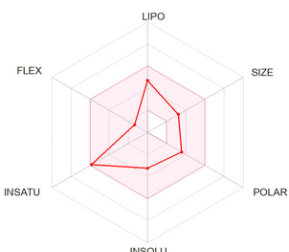
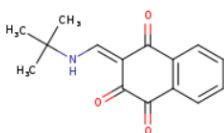
SMILES CCCCNc1oc2c(c1C1CCN(CC1)Cc1ccccc1)C(=O)c1c(C2=O)cccc1

Physicochemical Properties	
Formula	C ₂₈ H ₃₀ N ₂ O ₃
Molecular weight	442.55 g/mol
Num. heavy atoms	33
Num. arom. heavy atoms	17
Fraction Csp ³	0.36
Num. rotatable bonds	7
Num. H-bond acceptors	4
Num. H-bond donors	1
Molar Refractivity	133.93
TPSA	62.55 Å ²
Lipophilicity	
Log <i>P</i> _{o/w} (iLOGP)	4.04
Log <i>P</i> _{o/w} (XLOGP3)	5.91
Log <i>P</i> _{o/w} (WLOGP)	4.92
Log <i>P</i> _{o/w} (MLOGP)	2.92
Log <i>P</i> _{o/w} (SILICOS-IT)	5.89
Consensus Log <i>P</i> _{o/w}	4.74

Water Solubility	
Log S (ESOL)	-6.23
Solubility	2.63e-04 mg/ml ; 5.94e-07 mol/l
Class	Poorly soluble
Log S (Ali)	-7.00
Solubility	4.45e-05 mg/ml ; 1.01e-07 mol/l
Class	Poorly soluble
Log S (SILICOS-IT)	-9.41
Solubility	1.73e-07 mg/ml ; 3.91e-10 mol/l
Class	Poorly soluble
Pharmacokinetics	
GI absorption	High
BBB permeant	Yes
P-gp substrate	Yes
CYP1A2 inhibitor	No
CYP2C19 inhibitor	Yes
CYP2C9 inhibitor	Yes
CYP2D6 inhibitor	Yes
CYP3A4 inhibitor	Yes
Log <i>K</i> _p (skin permeation)	-4.80 cm/s
Druglikeness	
Lipinski	Yes; 0 violation
Ghose	No; 1 violation: MR>130
Veber	Yes
Egan	Yes
Muegge	No; 1 violation: XLOGP3>5
Bioavailability Score	0.55
Medicinal Chemistry	
PAINS	1 alert: quinone_A
Brenk	0 alert
Leadlikeness	No; 2 violations: MW>350, XLOGP3>3.5
Synthetic accessibility	4.66

3.2 Naphthoenaminones

Compound 2.91

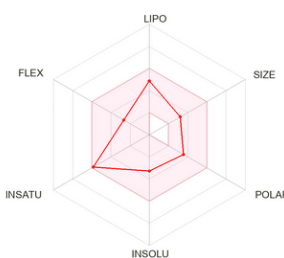
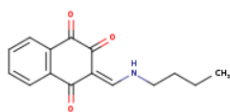


SMILES O=C1C(=O)/C(=C/N(C)C)C(C)C(=O)c2c1cccc2

Physicochemical Properties	
Formula	C ₁₅ H ₁₅ N ₃ O ₃
Molecular weight	257.28 g/mol
Num. heavy atoms	19
Num. arom. heavy atoms	6
Fraction Csp ³	0.27
Num. rotatable bonds	2
Num. H-bond acceptors	3
Num. H-bond donors	1
Molar Refractivity	71.32
TPSA	63.24 Å ²
Lipophilicity	
Log <i>P</i> _{o/w} (iLOGP)	2.00
Log <i>P</i> _{o/w} (XLOGP3)	2.73
Log <i>P</i> _{o/w} (WLOGP)	1.91
Log <i>P</i> _{o/w} (MLOGP)	0.47
Log <i>P</i> _{o/w} (SILICOS-IT)	2.86
Consensus Log <i>P</i> _{o/w}	1.99

Water Solubility	
Log S (ESOL)	-3.26
Solubility	1.42e-01 mg/ml ; 5.54e-04 mol/l
Class	Soluble
Log S (Ali)	-3.71
Solubility	4.99e-02 mg/ml ; 1.94e-04 mol/l
Class	Soluble
Log S (SILICOS-IT)	-4.47
Solubility	8.74e-03 mg/ml ; 3.40e-05 mol/l
Class	Moderately soluble
Pharmacokinetics	
GI absorption	High
BBB permeant	Yes
P-gp substrate	No
CYP1A2 inhibitor	Yes
CYP2C19 inhibitor	Yes
CYP2C9 inhibitor	No
CYP2D6 inhibitor	No
CYP3A4 inhibitor	No
Log <i>K</i> _p (skin permeation)	-5.93 cm/s
Druglikeness	
Lipinski	Yes; 0 violation
Ghose	Yes
Veber	Yes
Egan	Yes
Muegge	Yes
Bioavailability Score	0.55
Medicinal Chemistry	
PAINS	1 alert: imine_one_A
Brenk	3 alerts: diketo_group, michael_acceptor_1, michael_acceptor_4
Leadlikeness	Yes
Synthetic accessibility	2.99

Compound 2.92



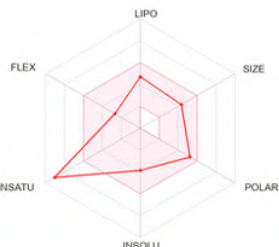
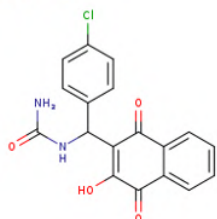
SMILES CCCCN/C=C/C1C(=O)C(=O)c2c(C1=O)cccc2

Physicochemical Properties	
Formula	C15H15NO3
Molecular weight	257.28 g/mol
Num. heavy atoms	19
Num. arom. heavy atoms	6
Fraction Csp3	0.27
Num. rotatable bonds	4
Num. H-bond acceptors	3
Num. H-bond donors	1
Molar Refractivity	71.28
TPSA	63.24 Å²
Lipophilicity	
Log $P_{o/w}$ (ILOGP)	2.03
Log $P_{o/w}$ (XLOGP3)	3.00
Log $P_{o/w}$ (WLOGP)	1.91
Log $P_{o/w}$ (MLOGP)	0.47
Log $P_{o/w}$ (SILICOS-IT)	3.18
Consensus Log $P_{o/w}$	2.12

Water Solubility	
Log S (ESOL)	-3.29
Solubility	1.30e-01 mg/ml ; 5.07e-04 mol/l
Class	Soluble
Log S (Ali)	-3.99
Solubility	2.62e-02 mg/ml ; 1.02e-04 mol/l
Class	Soluble
Log S (SILICOS-IT)	-4.86
Solubility	3.55e-03 mg/ml ; 1.38e-05 mol/l
Class	Moderately soluble
Pharmacokinetics	
GI absorption	High
BBB permeant	Yes
P-gp substrate	No
CYP1A2 inhibitor	Yes
CYP2C19 inhibitor	Yes
CYP2C9 inhibitor	No
CYP2D6 inhibitor	No
CYP3A4 inhibitor	No
Log K_p (skin permeation)	-5.74 cm/s
Druglikeness	
Lipinski	Yes; 0 violation
Ghose	Yes
Veber	Yes
Egan	Yes
Muegge	Yes
Bioavailability Score	0.55
Medicinal Chemistry	
PAINS	1 alert: imine_one_A
Brenk	3 alerts: diketo_group, michael_acceptor_1, michael_acceptor_4
Leadlikeness	Yes
Synthetic accessibility	2.98

3.3 Biginelli-linear series

Compound 3.43

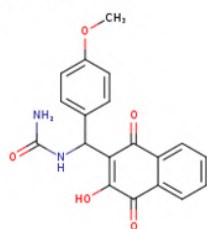


SMILES NC(=O)NC(C1=C(O)C(=O)c2c(C1=O)cccc2)c1ccc(cc1)Cl

Physicochemical Properties	
Formula	C18H13ClN2O4
Molecular weight	356.76 g/mol
Num. heavy atoms	25
Num. arom. heavy atoms	12
Fraction Csp3	0.06
Num. rotatable bonds	4
Num. H-bond acceptors	4
Num. H-bond donors	3
Molar Refractivity	91.02
TPSA	109.49 Å²
Lipophilicity	
Log $P_{o/w}$ (ILOGP)	1.34
Log $P_{o/w}$ (XLOGP3)	2.73
Log $P_{o/w}$ (WLOGP)	2.62
Log $P_{o/w}$ (MLOGP)	1.05
Log $P_{o/w}$ (SILICOS-IT)	2.42
Consensus Log $P_{o/w}$	2.03

Water Solubility	
Log S (ESOL)	-3.86
Solubility	4.89e-02 mg/ml ; 1.37e-04 mol/l
Class	Soluble
Log S (Ali)	-4.68
Solubility	7.40e-03 mg/ml ; 2.07e-05 mol/l
Class	Moderately soluble
Log S (SILICOS-IT)	-5.46
Solubility	1.24e-03 mg/ml ; 3.48e-06 mol/l
Class	Moderately soluble
Pharmacokinetics	
GI absorption	High
BBB permeant	No
P-gp substrate	No
CYP1A2 inhibitor	Yes
CYP2C19 inhibitor	No
CYP2C9 inhibitor	Yes
CYP2D6 inhibitor	No
CYP3A4 inhibitor	No
Log K_p (skin permeation)	-6.54 cm/s
Druglikeness	
Lipinski	Yes; 0 violation
Ghose	Yes
Veber	Yes
Egan	Yes
Muegge	Yes
Bioavailability Score	0.56
Medicinal Chemistry	
PAINS	1 alert: quinone_A
Brenk	0 alert
Leadlikeness	No; 1 violation: MW>350
Synthetic accessibility	3.36

Compound 3.45

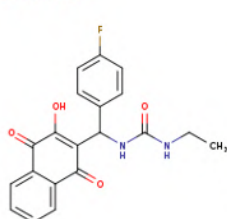


SMILES COc1ccc(cc1)C(C1=C(O)C(=O)c2c(C1=O)cccc2)NC(=O)N

Physicochemical Properties	
Formula	C ₁₉ H ₁₆ N ₂ O ₅
Molecular weight	352.34 g/mol
Num. heavy atoms	26
Num. arom. heavy atoms	12
Fraction Csp ³	0.11
Num. rotatable bonds	5
Num. H-bond acceptors	5
Num. H-bond donors	3
Molar Refractivity	92.51
TPSA	118.72 Å ²
Lipophilicity	
Log <i>P</i> _{o/w} (ILOGP)	1.68
Log <i>P</i> _{o/w} (XLOGP3)	2.07
Log <i>P</i> _{o/w} (WLOGP)	1.97
Log <i>P</i> _{o/w} (MLOGP)	0.25
Log <i>P</i> _{o/w} (SILICOS-IT)	1.84
Consensus Log <i>P</i> _{o/w}	1.56

Water Solubility	
Log S (ESOL)	-3.34
Solubility	1.61e-01 mg/ml ; 4.57e-04 mol/l
Class	Soluble
Log S (Ali)	-4.19
Solubility	2.26e-02 mg/ml ; 6.42e-05 mol/l
Class	Moderately soluble
Log S (SILICOS-IT)	-4.97
Solubility	3.75e-03 mg/ml ; 1.06e-05 mol/l
Class	Moderately soluble
Pharmacokinetics	
GI absorption	High
BBB permeant	No
P-gp substrate	Yes
CYP1A2 inhibitor	No
CYP2C19 inhibitor	No
CYP2C9 inhibitor	No
CYP2D6 inhibitor	No
CYP3A4 inhibitor	No
Log <i>K</i> _p (skin permeation)	-6.98 cm/s
Druglikeness	
Lipinski	Yes; 0 violation
Ghose	Yes
Veber	Yes
Egan	Yes
Muegge	Yes
Bioavailability Score	0.56
Medicinal Chemistry	
PAINS	1 alert: quinone_A
Brenk	0 alert
Leadlikeness	No; 1 violation: MW>350
Synthetic accessibility	3.43

Compound 3.46

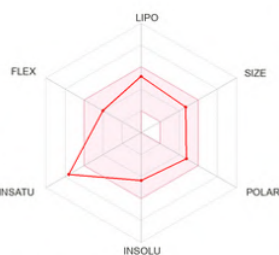
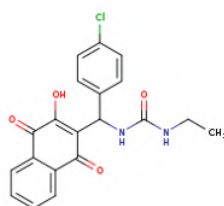


SMILES CCNC(=O)NC(C1=C(O)C(=O)c2c(C1=O)cccc2)c1ccc(cc1)F

Physicochemical Properties	
Formula	C ₂₀ H ₁₇ N ₂ O ₄
Molecular weight	368.36 g/mol
Num. heavy atoms	27
Num. arom. heavy atoms	12
Fraction Csp ³	0.15
Num. rotatable bonds	6
Num. H-bond acceptors	5
Num. H-bond donors	3
Molar Refractivity	95.68
TPSA	95.50 Å ²
Lipophilicity	
Log <i>P</i> _{o/w} (ILOGP)	2.43
Log <i>P</i> _{o/w} (XLOGP3)	2.97
Log <i>P</i> _{o/w} (WLOGP)	3.17
Log <i>P</i> _{o/w} (MLOGP)	1.38
Log <i>P</i> _{o/w} (SILICOS-IT)	3.05
Consensus Log <i>P</i> _{o/w}	2.60

Water Solubility	
Log S (ESOL)	-3.93
Solubility	4.35e-02 mg/ml ; 1.18e-04 mol/l
Class	Soluble
Log S (Ali)	-4.64
Solubility	8.46e-03 mg/ml ; 2.30e-05 mol/l
Class	Moderately soluble
Log S (SILICOS-IT)	-6.32
Solubility	1.78e-04 mg/ml ; 4.83e-07 mol/l
Class	Poorly soluble
Pharmacokinetics	
GI absorption	High
BBB permeant	No
P-gp substrate	Yes
CYP1A2 inhibitor	No
CYP2C19 inhibitor	No
CYP2C9 inhibitor	Yes
CYP2D6 inhibitor	No
CYP3A4 inhibitor	Yes
Log <i>K</i> _p (skin permeation)	-6.44 cm/s
Druglikeness	
Lipinski	Yes; 0 violation
Ghose	Yes
Veber	Yes
Egan	Yes
Muegge	Yes
Bioavailability Score	0.56
Medicinal Chemistry	
PAINS	1 alert: quinone_A
Brenk	0 alert
Leadlikeness	No; 1 violation: MW>350
Synthetic accessibility	3.63

Compound 3.47

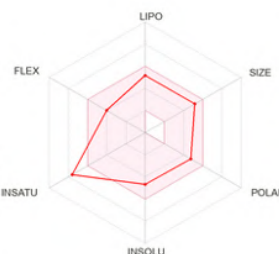
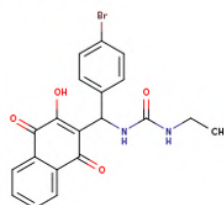


SMILES CCNC(=O)NC(C1=C(O)C(=O)c2c(C1=O)cccc2)c1ccc(cc1)Cl

Physicochemical Properties	
Formula	C20H17ClN2O4
Molecular weight	384.81 g/mol
Num. heavy atoms	27
Num. arom. heavy atoms	12
Fraction Csp3	0.15
Num. rotatable bonds	6
Num. H-bond acceptors	4
Num. H-bond donors	3
Molar Refractivity	100.73
TPSA	95.50 Å²
Lipophilicity	
Log $P_{o/w}$ (ILOGP)	2.48
Log $P_{o/w}$ (XLOGP3)	3.50
Log $P_{o/w}$ (WLOGP)	3.27
Log $P_{o/w}$ (MLOGP)	1.50
Log $P_{o/w}$ (SILICOS-IT)	3.27
Consensus Log $P_{o/w}$	2.80

Water Solubility	
Log S (ESOL)	-4.36
Solubility	1.67e-02 mg/ml ; 4.33e-05 mol/l
Class	Moderately soluble
Log S (Ali)	-5.19
Solubility	2.49e-03 mg/ml ; 6.48e-06 mol/l
Class	Moderately soluble
Log S (SILICOS-IT)	-6.64
Solubility	8.82e-05 mg/ml ; 2.29e-07 mol/l
Class	Poorly soluble
Pharmacokinetics	
GI absorption	High
BBB permeant	No
P-gp substrate	No
CYP1A2 inhibitor	Yes
CYP2C19 inhibitor	Yes
CYP2C9 inhibitor	Yes
CYP2D6 inhibitor	No
CYP3A4 inhibitor	Yes
Log K_p (skin permeation)	-6.16 cm/s
Druglikeness	
Lipinski	Yes; 0 violation
Ghose	Yes
Veber	Yes
Egan	Yes
Muegge	Yes
Bioavailability Score	0.56
Medicinal Chemistry	
PAINS	1 alert: quinone_A
Brenk	0 alert
Leadlikeness	No; 1 violation: MW>350
Synthetic accessibility	3.62

Compound 3.48

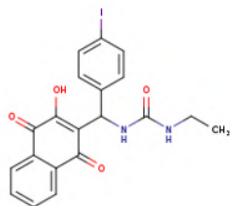


SMILES CCNC(=O)NC(C1=C(O)C(=O)c2c(C1=O)cccc2)c1ccc(cc1)Br

Physicochemical Properties	
Formula	C20H17BrN2O4
Molecular weight	429.26 g/mol
Num. heavy atoms	27
Num. arom. heavy atoms	12
Fraction Csp3	0.15
Num. rotatable bonds	6
Num. H-bond acceptors	4
Num. H-bond donors	3
Molar Refractivity	103.42
TPSA	95.50 Å²
Lipophilicity	
Log $P_{o/w}$ (ILOGP)	2.59
Log $P_{o/w}$ (XLOGP3)	3.56
Log $P_{o/w}$ (WLOGP)	3.38
Log $P_{o/w}$ (MLOGP)	1.61
Log $P_{o/w}$ (SILICOS-IT)	3.31
Consensus Log $P_{o/w}$	2.89

Water Solubility	
Log S (ESOL)	-4.68
Solubility	9.03e-03 mg/ml ; 2.10e-05 mol/l
Class	Moderately soluble
Log S (Ali)	-5.25
Solubility	2.41e-03 mg/ml ; 5.61e-06 mol/l
Class	Moderately soluble
Log S (SILICOS-IT)	-6.84
Solubility	6.26e-05 mg/ml ; 1.46e-07 mol/l
Class	Poorly soluble
Pharmacokinetics	
GI absorption	High
BBB permeant	No
P-gp substrate	No
CYP1A2 inhibitor	Yes
CYP2C19 inhibitor	Yes
CYP2C9 inhibitor	Yes
CYP2D6 inhibitor	No
CYP3A4 inhibitor	Yes
Log K_p (skin permeation)	-6.39 cm/s
Druglikeness	
Lipinski	Yes; 0 violation
Ghose	Yes
Veber	Yes
Egan	Yes
Muegge	Yes
Bioavailability Score	0.56
Medicinal Chemistry	
PAINS	1 alert: quinone_A
Brenk	0 alert
Leadlikeness	No; 2 violations: MW>350, XLOGP3>3.5
Synthetic accessibility	3.64

Compound 3.49



SMILES CCNC(=O)NC(C1=C(O)C(=O)c2c(C1=O)cccc2)c1ccc(cc1)I

Physicochemical Properties

Formula	C ₂₀ H ₁₇ IN ₂ O ₄
Molecular weight	476.26 g/mol
Num. heavy atoms	27
Num. arom. heavy atoms	12
Fraction Csp ³	0.15
Num. rotatable bonds	6
Num. H-bond acceptors	4
Num. H-bond donors	3
Molar Refractivity	108.44
TPSA	95.50 Å ²

Lipophilicity

Log <i>P</i> _{o/w} (iLOGP)	2.66
Log <i>P</i> _{o/w} (XLOGP3)	3.52
Log <i>P</i> _{o/w} (WLOGP)	3.22
Log <i>P</i> _{o/w} (MLOGP)	1.71
Log <i>P</i> _{o/w} (SILICOS-IT)	3.60
Consensus Log <i>P</i> _{o/w}	2.94

Water Solubility	
Log S (ESOL)	-4.94
Solubility	5.43e-03 mg/ml ; 1.14e-05 mol/l
Class	Moderately soluble
Log S (Ali)	-5.21
Solubility	2.94e-03 mg/ml ; 6.17e-06 mol/l
Class	Moderately soluble
Log S (SILICOS-IT)	-6.89
Solubility	6.18e-05 mg/ml ; 1.30e-07 mol/l
Class	Poorly soluble

Pharmacokinetics

GI absorption	High
BBB permeant	No
P-gp substrate	No
CYP1A2 inhibitor	Yes
CYP2C19 inhibitor	Yes
CYP2C9 inhibitor	Yes
CYP2D6 inhibitor	No
CYP3A4 inhibitor	Yes
Log <i>K</i> _p (skin permeation)	-6.71 cm/s

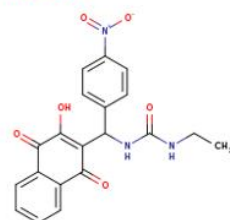
Druglikeness

Lipinski	Yes; 0 violation
Ghose	Yes
Veber	Yes
Egan	Yes
Muegge	Yes
Bioavailability Score	0.56

Medicinal Chemistry

PAINS	1 alert: quinone_A
Brenk	1 alert: iodine
Leadlikeness	No; 2 violations: MW>350, XLOGP3>3.5
Synthetic accessibility	3.73

Compound 3.50



SMILES CCNC(=O)NC(C1=C(O)C(=O)c2c(C1=O)cccc2)c1ccc(cc1)[N+](=O)[O-]

Physicochemical Properties

Formula	C ₂₀ H ₁₇ N ₃ O ₆
Molecular weight	395.37 g/mol
Num. heavy atoms	29
Num. arom. heavy atoms	12
Fraction Csp ³	0.15
Num. rotatable bonds	7
Num. H-bond acceptors	6
Num. H-bond donors	3
Molar Refractivity	104.54
TPSA	141.32 Å ²

Lipophilicity

Log <i>P</i> _{o/w} (iLOGP)	1.99
Log <i>P</i> _{o/w} (XLOGP3)	2.70
Log <i>P</i> _{o/w} (WLOGP)	2.52
Log <i>P</i> _{o/w} (MLOGP)	0.12
Log <i>P</i> _{o/w} (SILICOS-IT)	0.49
Consensus Log <i>P</i> _{o/w}	1.56

Water Solubility	
Log S (ESOL)	-3.84
Solubility	5.76e-02 mg/ml ; 1.46e-04 mol/l
Class	Soluble
Log S (Ali)	-5.32
Solubility	1.89e-03 mg/ml ; 4.78e-06 mol/l
Class	Moderately soluble
Log S (SILICOS-IT)	-5.39
Solubility	1.59e-03 mg/ml ; 4.03e-06 mol/l
Class	Moderately soluble

Pharmacokinetics

GI absorption	Low
BBB permeant	No
P-gp substrate	Yes
CYP1A2 inhibitor	No
CYP2C19 inhibitor	No
CYP2C9 inhibitor	Yes
CYP2D6 inhibitor	No
CYP3A4 inhibitor	No
Log <i>K</i> _p (skin permeation)	-6.79 cm/s

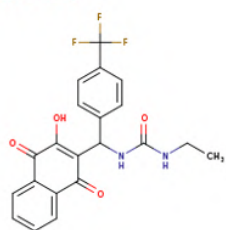
Druglikeness

Lipinski	Yes; 0 violation
Ghose	Yes
Veber	No; 1 violation: TPSA>140
Egan	No; 1 violation: TPSA>131.6
Muegge	Yes
Bioavailability Score	0.56

Medicinal Chemistry

PAINS	1 alert: quinone_A
Brenk	2 alerts: nitro_group, oxygen-nitrogen_single_bond
Leadlikeness	No; 1 violation: MW>350
Synthetic accessibility	3.70

Compound 3.51

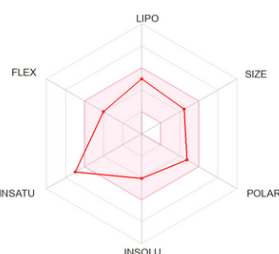
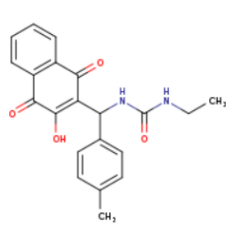


SMILES CCNC(=O)NC(C=C(O)C(=O)c2c(C1=O)cccc2)c1ccc(cc1)C(F)(F)F

Physicochemical Properties	
Formula	C ₂₁ H ₁₇ F ₃ N ₂ O ₄
Molecular weight	418.37 g/mol
Num. heavy atoms	30
Num. arom. heavy atoms	12
Fraction Csp ³	0.19
Num. rotatable bonds	7
Num. H-bond acceptors	7
Num. H-bond donors	3
Molar Refractivity	100.72
TPSA	95.50 Å ²
Lipophilicity	
Log <i>P</i> _{o/w} (iLOGP)	2.39
Log <i>P</i> _{o/w} (XLOGP3)	3.75
Log <i>P</i> _{o/w} (WLOGP)	4.78
Log <i>P</i> _{o/w} (MLOGP)	1.82
Log <i>P</i> _{o/w} (SILICOS-IT)	3.73
Consensus Log <i>P</i> _{o/w}	3.30

Water Solubility	
Log S (ESOL)	-4.63
Solubility	9.80e-03 mg/ml ; 2.34e-05 mol/l
Class	Moderately soluble
Log S (Ali)	-5.45
Solubility	1.49e-03 mg/ml ; 3.56e-06 mol/l
Class	Moderately soluble
Log S (SILICOS-IT)	-6.88
Solubility	5.50e-05 mg/ml ; 1.32e-07 mol/l
Class	Poorly soluble
Pharmacokinetics	
GI absorption	High
BBB permeant	No
P-gp substrate	Yes
CYP1A2 inhibitor	No
CYP2C19 inhibitor	No
CYP2C9 inhibitor	Yes
CYP2D6 inhibitor	No
CYP3A4 inhibitor	Yes
Log <i>K</i> _p (skin permeation)	-6.19 cm/s
Druglikeness	
Lipinski	Yes; 0 violation
Ghose	Yes
Veber	Yes
Egan	Yes
Muegge	Yes
Bioavailability Score	0.56
Medicinal Chemistry	
PAINS	1 alert: quinone_A
Brenk	0 alert
Leadlikeness	No; 2 violations: MW>350, XLOGP3>3.5
Synthetic accessibility	3.76

Compound 3.52

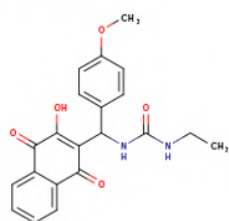


SMILES CCNC(=O)NC(C=C(O)C(=O)c2c(C1=O)cccc2)c1ccc(cc1)C

Physicochemical Properties	
Formula	C ₂₁ H ₂₀ N ₂ O ₄
Molecular weight	364.39 g/mol
Num. heavy atoms	27
Num. arom. heavy atoms	12
Fraction Csp ³	0.19
Num. rotatable bonds	6
Num. H-bond acceptors	4
Num. H-bond donors	3
Molar Refractivity	100.69
TPSA	95.50 Å ²
Lipophilicity	
Log <i>P</i> _{o/w} (iLOGP)	2.43
Log <i>P</i> _{o/w} (XLOGP3)	3.23
Log <i>P</i> _{o/w} (WLOGP)	2.92
Log <i>P</i> _{o/w} (MLOGP)	1.23
Log <i>P</i> _{o/w} (SILICOS-IT)	3.15
Consensus Log <i>P</i> _{o/w}	2.59

Water Solubility	
Log S (ESOL)	-4.07
Solubility	3.12e-02 mg/ml ; 8.57e-05 mol/l
Class	Moderately soluble
Log S (Ali)	-4.91
Solubility	4.50e-03 mg/ml ; 1.23e-05 mol/l
Class	Moderately soluble
Log S (SILICOS-IT)	-6.43
Solubility	1.36e-04 mg/ml ; 3.74e-07 mol/l
Class	Poorly soluble
Pharmacokinetics	
GI absorption	High
BBB permeant	No
P-gp substrate	Yes
CYP1A2 inhibitor	No
CYP2C19 inhibitor	No
CYP2C9 inhibitor	Yes
CYP2D6 inhibitor	No
CYP3A4 inhibitor	Yes
Log <i>K</i> _p (skin permeation)	-6.23 cm/s
Druglikeness	
Lipinski	Yes; 0 violation
Ghose	Yes
Veber	Yes
Egan	Yes
Muegge	Yes
Bioavailability Score	0.56
Medicinal Chemistry	
PAINS	1 alert: quinone_A
Brenk	0 alert
Leadlikeness	No; 1 violation: MW>350
Synthetic accessibility	3.71

Compound 3.53

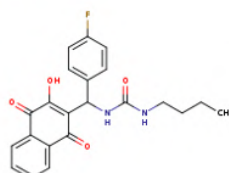


SMILES CCNC(=O)NC(C=C(O)C(=O)c2c(C1=O)cccc2)c1ccc(cc1)OC

Physicochemical Properties	
Formula	C ₂₁ H ₂₀ N ₂ O ₅
Molecular weight	380.39 g/mol
Num. heavy atoms	28
Num. arom. heavy atoms	12
Fraction Csp ³	0.19
Num. rotatable bonds	7
Num. H-bond acceptors	5
Num. H-bond donors	3
Molar Refractivity	102.21
TPSA	104.73 Å ²
Lipophilicity	
Log <i>P</i> _{o/w} (ILOGP)	2.42
Log <i>P</i> _{o/w} (XLOGP3)	2.84
Log <i>P</i> _{o/w} (WLOGP)	2.62
Log <i>P</i> _{o/w} (MLOGP)	0.70
Log <i>P</i> _{o/w} (SILICOS-IT)	2.70
Consensus Log <i>P</i> _{o/w}	2.26

Water Solubility	
Log S (ESOL)	-3.84
Solubility	5.46e-02 mg/ml ; 1.44e-04 mol/l
Class	Soluble
Log S (Ali)	-4.70
Solubility	7.63e-03 mg/ml ; 2.01e-05 mol/l
Class	Moderately soluble
Log S (SILICOS-IT)	-6.16
Solubility	2.66e-04 mg/ml ; 7.00e-07 mol/l
Class	Poorly soluble
Pharmacokinetics	
GI absorption	High
BBB permeant	No
P-gp substrate	Yes
CYP1A2 inhibitor	No
CYP2C19 inhibitor	No
CYP2C9 inhibitor	Yes
CYP2D6 inhibitor	No
CYP3A4 inhibitor	Yes
Log <i>K</i> _p (skin permeation)	-6.60 cm/s
Druglikeness	
Lipinski	Yes; 0 violation
Ghose	Yes
Veber	Yes
Egan	Yes
Muegge	Yes
Bioavailability Score	0.56
Medicinal Chemistry	
PAINS	1 alert: quinone_A
Brenk	0 alert
Leadlikeness	No; 1 violation: MW>350
Synthetic accessibility	3.69

Compound 3.54

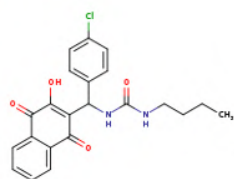


SMILES CCCCNC(=O)NC(C=C(O)C(=O)c2c(C1=O)cccc2)c1ccc(cc1)F

Physicochemical Properties	
Formula	C ₂₂ H ₂₁ N ₂ O ₄ F
Molecular weight	396.41 g/mol
Num. heavy atoms	29
Num. arom. heavy atoms	12
Fraction Csp ³	0.23
Num. rotatable bonds	8
Num. H-bond acceptors	5
Num. H-bond donors	3
Molar Refractivity	105.29
TPSA	95.50 Å ²
Lipophilicity	
Log <i>P</i> _{o/w} (ILOGP)	2.86
Log <i>P</i> _{o/w} (XLOGP3)	3.85
Log <i>P</i> _{o/w} (WLOGP)	3.95
Log <i>P</i> _{o/w} (MLOGP)	1.82
Log <i>P</i> _{o/w} (SILICOS-IT)	3.85
Consensus Log <i>P</i> _{o/w}	3.27

Water Solubility	
Log S (ESOL)	-4.50
Solubility	1.25e-02 mg/ml ; 3.15e-05 mol/l
Class	Moderately soluble
Log S (Ali)	-5.55
Solubility	1.11e-03 mg/ml ; 2.81e-06 mol/l
Class	Moderately soluble
Log S (SILICOS-IT)	-7.10
Solubility	3.13e-05 mg/ml ; 7.89e-08 mol/l
Class	Poorly soluble
Pharmacokinetics	
GI absorption	High
BBB permeant	No
P-gp substrate	Yes
CYP1A2 inhibitor	No
CYP2C19 inhibitor	Yes
CYP2C9 inhibitor	Yes
CYP2D6 inhibitor	No
CYP3A4 inhibitor	Yes
Log <i>K</i> _p (skin permeation)	-5.98 cm/s
Druglikeness	
Lipinski	Yes; 0 violation
Ghose	Yes
Veber	Yes
Egan	Yes
Muegge	Yes
Bioavailability Score	0.56
Medicinal Chemistry	
PAINS	1 alert: quinone_A
Brenk	0 alert
Leadlikeness	No; 3 violations: MW>350, Rotors>7, XLOGP3>3.5
Synthetic accessibility	3.85

Compound 3.55



SMILES CCCCNC(=O)NC(C1=C(O)C(=O)c2c(C1=O)cccc2)c1ccc(cc1)Cl

Physicochemical Properties

Formula	C ₂₂ H ₂₁ ClN ₂ O ₄
Molecular weight	412.87 g/mol
Num. heavy atoms	29
Num. arom. heavy atoms	12
Fraction Csp ³	0.23
Num. rotatable bonds	8
Num. H-bond acceptors	4
Num. H-bond donors	3
Molar Refractivity	110.35
TPSA	95.50 Å ²

Lipophilicity

Log <i>P</i> _{o/w} (ILOGP)	3.01
Log <i>P</i> _{o/w} (XLOGP3)	4.38
Log <i>P</i> _{o/w} (WLOGP)	4.05
Log <i>P</i> _{o/w} (MLOGP)	1.93
Log <i>P</i> _{o/w} (SILICOS-IT)	4.07
Consensus Log <i>P</i> _{o/w}	3.49

Water Solubility	
Log S (ESOL)	-4.94
Solubility	4.77e-03 mg/ml ; 1.16e-05 mol/l
Class	Moderately soluble
Log S (Ali)	-6.10
Solubility	3.27e-04 mg/ml ; 7.91e-07 mol/l
Class	Poorly soluble
Log S (SILICOS-IT)	-7.42
Solubility	1.55e-05 mg/ml ; 3.76e-08 mol/l
Class	Poorly soluble

Pharmacokinetics

GI absorption	High
BBB permeant	No
P-gp substrate	No
CYP1A2 inhibitor	No
CYP2C19 inhibitor	Yes
CYP2C9 inhibitor	Yes
CYP2D6 inhibitor	No
CYP3A4 inhibitor	Yes
Log <i>K</i> _p (skin permeation)	-5.71 cm/s

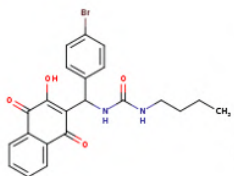
Druglikeness

Lipinski	Yes; 0 violation
Ghose	Yes
Veber	Yes
Egan	Yes
Muegge	Yes
Bioavailability Score	0.56

Medicinal Chemistry

PAINS	1 alert: quinone_A
Brenk	0 alert
Leadlikeness	No; 3 violations: MW>350, Rotors>7, XLOGP3>3.5
Synthetic accessibility	3.84

Compound 3.56



SMILES CCCCNC(=O)NC(C1=C(O)C(=O)c2c(C1=O)cccc2)c1ccc(cc1)Br

Physicochemical Properties

Formula	C ₂₂ H ₂₁ BrN ₂ O ₄
Molecular weight	457.32 g/mol
Num. heavy atoms	29
Num. arom. heavy atoms	12
Fraction Csp ³	0.23
Num. rotatable bonds	8
Num. H-bond acceptors	4
Num. H-bond donors	3
Molar Refractivity	113.04
TPSA	95.50 Å ²

Lipophilicity

Log <i>P</i> _{o/w} (ILOGP)	3.03
Log <i>P</i> _{o/w} (XLOGP3)	4.44
Log <i>P</i> _{o/w} (WLOGP)	4.16
Log <i>P</i> _{o/w} (MLOGP)	2.04
Log <i>P</i> _{o/w} (SILICOS-IT)	4.11
Consensus Log <i>P</i> _{o/w}	3.55

Water Solubility	
Log S (ESOL)	-5.25
Solubility	2.57e-03 mg/ml ; 5.61e-06 mol/l
Class	Moderately soluble
Log S (Ali)	-6.16
Solubility	3.13e-04 mg/ml ; 6.85e-07 mol/l
Class	Poorly soluble
Log S (SILICOS-IT)	-7.62
Solubility	1.10e-05 mg/ml ; 2.41e-08 mol/l
Class	Poorly soluble

Pharmacokinetics

GI absorption	High
BBB permeant	No
P-gp substrate	No
CYP1A2 inhibitor	No
CYP2C19 inhibitor	Yes
CYP2C9 inhibitor	Yes
CYP2D6 inhibitor	No
CYP3A4 inhibitor	Yes
Log <i>K</i> _p (skin permeation)	-5.94 cm/s

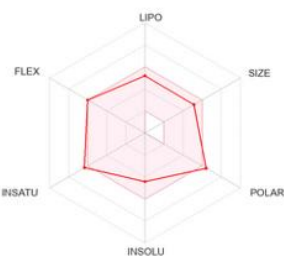
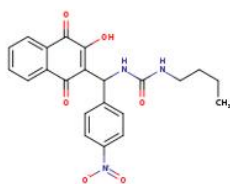
Druglikeness

Lipinski	Yes; 0 violation
Ghose	Yes
Veber	Yes
Egan	Yes
Muegge	Yes
Bioavailability Score	0.56

Medicinal Chemistry

PAINS	1 alert: quinone_A
Brenk	0 alert
Leadlikeness	No; 3 violations: MW>350, Rotors>7, XLOGP3>3.5
Synthetic accessibility	3.86

Compound 3.57

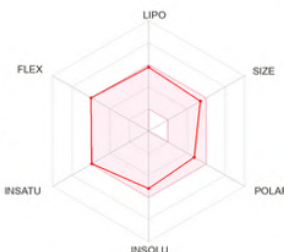
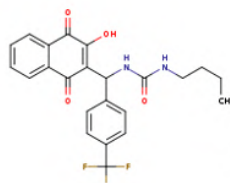


SMILES CCCCNC(=O)NC(C1=C(O)C(=O)c2c(C1=O)cccc2)c1ccc(cc1)[N+](=O)[O-]

Physicochemical Properties	
Formula	C ₂₂ H ₂₁ N ₃ O ₆
Molecular weight	423.42 g/mol
Num. heavy atoms	31
Num. arom. heavy atoms	12
Fraction Csp ³	0.23
Num. rotatable bonds	9
Num. H-bond acceptors	6
Num. H-bond donors	3
Molar Refractivity	114.16
TPSA	141.32 Å ²
Lipophilicity	
Log P _{o/w} (ILOGP)	2.54
Log P _{o/w} (XLOGP3)	3.58
Log P _{o/w} (WLOGP)	3.30
Log P _{o/w} (MLOGP)	0.56
Log P _{o/w} (SILICOS-IT)	1.29
Consensus Log P _{o/w}	2.25

Water Solubility	
Log S (ESOL)	-4.41
Solubility	1.64e-02 mg/ml ; 3.86e-05 mol/l
Class	Moderately soluble
Log S (Ali)	-6.23
Solubility	2.47e-04 mg/ml ; 5.84e-07 mol/l
Class	Poorly soluble
Log S (SILICOS-IT)	-6.18
Solubility	2.80e-04 mg/ml ; 6.62e-07 mol/l
Class	Poorly soluble
Pharmacokinetics	
GI absorption	Low
BBB permeant	No
P-gp substrate	Yes
CYP1A2 inhibitor	No
CYP2C19 inhibitor	No
CYP2C9 inhibitor	Yes
CYP2D6 inhibitor	Yes
CYP3A4 inhibitor	Yes
Log K _p (skin permeation)	-6.34 cm/s
Druglikeness	
Lipinski	Yes; 0 violation
Ghose	Yes
Veber	No; 1 violation: TPSA>140
Egan	No; 1 violation: TPSA>131.6
Muegge	Yes
Bioavailability Score	0.56
Medicinal Chemistry	
PAINS	1 alert: quinone_A
Brenk	2 alerts: nitro_group, oxygen-nitrogen_single_bond
Leadlikeness	No; 3 violations: MW>350, Rotors>7, XLOGP3>3.5
Synthetic accessibility	3.92

Compound 3.58

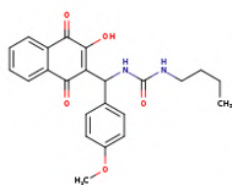


SMILES CCCCNC(=O)NC(C1=C(O)C(=O)c2c(C1=O)cccc2)c1ccc(cc1)C(F)(F)F

Physicochemical Properties	
Formula	C ₂₃ H ₂₁ F ₃ N ₂ O ₄
Molecular weight	446.42 g/mol
Num. heavy atoms	32
Num. arom. heavy atoms	12
Fraction Csp ³	0.26
Num. rotatable bonds	9
Num. H-bond acceptors	7
Num. H-bond donors	3
Molar Refractivity	110.34
TPSA	95.50 Å ²
Lipophilicity	
Log P _{o/w} (ILOGP)	3.12
Log P _{o/w} (XLOGP3)	4.64
Log P _{o/w} (WLOGP)	5.56
Log P _{o/w} (MLOGP)	2.24
Log P _{o/w} (SILICOS-IT)	4.54
Consensus Log P _{o/w}	4.02

Water Solubility	
Log S (ESOL)	-5.21
Solubility	2.72e-03 mg/ml ; 6.10e-06 mol/l
Class	Moderately soluble
Log S (Ali)	-6.37
Solubility	1.90e-04 mg/ml ; 4.25e-07 mol/l
Class	Poorly soluble
Log S (SILICOS-IT)	-7.66
Solubility	9.68e-06 mg/ml ; 2.17e-08 mol/l
Class	Poorly soluble
Pharmacokinetics	
GI absorption	High
BBB permeant	No
P-gp substrate	Yes
CYP1A2 inhibitor	No
CYP2C19 inhibitor	Yes
CYP2C9 inhibitor	Yes
CYP2D6 inhibitor	No
CYP3A4 inhibitor	Yes
Log K _p (skin permeation)	-5.73 cm/s
Druglikeness	
Lipinski	Yes; 0 violation
Ghose	Yes
Veber	Yes
Egan	Yes
Muegge	Yes
Bioavailability Score	0.56
Medicinal Chemistry	
PAINS	1 alert: quinone_A
Brenk	0 alert
Leadlikeness	No; 3 violations: MW>350, Rotors>7, XLOGP3>3.5
Synthetic accessibility	3.98

Compound 3.59

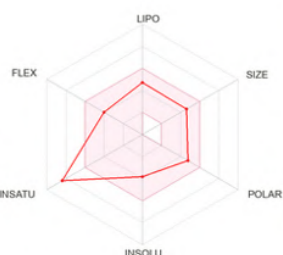
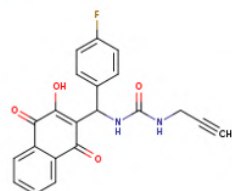


SMILES CCCCNC(=O)NC(C1=C(O)C(=O)c2c(C1=O)cccc2)c1ccc(cc1)OC

Physicochemical Properties	
Formula	C23H24N2O5
Molecular weight	408.45 g/mol
Num. heavy atoms	30
Num. arom. heavy atoms	12
Fraction Csp3	0.26
Num. rotatable bonds	9
Num. H-bond acceptors	5
Num. H-bond donors	3
Molar Refractivity	111.83
TPSA	104.73 Å²
Lipophilicity	
Log $P_{o/w}$ (iLOGP)	2.85
Log $P_{o/w}$ (XLOGP3)	3.72
Log $P_{o/w}$ (WLOGP)	3.40
Log $P_{o/w}$ (MLOGP)	1.13
Log $P_{o/w}$ (SILICOS-IT)	3.50
Consensus Log $P_{o/w}$	2.92

Water Solubility	
Log S (ESOL)	-4.42
Solubility	1.56e-02 mg/ml ; 3.82e-05 mol/l
Class	Moderately soluble
Log S (Ali)	-5.61
Solubility	1.00e-03 mg/ml ; 2.45e-06 mol/l
Class	Moderately soluble
Log S (SILICOS-IT)	-6.94
Solubility	4.68e-05 mg/ml ; 1.15e-07 mol/l
Class	Poorly soluble
Pharmacokinetics	
GI absorption	High
BBB permeant	No
P-gp substrate	Yes
CYP1A2 inhibitor	No
CYP2C19 inhibitor	Yes
CYP2C9 inhibitor	Yes
CYP2D6 inhibitor	Yes
CYP3A4 inhibitor	Yes
Log K_p (skin permeation)	-6.15 cm/s
Druglikeness	
Lipinski	Yes; 0 violation
Ghose	Yes
Veber	Yes
Egan	Yes
Muegge	Yes
Bioavailability Score	0.56
Medicinal Chemistry	
PAINS	1 alert: quinone_A
Brenk	0 alert
Leadlikeness	No; 3 violations: MW>350, Rotors>7, XLOGP3>3.5
Synthetic accessibility	3.92

Compound 3.60

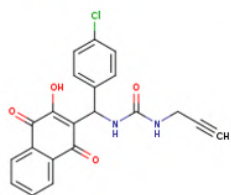


SMILES C#CCNC(=O)NC(C1=C(O)C(=O)c2c(C1=O)cccc2)c1ccc(cc1)F

Physicochemical Properties	
Formula	C21H15FN2O4
Molecular weight	378.35 g/mol
Num. heavy atoms	28
Num. arom. heavy atoms	12
Fraction Csp3	0.10
Num. rotatable bonds	6
Num. H-bond acceptors	5
Num. H-bond donors	3
Molar Refractivity	98.65
TPSA	95.50 Å²
Lipophilicity	
Log $P_{o/w}$ (iLOGP)	2.64
Log $P_{o/w}$ (XLOGP3)	2.72
Log $P_{o/w}$ (WLOGP)	2.87
Log $P_{o/w}$ (MLOGP)	1.53
Log $P_{o/w}$ (SILICOS-IT)	3.28
Consensus Log $P_{o/w}$	2.61

Water Solubility	
Log S (ESOL)	-3.82
Solubility	5.72e-02 mg/ml ; 1.51e-04 mol/l
Class	Soluble
Log S (Ali)	-4.38
Solubility	1.58e-02 mg/ml ; 4.18e-05 mol/l
Class	Moderately soluble
Log S (SILICOS-IT)	-6.00
Solubility	3.75e-04 mg/ml ; 9.91e-07 mol/l
Class	Poorly soluble
Pharmacokinetics	
GI absorption	High
BBB permeant	No
P-gp substrate	No
CYP1A2 inhibitor	No
CYP2C19 inhibitor	No
CYP2C9 inhibitor	Yes
CYP2D6 inhibitor	No
CYP3A4 inhibitor	No
Log K_p (skin permeation)	-6.68 cm/s
Druglikeness	
Lipinski	Yes; 0 violation
Ghose	Yes
Veber	Yes
Egan	Yes
Muegge	Yes
Bioavailability Score	0.56
Medicinal Chemistry	
PAINS	1 alert: quinone_A
Brenk	1 alert: triple_bond
Leadlikeness	No; 1 violation: MW>350
Synthetic accessibility	3.68

Compound 3.61

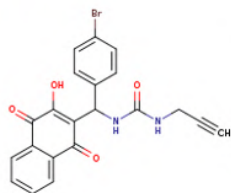


SMILES C#CCNC(=O)NC(C1=C(O)C(=O)c2c(C1=O)cccc2)c1ccc(cc1)Cl

Physicochemical Properties	
Formula	C ₂₁ H ₁₅ ClN ₂ O ₄
Molecular weight	394.81 g/mol
Num. heavy atoms	28
Num. arom. heavy atoms	12
Fraction Csp ³	0.10
Num. rotatable bonds	6
Num. H-bond acceptors	4
Num. H-bond donors	3
Molar Refractivity	103.70
TPSA	95.50 Å ²
Lipophilicity	
Log <i>P</i> _{o/w} (ILOGP)	2.73
Log <i>P</i> _{o/w} (XLOGP3)	3.24
Log <i>P</i> _{o/w} (WLOGP)	2.96
Log <i>P</i> _{o/w} (MLOGP)	1.64
Log <i>P</i> _{o/w} (SILICOS-IT)	3.50
Consensus Log <i>P</i> _{o/w}	2.81

Water Solubility	
Log S (ESOL)	-4.25
Solubility	2.22e-02 mg/ml ; 5.62e-05 mol/l
Class	Moderately soluble
Log S (Ali)	-4.92
Solubility	4.76e-03 mg/ml ; 1.21e-05 mol/l
Class	Moderately soluble
Log S (SILICOS-IT)	-6.33
Solubility	1.86e-04 mg/ml ; 4.71e-07 mol/l
Class	Poorly soluble
Pharmacokinetics	
GI absorption	High
BBB permeant	No
P-gp substrate	No
CYP1A2 inhibitor	Yes
CYP2C19 inhibitor	Yes
CYP2C9 inhibitor	Yes
CYP2D6 inhibitor	No
CYP3A4 inhibitor	Yes
Log <i>K</i> _p (skin permeation)	-6.41 cm/s
Druglikeness	
Lipinski	Yes; 0 violation
Ghose	Yes
Veber	Yes
Egan	Yes
Muegge	Yes
Bioavailability Score	0.56
Medicinal Chemistry	
PAINS	1 alert: quinone_A
Brenk	1 alert: triple_bond
Leadlikeness	No; 1 violation: MW>350
Synthetic accessibility	3.66

Compound 3.62

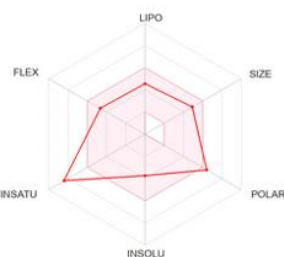
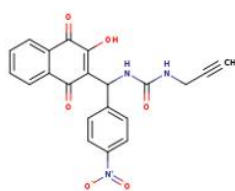


SMILES C#CCNC(=O)NC(C1=C(O)C(=O)c2c(C1=O)cccc2)c1ccc(cc1)Br

Physicochemical Properties	
Formula	C ₂₁ H ₁₅ BrN ₂ O ₄
Molecular weight	439.26 g/mol
Num. heavy atoms	28
Num. arom. heavy atoms	12
Fraction Csp ³	0.10
Num. rotatable bonds	6
Num. H-bond acceptors	4
Num. H-bond donors	3
Molar Refractivity	106.39
TPSA	95.50 Å ²
Lipophilicity	
Log <i>P</i> _{o/w} (ILOGP)	2.89
Log <i>P</i> _{o/w} (XLOGP3)	3.31
Log <i>P</i> _{o/w} (WLOGP)	3.07
Log <i>P</i> _{o/w} (MLOGP)	1.75
Log <i>P</i> _{o/w} (SILICOS-IT)	3.53
Consensus Log <i>P</i> _{o/w}	2.91

Water Solubility	
Log S (ESOL)	-4.57
Solubility	1.18e-02 mg/ml ; 2.69e-05 mol/l
Class	Moderately soluble
Log S (Ali)	-4.99
Solubility	4.48e-03 mg/ml ; 1.02e-05 mol/l
Class	Moderately soluble
Log S (SILICOS-IT)	-6.52
Solubility	1.32e-04 mg/ml ; 3.01e-07 mol/l
Class	Poorly soluble
Pharmacokinetics	
GI absorption	High
BBB permeant	No
P-gp substrate	No
CYP1A2 inhibitor	Yes
CYP2C19 inhibitor	Yes
CYP2C9 inhibitor	Yes
CYP2D6 inhibitor	No
CYP3A4 inhibitor	Yes
Log <i>K</i> _p (skin permeation)	-6.63 cm/s
Druglikeness	
Lipinski	Yes; 0 violation
Ghose	Yes
Veber	Yes
Egan	Yes
Muegge	Yes
Bioavailability Score	0.56
Medicinal Chemistry	
PAINS	1 alert: quinone_A
Brenk	1 alert: triple_bond
Leadlikeness	No; 1 violation: MW>350
Synthetic accessibility	3.68

Compound 3.63

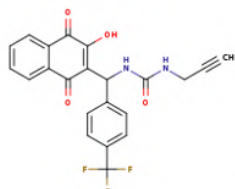


SMILES C#CCNC(=O)NC(C1=C(O)C(=O)c2c(C1=O)cccc2)c1ccc(cc1)[N+](=O)[O-]

Physicochemical Properties	
Formula	C21H15N3O6
Molecular weight	405.36 g/mol
Num. heavy atoms	30
Num. arom. heavy atoms	12
Fraction Csp3	0.10
Num. rotatable bonds	7
Num. H-bond acceptors	6
Num. H-bond donors	3
Molar Refractivity	107.51
TPSA	141.32 Å²
Lipophilicity	
Log $P_{o/w}$ (ILOGP)	2.02
Log $P_{o/w}$ (XLOGP3)	2.44
Log $P_{o/w}$ (WLOGP)	2.21
Log $P_{o/w}$ (MLOGP)	0.27
Log $P_{o/w}$ (SILICOS-IT)	0.71
Consensus Log $P_{o/w}$	1.53

Water Solubility	
Log S (ESOL)	-3.72
Solubility	7.65e-02 mg/ml ; 1.89e-04 mol/l
Class	Soluble
Log S (Ali)	-5.05
Solubility	3.61e-03 mg/ml ; 8.89e-06 mol/l
Class	Moderately soluble
Log S (SILICOS-IT)	-5.08
Solubility	3.36e-03 mg/ml ; 8.28e-06 mol/l
Class	Moderately soluble
Pharmacokinetics	
GI absorption	Low
BBB permeant	No
P-gp substrate	No
CYP1A2 inhibitor	No
CYP2C19 inhibitor	No
CYP2C9 inhibitor	Yes
CYP2D6 inhibitor	No
CYP3A4 inhibitor	No
Log K_p (skin permeation)	-7.04 cm/s
Druglikeness	
Lipinski	Yes; 0 violation
Ghose	Yes
Weber	No; 1 violation: TPSA>140
Egan	No; 1 violation: TPSA>131.6
Muegge	Yes
Bioavailability Score	0.56
Medicinal Chemistry	
PAINS	1 alert: quinone_A
Brenk	3 alerts: nitro_group, oxygen-nitrogen_single_bond, triple_bond
Leadlikeness	No; 1 violation: MW>350
Synthetic accessibility	3.73

Compound 3.64

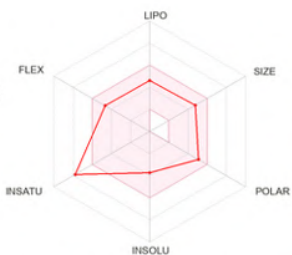
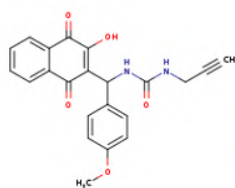


SMILES C#CCNC(=O)NC(C1=C(O)C(=O)c2c(C1=O)cccc2)c1ccc(cc1)C(F)(F)F

Physicochemical Properties	
Formula	C22H15F3N2O4
Molecular weight	428.36 g/mol
Num. heavy atoms	31
Num. arom. heavy atoms	12
Fraction Csp3	0.14
Num. rotatable bonds	7
Num. H-bond acceptors	7
Num. H-bond donors	3
Molar Refractivity	103.69
TPSA	95.50 Å²
Lipophilicity	
Log $P_{o/w}$ (ILOGP)	2.68
Log $P_{o/w}$ (XLOGP3)	3.50
Log $P_{o/w}$ (WLOGP)	4.48
Log $P_{o/w}$ (MLOGP)	1.96
Log $P_{o/w}$ (SILICOS-IT)	3.96
Consensus Log $P_{o/w}$	3.32

Water Solubility	
Log S (ESOL)	-4.53
Solubility	1.28e-02 mg/ml ; 2.98e-05 mol/l
Class	Moderately soluble
Log S (Ali)	-5.19
Solubility	2.77e-03 mg/ml ; 6.48e-06 mol/l
Class	Moderately soluble
Log S (SILICOS-IT)	-6.57
Solubility	1.16e-04 mg/ml ; 2.71e-07 mol/l
Class	Poorly soluble
Pharmacokinetics	
GI absorption	High
BBB permeant	No
P-gp substrate	No
CYP1A2 inhibitor	No
CYP2C19 inhibitor	No
CYP2C9 inhibitor	Yes
CYP2D6 inhibitor	No
CYP3A4 inhibitor	Yes
Log K_p (skin permeation)	-6.43 cm/s
Druglikeness	
Lipinski	Yes; 0 violation
Ghose	Yes
Weber	Yes
Egan	Yes
Muegge	Yes
Bioavailability Score	0.56
Medicinal Chemistry	
PAINS	1 alert: quinone_A
Brenk	1 alert: triple_bond
Leadlikeness	No; 1 violation: MW>350
Synthetic accessibility	3.80

Compound 3.65

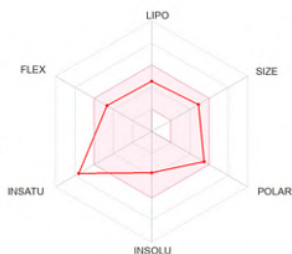
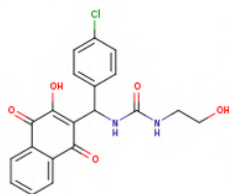


SMILES C#CCNC(=O)NC(C1=C(O)C(=O)c2c(C1=O)cccc2)c1ccc(cc1)OC

Physicochemical Properties	
Formula	C ₂₂ H ₁₈ N ₂ O ₅
Molecular weight	390.39 g/mol
Num. heavy atoms	29
Num. arom. heavy atoms	12
Fraction Csp ³	0.14
Num. rotatable bonds	7
Num. H-bond acceptors	5
Num. H-bond donors	3
Molar Refractivity	105.18
TPSA	104.73 Å ²
Lipophilicity	
Log P _{o/w} (ILOGP)	2.59
Log P _{o/w} (XLOGP3)	2.59
Log P _{o/w} (WLOGP)	2.32
Log P _{o/w} (MLOGP)	0.84
Log P _{o/w} (SILICOS-IT)	2.93
Consensus Log P _{o/w}	2.25

Water Solubility	
Log S (ESOL)	-3.74
Solubility	7.16e-02 mg/ml ; 1.84e-04 mol/l
Class	Soluble
Log S (Ali)	-4.44
Solubility	1.42e-02 mg/ml ; 3.65e-05 mol/l
Class	Moderately soluble
Log S (SILICOS-IT)	-5.84
Solubility	5.62e-04 mg/ml ; 1.44e-06 mol/l
Class	Moderately soluble
Pharmacokinetics	
GI absorption	High
BBB permeant	No
P-gp substrate	Yes
CYP1A2 inhibitor	No
CYP2C19 inhibitor	No
CYP2C9 inhibitor	Yes
CYP2D6 inhibitor	No
CYP3A4 inhibitor	Yes
Log K _p (skin permeation)	-6.84 cm/s
Druglikeness	
Lipinski	Yes; 0 violation
Ghose	Yes
Veber	Yes
Egan	Yes
Muegge	Yes
Bioavailability Score	0.56
Medicinal Chemistry	
PAINS	1 alert: quinone_A
Brenk	1 alert: triple_bond
Leadlikeness	No; 1 violation: MW>350
Synthetic accessibility	3.74

Compound 3.66

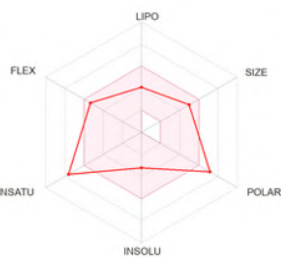
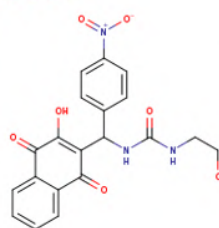


SMILES OCCNC(=O)NC(C1=C(O)C(=O)c2c(C1=O)cccc2)c1ccc(cc1)Cl

Physicochemical Properties	
Formula	C ₂₀ H ₁₇ ClN ₂ O ₅
Molecular weight	400.81 g/mol
Num. heavy atoms	28
Num. arom. heavy atoms	12
Fraction Csp ³	0.15
Num. rotatable bonds	7
Num. H-bond acceptors	5
Num. H-bond donors	4
Molar Refractivity	101.89
TPSA	115.73 Å ²
Lipophilicity	
Log P _{o/w} (ILOGP)	2.28
Log P _{o/w} (XLOGP3)	2.45
Log P _{o/w} (WLOGP)	2.24
Log P _{o/w} (MLOGP)	0.70
Log P _{o/w} (SILICOS-IT)	2.67
Consensus Log P _{o/w}	2.07

Water Solubility	
Log S (ESOL)	-3.72
Solubility	7.57e-02 mg/ml ; 1.89e-04 mol/l
Class	Soluble
Log S (Ali)	-4.52
Solubility	1.20e-02 mg/ml ; 2.99e-05 mol/l
Class	Moderately soluble
Log S (SILICOS-IT)	-6.07
Solubility	3.42e-04 mg/ml ; 8.53e-07 mol/l
Class	Poorly soluble
Pharmacokinetics	
GI absorption	High
BBB permeant	No
P-gp substrate	Yes
CYP1A2 inhibitor	No
CYP2C19 inhibitor	No
CYP2C9 inhibitor	Yes
CYP2D6 inhibitor	No
CYP3A4 inhibitor	No
Log K _p (skin permeation)	-7.01 cm/s
Druglikeness	
Lipinski	Yes; 0 violation
Ghose	Yes
Veber	Yes
Egan	Yes
Muegge	Yes
Bioavailability Score	0.56
Medicinal Chemistry	
PAINS	1 alert: quinone_A
Brenk	0 alert
Leadlikeness	No; 1 violation: MW>350
Synthetic accessibility	3.66

Compound 3.67

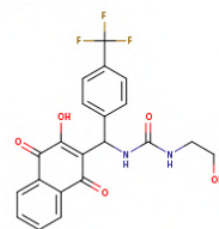


SMILES OCCNC(=O)NC(C1=C(O)C(=O)c2c(C1=O)cccc2)c1ccc(cc1)[N+](=O)[O-]

Physicochemical Properties	
Formula	C20H17N3O7
Molecular weight	411.36 g/mol
Num. heavy atoms	30
Num. arom. heavy atoms	12
Fraction Csp3	0.15
Num. rotatable bonds	8
Num. H-bond acceptors	7
Num. H-bond donors	4
Molar Refractivity	105.71
TPSA	161.55 Å²
Lipophilicity	
Log $P_{o/w}$ (ILOGP)	1.81
Log $P_{o/w}$ (XLOGP3)	1.65
Log $P_{o/w}$ (WLOGP)	1.49
Log $P_{o/w}$ (MLOGP)	-0.65
Log $P_{o/w}$ (SILICOS-IT)	-0.11
Consensus Log $P_{o/w}$	0.84

Water Solubility	
Log S (ESOL)	-3.20
Solubility	2.61e-01 mg/ml ; 6.34e-04 mol/l
Class	Soluble
Log S (Ali)	-4.66
Solubility	9.08e-03 mg/ml ; 2.21e-05 mol/l
Class	Moderately soluble
Log S (SILICOS-IT)	-4.82
Solubility	6.17e-03 mg/ml ; 1.50e-05 mol/l
Class	Moderately soluble
Pharmacokinetics	
GI absorption	Low
BBB permeant	No
P-gp substrate	Yes
CYP1A2 inhibitor	No
CYP2C19 inhibitor	No
CYP2C9 inhibitor	Yes
CYP2D6 inhibitor	No
CYP3A4 inhibitor	No
Log K_p (skin permeation)	-7.64 cm/s
Druglikeness	
Lipinski	Yes; 0 violation
Ghose	Yes
Veber	No; 1 violation: TPSA>140
Egan	No; 1 violation: TPSA>131.6
Muegge	No; 1 violation: TPSA>150
Bioavailability Score	0.11
Medicinal Chemistry	
PAINS	1 alert: quinone_A
Brenk	2 alerts: nitro_group, oxygen-nitrogen_single_bond
Leadlikeness	No; 2 violations: MW>350, Rotors>7
Synthetic accessibility	3.74

Compound 3.68



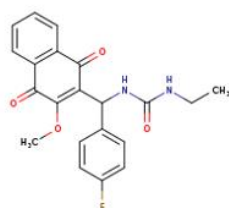
SMILES OCCNC(=O)NC(C1=C(O)C(=O)c2c(C1=O)cccc2)c1ccc(cc1)C(F)(F)F

Physicochemical Properties	
Formula	C21H17F3N2O5
Molecular weight	434.37 g/mol
Num. heavy atoms	31
Num. arom. heavy atoms	12
Fraction Csp3	0.19
Num. rotatable bonds	8
Num. H-bond acceptors	8
Num. H-bond donors	4
Molar Refractivity	101.89
TPSA	115.73 Å²
Lipophilicity	
Log $P_{o/w}$ (ILOGP)	2.38
Log $P_{o/w}$ (XLOGP3)	2.70
Log $P_{o/w}$ (WLOGP)	3.76
Log $P_{o/w}$ (MLOGP)	1.02
Log $P_{o/w}$ (SILICOS-IT)	3.13
Consensus Log $P_{o/w}$	2.60

Water Solubility	
Log S (ESOL)	-3.99
Solubility	4.42e-02 mg/ml ; 1.02e-04 mol/l
Class	Soluble
Log S (Ali)	-4.78
Solubility	7.15e-03 mg/ml ; 1.65e-05 mol/l
Class	Moderately soluble
Log S (SILICOS-IT)	-6.31
Solubility	2.13e-04 mg/ml ; 4.91e-07 mol/l
Class	Poorly soluble
Pharmacokinetics	
GI absorption	High
BBB permeant	No
P-gp substrate	Yes
CYP1A2 inhibitor	No
CYP2C19 inhibitor	No
CYP2C9 inhibitor	Yes
CYP2D6 inhibitor	No
CYP3A4 inhibitor	No
Log K_p (skin permeation)	-7.03 cm/s
Druglikeness	
Lipinski	Yes; 0 violation
Ghose	Yes
Veber	Yes
Egan	Yes
Muegge	Yes
Bioavailability Score	0.56
Medicinal Chemistry	
PAINS	1 alert: quinone_A
Brenk	0 alert
Leadlikeness	No; 2 violations: MW>350, Rotors>7
Synthetic accessibility	3.80

3.4 Methylated Biginelli-linear series

Compound 3.72

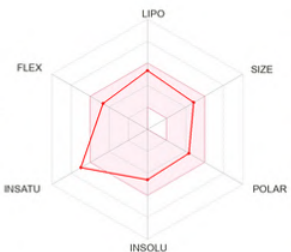
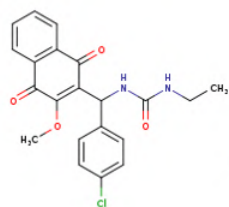


SMILES CCNC(=O)NC(C=C(OC)C(=O)c2c(C1=O)cccc2)c1ccc(cc1)F

Physicochemical Properties	
Formula	C ₂₁ H ₁₉ FN ₂ O ₄
Molecular weight	382.38 g/mol
Num. heavy atoms	28
Num. arom. heavy atoms	12
Fraction Csp ³	0.19
Num. rotatable bonds	7
Num. H-bond acceptors	5
Num. H-bond donors	2
Molar Refractivity	100.00
TPSA	84.50 Å ²
Lipophilicity	
Log <i>P</i> _{o/w} (iLOGP)	2.60
Log <i>P</i> _{o/w} (XLOGP3)	3.30
Log <i>P</i> _{o/w} (WLOGP)	3.26
Log <i>P</i> _{o/w} (MLOGP)	1.61
Log <i>P</i> _{o/w} (SILICOS-IT)	3.60
Consensus Log <i>P</i> _{o/w}	2.87

Water Solubility	
Log S (ESOL)	-4.14
Solubility	2.74e-02 mg/ml ; 7.16e-05 mol/l
Class	Moderately soluble
Log S (All)	-4.75
Solubility	6.80e-03 mg/ml ; 1.78e-05 mol/l
Class	Moderately soluble
Log S (SILICOS-IT)	-7.01
Solubility	3.76e-05 mg/ml ; 9.84e-08 mol/l
Class	Poorly soluble
Pharmacokinetics	
GI absorption	High
BBB permeant	No
P-gp substrate	No
CYP1A2 inhibitor	No
CYP2C19 inhibitor	Yes
CYP2C9 inhibitor	Yes
CYP2D6 inhibitor	No
CYP3A4 inhibitor	Yes
Log <i>K</i> _p (skin permeation)	-6.29 cm/s
Druglikeness	
Lipinski	Yes; 0 violation
Ghose	Yes
Veber	Yes
Egan	Yes
Muegge	Yes
Bioavailability Score	0.56
Medicinal Chemistry	
PAINS	1 alert: quinone_A
Brenk	0 alert
Leadlikeness	No; 1 violation: MW>350
Synthetic accessibility	3.82

Compound 3.73

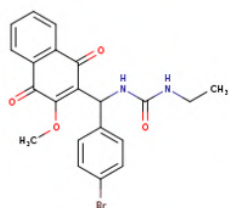


SMILES CCNC(=O)NC(C=C(OC)C(=O)c2c(C1=O)cccc2)c1ccc(cc1)Cl

Physicochemical Properties	
Formula	C ₂₁ H ₁₉ ClN ₂ O ₄
Molecular weight	398.84 g/mol
Num. heavy atoms	28
Num. arom. heavy atoms	12
Fraction Csp ³	0.19
Num. rotatable bonds	7
Num. H-bond acceptors	4
Num. H-bond donors	2
Molar Refractivity	105.05
TPSA	84.50 Å ²
Lipophilicity	
Log <i>P</i> _{o/w} (iLOGP)	2.85
Log <i>P</i> _{o/w} (XLOGP3)	3.82
Log <i>P</i> _{o/w} (WLOGP)	3.36
Log <i>P</i> _{o/w} (MLOGP)	1.71
Log <i>P</i> _{o/w} (SILICOS-IT)	3.82
Consensus Log <i>P</i> _{o/w}	3.11

Water Solubility	
Log S (ESOL)	-4.57
Solubility	1.06e-02 mg/ml ; 2.66e-05 mol/l
Class	Moderately soluble
Log S (All)	-5.29
Solubility	2.05e-03 mg/ml ; 5.13e-06 mol/l
Class	Moderately soluble
Log S (SILICOS-IT)	-7.33
Solubility	1.87e-05 mg/ml ; 4.68e-08 mol/l
Class	Poorly soluble
Pharmacokinetics	
GI absorption	High
BBB permeant	No
P-gp substrate	No
CYP1A2 inhibitor	Yes
CYP2C19 inhibitor	Yes
CYP2C9 inhibitor	Yes
CYP2D6 inhibitor	No
CYP3A4 inhibitor	Yes
Log <i>K</i> _p (skin permeation)	-6.02 cm/s
Druglikeness	
Lipinski	Yes; 0 violation
Ghose	Yes
Veber	Yes
Egan	Yes
Muegge	Yes
Bioavailability Score	0.56
Medicinal Chemistry	
PAINS	1 alert: quinone_A
Brenk	0 alert
Leadlikeness	No; 2 violations: MW>350, XLOGP3>3.5
Synthetic accessibility	3.81

Compound 3.74

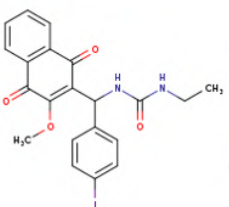


SMILES CCNC(=O)NC(C=C(OC)C(=O)c2c(C1=O)cccc2)c1ccc(cc1)Br

Physicochemical Properties	
Formula	C ₂₁ H ₁₉ BrN ₂ O ₄
Molecular weight	443.29 g/mol
Num. heavy atoms	28
Num. arom. heavy atoms	12
Fraction Csp ³	0.19
Num. rotatable bonds	7
Num. H-bond acceptors	4
Num. H-bond donors	2
Molar Refractivity	107.74
TPSA	84.50 Å ²
Lipophilicity	
Log <i>P</i> _{o/w} (ILOGP)	3.03
Log <i>P</i> _{o/w} (XLOGP3)	3.89
Log <i>P</i> _{o/w} (WLOGP)	3.46
Log <i>P</i> _{o/w} (MLOGP)	1.82
Log <i>P</i> _{o/w} (SILICOS-IT)	3.85
Consensus Log <i>P</i> _{o/w}	3.21

Water Solubility	
Log S (ESOL)	-4.89
Solubility	5.66e-03 mg/ml ; 1.28e-05 mol/l
Class	Moderately soluble
Log S (Ali)	-5.36
Solubility	1.92e-03 mg/ml ; 4.34e-06 mol/l
Class	Moderately soluble
Log S (SILICOS-IT)	-7.53
Solubility	1.32e-05 mg/ml ; 2.99e-08 mol/l
Class	Poorly soluble
Pharmacokinetics	
GI absorption	High
BBB permeant	No
P-gp substrate	No
CYP1A2 inhibitor	Yes
CYP2C19 inhibitor	Yes
CYP2C9 inhibitor	Yes
CYP2D6 inhibitor	No
CYP3A4 inhibitor	Yes
Log <i>K</i> _p (skin permeation)	-6.24 cm/s
Druglikeness	
Lipinski	Yes; 0 violation
Ghose	Yes
Veber	Yes
Egan	Yes
Muegge	Yes
Bioavailability Score	0.56
Medicinal Chemistry	
PAINS	1 alert: quinone_A
Brenk	0 alert
Leadlikeness	No; 2 violations: MW>350, XLOGP3>3.5
Synthetic accessibility	3.83

Compound 3.75

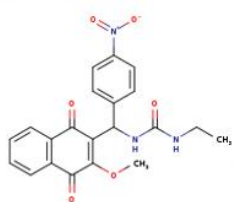


SMILES CCNC(=O)NC(C=C(OC)C(=O)c2c(C1=O)cccc2)c1ccc(cc1)I

Physicochemical Properties	
Formula	C ₂₁ H ₁₉ I ₂ N ₂ O ₄
Molecular weight	490.29 g/mol
Num. heavy atoms	28
Num. arom. heavy atoms	12
Fraction Csp ³	0.19
Num. rotatable bonds	7
Num. H-bond acceptors	4
Num. H-bond donors	2
Molar Refractivity	112.76
TPSA	84.50 Å ²
Lipophilicity	
Log <i>P</i> _{o/w} (ILOGP)	2.90
Log <i>P</i> _{o/w} (XLOGP3)	3.84
Log <i>P</i> _{o/w} (WLOGP)	3.31
Log <i>P</i> _{o/w} (MLOGP)	1.93
Log <i>P</i> _{o/w} (SILICOS-IT)	4.14
Consensus Log <i>P</i> _{o/w}	3.22

Water Solubility	
Log S (ESOL)	-5.15
Solubility	3.44e-03 mg/ml ; 7.01e-06 mol/l
Class	Moderately soluble
Log S (Ali)	-5.31
Solubility	2.40e-03 mg/ml ; 4.89e-06 mol/l
Class	Moderately soluble
Log S (SILICOS-IT)	-7.57
Solubility	1.31e-05 mg/ml ; 2.67e-08 mol/l
Class	Poorly soluble
Pharmacokinetics	
GI absorption	High
BBB permeant	No
P-gp substrate	No
CYP1A2 inhibitor	Yes
CYP2C19 inhibitor	Yes
CYP2C9 inhibitor	Yes
CYP2D6 inhibitor	No
CYP3A4 inhibitor	Yes
Log <i>K</i> _p (skin permeation)	-6.56 cm/s
Druglikeness	
Lipinski	Yes; 0 violation
Ghose	No; 1 violation: MW>480
Veber	Yes
Egan	Yes
Muegge	Yes
Bioavailability Score	0.56
Medicinal Chemistry	
PAINS	1 alert: quinone_A
Brenk	1 alert: iodine
Leadlikeness	No; 2 violations: MW>350, XLOGP3>3.5
Synthetic accessibility	3.91

Compound 3.76

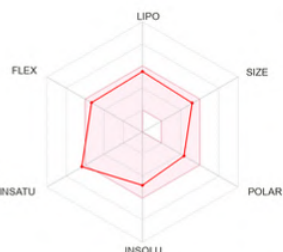
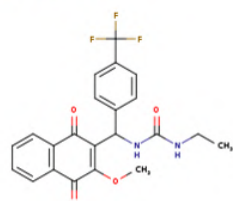


SMILES CCNC(=O)NC(C1=C(OC)C(=O)c2c(C1=O)cccc2)c1ccc(cc1)[N+](=O)[O-]

Physicochemical Properties	
Formula	C ₂₁ H ₁₉ N ₃ O ₆
Molecular weight	409.39 g/mol
Num. heavy atoms	30
Num. arom. heavy atoms	12
Fraction Csp ³	0.19
Num. rotatable bonds	8
Num. H-bond acceptors	6
Num. H-bond donors	2
Molar Refractivity	108.86
TPSA	130.32 Å ²
Lipophilicity	
Log <i>P</i> _{o/w} (iLOGP)	2.33
Log <i>P</i> _{o/w} (XLOGP3)	3.02
Log <i>P</i> _{o/w} (WLOGP)	2.61
Log <i>P</i> _{o/w} (MLOGP)	0.34
Log <i>P</i> _{o/w} (SILICOS-IT)	1.03
Consensus Log <i>P</i> _{o/w}	1.87

Water Solubility	
Log S (ESOL)	-4.05
Solubility	3.66e-02 mg/ml ; 8.94e-05 mol/l
Class	Moderately soluble
Log S (Ali)	-5.42
Solubility	1.55e-03 mg/ml ; 3.79e-06 mol/l
Class	Moderately soluble
Log S (SILICOS-IT)	-6.08
Solubility	3.37e-04 mg/ml ; 8.22e-07 mol/l
Class	Poorly soluble
Pharmacokinetics	
GI absorption	High
BBB permeant	No
P-gp substrate	No
CYP1A2 inhibitor	No
CYP2C19 inhibitor	Yes
CYP2C9 inhibitor	Yes
CYP2D6 inhibitor	Yes
CYP3A4 inhibitor	Yes
Log <i>K</i> _p (skin permeation)	-6.65 cm/s
Druglikeness	
Lipinski	Yes; 0 violation
Ghose	Yes
Veber	Yes
Egan	Yes
Muegge	Yes
Bioavailability Score	0.56
Medicinal Chemistry	
PAINS	1 alert: quinone_A
Brenk	2 alerts: nitro_group, oxygen-nitrogen_single_bond
Leadlikeness	No; 2 violations: MW>350, Rotors>7
Synthetic accessibility	3.88

Compound 3.77

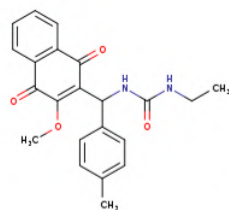


SMILES CCNC(=O)NC(C1=C(OC)C(=O)c2c(C1=O)cccc2)c1ccc(cc1)C(F)F

Physicochemical Properties	
Formula	C ₂₂ H ₁₉ F ₃ N ₂ O ₄
Molecular weight	432.39 g/mol
Num. heavy atoms	31
Num. arom. heavy atoms	12
Fraction Csp ³	0.23
Num. rotatable bonds	8
Num. H-bond acceptors	7
Num. H-bond donors	2
Molar Refractivity	105.04
TPSA	84.50 Å ²
Lipophilicity	
Log <i>P</i> _{o/w} (iLOGP)	2.95
Log <i>P</i> _{o/w} (XLOGP3)	4.08
Log <i>P</i> _{o/w} (WLOGP)	4.87
Log <i>P</i> _{o/w} (MLOGP)	2.04
Log <i>P</i> _{o/w} (SILICOS-IT)	4.28
Consensus Log <i>P</i> _{o/w}	3.64

Water Solubility	
Log S (ESOL)	-4.85
Solubility	6.11e-03 mg/ml ; 1.41e-05 mol/l
Class	Moderately soluble
Log S (Ali)	-5.56
Solubility	1.19e-03 mg/ml ; 2.76e-06 mol/l
Class	Moderately soluble
Log S (SILICOS-IT)	-7.57
Solubility	1.16e-05 mg/ml ; 2.69e-08 mol/l
Class	Poorly soluble
Pharmacokinetics	
GI absorption	High
BBB permeant	No
P-gp substrate	No
CYP1A2 inhibitor	No
CYP2C19 inhibitor	Yes
CYP2C9 inhibitor	Yes
CYP2D6 inhibitor	No
CYP3A4 inhibitor	Yes
Log <i>K</i> _p (skin permeation)	-6.04 cm/s
Druglikeness	
Lipinski	Yes; 0 violation
Ghose	Yes
Veber	Yes
Egan	Yes
Muegge	Yes
Bioavailability Score	0.56
Medicinal Chemistry	
PAINS	1 alert: quinone_A
Brenk	0 alert
Leadlikeness	No; 3 violations: MW>350, Rotors>7, XLOGP3>3.5
Synthetic accessibility	3.95

Compound 3.78

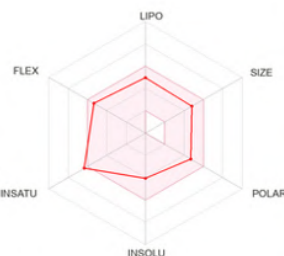
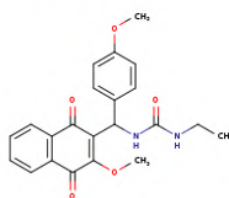


SMILES CCNC(=O)NC(C=C(OC)C(=O)c2c(C1=O)cccc2)c1ccc(cc1)C

Physicochemical Properties	
Formula	C ₂₂ H ₂₂ N ₂ O ₄
Molecular weight	378.42 g/mol
Num. heavy atoms	28
Num. arom. heavy atoms	12
Fraction Csp ³	0.23
Num. rotatable bonds	7
Num. H-bond acceptors	4
Num. H-bond donors	2
Molar Refractivity	105.01
TPSA	84.50 Å ²
Lipophilicity	
Log <i>P</i> _{o/w} (ILOGP)	2.79
Log <i>P</i> _{o/w} (XLOGP3)	3.56
Log <i>P</i> _{o/w} (WLOGP)	3.01
Log <i>P</i> _{o/w} (MLOGP)	1.45
Log <i>P</i> _{o/w} (SILICOS-IT)	3.70
Consensus Log <i>P</i> _{o/w}	2.90

Water Solubility	
Log S (ESOL)	-4.28
Solubility	1.97e-02 mg/ml ; 5.20e-05 mol/l
Class	Moderately soluble
Log S (Ali)	-5.02
Solubility	3.61e-03 mg/ml ; 9.55e-06 mol/l
Class	Moderately soluble
Log S (SILICOS-IT)	-7.12
Solubility	2.88e-05 mg/ml ; 7.62e-08 mol/l
Class	Poorly soluble
Pharmacokinetics	
GI absorption	High
BBB permeant	No
P-gp substrate	No
CYP1A2 inhibitor	No
CYP2C19 inhibitor	Yes
CYP2C9 inhibitor	Yes
CYP2D6 inhibitor	No
CYP3A4 inhibitor	Yes
Log <i>K</i> _p (skin permeation)	-6.08 cm/s
Druglikeness	
Lipinski	Yes; 0 violation
Ghose	Yes
Veber	Yes
Egan	Yes
Muegge	Yes
Bioavailability Score	0.56
Medicinal Chemistry	
PAINS	1 alert: quinone_A
Brenk	0 alert
Leadlikeness	No; 2 violations: MW>350, XLOGP3>3.5
Synthetic accessibility	3.91

Compound 3.79

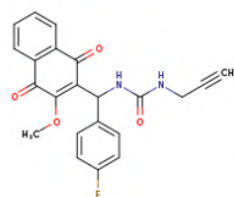


SMILES CCNC(=O)NC(C=C(OC)C(=O)c2c(C1=O)cccc2)c1ccc(cc1)OC

Physicochemical Properties	
Formula	C ₂₂ H ₂₂ N ₂ O ₅
Molecular weight	394.42 g/mol
Num. heavy atoms	29
Num. arom. heavy atoms	12
Fraction Csp ³	0.23
Num. rotatable bonds	8
Num. H-bond acceptors	5
Num. H-bond donors	2
Molar Refractivity	106.53
TPSA	93.73 Å ²
Lipophilicity	
Log <i>P</i> _{o/w} (ILOGP)	2.92
Log <i>P</i> _{o/w} (XLOGP3)	3.17
Log <i>P</i> _{o/w} (WLOGP)	2.71
Log <i>P</i> _{o/w} (MLOGP)	0.92
Log <i>P</i> _{o/w} (SILICOS-IT)	3.25
Consensus Log <i>P</i> _{o/w}	2.59

Water Solubility	
Log S (ESOL)	-4.06
Solubility	3.43e-02 mg/ml ; 8.70e-05 mol/l
Class	Moderately soluble
Log S (Ali)	-4.81
Solubility	6.12e-03 mg/ml ; 1.55e-05 mol/l
Class	Moderately soluble
Log S (SILICOS-IT)	-6.85
Solubility	5.62e-05 mg/ml ; 1.43e-07 mol/l
Class	Poorly soluble
Pharmacokinetics	
GI absorption	High
BBB permeant	No
P-gp substrate	Yes
CYP1A2 inhibitor	No
CYP2C19 inhibitor	Yes
CYP2C9 inhibitor	Yes
CYP2D6 inhibitor	Yes
CYP3A4 inhibitor	Yes
Log <i>K</i> _p (skin permeation)	-6.46 cm/s
Druglikeness	
Lipinski	Yes; 0 violation
Ghose	Yes
Veber	Yes
Egan	Yes
Muegge	Yes
Bioavailability Score	0.56
Medicinal Chemistry	
PAINS	1 alert: quinone_A
Brenk	0 alert
Leadlikeness	No; 2 violations: MW>350, Rotors>7
Synthetic accessibility	3.90

Compound 3.80

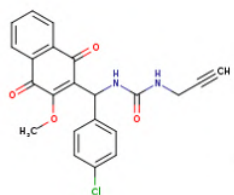


SMILES C#CCNC(=O)NC(C1=C(OC)C(=O)c2c(C1=O)cccc2)c1ccc(cc1)F

Physicochemical Properties	
Formula	C ₂₂ H ₁₇ N ₂ O ₄
Molecular weight	392.38 g/mol
Num. heavy atoms	29
Num. arom. heavy atoms	12
Fraction Csp ³	0.14
Num. rotatable bonds	7
Num. H-bond acceptors	5
Num. H-bond donors	2
Molar Refractivity	102.97
TPSA	84.50 Å ²
Lipophilicity	
Log <i>P</i> _{o/w} (iLOGP)	2.83
Log <i>P</i> _{o/w} (XLOGP3)	3.04
Log <i>P</i> _{o/w} (WLOGP)	2.95
Log <i>P</i> _{o/w} (MLOGP)	1.75
Log <i>P</i> _{o/w} (SILICOS-IT)	3.83
Consensus Log <i>P</i> _{o/w}	2.88

Water Solubility	
Log S (ESOL)	-4.03
Solubility	3.64e-02 mg/ml ; 9.29e-05 mol/l
Class	Moderately soluble
Log S (Ali)	-4.48
Solubility	1.30e-02 mg/ml ; 3.31e-05 mol/l
Class	Moderately soluble
Log S (SILICOS-IT)	-6.70
Solubility	7.92e-05 mg/ml ; 2.02e-07 mol/l
Class	Poorly soluble
Pharmacokinetics	
GI absorption	High
BBB permeant	No
P-gp substrate	No
CYP1A2 inhibitor	No
CYP2C19 inhibitor	Yes
CYP2C9 inhibitor	Yes
CYP2D6 inhibitor	No
CYP3A4 inhibitor	Yes
Log <i>K</i> _p (skin permeation)	-6.54 cm/s
Druglikeness	
Lipinski	Yes; 0 violation
Ghose	Yes
Veber	Yes
Egan	Yes
Muegge	Yes
Bioavailability Score	0.56
Medicinal Chemistry	
PAINS	1 alert: quinone_A
Brenk	1 alert: triple_bond
Leadlikeness	No; 1 violation: MW>350
Synthetic accessibility	3.86

Compound 3.81

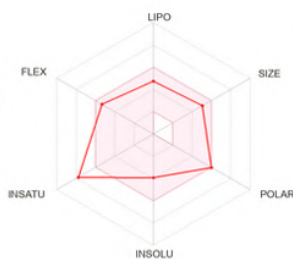
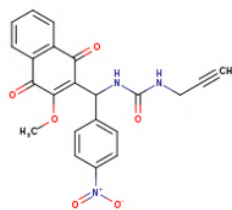


SMILES C#CCNC(=O)NC(C1=C(OC)C(=O)c2c(C1=O)cccc2)c1ccc(cc1)Cl

Physicochemical Properties	
Formula	C ₂₂ H ₁₇ ClN ₂ O ₄
Molecular weight	408.83 g/mol
Num. heavy atoms	29
Num. arom. heavy atoms	12
Fraction Csp ³	0.14
Num. rotatable bonds	7
Num. H-bond acceptors	4
Num. H-bond donors	2
Molar Refractivity	108.02
TPSA	84.50 Å ²
Lipophilicity	
Log <i>P</i> _{o/w} (iLOGP)	3.06
Log <i>P</i> _{o/w} (XLOGP3)	3.57
Log <i>P</i> _{o/w} (WLOGP)	3.05
Log <i>P</i> _{o/w} (MLOGP)	1.86
Log <i>P</i> _{o/w} (SILICOS-IT)	4.05
Consensus Log <i>P</i> _{o/w}	3.12

Water Solubility	
Log S (ESOL)	-4.47
Solubility	1.39e-02 mg/ml ; 3.40e-05 mol/l
Class	Moderately soluble
Log S (Ali)	-5.03
Solubility	3.81e-03 mg/ml ; 9.33e-06 mol/l
Class	Moderately soluble
Log S (SILICOS-IT)	-7.02
Solubility	3.93e-05 mg/ml ; 9.62e-08 mol/l
Class	Poorly soluble
Pharmacokinetics	
GI absorption	High
BBB permeant	No
P-gp substrate	No
CYP1A2 inhibitor	Yes
CYP2C19 inhibitor	Yes
CYP2C9 inhibitor	Yes
CYP2D6 inhibitor	No
CYP3A4 inhibitor	Yes
Log <i>K</i> _p (skin permeation)	-6.26 cm/s
Druglikeness	
Lipinski	Yes; 0 violation
Ghose	Yes
Veber	Yes
Egan	Yes
Muegge	Yes
Bioavailability Score	0.56
Medicinal Chemistry	
PAINS	1 alert: quinone_A
Brenk	1 alert: triple_bond
Leadlikeness	No; 2 violations: MW>350, XLOGP3>3.5
Synthetic accessibility	3.85

Compound 3.82

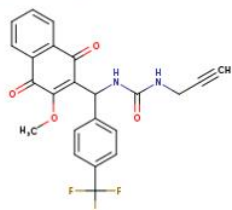


SMILES C#CCNC(=O)NC(C1=C(OC)C(=O)c2c(C1=O)cccc2)c1ccc(cc1)[N+](=O)[O-]

Physicochemical Properties	
Formula	C22H17N3O6
Molecular weight	419.39 g/mol
Num. heavy atoms	31
Num. arom. heavy atoms	12
Fraction Csp3	0.14
Num. rotatable bonds	8
Num. H-bond acceptors	6
Num. H-bond donors	2
Molar Refractivity	111.83
TPSA	130.32 Å²
Lipophilicity	
Log $P_{o/w}$ (ILOGP)	2.41
Log $P_{o/w}$ (XLOGP3)	2.77
Log $P_{o/w}$ (WLOGP)	2.30
Log $P_{o/w}$ (MLOGP)	0.49
Log $P_{o/w}$ (SILICOS-IT)	1.27
Consensus Log $P_{o/w}$	1.85

Water Solubility	
Log S (ESOL)	-3.94
Solubility	4.77e-02 mg/ml ; 1.14e-04 mol/l
Class	Soluble
Log S (Ali)	-5.16
Solubility	2.89e-03 mg/ml ; 6.88e-06 mol/l
Class	Moderately soluble
Log S (SILICOS-IT)	-5.77
Solubility	7.09e-04 mg/ml ; 1.69e-06 mol/l
Class	Moderately soluble
Pharmacokinetics	
GI absorption	High
BBB permeant	No
P-gp substrate	No
CYP1A2 inhibitor	No
CYP2C19 inhibitor	No
CYP2C9 inhibitor	Yes
CYP2D6 inhibitor	No
CYP3A4 inhibitor	Yes
Log K_p (skin permeation)	-6.89 cm/s
Druglikeness	
Lipinski	Yes; 0 violation
Ghose	Yes
Veber	Yes
Egan	Yes
Muegge	Yes
Bioavailability Score	0.56
Medicinal Chemistry	
PAINS	1 alert: quinone_A
Brenk	3 alerts: nitro_group, oxygen-nitrogen_single_bond, triple_bond
Leadlikeness	No; 2 violations: MW>350, Rotors>7
Synthetic accessibility	3.91

Compound 3.83

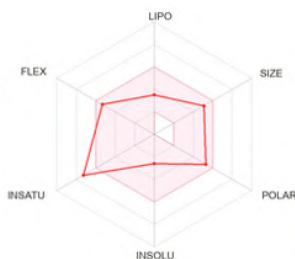
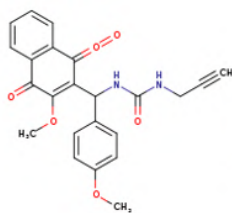


SMILES C#CCNC(=O)NC(C1=C(OC)C(=O)c2c(C1=O)cccc2)c1ccc(cc1)C(F)(F)F

Physicochemical Properties	
Formula	C23H17F3N2O4
Molecular weight	442.39 g/mol
Num. heavy atoms	32
Num. arom. heavy atoms	12
Fraction Csp3	0.17
Num. rotatable bonds	8
Num. H-bond acceptors	7
Num. H-bond donors	2
Molar Refractivity	108.01
TPSA	84.50 Å²
Lipophilicity	
Log $P_{o/w}$ (ILOGP)	2.87
Log $P_{o/w}$ (XLOGP3)	3.83
Log $P_{o/w}$ (WLOGP)	4.57
Log $P_{o/w}$ (MLOGP)	2.17
Log $P_{o/w}$ (SILICOS-IT)	4.51
Consensus Log $P_{o/w}$	3.59

Water Solubility	
Log S (ESOL)	-4.75
Solubility	7.95e-03 mg/ml ; 1.80e-05 mol/l
Class	Moderately soluble
Log S (Ali)	-5.30
Solubility	2.22e-03 mg/ml ; 5.01e-06 mol/l
Class	Moderately soluble
Log S (SILICOS-IT)	-7.26
Solubility	2.45e-05 mg/ml ; 5.55e-08 mol/l
Class	Poorly soluble
Pharmacokinetics	
GI absorption	High
BBB permeant	No
P-gp substrate	No
CYP1A2 inhibitor	Yes
CYP2C19 inhibitor	Yes
CYP2C9 inhibitor	Yes
CYP2D6 inhibitor	No
CYP3A4 inhibitor	Yes
Log K_p (skin permeation)	-6.28 cm/s
Druglikeness	
Lipinski	Yes; 0 violation
Ghose	Yes
Veber	Yes
Egan	Yes
Muegge	Yes
Bioavailability Score	0.56
Medicinal Chemistry	
PAINS	1 alert: quinone_A
Brenk	1 alert: triple_bond
Leadlikeness	No; 3 violations: MW>350, Rotors>7, XLOGP3>3.5
Synthetic accessibility	3.98

Compound 3.84



SMILES C#CCNC(=O)NC(C1=C(C(OC)C(=O)c2c(C1=O)=O)cccc2)c1ccc(cc1)OC

Physicochemical Properties	
Formula	C ₂₃ H ₂₀ N ₂ O ₆
Molecular weight	420.41 g/mol
Num. heavy atoms	31
Num. arom. heavy atoms	12
Fraction Csp ³	0.17
Num. rotatable bonds	8
Num. H-bond acceptors	6
Num. H-bond donors	2
Molar Refractivity	112.87
TPSA	110.80 Å ²
Lipophilicity	
Log <i>P</i> _{o/w} (iLOGP)	0.00
Log <i>P</i> _{o/w} (XLOGP3)	0.61
Log <i>P</i> _{o/w} (WLOGP)	2.21
Log <i>P</i> _{o/w} (MLOGP)	1.01
Log <i>P</i> _{o/w} (SILICOS-IT)	2.11
Consensus Log <i>P</i> _{o/w}	1.19

Water Solubility	
Log S (ESOL)	-2.59
Solubility	1.08e+00 mg/ml ; 2.57e-03 mol/l
Class	Soluble
Log S (Ali)	-2.51
Solubility	1.30e+00 mg/ml ; 3.08e-03 mol/l
Class	Soluble
Log S (SILICOS-IT)	-6.57
Solubility	1.12e-04 mg/ml ; 2.67e-07 mol/l
Class	Poorly soluble
Pharmacokinetics	
GI absorption	High
BBB permeant	No
P-gp substrate	Yes
CYP1A2 inhibitor	No
CYP2C19 inhibitor	No
CYP2C9 inhibitor	No
CYP2D6 inhibitor	No
CYP3A4 inhibitor	No
Log <i>K</i> _p (skin permeation)	-8.43 cm/s
Druglikeness	
Lipinski	Yes; 0 violation
Ghose	Yes
Veber	Yes
Egan	Yes
Muegge	Yes
Bioavailability Score	0.56
Medicinal Chemistry	
PAINS	1 alert: quinone_A
Brenk	1 alert: triple_bond
Leadlikeness	No; 2 violations: MW>350, Rotors>7
Synthetic accessibility	4.09

4. List of publications

1. Koumpoura, C. L.; Robert, A.; Athanassopoulos, C. M.; Baltas, M. Antimalarial Inhibitors Targeting Epigenetics or Mitochondria in *Plasmodium Falciparum*: Recent Survey upon Synthesis and Biological Evaluation of Potential Drugs against Malaria. *Molecules* **2021**, *26* (18), 5711. <https://doi.org/10.3390/molecules26185711>.
2. Koumpoura, C. L.; Nguyen, M.; Bijani, C.; Vendier, L.; Salina, E. G.; Buroni, S.; Degiacomi, G.; Cojean, S.; Loiseau, P. M.; Benoit-Vical, F.; Garcia-Sosa, A. T.; Robert, A.; Baltas, M. Design of Anti-Infectious Agents from Lawsone in a Three-Component Reaction with Aldehydes and Isocyanides. *ACS Omega* **2022**, *7* (40), 35635–35655. <https://doi.org/10.1021/acsomega.2c03421>.
3. Koumpoura, C. L.; Vendier, L.; Bijani, C.; Robert, A.; Carbonnière, P.; Sotiropoulos, J.-M.; Baltas, M. An Uncommon Multicomponent Reaction Activated by Mechanochemical Means Involving Lawsone. First-time Biginelli-type Linear Products. *Submitted to RSC Mechanochemistry*, **2023**.

NOM et prénom: KOUMPOURA Christina
Ecole doctorale : SDM - SCIENCES DE LA MATIERE - Toulouse
Diplôme de doctorat : Chimie-Biologie-Santé

Résumé:

Le paludisme et la leishmaniose sont deux maladies à transmission vectorielle (MVC) causées par des parasites (*Plasmodium* et *Leishmania* respectivement), transmises à l'homme par des insectes infectés. De nombreux groupes à travers le monde sont à la recherche de molécules capables de contourner le problème (multi)résistance aux médicaments, des pathogènes responsables.

Les dérivés de la naphtoquinone ont attiré une attention considérable au cours des dernières décennies à cause de l'atovaquone, médicament antipaludique comportant un fragment 2-hydroxy-1,4-naphtoquinone (ou lawsone), qui cible le complexe cytochrome bc1 dans la mitochondrie de *Plasmodium falciparum*. Ce motif est également présent dans des composés actifs contre *Leishmania*. Nous souhaitons donc concevoir et développer des composés possédant le motif lawsone qui pourraient être actifs contre ces deux parasites.

Notre approche se concentre sur l'utilisation de réactions multicomposants pour construire des composés à base de naphtoquinone. Dans ce cadre, nous avons étudié et développé deux réactions multicomposants impliquant la lawsone : la réaction domino et la réaction de Biginelli. Les conditions optimales pour la réaction domino ont été recherchées avec succès. Une série de 19 nouvelles naphtofuroquinones et 2 naphto-énaminodiones a été élaborée. Tous les composés ont été évalués *in vitro* contre *P. falciparum* (P.f.) et *L. donovani* (L.d.). Six composés sont actifs contre P.f. et trois contre L.d. Les deux naphto-énaminodiones sont actives sur les deux cibles. Les indices de sélectivité (SI) varient de 6 à 36. La réaction multicomposant de Biginelli, faisant intervenir la lawsone, diverses urées et des benzaldéhydes a été étudiée en solution et par mécano-chimie. Seule, l'activation mécano-chimique conduit avec des très bons rendements aux composés uniques issus du couplage des trois réactifs de manière linéaire, ainsi appelés « linéaires de Biginelli ». Ces composés n'ont jamais été décrits auparavant. Les dihydropyrimidinones de Biginelli, dérivés cycliques attendus n'ont pas pu être isolés. Pour expliquer ce résultat, une première approche de calcul théorique a été réalisée. Sur les composés linéaires de Biginelli, une étude a été menée pour obtenir de manière sélective les dérivés méthylés de la fonction éno. Nous avons également jeté les bases d'une réaction de cyclisation originale, conduisant à des carbamates.

Tous les composés linéaires de cette série ont été évalués *in vitro* contre P.f. et L.d. Les activités contre P.f. sont faibles, les meilleurs étant les composés méthylés ($CI_{50} < 10 \mu M$). Contre L.d., tous les dérivés méthylés sont actifs, car 7/13 ont des $CI_{50} < 2 \mu M$, par comparaison avec la miltéfosine ($CI_{50} = 1.5 \mu M$) qui est le médicament de référence.

Tous les composés ont été également évalués *in silico* contre les deux cibles mitochondriales de P.f. bc1 et dihydroorotate déshydrogénase (DHODH).